Proceedings of the 16th International Workshop on Laser Ranging

SLR – the Next Generation

Volume 1

October 13-17, 2008
Poznań, Poland

Book Title
Proceedings of the 16th International Workshop on Laser Ranging
October 2008, Poznań, Poland
Volume 1

Publisher
Space Research Centre, Polish Academy of Sciences
ul. Bartycka 18A
00-716 Warszawa
Poland
Tel: +48 22 840 3766
Fax: +48 22 840 3131

Published
December 2009

Printer
Drukarnia Oświatowa
ul. Głogowska 149
60-313 Poznań
drukoswiat@neostrada.pl

Edited by
Stanisław Schillak

SPONSORS

European Office of Aerospace Research and Development

We wish to thank the following for their contribution to the success of this conference: European Office of Aerospace Research and Development, Air Force Office of Scientific Research, United States Air Force Research Laboratory <http://www.london.af.mil>.

Polish Academy of Sciences, Committee on Space Research
http://www.kbkis.pan.pl/

IBB Andersia Hotel http://www.andersiahotel.pl/
Host of the Workshop

Kompania Piwowarska SA http://www.kp.pl/en
Kompania Piwowarska (KP), the best brews of beer
Making Beer, Making Friends

16th International Workshop on Laser Ranging
Poznań, Poland
13-17 October 2008

ORGANIZATION

Theme: "SLR – the Next Generation"

Venue: IBB Andersia Hotel

Program Committee

Dr. Graham Appleby	NERC Space Geodesy Facility, UK
Dr. John Degnan	Sigma Space Corporation, USA
Prof. Yang Fumin	Shanghai Astronomical Observatory, Chinese Academy of Sciences
Dr. Ben Greene	Electro Optic Systems Pty Ltd, Australia
Prof. Werner Gurtner	Astronomical Institute, University of Bern, Switzerland
Dr. Georg Kirchner	Austrian Academy of Sciences
Dr. Toshimichi Otsubo	Hitotsubashi University, Japan
Dr. Erricos Pavlis	Joint Center for Earth System Technology/Goddard Space Flight Center NASA, USA
Dr. Michael Pearlman	Harvard-Smithsonian Center for Astrophysics, USA
Dr. Stanisław Schillak	Space Research Centre, Polish Academy of Sciences

Honorary Organizing Committee

Dr. Marek Banaszkiewicz	Director of the Space Research Centre, Polish Academy of Sciences
Prof. Lubomir Włodzimierz Baran	Member of the Presidium of the Polish Academy of Sciences, Chairman of the Committee on Geodesy, Polish Academy of Sciences
Prof. Hieronim Hurnik	Astronomical Observatory, A.Mickiewicz University
Dr. Jan Kazimierz Łatka	Space Research Centre, Polish Academy of Sciences
Prof. Jan Węglarz	President of the Poznań Branch of the Polish Academy of Sciences
Prof. Piotr Wolański	Chairman of the Committee on Space Research, Polish Academy of Sciences
Prof. Janusz B. Zieliński	Member of the COSPAR Bureau, Space Research Centre, Polish Academy of Sciences

Local Organizing Committee

Dr. Stanisław Schillak (Head LOC)	Space Research Centre, Polish Academy of Science
Prof. Aleksander Brzeziński	Space Research Centre, Polish Academy of Science
Prof. Edwin Wnuk	Astronomical Observatory, A.Mickiewicz University
Dr. Michael Pearlman	Director, ILRS Central Bureau, Harvard-Smithsonian Center for Astrophysics
Carey Noll	Secretary, ILRS Central Bureau, NASA
Alicja Gąsiorowska	Astronomical Observatory, A.Mickiewicz University
Dr. Justyna Gołębiewska	Astronomical Observatory, A.Mickiewicz University
Roman Hirsch	Astronomical Observatory, A.Mickiewicz University
Dr. Paweł Lejba	Space Research Centre, Polish Academy of Science
Piotr Michałek	Space Research Centre, Polish Academy of Science
Franciszek Nowak	Space Research Centre, Polish Academy of Science
Danuta Schillak	Space Research Centre, Polish Academy of Science

Session Chairs

Opening Ceremony	Stanisław Schillak
Scientific Achievements, Applications and Future Requirements (1st)	Zuheir Altamimi, Steve Klosko
Scientific Achievements, Applications and Future Requirements (2nd)	Richard Gross, Aleksander Brzeziński
The role of Satellite Laser Ranging in Global Geodetic Observing System	Erricos Pavlis, Horst Mueller
Network and Station Performance	Vincenza Luceri, Mark Torrence
Lunar and Interplanetary Laser Ranging	Juergen Mueller, Tom Murphy
High Repetition-rate Systems	Georg Kirchner, Jan McGarry
Lasers, Detectors and Timers	Ivan Prochazka, Yuri Artyukh
Software and Automation	Randall Ricklefs
New and Upgraded Stations, Extended Facilities	Francis Pierron, Stanisław Schillak
Operational Issues and New Missions	Michael Pearlman, Ben Greene
Targets, Signatures and Biases	Graham Appleby, Toshimichi Otsubo
Advanced Systems and Techniques: Transponders, Altimeters, and Time Transfer	John Degnan, Ulrich Schreiber
Closing Session	Michael Pearlman

Editorial Committee

Stanisław Schillak, Paweł Lejba, Stanisław Zapaśnik and Session Chairs

PROGRAM

Saturday, October 11

	ILRS Working Group Meetings
17:00	Data Formats and Procedures Working Group meeting

Sunday, October 12

9:00 - 17:00	Analysis Working Group meeting
19:00	Program Committee Meeting
17:00 - 21:00	On-Site Registration

Monday, October 13

8:00 - 9:00	On-Site Registration
9:00 - 10:00	Welcome/Introduction
10:30 - 12:30	Scientific Achievements, Applications and Future Requirements (first session)
14:00 - 16:00	Scientific Achievements, Applications and Future Requirements (second session)
16:30 - 18:00	Scientific Achievements, Applications and Future Requirements (second session) (continued)
19:00	Reception at Andersia hotel

Tuesday, October 14

8:00 - 9:20	The role of Satellite Laser Ranging in the Global Geodetic Observing System
9:20 - 10:05	Network and Station Performance
10:30 - 12:15	Network and Station Performance(continued)
13:45 - 16:05	Lunar and Interplanetary Laser Ranging
16:30 - 18:00	Transponder Working Group - LRO meeting
18:30	Trip to Borowiec Observatory, Reception

Wednesday, October 15

8:30 - 10:00	High repetition-rate systems
10:30 - 12:00	High repetition-rate systems (continued)
12:00 - 12:30	Lasers, Detectors, and Timers
12:30 - 13:00	Signal Processing WG meeting
14:00 - 15:30	Lasers, Detectors, and Timers (continued)
15:30 - 16:00	Software and Automation
16:30 - 18:00	Software and Automation (continued)
19:00	ILRS Governing Board Meeting

Thursday, October 16

8:30 - 10:00	New and Upgraded Stations, Extended Facilities
10:30 - 10:55	New and Upgraded Stations, Extended Facilities (continued)
10:55 - 12:30	Operational Issues and New Missions
14:00 - 15:00	Operational Issues and New Missions (continued)
14:00 - 15:00	Targets, Signatures and Biases
16:28 - 16:45	Targets, Signatures and Biases (continued)
16:45 - 18:15	Advanced Systems and Techniques: Transponders, Altimeters, and Time Transfer
19:00	Banquet

Friday, October 17

8:30 - 10:00	Advanced Systems and Techniques: Transponders, Altimeters, and Time Transfer (continued)
10:30 - 13:00	ILRS General Assembly
	Workshop Summary, Resolutions, Closure
15:00	Tour around Poznań City

Saturday, October 18

8:00	Excursion to Toruń City, place Nicolaus Copernicus birth

TABLE OF CONTENTS

Scientific Achievements, Applications and Future Requirements (second session)

The role of Satellite Laser Ranging in the Global Geodetic Observing System

Network and Station Performance

Lunar and Interplanetary Laser Ranging

High repetition-rate systems

Lasers, Detectors, and Timers

Software and Automation

New and Upgraded Stations, Extended Facilities

Operational Issues and New Missions

Targets, Signatures and Biases

Advanced Systems and Techniques: Transponders, Altimeters, and Time Transfer

Obituary

WERNER GURTNER, 1949 – 2009

Professor, Astronomical Institute of Bern
Chair of the ILRS Governing Board

Passed away, 24 October 2009

Professor Dr. Werner Gurtner, 1949-2009
Astronomical Institute of Bern, Switzerland

It is with deep sadness that the ILRS community learned of the death of Prof. Dr. Werner Gurtner from cancer on October 24, 2009 shortly after his sixtieth birthday.

Werner Gurtner completed his studies in Surveying Engineering in 1973 at the Institute of Geodesy and Photogrammetry of the ETH in Zurich, Switzerland. From 1974 to 1979 he was a research assistant and Ph.D. candidate with Prof. Max Schuerer, who was a lecturer at the ETH in addition to his position as director of the AIUB. Werner's Ph.D. thesis, partly written in Bern, resulted in a well-known reference, the "Geoid of Switzerland" using astrometric observations.

Werner started his official employment with the AIUB in January 1980. As early as 1978, at the ETH, he started work on the new Zimmerwald observatory, dedicated to Satellite Laser Ranging (SLR) and in 1987 he became the director of the Zimmerwald Fundamental Observatory. Between 1992 and 1996 he led the AIUB team, which planned and realized the new SLR and astrometry telescope in Zimmerwald. In collaboration with the Canton of Bern, the University of Bern, the Swiss National Science Foundation, and the Swiss Federal Office of Topography, the one-meter combined SLR and astrometry telescope was deployed at Zimmerwald and became one of the essential pillars of the International Laser Ranging Service (ILRS). With this same energy, Werner organized the upgrade of the observatory during 2005-2008. This upgrade included a new laser capable of performing dual-color measurements as well as supporting future one-way ranging and transponder experiments. The Zimmerwald Observatory as established by Werner is recognized now as one of the foremost stations in the global space geodesy community from the scientific, technical, and administrative points of view.

During the 1980's Werner also worked on the team that successfully developed what would eventually be known as the Bernese GPS Software package. In the 1990's, he was one of the key persons in the development of the International GNSS Service (IGS). His contributions related to IGS data transfer and information dissemination were of great importance and at least in part responsible for the worldwide acceptance of the IGS. The Receiver INdependent

EXchange (RINEX) format, which he initiated and coined to a great extent, became a standard as the platform for exchanging GNSS data in both science and engineering applications. Werner continued to work on enhancements to RINEX until very recently. The global acceptance of RINEX in both the science and receiver technology communities is a tribute to Werner's foresight.

Werner helped the International Association of Geodesy (IAG) to develop essential structural elements related to space geodesy. He was a member of the very active EUREF Technical Working Group since 1992; he chaired this group from 1999 to 2003. He was not only a key person on the development of the IGS, but also, even to a much greater extent, for the development of the ILRS. Werner Gurtner was a member of the ILRS Governing Board since its inception in 1998 and served as Chair of the Board from 2002 to 2009. Before that time he chaired EUROLAS, an association of European SLR observatories. Werner was an important link between the various space geodesy communities, particularly the ILRS and IGS.

The Faculty of Sciences of the University of Bern acknowledged the achievements of this eminent engineer and scientist by awarding him the title of professor in 1999. Werner Gurtner will be remembered as competent collaborator, good friend and dear colleague.

We all will miss our association and interactions with Werner.

Gerhard Beutler, Astronomical Institute University of Bern, Switzerland
Michael Pearlman, Harvard-Smithsonian Center for Astrophysics, USA

Foreword

The 16th International Workshop on Laser Ranging was held at the IBB Andersia Hotel on October 13 through 17, 2008. The International Laser Ranging Service (ILRS) and the laser ranging community organize this event every two years to discuss progress in satellite and lunar laser ranging, and their application to scientific programs. Over 140 people from 19 countries participated in the meeting, which included presentations, posters, and discussions on hardware, software, operations, analysis, and science topics.

With a few exceptions, all the papers from the eleven sessions of the Workshop are included in this Proceedings, the presentations, and posters are available in electronic form at the website
http://www.astro.amu.edu.pl/ILRS_Workshop_2008/index.php or
http://cddis.gsfc.nasa.gov/lw16/.
Much of the planning for the Workshop was facilitated through the local website at the AMU Astronomical Observatory. In the months following the Workshop, the website was enhanced to provide summary information, links to papers from the proceedings, and photos from the week's meetings and social events.

The Local Organizers of the Workshop would like to thank the many people who contributed to the success of this international meeting. We would first like to thank the Program Committee and session chairs for their active participation and efforts in coordinating the Workshop sessions, papers, and summaries. We would also like to thank the attendees for taking time from their busy schedules to travel to Poznań and participate in the sessions, through both their excellent presentations and the lively discussions that followed.

We wish to thank our opening speakers, Mr. Tomasz Jerzy Kayser, Deputy Major of the Poznań City, Prof. Piotr Wolański, President, Committee on Space Research, Polish Academy of Sciences, Prof. Jacek Witkoś, Rector on Science and International Cooperation, Adam Mickiewicz University, Prof. Ryszard Naskręcki, Dean, Faculty of Physics, Adam Mickiewicz University. We are also grateful to the organizations and companies that supported the Workshop: Committee on Space Research, Polish Academy of Sciences, European Office of Aerospace Research and Development, Kompania Piwowarska and IBB Andersia Hotel.

Local Organizing Committee:
Stanisław Schillak, Edwin Wnuk, Michael Pearlman, Carey Noll

Workshop Summary

Michael Pearlman

The Committee on Space Research of the Polish Academy of Sciences, the Space Research Centre of the Polish Academy of Sciences, the Adam Mickiewicz University in Poznań and the ILRS hosted the 16th International Workshop on Laser Ranging in Poznań, Poland, October 13-17, 2008. The theme of the workshop was "SLR – The Next Generation". The Web site *http://www.astro.amu.edu.pl/ILRS_Workshop_2008/index.php* provides information about the workshop; proceedings and session summaries can also be found on the Web at *http://cddis.gsfc.nasa.gov/lw16/*.

Over 140 people from 19 countries participated in the workshop, which included oral and poster presentations on scientific achievements, applications and future requirements, system hardware and software, operations, advanced systems, and analysis. ILRS working group and Governing Board meetings and the ILRS General Assembly were held in conjunction with the workshop. The local organizers also entertained the delegates with a reception and banquet and tours of the Borowiec laser station and Poznań city.

The workshop brought together an exceptional group of researchers who provided reports on the spectrum of science investigations being supported by Satellite and Lunar Laser Ranging (SLR and LLR) and Laser Altimetry. The three sessions comprising this portion of the meeting, containing over twenty oral presentations and three posters, covered a wide range of activities. These sessions where structured as follows.

The first science session focused on the reference frame, positioning SLR stations with high precision within this frame, and time variations in the gravity field, which both perturb the SLR satellite orbits and cause changes of the location of the geocenter with respect to the polyhedron realized by the geographic distribution of the SLR stations. The legacy of SLR over the 1970s and 1980s where it alone provided precise Earth orientation information and through the 1990s for monitoring changes in the longest wavelengths of the gravity field were described. Also presented were results showing the SLR contribution to the International Terrestrial Reference Frame (ITRF) both in terms of providing scale and in monitoring geocenter motion. New missions, like GRACE, which now provide far more detailed information on mass flux within the Earth's system, were also discussed with regard to improving SLR orbit accuracies.

Session two focused on orbit determination capabilities, analyses, and new applications for SLR including support for upcoming Lunar Reconnaissance Orbiter (LRO) mission. This session also discussed various highly interesting investigations made possible through the availability of detailed topographic mapping capabilities delivered by laser altimeters and the Lunar Laser Ranging acquired on the moon. SLR remains one of the surest ways to provide precision orbits in its own right, and for independent orbit verification for solutions produced by GPS and DORIS. A laser transponder being deployed on LRO will provide significantly improved orbits for this lunar orbiter enhancing mission science objectives. The second half of this session focused on the outstanding results for both Earth and Planetary applications, made possible with laser altimetry. Excellent papers were presented on ICESat, the MOLA system flown on Mars Global Surveyor (MGS), and a survey of applications including NEAR, MESSENGER, and LRO.

The third science session highlighted SLR and LLR contributions to planetary and lunar geophysics, fundamental physics (e.g. the Lens Thirring effect, the geophysical properties of the moon deduced from LLR) and the upcoming LARES experiment. SLR and LLR, given the long time history and stability of these systems, have made significant contributions to the study of fundamental physics in the field of General Relativity.

The science presentations at this workshop both individually and in total, were some of the most comprehensive ever presented within the ILRS Workshop framework. These papers clearly demonstrated the continuing role that SLR, LLR, and laser altimetry has in furthering our understanding of the dynamics ongoing in the Earth and its terrestrial-like planetary companions.

The session "The Role of Satellite Laser Ranging in the Global Geodetic Observing System" highlighted the central role that SLR plays within GGOS. The opening presentation summarized the main contributions of SLR to the three pillars of geodesy for GGOS with examples of the state-of-the-art in the definition of the origin and scale of the ITRF, the long history of SLR series of EOP, the longest of all space techniques, and mass load variations from long wavelength harmonics time series derived from SLR, with comparisons to other techniques (GRACE, GPS, hydrology, etc.). Efforts on a new ILRS product, daily delivery of fresh EOP estimates, show the product can be used to constraint the EOP forecasting process of the NEOS service of IERS. Other presentations highlighted the intercomparison and combination of SLR with other geodetic techniques. ESA's efforts to harmonize the reduction of GNSS and SLR data with a common analysis package would be an important contribution to GGOS for a combined and consistent estimation of geophysical parameters. Comparison between GPS- and SLR-derived time series of coordinates over a period of eleven years were shown, where the results indicated the general consistency of the results at the few millimeter level. This work demonstrated how well the two techniques compare at sites with data of exceptional quality, and how they can be used to identify problems in either technique when they are co-located and properly and accurately surveyed. Results of optimization studies in designing the future global geodetic networks that will support GGOS, focusing on the role of SLR and the possible products to be delivered, were shown. This presentation stressed the stringent requirements of GGOS and how the synergy of the geodetic techniques will meet this challenge. A poster illustrating the global map of the four networks of the space techniques as they exist today was shown. A second poster showed an example of how ILRS can make use of the Virtual Observatory on the web, following the example of astronomy.

The Network and Station Performance session covered three main topics: data quality control (at stations and at analysis centers), models, and the network in general. Presentations on data quality control reported on efforts to reach and maintain the highest data quality through the use of other on-site geodetic techniques (GNSS, absolute gravity), co-location, automation, and software monitoring development in cooperation with data analysts, engineers, and station operators. Data quality control at Analysis Centers included an overview of the routine quality control system for the ILRS global network is provided by the Hitotsubashi University, which is available via web, ftp and email. Results from the re-processing of data from selected missions using the most accurate orbit models and the latest ITRF (SLRF2005) were shown; the analysis has been used in development of a new model, LPOD2005. A presentation summarizing an ILRS proposal to IERS for modification of the analysis standards related to the products contributing to the establishment of future ITRF solutions. Analysis of the correlation between the TRF datum and the ILRS network geometry was shown with the goal to explain the discontinuity in the SLR scale. Difficulties in tracking the

future TanDEM-X mission were discussed with possible remedies for the various types of stations in the ILRS network.

There was significantly more activity in the Lunar Laser Ranging (LLR) and Interplanetary Laser Ranging session this year. A presentation on reference frames for lunar ranging analysis emphasized the need to avoid confusing gauge-dependent terms and physical effects. Two years of APOLLO operation has showed high photon rates and evidence for one-millimeter performance. There were also presentations on recent efforts to understand Earth orientation using 38 years of LLR data and the science that would be attainable with the next-generation (large) corner cubes on the lunar surface. There were several talks on one-way ranging to the lunar reconnaissance orbiter (LRO), focusing on technical parameters/capabilities, pointing strategies and verification, and scheduling and predictions. Preparations for the LRO experiment are taking place at the McDonald Observatory, where most of the software preparation is already completed. There was also a presentation on the science deliverables one may achieve through interplanetary laser ranging, including the successful ranging to the MESSENGER and Mars Orbiter, as well as plans for LRO. Posters were displayed on displayed pertaining to using LLR for Celestial pole determination, and the minimum duration necessary for sea level rise determination.

In the High Repetition Systems Session, the five-year success of the Graz station with two kHz laser operation was reviewed. Other stations including Herstmonceux, Zimmerwald, TIGO, NGSLR, several Chinese stations, a Russian system, and the Potsdam station have or are switching to higher repetition rate laser. New control systems for higher repetition rate lasers have been developed and implemented; most kHz stations are now using now Riga event timer. With the benefit of kHz ranging, several new results and additional areas of study are underway including very accurate satellite spin determination, fast optical response retrieving, mm resolution accuracy from cm targets like LAGEOS and AJISAI, LIDAR applications, seeing measurements, and kHz ranging to a Mars transponder. The SLR future is talking "kHz".

The Session on Lasers, Detectors and Timers included a review on commercially available kHz diode pumped lasers, and descriptions of a new high voltage Pockels cell driver for kHz SLR lasers, a new saturable absorber for laser transmitters, and a promising narrow-band holographic filters for ranging receivers. A new version of the Riga timer with improved resolution was introduced along with a presentation in the integration of Riga timers into Chinese SLR systems. The design for a commonly used TDC chips for high-speed event timers was presented as were the design and construction of compact event timing and laser fire control device for one-way laser ranging and a new, sub-picosecond timing device. A new photon counting detectors for future space missions was also presented.

Several themes ran through the Software and Automation Session; major topics included software modularity and robustness, automation, and remote access to geodetic systems. Also discussed were automated processing of SLR data. CRD file creation, handling, and analysis, SLR predictions, and innovations in telescope pointing. Finally, a topic that has gained importance in the software industry, XML, has been applied to SLR station processing at Stromlo and Riga.

In New and Upgraded Stations, Extended Facilities, the Chinese network stations are being modernized with kHz lasers, event timers, CSPADS, and gravimeters. The Chinese TROS transportable system is in operational in The Republic of Korea to support the ARGO project.

In France, the new MEO station is operational on both satellites and the Moon, and the mobile FTLRS system has been upgraded with Dassaults event timers for T2L2 project. The Herstmonceux station is testing a new kHz ranging laser and now has an absolute gravimeter operating on site. The Borowiec station has undergone major upgrading, and upgrades on the Simeiz and Katzively stations are underway. In South America, San Juan SLR station continues to perform exceptionally well and the TIGO system at Concepcion is operational again after delicate optical replacements. The Russian SLR network has been upgraded including the release of some of the data.

In the session on Operational Issues and New Missions, several reports were given on new missions. Several current and upcoming European missions with retroreflectors including ERS-2, GOCE, and SWARM are focused on Earth sensing and technology applications. SOHLA-1, to be launched in early 2009 by JAXA for a demonstration of small, low cost technical payloads; since the spacecraft will be spinning, it will pose a tracking challenge since access to the retroreflector array will only last a few seconds in every few minute revolution period. Astro-G, a space borne VLBI antenna, is planned for launch in 2012; the highly elliptical orbit and bi-modal, switching operation of the antenna; will also limit normal points to very short intervals and require some special data handling procedures. The Precision Expandable Radar Calibration Satellite being planned by NRL for calibrating radars and studying drag and electromagnetic conditions in orbit will carry over 1000 retroreflectors distributed inside and outside of a spherical deployable frame. Consideration for an Optical Link for the ACES Mission was discussed along with concepts for resolving the range biases in one-way ranging experiments and a novel application of SPADs using no optics. An IR camera and aircraft radio detection beacon using a patched antenna array offers promise of new aircraft detection safety systems for laser ranging. The implementation of the Consolidated Laser Ranging Format is underway with full implementation later in 2009. Moblas 8 returned to operations. Posters included some historical SLR information, a status on the ILRS website update, and the upcoming ANDE mission scheduled for May 2009.

Papers presented during the Targets, Signatures, and Biases session covered retro-reflector array design and optical response functions. The continuing development of new missions that will require laser tracking support is evident, as is the ongoing and welcome dialogue between mission engineers and the laser community in developing the best array solutions to maximize the effectiveness of the tracking. Work on retro array design and chamber testing was shown, with particular emphasis on concepts for the next generation GPS satellites. A presentation described experimental results to determine pulse energy levels leaving the telescope as a function of its attitude and initial pulse polarization. Presentations were also given describing the laser arrays on the GEO and MEO elements of the emerging Chinese COMPASS GNSS and on the HEO two-satellite STSAT-2 technology mission. An optical response simulation was described for the proposed HEO VLBI mission ASTRO-G, which very interestingly will see the ILRS supporting an astrophysics mission.

In the session on Advanced Systems and Techniques: Transponders, Altimeters, and Time Transfer, Altimeters, papers were presented on the development of simulators for planetary exploration and present and future airborne photonic 3D-imaging. Transponder topics included transponder simulations using artificial satellites preliminary hardware designs to demonstrate the feasibility of Mars links. Papers were given on time transfer including first data from T2L2 and some preliminary results from the Chinese LTT experiment and a discussion on One-Way System Calibration Techniques. Other talks included a paper on

ranging to uncooperative targets in China, and SLR engineering activities at Riga including new developments in their epoch timer work.

Scientific Achievements, Applications, and Future Requirements

Chairs: Zuheir Altamimi, Steve Klosko, Richard Gross, Aleksander Brzeziński

Session Summary

Steve Klosko

The 16th International Workshop on Laser Ranging brought together an exceptional group of researchers who provided reports on the spectrum of science investigations being supported by Satellite and Lunar Laser Ranging (SLR and LLR) and Laser Altimetry. The 3 Sessions comprising this portion of the meeting, containing 21 oral presentations and 4 posters, covered a wide range of activities. These sessions where structured as follows:

- Session 1 focused on the reference frame, positioning SLR stations with high precision within this frame, and time variations in the gravity field which both perturb the SLR satellite orbits and cause changes of the location of the geocenter with respect to the polyhedron realized by the geographic distribution of the SLR stations. The legacy of SLR over the 1970s and 1980s where it alone provided precise Earth orientation information and through the 1990s for monitoring changes in the longest wavelengths of the gravity field were described. Also presented were results showing SLR's contribution to the International Terrestrial Reference Frame (ITRF) both in terms of providing scale and in monitoring geocenter motion. New missions, like GRACE, which now provide far more detailed information on mass flux within the Earth's system were also discussed with regard to improving SLR orbit accuracies.

- Session 2 focused on orbit determination capabilities, analyses, and new applications for SLR including support for upcoming Lunar Reconnaissance Orbiter (LRO) mission. This session also discussed various highly interesting investigations made possible through the availability of detailed topographic mapping capabilities delivered by laser altimeters and the Lunar Laser Ranging acquired on the moon. SLR remains one of the surest ways to provide precision orbits in its own right, and for independent orbit verification for solutions produced by GPS and DORIS. A laser transponder being deployed on LRO, will provide significantly improved orbits for this lunar orbiter enhancing mission science objectives. The second half of this session focused on the outstanding results for both Earth and Planetary applications, made possible with laser altimetry. Excellent papers were presented on ICESat, the MOLA system flown on Mars Global Surveyor (MGS), and a survey of applications including NEAR, MESSENGER, and LRO.

- Session 3 highlighted SLR and LLR contributions to planetary and lunar geophysics, fundamental physics (e.g. the Lens Thirring effect, the geophysical properties of the moon deduced from LLR) and the upcoming LARES experiment. SLR and LLR, given the long time history and stability of these systems, have made significant contributions to the study of fundamental physics in the field of General Relativity.

The science presentations at this workshop both individually and in total, were some of the most comprehensive ever presented within the ILRS Workshop framework. These papers clearly demonstrated the continuing role that SLR, LLR, and laser altimetry has in furthering our understanding of the dynamics ongoing in the Earth and its terrestrial-like planetary companions.

Laser Ranging Contributions to Earth Rotation Studies

Richard S. Gross
Jet Propulsion Laboratory, California Institute of Technology, Pasadena
Richard.Gross@jpl.nasa.gov / Fax: + 1-818-393-4965

Abstract

The groundwork for a new field in the geophysical sciences, space geodesy, was laid in the 1960s with the development of satellite and lunar laser ranging systems, along with the development of very long baseline interferometry systems, for the purpose of studying crustal plate motion and deformation, the Earth's gravitational field, and Earth orientation changes. The availability of accurate, routine determinations of the Earth orientation parameters (EOPs) afforded by the launch of the LAser GEOdynamics Satellite (LAGEOS) on May 4, 1976, and the subsequent numerous studies of the LAGEOS observations, has led to a greater understanding of the causes of the observed changes in the Earth's orientation. LAGEOS observations of the EOPs now span 32 years, making it the longest available space-geodetic series of Earth orientation parameters. Such long duration homogenous series of accurate Earth orientation parameters are needed for studying long-period changes in the Earth's orientation, such as those caused by climate change. In addition, such long duration series are needed when combining Earth orientation measurements taken by different space-geodetic techniques. They provide the backbone to which shorter duration EOP series are attached, thereby ensuring the stability of the final combined series. And if rapidly reduced, lunar laser ranging measurements have the potential to contribute to near-real-time UTI determination.

Introduction

The Earth's rotation, encompassing both the rate of rotation and the location of the rotation axis with respect to the Earth's crust, is not constant but exhibits minute changes on all observable time scales from subdaily to decadal and longer [for a recent review see, e.g., *Gross*, 2007]. Changes in the Earth's rate of rotation amount to a few parts in 10^8, corresponding to changes of a few milliseconds (ms) in the length of the day; changes in the location of the rotation axis with respect to the Earth's crust, known as polar motion, amount to about a part in 10^6, or several hundred milliarcseconds (mas). Length-of-day (LOD) variations consist largely of: (1) decadal variations of a few milliseconds in amplitude thought to be caused by interactions between the Earth's core and mantle, (2) tidal variations having periods between 12 hours and 18.6 years caused directly by the deformation of the solid Earth in response to the action of the luni-solar tide raising potential and indirectly by the interaction of the ocean tides with the solid Earth, and (3) forced variations on intraseasonal to interannual time scales caused primarily by changes in the strength and direction of the winds with the effects of atmospheric surface pressure and oceanic currents and bottom pressure being of relatively minor importance.

Polar motion consists largely of: (1) a forced annual wobble having a nearly constant amplitude of about 100 mas, (2) the free Chandler wobble having a variable amplitude ranging between about 100 to 200 mas, (3) quasi-periodic variations on decadal time scales having amplitudes of about 30 mas known collectively as the Markowitz wobble, (4) a linear trend having a rate of about 3.5 mas/yr, and (5) smaller amplitude variations occurring on all

measurable time scales. In general, the causes of the observed polar motion are not as well understood as are those of the observed length-of-day variations, although a growing body of evidence suggests that on intraseasonal to interannual time scales polar motion is caused largely by a combination of atmospheric and oceanic processes, with atmospheric surface and ocean-bottom pressure variations being more important than those of winds and currents *[Gross et al.,* 2003]. However, on decadal time scales atmospheric and oceanic processes do not appear to be energetic enough to excite polar motion to its observed levels *[Gross et al.,* 2005]. Core-mantle interactions also appear to be ineffective in exciting polar motion on decadal time scales [e.g., *Greff-Lefftz and Legros,* 1995; *Hide et al.,* 1996]. If progress is to be made in understanding the cause of decadal polar motion, then of primary importance is the continued availability of accurate and stable polar motion series of long duration.

Decadal Polar Motion

Figure 1 shows three different decadal polar motion series that were produced by applying a lowpass filter with a cutoff period of 6 years to the series of International Latitude Service [ILS; *Yumi and Yokoyama,* 1980] optical astrometric polar motion measurements (top solid green curve), the series of Hipparcos [*Vondrak et al.,* 1998] optical astrometric polar motion measurements (middle solid blue curve), and the SPACE96 [*Gross,* 1997] combination of space-geodetic polar motion measurements (bottom solid red curve). As can be seen, the decadal variability exhibited by these three polar motion series is very different. There is very little agreement between the SPACE96 series, which is based on highly accurate space-geodetic measurements, and the ILS and Hipparcos series which are based on less accurate optical astrometric measurements.

The most reliable estimates of decadal polar motion are those determined from spacegeodetic measurements. The only space-geodetic polar motion series that span the entire duration of SPACE96 are those determined from lunar and satellite laser ranging [*Gross,* 1997]. Figure 1 therefore demonstrates that the very nature of decadal polar motion was not known until the advent of the space-geodetic measurement techniques of lunar and satellite laser ranging. These laser ranging measurements must continue to be taken and reduced for Earth orientation parameters in order to provide the accurate and stable series of long duration required to investigate and uncover the cause of decadal polar motion variations

Combined Earth Orientation Series

Each of the modem, space-geodetic measurement techniques of lunar laser ranging (LLR), satellite laser ranging (SLR), very long baseline interferometry (VLBI), and the global positioning system (GPS) is able to determine the Earth orientation parameters. But each technique has its own unique strengths and weaknesses in this regard. Not only is each technique sensitive to a different subset and/or linear combination of the Earth orientation parameters, but also the averaging time for their determination is different, as is their duration, the interval between observations, and the precision with which they can be determined. By combining the individual Earth orientation series determined by each technique, a series of the Earth's orientation can be obtained that is based upon independent measurements and that spans the greatest possible time interval. Such a combined Earth orientation series is useful for a number of purposes, including a variety of scientific studies, and as an a priori series for use in data reduction procedures.

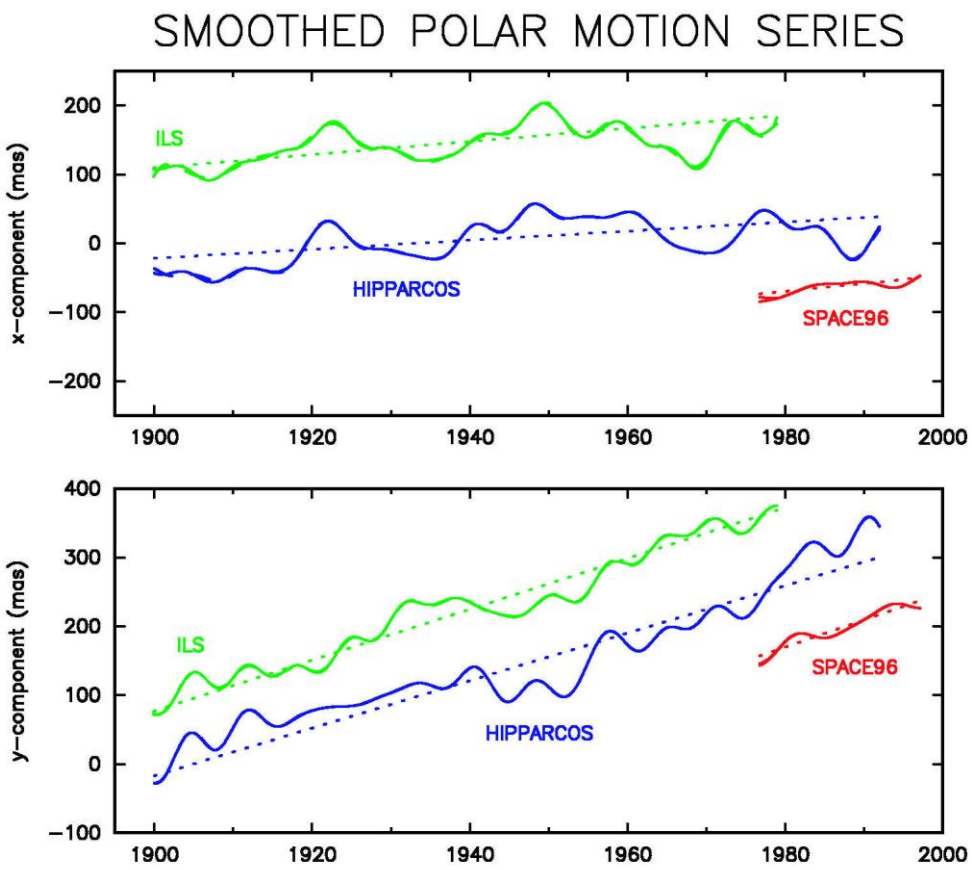

Figure 1. The x-component (top panel) and y-component (bottom panel) of decadal polar motion determined by applying a lowpass filter with a cutoff period of 6 years to the optical astrometric measurements of the International Latitude Service (top solid green curve), the Hipparcos optical astrometric polar motion series (middle solid blue curve), and the SPACE96 combination of space-geodetic polar motion measurements (bottom solid red curve). By convention, the x-component of polar motion is positive towards the Greenwich meridian and the y-component is positive towards 90°W longitude. For clarity of display, 100 mas have been added to the ILS series, and 100 mas have been subtracted from the SPACE96 series. After Figure 1 of *Gross and Vondrak* [1999].

For two decades, reference Earth orientation series have been generated at the Jet Propulsion Laboratory (JPL) in support of interplanetary spacecraft tracking and navigation. These series, the latest of which is known as SPACE2007, are produced by using a Kalman filter to combine Earth orientation series taken solely by space-geodetic measurement techniques [*Gross et al.*, 1998]. A number of corrections to the individual space-geodetic series must be made in order to ensure that they are consistent with each other prior to being combined. In particular, corrections to the bias and rate of each series must be determined and applied in order to make sure that they are aligned with each other prior to combination. Stable, internally self-consistent EOP series of long duration are required when determining these bias-rate corrections in order to ensure that the corrections made to the other shorter duration series are determined consistently with each other so that no residual bias-rate difference exists between the series being combined.

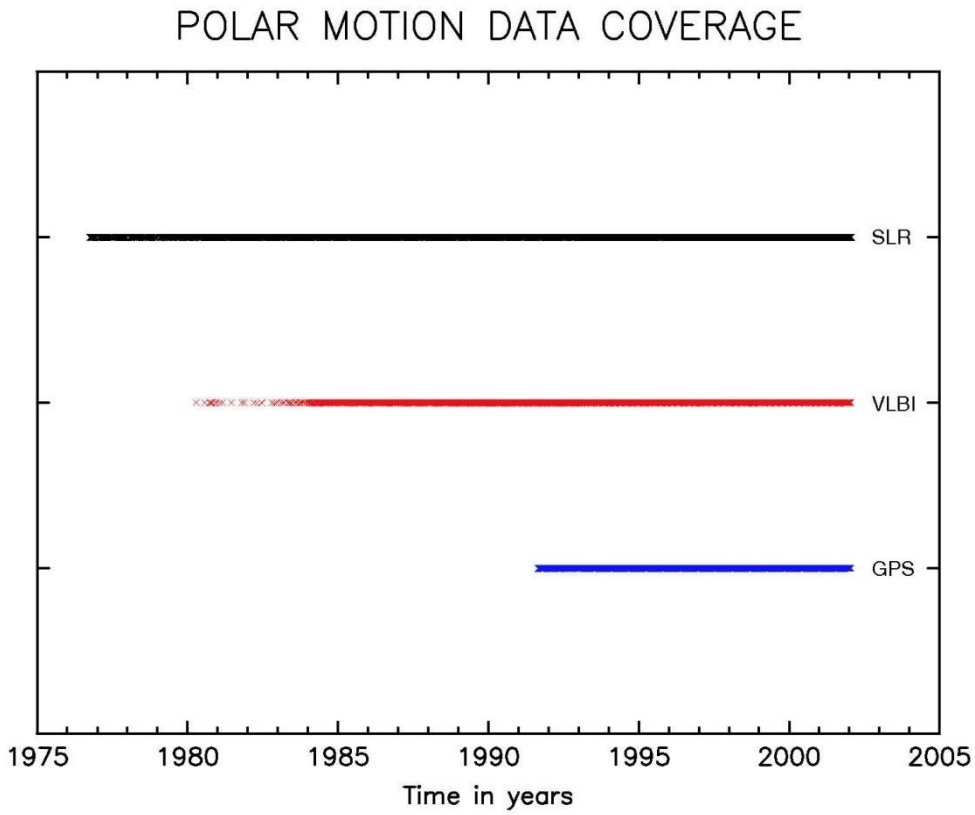

Figure 2. Epochs of the SLR, VLBI, and GPS polar motion measurements that were combined to form the SPACE2001 Earth orientation series.

Figure 2 shows the epochs of the SLR, VLBI, and GPS polar motion measurements that were combined to form the earlier SPACE2001 series [*Gross*, 2002]. The SLR measurements, which as can be seen are of longer duration than either the VLBI or GPS measurements, span the entire time interval of the SPACE2001 series. In fact, the starting epoch of SPACE2001 is determined by the starting epoch of the SLR series. The stability of the SLR series allows consistent bias-rate corrections to be determined for the shorter duration VLBI and GPS series, thereby ensuring the stability of the final combined EOP series. Due to its accuracy, stability, and long duration, the SLR series is the backbone to which other space-geodetic series are attached when combining them.

Near Real-Time UT1 Determination from LLR

Only two independent combinations of UT1 and the polar motion parameters $p_x(t)$ and $p_y(t)$ can be determined by analyzing lunar laser ranging measurements taken at a single station, namely, UT0 and the variation of latitude $\Delta\varphi_i(t)$ at that station (e.g., Moritz and Mueller, 1988, p. 425):

$$\Delta\phi_i(t) = x_p(t)\cos\lambda_i - y_p(t)\sin\lambda_i \quad \text{(1a)}$$

$$UT0_i(t) - TAI(t) = U(t) + x_p(t)\sin\lambda_i\tan\phi_i + y_p(t)\cos\lambda_i\tan\phi_i \quad \text{(1b)}$$

where (φ_i and λ_i are the nominal latitude and longitude of station i and the variable $U(t)$ is defined by $U(t) \equiv UT1(t) - TAI(t)$. A rotation of the Earth about an axis connecting the station with the origin of the terrestrial reference frame does not change the distance between the station and the Moon, and hence this component of the Earth's orientation cannot be determined from single station LLR observations.

Equation (1b) shows that LLR measurements of UT0 can be used to determine UT1 if independent estimates of polar motion are available. In particular, if UT0 could be rapidly determined from LLR measurements and if polar motion estimates were also rapidly available then LLR measurements could be used to rapidly determine UT1. In principle this should be possible because unlike VLBI the LLR observation files are quite small and could be rapidly sent electronically to analysis centers for rapid reduction to UT0. Since GPS estimates of polar motion are also rapidly available, LLR has the potential of determining UT1 within hours of data acquisition, making it competitive in latency with eVLBI.

Discussion and Summary

Earth orientation parameters determined from laser ranging measurements to the Moon and artificial satellites of the Earth span a greater time interval than do those determined by any other space-geodetic measurement technique. Simultaneously processing the entire history of laser ranging measurements ensures that the resulting series of Earth orientation parameters is stable and internally self-consistent. The accurate and stable Earth orientation series of long duration derived from laser ranging measurements are required for both investigating long-period changes in the Earth's orientation, which in the case of polar motion are still of unknown origin, and for combining Earth orientation measurements taken by different techniques. Analysis centers are encouraged to continue to derive Earth orientation parameters from all available laser ranging measurements, including those beginning with the launch of LAGEOS1 on May 4, 1976 and not just those taken since 1983. By using all available laser ranging measurements, an accurate and stable EOP series of ever increasing duration will continue to be available for investigating the causes and consequences of Earth orientation variations.

Of all the space-geodetic measurement techniques only lunar laser ranging and very long baseline interferometry are able to determine Universal Time. If lunar laser ranging measurements could be rapidly processed then they could contribute to near-real-time UT1 determination. Such rapidly available estimates of UT1 are needed for a number of purposes including the prediction of GNSS satellite orbits and the tracking and navigation of interplanetary spacecraft.

Acknowledgments

The work described in this paper was performed at the Jet Propulsion Laboratory, California Institute of Technology, under contract with the National Aeronautics and Space Administration.

References

Greff-Lefftz, M., and H. Legros, Core-mantle coupling and polar motion, *Phys. Earth Planet.*

Int., 91, 273-283, 1995

Gross, R. S., A combination of EOP measurements: SPACE96, summarized in *1996 IERS Annual Report,* pp. II29, Observatoire de Paris, Paris, France, 1997.

Gross, R. S., Combinations of Earth orientation measurements: SPACE2001, COMB2001, and POLE2001, Jet Propulsion Laboratory Publ. 02-08, 27 pp., Pasadena, Calif., 2002.

Gross, R. S., Earth rotation variations - long period, in *Physical Geodesy,* edited by T. A. Herring, pp. 239-294, Treatise on Geophysics vol. 3, Elsevier, Oxford, 2007.

Gross, R. S., and J. Vondrak, Astrometric and space-geodetic observations of polar wander, *Geophys. Res. Lett., 26,* 2085-2088, 1999.

Gross, R. S., T. M. Eubanks, J. A. Steppe, A. P. Freedman, J. O. Dickey, and T. F. Runge, A Kalman filter-based approach to combining independent Earth orientation series, *J. Geodesy, 72,* 215-235, 1998.

Gross, R. S., I. Fukumori, and D. Menemenlis, Atmospheric and oceanic excitation of the Earth's wobbles during 1980-2000, *J. Geophys. Res., 108*(B8), 2370, doi:10.1029/2002JB002143,2003.

Gross, R. S., I. Fukumori, and D. Menemenlis, Atmospheric and oceanic excitation of decadal-scale Earth orientation variations, *J. Geophys. Res., 110,* B09405, doi: 10.1 029/2004JB003565, 2005.

Hide, R., D. H. Boggs, J. O. Dickey, D. Dong, R. S. Gross, and A. Jackson, Topographic core-mantle coupling and polar motion on decadal time scales, *Geophys. J. Int., 125,* 599-607, 1996.

Moritz H., and I. I. Mueller, *Earth Rotation: Theory and Observation,* Ungar, New York, 1988.

Vondrak, J., I. Pesek, C. Ron, and A. Cepek, *Earth orientation parameters 1899.71992.0 in the ICRS based on the Hipparcos reference frame,* Publication No. 87 of the Astronomical Institute of the Academy of Sciences of the Czech Republic, 56 pp., Ondrejov, Czech Republic, 1998.

Yumi, S., and K. Yokoyama, *Results of the International Latitude Service in a Homogeneous System, 1899.9-1979.0,* Publication of the Central Bureau of the International Polar Motion Service and the International Latitude Observatory of Mizusawa, 199 pp., Mizusawa, Japan, 1980.

Geocenter Motion: Causes and Modeling Approaches

E. C. Pavlis, M. Kuźmicz-Cieślak
JCET/UMBC and NASA Goddard, Maryland, USA
epavlis@umbc.edu/Fax: +1-410-455-5868

Abstract

Since the first realization of the International Terrestrial Reference Frame (ITRF), its origin, defined to coincide with the geocenter, has been realized through the estimated coordinates of its defining set of positions and velocities at epoch. Satellite Laser Ranging (SLR) contributes to the ITRF realization this unique information along with that for its absolute scale, for over two decades. Over the past decade, the focus extended beyond the accuracy at epoch to include the stability of these realizations, given the increasingly more accurate observations of geophysical mass redistribution within the Earth system. Driven by numerous geophysical processes, the continuous mass redistribution within the Earth system causes concomitant changes in the long-wavelength terrestrial gravity field that result in geometric changes in the figure described by the tracking station network. The newly adopted ITRF development approach allows the simultaneous estimation of origin variations at weekly intervals through a geometric approach during the stacking step, and for the first time in the history of the ITRF accounts to some extent for these effects. Our dynamic approach has been used since the mid-90s, delivering, initially biweekly and later on, weekly variations of an "origin-to-geocenter" vector, simultaneously with an SLR-only TRF realization. Over the past year, the International Laser Ranging Service's (ILRS) Analysis Working Group adopted significant modeling improvements for the SLR data reduction of future as well as the historical SLR data. Based on this new standards, ILRS has embarked on a reanalysis of the LAGEOS 1 & 2 SLR data set up to present, to develop a uniformly consistent set of weekly variations with respect to a frame realized simultaneously by the ensemble of the data, closely approximating the current (scaled) ITRF2005. These series can complement the precise application of the ITRF when used as Cartesian offsets or the GRACE-derived monthly gravitational models, when converted to degree-1 harmonics. A simple model based on the dominant frequencies decomposition of the series can be easily used to account for the most significant part of the signal in various applications (examples).

Introduction

The origin of the Terrestrial Reference System (TRF) is realized through the adopted coordinates of its defining set of positions and velocities at epoch, constituting the conventional Terrestrial Reference Frame. Since many decades now, these coordinates are determined with space geodetic techniques, in terms of absolute or relative positions of the sites and their linear motions. Satellite tracking techniques use dynamics to define the origin and scale of the tracking station network since satellites "fall" naturally towards the center of mass of the central body and the size of their orbit is governed by the total mass of that central body. Today, late 2008, the state of the art TRF is the International Terrestrial Reference Frame (ITRF) with the latest realization being that of 2005—ITRF2005, [Altamimi et al., 2007]. An international and multi-technique effort is underway though to update this realization with a new one in late 2009, the ITRF2008 realization. This contribution focuses on the "origin to geocenter" vector variations and how these are monitored from the SLR network. We will examine first some theoretical estimates of the order of magnitude of

expected variations and their nature, followed by examples of the recently determined series from SLR data, and we will conclude with examples of how their incorporation in the interpretation of geophysical signals leads to improved results.

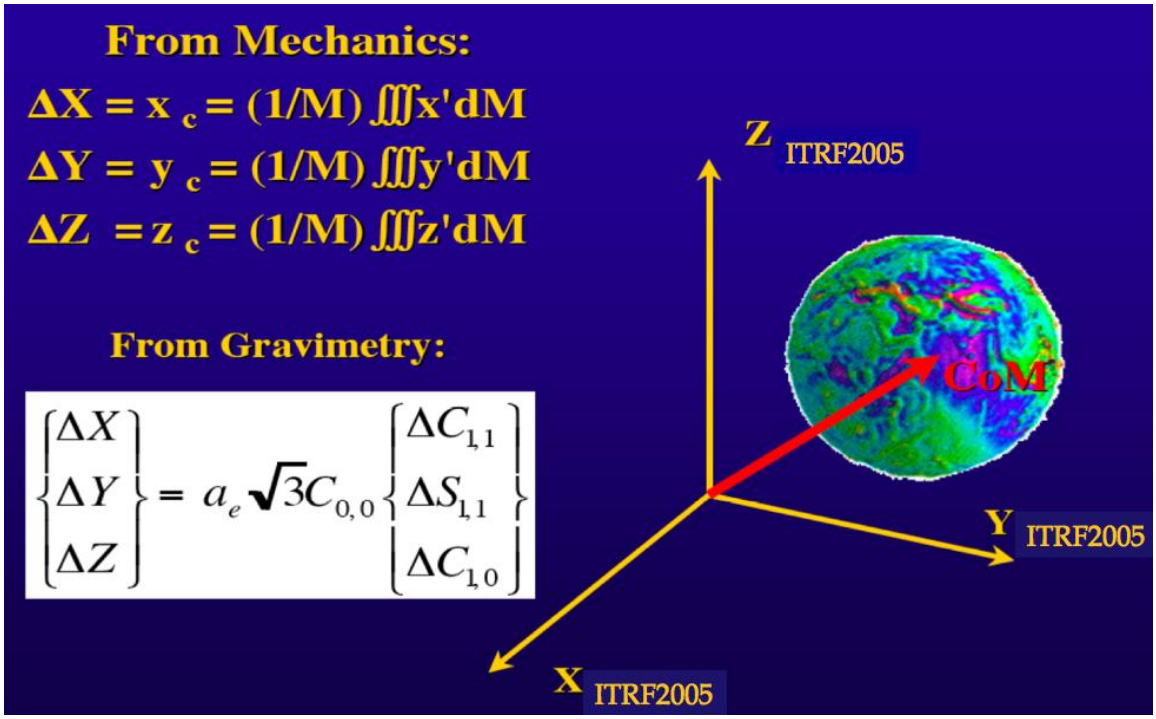

Figure 1. Center-of-mass (geocenter) definition and its relationship to gravity.

Temporal Gravitational Variations (TVG)

Despite the early use of space geodesy to develop accurate models of the terrestrial gravitational field, for many decades the field was viewed primarily as static, apart from the well known tidal variations. It soon became apparent that if not throughout its spectrum, at least the long wavelength part was exhibiting changes in time, because of reasons that were quickly traced to geophysical processes [Yoder et al., 1983]. Theoretical studies that followed over the coming years predicted further changes due to the redistribution of masses within the individual components of system Earth: atmosphere, oceans and solid Earth. This opened up an entirely new research area, temporal gravitational variations (TGV), and with it, it provided the missing link between space geodesy and climate change. As a result, it was widely accepted that since the "change" in climate change meant temporal change, the problem could not be properly addressed without a good handle on temporally changing gravitational signals with respect to a stable, well defined, and very accurate reference frame. Our focus here is in the degree-one terms that describe the non-geocentricity of the frame (Fig.1), with our primary concern being long-term, secular stability for that frame. Table 1 provides order of magnitude estimates of the plausible geophysical process that could contribute a secular component in the otherwise stable geocenter, with reference to the solid Earth component of the system.

Table 1. Plausible causes of secular geocenter change with expected order of magnitude.

Source	Magnitude	Induced motion
Sea level(2)	1.2 mm/y	0.064 ±0.02 mm/y
Ice sheets (G) (2)	2 mm/y	0.046±0.20 mm/y
Tectonics(2)	AMO-2	0.309±0.05 mm/y
Postglacial rebound(1)	ICE-3G	0.2 - 0.5 mm/y

(1) : Marianne Greff-Lefftz (2000)
(2) : Yu. Barkin (1997)

Seasonal changes in the long wavelength harmonic coefficients of the gravitational potential have been closely correlated with mass transfer in the atmosphere, hydrosphere and oceans, from independent observations of other than SLR techniques and different space missions. Gravity-mapping missions, (e.g. GRACE), and to a lesser extent the future mission GOCE, address temporal changes directly from the gravimetric point of view. For the very low degree and order terms though, there is also a geometric effect on the origin between the instantaneous and the mean (over very long time periods) reference frame as shown in Figure 1. This is one of the "couplings" between satellite dynamics and Earth geophysics and geokinematics.

SLR contribution to the Terrestrial Reference Frame

SLR has been for decades a primary tool in the establishment and maintenance of the TRF and monitoring of Earth's Orientation Parameters (EOP), in addition to being an extremely simple, precise and failsafe tracking technique. SLR data contributed in this effort the most accurate results yet, demonstrating early enough millimeter-level accuracy for short-term averages for these quantities [Pavlis, 1999, 2002]. Other satellite techniques, like GPS and DORIS, can potentially contribute to the definition of these quantities, however, due to the nature of these techniques, their contribution is limited in accuracy due to confounding with other parameters. SLR can determine a "SLR-realization" of the TRF at present on a weekly basis with accuracy at the centimeter level. These weekly series are "stacked" over time, and subsequently, combined with the contributions from other space techniques, they produce the new, global TRF. This process was first used in the development of ITRF2005 [Altamimi et al., 2007] and will be followed also in the development of the new TRF realization "ITRF2008", due sometime in 2009.

Although the SLR ground network of prime contributing sites has evolved considerably over these years, it still remains very poor in its global coverage, with a profound imbalance between north and south hemisphere stations (Fig. 2). It also suffers from long outages at sites that cease operations for extended time periods for upgrades or other reasons, due to redundancy gaps over certain areas. Finally, as [Angermann and Müller, 2008] point out, an examination of the 1993 to 2007 data set from the two LAGEOS targets that almost exclusively support the ITRF development, indicates that in addition to the geometric imbalance of the two hemispheres there is also a huge imbalance in terms of contributions between southern hemisphere sites. In particular, the two sites in Australia are responsible for almost all of the data collected in the southern hemisphere. These issues have a direct impact

on the development of a stable TRF and they are being addressed now in studies for an improved network of space geodetic techniques that will replace the currently operating ones, with an emphasis on multi-technique co-locations and uniform global distribution [Pavlis and Kuźmicz-Cieślak, these proceedings].

Figure 2. The ILRS network of stations with the most productive stations highlighted in ellipses and the lopsided nature of the network indicated by the large difference of sites between the north and south hemispheres. The loss of Tahiti over a significant time period created also a huge gap in longitude (~135°) in the southern Pacific region.

In preparation for the new ITRF2008, all of the LAGEOS and LAGEOS2 data are being reanalyzed by the ILRS Analysis Centers (AC), using improved modeling of biases, spacecraft dynamics and geometry, and background models. This time around the ILRS has extended the analysis to include the majority of the "historical" LAGEOS data, prior to 1993, starting with 1983. The extension to 1983 and not all the way back to the launch of LAGEOS, May of 1976, was decided after preliminary analyses indicated that the data prior to 1983 were not of the quality required for the definition of the TRF, suffering from large and unstable biases and poor network geometry. From the preliminary analyses at the JCET/GSFC AC, the evolution of the geocenter compared to the a priori definition from the underlying SLRF2005 TRF (compatible with ITRF2005S, but extended to apply to the period 1983 to 1993), seems very stable, indicating no significant secular variations as the prior models did with respect to ITRF2000, and with a clear annual signal. These preliminary series are displayed in Figure 3 for the recent period 1993 to end of 2008, when the resolution of the series is at weekly intervals. Note the lack of secular trends in the series. The years before 1993 do not support such a resolution and the official ILRS contribution is provided in 15-day averages. These series are obtained from a multi-year solution for a SLR-only TRF in the form of a set of coordinates at a fixed epoch (2000.0) and associated linear velocities. During the solution, we are determining weekly offsets of the frame determined with each weekly data set from the mean frame that is determined by the ensemble of the data. This approach delivers a consistent frame and geocenter series and it is applicable for a sequential approach of augmenting an established TRF with additional data as they are collected in time, to extend its validity without changing its definition.

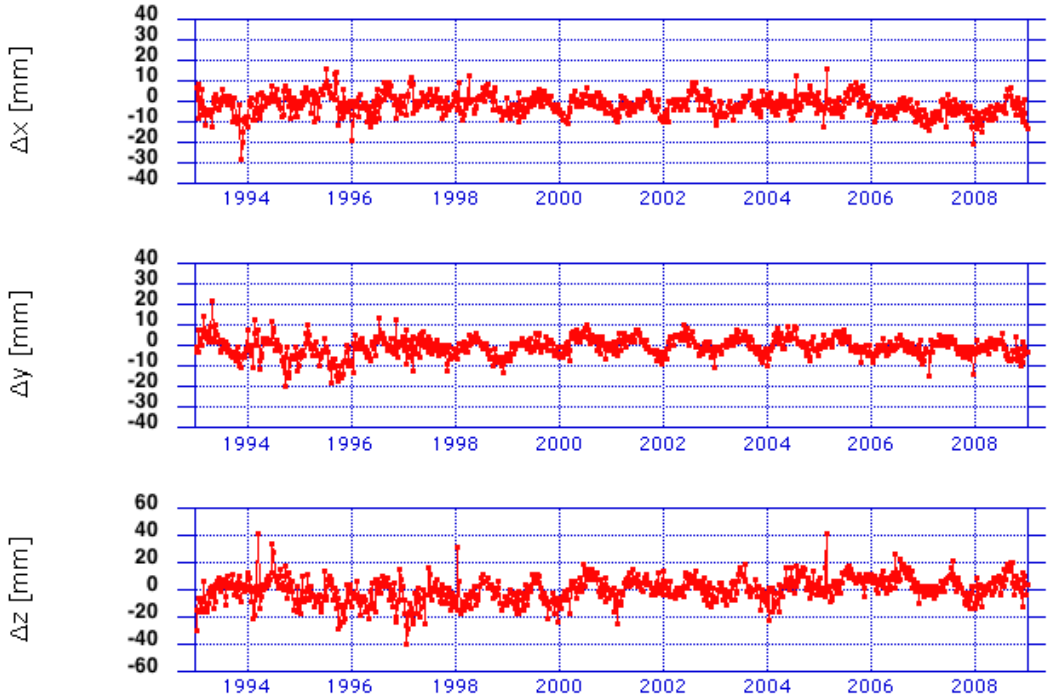

Figure 3. The new SSC(JCET) L 08 geocenter series based on SLRF2005 a priori and improved modeling of the LAGEOS SLR data.

Since the ITRF is not a SLR-only affair, harmonizing the modeling standards and the analysis principles to those commonly accepted by all the other space geodesy services and sanctioned by the International Earth Rotation and Reference Systems Service (IERS), it is vital in the development of a high quality product. Our recent reanalysis enforced as a prerequisite of all contributing ACs to follow the presently adopted IERS Conventions and Standards 2003, [McCarthy and Petit, 2004]. We hope that similar strict enforcement of these standards by the other techniques will help avoid the problems that the community faced with the release of ITRF2005 due to the erroneous application of the pole tide correction by a number of VLBI ACs. The consistency amongst the ILRS AC preliminary submissions is perhaps a strong indication of the benefit one can expect from enforcement of these standards throughout the contributing services.

Network geometry and data quality impacts on the SLR TRF

We have already discussed the poor quality of the SLR network and hinted at the large changes that it has undergone over time, in terms of both system quality and spatial coverage. In an attempt to gauge the level of TRF accuracy that these “different” networks could support during the years of evolution, we have generated a number of variants of the SLR-only TRF with subsets of the data (Fig. 4).

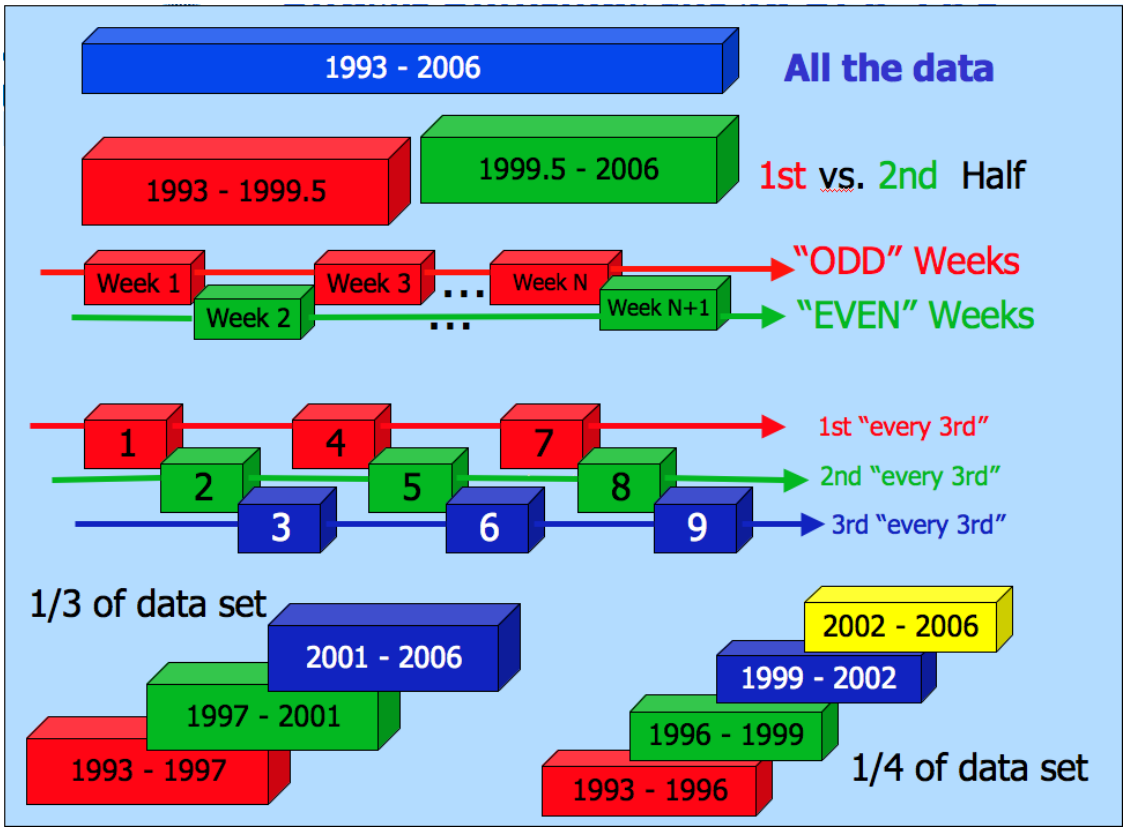

Figure 4. A graphical representation of input data variations for the development of a SLR-only TRF from subsets of the LAGEOS SLR data.

The idea behind these solutions is that the data set that is used in each case is strong enough to support the development of a TRF realization and if the data are of the same quality and represent the same geometry, then a comparison of the resulting TRF to the one obtained with the entire data set should give us some reasonable estimate of the relative accuracy between these variations. Accounting for the different number of observations between these solutions provides a good measure of the sought-for figure of merit for the variable accuracy of the geocenter definition in the 1993 to 2006 period. The tested variations were designed to provide information on the inherent strength in the data as a whole, as well as the evolution of this strength over the years, due to the evolution of the size, shape and technological advances of the ground network.

Solutions that spanned the same period of time, e.g. using the "odd-numbered" vs. "even-numbered" weeks (two different solutions), or picking every 3rd week (three different solutions), picking every 4th week (four different solutions), gave us a feeling of how much dependent are these solutions to the underlying data. Assuming that data obtained within one, two or three weeks apart should more or less contain the same information and they should thus yield the same TRF origin, the differences that we found between these realizations in terms of their origin with respect to that defined by the ensemble of the data gives a realistic estimate of how the technique can determine the origin of the TRF.

Table 2. Origin difference statistics between various subset SLR-only TRF realizations. All results are in [mm].

Case	ΔX $\sigma_{\Delta X}$	ΔY $\sigma_{\Delta Y}$	ΔZ $\sigma_{\Delta Z}$	3D |Δ| $\sigma_{3D\,\Delta}$
3 **Odd**	-8.37 ±10.91	19.25 ±10.78	-4.20 ±10.32	**21 ± 17**
4 **Even**	-12.62 ± 8.93	5.15 ± 8.82	-12.50 ± 8.44	**18 ± 16**
1 **1/2**	-41.20 ±35.82	6.26 ±35.38	-10.10 ±33.86	**43 ± 61**
2	1.74 ± 6.76	8.06 ± 6.68	7.28 ± 6.39	**11 ± 11**
15 **1/4**	-60.49 ± 23.68	57.43 ±23.39	7.48 ±22.39	**84 ± 40**
16	18.65 ± 31.40	-57.81 ±30.88	-6.19 ±29.50	**61 ± 53**
17	-0.27 ± 18.01	-4.74 ±17.79	15.72 ±17.03	**16 ± 31**
18	2.07 ± 12.29	7.16 ±12.18	1.73 ±11.60	**8 ± 21**

On the other hand, decimating the data set in subsets over time, examines more the effect that the evolution of the network size, shape and hardware have on the resulting TRF. Some of the results of these TRF comparisons in the three origin components are shown in Table 2 by component, as well as a root sum square (RSS) of the three. Examining these results we can reach some conclusions on the present state-of-the-art:

- The TRF origin defined by SLR is accurate at no better than 10 mm at present;
- The first half of the data is of much less quality than the second, possibly by a factor of four or so;
- Finer breakdown of the data set (e.g. in four parts) reveals an even clearer trend in the quality of the data and the network, indicating that the very early years were as bad as ten times the later years, with a linear transition in between.

This fact along with the large secular trends that were observed between the last two ITRF realizations, cast serious doubts on the ability of current SLR to support the accuracy requirements set forth by GGOS and primarily driven by the need to monitor sea level change with an accuracy of 0.1 mm/y [Pavlis et al., 2008].

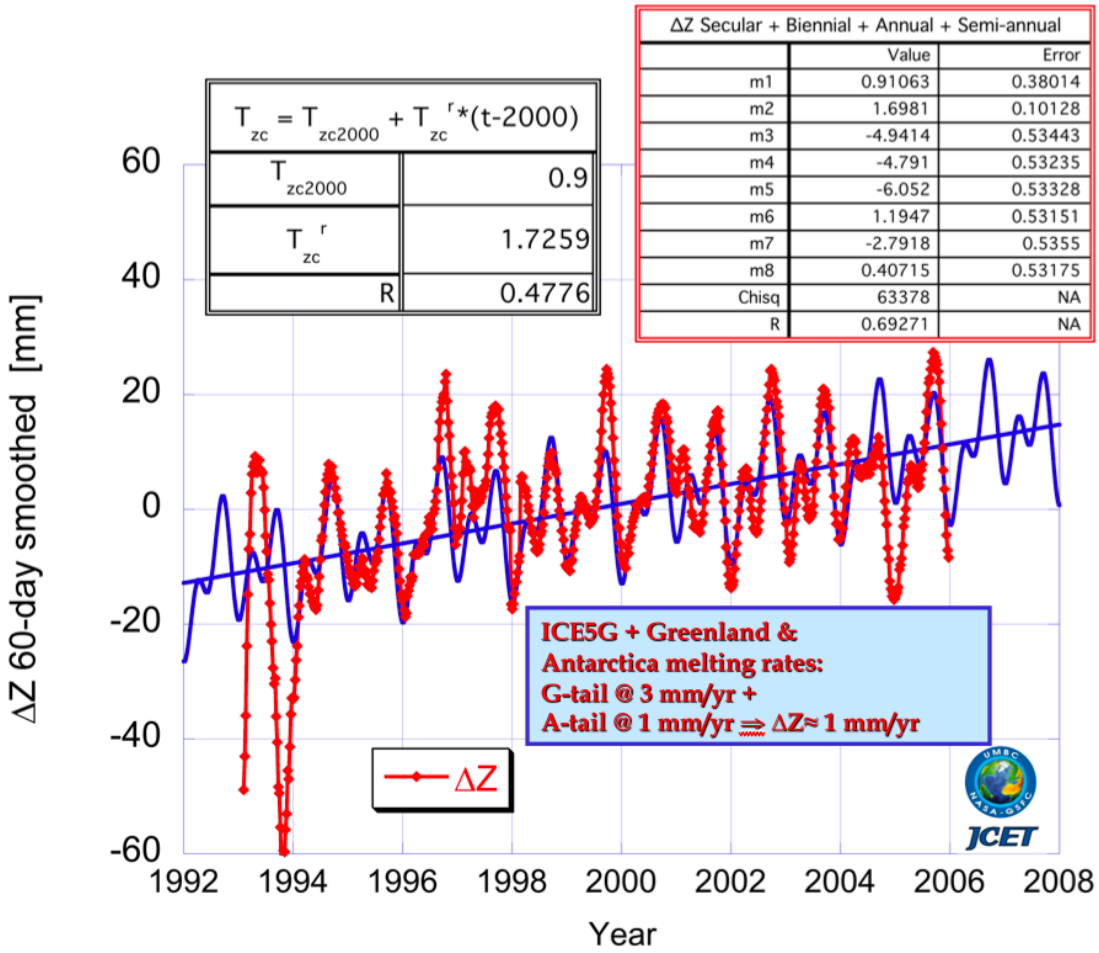

Figure 5. Variation of the Z-component of the geocenter from SLR, referenced to ITRF2000, from weekly solutions, smoothed with a 60-day boxcar filter. A four-component fit is also shown along with some estimates of plausible trends due to Greenland and Antarctica melting.

Applications of the SLR TRF and geocenter series

One of the most demanding in terms of accuracy geophysical investigations is monitoring mean sea level (MSL) variations over decades. The fact that it has huge societal implications makes this effort important and requires the utmost care in maintaining current estimates and understanding the processes that drive this change. The underlying TRF is terribly important because it relates estimates obtained from various oceanographic missions that can be decades apart, along with local, regional and global estimates from *in situ* data like tide gauges.

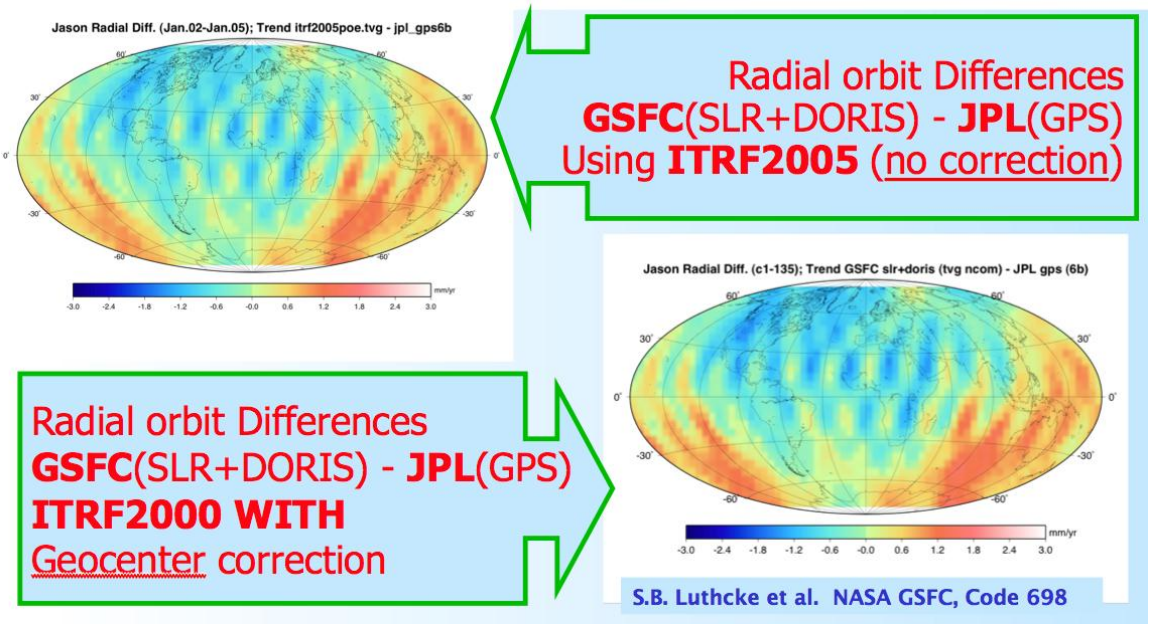

Figure 6. ΔMSL trends from JASON-2 observations (Jan. '02 – Jan. '05) reduced with ITRF2005 (left) and ITRF2000 plus the geocenter corrections shown in Figure 5. Both are differenced from JPL reductions that use GPS-based orbits with little dependence on dynamics (nearly geometric solutions).

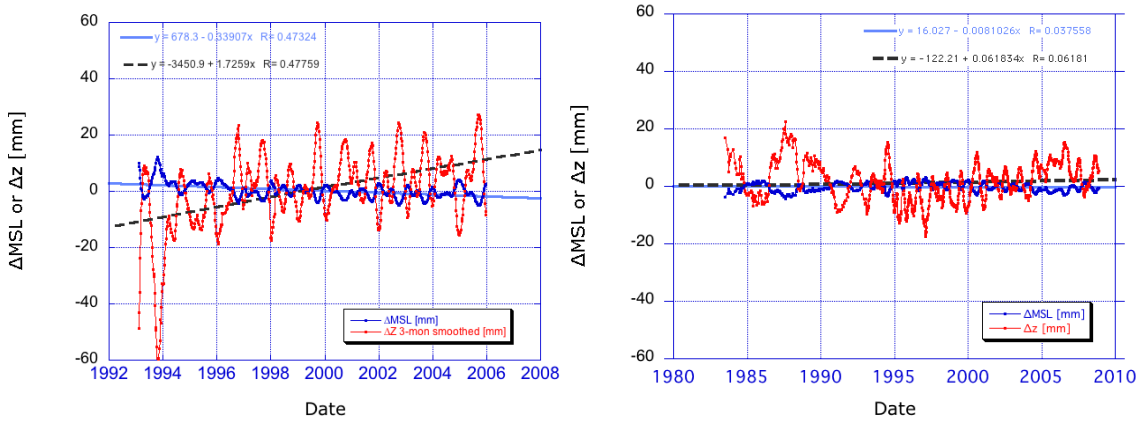

Figure 7. ΔZ_{COM}-induced trend in MSL for the new ITRF realization on the right and the past one on the left.

The application of the ITRF2000 had contaminated the observed trends of MSL due to the unstable origin definition, primarily the secular trend in the Z component that was clearly determined by SLR (Fig. 5). When the geocenter variation series was used in the reduction of the MSL data, the global picture that was obtained looked identical to that when the new ITRF2005 realization was used (Fig. 6), which had a much less prominent trend in the origin components. This was a clear indication that SLR was all along observing the correct geocenter, however, the construction of ITRF2000 was such that it could not account for it. The adoption of a new approach in the construction of the ITRF since the ITRF2005 realization has corrected the problem, as it can be verified by looking at Figure 7. The left figure shows the effect that the ITRF2000 vs. ITRF2005 Δz_{COM} has on the MSL trend, while the right side figure does the same between ITRF2005 and our preliminary version of a SLR-only ITRF2008. The linear fits to these "aliased" signals are 0.339 mm/y for the past realization and 0.008mm/y for the new one. Given the associated statistics for the MSL

estimates (on the order of 0.1 – 0.3 mm/y), the former error is very significant, while the latter is clearly insignificant. Unfortunately, these are estimates over the period that is covered by data used in the construction of these ITRF realizations, so they are really not able to tell us how the new ITRF will perform in the future. The fact though that there is no significant trend over the past 25 years is rather reassuring for its future performance.

Summary

The establishment of the Terrestrial Reference Frame is a collective effort of many research institutions and all of the space geodetic techniques. Although many of the techniques share strengths and weaknesses, each technique has some unique role in this effort. Satellite Laser Ranging, one of the very first precise space geodetic techniques to contribute to this effort, uniquely defines the origin of the TRF and its temporal variations, and in part its scale and its variable orientation. As the development of the TRF over time improved, so did our ability to analyze SLR data, thereby contributing higher quality products for subsequent realizations. This presentation gave some examples of SLR contributions in the past (ITRF2000 and ITRF2005), and discussed with examples, the improvements in the analysis and modeling of SLR observations used in the development of a new realization of the TRF (ITRF2008). These few examples show clearly that the usual tag-war between science and technology is alive and well, and guarantees that our knowledge about Earth and its environment will continuously improve, as long as we continue to invest in these efforts.

Tracking-network origin definition varies from week to week due to geophysical fluid redistribution in the Earth system, ILRS however monitors these variations with mm-level accuracy, including linear rates. SLR network non-uniformity and varying data yield result in variable quality of the above results over the past decade. Future requirement of definition at epoch at < 1mm and rates of < 0.1mm/y are dictated by MSL change studies and they will need a revised network and analysis approach to meet consistently and over decades. Application of SLR monitoring of the “geocenter” in altimetry data reductions produces MSL results qualitatively equivalent to those derived from the newer and more correct ITRF realizations, demonstrating SLR’s ability to accurately monitor such variations.

References

Altamimi, Z., X. Collilieux, J. Legrand, B. Garayt, and C. Boucher (2007), ITRF2005: A new release of the International Terrestrial Reference Frame based on time series of station positions and Earth Orientation Parameters, J. Geophys. Res., 112, B09401, doi:10.1029/2007JB004949.

Angermann, D. and H. Müller (2008), On the strengths of SLR observations to realize the scale and origin of the terrestrial reference system, *Observing our changing earth: proceedings of the 2007 IAG General Assembly, Perugia, Italy, July 2 - 13, 2007*, vol. 133, M. G. Sideris (ed.), pp. 21-29, Springer.

McCarthy, D. D. and G. Petit, (2004), IERS Conventions 2003, IERS Technical Note (32), pp. 127, Verlag des Bundesamts für Kartographie und Geodäsie, Frankfurt am Main, 2004.

Mendes, V. and E. C. Pavlis "High-Accuracy Zenith Delay Prediction at Optical Wavelengths", Geophysical Res. Lett., 31, L14602, doi:10.1029/2004GL020308, 2004.

Pavlis, E. C. (1999), "Fortnightly Resolution Geocenter Series: A Combined Analysis of LAGEOS 1 and 2 SLR Data (1993-96)", in *IERS Technical Note 25*, Observatoire de Paris, April 1999.

Pavlis, E. C. (2002), Dynamical Determination of Origin and Scale in the Earth System from Satellite Laser Ranging, in *Vistas for Geodesy in the New Millennium*, proceedings of the 2001 International Association of Geodesy Scientific Assembly, Budapest, Hungary, September 2-7, 2001, J. Adam and K.-P. Schwarz (eds.), Springer-Verlag, New York, pp. 36-41, 2002.

Pavlis, E. C. et al., (2008), "Observing Systems Needed to Address Sea-level Rise and Variability", in *Understanding Sea-level Rise and Variability*, Aarup, T., J. Church, S. Wilson, and P. Woodworth (eds.), Blackwell, Oxford (*in press*).

Yoder, C. F., Williams, J. G., Dickey, J. O., Schutz, B. E., Eanes, R. J., and Tapley, B. D., (1983), "Secular Variation of Earth's Gravitational Harmonic J_2 Coefficient from LAGEOS and Nontidal Acceleration of Earth Rotation", Nature, V.303, pp. 757-762, 1983.

The International Terrestrial Reference Frame - Latest Developments

Horst Müller, Detlef Angermann
Deutsches Geodätisches Forschungsinstitut, DGFI, Germany
mueller@dgfi.badw.de, angermann@dgfi.badw.de

Abstract

The major goal of this paper is to give an overview about latest developments regarding terrestrial reference frame computations. Some aspects related to the latest ITRS realization, the ITRF2005, are addressed. The combination strategies of the ITRS Combination Centres of IGN and DGFI are compared and the impact of the different strategies on the terrestrial reference frame results is discussed. The paper also summarizes some of the latest developments performed by the technique centres (i.e., IGS, ILRS, IVS, IDS) to achieve further improvements for the generation of new time series for the computation of the ITRF2008, which is currently under examination. Another issue is the identification of remaining deficiencies and the development of improved concepts for future terrestrial reference frame computations.

1. Introduction

The latest version of the International Terrestrial Reference Frame, the ITRF2005, has been released by the ITRS Center in October 2006. The situation after the release of the ITRF2005 was dominated by the discussion on the scale problem, mainly the inconsistency between the VLBI and the SLR scale. For the first time in ITRF history, SLR did not contribute to the scale definition, instead this was solely determined by VLBI. SLR observations showed a significant bias w.r.t. the ITRF2005 scale, which makes it impossible to use the ITRF2005 directly for the SLR processing. As a consequence of this problem, IGN has provided a second (re-scaled) ITRF2005 solution for SLR users in December 2006. During the analyses of the ITRF2005 results it was found, that the scale of the ITRF2005 solution computed by the ITRS Combination Center of DGFI (ITRF2005-D) is consistent with the SLR observations (Angermann et al., 2009a; Müller and Angermann, 2008). A comparison between the ITRF2005 solutions of IGN and DGFI has shown, that the station positions and velocities are in good agreement (small R.M.S. differences after similarity transformations). Also most of the transformation parameters agree within their estimated standard deviations, except for the scale and its time variation of the SLR network. A significant difference of about 1 ppb (offset at epoch 2000.0) and 0.13 ppb/yr (drift) between the IGN and DGFI solutions has been found, which accumulates to more than 2 ppb in 2008 (Angermann et al., 2009a).

Several analyses have been performed to investigate the discrepancies reported above and to achieve improvements for future realizations of the terrestrial reference frame. In this context the combination strategies of both ITRS Combination Centers have been compared and their effect on the ITRF results has been investigated (see chapter 2). In chapter 3 some technique-specific issues, primarily related to the scale realization, are addressed. Chapter 4 presents various SLR test computations to investigate the impact of range bias estimation on the scale. Remaining deficiencies and concepts for future improvements are addressed in chapter 5, and finally, conclusions are given in chapter 6.

2. Comparison of IGN and DGFI combination strategies for ITRF2005

The ITRS Combination Centres of IGN and DGFI computed each a solution of the ITRF2005. The computation strategy of IGN is on the solution level by simultaneously estimating similarity transformation parameters with respect to the combined frame along with the adjustment of station positions, velocities and EOP (Altamimi et al., 2007). The strategy applied at DGFI is based on the combination of normal equations and the common adjustment of station positions, velocities and EOP (see e.g., Angermann et al., 2004; Drewes et al., 2006; Angermann et al., 2009a). A comparison of the combination strategies of both ITRS Combination Centres is provided in Tab. 1.

Table 1. Comparison of the combination strategies of IGN and DGFI

	IGN	**DGFI**
Software	CATREF	DOGS-CS
Time series combination	Stacking of minimum constrained Solutions by 7 parameter transformations	Accumulation of normal equations, without transformations
Inter-technique combination	Combination of per-technique solutions by 14 parameter transformations IGN used all available local ties with appropriate weighting	Accumulation of per-technique datum-free normal equations, without transformations DGFI used a selected set of local ties with appropriate weighting
ITRF2005 datum - Origin - Scale - Rotation - Rotation rate	 SLR VLBI 3 NNR conditions w.r.t. ITRF2000 3 NNR conditions w.r.t. NNR NUVEL-1A	 SLR VLBI + SLR (weighted mean) 3 NNR conditions w.r.t. ITRF2000 3 NNR conditions w.r.t. APKIM2005

A major difference is that IGN is estimating similarity transformation parameters between epoch solutions as well as between per-technique solutions and the combined frame. DGFI accumulates normal equations without performing similarity transformations. As outlined for example in Drewes (2009a), the estimation of similarity transformation parameters may be critical. One problem is, that all common motions of the stations of the reference network are transformed into the similarity parameters (translation, orientation, scale factor). According to the ITRS definition, the origin of the terrestrial reference system shall be fixed in the geocenter, and coordinate changes caused by the station movements must go to the individual station coordinates and not into the datum. Another difference between the IGN and DGFI solutions is, that different sets of local ties have been used for the inter-technique combinations. It was found, that this can produce an effect on the scale of the SLR network in the order of 1 ppb (see Müller and Angermann, 2008). Furthermore the datum definition is different in both ITRF2005 solutions: The scale of the IGN solution is defined by VLBI only, whereas the scale of the DGFI solution is realized by a weighted mean of the SLR and VLBI solutions. For the definition of the rotation rate, IGN uses the geophysical model NNR NUVEL-1A and DGFI the APKIM2005 model based on ITRF2005 station velocities (Drewes, 2009b).

3. Technique-specific issues

The technique centres for the different space techniques (i.e., IVS, ILRS, IGS, IDS) investigated the modelling and processing strategies to identify remaining deficiencies and to improve the consistency of their observation time series as input for the ITRF2008 computation, which is currently under examination. Below some of the latest developments are addressed for the different space techniques:

- ***VLBI***: From a refined analysis and comparison of VLBI time series generated by different analysis centres using different software systems it was found, that some of the

analysis centres using CALC/Solve have obviously not correctly applied the pole tide model. The impact on the scale of the VLBI data submitted for ITRF2005 is in the order of 0.5 ppb (in direction to the SLR scale). Other issues that were addressed by the IVS include the modeling of antenna thermal deformation, investigations regarding the impact of loading effects (hydrology, pressure) and the implementation of improved tropospheric models (e.g., Nothnagel et al., 2009; Tesmer et al., 2008).

- ***SLR***: Because of the scale problems between SLR and the ITRF2005 a second realization (ITRF2005_rescaled) was computed by IGN. This solution is consistent with the SLR scale and has been used by the ILRS analysis working group for the computation of a new set of station coordinates and velocities, the SLRF2005. This SLR reference frame includes all ITRF2005 SLR stations, and in addition also some newer and older sites that were not included in the ITRF2005. Because of possible technical problems of the laser ranging systems (e.g., counter problems) the estimation of range biases may be required. Various test computations have been performed to investigate the impact of range bias estimation on the scale definition. Some results of these computations are presented in chapter 4 (see also Angermann and Müller, 2009).
- ***GPS***: Major shortcomings regarding the input data for ITRF2005 were that the data were not homogeneously reprocessed by the contributing analysis centres, and that relative antenna phase centre corrections were applied for the processing. In order to be consistent with absolute antenna phase centre corrections, the IGS has computed the IGS05 reference frame, which is currently used for the computation of the IGS products. The new submissions for the ITRF2008 are homogeneously processed and combined series based on absolute antenna phase center corrections. A serious problem in case of GPS is that there are many stations with several equipment changes resulting in a large number of discontinuities. This weakens the long-term stability of the solutions and complicates the co-location with the other space techniques.
- ***DORIS***: For precise orbit determinations (POD), the so-called DPOP2005 solution with updated DORIS station coordinates and velocities was computed in the ITRF2005 frame (Willis et al., 2009). Furthermore, the modelling and parameterization for the processing of the DORIS data was improved by the contributing analysis centres. Progress has also been achieved regarding the generation of ITRF2008 input data, which are now combined time series SINEX files.

4. Tests of SLR-dependent influences on the ITRF scale

Based on the SLRF2005, DGFI has reprocessed the SLR time series from 1993 to 2005 using the new bias values. As shown in figure 1, the new biases did not significantly change the SLR scale. There is no offset and only a slight drift of 0.1 ppb/year between the old and the new SLR solutions. Furthermore, the SLR observations were processed backwards for the period 1983 to 1992 by computing 15-day arc solutions. The corresponding time series of the SLR scale w.r.t. the SLRF2005 are shown in figure 2. The results indicate that also for the earlier data the SLR scale is consistent with the SLRF2005. However, there are some systematic deviations in the year 1992 (which need to be further investigated), and the data before 1984 show higher variations which is mainly due to a weak SLR station network geometry during that earlier period.

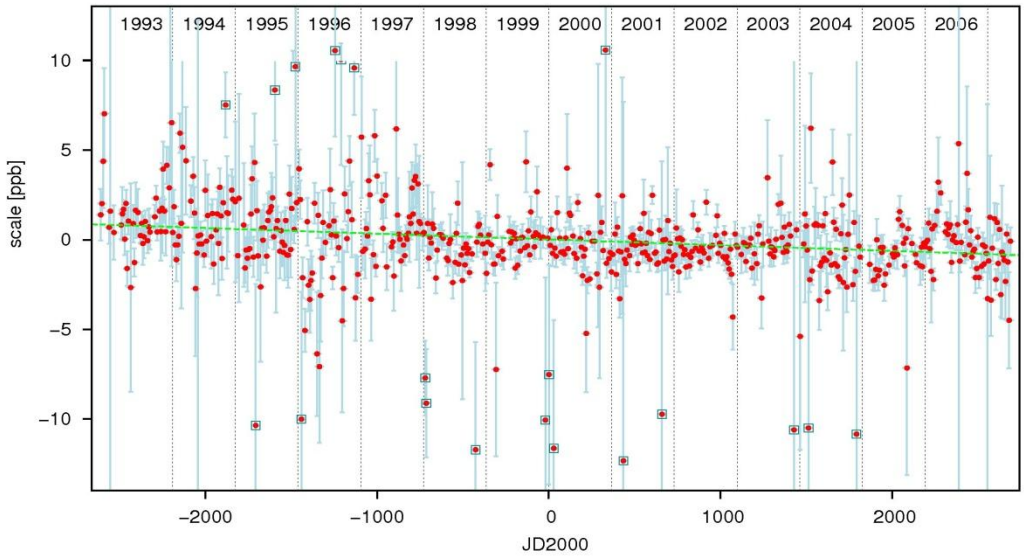

Figure 1. Time series for the scale obtained from the weekly SLR solutions (new bias values) w.r.t. SLRF2005 (offset: 0.0 ± 0.1 ppb , drift –0.1 ± 0.03 ppb/year).

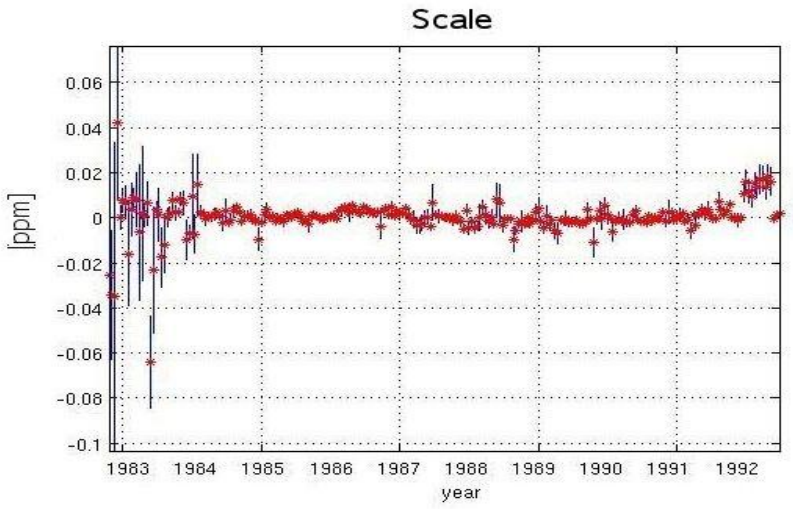

Figure 2. Scale difference from 15 arcs between SLRF2005 and the newly processed DGFI solution between 1983 and 1992

The major outcome of this test computations is that the SLR scale has a high long-term stability, that it is consistent with the SLRF2005, and that there is no significant effect of the bias handling strategy on the SLR scale. Similar results were obtained in earlier test computations performed at DGFI (for more details see Angermann and Müller, 2009).

5. Developments and future concepts

Although a remarkable progress has been achieved for the analysis and combination of the different space techniques in the last years, there are still some remaining deficiencies for the computation of the terrestrial reference frame. One problem is, that the input data sets are not fully consistent. On the international level, the standards for modeling and parameterization have not yet been (totally) unified among the analysis centres.

Within the GGOS-D project, homogeneously processed observation time series have been generated for the different space geodetic observation techniques, as the basis for the computation of a GGOS-D terrestrial reference frame and for the generation of consistent, high-quality time series of geodetic-geophysical parameters. The project involves four German institutions: GeoForschungsZentrum Potsdam (GFZ), Bundesamt für Kartographie und Geodäsie (BKG) in Frankfurt/Main, Institut für Geodäsie und Geoinformation, Universität Bonn (IGG) and DGFI. An overview about the project as well as the standards for modelling and parameterization used for the processing of the GGOS-D data are given in Rothacher et al., (2007). Table 2 shows the VLBI, SLR and GPS observation time series, which were provided as unconstrained datum-free normal equations (Krügel et al., 2007; Angermann et al., 2009a).

Table 2. GGOS-D input data used for the TRF computation.

Technique	Institutions	Software	Data	Time period
GPS	GFZ	Bernese	Daily NEQ	1994 – 2007
VLBI	IGG	CALC/SOLVE	24 h session NEQ	1984 – 2007
	DGFI	OCCAM	24 h session NEQ	1984 – 2007
SLR	DGFI	DOGS	Weekly NEQ	1993 – 2007
	GFZ	EOPS	Weekly NEQ	1993 - 2007

Compared to the ITRF2005 input data, there are some major advantages: (1) The observation time series of the different space techniques were homogeneously reprocessed based on unified standards; (2) in case of GPS consistently reprocessed observation time series were used (see Steigenberger et al., 2006, Rülke et al., 2008); (3) the modelling of the observations was improved (e.g., absolute instead of relative phase centre corrections, the pole tide model was correctly applied in the VLBI software CALC/SOLVE); and (4) the type of input data is nearly identical to the original observation equations and is much more appropriate for the combination than for example loosely constrained solutions or solutions with removable mimimum constraints. Another advantage is, that the total number of discontinuities could significantly be reduced compared to the ITRF2005 computation (Krügel et al., 2007). This was mainly achieved by the homogeneously processed GGOS-D data sets and the implementation of absolute antenna phase centre corrections for the GPS processing.

The time series analysis has shown seasonal variations for many stations, especially in the height component. Fig. 3 shows the mean average shape of such annual variations for four GPS-VLBI co-location sites. These seasonal signals may be caused by atmospherical, hydrological and non-tidal oceanic loading effects, which are presently not reduced from the original observations. In other cases, instrumentation effects (rather than geophysical ones) may be also responsible for the observed signals.

A deficiency in the current reference frame computation is that the temporal variations of station positions are described only by constant velocities. Deviations of the station motions from a linear model (e.g., seasonal variations) will produce errors in the combination results. Seasonal variations will affect the velocity estimations, in particular for stations with relatively short observation time spans (i.e., < 2 years). The alignment of epoch solutions to a reference frame with positions and constant velocities is also affected by non-linear station motions. As shown in figure 3, the shape of these non-linear motions differs between stations. A suitable handling (parameterization) of the seasonal variations in station positions is a challenge for future ITRF computations.

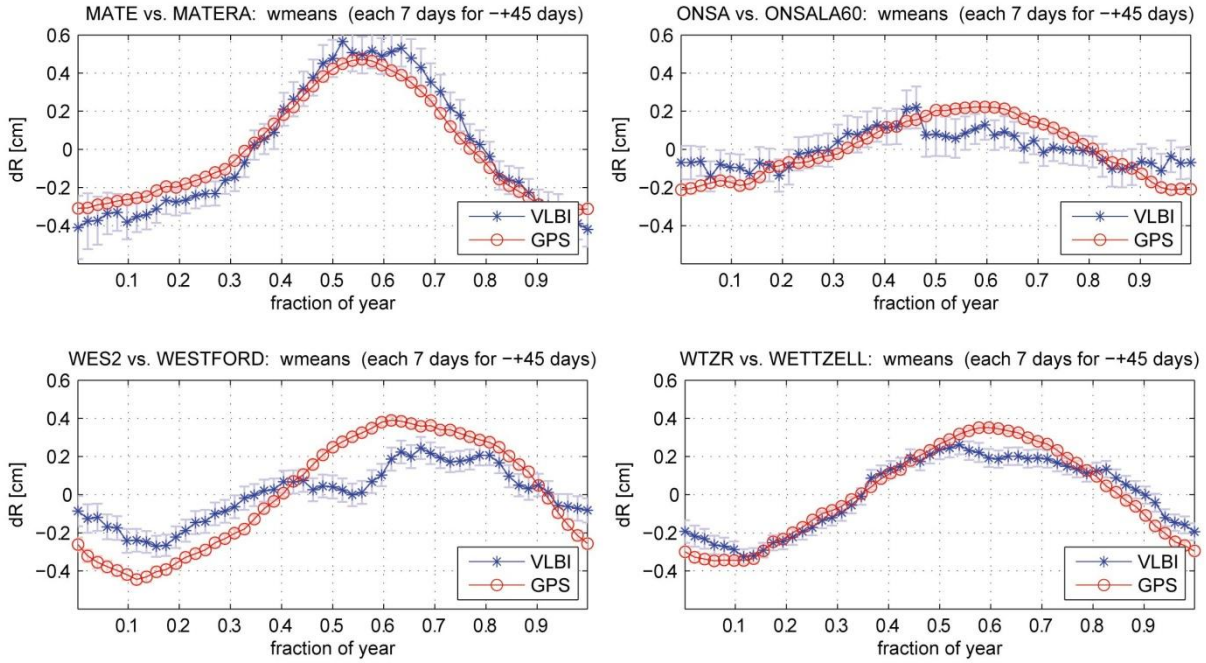

Figure 3. Mean annual behaviour of homogeneously processed VLBI (blue stars) and GPS (red circles) height time series at four co-location sites. The figures illustrate 90 days moving weighted means and their formal errors, computed each 7 days from the daily height estimates

6. Conclusions

The ITRF2005 results and in particular the inconsistency between the VLBI and SLR scale have stimulated intensive discussions within the space geodetic community. The combination strategies of the ITRS Combination Centres of IGN and DGFI were analysed and the differences were discussed. Also the technique centres (i.e. IGS, ILRS, IVS and IDS) have carried out various activities to study the existing inconsistencies and to perform investigations regarding modelling and parameterizations for the processing of the different space geodetic observations. As a result improvements have been achieved for all space techniques and reprocessed observation time series are available for the computation of the new ITRF2008, which is currently under examination.

Another objective was the identification of remaining deficiencies regarding terrestrial reference frame computations and the development of new concepts. A remarkable progress has been achieved within the GGOS-D project due to the generation of fully consistent and homogeneously processed observation techniques and due to the development of advanced combination methods. The results of the time series analysis have shown non-linear variations for most of the stations. Deficiencies regarding current reference frame computations are that the temporal variations are described only by constant velocities, and hence deviations of the station positions from a linear model (e.g., seasonal variations) will produce errors in the ITRF results. Thus, the handling and parameterization of non-linear station motions is a challenge for future TRF realizations.

Acknowledgement

This work was partly funded by the project GGOS-D within the GEOTECHNOLOGIEN programme of the Federal Ministry of Education and Research (BMBF: Bundesministerium für Forschung und Technologie), FKZ 03F0425C.

References

ALTAMIMI,Z., X. COLLILIEUX, J. LEGRAND, B. GARAYT, C. BOUCHER: *ITRF2005: A new release of the International Terrestrial Reference Frame based on time series of station positions and Earth Orientation Parameters.* Journal of Geophyiscal Research, Vol. 112, B09401, doi:10.1029/2007/JB004949, 2007.

ANGERMANN D, DREWES H, KRÜGEL M, MEISEL B, GERSTL M, KELM R, MÜLLER H, SEEMÜLLER W, TESMER V: *ITRS Combination Center at DGFI: A terrestrial reference frame realization 2003,* Deutsche Geodätische Kommission, Reihe B, Heft Nr. 313, 2004.

ANGERMANN D., DREWES H., GERSTL M., KRÜGEL M., MEISEL B.: *DGFI combination methodology for ITRF2005 computation,* Proceedings of the IAG Symposium Geodetic Reference Frames GRF 2006 Munich, Springer, 2009, in press.

ANGERMANN, D., H. MÜLLER: *On the strengths of SLR observations to realize the scale and origin of the terrestrial reference system.* IAG Symposia, Vol. 133, 3-9, Springer, 2009.

ANGERMANN, D., H. DREWES, M. GERSTL, B. MEISEL, M. SEITZ, D. THALLER: *GGOS-D Global Terrestrial Reference Frame*, Springer, 2009, in press.

DREWES, H., D. ANGERMANN, M. GERSTL, M. KRÜGEL, B. MEISEL, W. SEEMÜLLER*: Analysis and refined computations of the International Terrestrial Reference Frame*. Observation of the Earth System from Space, Flury, Rummel, Reigber, Rothacher, Bödecker, Schreiber, (Eds), Springer, 2006.

DREWES H.: *Reference Systems, Reference Frames, and the Geodetic Datum – basic considerations,* IAG Symposia, Vol. 133, 3-9, Springer, 2009a.

DREWES H.: *The APKIM2005 as basis for a non-rotating ITRF*, Proceedings of the IAG Symposium Geodetic Reference Frames GRF 2006 Munich, Springer, 2009b, in press.

KRÜGEL, M, ANGERMANN, D., DREWES, H., GERSTL, M., MEISEL, B., TESMER, V., THALLER, D.: *GGOS-D Reference Frame Computations*. GEOTECHNOLOGIEN Sciene Report, No. 11, ISSN 1619-7399, 2007a.

MEISEL, B., D. ANGERMANN, M. KRÜGEL, H. DREWES, M. GERSTL, R. KELM, H. MÜLLER, V. TESMER: Refined approaches for terrestrial reference frame computations. Adv. Space Res., 2005.

MÜLLER, H., D. ANGERMANN: Some aspects concerning the SLR part of ITRF2005. In: Luck, J., Moore, Ch., Wilson P. (Eds.): Proceedings of the 15th International Workshop on laser ranging, EOS Space Systems PTY Limited, Canberra, 2008.

NOTHNAGEL A.: *Short Note: Conventions on thermal expansion modelling of radio telescopes for geodetic and astrometric VLBI*. JoG online first, doi 1.1007/s00190-008-0284-z, 2008

ROTHACHER, M., DREWES, H., NOTHNAGEL, A., RICHTER, B.: *Integration of space geodetic techniques as the basis for a Global Geodetic-geophysical Observing System (GGOS-D): An overview.* GEOTECHNOLOGIEN Sciene Report, No. 11, ISSN 1619-7399, 2007.

RÜLKE, A., R. DIETRICH, M. FRITSCHE, M. ROTHACHER, P. STEIGENBERGER: *Realization of the terrestrial reference system by a reprocessed global GPS network*, Journal of Geophysical Research, DOI: 10.1029/2007JB005231, 2008.

STEIGENBERGER, P., ROTHACHER, M., DIETRICH, R., FRITSCHE, M., RÜLKE, A., VEY, S.: *Reprocessing of a global GPS Network*. Journal of Geophysical Research, Vol. 111, B05402, 2006.

TESMER V., J. BÖHM, R. HEINKELMANN, H. SCHUH: Effect of different tropospheric mapping functions on the TRF, CRF and position time-series estimated from VLBI. JoG Vol. 81, Nos. 6-8, 409-421, 2007.

WILLIS, P., J.C. RIES, N.P. ZELENSKY, L. SOUDARIN, H. FAGARD, E.C. PAVLIS, F.G. LEMOINE: DPOD2005: An extension of ITRF2005 for precise orbit determination, Adv. Space Res., 2009, in press.

Status of the ITRF development and SLR contribution

Z. Altamimi, D. Coulot, X. Collilieux
IGN/LAREG/ and GRGS, Marne-La-Vallée France
altamimi@ensg.ign.fr /Fax: +33164153255

Abstract

It is expected to start preparing for a new version of the International Terrestrial Reference Frame, namely the ITRF2008. Before initiating this new solution, some conditions have to be satisfied, mainly the need of reprocessed and consistent solutions from each technique: a new reprocessed IGS solution involving the absolute PCV models, an improved reanalysis solution from IVS accounting for the mean pole tide correction and better troposphere modeling, an improved ILRS solution taking into account all range biases and other station-dependent corrections, and new DORIS solutions where improvements are expected in the frame Z translation and the scale. In preparation of the ITRF2008, we analyze here individual SLR and the IVS regular time series solutions of station positions. A particular emphasis is given to the time behavior of the frame physical parameters (origin and scale). In an attempt to evaluate the pertinence of the estimated vertical velocities of SLR and VLBI stations co-located with GPS, we confront both estimations to GIA model predictions. This confrontation suggests poor agreement between the model predictions and space geodesy estimates on a site-by-site basis.

Introduction

The science requirement for the reference frame is to have an ITRF that is stable at the level of 0.1 mm/yr. The notion of stability used here is that the frame parameters and, in particular, its origin and scale should have linear behavior with no discontinuity over the time-span of the implied observation. The power of using time series of station positions as input data for the ITRF formation is that they allow the assessment of the time behavior of its defining parameters, notably the origin and the scale. Without being exhaustive, one example of Earth science applications of the reference frame is the mean sea level rise and its variability. Therefore any bias in the ITRF scale or origin will directly map to the mean sea level estimation through the usage of the ITRF data [Beckley et al, 2007, Morel and Willis, 2005].
The Satellite Laser Ranging technique is essential to the ITRF, being used to define its origin and contributing to the definition of its scale. In view of the ITRF2008, we present in the following sections analysis of some preliminary SLR and VLBI solutions and focus mainly on their origin and scale behavior. We also evaluate the station vertical velocities, as determined by some of these solutions and perform confrontation to Glacial Isostatic Adjustment model ICE-5G VM4 of Peltier (2004), [SBL 2005, Peltier, 2004].

Input data

We use the following time series solutions provided in SINEX format and which were available at the time of the ILRS workshop:

- IVS routine solutions sampled at the regular 24-hour sessions;
- SLR time series: ASI-12, GRGS-11, NCL test solutions from Philip Moore (private communication) and three IGN tests solutions (computed by the 3rd author of this paper) using data from separately Lageos I, Lageos II, and both satellites.

Data analysis

We use the CATREF software approaches of (1) internal or intrinsic conditions and (2) minimum constraints when stacking the various time series (Altamimi et al., 2007). The first approach allows indeed preserving the intrinsic origin (of SLR) and the scale (of SLR and VLB), by taking the mean of the analyzed time series of station positions, imposing neither shift nor drift of these parameters. In this case, the weekly translation and scale parameters are estimated with respect to the long-term averaged origin and scale of the accumulated solution. The second approach permits not only the expression of the long-term accumulated solution in a given reference frame, but also the estimation of the weekly transformation parameters with respect to the selected external reference frame.

Origin and scale analysis

Figure 1 displays the annual averages of the translations and scale factors with respect to ITRF2005, where good agreement between the three analyzed solutions can be noticed. We see in particular the origin consistency with the ITRF2005, whereas the scale behavior exhibits a significant drift.

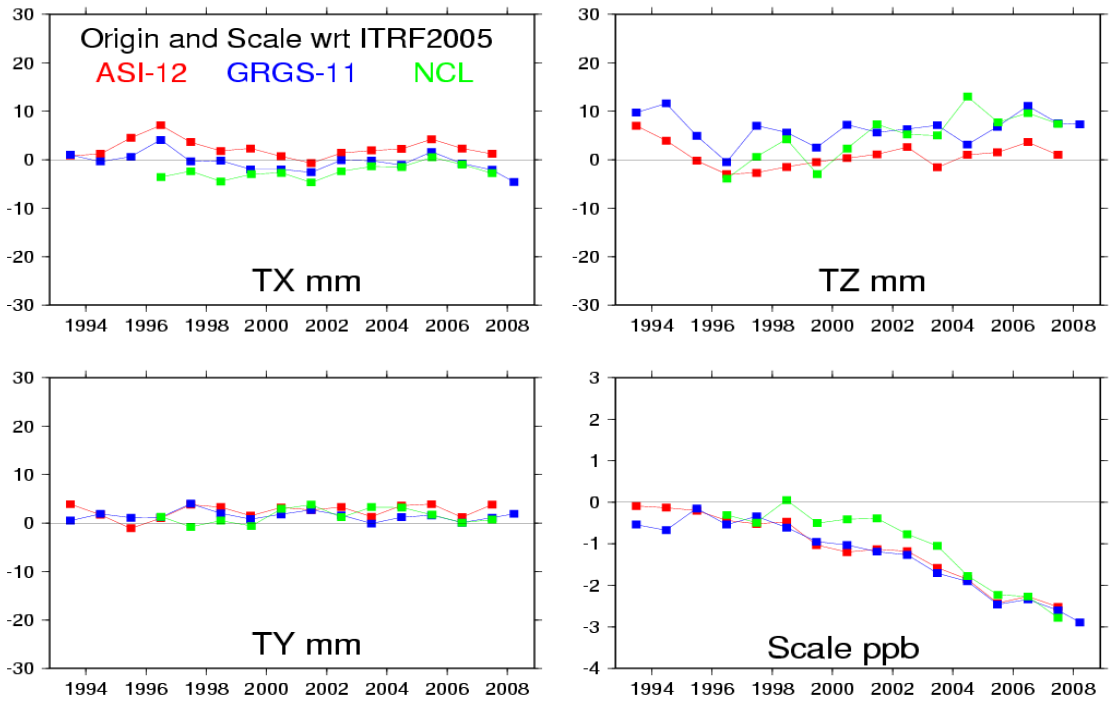

Figure 1. Averaged annual origin components and scale factors of the analyzed solutions with respect to ITRF2005

Figure 2 shows the averaged annual origin parameters and scale factors with respect to the ITRF2005 of the three solutions determined using separately data from Lageos I, Lageos II, and data from both satellites. This figure demonstrates that these parameters are roughly the same for either satellites (taken separately) or their combination.

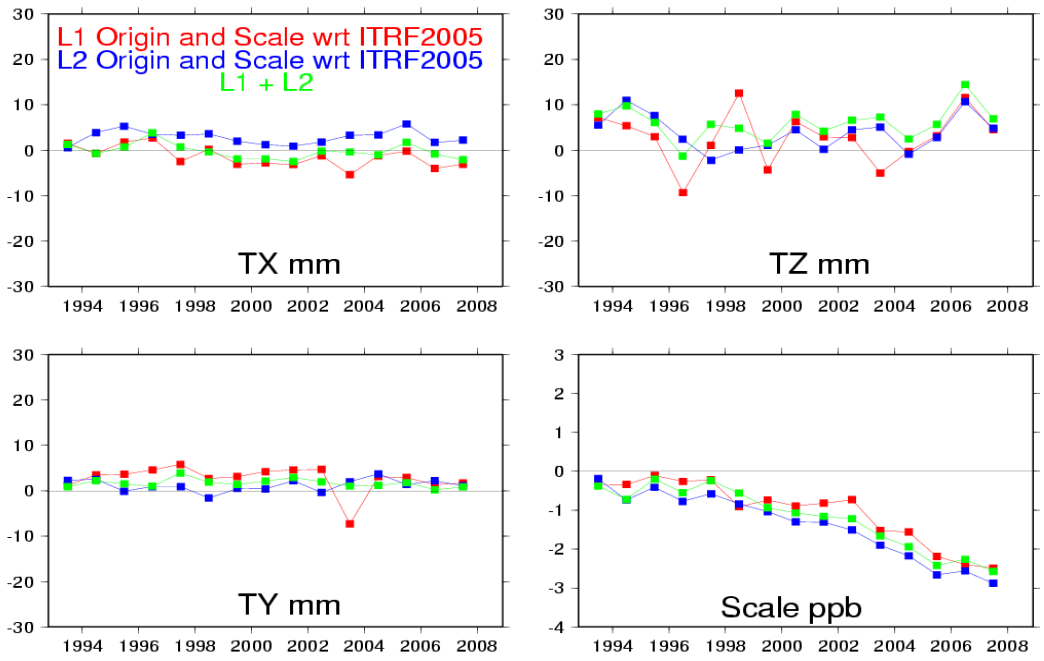

Figure 2. Averaged annual origin components and scale factors of three solutions determined using data from Lageos I in red, Lageos II in blue, and both satellites in green

Figure 3 displays the averaged annual scale factors with respect to ITRF2005 for IVS VLBI and SLR ASI-12 time series. We distinctively see the scale factor offset of VLBI solution with respect to ITRF2005 which is due to the fact the IVS is now applying for the mean pole tide correction [McCarthy and Petit, 2003]. The apparent scale drift difference between IVS VLBI and SLR ASI-12 solutions is still to be understood.

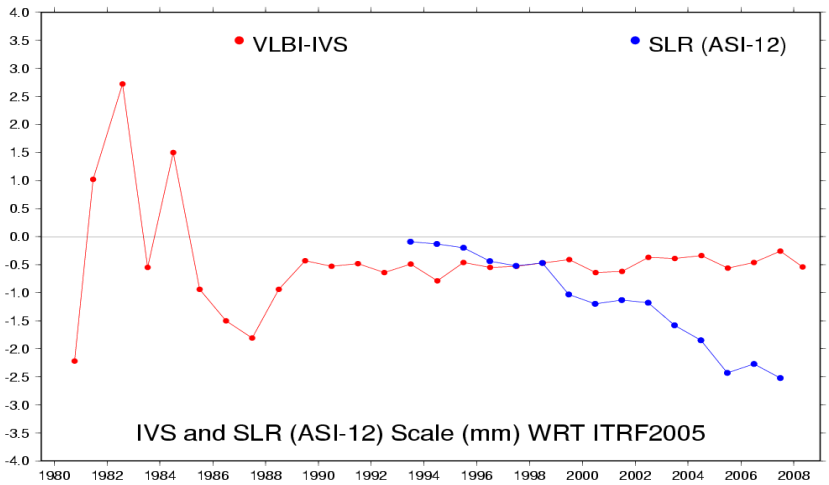

Figure 3. Averaged annual scale factors of VLBI IVS and SLR ASI-12 time series with respect to ITRF2005

Analysis of station vertical velocities

In order to investigate the significance and accuracy of station vertical velocities as estimated by SLR and VLBI, we selected from both networks the core sites that are co-located with GPS as depicted on Figure 4. The reasons for this selection are (1) there are very few sites (7 in total) where VLBI and SLR are co-located; (2) both techniques are co-located with GPS in all sites and (3) the scale and its drift between both techniques are fully determined over these co-located sites. Therefore GPS is playing the important role of connecting the SLR and VLBI networks. The reason for investigating the station vertical velocities is due to their dependency on the frame origin and scale time evolution definition. It could be shown that a drift in the Z-translation (δTz) component produces velocity changes of any site at latitude ϕ by $\delta Tz \times \cos(\phi)$ and by $\delta Tz \times \sin(\phi)$ along the north and vertical directions, respectively (Altamimi et al, 2007). On the other hand, any scale drift introduces vertical velocity changes with one-to-one ratio.

Supposedly, if the scale determined by both techniques is accurate and has no drift or discontinuities, and in the absence of systematic errors, there should be no physical reason of significant difference between both scale estimates. However, given the different natures of the shapes of both networks (see Figure 4), sampling the crust vertical motion in two different ways, this network effect might be one cause, among others, of the scale rate difference between the two technique solutions. The intrinsic conditions were used over the origin and the scale to generate the SLR ASI-12 long term solution. As the VLBI frame cannot be formed without inheriting its origin from SLR, two long-term VLBI solutions we generated by stacking the time series, and are expressed in the ITRF2005 and ITRF2000 origins, respectively, whereas the scale is determined by the intrinsic conditions.

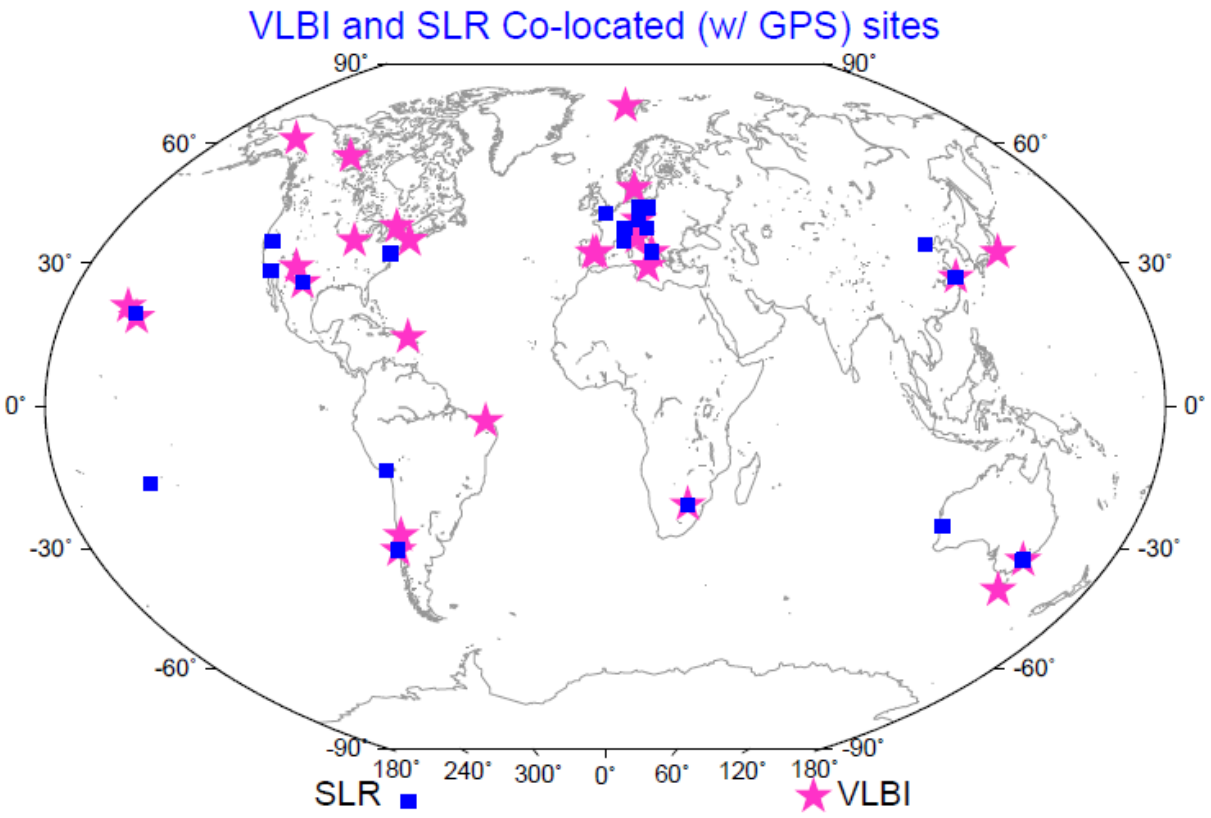

Figure 4. VLBI and SLR sites co-located with GPS

In order to evaluate the pertinence of the estimated vertical velocities by both technique solutions (VLBI IVS and SLR ASI-12), we attempted to confront them to the GIA model of Peltier (2004). Figure 5 depicts the SLR ASI-12 station vertical velocities corrected by the predictions of the GIA model, whereas Figures 6 and 7 show the GIA-corrected vertical velocities of the VLBI sites, expressed in the ITRF2005 and ITRF2000 origins, respectively.

If the GIA model and space geodesy estimates were perfect, with the assumption that all station vertical velocities are only due to GIA, correcting the station vertical velocities by the model predictions would lead to zero velocities at all sites. From Figures 5, 6 and 7, it becomes clear that on a site-by-site basis, not all the sites have zero vertical velocities after GIA model corrections. However, we computed the weighted means of the uncorrected and GIA-corrected vertical velocities of both co-located (via GPS) networks and reported these values in Table 1. The reasons for computing these averages are that they represent the mean vertical motions of each network and because of their possible correlations with the scale rate estimation. From these values we can notice that GIA corrections induce a mean change of +0.4 mm/yr for SLR and VLBI (expressed in ITRF2005 origin) solutions, whereas the change is about -0.4 mm/yr for VLBI solution expressed in ITRF2000 origin. We also notice that expressing the VLBI solution in the ITRF2000 origin reduces significantly the weighted mean of the vertical velocities. Therefore the reference frame stability in origin and scale definition is probably not better than 1 mm/yr, which corresponds to about 0.17 ppb/yr in scale rate.

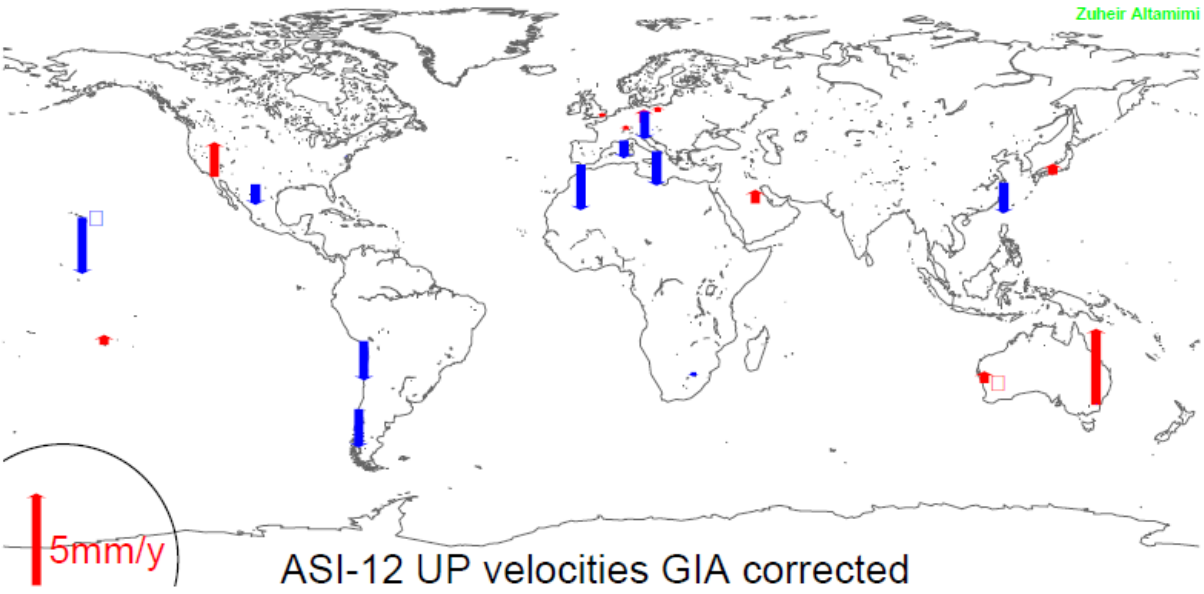

Figure 5. Vertical velocities of ASI-12 SLR core network, corrected by ICE-5G V1.2 GIA model of Peltier (2004). Red vectors represent positive velocities and blue vectors negative velocities.

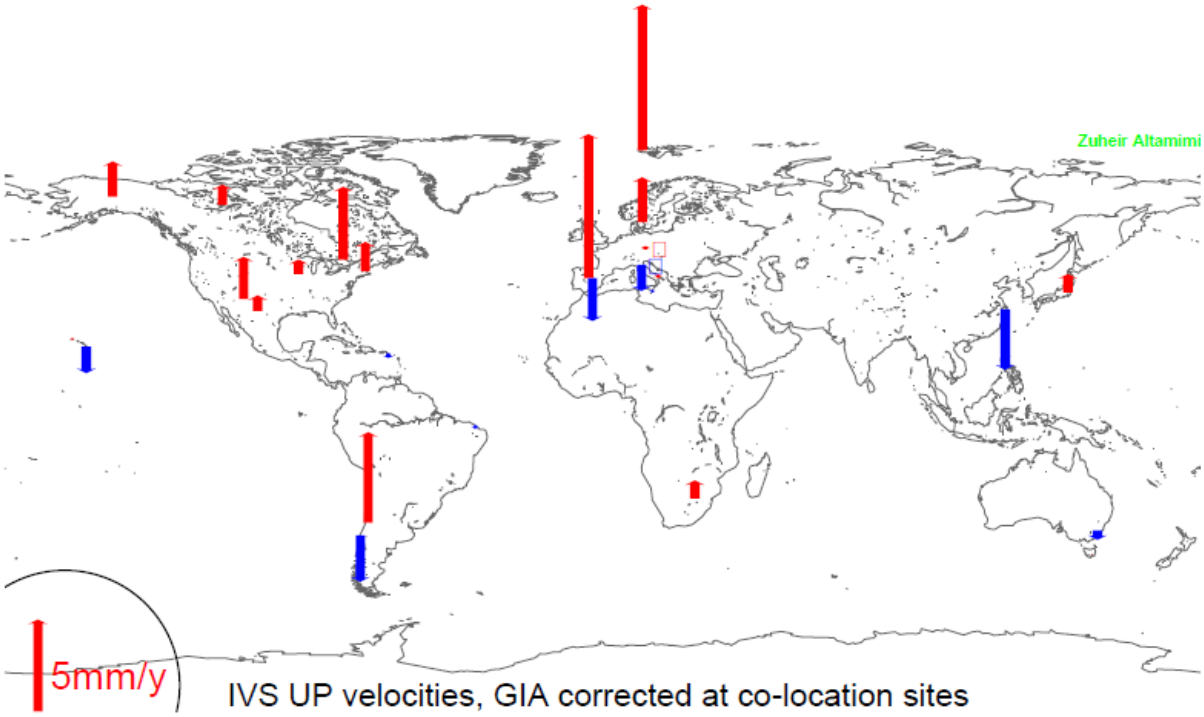

Figure 6. Vertical velocities of IVS-VLBI (intrinsic scale and ITRF2005 origin) co-located stations, corrected by ICE-5G V1.2 GIA model of Peltier (2004). Red vectors represent positive velocities and blue vectors negative velocities.

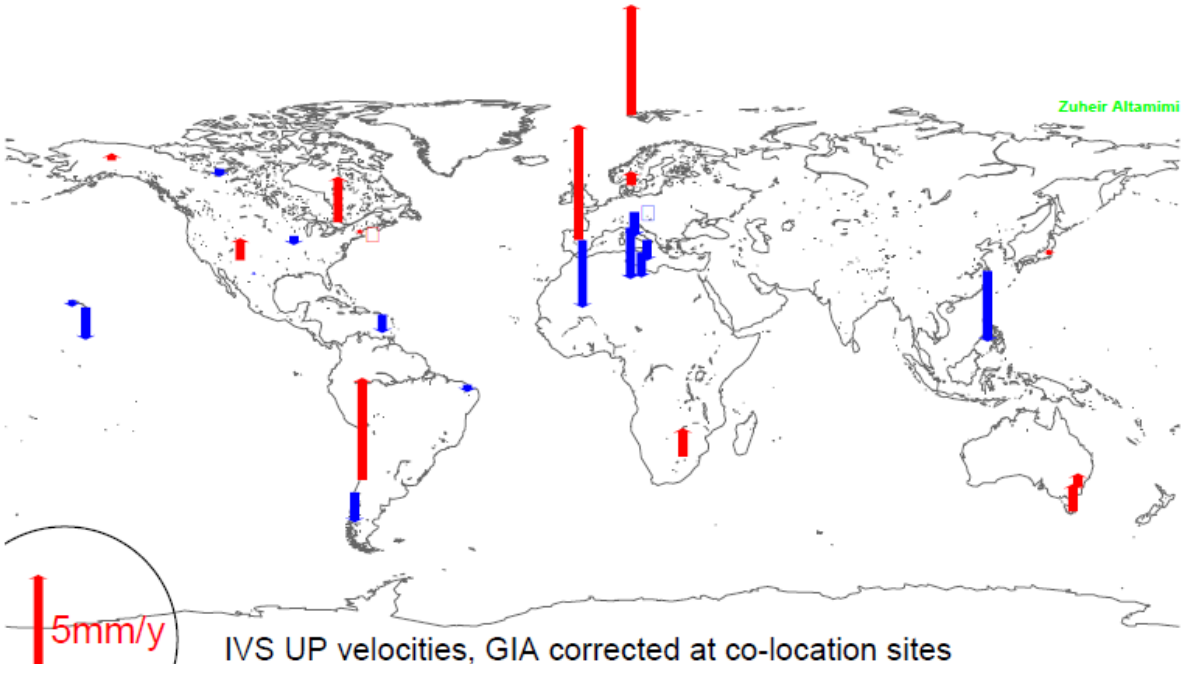

Figure 7. Vertical velocities of IVS-VLBI (intrinsic scale and ITRF2000 origin) co-located stations, corrected by ICE-5G V1.2 GIA model of Peltier (2004). Red vectors represent positive velocities and blue vectors negative velocities.

Table 1. Weighted mean of vertical velocities

	Weighted Mean of Vertical Velocities (GIA not corrected) (mm/yr)	Weighted Mean of Vertical Velocities (GIA corrected) (mm/yr)
SLR ASI-12 (intrinsic origin and scale)	-0.24	+0.16
VLBI IVS (intrinsic scale and ITRF2005 origin)	+0.89	+1.26
VLBI IVS (intrinsic scale and ITRF2000 origin)	+0.19	-0.24

Conclusion

We presented in this paper some preliminary analysis in preparation of the upcoming ITRF2008. We evaluated the origin and scale temporal behaviors of individual SLR and the regular IVS solutions of time series of station positions. Based on these preliminary analyses, we expect no significant change of the ITRF2008 origin, compared to ITRF2005. The difference in scale rate between VLBI and SLR solutions is still to be investigated and understood. Confronting the station vertical velocities estimated by both technique solutions to the predictions of the GIA model of Peltier (2004) yielded poor agreement between the two estimates on a site-by-site basis. The difference between the weighted averages of vertical velocities of VLBI and SLR network solutions is about 1 mm/yr, suggesting the same level of the scale and origin stability of the reference frame.

References

Altamimi, Z., Collilieux, X., Legrand, J., Garayt B. and Boucher, C., 2007, ITRF2005: A New Release of the International Terrestrial Reference Frame based on time series of station positions and Earth Orientation Parameters, *J. Geophys. Res.*, doi: 10.1029/2007JB004949.

Beckley B., F. Lemoine, S. Luthcke, R. Ray, and N. Zelensky, 2007, A reassessment of global and regional mean sea level trends from TOPEX and Jason-1 altimetry based on revised reference frame and orbits, *Geophysical Research Letters*, doi:101029/2007GL030002

McCarthy D. D. and G. Petit, IERS Conventions (2003) (IERS Technical Note ; 32), Frankfurt am Main: Verlag des Bundesamts für Kartographie und Geodäsie, 2004. 127 pp.

Morel, L. and P. Willis, 2005, Terrestrial reference frame effects on global sea level rise determination from TOPEX/Poseidon altimetric data, Advances in Space Research, DOI:10.1016/j.asr.2005.05.113

Peltier, W. R., 2004, Global Glacial Isostasy and the Surface of the Ice-Age Earth: The ICE-5G (VM2) model and GRACE, Ann. Rev. Earth Planet. Sci., doi:10.1146/annurev.earth.32.082503.144359

SBL web site, 2005, Predictions of present-day PGS signal in 3-d Displacements, http://www.sbl.statkart.no/projects/pgs/displacements/, May 2009.

Determination of the SLR station coordinates and velocities on the basis of laser observations of low satellites

P. Lejba, S. Schillak
Space Research Center of the Polish Academy of Sciences
Astrogeodynamic Observatory, Borowiec
plejba@cbk.poznan.pl

Abstract

The orbits of three low satellites Ajisai, Starlette and Stella have been determined on the basis of the data collected in 2001-2005 from the best 14 Satellite Laser Ranging stations. The positions and velocities of four SLR stations Graz (7839), Greenbelt (7105), Herstmonceux (7840) and Yarragadee (7090) were determined. Additionally, the station velocities were compared with the geological model NNR-NUVEL1A. All calculations have been made assuming the model of the Earth gravity field EIGEN-GRACE02S. All the calculations have been performed with the use of GEODYN-II program. The results presented in this work show that the data from low satellites such as Ajisai, Starlette or Stella can be successfully applied for determination of the SLR station coordinates and velocities.

1. Introduction

The high accuracy of laser observations and large number of observations allow for determination of the stations' coordinates and velocities from orbits of low satellites such as Ajisai, Starlette and Stella. Ajisai was launched by the JAXA on August 12, 1986. It is a spherical satellite covered with 1436 corner cube reflectors for SLR tracking and 318 mirrors for photography. The main purpose of the Ajisai was determination of the position of Japanese islands situated on the border of four tectonic plates Eurasian, Pacific, North American and Philippine and determination of plate motion. The laser data of Ajisai are used for definition and realization of ITRF and determination it changes in time, determination of geopotential coefficients (Bianco et al., 1997) and determination of spin axis of the satellite (Kirchner et al., 2006).

The twins Starlette and Stella with 60 corner cube reflectors were launched by the CNES, on February 6, 1975 and September 26, 1993, respectively. The laser observations to these satellites are used mainly for determination of Earth's gravity field coefficients, investigation of Earth and ocean tides, and determination of Earth rotation parameters (Cheng et al., 1990, Cheng et al., 1991, Schutz et al., 1989). The orbital and technical characteristics of the three satellites are presented in Table 1.
The first promising results of the stations' coordinates determination were obtained for Starlette and Stella (Lejba et al., 2007). In this work the period of the laser data were expanded to 5 years (2001-2005). Such period is taking as a minimum for determination of stations' velocities.

Table 1. Characterisation of the satellites Ajisai, Starlette and Stella.

	AJISAI	STARLETTE	STELLA
Sponsor	JAXA (JAPAN)	CNES (FRANCE)	CNES (FRANCE)
Launch date	August 12 1986	February 6 1975	September 26 1993
ID number	8606101	7501001	9306102
TECHNICAL AND PHYSICAL PARAMETERS			
Number of retroreflectors	1436	60	60
Shape	sphere	sphere	sphere
Diameter [cm]	214	24	24
Centre of mass correction [mm]	1010	75	75
Mass [kg]	685	47.25	48
CSA [m²]	3.5968	0.0452	0.0452
CSA/Mass [m²/kg]	0.00525	0.00096	0.00094
ORBITAL PARAMETERS OF THE SATELLITES			
Inclination	50.0°	49.8°	98.6°
Eccentricity	0.001	0.02	0.002
Perigee [km]	1480	810	800
Period [min.]	116	104	101

2. Determination of orbital arcs

The orbits of Ajisai, Starlette and Stella were determined using the program GEODYN-II (Pavlis et al., 1998) in two cases with empirical acceleration coefficients determined every 6 and 12 hours. The perturbing forces, constants and parameters used are listed in Table 3.

The satellites arcs were calculated using the observation data from the 14 best ILRS stations (Table 2), collected during the period from January 1st 2001 to December 25th, 2005 (Pearlman et al., 2002). This period was divided into 130 orbital arcs of 14-days each for Ajisai and 182 orbital arcs of 10-days each for Starlette and Stella. Due to similar orbital and technical parameters the data of Starlette and Stella were combined in the calculations.

Table 2. List of the stations.

	Station	ID Number
1	McDonald	70802419
2	Yarragadee	70900513
3	Greenbelt	71050725
4	Monument Peak	71100411
5	Haleakala	72102313
6	Zimmerwald	78106801
7	Borowiec	78113802
8	Mount Stromlo	78259001
9	Grasse SLR	78353102
10	Potsdam	78365801
11	Graz	78393402
12	Herstmonceux	78403501
13	Mount Stromlo	78498001
14	Wettzell	88341001

472259 normal points of Ajisai, 265282 for Starlette and 133093 for Stella were accepted by the GEODYN. The number of rejected normal points is 2335 for Ajisai and 3729 together for Starlette and Stella. The obtained mean RMS of fit values for the calculated orbits for Ajisai are 1.61 cm and 1.98 cm for 6 and 12-hour interval of empirical acceleration coefficients, respectively. For Starlette and Stella the mean RMS of fit values are 1.15 cm and 1.63 cm, respectively.

Table 3. GEODYN II – force models and parameters

Force Model
Earth gravity field: EIGEN-GRACE02S (Reigber et al., 2005), 45x45 solution for Ajisai and 75x75 solution for Starlette and Stella
Earth and ocean tide model: EGM96 (Lemoine et al., 1998)
Third body gravity: Moon, Sun and all planets – DE200 (Standish, 1990)
Solar radiation pressure: C_R coefficient *a priori* 1.13 for Starlette and Stella and 1.0 for Ajisai
Earth albedo (Pavlis et al., 1998)
Dynamic polar motion (Pavlis et al., 1998)
Relativistic correction (Pavlis et al., 1998)
Constants
Gravitational constant times the mass of the Earth (GM): $3.986004415 \times 10^{14}$ m^3/s^2 (EIGEN-GRACE02S Earth gravity field model)
Speed of light: 299792.458 km/s (McCarthy et al., 2004)
Semi-major axis of the Earth: 6378.13630 km (EIGEN-GRACE02S Earth gravity field model)
Inverse of the Earth's flattening: 298.2570 (EIGEN-GRACE02S Earth gravity field model)
Reference Frame
Inertial reference system: true of date defined at 0^h of the first day of each arc (Pavlis et al., 1998)
Stations coordinates and stations velocities: ITRF2005 solution, epoch 2000.0 (Altamimi et al., 2007)
Precession: IAU 1976 (Lieske et al., 1977)
Nutation: IAU 1980 (Seidelmann 1982)
Polar motion: C04 IERS (IERS 2001)
Tidal uplift: Love model H2 = 0.609, L2 = 0.0852 (Pavlis et al., 1998)
Pole tide (Pavlis et al., 1998)
Estimated parameters
Satellite state vector
Station geocentric coordinates
Drag coefficients C_D determined every 15 hours for Ajisai and 12 hours for Starlette, Stella
Acceleration parameters along-track, cross-track and radial at 6 and 12 hours intervals
Measurement Model
Observations; 30 seconds normal points from Eurolas Data Center
Laser pulse wavelength: 532 nm (Zimmerwald 423 nm)
Tropospheric refraction: Marini/Murray model (Marini and Murray, 1973)
Editing criteria:
$5\sigma \approx \pm 11$ cm for arc (Ajisai), $5\sigma \approx \pm 12$ cm for arc (Starlette, Stella)
cut-off elevation 10 deg.
Numerical Integration
Integration: Cowell's method
Orbit integration step size: 110 sec for Ajisai and 90 sec for Starlette and Stella
Arc length: 14 days for Ajisai and 10 days for Starlette and Stella

3. Determination of SLR station coordinates and velocities

The coordinates and velocities of the following stations were determined: Yarragadee (7090), Greenbelt (7105), Graz (7839) and Herstmonceux (7840). These stations provide the best quality of observation results. Besides these stations provided the largest number of normal points of Ajisai, Starlette and Stella in the mentioned period. The calculated X, Y, Z

geocentric coordinates referenced to the epoch of ITRF2005 were transformed to the topocentric coordinates N, E, Up. These results were related to ITRF2005. In order to determine the movement of station the calculated X, Y, Z geocentric coordinates were referenced to the epoch of each orbital arc. Also in this case the calculated X, Y, Z components were transformed to N, E, Up components. On figures 1-4 the results obtained from Ajisai data were presented in two cases with empirical acceleration coefficients determined every 6 (blue line) and 12 (red line) hours. The left site of each figure shows determined station coordinates in reference to ITRF2005, the right one the movement of each topocentric component for a given epoch of orbital arc. Analogous results were presented for Starlette and Stella on figures 5-8. The gaps on the figures mean the lack or less than 50 number of normal points of the station for the given orbital arc. The RMS of the determined coordinates amount from 14.7 to 20.1 mm for Ajisai and 9.3 to 17.1 mm for Starlette and Stella depending on the number of the empirical acceleration coefficients. In case of Ajisai results the noticable systematical shifts of Up component for each station are visible. Probably they are caused by the inaccurate definite centre of mass correction of Ajisai. This parameter changes within the range of 5 cm (Otsubo et al., 2003).

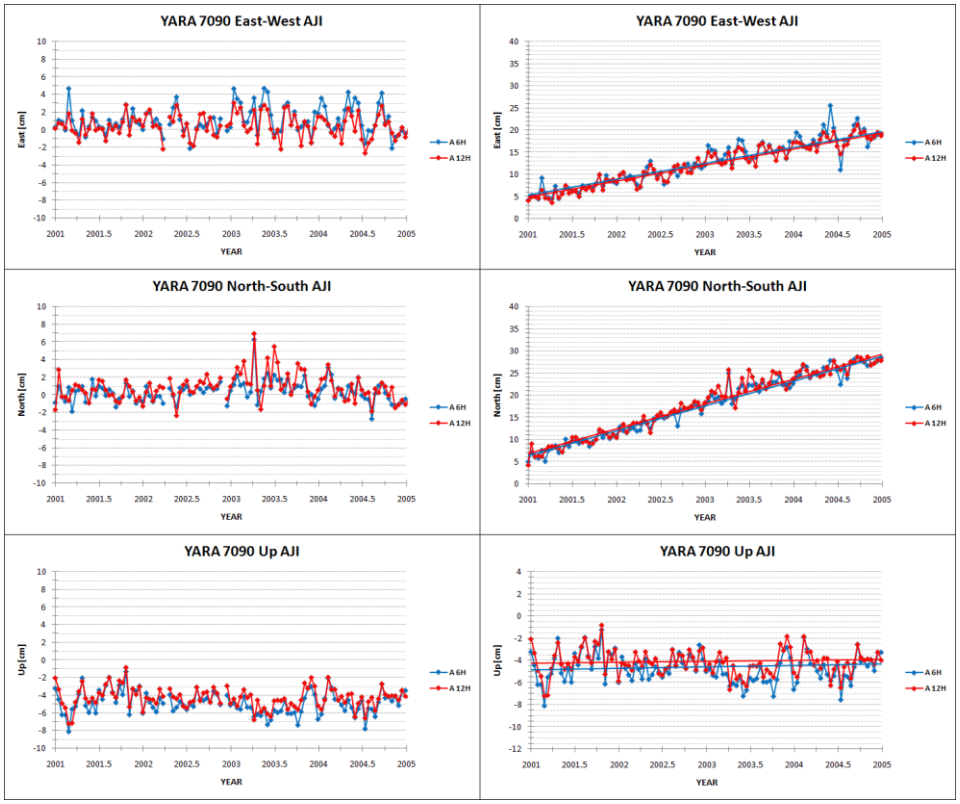

Figure 1. The topocentric coordinates N, E, Up of the station Yarragadee (7090) obtained from laser observations of Ajisai.

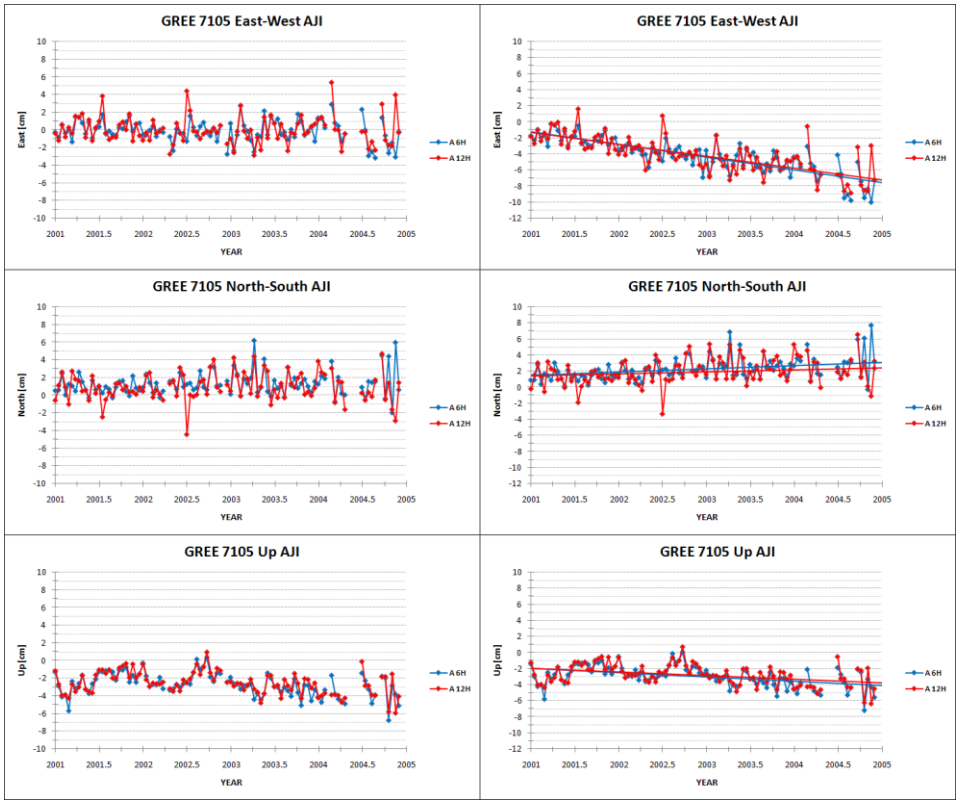

Figure 2. The topocentric coordinates N, E, Up of the station Greenbelt (7105) obtained from laser observations of Ajisai.

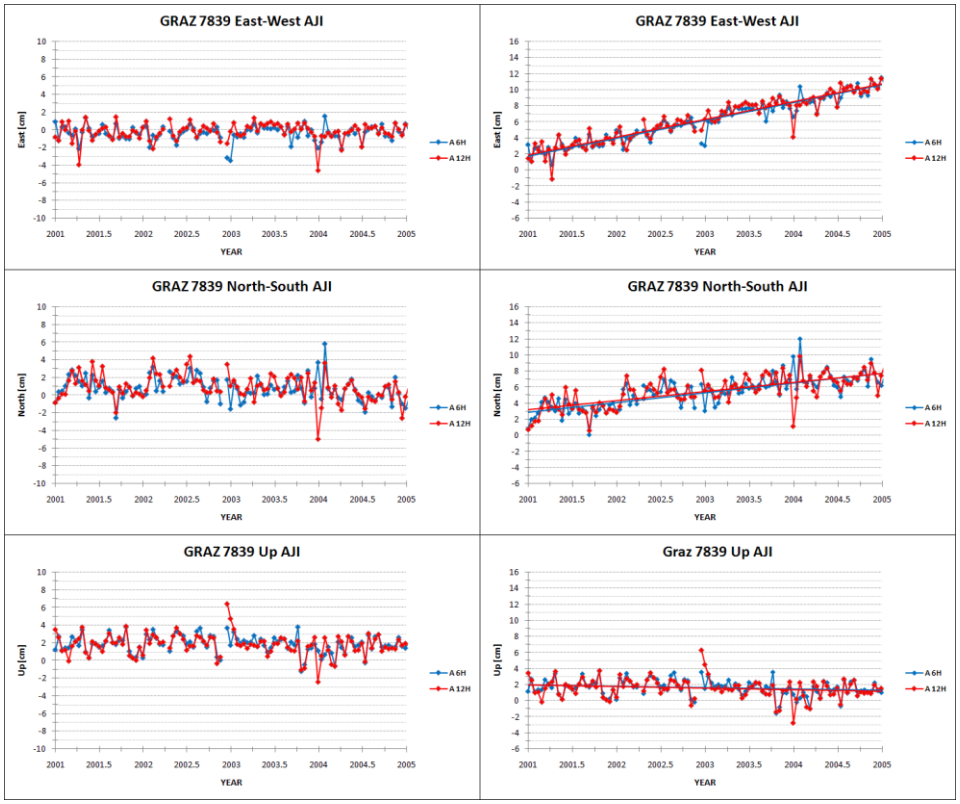

Figure 3. The topocentric coordinates N, E, Up of the station Graz (7839) obtained from laser observations of Ajisai.

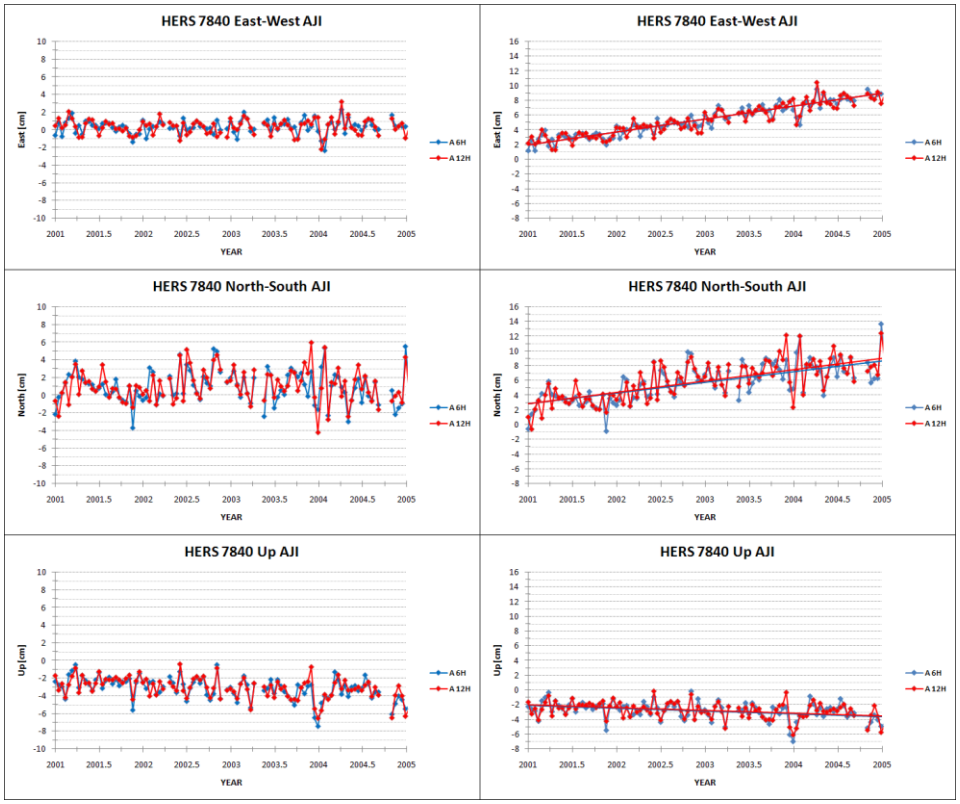

Figure 4. The topocentric coordinates N, E, Up of the station Herstmonceux (7840) obtained from laser observations of Ajisai.

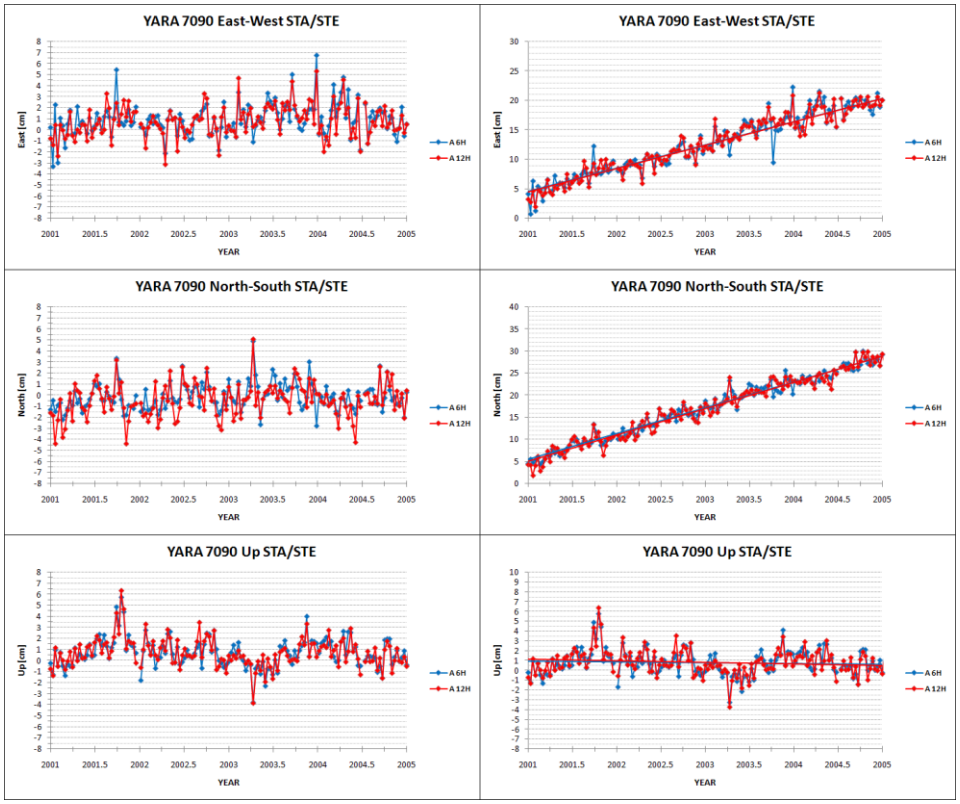

Figure 5. The topocentric coordinates N, E, Up of the station Yarragadee (7090) obtained from laser observations of Starlette and Stella.

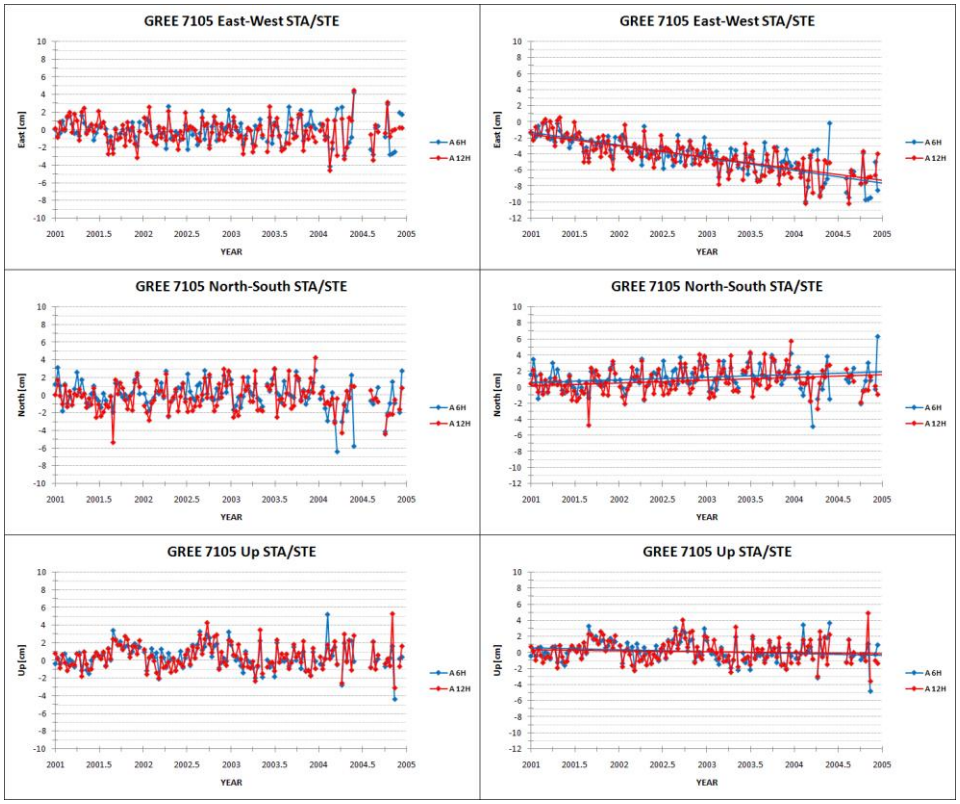

Figure 6. The topocentric coordinates N, E, Up of the station Greenbelt (7105) obtained from laser observations of Starlette and Stella.

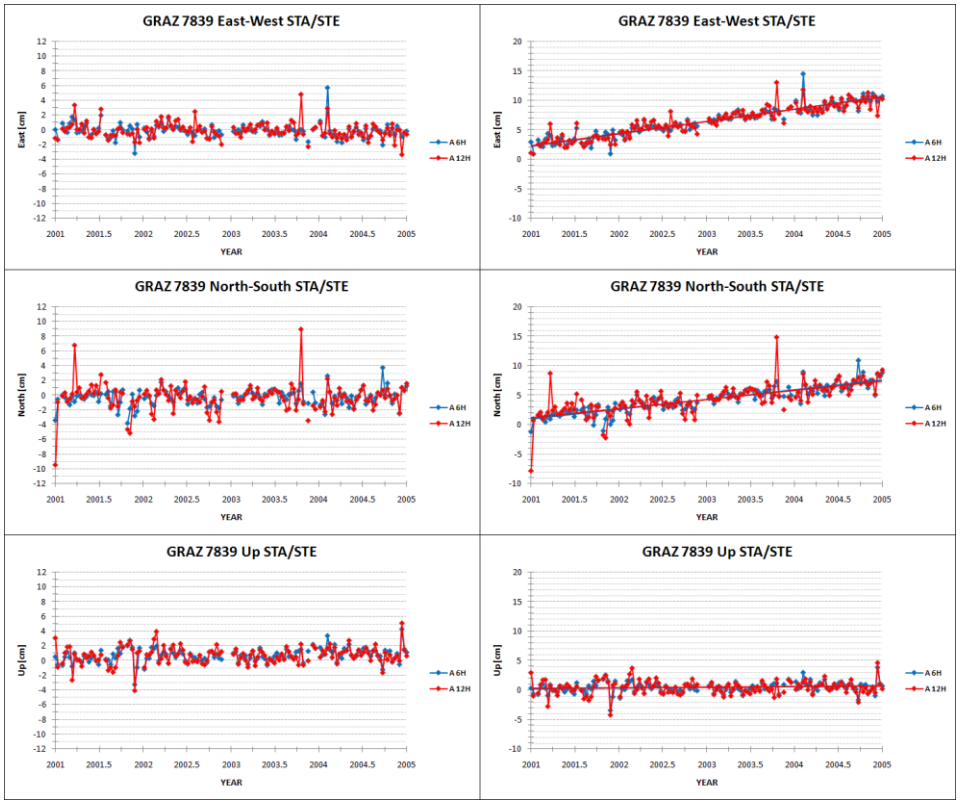

Figure 7. The topocentric coordinates N, E, Up of the station Graz (7839) obtained from laser observations of Starlette and Stella.

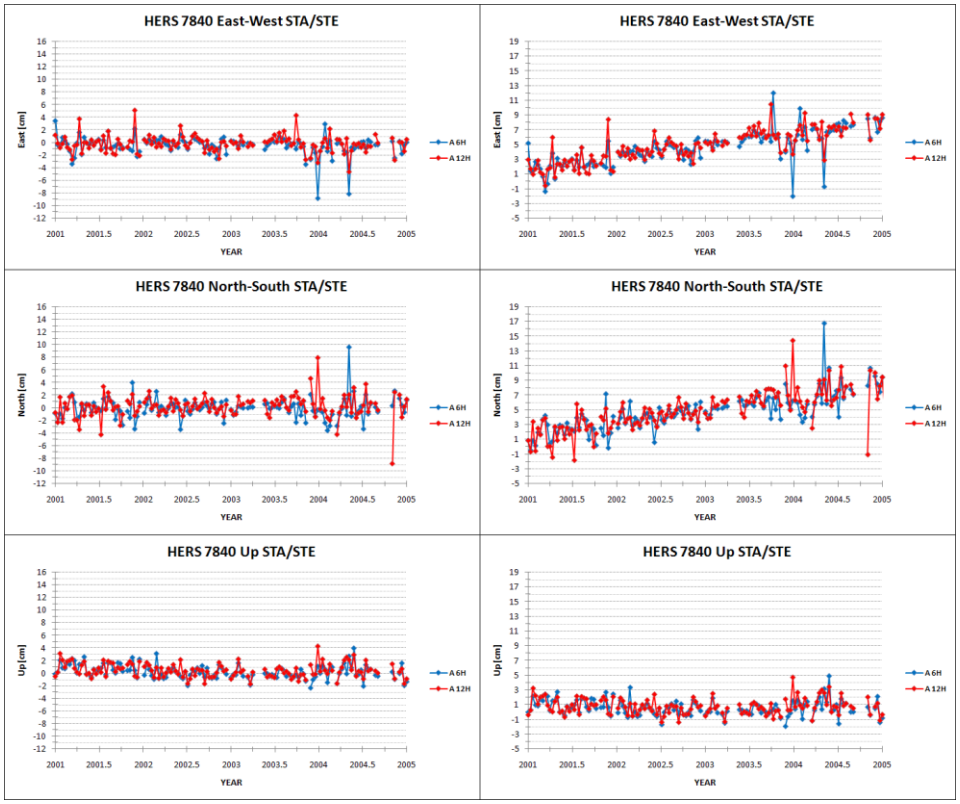

Figure 8. The topocentric coordinates N, E, Up of the station Herstmonceux (7840) obtained from laser observations of Starlette and Stella.

Table 4. The velocities in horizontal plane of the stations determined for Ajisai, Starlette/Stella, LAGEOS, ITRF2005 and geological model NNR-NUVEL1A.

	V 2D [mm/rok]				
	AJISAI	STARLETTE STELLA	LAGEOS	ITRF2005	NNR NUVEL1A
Yarragadee	66.5 67.0	65.7 71.5	68.3	68.1	66.6
Greenbelt	16.1 15.0	16.2 14.7	15.6	15.7	15.4
Graz	25.3 25.0	26.7 25.8	26.6	26.7	24.8
Herstmonceux	22.8 23.4	22.7 23.3	23.3	23.4	23.3

Table 4 shows the velocities of the stations in horizontal plane determined for Ajisai and Starlette and Stella in comparison to the same results obtained for LAGEOS, ITRF2005 and geological model NNR-NUVEL1A (DeMets et al., 1994). In case of LAGEOS the velocity of the station were computed for the period 1999-2004 (Schillak, 2008). For Ajisai and Starlette and Stella two values of the V2D velocity were presented. The upper value is in Table 4 for variant with empirical acceleration coefficients determined every 6 hours. For this solution the differences come from 0.4 to 2.6 mm/year. The bottom is for variant with empirical

acceleration coefficients determined every 12 hours. For this solution the differences don't exceed 1.6 mm/year for Ajisai and 4.9 mm/year for Starlette and Stella. The fastest station is Yarragade moving about 7.0 cm/year in North-East direction. The European stations like Graz and Herstmonceux 2.5 and 2.3 cm/year in Nort-East direction, rspectively. The slowest is Greenbelt moving in North-West direction about 1.5 cm/year.

5. Summary and conclusions

The results presented in this work show, that observations of low satellites such as Ajisai, Starlette and Stella can be used for determination of the SLR station coordinates and velocities. The obtained results permit verification of results derived from the LAGEOS observations are in a good agreement with those determined from LAGEOS observations, for ITRF2005 and geological model NNR-NUVEL1A. The stations' coordinates and velocities were counted for 5-years period. Approximately 0.5% of all normal points of Ajisai were rejected by the orbital program and about 1% for Starlette and Stella. The RMS of fit is on the level 1.61-1.98 cm for Ajisai and 1.15-1.63 cm for Starlette and Stella. The RMS of the calculated coordinates amount from 9.3 to 20.1 mm depending on the number of the empirical acceleration coefficients. The stations are moving in horizontal plane from 1.5 to 7.0 cm/year. These results show, that the laser observations of low satellites could be included to the global solution of the stations' coordinates and velocities.

Acknowledgements

The authors wish to thank the NASA geodesy group for consent to use of GEODYN-II orbital program and to thank all ILRS stations and data centers for their continuous efforts to provide high-quality global SLR data for this work. This work has been supported by financial resources for science in 2006-2009 as a research project No. 4T12E 007 30.

References

Altamimi, Z., Collilieux, X., Legrand J., Garayt B., Boucher C., ITRF2005: A new release of the International Terrestrial Reference Frame based on time series of station positions and Earth Orientation Parameters, J. Geophys. Res., 112, B09401, 2007.

Bianco, G., Devoti, R., Fermi, M., Luceri, V., Rutigliano, P., Sciarretta, C., Estimation of low degree geopotential coefficients using SLR data, Planet Space Sci., vol. 46, no.11/12, pp.1633-1638, 1997.

Cheng, M.K., Shum, C.K., Eanes, R.J., Shutz, B.E. and Tapley, B.D., Long-Period Perturbations in Starlette Orbit and Tide Solution, Journal of Geophysical Research., 95, B6, pp. 8723-8736, 1990.

Cheng, M.K., Shum, C.K., Eanes, R.J., Schutz, B.E. and Tapley, B.D., Observed temporal variations in the Earth's gravity field from 16-years of Starlette orbit analysis, Processing XX General Assembly of the IUGG, IAG Symp. No. 3, Vienna, Austria, August, 1991.

DeMets, C., Gordon, R. G., Argus, D. F., Stein, S., Effect of recent revisions to the geomagnetic reversal time scale on estimates of current plate motions, Geophysical Research Letters, 21, pp. 2191-2194, 1994.

Kirchner, G., Kucharski, D., Cristea, E., Hausleitner, W., Spin Parameters of GP-B and AJISAI with Kilohertz SLR Data, 15th International Workshop on Laser Ranging, Canberra, Australia, October 15-20, 2006.

Lejba, P., Schillak, S., Wnuk, E., Determination of orbits and SLR stations' coordinates on the basis of laser observations of the satellites Starlette and Stella, Advances in Space Research, Volume 40, Issue 1, p.143-149, 2007.

Lemoine, F.G., Kenyon, S.C., Factor, J.K., Trimmer, R.G., Pavlis, N.K., Chinn, D.S., Cox, C.M., Klosko, S.M., Luthcke, S.B., Torrence, M.H., Wang, Y.M., Williamson, R.G., Pavlis, E.C., Rapp, R.H., Olson, T.R., The development of the joint NASA GSFC and the National Imagery and Mapping Agency (NIMA) Geopotential Model EGM96, NASA/TP-1998-206861, Goddard Space Flight Center, Greenbelt,1998.

Lieske, J. H., Lederle, T., Fricke, W., Morando, B., Expression for the precession quantities based upon the IAU (1976) system of astronomical constants, Astronomy & Astrophysics, 58:1-16, 1977.

McCarthy, D. D., Petit, G., IERS Conventions 2003, Frankfurt am Main, 2004.

Otsubo, T., Appleby, G. M., System-dependent center-of-mass correction for spherical geodetic satellites, Journal of Geophysical Research, 108(B4), 2201, doi:10.1029/2002JB00-2209, 2003.

Pearlman, M.R., Degnan, J.J., and Bosworth, J.M., "The International Laser Ranging Service", Advances in Space Research, Vol. 30, No. 2, pp. 135-143, July 2002, DOI:10.1016/S0273-1177(02)00277-6.

Pavlis, D. E., Luo, S., Dahiroc, P., McCarthy, J. J., Luthcke, S. B., GEODYN II System Description, Hughes STX Contractor Report, Greenbelt, Marylnad, July, 1998.

Reigber, C., Schmidt, R., Flechtner, F., Koenig, R., Meyer, U., Neumayer, K.H., Schwiatzer, P., Zhu, S.Y., An Earth gravity field model complete to degree and order 150 from GRACE: EIGEN-GRACE02S, Journal of Geodynamics 39 (1): 1-10, 2005.

Schillak, S., The comparison of the reference frames ITRF2000 and ITRF2005 in the determination SLR station positions and velocities, European Geosciences Union, General Assembly 2008, Vienna, Austria, April 13-18, 2008.

Schutz, B. E., Cheng, M. K., Shum, C. K., Eanes, R. J., Tapley, B. D., Analysis of Earth Rotation Solution from Starlette, Journal of Geophysical Research 94, pp. 10167-10174, 1989.

Seidelmann, P. K., 1980 IAU nutation: The final report of the IAU Working Group on nutation, Celestial Mechanics, 27:79-106, 1982.

Standish E.M., The observational basis for JPL's DE200, the Planetary Ephemerides of the Astronomical Almanac, Astron. Astrophys., Vol. 233, pp. 252-271, 1990.

Temporal variations of the Earth's gravity field derived from SLR data over a long period of time

F. Deleflie (1)**, J.-M. Lemoine** (2)**, O. Laurain** (1)**, D. Feraudy** (1)

(1) Observatoire de la Côte d'Azur – Geoazur / GRGS, Grasse, France
(2) Centre National d'Etudes Spatiales / GRGS, Toulouse, France

Florent.Deleflie@obs-azur.fr /Fax: +33-4-93405333

Abstract

In addition to the products built by the GRGS Analysis Center and delivered to the ILRS community through the Analysis Working Group, the authors now provide as well, routinely on a weekly basis, time series of the low wavelengths of the Earth's gravity field, namely for degree 2, 3, 4, 5. Over a long period of time, we enlighten temporal variations due to mass redistribution within the Earth's system, as shown by many authors, and especially at the beginning of the decade. We present here our own preliminary results.

Introduction

We use SLR data tracked by the ILRS network (Pearlmann et al., 2002) since more than twenty years to derive long time series of the low wavelengths of the Earth's gravity field. The work is based on a post-fit residuals analysis, performed with the computation of the orbits of geodetic satellites, LAGEOS-1, LAGEOS-2, Starlette in particular. On a weekly basis, normal matrices deduced from each orbital arc are stacked and then inversed to perform time series of gravity field parameters.

1. Post-fit residuals analysis of weekly arcs

1.1. LAGEOS-1

As mentioned in (Métris *et al.*, 1997), a main difficulty to study non gravitational effects acting on LAGEOS-1 orbit is a "lack of firm knowledge of the satellite spin axis evolution. Several important effects, notably the thermal phenomena and the optical anisotropy effect, depend criticaly on the spin axis orientation. A lack of the theoretical understanding of this evolution has posed (and still poses) an important obstacle in the non gravitational force modeling process." This difficulty to model the spin axis orientation has been increased since the middle of the 90's, because the rotation LAGEOS-1 rotation period has been considerably decreased by the action of the eddy current dissipation. In addition to the well-known radiation pressure, and to the discover in 1981 by Smith and Dunn of an unexplained decreasing of the semi-major axis of about 1.1mm/day, (corresponding to a constant along track acceleration of $-3.3\ 10^{-12}$ m.s^{-2}), different non gravitational effects have been enlightened in the LAGEOS-1 orbit, and produce specific perturbations on the orbital motion (Yarkovsky-Shah thermal effect, asymmetric reflectivity of the satellite surface, asymmetric thermal emissivity of the Earth).

The level of residuals strongly depends, not only on the quality of the orbital model, but also on the number of the adjusted parameters. Hence, some small effects can be "absorbed" through some of the parameters accounting for empirical forces, especially the odd degrees of the Earth's gravity field. Nevertheless, since the periods appearing in the orbital motion and

the gravity field are slightly different, we think that we can trust on the temporal variations for the odd parameters (see below).

Weekly orbital arcs of LAGEOS-1 have been built from 1990 to 2006. Figure 1 shows time series of the adjusted empirical parameters, towards the radial, tangential and normal directions, respectively (two sets per week). Some characteristic signals can easily be observed, in particular on the normal direction. Let us note that since there is no physical reason why the radiation pressure coefficient should vary, this coefficient has been constrained to its averaged value (1,02). The averaged rms for weekly arcs is of the order of 1,4cm.

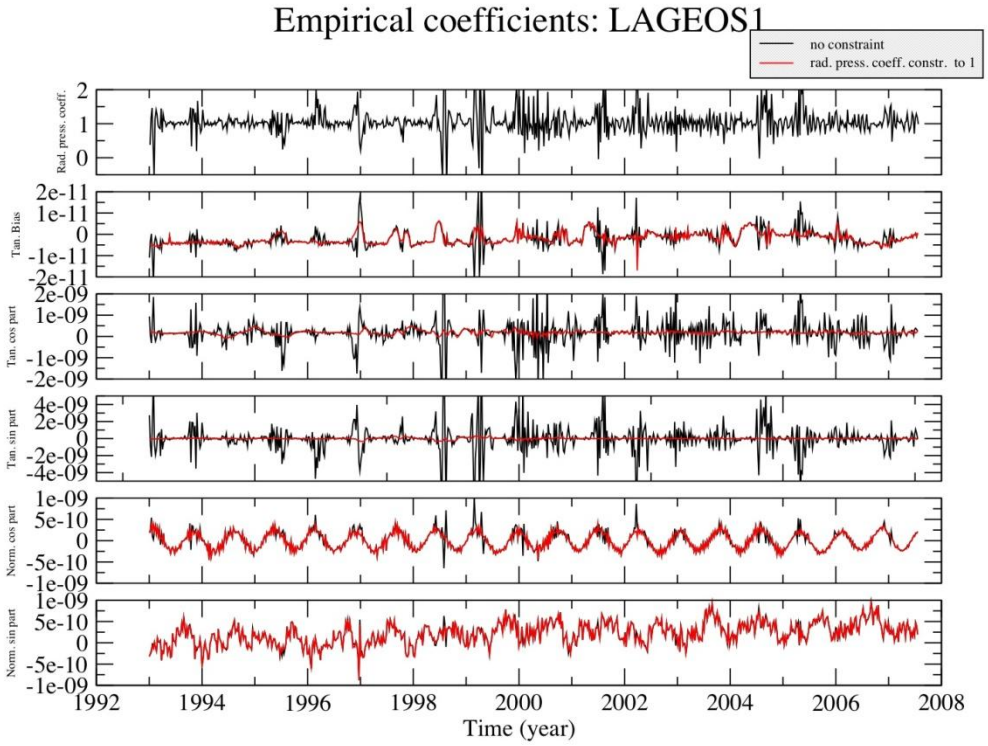

Figure 1. Time series of empirical parameters for LA-1

1.2. LAGEOS-2, and other satellites

The same kind of strategy was used to build weekly arcs of other geodetic satellites. Figure 2 shows the weighted rms for LAGEOS-1, with an orbit modeling very close to the one used for LAGEOS-1, and the number of normal points used for each weekly computation. Some arcs of ETALON-1 have also been used, as well as Starlette (orbital modeling accounting for additional perturbations, such as the atmospheric drag).

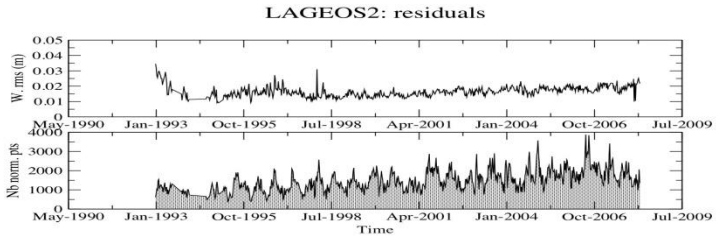

Figure 2. LA-2 weekly post-fit residuals

2. Time series of gravity field parameters

SLR tracking data of geodetic satellites have been used to determine time series of gravitational field harmonics up to degree 5. We show here the results for the degree 2 and the degree 3.

2.1. Degrees 2, 3

Figure 3 shows the time series for the whole degree 2, Figure 5 the time series for the whole degree 3.The black curve is composed by one point every 10 days, and the red one is a running averaging, enlightening seasonal variations. The blue curve shows the temporal variations determined by GRACE measurements (courtesy J.M. Lemoine). The zero line corresponds to the value of the EIGEN-GL04S model.

We compared these temporal variations with the one determined by geophysical models (courtesy O. de Viron), modeling changes in ocean-bottom pressure, and land hydrology. The ocean-bottom pressure series is from "a data assimilating oceanic general circulation model, ECCO (Stammer et al., 2002), constrained by in situ and satellite data including expandable bathyther-mograph data and altimetric measurements of sea surface height. (…) The land hydrology model is the land Dynamics (LaD) model of Milly and Shmakin (2002), which consists of gridded values of the surface mass density of snow, root-zone soil water, an groundwater given at monthly intervals." (Gross et al., 2009). This comparison is shown Figure 4. The correlation between the two curves gives a poor value. It appears that it seems to exist a good correlation over significant periods of time, but the consistency between values obtained from space data and geophysical models still needs to be improved significantly over the whole period.

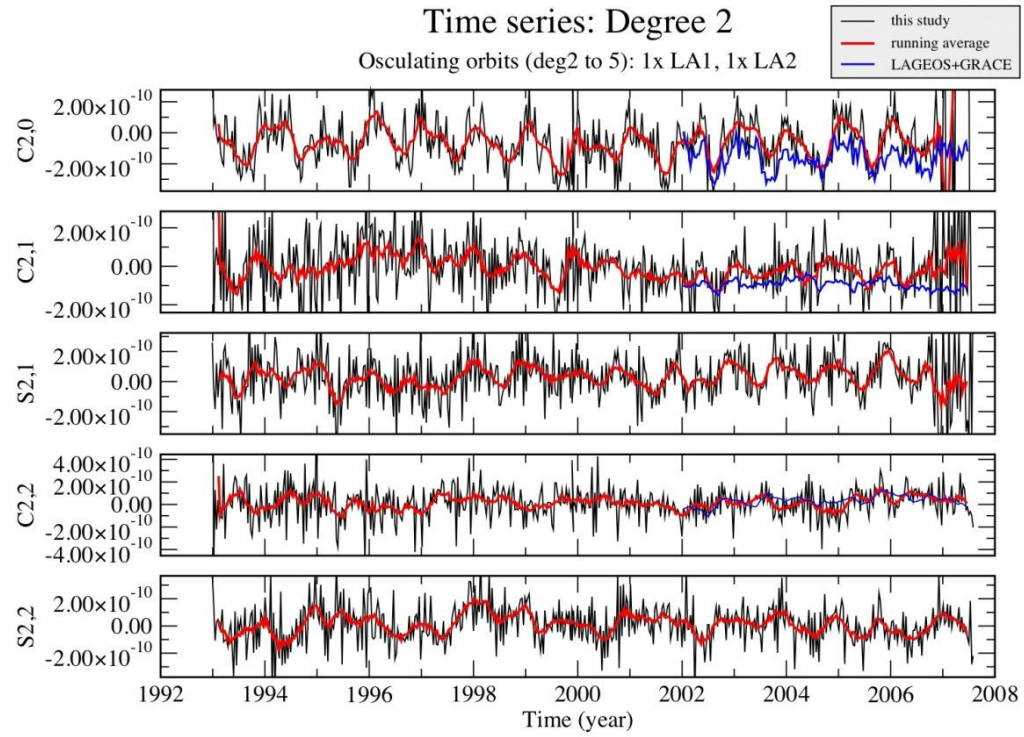

Figure 3. Degree 2 time series (zonal and tesseral coefficients)

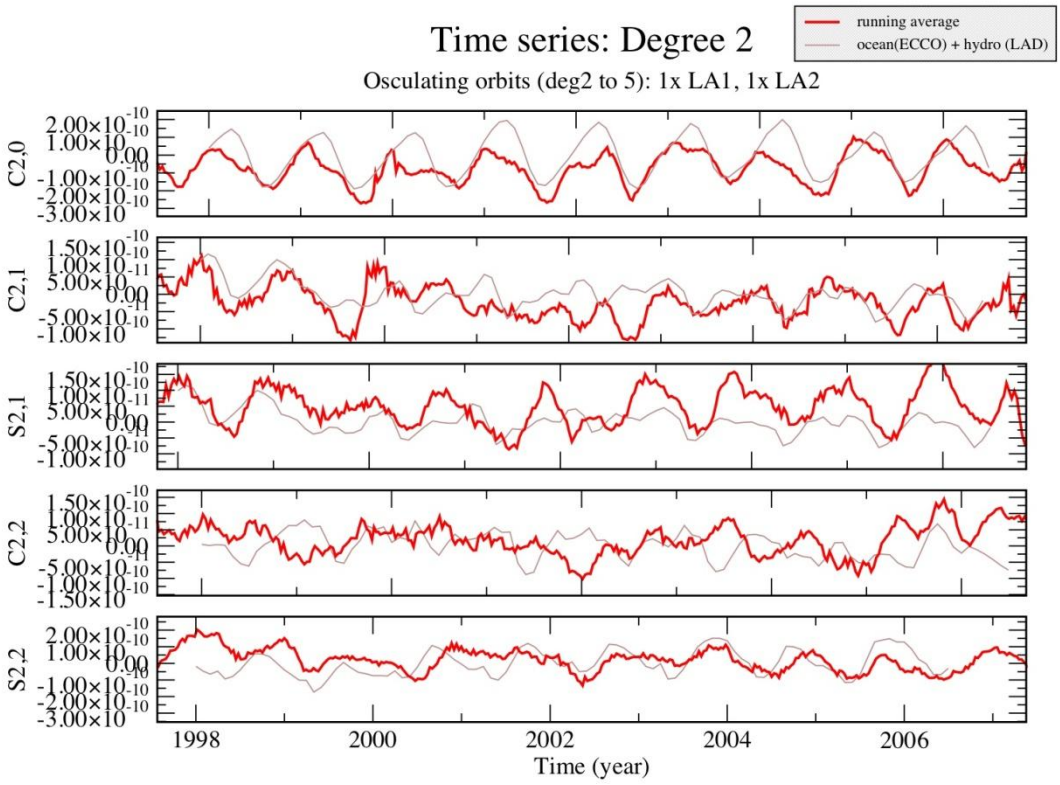

Figure 4. Degree 2: comparison with geophysical models

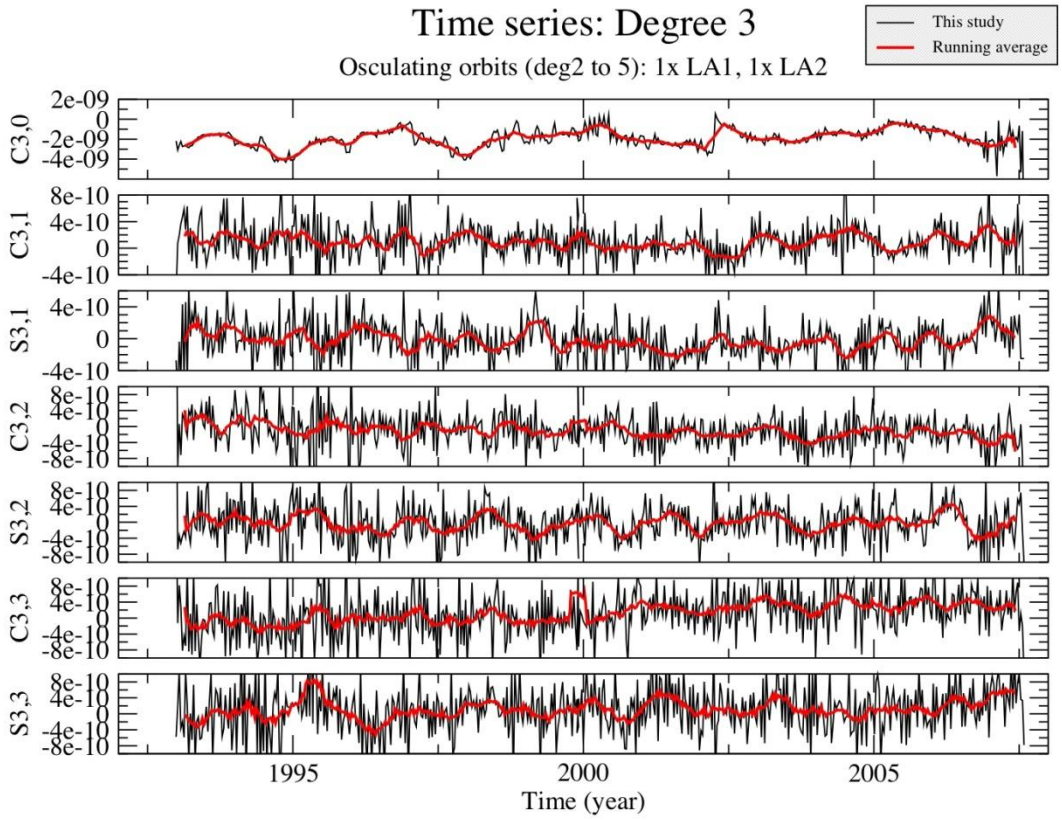

Figure 5. Degree 3 time series (zonal and tesseral coefficients)

2.2. Particular case of the J2 zonal coefficient

Figure 6 is a blow-up of Figure 3 for the C(2,0)=-J2 coefficient. As it is well known SLR data analyses indicate that the earth's dynamic oblateness has undergone significant variations. The dominant signature in the observed variations are mainly (i) a secular decrease linked more or less to the post-glacial rebound, at the level of 4,88 10^{-12} / yr, obtained from a least square fitting to the whole time series (value affected by the 1996-2002 event) (ii) seasonal variations with a mean amplitude of the order of 1.62 10^{-10} (to be compared to the value of (Cheng & Tapley, 2004) of about 3 10^{-10}) and a phase of 187°. There are as well significant interannual variations related to El Nino Southern Oscillation event, especially during the 1996-2002 period.

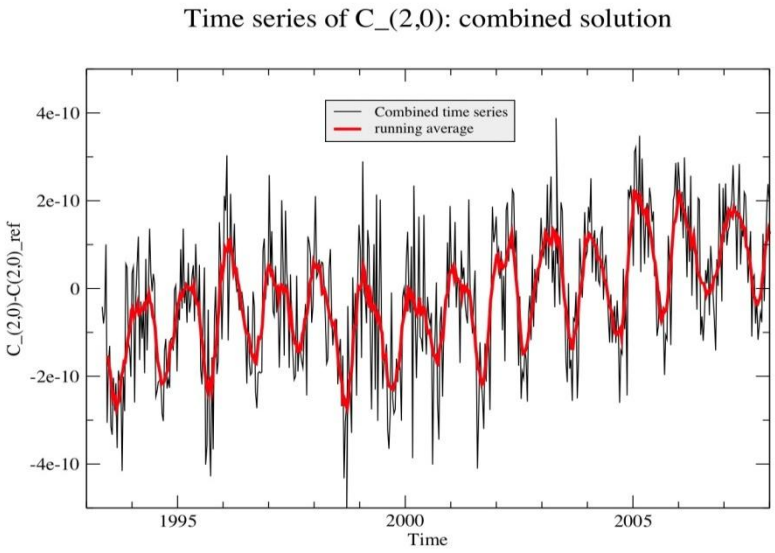

Figure 6. C (2,0) time series

3. Conclusions

Mass variations within the Earth's dynamic system have a temporal spectrum ranging from hours to decades, and even longer. Many of them are related to both long term and short term climate forcing, and many papers showed that the annual variations of the low wavelengths of the gravity field, and the J2 parameter in particular, can be explained by the existing geophysical models of mass redistribution in the atmosphere, ocean, and continental water. Nevertheless, space data can still contribute to constrain some parameters of these geophysical models, and SLR data, because they are available over a very long period of time, have a strong role to play in that context. Geodetic satellite perturbations need to be carefully analyzed, in order to ensure the best accuracy and decorrelation of the low wavelengths of the gravity field, for the even and odd degrees, in particular for LAGEOS-1 because of the specific non gravitational perturbations. A next step of this work should be to provide an optimal weighting of the contribution of each satellite.

References

Chen, J.L., Wilson, C.R., Eanes, R.J., Tapley, B.D., *A new assessment of long-wavelength gravitational variations*, J. Geophys. Res., 105(B7), 16271-16277, 2000

Cheng, M.K., Tapley, B.D., *Variations in the Earth's oblateness during the past 28 years*, J. Geophys. Res., 109(B09402), 2004

Gross, R.S., Lavallée, D.A., Blewitt, G., Clarke, P.J., *Consistency of Earth Rotation, Gravity, and Shape Measurements*, Observing our Changing Earth, IAG Symposia 133, M.G. Sideris eds., 2009

Métris, G., Vokrouhlicky, D., Ries, J.C., Eanes, R.J., *Non gravitational effects and the LAGEOS eccentricity excitations*, J. Geophys. Res., 102(B2), 2711-2729, 1997

Milly, P.C.D., Smakin, A.B., *Global modeling of land water and energy balances. Part I: the Land Dynaics (LaD) model*, J. Hydrometeor, 3(3), pp. 283-299, 2002

Pearlmann, M.R., Degnan, J.J.,, and Bosworth, J.M., *The International Laser Ranging Service*, Adv. In Sp. R., Vol 30, No 2, pp 135-143, 2002

Stammer, D., Wunsch,, C., Fukumori, I., Marshall, J., *State estimation improves prospects for ocean research*, Eos Trans. Amer. Geophys. Union, 83(27), pp. 289-295, 2002

A 33 Year Time History of the Earth Dynamic Oblateness changes from SLR data

Minkang Cheng, Byron D. Tapley
Center for Space Research, University of Texas at Austin, USA
cheng@csr.utexas.edu

Abstract

Satellite Laser Ranging (SLR) data tracked by the ILRS network have recorded the global nature of long-wavelength mass redistribution occurring within the Earth system for more than three decades. The second degree zonal harmonics of the Earth's gravity field, or the J2 coefficient is directly related to the Earth dynamic oblateness, or the dynamic shape factor, which represents how much its rounded shape flattens at the poles and widens at the equator. The variations in J2 are the results of imbalance of the climate induced mass changes between the tropical' area (in the range of the north and south 35 degree latitude) and the extra tropical area. Studying the variations in J2 has provided a clear vision of the large-scale mass redistribution with a long-term signature within the Earth system from analysis of SLR data. Early analysis of 28-year time series of monthly SLR estimates of J2 [Cheng and Tapley, 2004] has indicated that in addition to the secular, 18.6 year tidal and seasonal variations, the J2 has undergone significant interannual variations with time scales of ~4-6 years and a decadal variation with a period of ~21 years. Two large interannual variations are related to the strong El Ninio-Southern Oscillation (ENSO) events during the periods of 1986-1991 and 1996-2002. Recent analysis including an additional five years of data suggests that the Earth has undergone another 3 fluctuations cycles starting from middle of 2002.

Because of the significant aliasing effects in the GRACE data derived J2 coefficient and the J2 variations from SLR data is the most accurate measurement for the application of GRACE product to extract the signal of mass variations in ocean and hydrological. This paper presents detail analysis for the variations in J2 from analysis of multiple geodetic satellites over the period from 1976 to 2008, and a comparison with the monthly solutions from GRACE measurements.

ICESat, GRACE, and Time Varying Gravity: SLR Contributions and Applications

S B Luthcke (1)**, D D Rowlands** (1)**, F G Lemoine** (1)**, H J Zwally** (1)**, S M Klosko** (2)**, D S Chinn** (2)**, J J McCarthy** (2)**, T A Williams** (2)

(1) NASA GSFC, Greenbelt, MD, USA (2) SGT Inc., Greenbelt, MD, USA

Abstract

Temporal changes in the Earth's gravity field have a rich history of study, prediction, measurement, and with today's technologies, monitoring. Over the past 25 years, the need to improve the modeling of these effects within SLR precision orbit determination investigations and in the context of the geophysical interpretations of the results developed from SLR, has progressed significantly and added challenging complexity to SLR pursuits. Laser altimeter missions, like ICESat and DESDynI provide another component for better understanding and monitoring geodynamical systems having topographical manifestations.
The GRACE mission, launched in 2002, has now operated for approximately 6 years, producing monthly and ten-day snapshots of the variations of the gravity field of the Earth. The available solutions either from spherical harmonics or from mascons provide new monitoring capabilities for integrated surface mass flux. Through extensive validation with independent sources, GRACE derived products have been shown to be highly reliable. A wide range of independent sources of derived time gravity variations, when tested in forward modeling approaches for GRACE, have been shown to significantly reduce the variance levels seen in GRACE highly precise KBRR data analyses. This paper will review some of the comparisons which have been made comparing GRACE-derived science products with these independent sources – including ocean tides, atmospheric pressure variations, surface hydrological mass variations, and ice sheet mass changes from ICESat. We will also show the significant improvement obtainable in SLR orbit recoveries if these same forward models are applied.

Introduction

Satellite Laser Ranging was the first satellite tracking technology with sensitivity to gravity field variations ongoing within the Earth's system like tides. Given that SLR alone was able to deliver high measurement precision in the 1970s and 1980s, the study of global-scale mass motion was coupled with many SLR analysis activities with SLR contributing significantly to improving tide models at their longest wavelengths (e.g. Christodoulidis et al, 1988).

SLR analyses over the last two decade, in addition to improving models of the tides and static gravity model, have also allowed time histories of the longest wavelength components of the gravity field to be estimated. These investigations both confirmed and at times confounded geophysical models which predicted these changes (e.g. Cox and Chao, 1998) where for example, the anticipated secular rate of J_2 was observed to have significant deviations. .

Starting in 1980, a major effort was expended to meet the orbit accuracy requirements needed to support the TOPEX/Poseidon (T/P) mission. These investigations were afforded a lead time of more than a decade before the 1992 launch of T/P. A central component of this effort was to improve the time-averaged gravity model while also assessing the sensitivity of the radial component of this orbit to various sources of mass redistribution. As a result of these analyses

and the requirements they defined, accurate tide modeling goals were developed, and long wavelength models improved and tested for orbit applications using SLR. The SLR and DORIS tracking systems were also simultaneously assessed to ensure that their data could support the orbit determination refinements delivered from much more complicated tide models. .

TOPEX/Poseidon was highly successful in delivering radial orbit accuracies which significantly exceeded pre-launch mission goals and ushered in a new era in the remote sensing of the ocean using radar altimetry. Whereas ±14 cm RMS orbits were sought, ±3 cm orbits were delivered. This in turn compelled the orbit determination teams to revisit both the time averaged and time variable gravity models. These investigations resulted in significantly more complex models, especially for ocean and solid earth tides, and improved gravity fields, which when adopted, improved the orbits henceforth. This cycle has been repeated until the present where we are now realizing nearly ±1 cm radial RMS orbits on Jason and reprocessed TOPEX/Poseidon orbits are close to approaching this level of accuracy. The history of these improvements is depicted in Figure 1.

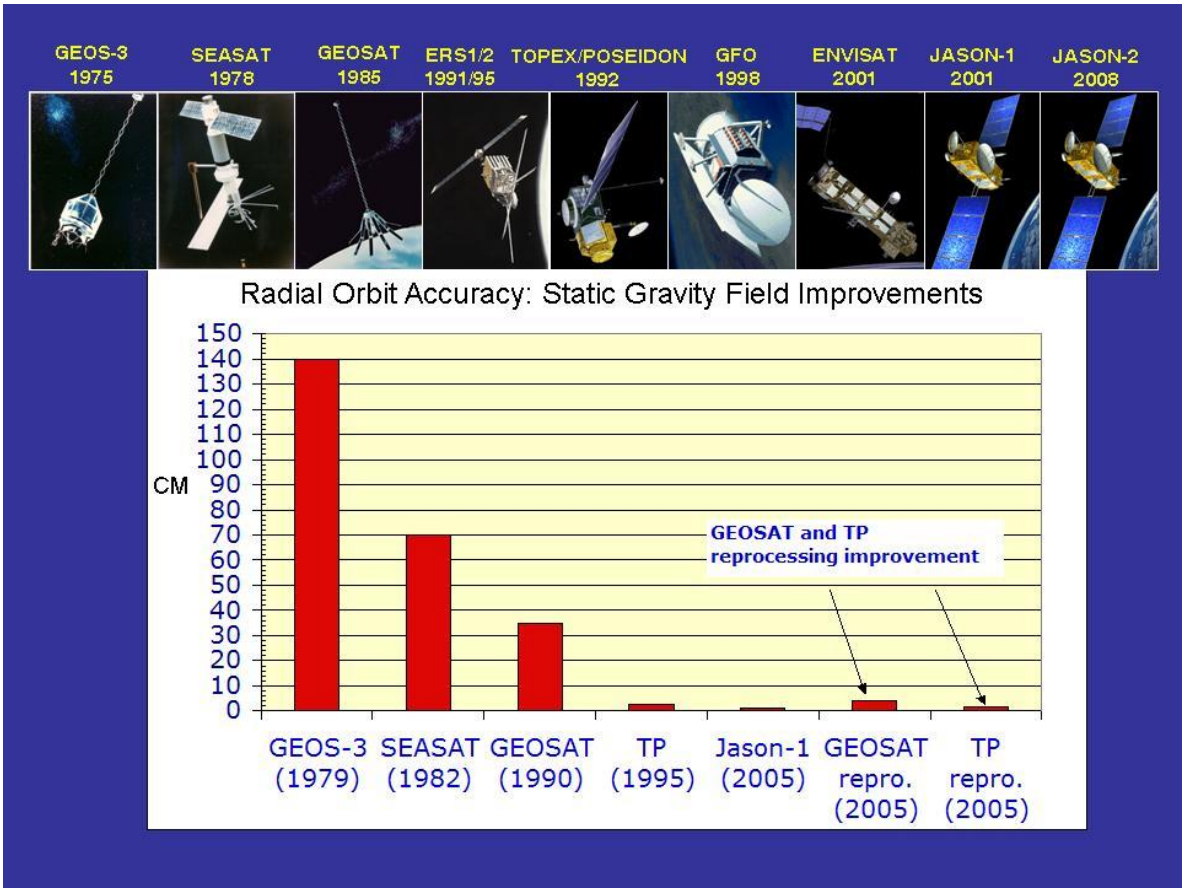

Figure 1. Improved force modeling including large models for tides have yielded a steady improvement in orbit accuracy for altimeter missions.

In parallel, the ability to measure changes in the gravity field with high temporal and spatial resolution has been a major goal for space geodesy missions over the last three decades. Today there are multiple missions that are focused on accurately monitoring mass variations, and using these capabilities to directly measure important manifestations of climate change (GRACE, ICESat, CryoSat, GOCE).

The GRACE Mission stands out given its seven years on orbit continuously acquiring exquisitely accurate intersatellite tracking at the 0.3 micron/sec level, and has driven major advancements in all aspects of monitoring mass motion to isolate signals arising from hydrological and geophysical sources which heretofore could not be measured synoptically. As this paper will show, SLR investigations can benefit from inclusion of a significantly improved time varying gravity time series for precision orbit and reference frame improvements.

GRACE.

The Gravity Recovery and Climate Experiment (GRACE) Mission was designed to monitor local, regional, and global changes in the Earth's gravity field. GRACE is sensitive to changes in the gravity field due to any mass being transported in the Earth's oceans, atmosphere, and on land surfaces within its bandwidth of resolution. Analysis of the data delivered by GRACE yields a direct measure of mass flux with high spatial resolution on the Earth's surface. This is accomplished at one month intervals through the estimation of monthly gravity fields [Tapley et al., 2004]. The spherical harmonic models of the gravity field produced to date from GRACE are at least a two orders of magnitude improvement over any former modeling effort (e.g. Lemoine et al., 1998). This is a result of the special design of the GRACE Mission and its exquisitely accurate measurement of the range-rate between two co-orbiting satellites separated by approximately 250 km using a highly stable K-Band link (KBRR). These data give GRACE unique sensitivity to the accelerations induced on low Earth orbiting satellites from the surface mass along the satellite's ground track

In the analysis of the GRACE data, it has been desirable to forward model time varying gravity signals that are captured in independent and well tested models. The forward models include extensive high degree and order spherical harmonic representations of the solid Earth and ocean tides, global variations in atmospheric surface pressure, and the response of the oceans to atmospheric pressure loading that is non-barothropic. Figure 2 shows a comparison of the atmospheric pressure modeling delivered by two different forecasts. These are large effects clearly sensed by GRACE. To eliminate atmospheric pressure changes through forward modeling, we are now using 3hr global time series in our analyses.

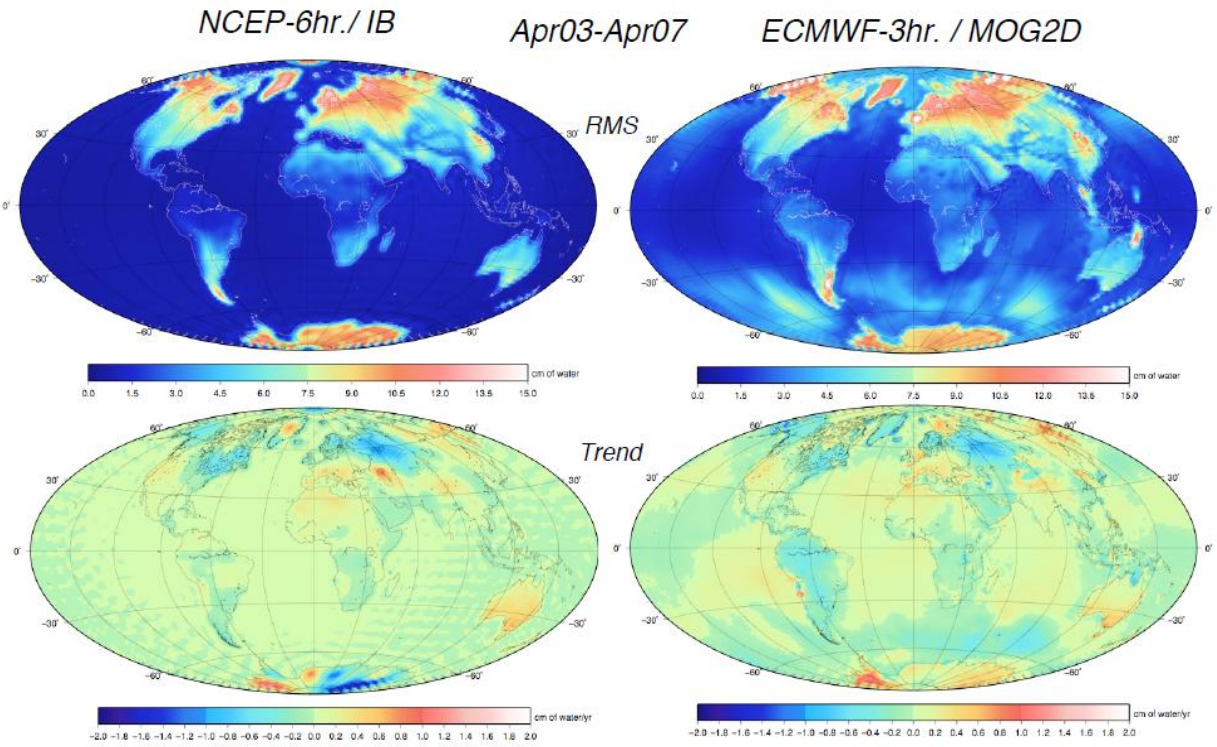

Figure 2. Atmospheric pressure variations are forward modeled in GRACE data reductions. Herein we show the 4 year average variation and secular trend from two independent atmospheric forecasts. Units are surface mass in equivalent cm of water.

With these forward models being applied, the continental hydrological mass flux can be isolated and monitored using GRACE. For example, at GSFC we have made regional solutions for mass flux using a mascon representation (Rowlands, et al, 2005). Shown below (Figure 3) is a ten-day GRACE-recovered time series of the surface mass change over India. Each cell is 4x4 degrees in spatial resolution. Clearly seen is the mass change occurring due to monsoon rains.

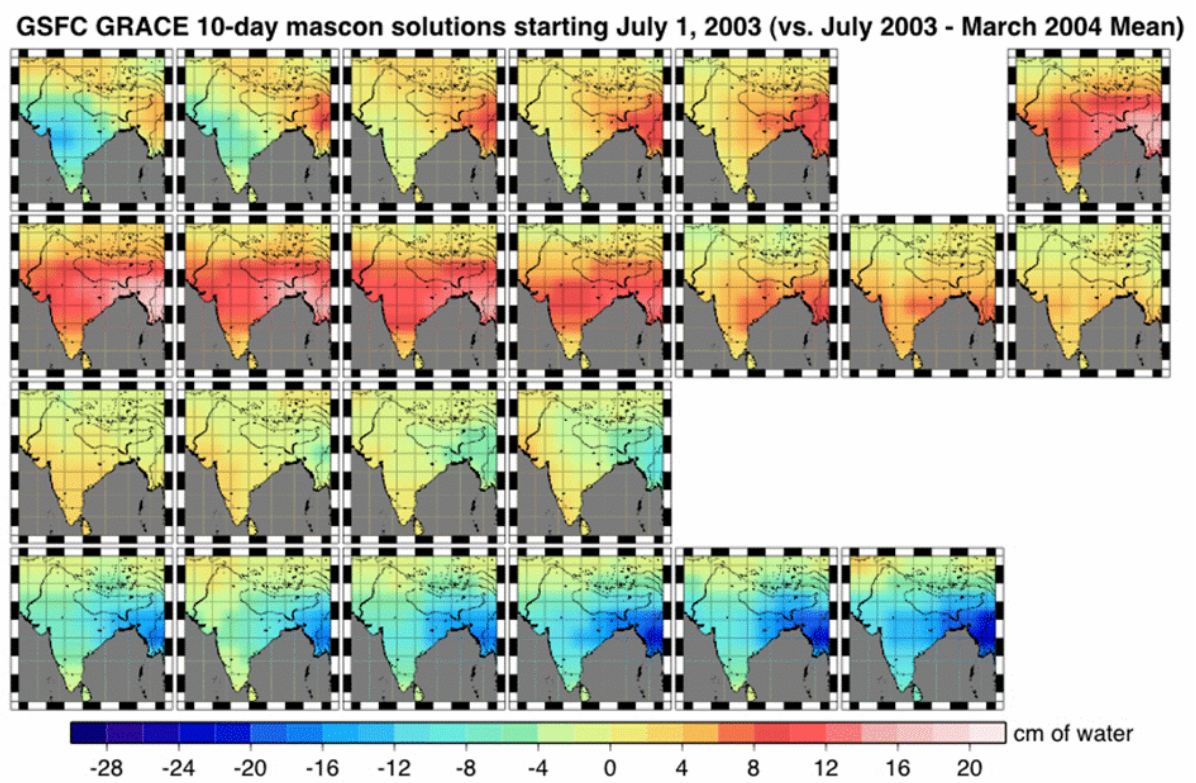

Figure 3. Mascons over the Indian Subcontinent with 400 km spatial resolution and 10-day temporal resolution for 2003-2004. GRACE is capable of observing coherent mass change signal at 400 km spatial and 10-day temporal resolution. Gaps in time series are due to GRACE data outages.

Validation of GRACE Time Series

Before adopting GRACE and the forward models used to support these analyses, it is important to verify GRACE mass flux estimates. The GRACE Science Team has made an extensive effort to verify that the GRACE mass flux estimates are confirmed using independent data sources. Described below are two comparisons performed by our group.

The first study was a comparison of GRACE derived hydrology versus *in situ* data in the Mississippi Basin (Klosko et al, 2009 in press). The Mississippi Basin has accurate surface hydrological modeling available from the Global Land Data Assimilation System (GLDAS, Rodell et al, 2004), which uses advanced land surface modeling and data assimilation techniques. There is also a wealth of groundwater data obtained from a regional well network. This provided an opportunity to quantitatively compare GRACE estimates of the mass flux in the entire hydrological column with those available from independent and reliable sources. The Mississippi Basin is one of the few regions having a large hydrological signal that can support a meaningful GRACE comparison on the spatial scale resolved by GRACE. As noted above, the isolation of the hydrological signal is dependent on the adequacy of the forward mass flux modeling for tides and atmospheric pressure variations. While these models have non-uniform global performance they are excellent over the Mississippi Basin.

As shown in Figure 4, we found that the mass anomalies, as represented by surface layer of water within regional cells have accuracy estimates of ±2-3 cm on par with the best hydrological estimates and consistent with our accuracy estimates for GRACE mass anomaly

estimates. This validation confirmed that GRACE could provide critical environmental data records for a wide range of applications including monitoring ground water mass changes.

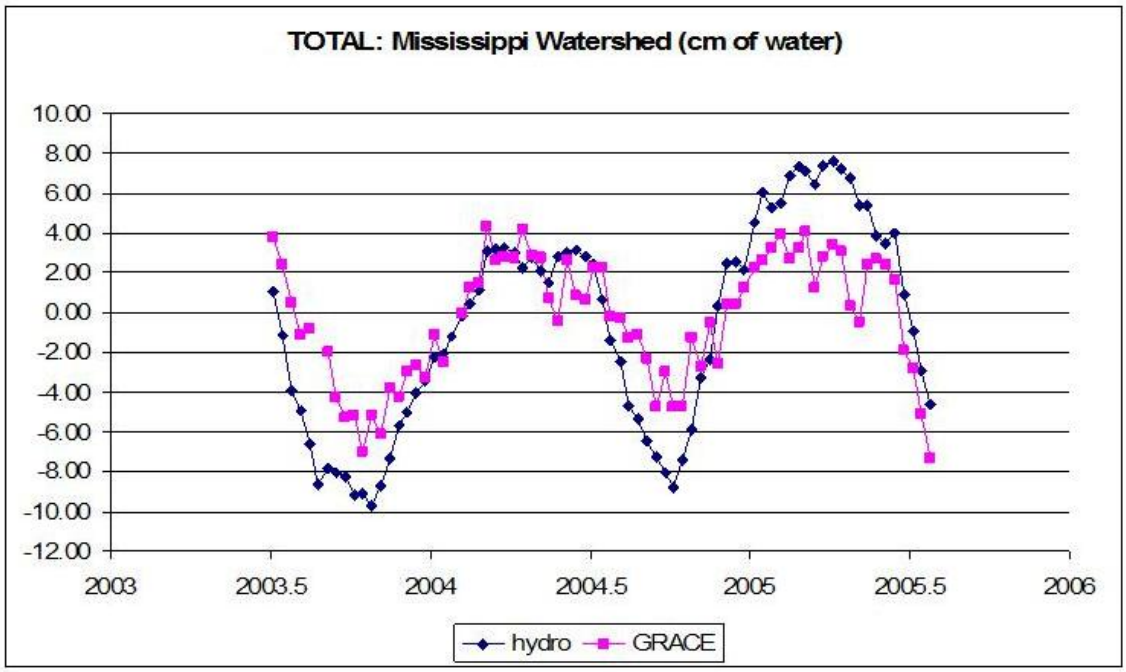

Figure 4. GRACE masons in cm of equivalent water (purple) compared to hydrology (blue) spatially averaged across entire Mississippi watershed. Cross correlation is shown between time series. The RMS agreement between the two time series is 2.9 cm representing the combined error for each independent source.

A second example of our verification activities compares the mass flux occurring over Greenland from two independent sources (Luthcke, private communications) – GRACE, which directly supports estimation of mass changes, and ICESat, which measures changes in the ice surface topography. While the ICESat time series provides distinct measures only twice per year, the GRACE time series is continuous. In order to make this comparison, the density of Greenland's ice was modeled at 0.77 g/cm^3. As shown in Figure 5, there is a remarkable level of agreement of the mass loss occurring over Greenland from these independent systems.

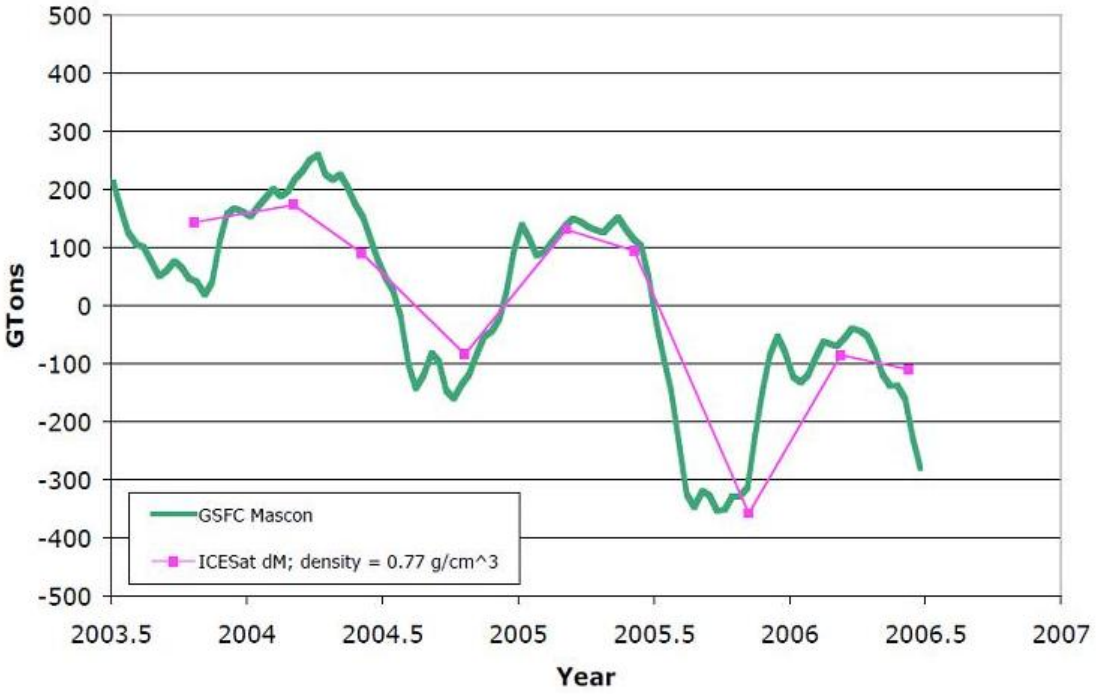

Figure 5. The mass flux over Greenland is estimate using two independent remote sensing systems. GRACE measures the dm/dt whereas ICESat provides a measure of di/dt where m is mass, and i is ice surface height changes. Both systems recover a compatible time series.

SLR Orbit Improvements

Clearly, from the above discussion, one can see that there is a wealth of high fidelity information about the mass flux occurring across the Earth's systems. Furthermore, based on the post solution fit to the GRACE data, we are confident that these series are quite accurate and should not be ignored by other studies requiring precision orbit determination.

As discussed above, one of the most demanding orbit determination applications is found in supporting ocean radar altimeter missions. All orbit errors translate into a corruption of the sea surface heights obtained by these orbiting radars. In Figure 6 we review the mass flux signals and their effect on the orbit of Jason. Clearly, with 1 cm orbits being sought, these are important effects and their neglect results in systematic long wavelength errors in surface height measurements across key ocean basins.

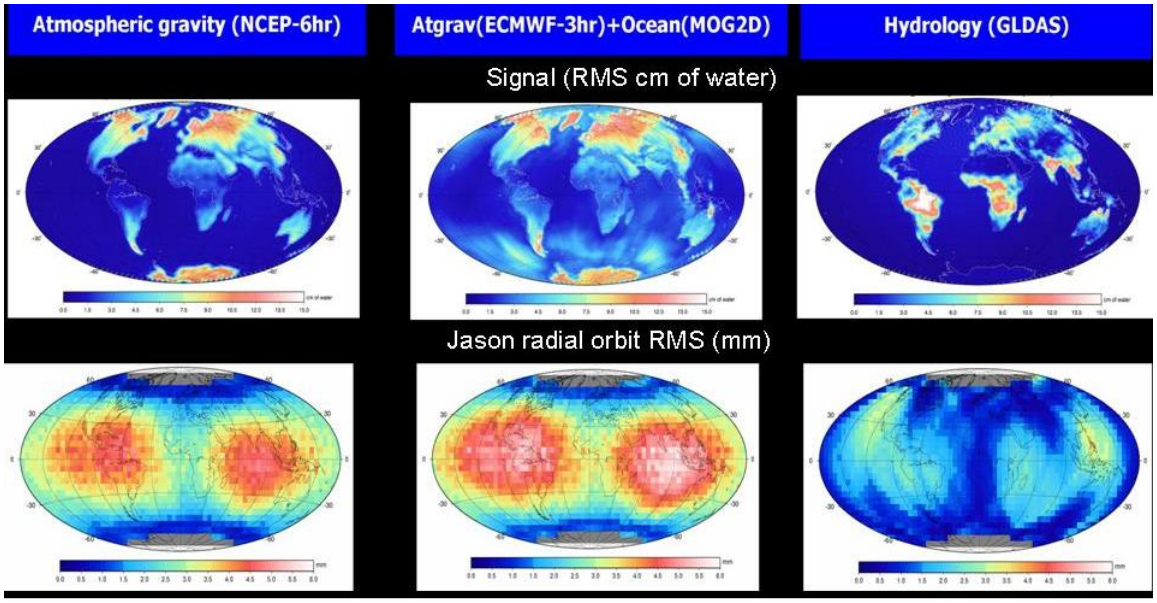

Figure 6. High fidelity mass flux modeling for the well resolved atmospheric pressure, non-barotrophic ocean response to atmospheric loading, and within the continental hydrosphere significantly improves orbit accuracies for altimeter missions. The scale for the top row of figures is mass flux of from 0 to 15 cm of equivalent water; the bottom row is 0 to 6 mm RMS of radial orbit effect (with blue being no change).

In the following tables we provide a direct comparison of these mass flux models on the orbits of Jason and LAGEOS 1 and 2. We provide the RMS of fit to the laser and DORIS tracking data to show that SLR is sensitive to these mass flux sources, and the variance of fit to the data is reduced as these models are employed in orbital solutions.
Table 1 presents the results for Jason.

Table 1. Shown are the RMS of fit to the Jason DORIS, SLR and Altimeter Crossover measurement types tested over 23 cycles when using different time varying gravity models.

Jason Solution	DORIS RMS (mm/s)	SLR RMS (cm)	Alt xover RMS (cm)
No non-tidal time varying gravity (GDR release)	0.4034	1.484	5.579
Atmospheric Gravity using NCEP-6 hr	0.4033	1.444	5.564
ECMWF-3hr + Barotropic Ocean (MOG2d)	0.4033	1.441	5.562
ECMWF- 3hr + Barotropic Ocean (MOG2d) + Hydrology (GLDAS)	0.4033	1.427	5.560

Table 2 presents the results for the LAGEOS 1 and 2 satellites.

Table 2a and 2b. Shown are the RMS of fit to the LAGEOS 1 and 2, SLR measurements tested for all monthly arcs for years 2003 through 2007. Table 2a shows the reduced variance from improved when using different time varying gravity models. Note, annual models complete to degree and order 20 for the mass variations derived from GRACE are inadequate to explain the full hydrological signal.

2(a)

Solution	Description	LAGEOS 1 RMS (cm)	LAGEOS 2 RMS (cm)
Slrtest N (Nominal)	ITRF2005 stations/oloads; GGM02C 10 day empirical corrections	1.6379	1.4782
N_ecmwf6	N + Atmosphere (ECMWF 50x50_6hr)	1.5808	1.4350
N_ecmwf3	N_ecmwf6 + ATGRAV_apr02_jul07_ecmwf_mog2d_boy3hrn9	1.5745	1.4225
N_eigen	N_ecmwf3 + EIGEN GLl04S1	1.5804	1.4197
N_eop	N_EIGEN + improved ocean loading	1.4748	1.3395
N_hydro	N_eop + grvtim_sph_v02_annual20x20_apr03_apr07.osts	1.4372	1.3074
N_opr5day	Slrtest +_hydro + 5 day empirical corrections	1.1452	1.1465

2(b)

Solution	Lageos 1 RMS (cm)	Lageos 2 RMS (cm)
Slrtest N (Nominal)	-	-
N_ecmwf6	0.43	0.35
N_ecmwf3	0.45	0.40
N_eigen	0.43	0.41
N_eop	0.71	0.63
N_hydro	0.79	0.69
N_opr5day	1.17	0.93

From both set of tests it is clear that significantly improved orbits and fits to SLR data are obtained with more complete force modeling. It is therefore recommended that the standards adopted for orbit analyses when producing solutions for the ITRF or for altimeter mission support be augmented to include the complete suite of now available time varying gravity models.

Summary

This paper has shown comparisons which have been made comparing GRACE-derived science products with these independent sources – including ocean tides, atmospheric pressure variations, surface hydrological mass variations, and ice sheet mass changes from ICESat. We then show that there is significant improvement obtainable in SLR orbit recoveries if these same models are applied.

References

Christodoulidis, D., D.E. Smith, R.G. Williamson, S.M. Klosko, "Observed tidal braking in the Earth/Moon/Sun System", **J. Geophys. Res.**, 93, B6, 6216-6236, 1988.

Cox, C. M., and B. F. Chao, Detection of a large-scale mass redistribution in the terrestrial system since 1998, **Science**, 297, 831– 833, 1998.

Lemoine, et al. (1998), The Development of the Joint NASA GSFC and National Imagery and Mapping Agency (NIMA) Geopotential Model EGM96, NASA/TP-1998-206861, NASA Goddard Space Flight Center, 1998.

Luthcke, S.B., H.J. Zwally, W. Abdalati, D.D. Rowlands, R.D. Ray, R.S. Nerem, F.G. Lemoine, J.J. McCarthy and D.S. Chinn Recent Greenland Ice Mass Loss by Drainage System from Satellite Gravity Observations. **Science** 314(1286), 1286-1289, 2006a.

Luthcke, S.B., D.D. Rowlands, F.G. Lemoine, S.M. Klosko, D. Chinn and J.J. McCarthy Monthly spherical harmonic gravity field solutions determined from GRACE inter-satellite range-rate data alone. **Geophysical Research Letters**, 33, L02402, doi:10.1029/2005GL024846, 2006b.

Rodell, M., et al., "The global land data assimilation system", **Bull. Am. Meteorol. Soc**., 85 (3), 381-394, 2004.

Rowlands, D.D., S.B. Luthcke, S.M. Klosko, F.G. Lemoine, D.S. Chinn, J.J. McCarthy, C.M. Cox and O.B. Anderson) Resolving mass flux at high spatial and temporal resolution using GRACE intersatellite measurements. **Geophysical Research Letters**, 32, L04310, doi:10.1029/2004GL021908, 2005.

Tapley, B.D., S. Bettadpur, M. Watkins, and C. Reigber (2004a), The gravity recovery and climate experiment: Mission overview and early results, **Geophys. Res. Lett**., 31, L09607, doi:10.1029/2004GL019920, 2004.

Use of SLR observations to improve GIOVE-B orbit and clock determination

I. Hidalgo, A. Mozo, P. Navarro, R. Piriz (1)**, D. Navarro-Reyes** (2)

(1) GMV, Madrid, Spain
(2) ESA - ESTEC, Noordwijk, Netherlands

pfnavarro@gmv.com, Daniel.Navarro-Reyes@esa.int

Abstract

GIOVE-A and GIOVE-B (Galileo In Orbit Validation Elements) are experimental satellites that have been launched by ESA in order to verify some of the critical technologies of the future Galileo system, such as on-board atomic clocks and the generation of the navigation signal, in addition to characterizing the processing of the Galileo signal by user receivers, all in the frame of the GIOVE Mission.

As a primary tool in the experimentation activities, the GIOVE Mission E-OSPF software (Experimental Orbitography and Synchronization Processing Facility) receives the navigation observations gathered by a network of dual GPS/Galileo receivers and estimates the orbit and clock offsets of the GPS and GIOVE satellites. The inclusion of GPS satellites is necessary to achieve the required level of redundancy in the clock estimation. The clock offsets are obtained every 5 *minutes, and their time series is essential to characterize the behavior of the on-board atomic clocks, both the RAFS (Rubidium Atomic Frequency Standard) and the Passive Hydrogen Maser clock (PHM) of GIOVE-B, the most stable clock ever flown in space.*

The main problem in the determination of the offsets of the on-board clocks is that the radial error in orbits and the clock offsets are highly correlated, so that it is difficult to disentangle them. A good way of overcoming this effect is to have a complementary means to compute the estimated orbits, such as SLR measurements. The GIOVE satellites are equipped with laser reflectors, and dedicated campaigns of laser tracking are being carried by ILRS in coordination with ESA. The E-OSPF is able to process SLR observations together with the navigation ones. In this way, the orbit determination can be improved and decorrelated from the clock estimation.

This paper describes the process of orbit and clock determination from the navigation signal, and how the SLR measurements can be added to have better orbits and a better observability of the on-board clocks. It presents the results of the experimentation carried to characterize the behavior of the GIOVE-B PHM, with the help of SLR measurements, and to assess the improvement obtained by using them.

Introduction

In preparation for the deployment of the Galileo System, the European Space Agency (ESA) initiated in the late 90ies the development and industrialization of two on-board clock technologies: Rubidium Atomic Frequency Standard (RAFS) and Passive Hydrogen Maser (PHM). In 2004, both technologies successfully passed ground environmental qualification tests (including vibration, shock, radiation, etc). In 2005, 6 RAFS and 2 PHM flight models

were delivered for first in-orbit validation.

In parallel, ESA began development in 2002 of an experimental Ground Mission Segment, called Galileo System Test Bed Version 1. Within the GSTB-Vl project, tests of Galileo orbit determination, integrity and time synchronization algorithms were conducted in order to generate navigation and integrity core products based on GPS data.

In 2003 the second step of the overall Galileo System Test Bed (GSTB-V2) implementation began with the development of two Galileo In-Orbit Validation Element (GIOVE) satellites: GIOVE-A (launched on 28th December 2005) and GIOVE-B (launched on 27th April 2008). In order to mitigate programmatic and technical risks of the Galileo IOV phase the main objectives of the GSTB-V2 or GIOVE Mission are:

- Secure the use of the frequencies allocated by the International Telecommunications Union (ITU) for the Galileo System
- Validate Signal In Space performance in representative environment (RFI and multi-path) conditions
- Characterize the On-Board Clock (RAFS and PHM) technology in space
- Characterize the Radiation Environment for the Galileo Medium Earth Orbit (MEO)
- Collect lessons learned on Ground Mission Segment development, deployment and validation especially as far as Galileo Sensor Station are concerned
- Collect lessons learned on Space Segment on-board units pre-development and in-orbit operations
- Early demonstration and performance assessment of the navigation service (including navigation message uplink and broadcast)
- Validation of ground algorithm prototypes (evolved from GSTB-Vl) and testing of new ones
- Overall testing of timeliness and operational aspects (including data collection from GESS, data processing, message generation and uplink)

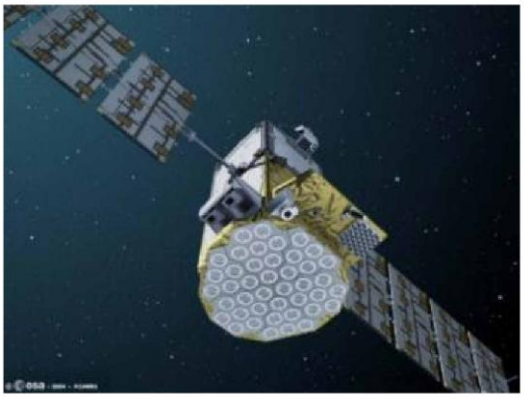

Figure 1. Artist's view of GIOVE-B satellite

The overall GIOVE system architecture with the necessary components to achieve the above mentioned objectives are as listed here:

- The space segment is composed of GIOVE-A and GIOVE-B satellites
- The Ground Control Segment is composed of both GIOVE Ground Control Centers (GSC), in Guildford for GIOVE-A and in Fucino for GIOVE-B
- The GIOVE Mission Segment infrastructure

The present paper focuses in one of the aforementioned objectives of the GIOVE mission: the characterization of the PHM clock of GIOVE-B. From the user point of view, the stability of the on-board clocks is essential, since the computation of the navigation solution is partly based on the prediction of the satellite clock offsets. An unstable clock cannot be accurately predicted, and leads to a degradation of the user performances. On the other hand, the PHM clock onboard GIOVE-B sets a new standard of stability on a satellite, which has to be assessed as part of the GIOVE Mission activities.
The analysis of the satellite clock behavior is based on the determination of the clock offsets with respect to a very stable reference, obtained by processing the microwave measurements gathered from a network of stations. As will be explained in more detail below, the precise estimation of these offsets is hindered by the strong correlation between orbit and clock errors. The use of SLR measurements, that are only dependent on the orbit of the satellite, is expected to help separating both components, and hence improving the accuracy of the clock offsets estimation.

The GIOVE Mission Segment

The GIOVE Mission Segment provides all the necessary facilities and tools for the requested experimentations, covering the data acquisition (from external providers such as IGS [Dow 2005], IERS, BIPM and ILRS [Pearlman 2002]) and archiving, the operations of the major processing facilities and the management and wide dispatching of the results to internal and external users. The GIOVE Mission Segment includes:

- GIOVE Processing Center (GPC) located in ESTEC (Noordwijk, The Netherlands), composed of the Data Server Facility (DSF), the interface with the GIOVE-A and -B Ground Control Centers (GPCI) and the Experimental Orbit & Synchronization Processing Facility (E-OSPF)
- A word-wide network of 13 Galileo Experimental Sensor Stations (GESS), each of which operates a GIOVE/GPS dual receiver connected to an atomic clock, and a Communication Network

A key element of the GPC is the Experimental Orbit Determination and Time Synchronisation Processing Facility (E-OSPF). This element processes pseudo-range and carrier phase measurements collected from the GESSs in order to provide GIOVE orbit and clock estimations and predictions and generate the experimental navigation message to be broadcast by the satellite. The E-OSPF features sophisticated Orbit Determination and Time Synchronisation algorithms, similar to the algorithms that will compute the Galileo navigation message in the operational system. Since these algorithms are based on the processing of data from several satellites and stations simultaneously, complementary GPS data have to be used. This brings some difficulties (such as the need for dual GIOVE/GPS receivers and the existence of so-called Inter-System Biases - ISBs -) that have to be tackled.

The GIOVE orbit and clock estimations and predictions generated by the E-OSPF are input to a number of operational and experimental activities, such as:

- Generation of experimental GIOVE navigation messages in a routine basis
- Assessment of navigation performances
- Characterization of the on-board clock performances

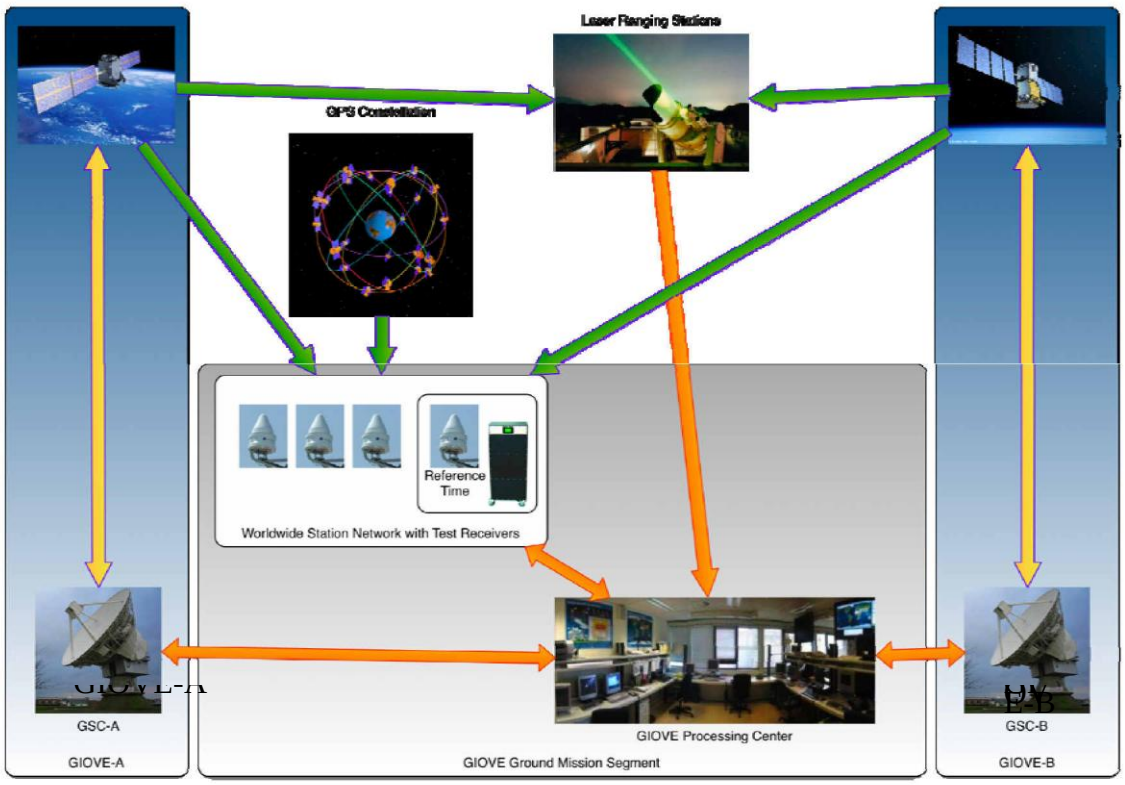

Figure 2. Overview of GIOVE Mission Architecture

Experimentation Setup

The GIOVE signal in space is continuously acquired by the GESS network, together with the GPS signals. The DSF acquires periodically the data files and converts them to standard RINEX 3.00 format. In addition, the GIOVE flight dynamics data and the telemetry and telecommand processed by the GSC-A and -B are also archived in the Data Server, through the GPCI. Finally, GIOVE laser ranging data collected from the International Laser Ranging Service (ILRS, [Pearlman 2002]) are also retrieved and stored. These data are the basis for the routine generation of experimental GIOVE navigation messages at the GPC, as well as for the off-line experimentation process.

The time span covered in this experimentation ranges from 29th August to 8th September 2008. The satellites processed were 25 GPS plus the GIOVE-B. During this period, GIOVE-B used the PHM clock for the signal generation. Unfortunately, the experimentation period could not be extended to the end of September, as initially foreseen.

The sensor station network of the GSTBV2 includes 13 GESS stations distributed as

the following map and table show:

Table 1. GSTB-v2 GESS list

Site Code	Site Name	Country
GIEN	INRiM, Turin	Italy
GKIR	Kiruna	Sweeden
GKOU	Kourou	French Guyana
GLPG	La Plata	Argentina
GMAL	Malindi	Kenya
GMIZ	Mizusawa	Japan
GNNO	New Norcia	Australia
GOUS	Dunedin	New Zealand
GTHT	Tahiti	French Polynesia
GUSN	USNO, Washington	USA
GVES	Vesleskarvet	Antarctica
GWUH	Wuhan	China

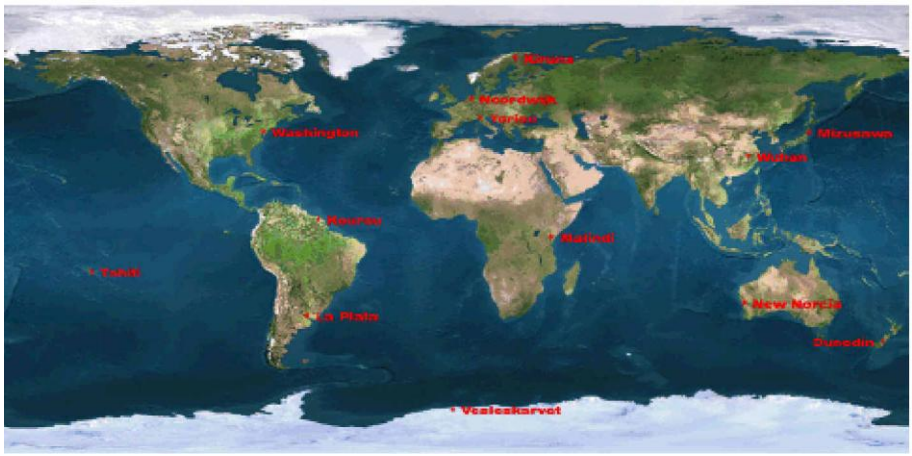

Figure 3. GSTB-v2 GSS network distribution

The SLR stations that have been employed in the experimentation are the following:

Table 2. GSTB-v2 SLR stations list

Site Code	Site Name	Num. Obs.
7237	Changchun	15
7839	Graz	50
7105	Greenbelt	20
7840	Herstmonceux	16
7308	Koganei	5
7110	Monument Peak	5
7825	Mount Stromlo	6
7406	San Juan	41
8834	Wetzell	4
7090	Yagardee	32
7810	Zimmerwald	34

Note that the number of available SLR measurements is low, so that they cannot be expected to have a big impact in the performances.

The microwave channels processed are listed in the table below:

Table 3. Processed microwave channels

	Frequency Band	Frequency (Mhz)	Code	Phase
GPS	L1	1575.42	P1	L1
	L2	1227.60	P2	L2
GIOVE-B	L1	1575.42	C1C	L1C
	E5b	1207.140	C7Q	L7Q

ODTS Processing Overview

The orbit and clock determination is mainly based on the microwave measurements from the GESS network. Since they involve the positions and the clock offsets of the satellites, both orbits and clocks have to be estimated in the same process. The estimation algorithm (ODTS: Orbit Determination and Time Synchronisation) is a batch least-squares algorithm that is able to process microwave and SLR measurements. The code measurements, coming at l-second rate from the tracking stations, are smoothed with the phase observations using a Hatch filter. The ODTS process solves for orbits (dynamics parameters, i.e. parameters of a high-accuracy orbit model), clocks, troposphere, and the so-called station inter-system bias (ISB), following a dedicated strategy in order to deal with different effects (ionosphere, troposphere, relativity, phase center offsets, phase wind-up, tides, site displacements, ocean-atmosphere loading, etc).

Unlike SLR, the use of microwave measurements requires a good number of satellites and stations to be processed simultaneously, to attain a reasonable level of accuracy. It does not make sense to configure one or two GIOVE satellites alone in ODTS. A sound approach is to include the GPS satellites in ODTS, although this will make necessary to estimate an intersystem bias per receiver, as explained below. On the receiver side, the results will be better if the GESS network is enlarged, but at the time of the experimentation there were only thirteen stations available.

The E-OSPF implements a version of the ODTS algorithm. But for the current experimentation, the tool magicODTS (GMV) has been used, that provides additional features as the capability of fixing orbits and clock of certain satellites to the values taken from input files (like IGS products). Nevertheless, it has been checked that for the conventional mode, both tools provide similar results.

The experimentation is carried out by executing consecutive and overlapping ODTS arcs. The length of the arcs has been chosen to be 2 and 3 days, with 1 day of overlapping. Longer arcs have not been considered, since for the short period of data available, there were to few overlaps for the analysis.

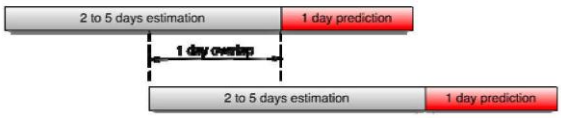

Figure 4. ODTS Overlapping Arcs

While the GPS satellites solutions can be compared with the IGS reference, there is no direct way to assess the quality of the GIOVE orbit and clock estimations. However, a good indicator is the differences in the overlap of successive ODTS estimation arcs.
Additionally, when the clock estimation errors dominate over the clock instability, an improvement in the solutions should carry a better fit to a quadratic model. So, a useful metric is the RMS of the residuals of the quadratic fit.

In summary, the following metrics are used in the analysis of the results:

- Comparison of orbits and clocks from consecutive arcs in the overlapping period
- Comparison of GPS estimated orbits and clocks with those computed by the International GNSS service (IGS)
- Analysis of the residuals of the clock estimation to a quadratic fit.
- Analysis of SLR residuals

The whole experimentation set-up is depicted in the figure below:

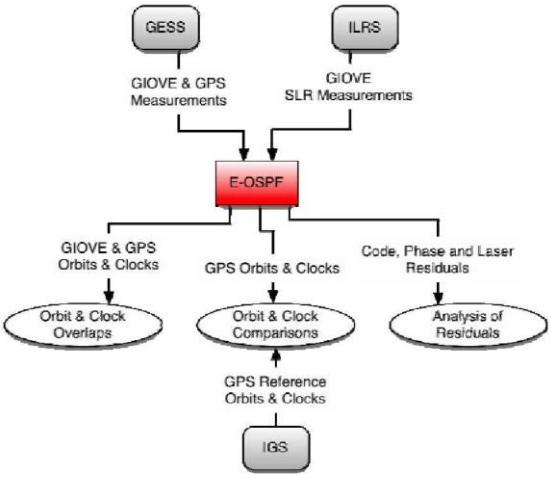

Figure 5. ODTS Experimentation Setup

Clock bias estimation

The microwave measurements are sampled at fixed intervals (every 5 minutes). At each such epoch, a clock bias is estimated for all the satellite and receiver clocks. However, the measurements do not provide enough information to fix a global reference for the clock estimation, the associated system of equations being degenerate. The solution adopted is to use the clock of a GSS as reference, constraining its bias to zero. So, what is finally estimated is the clock difference of all stations and satellites with respect to this reference clock. The reference clock for the GIOVE experimentation is a free-running Active Hydrogen Maser (AHM) connected to the GIEN station, a GESS at the Italian national metrological laboratory

(INRiM) in Turin. All clocks in the GIOVE segment are synchronized to the INRiM master clock. The AHM output signal, both 10 MHz and 1 Pulse Per Second (PPS), is fed to the GIEN station as an external reference time scale. The clock is continuously monitored versus the ensemble of atomic clocks of INRiM and also compared versus external reference time scales as the Universal Coordinated Time (UTC) realized by the BIPM.

The clock estimated by ODTS is not the 'true' clock connected to the satellite or the receiver, but an 'apparent clock' that is the sum of the clock signal plus some hardware delays of the satellite/receiver due to different effects (clock connection to the signal generator on board of the satellite, path from the signal generator to the transmitting antenna array, cable from the antenna to the receiver, etc). These delays are not the same for code and phase observations, or for different frequencies or satellites, but can be safely ignored as far as:

- The biases are stable (close to a constant value during ODTS estimation intervals).
- At each receiver, the delays introduced for different satellites are similar, with negligible differences.

If the latter is not true, an inter-satellite bias has to be estimated for each receiver-satellite link, as is the case when GLONASS satellites are configured. However, the dual receivers of the GESS have similar delays for satellites of the same constellation (GPS or GIOVE), so it is enough to estimate the bias between GPS and GIOVE satellite clocks. This parameter is called inter-system bias, and is typically estimated at constant by intervals (24 hours long, or the whole estimation arc). Even if the code and phase hardware delays are not the same, there is no need to estimate an inter-system bias parameter for the phase measurements, since the ambiguity parameters can absorb the constant difference. As in the clock estimation, all the inter-system bias values obtained in ODTS are relative to the master GSS.

The above scheme works in a proper way if the hardware delays are very stable and remain approximately constant in the term of several hours. Nevertheless, if this assumption is not fulfilled, there will be a negative impact in the performances. Since the GIOVE-B is the only GIOVE satellite processed, ODTS will tend to set the clock biases to the values that best suit the GPS satellites, while the GIOVE-B residuals will tend to absorb most of the modeling error. Hence, the errors derived from the instability of the inter-system bias will mainly affect the GIOVE-B satellite estimations.

The satellite clock estimation is better when more ground stations are tracking the satellite. The number of stations in view from a satellite, when the satellite is flying over a particular area, is called. Depth-of-Coverage (DOC). At least a DOC-2 is required to have a minimum quality in the estimation but it is better to have higher values. The following picture shows the geographical coverage provided by the 13-GESS network.

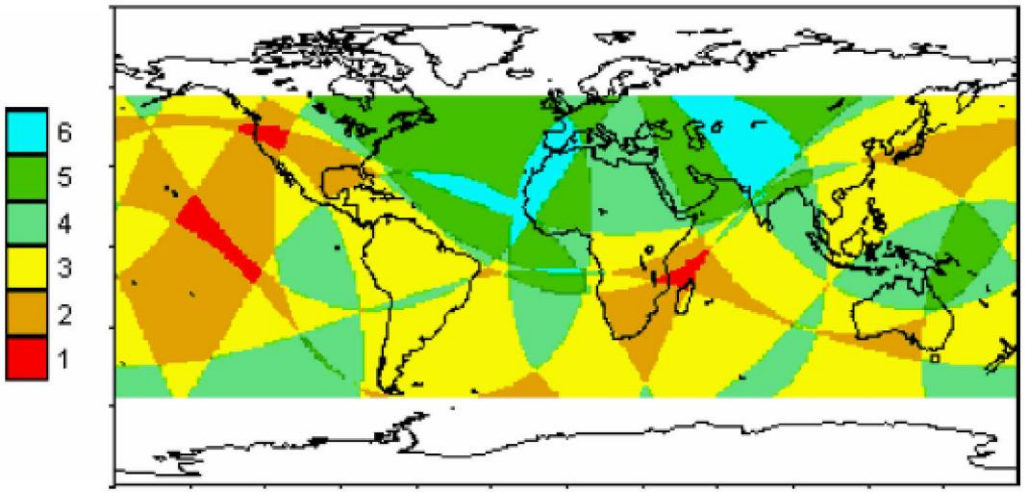

Figure 6. DOC provided by the GSTB-v2 GSS network

One of the difficulties in the current scenario is the reduced GESS network, which provides a poor DOC coverage.

Use of IGS solutions

In order to improve the results, the ODTS process can be forced to use the orbit and clock estimations provided by IGS for the GPS satellites. Meanwhile, the GIOVE solutions and the station clocks, tropospheric zenith delay and Inter-system biases are still estimated. This improves the quality of the station and GIOVE satellites parameters estimation, and hence of the GIOVE-B clock determination. Note that the 25 GPS satellites weight much more than a single GIOVE satellite in the receivers clock and troposphere estimations. Hence, the results based on this technique are similar to those obtained by fixing these parameters to the solution obtained from the GPS IGS products only, and later using them to process the GIOVE satellite.

Use of SLR measurements

The use of thirteen stations and thousands of microwave measurements does not necessarily give very accurate solutions, in contrast with SLR processing, where a smaller number of observations is required. Two reasons for this fact are:

- the need to estimate a large amount of clock parameters at each observation epoch.
- the high correlation between the radial part of the orbital error and the clock error.

To illustrate the second point, the figure below shows an overlap difference of two orbit and clock solutions of satellite GIOVE-B, where in particular the (radial+clock) and (radial-clock) error components are depicted. The observation of the satellites from the ground stations privileges the radial direction over the transversal ones (along-track, cross-track), but the radial component is highly correlated with the clock, so that:

- the (radial+clock) combination is well observed, since it is the essential contribution to the observations;
- the (radial-clock) is not well determined, and this is the main source of the radial and clock errors, where it appears with opposite sign. So, any technique used to improve the clock determination has to reduce this component, either directly or indirectly.

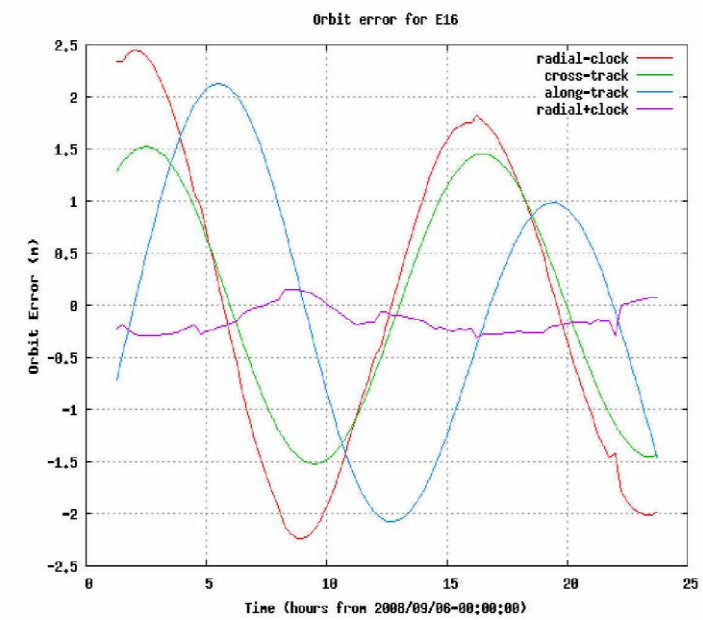

Figure 7. Overlap difference of two consecutive GIOVE-B estimations

On the other hand, the SLR measurements are independent of the satellite clock, so they can improve the accuracy of the satellite orbit alone. But a better determination of the orbit in the radial direction will imply an improvement in the determination of the (radial-clock) component, and hence in the clock estimation.

GIOVE-B Orbit and Clock Determination Results

As a first step, the scenarios have been run including SLR measurements with a negligible weight. Then the solution are based in the microwave signals only, but ODTS computes the SLR residuals.
The following tables summarize the results obtained by running arcs 2 and 3 days long. The performance metrics are obtained either by comparing the estimation of GPS orbits and clocks with the IGS final products, or by comparing the results of two consecutive ODTS runs in the 1-day overlapping period. The final value is the RMS of the orbit or clock differences (in the case of the orbits, the typical RMS).

Table 4. Orbits and clocks results for 2 days arcs

	GPS satellites	GIOVE-B
Estimated GPS Solutions		
Orbit error wrt IGS (2 days RMS)	10.1cm	--
Clock error wrt IGS (2 days RMS)	0.60ns	--
Orbit overlap (1 day RMS)	10.2cm	14.5cm
Clock overlap (1 day RMS)	0.25ns	0.56ns
GPS fixed to IGS solutions		
Orbit overlap (1 day RMS)	--	14.6cm
Clock overlap (1 day RMS)	--	0.46ns

Table 5. Orbits and clocks results for 2 days arcs

	GPS satellites	GIOVE-B
Estimated GPS Solutions		
Orbit error wrt IGS (3 days RMS)	10.6cm	--
Clock error wrt IGS (3 days RMS)	0.61ns	--
Orbit overlap (1 day RMS)	14.3cm	10.1cm
Clock overlap (1 day RMS)	0.29ns	0.40ns
GPS fixed to IGS solutions		
Orbit overlap (1 day RMS)	--	8.8cm
Clock overlap (1 day RMS)	--	0.38ns

The most relevant conclusions are:

- The orbit overlaps for GIOVE-B give results of the same order as the GPS satellites. However, the GIOVE clock overlaps are worse, due to variations in the estimations of the inter-system bias.
- The use of estimation arcs of 3 days lead to better results for the GIOVE-B satellite, while the GPS results are very similar in both configurations. This is probably related to the inter-system bias, which is more consistently estimated in longer arcs.
- The overlap results for clocks are better for GPS than the comparison with IGS. This is because the differences with IGS show average offsets that are cancelled out in the overlaps. As these constant offsets do not affect the clock stability analysis, they can be neglected, and the clock overlap RMS taken as a valid indicator.
- The use of IGS solutions for the GPS satellites brings a small improvement.

The next step has been to run the scenarios again, but assigning a proper weight to the SLR measurements. The scenarios with the GPS solutions fixed to IGS as reference, has been chosen as a reference for the comparison. The following tables present the values of several performance metrics with and without the use of SLR measurements:

Table 6. SLR values for 2 days arcs

	Without SLR	With SLR
Orbit overlap (RMS)	14.5cm	12.6cm
Clock overlap (RMS)	0.46ns	0.39ns
(Radial – clock) overlap (std)	12.1cm	10.1cm
GIOVE-B clock fit residuals (RMS)	0.29ns	0.21ns

Table 7. Metrics values for 3 days arcs

	Without SLR	With SLR
Orbit overlap (RMS)	8.8cm	8.6cm
Clock overlap (RMS)	0.38ns	0.38ns
(Radial – clock) overlap (std)	8.5cm	8.0cm
GIOVE-B clock fit residuals (RMS)	0.26ns	0.23ns

As a main conclusion, the use of SLR measurements brings an improvement in the case of estimation arcs of 2 days, but not in the longer 3 days scenarios. This is not unexpected, since the microwave-only performance is clearly better in the latter case, and the SLR contribution is possibly not enough to make a difference.
It must be stressed that during the period analyzed, only 228 SLR measurements were available, which are too few. This is due to the small size of the GIOVE-B LRA. A larger number would be required to have a significant effect in the results. But the previous analysis shows a promising tendency that could be used in the future to better assess the quality of the GIOVE/Galileo on board clocks, if the appropriate SLR campaigns are performed.

Finally, as an example, the orbit and clock differences in the overlap period for two typical arcs with SLR is shown in Figure 8.

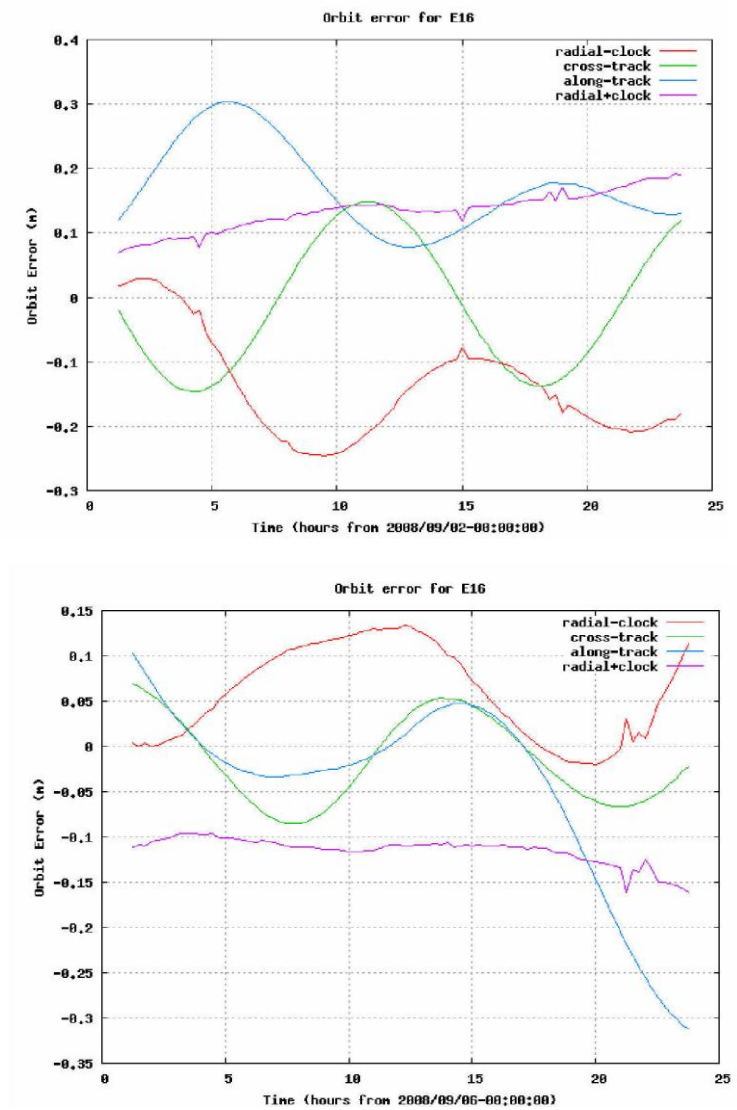

Figure 8. GIOVE-B Orbit and Clock Overlaps Examples

SLR Measurement Residuals

Table 8 shows the statistics of SLR residuals in the ODTS arcs, in the 3 days long scenarios. As expected, the results are better when the SLR observations contribute to the solution, although it is remarkable that the improvement is so evident with so few SLR measurements available. As SLR gives clock-free observations completely independent from the navigation signal, these residuals provide a good indication of the orbit performances: around 10cm in the radial direction, which is in line with the observed internal orbit consistency.

Table 8. SLR two-way residuals

	Microwave only	Microwave + SLR
3 days /est GPS	16cm	12cm
3 days / fix GPS	18cm	14cm

Conclusions

The on-board Passive Hydrogen Maser clock of GIOVE-B represents an important step in the testing of the new technologies that will be integrated in Galileo. The assessment of the stability of the clock is done from the products of an orbit and clock determination process, based on the measurements gathered by the GESS network that is part of the GIOVE Mission. Due the expected level of performance of the PHM, the accuracy of the clock determination has to be as high as possible, in spite of the limited size of the GESS network. A way of improving the quality of the estimations is to use the SLR measurements as a complementary mean to fix the GIOVE satellite orbits and help disentangling orbits and clock solutions.

Several SLR stations from the ILRS are tracking the GIOVE satellites. For the present paper, experimentation has been carried out by processing microwave together with SLR measurements, to confirm the viability of using laser ranging to improve the accuracy of the GIOVE-B clock estimations. The main conclusions are:

- Microwave and SLR observations show a good consistency between them, thus confirming the very good performance of the orbit and clock determination performed in the GIOVE Mission.
- For GIOVE-B, the use of arcs of 3 days has shown a clear improvement over two-day arcs.
- There is a clear improvement in the results when using SLR together with the microwave measurements, for the 2 days scenarios, even if there are very few SLR observations available. For longer arcs (3 days), the improvement is smaller.
- Due to small size of the GIOVE-B LRA, the number of SLR measurement is limited. The improvements could be much more significant if the number of SLR measurements per day were higher.

The processing of longer periods of data should give more conclusive results.

References

J.M. Dow, R.E. Neilan and G. Gendt: *The International GPS Service (IGS): Celebrating the 10th Anniversary and Looking to the Next Decade,* Adv. Space Res. 36 vol. 36, no. 3,

pp. 320-326,2005. DOl: 10-1 06/J.ASR.2005.05.125

M.R. Pearlman, J.J. Degnan and J.M. Bosworth: *The International Laser Ranging Service,* Advances in Space Research, Vol. 30, No.2, pp. 135-143, July 2002, DOl: 10.1016/S0273-1177(02)00277-6

Orbit Determination of LRO at the Moon

David E. Smith, Maria T. Zuber, Frank G. Lemoine, Mark H. Torrence, Erwan Mazarico
NASA-GSFC, USA
Mark.H.Torrence@nasa.gov

Abstract

The orbit determination of LRO is particularly important because the mission is designed to select landing sites for future robotic and human landings. For these purposes the program needs an accurate geodetic model of the Moon that provides the best knowledge of the positions of features on the surface, including the far side, and the gravity field to enable spacecraft to return to, or visit, a particular location. LRO is expected to provide this information. The baseline tracking system for LRO is S-band with Doppler accuracy of ~1 mm/s for approx. 20 hours per day but this will not be accurate enough for the LRO requirements which are estimated to be ±50m or better in along track position . One-way laser ranging at 10 cm precision has been added to the spacecraft to assist in orbit determination, and in conjunction with the laser altimeter (LOLA) at 10 cm accuracy is expected to provide the position of LRO and, by inference, the position of surface features to the desired accuracy. Important aspects of LRO orbit determination are gravity model improvement, improvement of spacecraft timing and pointing knowledge, and laser altimetry and laser tracking of LRO are expected to be critical components.

Comparison and Combination of SLR Solutions Including Gravity Field Coefficients and Range Biases

N. Panafidina (1)**, M. Rothacher** (2)**, D. Thaller** (3)

(1) GFZ Potsdam, Germany
(2) ETH Zurich, Switzerland
(3) AIUB, Bern, Switzerland

natasha@gfz-potsdam.de

Abstract

Within the GGOS-D project SLR solutions containing station coordinates, Earth rotation parameters (ERPs), range biases and low-degree gravity field coefficients were generated by GFZ and DGFI for the time span 1993-2007. We used these two long-term weekly solutions to study the impact of estimating different parameter sets on the solution. First, all gravity field coefficients were fixed to an accurate a priori gravity field model and the influence of range biases on the station coordinates and ERPs of the weekly solutions was considered. In the second step we considered the influence of estimation of gravity field coefficients of degree one on the solution.

Introduction

Analysis Centres at GFZ and DGFI obtained within the GGOS-D project weekly SLR solutions (Koenig and Mueller, 2006) where in addition to usually estimated from SLR observations parameters (satellite orbits, station coordinates, Earth rotation parameters, range biases etc.) low-degree gravity field coefficients up to degree and order 2 were set up and estimated. The generated weekly solutions cover the time span 1993-2007. The processing strategy, models and parameterization used by GFZ and DGFI were selected to be as consistent as possible to insure the compatibility of the solutions for future combination studies. Differences in the processing strategies within GGOS-D project at DGFI and GFZ concern mainly the cut-off elevation angle and the observations screening procedure what lead to different level of noise in the resulting solutions. Also the list of stations with range biases shows some differences. In principle, range biases are estimated for some stations and for some stations the known values of range biases are applied in the processing. The ILRS lists of stations for which range biases should be applied or estimated are changed from time to time, so the compatibility of different solutions concerning the range biases cannot be always ensured. In this contribution we focus on the properties of individual and combined GGOS-D SLR solutions. We show the influence of range biases and low-degree harmonics on the solution.

GFZ and DGFI SLR solutions

Both GFZ and DGFI GGOS-D weekly solutions contain station coordinates, range biases for some stations and gravity field coefficients for the middle of the week and daily Earth Rotation Parameters (x-pole, y-pole and UT1). Starting from the free normal equations from both analysis centres we computed weekly SLR solutions using Bernese GPS Software (Dach et al., 2007). All the gravity field coefficients were first fixed to the model EIGEN-GL04C (Foerste et al., 2006). In this case we need to constrain only the rotations of the whole

network to adjust it to a certain terrestrial reference frame, because SLR observations provide direct access to the Earth's center of mass and the scale. The no-net-rotation condition was applied over a set of stable stations (6-9 stations for each week). Since in these solutions UT1 was set up as a parameter and not LOD which can only be directly estimated from satellite observations, we also always fixed the first daily UT1 estimate to the a priori value and the other daily UT1 parameters within a week were estimated as piece-wise linear functions. As a priori coordinates we used re-scaled ITRF2005 for SLR, and for a priori ERPs IERS time series C04 was used.

Figures 1 and 2 show as an example time series of ERPs w.r.t. a priori C04 values. DGFI solution is noticeably noisier than GFZ solution because it includes about 10% more observations due to the different cut-off elevation angle (1° for DGFI solution, 10° for GFZ) and different screening of the observations. Nevertheless the weighted root-mean-square values for x-pole, y-pole and UT1 estimates are on approximately the same level for both solutions, as can be seen from Table 1. To get an idea about possible systematic differences in the coordinates, we computed Helmert transformation parameters between GFZ and DGFI solutions. We do not show here pictures for the time series of transformation parameters, because there are no systematic components and all the parameters are scattered around zero. Differences between ERPs time series also do not show any systematic effects. Combined GFZ-DGFI solution shows a little bit better WRMS values for polar motion and somewhat worse value for UT1, what is seen from Table 1.

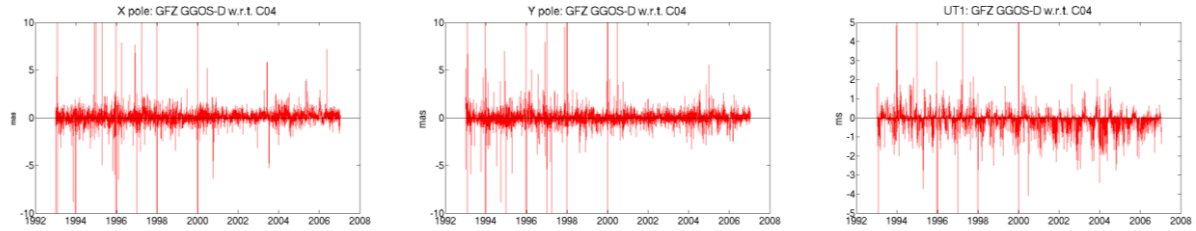

Figure 1. GFZ solution, x-pole (left), y-pole (middle), UT1 (right) w.r.t. C04

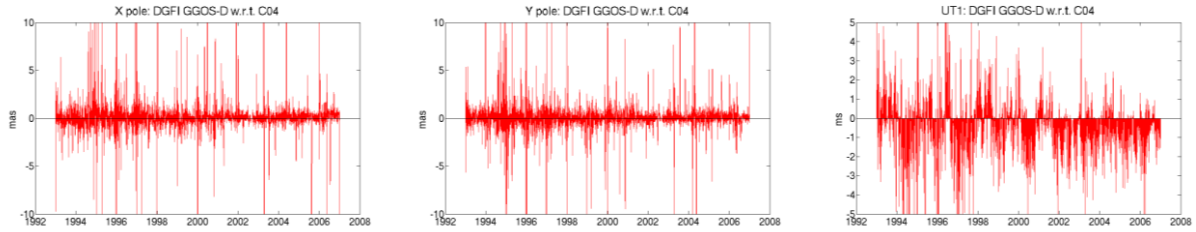

Figure 2. DGFI solution, x-pole (left), y-pole (middle), UT1 (right) w.r.t. C04

At the same time a comparison of GFZ GGOS-D weekly solutions with GFZ solutions for the ILRS shows some systematic differences both for the coordinates and ERPs. Weekly GFZ ILRS solutions, containing station coordinates and daily ERPs, were also re-processed starting from the free normal equations applying only no-net-rotation condition over the same set of stations as for GGOS-D solution. In Fig. 3 we show time series of scale parameter between GFZ GGOS-D and GFZ ILRS solutions, a clear periodic component is well-seen. Fig. 4 shows x-pole differences between the solutions, here we can see a systematic shift of about 0.2 mas. Y-pole differences do not show a systematic shift. The possible reasons for these systematic effects could be different processing options, such as using different a priori

models and different parameter sets. DGFI GGOS-D and ILRS solutions, although again more scattered than GFZ solutions, do not show these clear systematic differences.

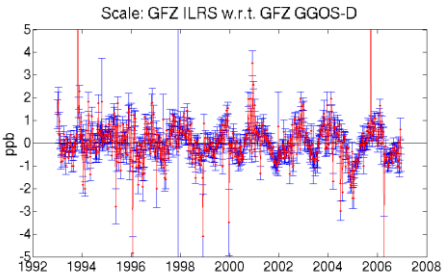

Figure 3. Scale between GFZ GGOS-D and GFZ ILRS weekly solutions

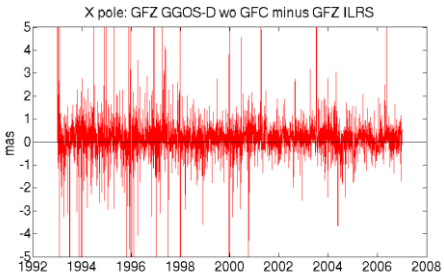

Figure 4. X-pole differences between GFZ GGOS-D and GFZ ILRS weekly solutions

Influence of range biases

Fig.5 shows an example of range biases estimates from GFZ solution for station Riga 1884. To get a general impression of the influence of range biases on the solution we computed a test GFZ solution where all the estimated range biases were fixed to zero. This test solution was compared to the normal GFZ solution with estimated range biases. Since the estimated values of range biases can vary from some millimetres to more than 10 cm, we can expect significant differences. Fig. 6 shows ERP differences between these solutions, it can be seen that the differences are more noticeable for the first part of time series, when the number of estimated range biases was also larger – about 4-8 till 1998, and about 1-2 afterwards. Helmert transformation parameters between the solutions show similar picture – more scatter in the first part of the time series and no noticeable systematic components, we do not show the corresponding graphics here. For the stations with range biases the coordinate difference between the solutions amounts to the range bias value, which is significant. This means that solutions obtained with different lists of range biases cannot be combined without distorting the solution.

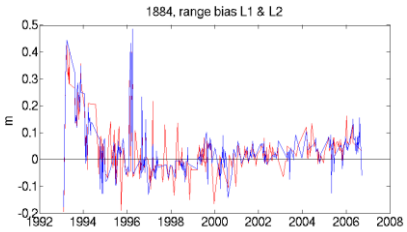

Figure 5. Range biases for station 1884 from GFZ GGOS-D solution.

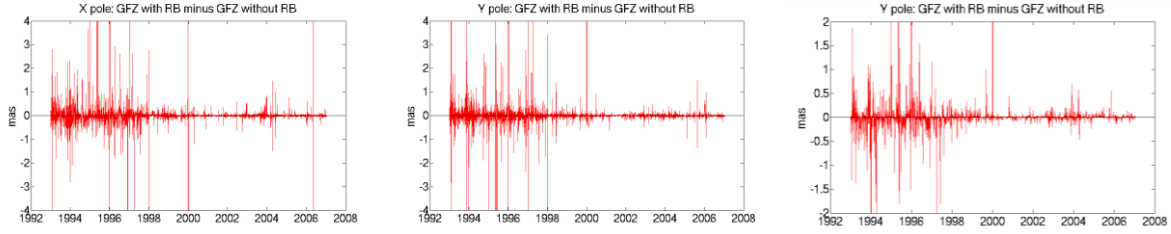

Figure 6. ERP differences for GFZ solutions with range biases estimated and range biases fixed to zero, x-pole (left), y-pole (middle), UT1 (right)

While computing a combined weekly solution we can estimate range biases from the individual solutions separately or we can stack them within a week. To estimate a possible influence of stacking range biases, we made a comparison between combined GFZ-DGFI weekly solutions with range biases stacked (separately for Lageos I and II) and with range biases estimated for both individual solutions. Fig. 7-9 show Helmert transformation parameters between these two combined solutions. As can be seen the coordinate differences are larger for the first part of the time series, what corresponds to the greater number of stations with range biases in the solutions, but still even for the most affected by range biases Z-translation the differences do not amount to 1 mm, so they can be considered negligible. The differences in the ERPs, which are not shown here, are also not significant. When we in addition stack range biases from Lageos I and II, the differences become more noticeable and amount for Tz component to 4-5 mm.

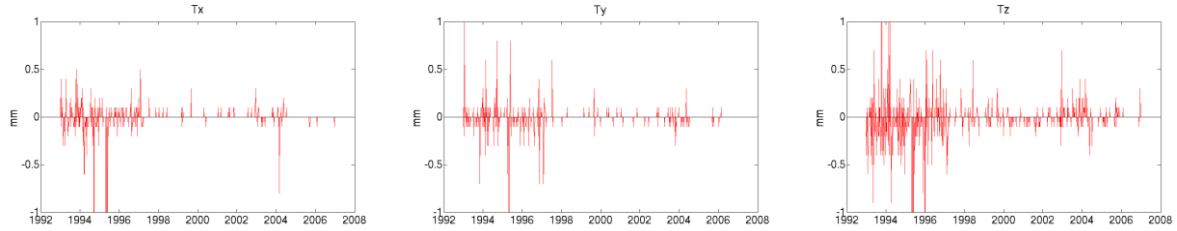

Figure 7. Translations between GFZ-DGFI combined weekly solutions with range biases stacked and not stacked

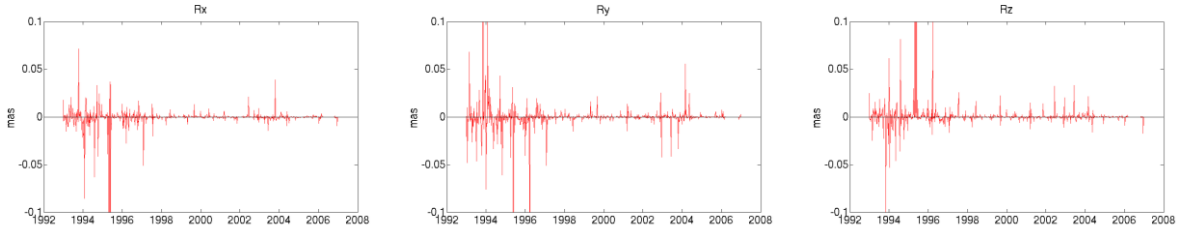

Figure 8. Rotations between GFZ-DGFI combined weekly solutions with range biases stacked and not stacked

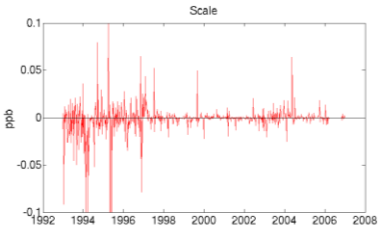

Figure 9. Scale between GFZ-DGFI combined weekly solutions with range biases stacked and not stacked

Estimation of 1st degree gravity field coefficients

To have a look at the influence of estimation in addition low degree harmonics on the solution we computed test GFZ GGOS-D weekly solutions where 1st degree gravity field coefficients (GFC) were estimated. In this case we need to apply (in addition to no-net-rotation condition) a no-net-translation condition to fix the solution to the ITRF. Gravity field coefficient C00 and all the coefficients of 2nd degree were kept fixed to a priori values to avoid the correlations with other parameters. The random errors of the ERPs from this solution remain on the same level as for the solution without GFC (see Table 1). The differences in ERPs between the solutions with estimated GFC and fixed GFC are shown in Fig. 10. Some periodic components can be seen there. The transformation parameters

between these two solutions should directly correspond to the estimated first degree gravity field coefficients, C11 corresponds to Tx, S11 to Ty and C10 to Tz (e.g. Cretaux et al., 2002). In the Fig. 11 and 12 we show translations between the solutions, the high level of correlation with the GFC is well seen. The annual and semiannual signals presented in Table 2 also show a good level of agreement. This periodic geocenter motion agrees quite well with the results from (Angermann et al, 2002), where the annual amplitudes were estimated to be 2.82 mm in Tx, 3.04 mm in Ty, 5.09 mm in Tz, and semiannual amplitudes 0.57 mm in Tx, 0.53 mm in Ty and 1.07 mm in Tz.

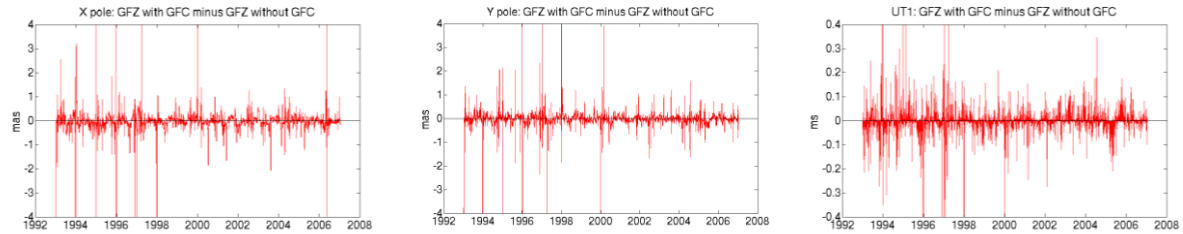

Figure 10. ERP differences between GFZ GGOS-D solutions with fixed gravity filed coefficients and estimated ones: x-pole (left), y-pole (middle), UT1 (right)

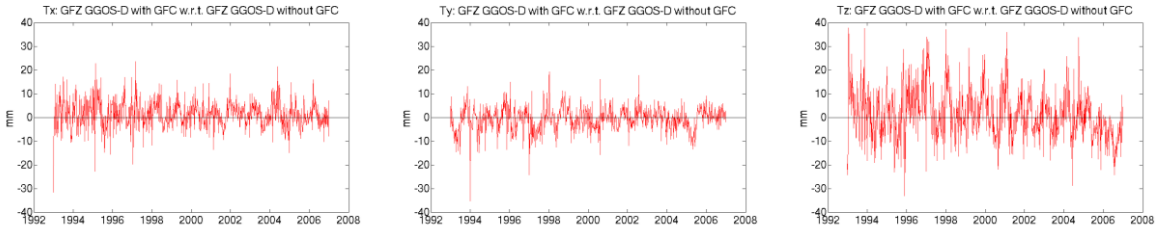

Figure 11. Translations between GFZ GGOS-D solutions with fixed gravity filed coefficients and estimated ones: Tx (left), Ty (middle), Tz (right)

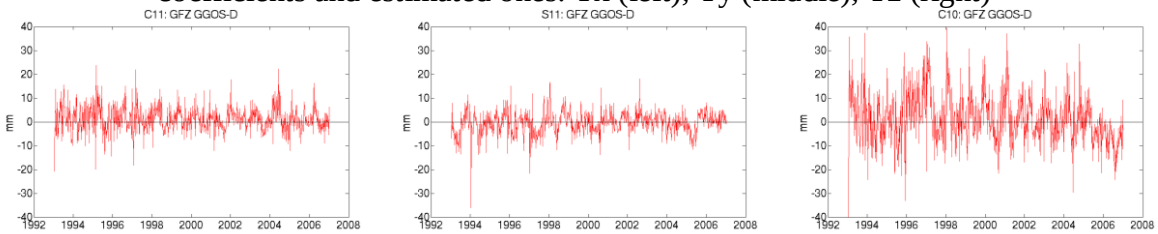

Figure 12. 1st degree gravity field coefficients: C11 (left), S11 (middle), C10 (right)

Table 1. Weighted RMS of ERPs from GFZ, DGFI and a combined solution

	GFZ, no GFC	DGFI, no GFC	comb, no GFC	GFZ, 1st deg. GFC	DGFI, 1st deg. GFC	comb, 1st deg. GFC
Xp, mas	0.35	0.38	0.33	0.37	0.38	0.35
Yp, mas	0.35	0.37	0.31	0.34	0.36	0.32
UT1, μs	0.11	0.12	0.14	0.11	0.12	0.15

Table 2. Annual and semiannual amplitudes (mm) in translation parameters and 1st degree gravity field coefficients.

	Annual amplitude, mm	Semiannual amplitude, mm
Tx	2.3 ± 0.3	0.6 ± 0.3
C11	1.9 ± 0.3	0.6 ±0.3
Ty	2.5 ± 0.2	0.3 ± 0.2
S11	2.2 ± 0.2	0.3 ± 0.2
Tz	4.8 ± 0.5	1.2 ± 0.5
C10	4.6 ± 0.5	1.3 ± 0.5

Conclusions

Within the GGOS-D project SLR weekly solutions including low-degree harmonics were generated by GFZ and DGFI. The standards adopted for these solutions were different than those used for ILRS Analysis Centre processing, what causes systematic differences in station coordinates and ERP between GGOS-D and ILRS solutions. The comparison shows no systematic differences between DGFI and GFZ GGOS-D solutions. Tests performed on these solutions concerning the stacking of range biases within a week showed no significant influence on the combined GFZ-DGFI solutions, although the differences in range biases applied in the processing will cause a distortion of station network. Estimating in addition 1st degree gravity field coefficients doesn't change the random error of the obtained parameters, but it introduces a periodic systematic difference in the station coordinates due to geocenter motion.

References

Angermann, D., H. Müller, M. Gerstl. Geocenter variations derived from SLR data to LAGEOS 1 and 2. In: Adam, J., K.-P. Schwarz (Eds.), Vistas for Geodesy in the New Millinium,. IAG Symposia, Springer, Vol. 125, pp. 30-35, 2002.

Cretaux Jean-Francois, Laurent Soudarin, Fraser J. M. Davidson, Marie-Claude Gennero, Muriel Berge-Nguyen, and Anny Cazenave. Seasonal and interannual geocenter motion from SLR and DORIS measurements: Comparison with surface loading data, Journal of Geophysical Research , vol. 107, NO. B12, 2374, doi:10.1029/2002JB001820, 2002.

Dach, R., U. Hugentobler, P. Fridez, M. Meindl (Eds.). Bernese GPS Software, Version 5.0. Astronomical Institute, University of Bern, February 2007.

Förste, C., Flechtner, F., Schmidt, R., König, R., Meyer, U., Stubenvoll, R., Rothacher, M., Barthelmes, F., Neumayer, H., Biancale, R., Bruinsma, S., Lemoine, J.-M., Loyer, S., A mean global gravity field model from the combination of satellite mission and altimetry/gravimetry surface data – EIGEN-GL04C. Geophysical Research Abstracts, 8, 03462, 2006

R Koenig, H Mueller, Station Coordinates, Earth Rotation Parameters and Low Degree Harmonics from SLR within GGOS-D, 15th ILRS Workshop Proceedings, 2006.

Measurement of anomalous angle of deviation of light during Satellite Laser Ranging

I. Ignatenko (2)**, Yu. Ignatenko** (1)**, A. Makeyev** (1)**, V. Tryapitsyn** (1)

(1) Crimean Laser Observatory, Katzively, Yalta, Crimea, Ukraine
(2) All-Russian Research Institute of Physicotechnical and Radiotechnical Measurements, Mendeleevo, Moscow Region, Russia

clogao@rambler.ru

Abstract

In this article the effect of anomalous deviation of light during satellite laser ranging is described. It is shown that it is not caused by telescope's deformations. Specially for study of this effect the measurement and data processing procedure was developed. First measurements' results are presented.

Introduction

The SLR station "Katzively-1893" of the Crimean Laser Observatory ranges satellites with laser beam with small angular divergence (about 5 arcseconds). Thus, we need high pointing accuracy to receive response signal from ranged objects. We discovered that in order to obtain strong signal, we have to make an advance not only for the velocity aberration, but also for an unknown factor that we call "anomalous deviation of light" that is comparable with velocity aberration by value but, as a rule, different by direction. First manual mostly qualitative observations were conducted in years 2001, 2002, 2004 [Ignatenko et al. 2004]. With installation of CCD camera in mid 2007 attached to computer with proper software we increased quality and quantity of observations. This allowed us to determine more precisely the anomalous deviation of light from the preset direction in the field of view of the telescope subtracting velocity aberration from apparent deviation of satellite's image.

Equipment

Scheme of the optical part of the Katzively SLR station is shown on the Fig. 1.
Main optical axes and focuses of the 1 m TPL-1 telescope with alt-azimuthal mount, the PMT, and the Nd:YAG laser with output wavelength 532 nm are superposed by means of the optical matching system (OMS). The OMS permits to set and control direction of emission and divergence of the transmitted laser beam. All elements of the OMS are mounted on immobile part of the telescope. Hence, all optical alignments are long-term stable. During the full telescope's alignment the artificial star of the OMS is set in the conjugate focal plane of the telescope so that its center represents telescope's main optical axis. Then all adjustments are made respectively to this star. Tuning mirror 8 (Fig. 1) is placed into its operating location unambiguously due to its special mount.

To prove that anomalous deviation of light is not caused by thermal or mechanical deformations of the telescope we conducted the following experiment: on the shutter of the dome two high-quality retroreflectors were set. The rotating mirror 7 (Fig. 1) is partially transparent (~ 1%). Through it and guide 6 we observed laser radiation reflected from corner cubes and passed twice through the telescope. While we rotated the dome and moved the

shutter up and down imitating change of angular coordinates, the center of the reflected spot never deviated from projection of the main telescope's optical axis onto the field of view more than on 2 arcseconds.

Specially for measurement of anomalous angle of deviation of light the CCD camera was installed onto the telescope's main guide and calibrated by pairs of stars with known angular distance between them. Inequality of horizontal and vertical scales of the camera images also was taken into account. We have written a special program (in C++) that stores camera images on PC hard disk when station's measuring equipment detects laser pulse reflected from the satellite. Also we have modified standard software in order to calculate the projection of the satellite's velocity aberration onto the telescope's focal plane. Post-processing software for detection of the satellite image center and computation of the anomalous deviation was written too (in MATLAB).

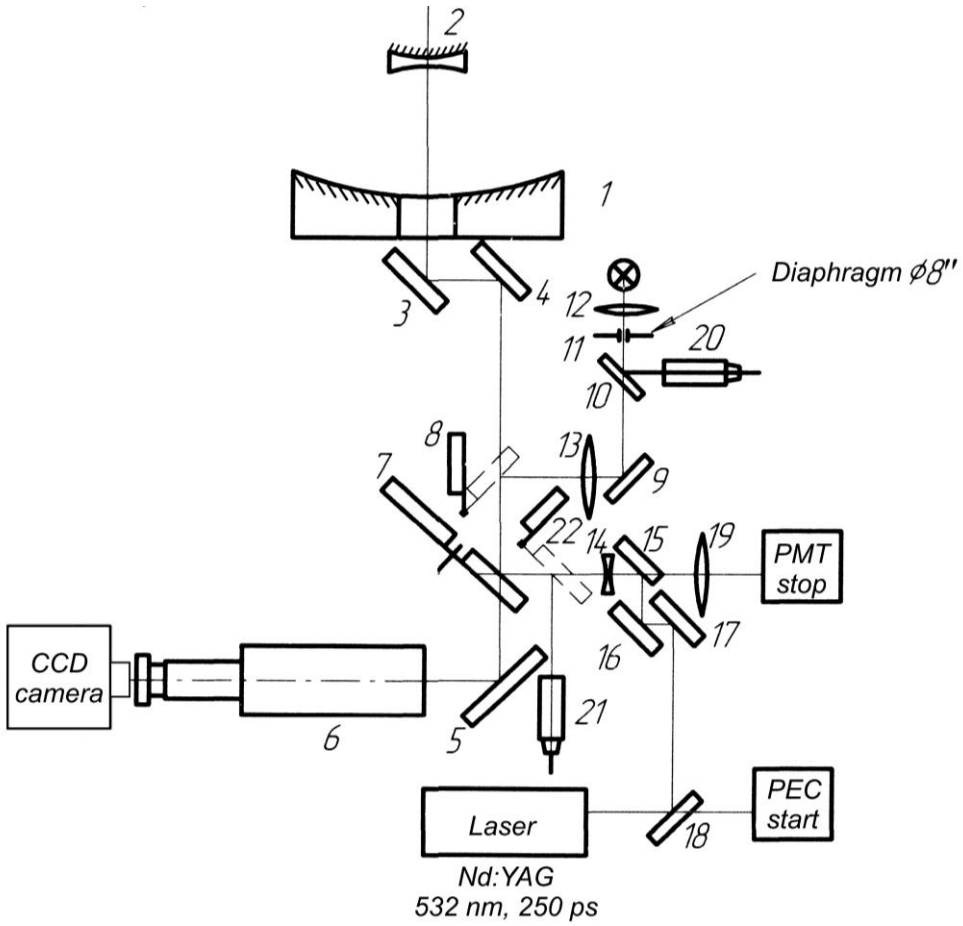

Figure 1. Optical part of the laser ranging system on the Katzively SLR station

i) *TPL-1 telescope:*
   1 – primary mirror; 2 – secondary mirror; 3, 4, 5 – diagonal mirrors;
   6 – main guide with chromatic aberrations compensator and image intensifier;
ii) *Optical matching system:*
   7 – rotating mirror; 8, 22 – tuning switch mirrors; 13, 14, 19 – matching lenses;
   9, 15..18 – mirrors; 10, 11, 12, 20 – artificial star; 20, 21 – oculars

Measurement and data processing procedure

During our observations laser radiation was directed along the telescope's main optical axis, divergence was 5 – 8 arcseconds. We checked it before each night, when observations were conducted, and corrected in case of need. At the same time the artificial star's image was captured and a virtual guide mark was placed on the monitoring computer's screen.

Throughout the satellite's passage operator corrected telescope's pointing in order to obtain strong response signal from satellite's retroreflectors. At moments, when we received echoes, video frames were stored on the PC.
While postprocessing of the obtained images we determined positions of the projection of the telescope's main optical axis onto the focal plane (from pictures of the artificial star) – point A on Fig. 2, and of the satellite's center – point B – in Cartesian coordinate system bounded to the telescope's focal plane. To remove outliers in determination of the satellite's position we used median filtering and sliding average by each coordinate. Then we found the sequence of vectors $\mathbf{AB}$ of the observed deviation of the satellite. For the corresponding instants we calculated the vectors of the satellite's velocity aberration $\mathbf{AC} = 2\mathbf{v}/c$, where c denotes the speed of light and $\mathbf{v}$ is for projection of the satellite's velocity onto the field of view of the telescope. In addition, the direction of the vector $\mathbf{AC}$ was controlled by sequence of frames with the same star passing through the telescope's field of view. So, the vector of anomalous deviation of light was computed as $\mathbf{CB} = \mathbf{AB} + (-\mathbf{AC})$.

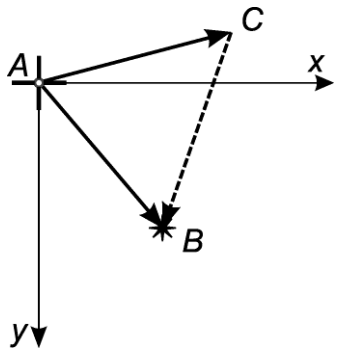

Figure 2. Computation of the anomalous deviation of light

Results

From March until November 2007 using described hereinbefore procedure we observed near a hundred passes of various satellites. We processed only those passes which satisfied the following criteria: the number of signal points was greater than 100 (operating laser rate is 3 Hz), the satellite's image was not too bright and its diameter was less than 8 arcseconds (this allowed to avoid image intensifier's afterglow and determine the image center more precisely), the duration of the pass was long enough (5 – 12 minutes for LEO, 15 – 30 minutes for LAGEOS, 30 – 60 minutes for HEO), the atmospheric conditions permitted to obtain more or less uniform sequence of signal points, the satellite's elevation was greater than 20° above horizon for LEO and exceeded 30° for LAGEOS and HEO.

On the Fig. 3, 4 the results for two LAGEOS-1 passes are shown. On the Fig. 3A, 4A the vector diagrams represent the change with time of the measured apparent deviation $\mathbf{AB}$ (curve number 1 on the figures), the vector opposite to velocity aberration $\mathbf{CA} = (-\mathbf{AC})$ (2), and the anomalous deviation $\mathbf{CB}$ (3) in the telescope's field of view. The arrows indicate the beginning of the observations. Angular scale is in degrees; absolute values are in arcseconds. On the Fig. 3B, 4B the time dependency of the absolute values of the vectors $\mathbf{AB}$ (1), (2) and $\mathbf{CB}$ (3) is plotted. We would like to note that there is a several months' interval between shown on these two figures observations. It is clear that the directions of the vector $\mathbf{CB}$ differ for different epochs.

On the Fig. 5 the maximal absolute values of the anomalous deviation of light **CB** for each processed pass of the LAGEOS-2 and Beacon-C satellites are presented. One can see the seasonal dependency of the investigated effect.

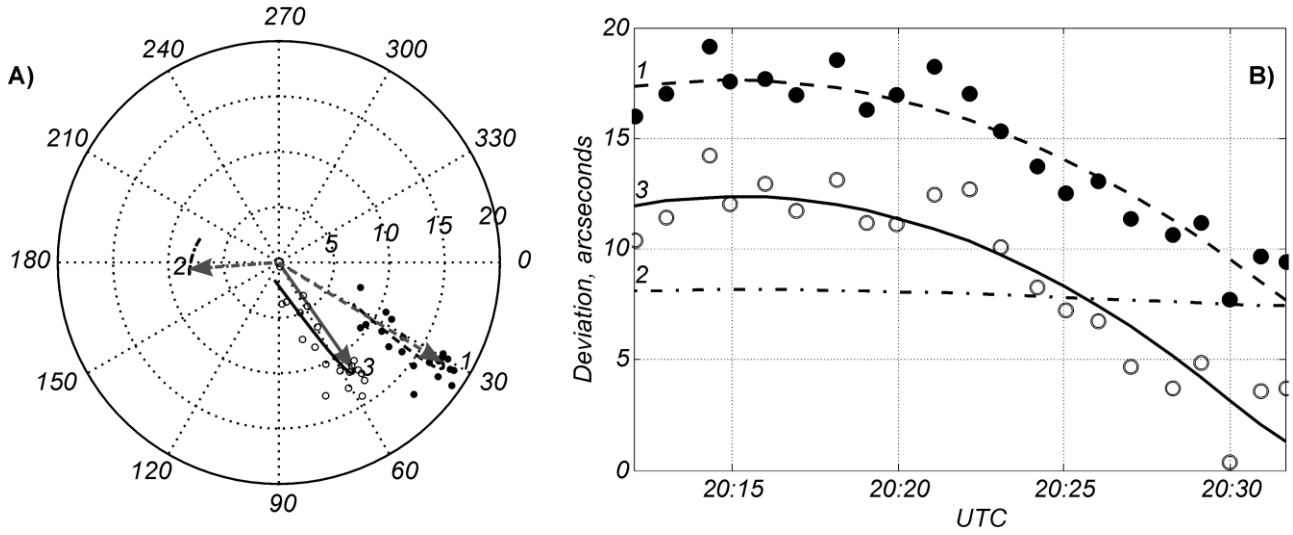

Figure 3. Satellite LAGEOS-1 March 20, 2007

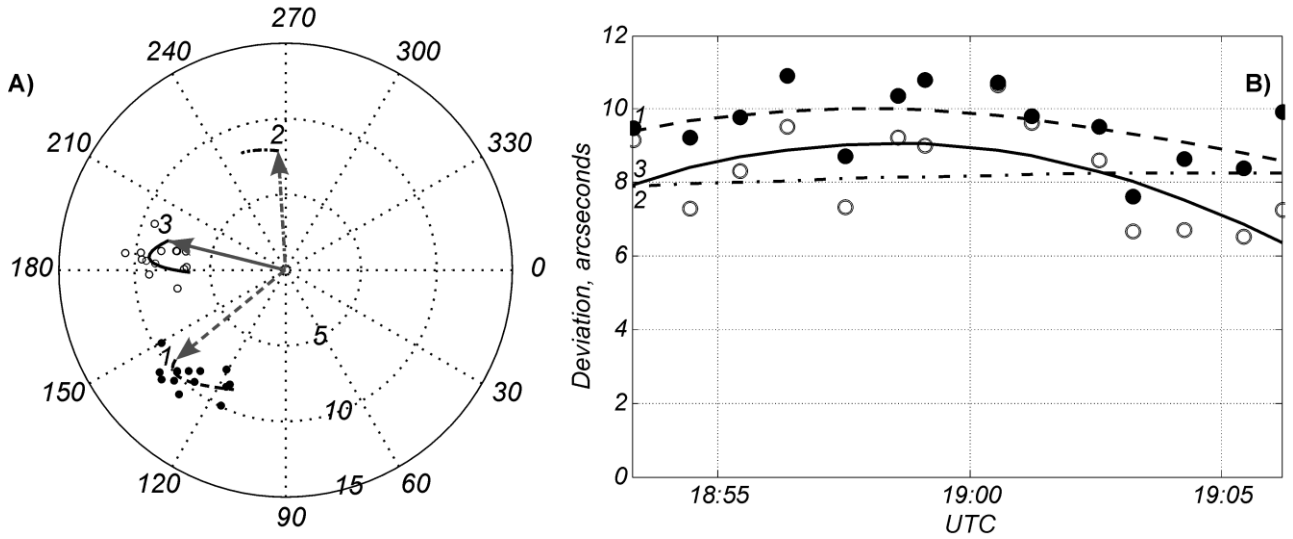

Figure 4. Satellite LAGEOS-1 July 28, 2007

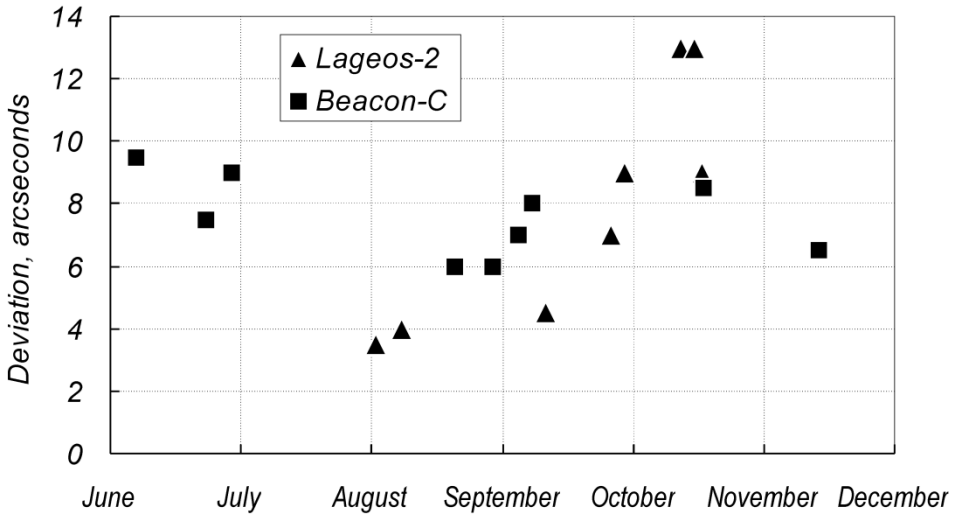

Figure 5. Seasonal dependency of the maximal absolute values of projections onto the telescope's focal plane of the anomalous deviation of light

Conclusion

Automation of measurements allowed us to improve quality and to increase quantity of observations as compared with ones held in 2004 and earlier. The method of automatic registration of anomalous deviation of light and data processing was developed.

First results indicate that the anomalous deviation of light attains 10 – 12 arcseconds and is comparable with velocity aberration by value but different in direction. The observed effect is seasonally dependent.

Further processing of obtained results needed. We are going to make an attempt to combine a 3D-vector of anomalous deviation from its different projections onto the telescope's field of view.

It is possible that observed anomalous deviation of light could be explained by motion of luminiferous medium in the near-Earth space relatively to the optical ranger.

Reference

Ignatenko Yu., Tryapitsyn V., Ignatenko I., *Determination of Speed Aberration While Laser Location of Earth Artificial Satellites*, Journal of Automation and Information Sciences, vol. 36, issue 4, 2004.

Overview of the Science Results from ICESat

B. E. Schutz, H. J. Zwally
The University of Texas at Austin, USA
schutz@csr.utexas.edu

Abstract

ICESat (ICE, Cloud and Land Elevation Satellite) was launched in January 2003 into a 94, 600 km altitude orbit and laser altimeter operations began one month after launch. Although laser life issues were identified after one month of operation, the adopted operation scenario has supported the creation of a time series of elevation from which elevation change has been measured. A variety of calibration/validation experiments have been executed which show that the elevation products, when fully calibrated, have an accuracy that meets the science requirements (e.g., radial orbit accuracy < 5 cm, laser spot geolocation accuracy < 5 meters). The elevation products from ICESat use GPS-derived orbits, but the SLR measurements collected through the ILRS are critical to verify the radial orbit accuracy. Results obtained from ICESat for elevation change correlate well with mass change results obtained from GRACE over the same time interval. This presentation will summarize the science results obtained from ICESat.

Planetary Laser Altimetry; Past and Present

David E. Smith[1], **Maria T. Zuber**[2]
[1]NASA-GSFC, [2]MIT, USA
David.E.Smith@nasa,gov

Abstract

After Apollo, laser altimetry in NASA began with Mars Observer (MOLA-1), launched in 1992 but lost on approach to Mars, and re-flown on Mars global Surveyor (MOLA-2) in 1996. In Jan 1994 the Clementine mission to the Moon carried the second laser altimeter into space that provided the first global shape of the Moon. In 1996 the NEAR spacecraft carrying the NEAR Laser Ranger (NLR) was launched to the asteroid 433 Eros, and in 2004 a laser altimeter was launched on the MESSENGER spacecraft to Mercury and is currently in cruise to the planet. Early next year the LRO spacecraft carrying LOLA will be launched to the Moon. Japan launched the SELENE spacecraft in 2007 carrying the LALT laser altimeter followed by Chang'E by China. Soon India will launch Chandrayaan carrying a laser altimeter. In nearly all the missions todate laser altimeters have been used for mapping of planetary bodies with remarkable success and played major roles in preparing for subsequent lander missions. All of the these missions and their laser instruments have helped make advances in the use of lasers for planetary science and helped convince skeptical space agencies that these kinds of instruments could be used with confidence and reliability on long planetary missions in some harsh environments. Laser altimetry is now accepted, albeit not with the same level of confidence as microwave instruments, and laser tracking of planetary spacecraft will be next challenge.

Volatile Exchange on Mars

Maria T. Zuber[1], **David E. Smith**[2]
MIT[1], NASA-GSFC[2], USA
zuber@mit.edu

Abstract

The movement of CO2 from the atmosphere of Mars to the polar caps on a seasonal basis and the subsequent sublimation of the material back into the atmosphere is the long-term dominating atmospheric processes on Mars. This process is observable in the orbits of Mars spacecraft determined from tracking data and the quantity of material can be estimated from changes in the gravity field. These observations of the motion of volatiles is not necessarily restricted to the exchange of CO2 between the atmosphere and polar caps but, like Earth, to any movement of mass on or in the planet, including the possible flow of ground water, and the escape of volatiles from the regolith. The measurement of these motions is largely dependent on the quality of the orbit determination and hence the tracking data. Laser tracking of spacecraft around other planets is potentially the most accurate source of data for observing and monitoring these changes.

Lunar Laser Ranging - A Science Tool for Geodesy and General Relativity

J. Müller
Institut für Erdmessung, Leibniz Universität Hannover, Germany
mueller@ife.uni-hannover.de

Abstract

Lunar Laser Ranging (LLR) has routinely provided observations for more than 38 years. A new site called APOLLO has just started with measurements reaching mm ranging accuracy. The main benefit of LLR is, e.g., to determine many parameters of the Earth-Moon dynamics (e.g. orbit and rotation of the Moon, a selenocentric reference frame or the secular increase of the Earth-Moon distance: 3.8 cm/year) and to test metric theories of gravity. LLR data analysis determines gravitational physics quantities such as the equivalence principle, any time variation of the gravitational constant, relativistic precessions, and several metric parameters. The gravitational physics parameters cause different spectral perturbations of the lunar orbit, which can be used to separate the various relativistic and Newtonian effects with high accuracy. We give an overview of the recent status of our LLR analysis procedure, present new results for the relativity parameters, and address potential capabilities of LLR in the near future.

Details of our LLR analysis procedure and new results for gravitational physics and Earth orientation parameters are given in the paper of L. Biskupek and J. Müller about "Relativity and Earth Orientation Parameters from Lunar Laser Ranging" in these proceedings, Session "Lunar and Interplanetary Laser Ranging**"**.

Lunar Core and Mantle. What Does LLR See?

James G. Williams, Dale H. Boggs
Jet Propulsion Laboratory, California Institute of Technology, Pasadena CA, 91109, USA
James.G.Williams@jpl.nasa.gov

Abstract

The lunar interior is hidden, but Lunar Laser Ranging (LLR) senses interior properties through physical librations and tides. The mean density of the Moon is like rock and the mean moment of inertia is only 1.6% less than a uniform body would have. Neither is compatible with a large dense core like the Earth's, though a small dense core is permitted. The solid-body tides are proportional to Love numbers that depend on interior structure and the radial dependence of elastic parameters and density. A small core, either solid or fluid, increases the Love numbers by a few percent, but uncertainty of deep elastic parameters also affects Love number computations. LLR sees three effects through the physical librations that indicate a fluid core. The strongest effect is from energy dissipation arising at the fluid-core/solid-mantle boundary (CMB). Since there is also dissipation from tides in the solid mantle, we separate tide and CMB dissipation by determining phase shifts in multiple periodic libration terms. The second indicator of a fluid core comes from the oblateness of the CMB which causes a torque as the fluid moves along the oblate surface. The third effect comes from the moment of inertia of the fluid core which affects the amplitude of a physical libration term. The fluid moment is difficult to detect, but it is now weakly seen and its determination should improve from future LLR data. LLR does not separate fluid core density and size, but if the fluid core has the density of iron then a radius of roughly 330-400 km is suggested. Lower density materials would have larger radii; Fe-FeS mixtures are attractive because they have lower freezing points. The dissipation analysis which gives CMB dissipation also gives tidal Q vs frequency. At one month Q is ~30, while Q is ~35 at one year. These low values may come from the lower mantle which is suspected to be a partial melt. How can the core and mantle parameter determinations be improved? Expanded modeling may improve fits and add parameters. Long LLR data spans are important, so future accurate ranges to the four retroreflector arrays are requested. Expanding the number and spread of lunar retroreflector sites, by finding the lost Lunokhod 1 rover or placing new retroreflectors on the Moon, would also benefit the extraction of scientific information from LLR data.

Introduction

Where does the Moon fit in solar system science including origin and evolution? The five terrestrial bodies ordered by increasing size are the Moon, Mercury, Mars, Venus and Earth. Thermal evolution depends on size. The Moon is the smallest and most primitive terrestrial body. The crust is still present, but it was subject to many early large impacts that broke up the surface; at the dark mare areas the original crust is covered with lava flows. Beneath the crust the lunar interior is hidden from direct view and our knowledge of it relies on a variety of evidence. The Moon is an end member in our solar system sample of terrestrial bodies and understanding it contributes to the larger problem of the origin and evolution of the solar system.

Lunar Laser Ranging (LLR) contributes to several scientific areas: lunar science, gravitational physics, geophysics and geodesy, ephemerides and astronomical constants (Dickey et al., 1994). LLR has made significant contributions to lunar science including the lunar interior. The interiors of the planets and satellites are hidden from sight and information on interior structure and properties is difficult to obtain. The lunar interior structure and properties are the subjects of this paper. This paper first reviews some of the relevant information gathered by other techniques, and then discusses what LLR has learned.

Information from Various Techniques

Knowledge of the lunar interior comes from a variety of techniques. To understand the LLR contribution in the larger context, a selective review of some of these results is given in this section. This is a narrow review omitting some topics and references for brevity. A broader modern review of lunar science, including a chapter on the lunar interior, is given in the book New Views of the Moon (Jolliff et al., 2006).

Basic properties of the Moon include mass and radius and the derived mean density. Orbiting spacecraft determine lunar GM (Konopliv et al., 1998), the product of the gravitational constant and the mass. Tracking distant spacecraft also gives the lunar GM since the displacement of the center of the Earth from the Earth-Moon center of mass gives sensitivity. A recent value from DE421 (Williams, Boggs, and Folkner, 2008; Folkner, Williams, and Boggs, 2008) depends most strongly on interplanetary tracking of spacecraft from Earth.

$$GM_{moon} = 4902.80008 \pm 0.00010 \text{ km}^3/\text{sec}^2$$

Dividing GM by the gravitational constant G gives the mass

$$M_{moon} = 7.3459 \pm 0.0011 \text{x} 10^{22} \text{ kg},$$

with the uncertainty in the mass dominated by the uncertainty in G.

From Moon orbiting spacecraft, both laser altimetry and overlapping images have been used to determine lunar topography and the mean radius. The Clementine mission laser altimetry gave a mean radius R of 1737.10 km (Smith et al., 1997). Recent Change'E-1 altimetry gets a mean radius of 1737.01 km (Ping et al., 2008). The recent Kaguya (SELENE) mean radius is 1737.15 km (Araki et al., 2009). With a 1737.1 km radius and the above mass, the mean density is

$$\rho = 3346 \text{ kg/m}^3.$$

This mean density is like rock so any much denser core material must be a small fraction of the total.

Another bulk property of the Moon is the moment of inertia. The three principal moments of inertia around three orthogonal principal axes are A<B<C. The principal axis z near the axis of rotation is associated with moment C while the principal axis x associated with A points near the mean Earth direction. The moments of inertia come from the combination of results from two techniques: orbiting spacecraft gravity field and LLR relative moment differences. From the physical librations, the three-axis rotation or time-variable lunar orientation, LLR determines the moment differences.

$$\beta = \frac{(C-A)}{B} \quad (1)$$

$$\gamma = \frac{(B-A)}{C} \quad (2)$$

The second-degree gravity coefficients are related to the moment differences through their definitions.

$$\frac{(C-A)}{MR^2} = J_2 + 2C_{22} \quad (3)$$

$$\frac{(C-B)}{MR^2} = J_2 - 2C_{22} \quad (4)$$

$$\frac{(B-A)}{MR^2} = 4C_{22} \quad (5)$$

Because we are using the principle axis x to define zero longitude, $S_{22} = 0$. The combination of the LLR and spacecraft results gives the normalized polar moment C/MR^2 and the mean moment I/MR^2. The Konopliv et al. (1998) combination used the R=1738.0 km reference radius that is standard for gravity fields. That radius is close to the mean equatorial radius.

$$C/MR^2 = 0.3932 \pm 0.0002$$
$$I/MR^2 = 0.3931 \pm 0.0002$$

The Clementine, Chang'E-1 and Kaguya mean radii are given above. Rescaling the Konopliv et al. moments to R=1737.1 km gives

$$C/MR^2 = 0.3936 \pm 0.0002$$
$$I/MR^2 = 0.3935 \pm 0.0002$$

The mean value is only 1.6% less than a homogeneous sphere's 0.4. Any increase of density with depth, including the lower density crust and any dense core, will reduce the moment ratios below 0.4, so any dense core must be small.

The detailed structure of the Earth's interior was revealed by seismology. Seismometers were placed on the Moon during the Apollo missions and instruments at four of the sites operated for several years. Two types of moonquakes were detected, shallow and deep moonquakes. The deep moonquakes, from ~750 to ~1100 km deep, were very weak but numerous. Over one hundred source locations are recognized (Nakamura, 2005) and deep moonquakes recur at the same locations, apparently triggered by deep solid-body tides. Impacts were also recognized, both meteoroids and spacecraft. Analysis of the P- and S-wave arrival times by several groups (Goins et al., 1981; Nakamura, 1983; Khan et al., 2000; Lognonné et al., 2003; Gagnepain-Beyneix et al., 2006) showed that the lunar crust was a few tens of kilometers thick and the mantle extended down from the crust through the deep moonquake zone. Deeper structure was not revealed because the damping of the seismic waves became strong below the deep moonquake zone, particularly for the S waves. This attenuating zone is suspected to be a partial melt (Nakamura, 1983). The loss of the S waves prevented deep structure from being determined. There was a second difficulty for lunar seismology; the crust has been broken up by early large impacts and this scatters most of the seismic energy away from the first arrivals of the waves. The damping of seismic waves is very low in the crust and the delayed arrival of scattered seismic waves obscures later arriving waves that

could have been useful. So the Apollo seismic data revealed the lunar crust and mantle, but little is known about the deep-mantle attenuating zone and there is uncertainty about which P waves might have passed through a lunar core (Sellers, 1992). We conclude that the core was undetected or unrecognized by seismology. Lunar seismology is reviewed by Lognonné (2005).

If the Moon had a strong dipole magnetic field it would be persuasive evidence for a liquid core since such fields are considered to arise from dynamos in conducting fluid cores. But there is no strong organized lunar field. The Moon's magnetic field consists of local patches with different polarities. It does not follow that the Moon's core must be solid since sluggish convection in a fluid core may not be vigorous enough to cause a dynamo. It is interesting that many of the basalts brought back from the Mare regions of the Moon are magnetized. This may be evidence for an ancient magnetic field at the time that the Mare flows solidified 3-4 billion years ago (Cisowski et al, 1983; Collinson, 1984; Cisowski and Fuller, 1986), but this explanation is not universally accepted. A 4.2×10^9 year old crustal rock, a troctolite, also shows magnetization so a dynamo could have been active early in the lunar history (Garrick-Bethell et al., 2009).

The Earth's magnetic field deflects the solar wind causing a cavity around the Earth. The Moon lacks a dipole field, so the solar wind impacts and flows around the Moon except when it is passing through the elongated tail of the Earth's cavity. So the Moon is subject to varying external magnetic fields from the solar wind most of the time, but occasionally experiences the quieter field of the geotail. Varying magnetic fields induce currents in the Moon that generate their own magnetic fields that can be sensed by spacecraft magnetometers on or orbiting the Moon. When passing through the geotail these currents decay, with the currents in the most conducting material damping slowest. Apollo-era and more recent Lunar Prospector magnetic data seem to show a long lasting induced field interpreted to be from a conducting core (Goldstein et al., 1976; Russell et al., 1981; Hood et al., 1999). For a core conducting like metals do, the radius inferred by Hood et al. is 340±90 km. For lower conductivity, such as a molten silicate core, the size could be larger.

Rocks brought back from the Moon are highly depleted in minerals involving water and other volatile compounds. The interpretation is that the upper part of the Moon, and perhaps the whole body, was melted when young. During this lunar magma ocean phase, low density materials would have floated to the surface forming the crust. As the Moon cooled the crust and mantle would have solidified. The basalts that make up the dark lunar Mare in low areas came up from partial melts in the upper mantle (Spohn et al., 2001). The basalts are modified mantle material and they have densities higher than the crust. The basalts brought back from the Moon are 3-4 billion years old. The extensive volcanic activity that flooded the dark Mare areas was early in the Moon's lifetime. The mantle convects slowly, radioactive heating is declining and the Moon slowly cools (Spohn et al., 2001). Orbital images show that the cooling Moon produced some lava flows until about 1×10^9 yr ago and there is evidence of very recent gas release (Schultz, Staid, and Pieters, 2006). Heat flow measurements made at two of the Apollo sites help constrain current heat production (Langseth et al., 1976; Warren and Rasmussen, 1987).

Can the core remain molten for the 4.5×10^9 yr age of the Moon? That depends on its composition as well as its initial temperature. A cooling pure iron core would solidify at about 1650˚ K. However, mixes of iron and other materials have lower melting points, sulfur and carbon are particularly effective. The optimum mixture of iron and sulfur, the eutectic,

stays molten down to ~1000˚ K (Brett and Bell, 1969). Because the melting point of iron can be lowered so much, Brett (1973) suggested that the lunar core could be molten. A cooling mixture of iron, sulfur and other materials does not solidify at a single temperature. Rather the iron solidifies over a range of decreasing temperatures before the iron-sulfur mixture freezes. This provides a natural way to form a solid iron core interior to the fluid mixture while concentrating the sulfur in the liquid, where it acts like antifreeze.

The liquid or solid state of a core is connected to its temperature and composition. While it is convenient to discuss pure iron as an extreme possibility, iron mixed with sulfur, carbon, nickel, etc are more realistic. It is suggestive that siderophile elements, which would be expected to migrate into a core along with iron, are depleted in lunar rocks when compared to primitive meteorites and the Earth's mantle (Righter and Drake, 1996). As an alternative to iron alloys, dense silicate cores have been proposed. The composition and density of any core should not be considered established.

In summary, any dense lunar core must be small to satisfy density and moment of inertia values, and there is magnetic induction evidence that it is conducting. Non-LLR evidence does not establish core composition, though iron alloys are plausible, or whether the core is liquid or solid, or whether there is an inner solid and outer liquid structure. More is known about the mantle. Its density and elastic properties are sampled down to the deep moonquake zone. There may be a partial melt in the deepest part of the mantle above the core.

LLR Evidence

Early LLR lunar science included moment of inertia differences and low-degree gravity field coefficients. Previous reviews are given by Dickey et al. (1994) and Williams and Dickey (2003). At the end of the 1970s LLR found a strong energy dissipation signature, a displacement in the direction of the precessing pole of rotation. It took two decades to separate the two causes, tidal dissipation in the Moon and dissipation at the fluid-core/solid-mantle boundary (CMB). LLR is also sensitive to potential Love number k_2, displacement Love numbers h_2 and l_2, tidal dissipation at several frequencies, flattening of the CMB, and moment of inertia of the fluid core. All of these parameters tell us something about the lunar interior.

LLR Data, Stations and Retroreflector Arrays

The LLR data analysis uses ranges from 1970-2008. The initial conditions for the lunar ephemeris and three dimensional lunar orientation (Euler angles and spin rates), lunar laser retroreflector array positions, lunar geophysical parameters, and other parameters including Earth orientation and station positions and rates were fit to Lunar Laser Ranging (LLR) data. A total of 16,941 ranges extend from March 16, 1970 to November 22, 2008. Modern range accuracies are more than an order-of-magnitude more accurate than the early data. Ranges were processed from McDonald Observatory, Texas (6,523 ranges), Observatoire de la Côte d'Azur (OCA), France (9,177), Haleakala Observatory, Hawaii (694), Apache Point Observatory, New Mexico (536), and Matera, Italy (11). LLR data are archived by the ILRS (Pearlman et al., 2002). The Apache Point Observatory is a high accuracy addition to the LLR network (Murphy et al., 2009). Figure 1 shows the annual weighted rms range residuals after fits. The weighted rms residual for the past 4 yr combined is 0.11 nsec or 1.67 cm. The Apache Point ranges and the best of the OCA data cannot be fit to their noise levels. Shortening the data span in the fit reduces the rms residual, so there is a long-time signature that is not being fit.

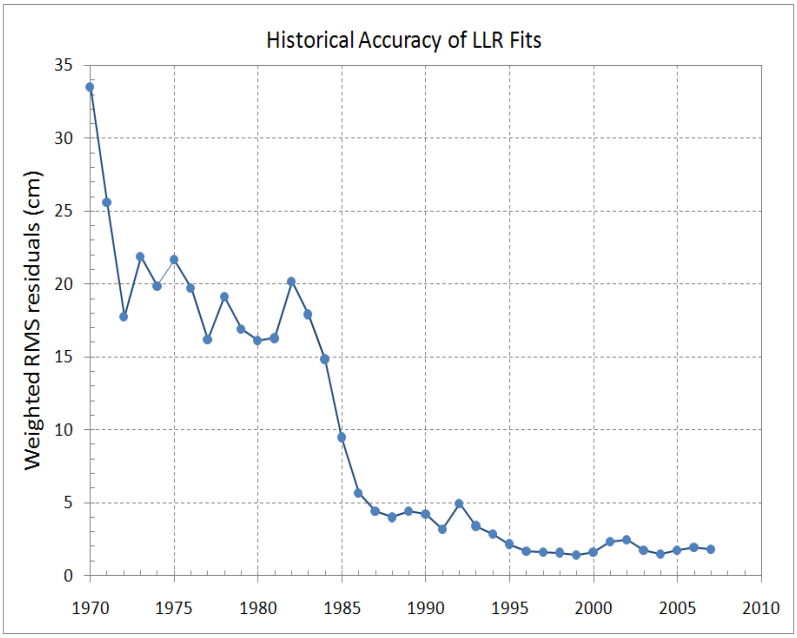

Figure 1. Weighted rms range residuals improve with time.

Ranges to four retroreflector arrays on the Moon are used in fits. Arrays are located at the Apollo 11, 14, 15 and Lunokhod 2 sites shown in Fig. 2. Lunar landing site maps, images and descriptions are presented by Stooke (2007). A majority of the ranges are to the largest array at the Apollo 15 site (77.5%), while Lunokhod 2 gets the fewest number of ranges (2.8%). Apollo 11 and 14 make up 9.9% and 9.7% of the total data set, respectively. The Lunokhod 1 position has not been known well enough to acquire ranges. A proposed location is given by Stooke (2005). Finding and ranging Lunokhod 1 would benefit the tide measurements. The Lunokhod 2 array now gives a weak return (Murphy et al., 2009) and Lunokhod 1 may also be weak and hard to find. The coordinates of known LLR sites are available (Williams, Newhall and Dickey, 1996; Williams, Boggs and Folkner, 2008) and are used for lunar geodesy. Figure 3 shows the four arrays. Ranges to multiple arrays are important for determining the physical librations, tides and lunar geophysical parameters.

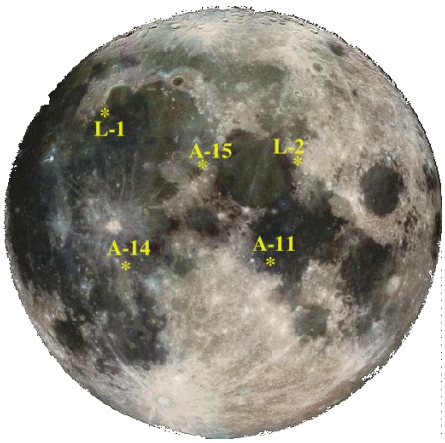

Figure 2. Locations of retroreflecting arrays on the Moon.

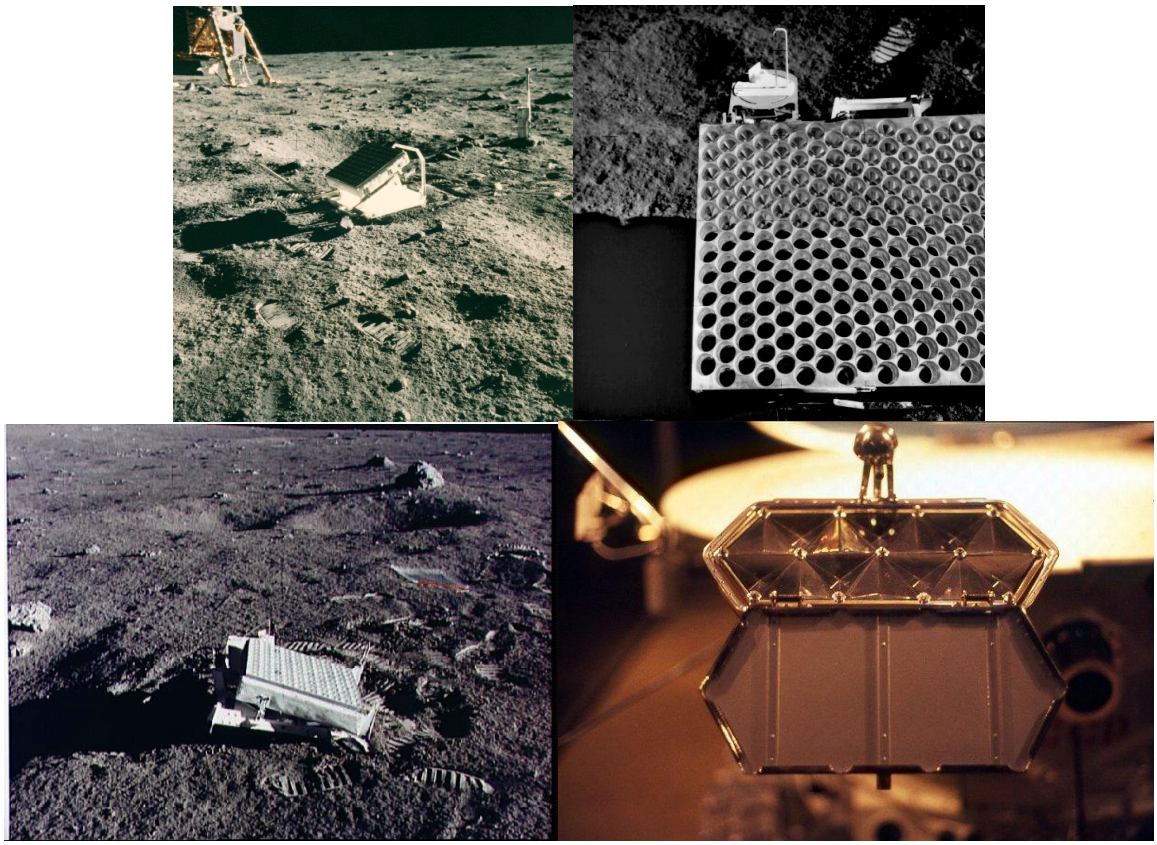

Figure 3. Retroreflecting arrays on the Moon at the Apollo 11 (upper left), 14 (lower left) and 15 (upper right) sites. The French-built array (lower right) projects out from the front of the Soviet Lunokhod rover.

Physical Librations

Many of the lunar geophysical parameters affect the 3-axis lunar rotation and orientation, the physical librations, and that gives LLR sensitivity to those effects. This sensitivity is illustrated by the equations of motion for the vector rotation of the lunar mantle and fluid core. Those three-dimensional rotations are coupled by two interactions at the core/mantle boundary (CMB).

$$\frac{dI_m\omega_m}{dt} + \omega_m \times I_m\omega_m = T_g + T_{cmb} \tag{6}$$

$$\frac{dI_f\omega_f}{dt} + \omega_m \times I_f\omega_f = -T_{cmb} \tag{7}$$

$$T_{cmb} = K_v(\omega_f - \omega_m) + (C_f - A_f)(\hat{z}\cdot\omega_f)(\hat{z}\times\omega_f) \tag{8}$$

The first differential equation is the Euler equation for the mantle with torques on the right-hand side. The rotating mantle provides the frame with axes aligned with the mean principal axes of the mantle.

- I_m is the mantle moment of inertia matrix including tidal deformation. The mean moment matrix is diagonal with principal moments A_m, B_m and C_m, but the tidal variation matrix is 3x3.
- ω_m is the spin rate vector for the mantle. The spin rate components are functions of the Euler angels and their rates.

- T_g is the gravitational torque vector from the lunar gravity field, degree 2-4, interacting with the Earth, Sun, Venus, Mars, and Jupiter. The degree-2 field is subject to variations due to tides and spin. Also included is the figure-figure torque from degree-2 Earth x degree-2 Moon.
- T_{cmb} is the torque vector from two interactions at the fluid-core/solid-mantle boundary. Since the core and mantle have different spin rate vectors, the fluid moves with respect to the solid mantle and forces arise. The CMB dissipation and oblateness forces are the two interactions. Integrating the local torques over the CMB surface gives the total torque. The unit z vector is the mantle principal axis corresponding to moment C_m.

The second differential equation is written for a uniform fluid core, assumed to be rotating like a solid, but using the frame of the mantle. The mantle frame is used because the mantle controls the CMB shape and the nonspherical moments of inertia of the fluid.

- I_f is the fluid moment of inertia tensor including an oblate CMB. The mean moment matrix is diagonal in the mantle frame with principal moments A_f, A_f and C_f.
- ω_f is the spin vector for the mantle.
- Torque $-T_{cmb}$ now enters with sign reversed from the mantle torque.

The above differential equations show that the rotation of the Moon is sensitive to moments of inertia of mantle and fluid core, lunar gravity field, tidal deformation (Love number k_2 with a time delayed response for dissipation), dissipation at the CMB, and flattening at the CMB. The differential equations for vector rotation and lunar and planetary orbits are integrated numerically.

Fluid Core Moment of Inertia

The fluid core moment of inertia is the latest lunar geophysical parameter to emerge from the LLR analysis. This is a valuable new result. Sensitivity comes because the orientations of both mantle and fluid core follow the slow motion of the ecliptic plane, while the core has diminished response to faster variations (see Sidereal Terms in Williams et al., 2001). The solution for the ratio of fluid moment to total moment gives $C_f/C = (12\pm4)\text{x}10^{-4}$. For a uniform liquid iron core without an inner core this value would correspond to a radius of 390±30 km while for the Fe-FeS eutectic the radius would be 415 km. Those two cases would correspond to fluid cores with 2.4% and 2.2% of the mass, respectively. With a solid inner core, assuming that the inner core orientation is gravitationally coupled to the mantle so that they precess together, the fluid moment depends on the fluid density and outer and inner radii, $(8/15)\pi\rho_f(R_f^5 - R_{ic}^5)$. So the outer (CMB) radius would be larger if there is a solid inner core.

In the past we have inferred the fluid core moment of inertia and radius from LLR dissipation results (Williams et al., 2001). Those inferred moments were about half of the new result. Our 2001 paper used Yoder's boundary layer theory for dissipation at the CMB (Yoder, 1995), but did not keep a factor of ½ in Yoder's expression for torque. That factor would reconcile the two approaches. Otherwise, the dissipation results tend to give an upper limit for fluid core moment because any topography on the CMB surface will increase the dissipative torque. Any inner core would provide a second surface for dissipation so that a smaller CMB radius would account for the dissipative torque.

While the new result for core moment is noisy, any core result that involves size and density is important. The moment uncertainty should improve as the LLR data span increases. The

main difficulty with using this direct approach comes from separating three effects, core moment and two free precessions, causing slow motions of the pole in space (Williams et al., 2001). The increasing LLR data span is improving the separation and reducing the uncertainty.

Tides

The elastic response of the Moon to a tide-raising force is given by Love numbers. At the Moon's distance from the Earth, >99% of the size of the tidal response is described by the three second-degree Love numbers. LLR sensitivity to the potential Love number k_2 comes from physical librations. In the above differential equations, our software distorts the mantle moment matrix I_m on the left-hand side while for the gravitational torque T_g on the right-hand side the total moment matrix is distorted (appropriate for a uniform fluid core without an inner core). For the solutions being presented I_f was not distorted in the model, though that refinement is being added to the software. There is a small contribution for spin distortion, but the variation of distortion from spin is small compared to tides. Orbiting spacecraft can determine the lunar Love number k_2 from tidal variation of the gravity field. Results are 0.026±0.003 (Konopliv et al., 2001), 0.0248 in the LP150Q gravity solution (Konopliv, PDS website), and 0.0213±0.0075 (Goossens and Matsumoto, 2008).

While k_2 is a dynamical parameter, the displacement Love numbers h_2 for the vertical tides and l_2 for the horizontal are determined from tidal displacement of the retroreflectors. Tidal variations are about ±0.1 m for vertical and half that for horizontal. If one solves for h_2 and l_2 the correlation is 0.73 and the separation is weakened by an unfavorable distribution of retroreflector X coordinates (toward the mean Earth direction) on the Moon. There is elastic information from the Apollo seismometers, but that information does not extend to the lower mantle and core. Of the three Love numbers, l_2 is least sensitive to the deep zones so we solve for k_2 and h_2 while fixing l_2 at a model value of 0.0105. Solutions give k_2 = 0.0199±0.0025 and h_2 = 0.042±0.008.

Model Love numbers are calculated using seismic P- and S-wave speeds deduced from Apollo seismometry. The seismic speeds have to be extrapolated from the sampled mantle regions into the deeper zone above the core. Figure 4 shows radial profiles for density and seismic speeds. A 340 km liquid iron core was added to a mantle model from Kuskov and Kronrod (1998). The resulting model Love numbers are k_2=0.0225, h_2=0.0394, and l_2=0.0106. Another model with a 390 km radius liquid iron core gives k_2 of 0.0233, h_2 of 0.0408, and l_2 of 0.0107. The Apollo seismic uncertainties contribute several percent uncertainty to the three model Love numbers and the core adds further uncertainty. A larger core increases the model k_2 and h_2 values, but has less effect on l_2. Any partial melt above the core would increase k_2 and h_2.

There are substantial uncertainties, but the k_2 values from LLR as well as Goossens and Matsumoto are more compatible with a smaller core while the Konopliv k_2 values and the LLR h_2 and core moment results favor a larger core. While this apparent conflict is not large compared to uncertainties, it does deserve attention as new results become available. We are exploring whether tidal deformation of the core/mantle boundary will make a significant difference for the LLR k_2 determination.

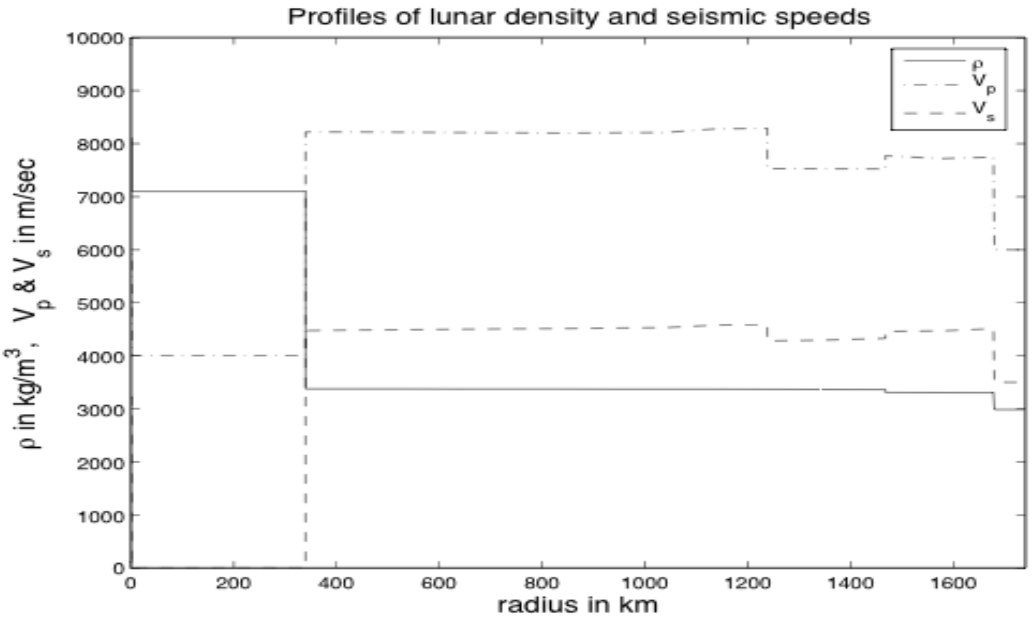

Figure 4. Lunar density and P- and S-wave speeds vs radius. The liquid iron core radius is 340 km. V_P is greater than V_S, and V_S is zero in the fluid.

Dissipation from Tides and Core

There are many small perturbations on the orientation of the lunar orbit and equator planes, but there is one big effect. The Moon's mean orbit plane is tilted by 5.145˚ to the ecliptic plane and the orbit plane precesses in a retrograde direction along the ecliptic plane with a retrograde 18.6 yr period. The lunar equator also precesses along the ecliptic plane with an 18.6 yr period, but the tilt of 1.543˚ is in the opposite direction from the orbit. So the angle between the orbit and equator is 6.69˚. Without dissipation, the ascending node of the orbit matches the descending node of the lunar equator so that the orbit, ecliptic and rotation poles are coplanar. When the rotation is subject to energy dissipation, either from tides or CMB effects, the rotation pole is shifted slightly in the direction of precession, and the alignment of three planes is no longer exact. Such a displacement of the mean pole of rotation/mean equator was seen three decades ago with the LLR data. While at least some of the displacement had to be due to tidal dissipation, it was not then known if the Moon had a fluid core though that possible explanation was proposed by Yoder (1981).

The key to separating the two causes of dissipation was the detection of small physical libration effects of a few milliarcseconds (mas) size. Guided by semi-analytical theories for tide and core dissipation (Williams et al., 2001), we solve for periodic terms in longitude physical librations at 1 yr (annual mean anomaly), 206 d, and 1095 d (1/2 period of argument of perigee) in addition to a tidal time delay and the fluid core K_ν. The tidal time delay and the CMB dissipation are both effective at introducing a phase shift in the precessing pole direction. The three small periodic terms allow for tide-induced phase shifts in physical libration periodicities. Third-degree gravity coefficients also cause phase shifts. We adopt C_{31}, S_{31}, and S_{33} from spacecraft determined LP150Q (Konopliv, website) and use the LLR data to solve for the four remaining third-degree coefficients. The solution gives dissipation from the CMB and tides. Both are strong contributors to the 0.27" offset of the precessing rotation pole from the dissipation-free pole, equivalent to a 10" shift in the node of the equator on the ecliptic plane. There is a weak dependence of tidal specific dissipation Q on

period. The Q increases from ~30 at a month to ~35 at one year. Q for rock is expected to have a weak dependence on tidal period, but it is expected to decrease with period rather than increase. The frequency dependence of Q deserves further attention and should be improved.

Core Oblateness

Detection of the oblateness of the fluid-core/solid-mantle boundary (CMB) is independent evidence for the existence of a liquid core. In the first approximation, CMB oblateness influences the tilt of the lunar equator to the ecliptic plane (Dickey et al., 1994). Parameters for CMB flattening, core moment of inertia, and core spin vector, are introduced into torque T_{cmb} in the numerical integration model used for lunar orientation and partial derivatives. Equator tilt is also influenced by moment-of-inertia differences, gravity harmonics and Love number k_2, solution parameters affected by CMB oblateness. Solutions can be made using the core and mantle parameters.

Torque from an oblate CMB shape depends on the product of the fluid core moment of inertia and the CMB flattening, $fC_f=(C_f-A_f)$. Both are uncertain and there is no information about flattening apart from these LLR solutions. The LLR solution gives $f=(C_f-A_f)/C_f=(2.0\pm2.3)\times10^{-4}$. For a 390 km core radius the flattening value would correspond to a difference between equatorial and polar radii of about 80 m with a comparable uncertainty. The f uncertainty seems to imply no detection, but the oblateness parameter f correlates –0.90 with core moment. The derived oblateness varies inversely with fluid core moment, as expected theoretically, so a smaller fluid core corresponds to a larger oblateness value. The product $fC_f/C=(C_f-A_f)/C=(3\pm1)\times10^{-7}$ is better determined than f alone. Core flattening appears to be detected and the foregoing product is more secure in a relative sense than the value of f itself. In the solution of this paper the corrections to core moment and CMB flattening were substantial compared to the prefit DE421 values. In the earlier solution leading to DE421 the fluid core moment was fixed (Williams, Boggs and Folkner, 2008). Updated values are anticipated with the next ephemeris.

The influence of the CMB flattening on the mantle's forced precession depends on the product of the flattening and core moment, as given above. Core oblateness can also cause a retrograde free precession in space of the orientation of the fluid core, which has a small influence on the mantle. In the case of the Earth, this free precession in space is often considered in a frame rotating with the body and it is often called the free core nutation (FCN). The free precession frequency is proportional to the flattening f (Gusev et al., 2005; Petrova and Gusev, 2005). Since the LLR solution shows a large correlation between core moment and flattening, we conclude that the forced term is more important to the LLR solution than the free precession. The fluid core free precession period (1/fn, where n is mean motion) appears to be greater than a century, >170 yr if we use the solution f plus its uncertainty. Small amplitude and long period make the core free precession difficult to distinguish directly from four decades of LLR data.

The Moon's figure is subject to tide and spin distortions. If the mantle supported no shear stresses, like a fluid, then the Moon's figure would be an equilibrium figure for the tides and spin. The model equilibrium value for the CMB flattening is $f_e=2.2\times10^{-5}$. The equilibrium product f_eC_f/C is an order-of-magnitude smaller than the fC_f/C value found by LLR and the latter would require a 3σ discrepancy to agree with the equilibrium value. Thus, the CMB flattening does not appear to be close to equilibrium. For comparison, the whole Moon degree-2 shape (Smith et al., 1997; Araki et al., 2009; Ping et al., 2008), gravity field (Konopliv et al., 1998, 2001) and moment of-inertia differences (Dickey et al., 1994) are an

order-of-magnitude larger than the equilibrium figure expected from the current tides and spin. The same appears to be true for the CMB flattening.

Free Librations

Dissipation has been recognized by LLR from both tidal flexing and the fluid/solid interaction at the core/mantle boundary. Dissipation introduces a phase shift in each periodic component of the forced physical librations. The differential equations for lunar rotation have normal modes, three for the mantle and one for the fluid core. It might be expected that that the free physical librations associated with these normal modes would be imperceptible since the damping times are short compared to the age of the Moon. However, substantial motions are found for two of the modes (Calame, 1976ab; Jin and Li, 1996; Newhall and Williams, 1997; Chapront et al., 1999; Rambaux and Williams, 2009ab) and we have to ask what is the source of stimulation.

Reported here are results from the recent effort with Rambaux that analyzed the DE421 physical librations. The free physical librations depend on the initial conditions for the Euler angles and spin rates, which are adjusted during the LLR fits. The integrated Euler angles were fit with polynomials plus amplitudes and amplitude rates for trigonometric series. More than 130 periodic terms were recognized in two latitude libration angles, while longitude libration yielded 68. The free libration terms were identified among many forced terms.

The longitude mode is a pendulum-like oscillation of the rotation about the (polar) principal axis associated with moment C. The period for this normal mode is 1056 d = 2.89 yr. Recovering the amplitude is complicated by two forced terms very close to the resonance period. A first approximation for the two forced terms results in a free amplitude of 1.3", or 11 m at the equator. From the dissipation results, the damping time is calculated to be 2×10^4 yr using expressions in Williams et al. (2001).

The lunar wobble mode is analogous to the Earth's polar motion Chandler wobble, but the period is much longer and the path is elliptical. Observed from a frame rotating with the lunar crust and mantle, the rotation axis traces out an elliptical path with a 74.6 yr period. The amplitudes are 3.3"x8.2" (28 m x 69 m). The minor axis of the ellipse is toward the mean Earth direction. LLR has followed this elliptical motion through half a cycle. The computed damping time is about 10^6 yr.

The two remaining free modes are retrograde precession modes when viewed from a nonrotating frame in space. The mantle free precession of the equator (or pole) has an 81 yr period. An amplitude of 0.03" is found for this mode, but there is uncertainty because the LLR fit for the integration initial conditions appears to be sensitive to the lunar interior model. The expected damping time is 2×10^5 yr. The fluid core free precession of the fluid spin vector has an expected period >170 yr, as previously discussed under Core Oblateness; it would be 197 yr for the DE421 integration. Based on the trigonometric analysis, this mode must have a small amplitude.

The two free modes with large amplitudes can be stimulated by internal lunar processes, but internal stimulation is an inefficient way to generate the free precession of the mantle. The longitude mode can also be stimulated by resonance passage, as has been proposed by Eckhardt (1993) and confirmed by Newhall and Williams (1997). Yoder (1981) proposed that the free wobble could be generated by fluid eddies formed at the core/mantle boundary.

Uncertain stimulating mechanisms for free librations, including the possible connection to the lunar interior, makes the free librations of continuing interest.

Search for a Solid Inner Core

It is reasonable to expect that the Moon would have a solid core interior to the fluid core, but it remains undetected. The phase diagram for Fe-FeS shows that cooling of fluid alloys of iron and sulfur would freeze out part of the iron while concentrating sulfur compounds in the fluid (Brett and Bell, 1969). There is no direct evidence for a solid inner core. An inner core might be detected through its influence on physical librations or gravity, or through seismology. Any detection would establish the last major unit of the Moon's structure.

Lunar Laser Ranging is sensitive to small effects in the lunar physical librations. Predicting the size of these effects depends on a number of unknown parameters including the inner core moment of inertia and gravity field, and the mantle's gravity field interior to the CMB. An inner core might be rotating independently or it might lock to the mantle rotation through gravitational interaction. The inner core and mantle interact through their nonspherical gravity fields. This gravitational interaction is probably very much stronger than torques from the fluid core so we assume that the mean rotation rates of mantle and inner core are the same. The inner core also interacts gravitationally with the Earth. Like the mantle, the orientation of the inner core is expected to precess at the same node rate as the mantle, but not necessarily with the equator of the inner core exactly aligned with the mantle's equator. The tilts between the two equators and the ecliptic plane will be different and this difference will cause a small variation in the external gravity field of the Moon that might be detected by spacecraft (Williams, 2007). A strong gravitational interaction between inner core and mantle tends to align their equator planes and a very weak interaction makes the orientations more independent. The inner core rotation dynamics has a resonance if the precession normal mode frequency of the inner core matches the forcing frequency of –1/18.6 yr. Close to such a resonance the two orientations could be very different. There are other forcing frequencies that can also resonate causing potentially observable effects in the physical librations. The frequency of the precession-like normal mode would determine which physical libration terms would get modified most strongly.

An inner core can also modify the physical librations in longitude. There are a large number of forcing terms for longitude librations. The inner core introduces a new normal mode with a natural frequency and that frequency will determine which longitude libration periodicities are most strongly affected. The period of the normal mode might be from less than one year to decades.

To look for inner core effects, the postfit LLR residuals for each retroreflector array have been analyzed to produce spectra. The Apollo 11 and 14 arrays are near the equator (see Fig. 2), so they will be most sensitive to longitude librations. The Apollo 15 array, well north of the equator with a small longitude, provides the most sensitivity to latitude librations. The Lunokhod 2 array is sensitive to both longitude and latitude librations, but the smallest number of observations (477 is 2.8%) gives this array the noisiest spectra. All of the spectra are highest for periods longer than a year. The Apollo 11 spectrum is highest on either side of the 1056 d mantle resonance: 9 mm at 850 d and 10 mm at 1350 d. The Apollo 14 spectral amplitudes are highest at 1200 d (9 mm) and 2200 days (11 mm). The latter period is very interesting because it coincides with a 2190 d = 6.0 yr argument of perigee period that is a forcing term. The phase aligns more closely with the cosine of argument of perigee. If from longitude librations, the amplitude at 6.0 yr should also show in the Apollo 11 spectrum with

opposite sign from Apollo 14, but we find a 5 mm amplitude with the same sign. So we cannot claim detection of an anomalous libration amplitude at 6.0 yr. The amplitudes for the Apollo 15 spectrum are all <5 mm.

The detection of the Moon's inner core will be a major accomplishment for any technique. For LLR it is a future possibility.

Orbit Evolution

Dissipation in the Moon and Earth causes slow changes in the lunar orbit. The semimajor axis and eccentricity increase with time and the inclination decreases. Dissipation in the Moon also deposits heat in the Moon. This is a minor effect now, but could have been much more important when the Moon was closer to the Earth. Here we summarize the orbit changes.

Table 1 presents dissipation-induced secular rates for mean motion n, eccentricity e, and Earth rotation rate ω. LLR results on two lines are compared with model computations on three. The LLR integration model for terrestrial tidal dissipation uses Love numbers and time delays for three frequency bands: zonal (long period), diurnal, and semidiurnal. For DE421 the three Love numbers and the zonal time delay were set to model values. The diurnal and semidiurnal delays were fit to LLR data in creating DE421. For the Moon, the lunar Love number k_2, time delay, and CMB dissipation parameter K_v were fit for DE421. The Earth and Moon related rates in the table are computed from the DE421 Earth and Moon parameters. For the LLR fits, the Earth tide parameters are sensed through the orbit changes, but the lunar parameters are mainly determined from the physical librations. The anomalous eccentricity rate is not present in the DE421 integration, but a rate of unknown cause is routinely found to be significant. For comparison, model values of dn/dt, de/dt and dω/dt were computed for the Earth based on the IERS Conventions (McCarthy and Petit, 2003) for the main body and FES2004 results for the ocean tides (Lyard et al., 2006; Ray, 2007). There is some uncertainty in converting the terrestrial Love numbers and time delays to orbit rates, but the same theoretical expressions were used for converting the LLR and Earth model parameters and that should minimize differences. The results are presented in Table 1.

Table 1. Dissipation-induced rates for mean motion, eccentricity, and Earth rotation comparing LLR to an Earth model.

	units	zonal	diur-nal	semi-diurnal	Earth sum	lunar tides	lunar CMB	Moon sum	anom-alous	total
LLR dn/dt	$''/cent^2$	0.12	-3.31	-22.88	-26.07	0.20	0.02	0.22		-25.85
LLR de/dt	10^{-11} /yr	-0.03	0.16	1.20	1.33	-0.40	0	-0.40	1.32	2.25
model dn/dt	$''/cent^2$	0.12	-3.76	-22.61	-26.25					
model de/dt	10^{-11} /yr	-0.03	0.22	1.54	1.73					
model dω/dt	$''/cent^2$	0	-196	-1125	-1321					

In the table note that the total Earth dn/dt from LLR and the Earth model differ by <1%. An independent LLR analysis for total dn/dt of –25.858 ”/cent^2 (Chapront et al., 2002) gives very good agreement with the DE421 mean longitude acceleration of –25.85 ”/cent^2 given here. The DE421 value corresponds to a 38.14 mm/yr rate for semimajor axis. There is less agreement between eccentricity rate from LLR and the Earth model because the LLR solutions mainly accommodate the tidal acceleration dn/dt that very strongly affects the LLR data. Most of the Earth tide de/dt comes from the N2 tide, while for dn/dt the M2 and O1 contributions are larger. For the lunar tides, the component with the anomalistic period is most important for de/dt. Accounting for the difference in de/dt from the simple LLR integration model and the more complete Earth model, the unexplained eccentricity rate is $(0.9\pm0.3)\text{x}10^{-11}$ /yr, equivalent to an extra 3.5 mm/yr in the perigee rate. The inclination rate is not given in the table since it is computed to be only $-1\text{x}10^{-6}$ ”/yr. The predicted Earth spin rate change is given in the last line of the table. In decreasing order, the most important tides for secular rotation acceleration are M2, S2, K1, O1, and N2. The S2 and K1 tides do not cause secular changes in lunar mean motion or eccentricity.

There is no evidence for any anomaly in the tidal acceleration in mean longitude. By contrast, the anomalous lunar eccentricity rate indicates that something is not understood well enough. Though it cannot be said with certainty that the anomaly comes from the Moon, the lunar interior is less well known than the Earth’s interior. Computation of lunar orbit evolution over long times needs a good understanding of the various contributions to the secular rates. Long-time evolution of the orbit is complex because of evolving lunar thermal conditions and changing ocean tides (Bills and Ray, 1999).

Lunar Ephemeris

Selected lunar and planetary ephemerides are made available for scientific and mission use. The latest recommended lunar and planetary ephemerides and lunar physical librations make up DE421. The DE421 ephemeris may be downloaded in an ascii version from

ftp://ssd.jpl.nasa.gov/pub/eph/planets/ascii/de421 .

The complete set of input parameters for the solar system integration is part of the file. The SPICE kernel version of DE421 is available at

ftp://ssd.jpl.nasa.gov/pub/eph/planets/bsp .

Documentation is available in two memos (Williams, Boggs, and Folkner, 2008; Folkner, Williams, and Boggs, 2008).

Conclusions and Future Possibilities

Among the five major terrestrial bodies, the Moon is a primitive end member. Most of the large surface features are ancient, $3\text{x}10^9$ to $4\text{x}10^9$ yr old compared to the $4.5\text{x}10^9$ yr age of the Earth and Moon. At very early times, at least the upper part of the Moon was molten, perhaps all of it was melted. As the Moon cooled, the crust and mantle solidified, volcanism flooded the Mare areas, became infrequent, and ended. Today’s Moon is slumbering, but not dead.

The analysis of data from several techniques provides clues about the lunar core and deep interior. The lunar mean density and moment of inertia permit a small dense core, but not a large core. That core could be solid or liquid. Analysis of Apollo-era seismic data provides

information on the elastic properties of crust and mantle and shows that S waves damp out for the deep mantle, possibly due to a deep partial melt. P waves penetrate the deepest mantle better, but the seismic data were not able to unambiguously detect a core. Magnetic induction data indicates a small conducting core.

Lunar laser ranging (LLR) physical libration analysis shows that there is a liquid lunar core, first detected from dissipation at the core mantle boundary (CMB) and more recently from detection of CMB flattening and core moment of inertia. The core moment would correspond to a 390 km radius core if the core density is like iron, or larger if it has lower density or if an inner core exists. The core moment is the most important new lunar science result to come out of LLR. The tidal Love numbers are sensitive to internal elastic properties and structure including a core. At present, the LLR determination of the displacement Love number h_2 is compatible with the foregoing core size, but the k_2 Love number would work better with a smaller core. Future lunar range data should improve the uncertainties of the core moment and Love numbers.

Future LLR data should also greatly improve the determination of the CMB flattening which, like the core moment, is a recent detection that needs improvement. Low tidal Qs may result from a partial melt just above the CMB. A better determination of tidal Q vs frequency would be valuable.

Two of the free libration modes have big amplitudes. Future range data should also give insight into the cause of the free librations. The finite free librations require stimulation, but was that stimulation in the past or is it ongoing and possibly observable? Free librations show that the Moon has some activity affecting the dynamics.

LLR also contributes to orbit evolution. The mean motion and eccentricity changes are observed. While the mean motion and semimajor axis rates are compatible with our understanding of dissipation in Earth and Moon, LLR solutions consistently find an anomalous eccentricity rate. The anomalous eccentricity rate is a puzzle that needs to be solved, both for physical understanding and computation of dynamical evolution.

Three years of very accurate ranges from Apache Point Observatory show that our software is not fitting modern ranges to the subcentimeter level when the entire four decades of data are processed. Physical libration signatures were first seen in the postfit OCA residuals and they are clearly visible in the Apache Point residuals. The long-period excess of the residual spectra, discussed under the search for an inner core, could be due to the model or it could imply new science. Our physical models and analysis programs need to be improved to advance the science.

Ranging to the Apollo and Lunokhod retroreflecting arrays has provided a four-decades-long data set that has benefitted several science disciplines. Range accuracies have improved by two orders of magnitude since the Apollo era. The existing arrays spread laser pulses and may be contaminated with dust. A new set of widely distributed retroreflectors would be welcome, as would the recovery of Lunokhod 1. New devices should minimize the pulse spread and should be capable of operating in daylight with minimum thermal degradation of signal strength. A wider geographical distribution than the current pattern (Fig. 2) would increase sensitivity to physical librations and tides. There might be new lunar landers with corner cubes and other geophysical instruments by the middle of the coming decade.

Continued LLR data, improved software and new retroreflectors may open up new science possibilities while improving uncertainties for current solution parameters. New possibilities include the search for an inner core and seeking causes for the free librations. Attention has turned back to the Moon decades after the Apollo era missions. The current set of lunar orbiting spacecraft will be followed by new lunar landers, and that will offer opportunities for new ranging sites and accurate laser ranging for years to come.

Acknowledgments

We thank Richard Gross for making the presentation at the Workshop. The research described in this paper was carried out at the Jet Propulsion Laboratory of the California Institute of Technology, under a contract with the National Aeronautics and Space Administration.

References

Araki, H., S. Tazawa, H. Noda, Y. Ishihara, S. Goossens, S. Sasaki, N. Kawano, I. Kamiya, H. Otake, J. Oberst, and C. Shum, Lunar global shape and polar topography derived from Kaguya-LALT laser altimetry, *Science, 323*, 897-900, 2009.

Bills, B. G., and R. D. Ray, Lunar orbital evolution: a synthesis of recent results, *Geophys. Res. Lett., 26,* 3045-3048, 1999.

Brett, R., A lunar core of Fe-Ni-S, *Geochim. Cosmochim. Acta*, *37*, 165-170, 1973.

Brett, R., and P. M. Bell, Melting relations in the Fe-rich portion of the system Fe-FeS at 30 kb pressure, *Earth and Planetary Sci. Lett., 6*, 479-482, 1969.

Calame, O., Determination des librations libres de la Lune, de l'analyse des mesures de distances par laser, *C. R. Acad. Sc. Paris, 282, Serie B,* 133-135, 1976a.

Calame, O., Free librations of the Moon determined by an analysis of laser range measurements, *The Moon, 15*, 343-352, 1976b.

Chapront, J., M. Chapront-Touzé, and G. Francou, Complements to Moons' lunar libration theory. Comparisons and fits to JPL numerical integrations, *Celestial Mechanics and Dynamical Astronomy, 73*, 317-328, 1999.

Chapront, J., M. Chapront-Touzé, and G. Francou, A new determination of lunar orbital parameters, precession constant and tidal acceleration from LLR measurements, *Astron. and Astrophys., 387*, 700-709, doi:10.1051/0004-6361:20020420, 2002.

Cisowski, S. M., D. W. Collinson, S. K. Runcorn, A. Stephenson, and M. Fuller, A review of lunar paleointensity data and implications for the origin of lunar magnetism, in *Proc. of the 13th Lunar and Planetary Sci. Conf., J. Geophys. Res., 88*, A691-A704, 1983.

Cisowski, S. M., and M. Fuller, Lunar paleointensities via the IRMs normalization method and the early magnetic history of the Moon, in *Origin of the Moon*, edited by W. K. Hartmann, R. J. Phillips, and G. J. Taylor, pp. 411-424, Lunar and Planetary Institute, Houston, 1986.

Collinson, D. W., On the existence of magnetic fields on the Moon between 3.6 Ga ago and the present, *Physics of the Earth and Planetary Interiors*, *34*, 102-116, 1984.

Dickey, J. O., P. L. Bender, J. E. Faller, X X Newhall, R. L. Ricklefs, J. G. Ries, P. J. Shelus, C. Veillet, A. L. Whipple, J. R. Wiant, J. G. Williams, and C. F. Yoder, Lunar laser ranging: a continuing legacy of the Apollo program, *Science, 265*, 482-490, 1994.

Eckhardt, D. H., Passing through resonance: The excitation and dissipation of the lunar free libration in longitude, *Celestial Mechanics and Dynamical Astronomy, 57*, 307-324, 1993.

Folkner, W. M., J. G. Williams, D. H. Boggs, The Planetary and Lunar Ephemeris DE 421, JPL IOM 343R-08-003, March 31, 2008.

Gagnepain-Beyneix, J., P. Lognonné, H. Chenet, D. Lombardi, and T. Spohn, Seismic model of the lunar mantle and constraints on temperature and mineralogy, *Physics of the Earth and Planetary Interiors, 159*, 140-166, 2006.

Garrick-Bethell, I., B. P. Weiss, D. L. Shuster, and J. Buz, Early lunar magnetism, *Science, 323*, 356-359, 2009.

Goins, N. R., A. M. Dainty, and M. N. Toksoz, Lunar seismology: the internal structure of the Moon, *J. Geophys. Res., 86*, 5061-5074, 1981.

Goldstein, B. E., R. J. Phillips, and C. T. Russell, Magnetic permeability measurements and a lunar core, *Geophys. Res. Lett., 3*, 289-292, 1976.

Goossens, S. and K. Matsumoto, Lunar degree 2 potential Love number determination from satellite tracking data, *Geophys. Res. Lett., 35*, L02204, doi:10.1029/2007GL031960, 2008.

Gusev, A., N. Kawano, and N. Petrova, Fine phenomena of the lunar libration, abstract No. 1447 of *Lunar and Planetary Science Conference XXXVI*, 2005.

Hood, L. L., D. L. Mitchell, R. P. Lin, M. H. Acuna, and A. B. Binder, Initial measurements of the lunar induced magnetic dipole moment using Lunar Prospector magnetometer data, *Geophys. Res. Lett., 26*, 2327-2330, 1999.

Jolliff, B. L., M. A. Wieczorek, C. K. Shearer, and C. R. Neal, editors., New Views of the Moon, Reviews in Mineralogy and Geochemistry, vol. 60, The Mineralogy Society of America, Chantilly, VA, USA, 2006.

Jin, W., and J. Li, Determination of some physical parameters of the Moon with lunar laser ranging data, *Earth, Moon and Planets, 73*, 259-265, 1996.

Khan, A., K. Mosegaard, and K. L. Rasmussen, A new seismic velocity model for the Moon from a Monte Carlo inversion of the Apollo lunar seismic data, *Geophys. Res. Lett., 27*, 1591-1594, 2000.

Konopliv, A. S., A. B. Binder, L. L. Hood, A. B. Kucinskas, W. L. Sjogren, and J. G. Williams, Improved gravity field of the Moon from Lunar Prospector, *Science 281*, 1476-1480, 1998.

Konopliv, A. S., S. W. Asmar, E. Carranza, W. L. Sjogren, and D. N. Yuan, Recent gravity models as a result of the lunar prospector mission, *Icarus, 150*, 1-18, 2001.

Konopliv, A. S., the LP150Q lunar gravity field is available on the PDS website http://pds-geosciences.wustl.edu/geo/lp-l-rss-5-gravity-v1/lp_1001/sha/jgl150q1.lbl

Kuskov, O. L., and V. A. Kronrod, Constitution of the Moon 5. Constraints on composition, density, temperature, and radius of a core, *Physics of the Earth and Planetary Interiors, 107*, 285-306, 1998.

Langseth, M. G., S. J. Keihm, and K. Peters, Revised lunar heat-flow values, in *Proc. Lunar Sci. Conf. 7th*, Pergamon Press, pp. 3143-3171, 1976.

Lognonné, P., J. Gagnepain-Beyneix, and H. Chenet, A new seismic model of the Moon: implications for structure, thermal evolution and formation of the Moon, *Earth and Planetary Science Lett.*, *211*, 27-44, 2003.

Lognonné, P., Planetary Seismology, Annual Reviews of Earth and Planetary Sci., 33, 19.1-19.34, doi: 10.1146/annurev.earth.33.092203.122604, 2005.

Lyard, F., F. Lefevre, T. Letellier, and O. Francis, Modelling the global ocean tides: insights from FES2004, *Ocean Dynamics*, *56*, 394-415, 2006.

McCarthy, D. D., G. Petit (eds.), IERS Conventions (2003), IERS Technical Note No. 32, 2003.

Murphy, T. W., E. G. Adelberger, J. B. R. Battat, C. D. Hoyle, R. L. McMillan, E. L. Michelsen, C. W. Stubbs, and H. E. Swanson, APOLLO: One-millimeter Lunar Laser Ranging, in proceedings of 16th International Workshop on Laser Ranging, Poznan, Poland, Oct 13-17, 2008, 2009.

Nakamura, Y., Seismic velocity structure of the lunar mantle, *J. Geophys. Res.*, *88*, 677-686, 1983.

Nakamura, Y., Far deep moonquakes and deep interior of the Moon, *J. Geophys. Res.*, *110*, E01001, doi:10.1029/2004JE002332, 2005.

Newhall, X X, and J. G. Williams, Estimation of the lunar physical librations, *Celestial Mechanics and Dynamical Astronomy*, *66*, 21-30, 1997.

Pearlman, M. R., J. J. Degnan, and J. M. Bosworth, The International Laser Ranging Service, in *Advances in Space Research*, *30 (#2)*, pp 135-143, doi:10.1016/S0273-1177(02)00277-6, 2002.

Petrova, N., and A. Gusev, Modeling of the free lunar libration, abstract No. 1448 of *Lunar and Planetary Science Conference XXXVI*, 2005.

Ping, J. S., Q. Huang, J. G. Yan, J. F. Cao, G. S. Tang, and R. Shu, Lunar topographic model CLTM-s01 from Chang'E-1 laser altimeter, submitted, 2008.

Ray, R., http://bowie.gsfc.nasa.gov/ggfc/tides/harm_fes04.html, 2007.

Rambaux, N., and J. G. Williams, A new determination of the normal modes of the Moon's libration, abstract for Division on Dynamical Astronomy meeting, Virginia Beach, VA, May 2-5, 2009a.

Rambaux, N., and J. G. Williams, The Moon's physical librations and determination of the free librations, in preparation, 2009b.

Righter, K., and M. J. Drake, Core formation in Earth's Moon, Mars, and Vesta, *Icarus*, *124*, 513-529, 1996.

Russell, C. T., P. J. Coleman Jr., and B. E. Goldstein, Measurements of the lunar induced magnetic moment in the geomagnetic tail: Evidence for a lunar core?, in *Proc. Lunar Planetary Science Conf. 12th*, pp. 831-836, 1981.

Schultz, P. H., M. I. Staid, and C. M. Pieters, Lunar activity from recent gas release, *Nature*, *444*, 184-186, doi: 10.1038/nature05303, 2006.

Sellers, P. C., Seismic evidence for a low-velocity lunar core, *J. Geophys. Res. Planets*, *97*, 11663-11672, 1992.

Smith, D. E., M. T. Zuber, G. A. Neumann, and F. G. Lemoine, Topography of the Moon from the Clementine lidar, *J. Geophys. Res., 102,* 1591-1611, 1997.

Spohn, T., W. Konrad, D. Breuer, and R. Ziethe, The longevity of lunar volcanism: implications of thermal evolution calculations with 2D and 3D mantle convection models, *Icarus, 149*, 54-65, 2001.

Stooke, P. J., Lunar laser ranging and the location of Lunokhod 1, abstract #1194, *Lunar and Planetary Science Conference XXXVI*, 2005.

Stooke, P. J., The International Atlas of Lunar Exploration, Cambridge University Press, New York, 2007.

Warren, P. H., and K. L. Rasmussen, Megaregolith insulation, internal temperatures, and bulk Uranium content of the Moon, *J. Geophys. Res., 92,* 3453-3465, 1987.

Williams, J. G., X X Newhall, and J. O. Dickey, Lunar Moments, Tides, Orientation, and Coordinate Frames, *Planetary and Space Science, 44*, 1077-1080, 1996.

Williams, J. G., D. H. Boggs, C. F. Yoder, J. T. Ratcliff, and J. O. Dickey, Lunar rotational dissipation in solid body and molten core, *J. Geophys. Res. Planets, 106,* 27933-27968, 2001.

Williams, J. G., and J. O. Dickey, Lunar Geophysics, Geodesy, and Dynamics, Proceedings of 13th International Workshop on Laser Ranging, October 7-11, 2002, Washington, D. C., eds. R. Noomen, S. Klosko, C. Noll, and M. Pearlman, NASA/CP-2003-212248, pp. 75-86, 2003. http://cddisa.gsfc.nasa.gov/lw13/lw_proceedings.html

Williams, J. G., S. G. Turyshev, D. H. Boggs, and J. T. Ratcliff, Lunar Laser Ranging Science: Gravitational Physics and Lunar Interior and Geodesy, in *Advances in Space Research, vol. 37, Issue 1*, The Moon and Near-Earth Objects, 67-71, doi: 10.1016/j.asr.2005.05.13, 2006. [arXiv:gr-qc/0412049]

Williams, J. G., A Scheme for Lunar Inner Core Detection, *Geophysical Research Letters*, *34*, L03202, doi:10.1029/2006GL028185, (Feb 9) 2007.

Williams, J. G., D. H. Boggs and W. M. Folkner, DE421 Lunar Orbit, Physical Librations, and Surface Coordinates, JPL IOM 335-JW,DB,WF-20080314-001, March 14, 2008.

Yoder, C. F., The free librations of a dissipative Moon, *Philos. Trans. R. Soc. London Ser. A, 303*, 327-338, 1981.

Yoder, C. F., Venus' free obliquity, *Icarus, 117,* 250-286, 1995.

Creation of the New Industry-standard Space Test of Laser Retroreflectors for GNSS, Fundamental Physics and Space Geodesy: the "SCF-Test"[1]

S. Dell'Agnello (1)**, G. O. Delle Monache** (1)**, D. G. Currie** (2)**, R. Vittori** (3)**, C. Cantone** (1)**, M. Garattini** (1)**, A. Boni** (1)**, M. Martini** (1)**, C. Lops** (1)**, N. Intaglietta** (1)**, R. Tauraso** (4)**, D. A. Arnold** (5)**, G. Bianco** (6)**, M. R. Pearlman** (5)**, M. Maiello** (1)

(1) Laboratori Nazionali di Frascati (LNF) dell'INFN, Frascati (Rome), Italy
(2) University of Maryland (UMD), College Part, MD, USA
(3) Italian Air Force, Rome, Italy
(4) University of Rome Tor Vergata and INFN-LNF, Rome, Italy
(5) Harvard-Smithsonian Center for Astrophysics (CfA), Cambridge, MA, USA
(6) ASI, Centro di Geodesia Spaziale "G. Colombo" (CGS), Matera, Italy

Abstract

We created a new experimental apparatus (the SCF[2]) and a new test procedure (the SCF-Test) to characterize and model the detailed thermal behavior and the optical performance of laser retroreflectors in space for industrial and scientific applications. One of the primary goals of this innovative tool is to provide critical capabilities in a timely fashion for the advent of the European GNSS, GALILEO: (i) validation of the functionality of GNSS laser retroreflector payloads; (ii) optimization of their design in order to maximize the efficiency of satellite laser ranging (SLR) observations by the International Laser Ranging Service (ILRS). This will allow for a significant improvement of the positioning of GNSS satellites, both in terms of absolute accuracy and of long-term stability. Thanks to its superior H-maser clocks and SCF-Tested retro-reflectors GALILEO will also provide a large improvement in the measurement of the gravitational redshift. The SCF-Test was developed in the context of the ETRUSCO [1] experiment of INFN (approved in Summer 2006) at INFN-LNF, Frascati (Italy), a large-scale infrastructure of the European Research "Framework Programme" (FP). This research has been funded by INFN and carried out at two dedicated LNF facilities, in collaboration with Italian and American partners. Since a comprehensive and non-invasive space characterization like the SCF-Test has never been performed before, the results reported in this paper are important to understand the SLR performance on current and future GNSS, as well as the fundamental physics reach of 2nd generation lunar laser ranging (LLR). We identified the SCF-Test as a missing industry standard for space applications and as a missing critical service/functionality for GALILEO. We proposed its adoption as a tool for the simulation and testing of GALILEO SLR and of 2nd generation LLR for the "International Lunar Network" (ILN) and for NASA's manned landings.

SCF-Test of the "GPS3" Laser Retroreflector Array Flight Model

The full description of ETRUSCO, the SCF, the SCF-Test and the test results obtained on cube corner retroreflector (CCR) prototypes of GLONASS/GIOVE and of LAGEOS can be found in [1]. Here we report the results of the SCF-Test of the 3rd and last existing laser retroreflector array (LRA) flight model built in Russia for the GPS-2 GNSS constellation. We call this LRA the "GPS3". The GPS3, now loaned to LNF, is property of UMD.

[1] Presented by S. Dell'Agnello at the 16th ILRS Workshop, Poznan, Poland, October 13-17, 2008.
[2] Satellite/lunar laser ranging Characterization Facility, Frascati (Rome), Italy.

The New Industry-Standard Space Test of Laser Retroreflectors: the "SCF-Test"

The SCF-Test consists of the integrated thermal and optical measurements described below performed on LRA breadboards, prototypes or payloads. The SCF-Test is innovative. Its comprehensive and non-invasive set of measurements was never performed before. For example, it was not done on LAGEOS I and LAGEOS II. It was also never done for GNSS. The SCF-Test concept for an orbital configuration corresponding to the sunlit to earth shadow transition is shown in Fig. 1.

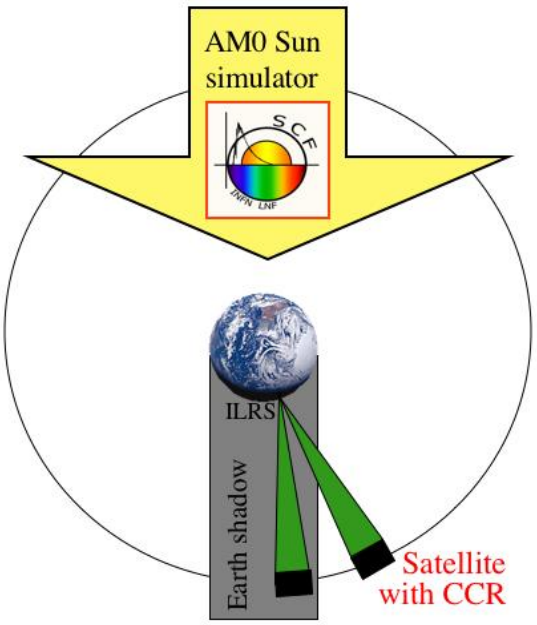

Figure 1. SCF-Test conceptual drawing.

The new test that we developed and validated with GNSS and LAGEOS CCRs consists of several measurements and software simulations, which include:

- Hold the average temperature of the LRA mechanical support structure (Al for LAGEOS, GLONASS, GPS-2, GIOVE-A/B), T_M, to the expected value, T_{AVG}. T_{AVG} has been estimated with thermal simulations for LAGEOS. T_{AVG} is an input to the SCF-Test. Evaluate with SCF data and TRS models:
    1. CCR surface temperature and τ_{CCR}.
    2. CCR far field diffraction patterns (FFDPs) in representative space conditions (see Fig. 2, left) and in air/isothermal conditions (Fig. 2, right). FFDPs are measured with the external optical circuit [1][2].
    3. Surface temperature of non-CCR components of the LRA.
    4. Temperature difference between the CCR outer face and its corner inside the cavity. This evaluation is a combination of measurement plus modeling to assess the CCR optical functionality.
    5. Repeat the above for T_M different from T_{AVG}, in the appropriate range.

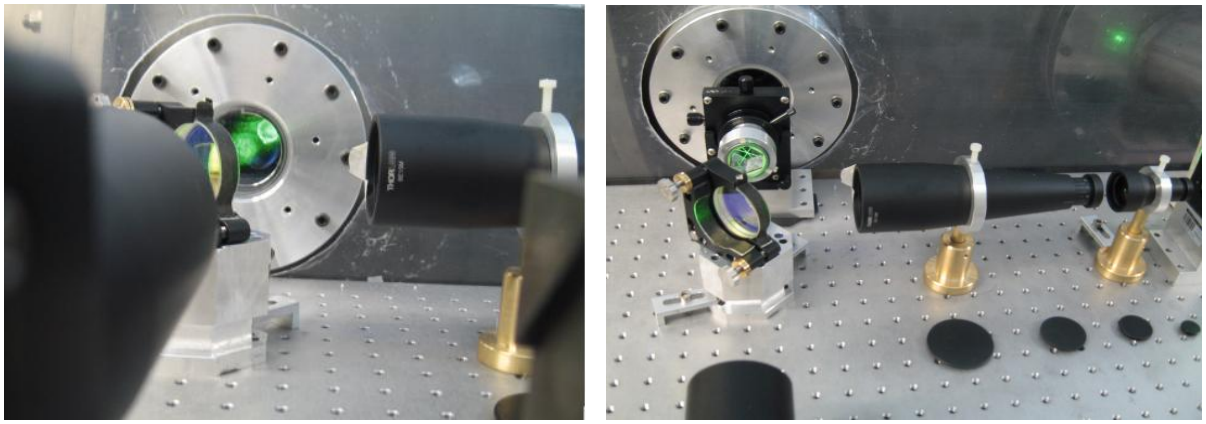

Figure 2. FFDP measurement of a Glonass CCR inside the SCF (left) and at STP (right).

- Repeat the above for different Sun illumination conditions:
    1. transition from SS turned off to on and vice versa (effect of Earth shadow)
    2. varying incidence angles of the Sun illumination
    3. different times along the thermal relaxation curve.
- Tune the TRS models to the *SCF data* for "static" climatic conditions, in which the Sun Simulator and Earth Simulator are turned on and off alternatively.
- Use validated TRS and CODEV simulations to model the LRA behavior for generic orbit and spin configurations (ie, *SPACE data*).

FFDP Test in Air/Isothermal Conditions of the GPS3 at 632 nm

We performed the FFDP test of each single CCR in air and isothermal conditions at 632 nm laser wavelength in the Optics Lab [2]. Figure 3 shows FFDPs of 4 CCRs mounted with different relative orientations. For 12 CCRs, like the bottom left of Fig. 3, the two peaks are almost blend into one. In the presence of thermal perturbations "blended" peaks will separate into two peaks; this has been demonstrated by the GLONASS SCF-Test reported in [1].

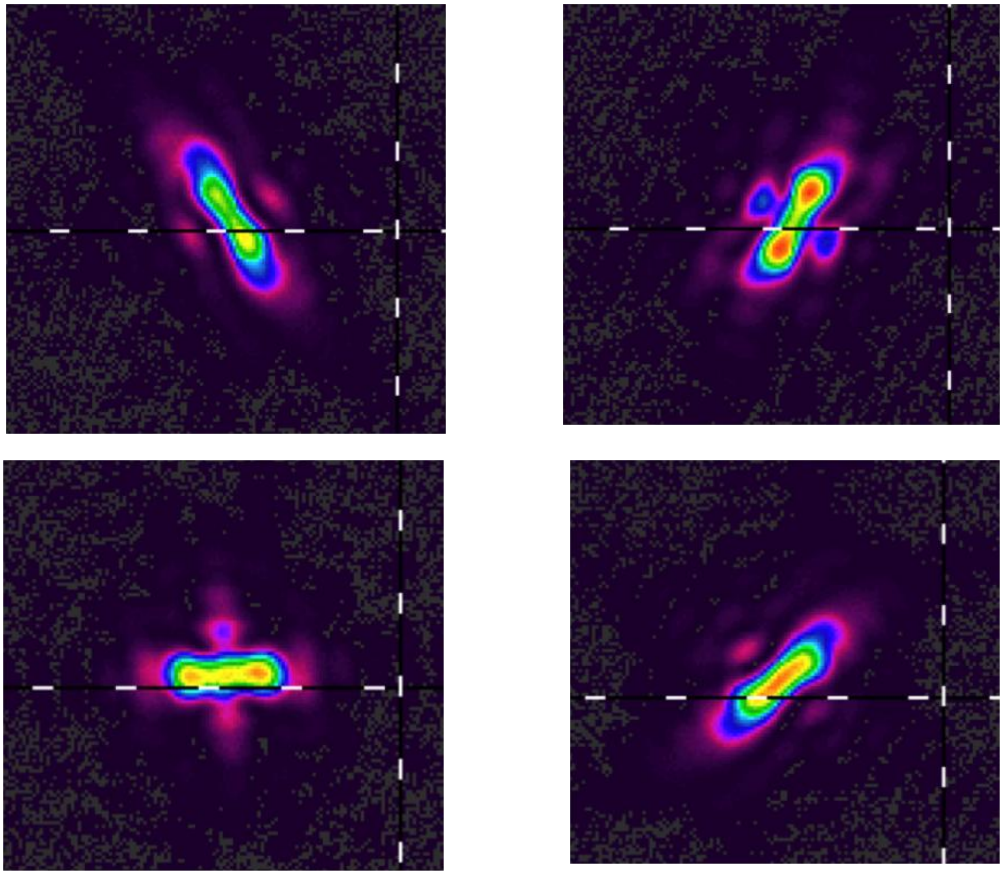

Figure 3. FFDPs of flight GPS3 retroreflectors in air, T = 22^{o}C and 632 nm.

Fig. 4 shows the distance between the two peaks of the 20 CCRs whose FFDP has two cleanly separated peaks. The CodeV prediction assumes the nominal 50 μrad central value of the GPS velocity aberration and a uncertainty of 5 μrad related to the inaccurate knowledge of the FFDP circuit.

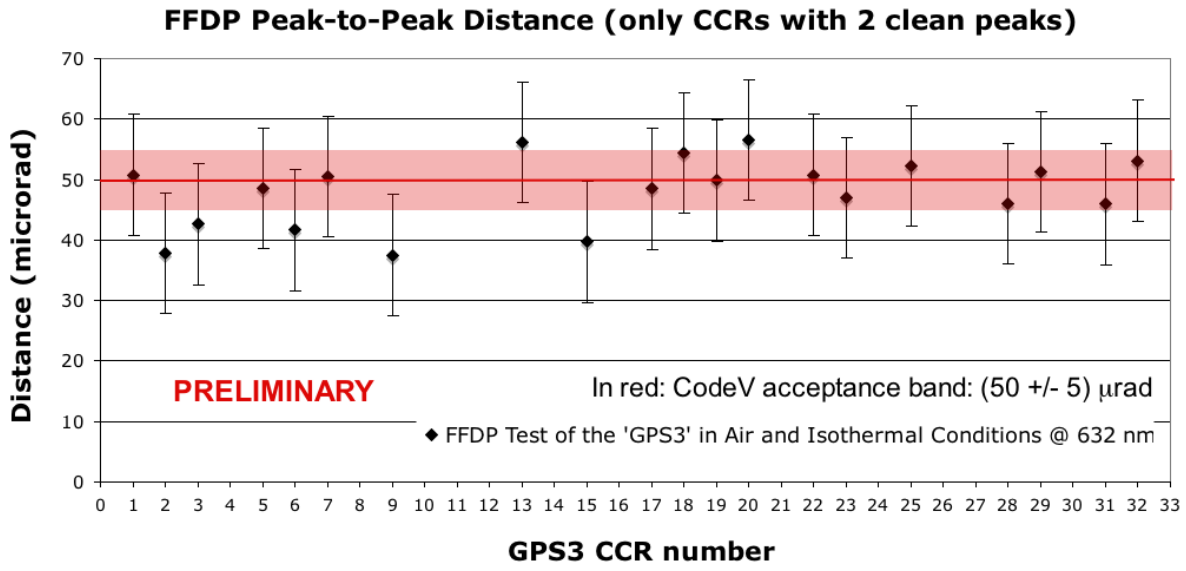

Figure 4. FFDP of the GPS3 retroreflectors with two separate peaks.

SCF-Test of the GPS3 at 532 nm

We performed the SCF-Test of four CCRs at 532 nm laser wavelength. The measurement and analysis is described in detail in [1]. The GPS3 temperature was controlled with a custom copper plate (Fig. 5, left) in thermal contact with the array Al base plate (Fig. 5, center) via indium washers. The copper plate is in turn thermally controlled with a fluid driven by an external chiller. The temperature of the array Al back plate is measured via a PT100 probe (Fig. 5, center) and during the test it was set to (19±1)^{o}C. The solar constant had a slightly reduced value of (0.92±0.02)×AM0 due to technical reasons.

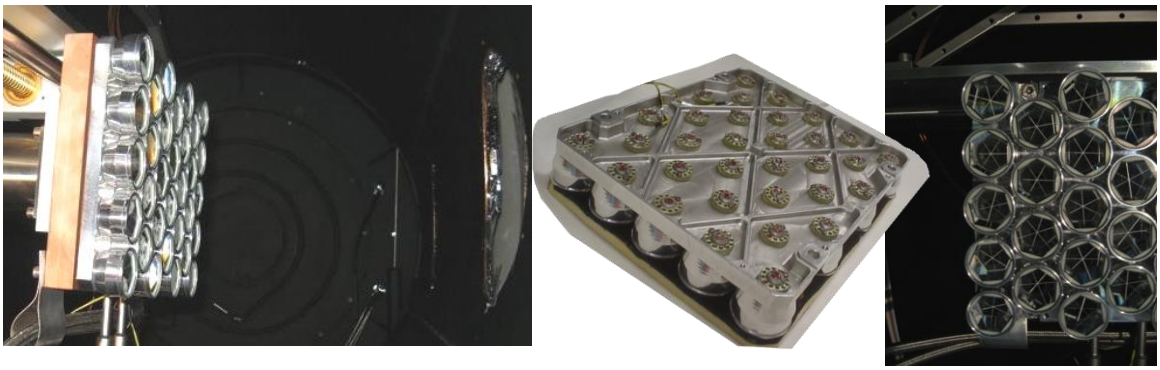

Figure 5. GPS3 in the SCF on the Cu thermal control plate and roto-translation system (left); GPS3 Al back with PT100s; (center); CCRs with staggered orientations (right).

Here we present the FFDP variations vs. time for one CCR of the GPS3. The temperature variation of the front face of this CCR, its "hot" and "cold" FFDPs are shown in Fig. 6. The FFDP behavior vs. time is shown in Fig. 7. The oscillation of the FFDP peak heights shown in Fig. 7 (top) for times above 2000 sec is due to a few degree instability of the thermal control system. This technical issue has now been solved, but it shows that small LRA bulk

temperature changes directly influence the LRA optical performance. This is a 20% effect due to a few-degree change.

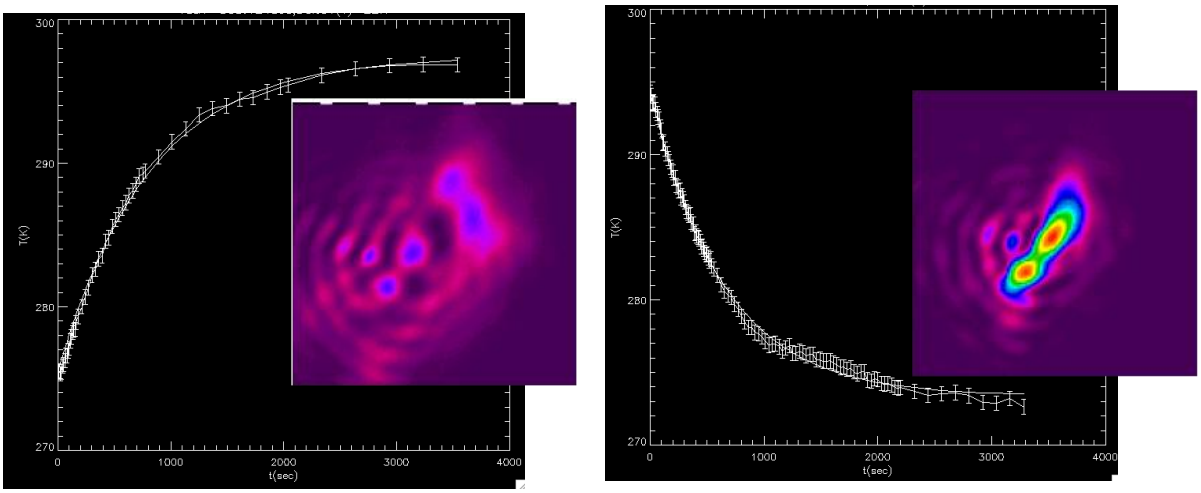

Figure 6. Front face CCR temperature and CCR FFDP at the end heating (left). Front face CCR cool-down curve and its FFDP 3000 sec after the SS has been turned off.

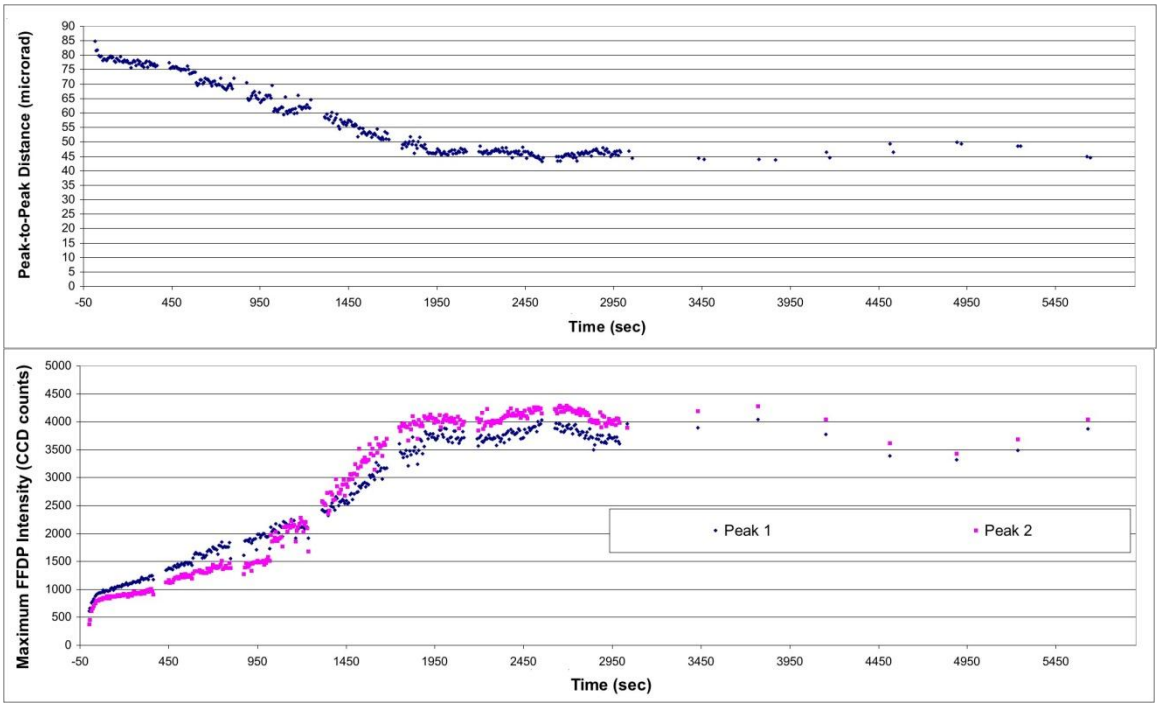

Figure 7. CCR cool-down: FFDP peak distance vs. time (top); maximum FFDP intensities at the average velocity aberration of ILRS stations vs. time (bottom).

These data show that the optical performance is significantly degraded for this geometric and thermal configuration. The FFDP peaks are disrupted and the FFDP intensity is scattered all over the place. For the first 10-20 seconds it is hard to define peaks. The fast decrease/increase of the peak distance/height that is clearly visible for the SCF-Test of the GLONASS 2007 CCRs [1] is less clearly visible for these late '80s GPS-2 CCR. The degradation of the initial "hot" FFDP is worse than for the GLONASS prototype, probably

because the GPS3 is an older and less optimized payload. However, the reduction in intensity between the hot and cold conditions is a factor about 7, exactly like for the SCF-Test of the more recent GLONASS CCR.

Based on their nominal specifications (number of cubes, their size, Al-coating, etc) and assuming isothermal conditions, the GPS LRAs are known to provide a LIDAR optical cross section about a factor 5 lower than the 100 million m^2 required by ILRS for GPS altitudes [3][4]. Thermal perturbations like those measured with our SCF-Test represent a dramatic degradation of this cross section, by a factor of about 7.
SCF-Tests help predict the SLR signal strength of the GPS3 in orbit. This requires correcting the data for the residual instrumental effects, differences between the SCF and orbital configurations, computing the optical cross section and correcting that for the $(\text{distance})^{-4}$ reduction. Since GALILEO is higher than GPS/GLONASS/Compass, greater care must be taken to make the return pattern uniform when the satellite moves across the sky and to avoid degradations due to on-board thermal effects. Our ultimate goals is provide data useful to optimize the LRA design and boost the signal strength to allow for daylight ranging by the majority of ILRS stations (unlike now). This in turn will allow SRL-only orbits to be computed more frequently than weekly. Week-average SLR-only orbits were computed during the important SLR tracking campaign of GIOVE-A in 2006 [5].

Acknowledgments

Very special thanks to E. Saggese and M. Bizzarri of ASI for encouraging and inspiring this work.
We then wish to warmly thank: C. O. Alley for making the GPS3 available to LNF; V. Vasiliev of the Institute of Precision Instrumentation Engineering (IPIE) of Moscow for making the GLONASS CCRs available to LNF; J. McGarry and T. Zagwodzki of NASA-GSFC for making the LAGEOS sector also available for testing at the LNF facilities.
We thank G. Giordano of INFN-LNF for allowing the use of the “Ex-Virgo” Optics Lab: this helped tremendously our work.
We are also indebted to M. Calvetti, U. Bottigli, S. Bertolucci, F. Ronga, B. D’Ettore Piazzoli, C. Sanelli and V. Chiarella of the INFN and LNF Management for supporting and encouraging this research activity.
The LNF Support Services, Cryogenics, SSCR, Electronics and Automation, also gave a significant help to the success of the experimental program.

References

[1] *Creation of the New Industry Standard Space Test for Laser Retroreflectors for GNSS, Fundamental Physics and Space Geodesy: the SCF-Test*, S. Dell'Agnello, G. O. Delle Monache, D. G. Currie, R. Vittori, et al, INFN-LNF Report LNF-09/02(P).
[2] *Optical Far Field Diffraction Pattern Test of Laser Retroreflectors for Space Applications in Air and Isothermal Conditions at INFN-LNF*, A. Boni, C. Cantone, S. Dell’Agnello, G. O. Delle Monache, M. Garattini, N. Intaglietta, C. Lops, M. Martini, L. Porcelli, INFN-LNF Report LNF-08/26(IR), 2008.
[3] The following document describes the rationale for LRAs on GNSS: http://ilrs.gsfc.nasa.gov/docs/retroreflector_specification_070416.pdf.

[4] This document reports the up-to-date *ILRS Standard for Retroreflector Arrays at GNSS Altitudes*: http://ilrs.gsfc.nasa.gov/docs/ILRSRetroreflectorStandards_200812.pdf. The ILRS has established a standard for the "effective cross section" (or active area times gain) to provide sufficient return signal strength.

[5] *GIOVE's Track*, M. Falcone, D. Navarro-Reyes, J. Hahn, M. Otten, R. Piriz, M. Pearlman, GPS World, page 34, November 2006; www.gpsworld.com.

Confirming the Frame-Dragging Effect with Satellite Laser Ranging

John C. Ries, Richard J. Eanes, Michael M. Watkins
The University of Texas at Austin, Center for Space Research, USA
ries@csr.utexas.edu

Abstract

The theory of General Relativity predicts several non-Newtonian effects that have been observed by experiment, but one that has proven to be challenging to directly confirm is the so-called 'frame dragging' effect. One manifestation of this effect is the Lense-Thirring precession of a satellite's orbital plane due to the Earth's rotation. While the signal is large enough to be easily observed with satellite laser ranging, the Lense-Thirring measurement uncertainty is limited by the knowledge of the even zonal harmonics of the Earth's gravity field that also produce Newtonian secular orbit precessions. In the late 1980's, it was proposed to launch the LAGEOS-3 satellite matching LAGEOS-1, except that the orbit inclination would be exactly supplementary to LAGEOS-1. This would have allowed the cancellation of the equal but opposite orbit precession due to the Earth's gravity field to reveal the Lense-Thirring precession. However, this satellite was never launched, and the orbit selected for LAGEOS-2 was not sufficiently close to the proposed LAGEOS-3 orbit specifications to support an accurate Lense-Thirring experiment with the available gravity models. However, this problem has been largely overcome with the dramatically improved models resulting from the joint NASA-DLR Gravity Recovery and Climate Experiment (GRACE) mission. Using laser ranging to LAGEOS-1 and LAGEOS-2, we demonstrate, with an error analysis based on several now-available GRACE gravity models, that the General Relativity prediction of the Lense-Thirring precession can be confirmed with an uncertainty better than 15%, in good agreement with previously published results. In addition, with extensive modeling improvements in the various models, including the terrestrial reference frame and solid earth and ocean tides, we show that a credible experiment can be conducted with just four years of SLR overlapping the GRACE mission.

Status of the LARES Experiment for Accurate Measurements of Earth Gravitomagnetism

Ignazio Ciufolini, Antonio Paolozzi, Erricos Pavlis
University of Salento, Italy
ignazio.ciufolini@unile.it

Abstract

LARES (LAser RElativity Satellite) is a laser ranged satellite of the Italian Space Agency (ASI) for accurate measurement of the Earth gravitomagnetic field (Lense-Thirring effect). We descibe the status of this experiment that will be launched with the VEGA maiden flight.

Accurate atmospheric correction of two-frequency SLR observations

Dudy D. Wijaya, Fritz K. Brunner
Institute of Engineering Geodesy and Measurement Systems
Graz University of Technology, Austria
dudy@gd.itb.ac.id & fritz.brunner@tugraz.at

Abstract

We have developed a new atmospheric correction formula for two-frequency SLR observations based on the theory of the two-frequency range correction. This new formula eliminates the total atmospheric density effects and takes into account all the remaining propagation effects except those caused by atmospheric turbulence. Numerical simulations show that this new formula completely reduces all propagation effects at any elevation angle with an accuracy better than 1 mm.
The required information about the water vapour distribution along the propagation path can be calculated using GPS or Water Vapour Radiometer data. The accuracy demand on this data is moderate, thus we propose to use a co-located GPS receiver. The curvature effects can be calculated by an accurate ray-tracing algorithm or a model. However, the required precision for the difference of the two-frequency SLR measurements, i.e. better than 30µm for a single epoch, exceeds the capability of the current state-of-the-art SLR systems.

1. Motivation

The International Association of Geodesy (IAG) has inagurated a new global service, namely, Global Geodetic Observing System (GGOS). This global service is dedicated to ensure precise long-term monitoring of the geodetic observables related to the global reference frame definition, the dynamic of atmosphere and ocean, the global hydrological cycle as well as natural hazards and disasters by integrating different geodetic techniques, different models and different approaches (see www.ggos.org). In the frame of GGOS, the accuracy requirement of Satellite Laser Ranging (SLR) observations has to be at the millimeter level (Rothacher, 2005). However, the demand to increase the accuracy of the measurements has shown that their ultimate accuracy is limited by the correction of the atmospheric propagation effects.

For the single frequency SLR system, Marini and Murray (1973) proposed in 1973 their model reflecting the precision requirement at that time. Since then all known developments of improved atmospheric correction formulae were based on the Marini-Murray scheme. For example, Mendes et al. (2002) developed new mapping functions (FCULa and FCULb) to scale the zenith delay to other elevation angles. Finally, Mendes and Pavlis (2004) proposed a new zenith delay model which was then adopted as the standard model for refraction modeling. The latest progress is due to Hulley and Pavlis (2007) who used a ray-tracing technique to calculate the propagation effects, including the effects of horizontal refractivity gradients.

The alternative to modeling is the use of two-frequency SLR measurements for the direct computation of the propagation effects by utilizing the dispersion in the electrically neutral atmosphere. The dispersion causes the optical path lengths (OPLs) at two different frequencies to differ in proportion to the path integrated atmospheric density. Thus, the

difference of the two OPLs can be used to calculate one of the propagation effects. This system obviously has the potential to improve the accuracy of SLR results. For a two-frequency SLR system, one atmospheric correction formula is known that originally was proposed by M.T. Prilepin (see ref [12] in Abshire and Gardner, 1985) and his formula was later studied by several investigators (e.g. Bender and Owens,1965; Abshire and Gardner, 1985; Greene and Herring, 1986). It has become the standard atmospheric correction formula for two-frequency SLR systems.

The standard formula can reduce the largest part of the propagation effects, namely the dry atmospheric density. The remaining effects such as the water vapor density and curvature effects are neglected. At the optical frequencies, water vapor contributes only about 1% of the group refractivity, however, it can introduce substantial errors. Numerical simulations show that the water vapor effects amount to a few mm for SLR observations in the zenith direction. Furthermore, the magnitude of the curvature effects could be a few cm for observations taken at an elevation angle lower than 10^0. Based on the above facts, it seems important to improve the standard formula by considering all propagation effects, so that the accuracy of SLR observations as required by the GGOS service can be fulfilled.

We have developed a new atmospheric correction formula for two-frequency SLR observations based on the theory of the two-frequency range correction of Gu and Brunner (1990). The propagation effects of the first and second frequency measurements are evaluated along the same ray path. This new formula eliminates the total atmospheric density effect including its gradient and provides two terms to calculate the water vapor and curvature effects. In the following sections, we first present briefly the derivations of the new formula. Then we summarize results from the investigations of the new formula.

2. Derivation of the new formula

Since the electrically neutral atmosphere is a dispersive medium for optical waves, the propagations of the first and second SLR frequencies are slightly different. In Figure 1, we depict a slight separation of the ray path p_1 of frequency f_1 from the ray path p_2 of frequency f_2, where $f_1 < f_2$ is assumed. Based on the theory of the two-frequency range correction, the propagation effects of frequency f_2 can be evaluated along the ray path p_1,or vice versa. Thus, we are able to investigate the propagation effects of both frequencies along the same ray path. Following the assumptions made by Gu and Brunner (1990), the derivations presented here also assume the applicability of the geometrical optics approximation and neglect atmospheric turbulence effects.

The OPLs for f_1 and f_2 are denoted by R_1 and R_2, respectively. The straight line distance between the two points O and X is denoted by S. For a specific time instance, the refractive index n can be expressed as a function of frequency f_1 and position $\vec{r}_i$, $n(f_i, \vec{r}_i)$. The OPL is obtained by integrating the refractive index along the ray path that satisfies the ray equation (Born and Wolf, 1999) and can then be expressed as

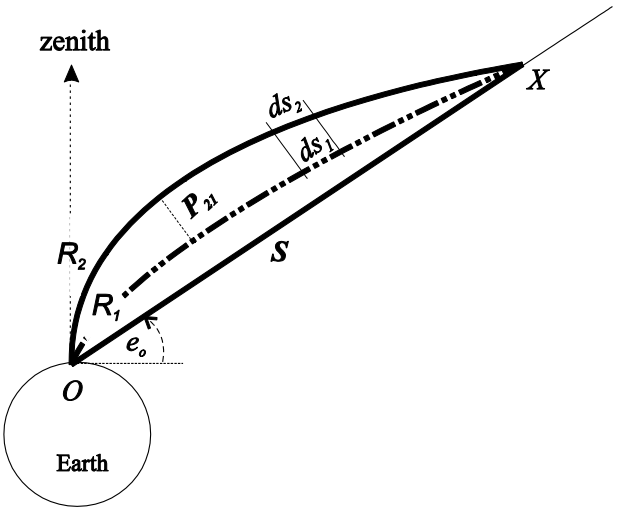

Figure 1. The geometrical scheme of the propagation of SLR signals through the electrically neutral atmosphere. The OPL for f_1 (R_1) is slightly different to that for f_2 (R_2). P_{21} is the propagation correction term and e_o is the chord elevation angle.

$$R_1 = \int_{p_1} n(f_1, \vec{r}_1)\, ds_1 \tag{1}$$

$$R_2 = \int_{p_2} n(f_2, \vec{r}_2)\, ds_2 \tag{2}$$

In order to use R_2 for the calculation of the propagation effects, the integral in Eq.(2) needs to be expressed along the ray path p_1 rather than p_2. Thus, following Gu and Brunner(1990), R_2 may be expressed as

$$R_2 = \int_{p_1} n(f_2, \vec{r}_1)\, ds_1 + P_{21} \tag{3}$$

where the term P_{21} represents the propagation corrections from the ray path p_1 to p_2 and is expressed as

$$P_{21} = \int_{p_2} n(f_2, \vec{r}_2)\, ds_2 - \int_{p_1} n(f_1, \vec{r}_1)\, ds_1 \tag{4}$$

Furthermore, we can express $S = \int_{p_1} ds_1 - K_1$ and by combining it with Eq.(1) and Eq.(3), we obtain

$$R_1 = S + \int_{p_1} \left[n(f_1, \vec{r}_1) - 1 \right] ds_1 + K_1 \tag{5}$$

$$R_2 = S + \int_{p_1} \left[n(f_2, \vec{r}_1) - 1 \right] ds_1 + K_1 + P_{21} \tag{6}$$

K_1 is the arc-to-chord correction for the ray path p_1. General expression for K_1 and P_{21} can be found in Gu and Brunner (1990).

The OPLs R_1 and R_2 are now expressed along the same ray path, which allows us to calculate the propagation effects along the ray path p_1 only. The next step is to provide an expression for the refractivity term $\left[n(f_i,\vec{r}_i)-1\right]$. A separation of a frequency term from the atmospheric variables would be very useful. Thus, we express the refractivity as a function of the atmospheric density ρ, which depends on time and position, and the dispersion constant k, which depends on frequency only. The refractivity can be expressed as

$$10^6\left[n(f_i,\vec{r}_i)-1\right]=k_d(f_i)\,\rho_t(\vec{r}_i)+k_v^*(f_i)\,\rho_v(\vec{r}_i) \tag{7}$$

where $k_v^*(f_i)=k_v(f_i)-k_d(f_i)$. $k_d(f_i)$ and $k_v(f_i)$ are the dispersion constants for dry air and water vapor, respectively. ρ_t and ρ_v are the atmospheric total density and the water vapor density, respectively. By substituting the above equation into Eq.(5) and Eq.(6), we obtain

$$R_1=S+10^{-6}k_d(f_1)\int_{p_1}\rho_t(\vec{r}_1)ds_1+10^{-6}k_v^*(f_1)\int_{p_1}\rho_v(\vec{r}_1)ds_1+K_1 \tag{8}$$

$$R_2=S+10^{-6}k_d(f_2)\int_{p_1}\rho_t(\vec{r}_1)ds_1+10^{-6}k_v^*(f_2)\int_{p_1}\rho_v(\vec{r}_1)ds_1+K_1+P_{21} \tag{9}$$

From the above equation, it is clear the OPLs R_1 and R_2 contain the same quantities of the atmospheric total density and the water vapor density as well as the curvature effects, which are evaluated along the same ray path p_1. Therefore, we can rigorously eliminate the unknown integral $\int_{p_1}\rho_t(\vec{r}_1)ds_1$, which now yields

$$S=R_1+\nu(R_1-R_2)+(\nu P_{21}-K_1)+\mathrm{H}_{21}.\mathrm{SIWV} \tag{10}$$

where the power of dispersion ν is

$$\nu=\frac{k_d(f_1)}{k_d(f_2)-k_d(f_1)} \tag{11}$$

the water vapor factor H_{21} is

$$\mathrm{H}_{21}=10^{-6}k_v^*(f_1)\,\nu\left(\frac{k_v^*(f_2)}{k_v^*(f_1)}-\frac{k_d(f_2)}{k_d(f_1)}\right) \tag{12}$$

the slant integrated water vapor (SIWV) is

$$\mathrm{SIWV}=\int_{p_1}\rho_v(\vec{r}_1)ds_1 \tag{13}$$

The second term in Eq.(10) contains the dispersion effects, the third term represents the curvature effects of the ray path p_1 and the propagation corrections from p_2 to p_1, and the last term represents effects of the water vapor density. Furthermore, the second term can be obtained from the observed $(R_1 - R_2)$ data. The terms K_1 and P_{21} can be calculated using a ray-tracing technique or a model. SIWV can be observed by using an external technique such as GNSS or Water Vapor Radiometer (WVR). The constants ν and H_{21} can be easily calculated using the dispersion formulae.

3. Evaluation and investigation

3.1 Numerical simulation

We have investigated the values of all terms in Eq.(10) using a 2D ray-tracing technique. The frequencies used in the numerical simulations are those of the two-frequency SLR system of the Graz station, λ_1 = 532 nm and λ_2 = 1068.4 nm (Kirchner, *personal communication*). Radiosonde data from World Meteorological Organization (WMO) during 2007 to 2008 are used in the calculations. The refractivity values are calculated based on the Ciddor (1996) procedures. The mean values of all correction terms are presented in Table 1. The constant values of ν and H_{21} are -22.2065 and 1.35×10^{-4} m^3 kg^{-1}, respectively.

The mean value of the term $(R_1 - R_2)$ is about -2.3275 m for observations in the zenith direction and it increases to -33.8711 m for observations down to 3^0 elevation angle. The mean values of the term $(\nu P_{21} - K_1)$ can be as large as 0.35 m at 3^0 elevation angle and its values become insignificant at elevation angles above 30^0. Furthermore, the mean values of term $(H_{21} . SIWV)$ is in the order of few mm to cm for all elevation angles.

Finally, to evaluate the performance of the new formula, we calculated the residual range error (RRE) that is defined as $RRE \equiv S - S_{RT}$. The term S_{RT} is the chord distance S that is calculated using the ray tracing technique. The mean values of RRE are listed in the last column of Table 1 (unit in nm) and indicate that the new formula can reduce all propagation effects at any elevation angle with an accuracy better than 1 mm.

Table 1. The 2-year mean and standard deviation of all correction terms and RRE

e_o (°)	$(R_1 - R_2)$ (m)	$(\nu P_{21} - K_1)$ (mm)	$H_{21} . SIWV$ (mm)	RRE (nm)
3	-33.8711 ± 0.2820	-351.84 ± 14.83	36.49 ± 17.54	-2.5
5	-23.5023 ± 0.1909	-128.55 ± 4.66	23.62 ± 11.39	-0.1
10	-12.9089 ± 0.1038	-22.51 ± 0.70	12.34 ± 5.96	7.8
15	-8.8409 ± 0.0709	-7.31 ± 0.23	8.35 ± 4.04	2.8
20	-6.7416± 0.0541	-3.04 ± 0.09	6.34 ± 3.06	-9.2
30	-4.6375 ± 0.0372	-0.84 ± 0.03	4.35 ± 2.10	3.7
40	-3.6145± 0.0290	< -0.3	3.38 ± 1.64	-0.2
60	-2.6864 ± 0.0215		2.51 ± 1.21	-4.9
90	-2.3275 ± 0.0187		2.18 ± 1.05	-3.6

3.2 Precision requirement

In order to calculate s with the 1 mm level of precision, we need to investigate precision requirements of all terms in Eq.(10). We have carried out the precision analysis using the variance propagation law with the assumption that the OPLs R_1 and R_2 are observed simultaneously. The results are briefly presented here.

An error of 1 kg m^{-2} of SIWV introduces an error of about 0.2 mm to s. Thus, the precision requirement of SIWV is moderate, which must only be better than 5 kg m^{-2}. The term SIWV can be calculated from a quantity SWD (slant wet delay). If this quantity is used to correct for the water vapor effect, then its precision must be better than 4 cm. This SWD requirement may be achieved by using GNSS or WVR technique.

The curvature term K_1 needs to be calculated with 1 mm precision. It was already mentioned that the magnitude of this term is only significant at low elevation angles. This term may be calculated using an accurate ray-tracing technique. Alternatively, a model could be derived for this term, however, the model's uncertainty has to be carefully considered.

The term $(R_1 - R_2)$ has to be observed with a precision better than 30μm for a single measurement epoch. This high requirement is due to the amplification by a large constant ν, which can be in the order of 10 to 200. Nowadays, modern kHz SLR systems can produce a precision of normal point data at the level of 0.37 mm (Hamal et al., 2005). Thus, the precision demand for this term exceeds the capability of the current state-of-the-art SLR systems. Similarly, the term P_{21} has to be also calculated with a precision better than 30 μm.

The precision of k_d and k_v, which are used to calculate the constant ν and H_{21}, must be better than 10^{-6}. According to Ciddor (1996), the uncertainties of the dispersion formulae proposed by some investigators (e.g. Edlen,1996; Owens,1967; Ciddor, 1996) are in the order of 10^{-6} to 10^{-9}. We recommend to use the formula developed by Ciddor (1996).

4. Concluding remarks

For the calculation of water vapor effects, we propose to use a co-located GPS receiver as it is readily available at all SLR stations and it also can produce the SWD values with a higher accuracy than required. There are two possible co-location scenarios: (i) co-located SLR and GPS observations to a satellite equipped with a retroreflector, and (ii) co-located SLR and GPS observations to different satellites. For the first scenario, the SWD can be calculated from a single GPS signal (e.g. GPS36 or GPS35). The propagation paths of SLR and GNSS signals deviate only slightly (optical and microwave paths) and hence they are assumed to carry the same information about the water vapor distribution. For the second scenario, the SWD values along the propagation paths of the SLR signal can be calculated by interpolating the SWD values obtained from processing the GPS data. It is important to mention that, the SWD observations by GPS include also the horizontal gradient of the SWD.

Since the current SLR systems can not fulfill the precision demand of the term $(R_1 - R_2)$, we are studying the application of averaging techniques to improve the precision. Using the new formula the bias (propagation effects) can be removed but the noise is amplified. The noise, however, can be reduced by averaging techniques. This, of course, requires a careful study of the turbulence effects.

The new formula developed in this paper improves the standard formula by adding two additional terms to calculate the curvature and water vapor effects. In particular, we thoroughly consider the propagation paths of f_1 and f_2 before eliminating one of the unknown terms. In this case, we take into account the propagation term P_{21} that allows us to evaluate the propagation effects of frequency f_2 along the ray path of frequency f_1. This makes the rigorous elimination of the term $\int_{p_1} \rho_t(\vec{r}_1) ds_1$ possible. Finally, we would like to emphasis that the new formula is derived based on the assumption of simultaneous R_1 and R_2 observations. Only for this situation can the instantaneous value of $\int_{p_1} \rho_t(\vec{r}_1) ds_1$ be eliminated accurately.

References

Abshire, J. B. and C. S. Gardner (1985). Atmospheric refractivity corrections in Satellite Laser Ranging.*IEEE Trans. Geosc. Rem. Sens., GE-23*(4), 414-425.

Bender, P. L. and J. C. Owens (1965). Correction of optical distance measurements for the fluctuating atmospheric index of refraction. *J. Geophys. Res., 70*,2461.

Born, M. and E. Wolf (1999). *Principles of optics* (7th ed.). Cambridge Univ. Press.

Ciddor, P. E. (1996). Refractive index of air: new equations for the visible and near infrared. *Appl. Opt., 35*(9), 1566-1573.

Edlen, B. (1966). The refractive index of air. *Metrologia, 2(*2),71-80.

Greene, B. A. and T. A. Herring (1986). Multiple wavelength laser ranging. In *The 6th International Workshop on Laser Ranging Instrumentation*.

Gu, M. and F. K. Brunner (1990). Theory of the two frequency dispersive range correction. *Manucsripta Geodaetica, 15*, 357-361.

Hamal, K., I. Prochazka, G. Kirchner, and F. Koidl (2005). Satellite laser ranging normal point precision limit. In *CTU Workshop,* Prague, Czech Republic, 21-25 March.

Hulley, G. C. and E. C. Pavlis (2007). A ray-tracing technique for improving Satellite Laser Ranging atmospheric delay corrections, including the effects of horizontal refractivity gradients. *J.Geophys. Res., 112* (B06417,doi10.1029/2006JB004834), 1-19.

Marini, J. W. and C. W. Murray (1973). Correction of laser range tracking data for atmospheric refraction at elevations above 10 degrees. Technical Report x-591-73-351, NASA Goddard Space Flight Center.

Mendes, V. B. and E. C. Pavlis (2004). High-accuracy zenith delay prediction at optical wavelengths. *Geophys. Res. Let., 31*, L14602, doi:10.1029.

Mendes, V. B., E. C. Pavlis, D. E. Pavlis, and R. B. Langley (2002). Improved mapping functions for atmospheric refraction correction in SLR. *Geophys. Res. Let., 29* (10), 10.1029-10.1032.

Owens, J. C. (1967). Optical refractive index of air: dependence on pressure, temperature and composition. *Appl. Opt. 6* (1), 51-59.

Rothacher, M. (2005). Role of the existing IAG services for GGOS. In *Dynamic Planet 2005*, August 22-26, Cairns, Australia.

Evaluation of PPN parameter Gamma as a test of General Relativity using SLR data

L. Combrinck
Hartebeesthoek Radio Astronomy Observatory.
ludwig@hartrao.ac.za

Abstract

The post Newtonian parameter Gamma is evaluated as a solve-for parameter utilizing recently developed satellite laser ranging analysis software. The analysis technique utilizes the radial acceleration component of the LAGEOS satellites. The Schwarzschild, Lense-Thirring and de Sitter terms, as well as relativistic time delay are considered in the present analysis.

Introduction

General Relativity (GR), in its weak-field and slow-motion approximation, is currently accepted as being compatible with several observations of various kinds in the Solar System. Nonetheless, searches for possible violations of GR, or further validations, continue to be an active area of research utilizing multiple approaches. The parameterized post-Newtonian (PPN) formalism pioneered by Nordvedt (1968) uniquely details the parameters in which a metric theory of gravity (e.g GR) can differ from Newtonian gravity. PPN formalism (Will and Nordtvedt, 1972) is valid for metric theories of gravitation in which all bodies satisfy the Einstein Equivalence Principle (EEP).

The formalism is particularly useful, even though normally expensive and difficult (Iorio, 2007), for its linearized weak-field and slow-motion approximation e.g in the proximity of the Earth. LAGEOS and LAGEOS II provide the opportunity for such tests, and the literature abounds with attempts on measuring the Lense-Thirring gravitomagnetic precessions of the longitude of the ascending node and argument of perigee of the orbits of these two satellites (Ciufolini et al. 2006). However, these results have yet to be confirmed or generally accepted (Iorio 2009).

Objective

The LAGEOS satellites are particularly suitable for testing GR through evaluation of the PPN parameters in that they have a low area to mass ratio and suffer proportionally less from non-gravitational orbital perturbations such as, e.g., solar radiation pressure. However, they still do suffer, even though modelling the direct solar radiation pressure and reflected solar radiation from Earth is possibly simpler due to their relatively uncomplicated shape. Currently this work has as objective testing the value of the PPN parameter γ by including it in the least squares orbital determination process as a solve-for parameter utilizing a strategy which minimizes the impact of mismodelling.

Method

The relativistic correction to the acceleration of a LAGEOS satellite according to the IERS 2003 conventions (McCarthy and Petit, 2004) is

$$\Delta\ddot{\vec{r}} = \frac{GM_E}{c^2 r^3}\left\{\left[2(\beta+\gamma)\frac{GM_E}{r} - \gamma\dot{\vec{r}}\cdot\dot{\vec{r}}\right]\vec{r} + 2(1+\gamma)\left(\vec{r}\cdot\dot{\vec{r}}\right)\dot{\vec{r}}\right\} +$$
$$(1+\gamma)\frac{GM_E}{c^2 r^3}\left[\frac{3}{r^2}\left(\vec{r}\times\dot{\vec{r}}\right)\left(\vec{r}\cdot\vec{J}\right) + \left(\dot{\vec{r}}\times\vec{J}\right)\right] +$$
$$\left\{(1+2\gamma)\left[\dot{\vec{R}}\times\left(\frac{-GM_s\vec{R}}{c^2 R^3}\right)\right]\times\dot{\vec{r}}\right\}$$

where

$c =$ speed of light,
β, γ = PPN parameters equal to 1 in General Relativity,
$\vec{r}$ is the position of the satellite with respect to the Earth,
$\vec{R}$ is the position of the Earth with respect to the Sun,
$\vec{J}$ is the Earth's angular momentum per unit mass, and
GM_E and GM_s are the gravitational coefficients of the Earth and Sun, respectively.

This formulation includes the Schwarzschild terms and the effects of rotational frame-dragging (Lense-Thirring precession) and de Sitter (geodesic) precession. Frame-dragging causes a displacement of about 1.8 m of the ascending node of a LAGEOS satellite in one year (about 30 mas/yr), whereas de Sitter precession on the nodal longitude is about 17.6 mas/yr.

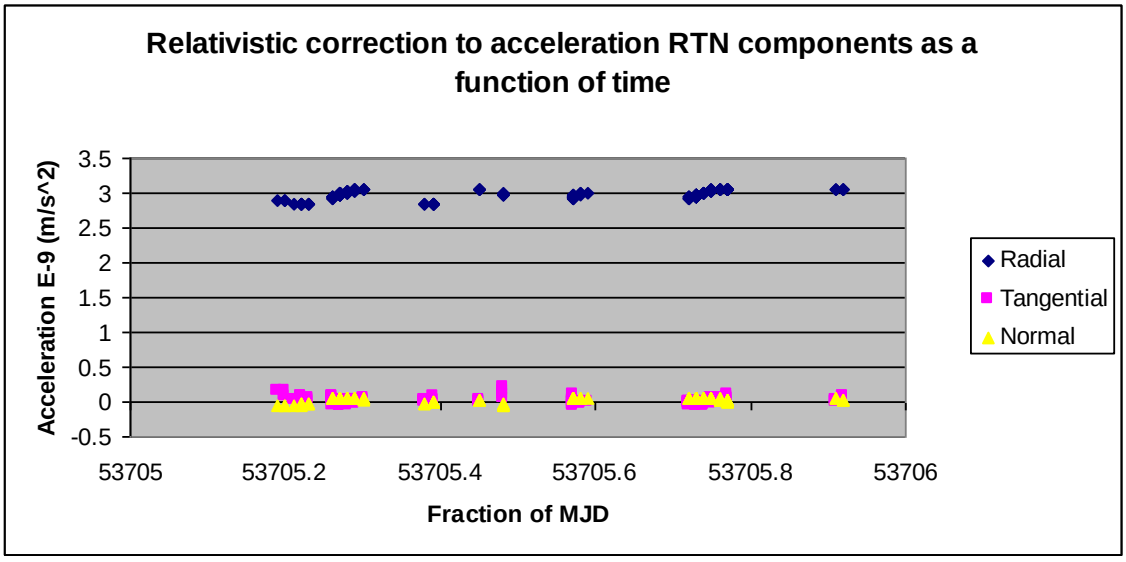

Figure 1. The major component of the correction to the acceleration of LAGEOS is radial.

Acceleration values for the Schwarzschild terms (line 1) are a factor of about 100 larger than Lense-Thirring (line 2) and de Sitter terms (line 3). The acceleration components are, for a random LAGEOS II sample arc of one day, $\sim 2E-9$ m.s^{-2}, $1E-11$ m.s^{-2} and $2E-11$ m.s^{-2}, respectively. When split into radial, tangential and normal components (Figure 1), it is clear that the major component of the relativistic correction to acceleration is radial. The effects of non-gravitational perturbations on the orbit of LAGEOS are mostly larger than the relativistic effects. Table 1 indicates these perturbations on LAGEOS II node and perigee rates (Lucchesi, 2004). Using SLR data to determine a 1.8 m shift in the ascending node is a

Table 1. Non-gravitational perturbations on LAGEOS orbits.

Perturbation	$\dot{\Omega}$ (mas yr^{-1})		$\dot{\omega}$ (mas yr^{-1})	
	LAGEOS	**LAGEOS II**	**LAGEOS**	**LAGEOS II**
Direct solar radiation	-7.3	36.2	-40 260.9	-2694.4
Earth albedo	1.1	-1.5	144.6	57.2
Yarkovsky-Scach	-0.07	-0.9	-143.2	280.5
Earth-Yarkovsky	0.2	-1.5	0.07	0.9
Asymmetric reflectivity	6×10^{-4}	52.9	52.9	152

daunting task due to the small eccentricity of the orbits and the influence of classical even zonal secular precessions. In this work however, the *radial component* of the SLR measurements is the strength of the technique, and the relativistic acceleration on LAGEOS is just *mainly* a radial component.

Therefore the strategy employed in this preliminary study is to solve for PPN parameter γ in the least squares sense utilising SLR data in a strategy where the O-C residuals indicate better observation/modelling fits, through different levels of O-C residual rejection levels. This strategy assigns greater weight to SLR measurement accuracy than to the modelling parameters. Basically the filter exists of a low-pass and high-pass criteria set to an O-C standard deviation based on a selected number of iterations during the least squares fitting process. This effectively creates a bandpass filter, which rejects observations which fall outside the rejection criteria level.

Other solve-for parameters such as nine 1-cycle-per revolution (1 CPR) empirical acceleration parameters are constrained at the 1×10^{-11} m.s^{-2} level. The 1 CPR values obtained during analysis are at the 1×10^{-11} m.s^{-2} to 1×10^{-14} m.s^{-2} level.

Results

A five month period of LAGEOS II data were processed to evaluate the strategy, using data from an average of 13 SLR stations. Table 2 lists the results for the PPN parameter γ and the mean of the observed minus computed (O-C) residuals per 1 day arc.

Figures 2 and 3 indicate the effect of the mean O-C RMS rejection filter and the obtained absolute values of (PPN Gamma -1) respectively.

Table 2. Results for various filter strategies.

Filter (σ)	PPN $\lvert\bar{\gamma}-1\rvert$	σ	Mean O-C RMS (m)	σ (m)
0.4	6.977×10^{-5}	0.000078014	0.005403	0.003136
0.6	1.0649×10^{-5}	0.000183666	0.007469	0.004251
0.8	3.947×10^{-6}	0.000525783	0.011888	0.006701
1.0	3.268×10^{-5}	0.001324442	0.017238	0.009609
1.2	2.6428×10^{-5}	0.001647755	0.023074	0.012702

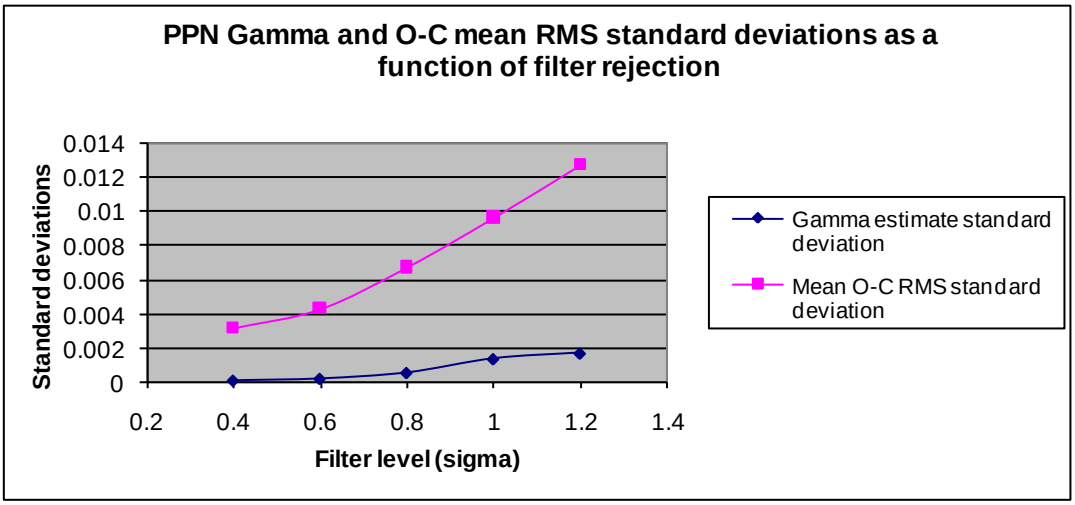

Figure 2. Plot indicating effect of filter on PPN Gamma estimate.

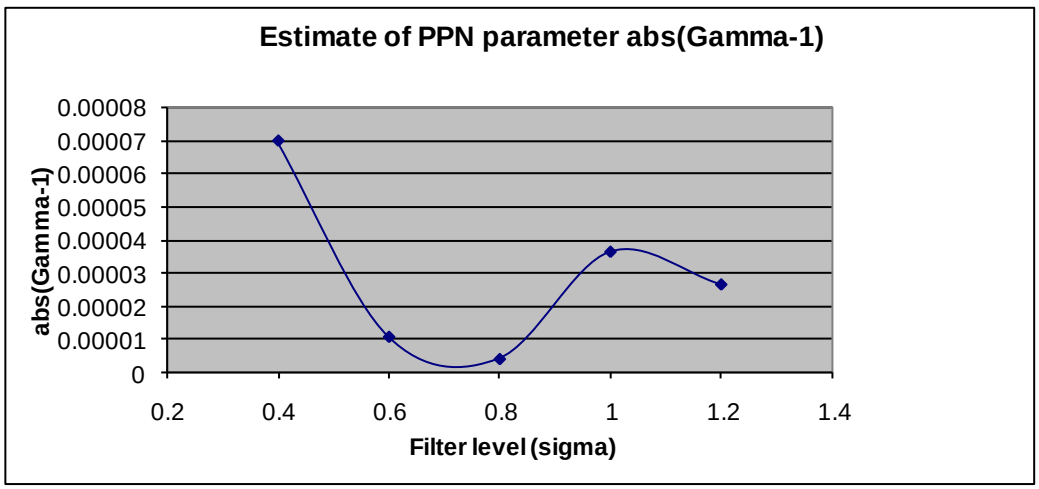

Figure 3. Absolute values of (PPN Gamma-1) estimate.

Figure 4 depicts the values for Gamma obtained as a solve-for parameter with the O-C RMS rejection filter set to 0.8 sigma. Some solutions towards the latter part of the period used indicate strong deviations from the mean. The reasons for these deviations are not clear at this time, although further investigation utilising co-variance analysis and data quantity dependency checks may shed light on these excursions. These points were included in the results. Processing longer data periods and including both LAGEOS satellite should improve the solutions.

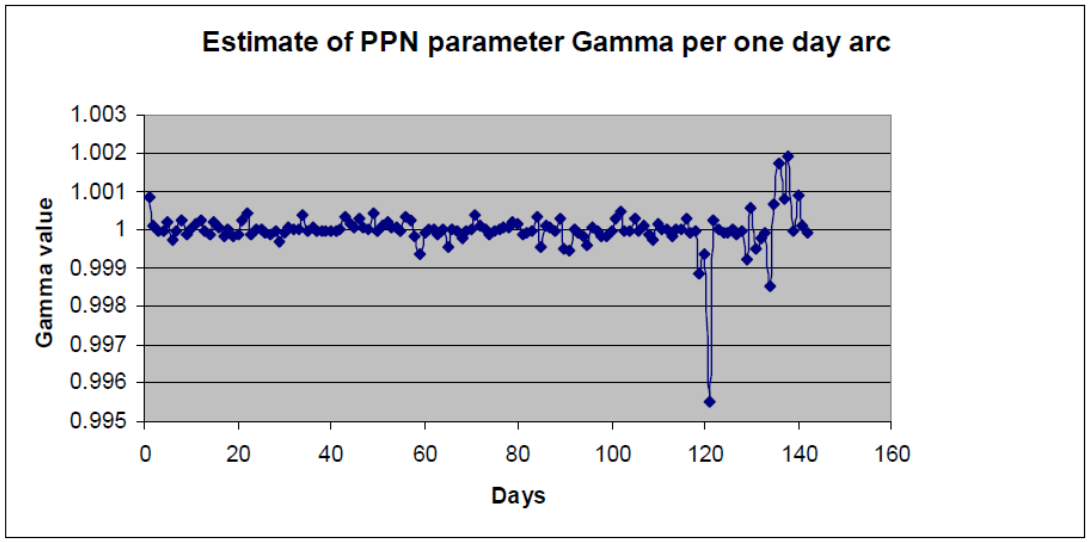

Figure 4. Estimate of PPN parameter Gamma.

Discussion

Table 2 indicates a range of values for Gamma-1, the best value being for a filter setting of 0.8 sigma (O-C RMS 1.2 cm), with 0.4 sigma indicating smallest standard deviation. Filter settings below 0.8 sigma are too constrained and too much data (>20 %) tends to be rejected. These values compare favourably with other determinations e.g. $\gamma - 1 = (2.1 \pm 2.3) \times 10^{-5}$ as determined by Bertotti et al., 2003, but standard deviations are larger. The filter technique has limitations in that it assumes that the SLR two way range accuracy is more reliable than orbital integration. This could lead to discarding good modelling in favour of bad data, although in general, the accepted normal point RMS values should preclude this scenario if incorporated into the processing strategy. Too strong filter levels (approximately < 0.8) degrades the solutions due to data volume decline. Further investigation utilising this approach will involve the evaluation of different gravity models and the addition or improvement of non-gravitational perturbation models.

Conclusion

The PPN parameter γ was evaluated to a level of 5×10^{-4} as a solve-for parameter in an analysis of five months of LAGEOS II satellite laser ranging data. The results of using a rejection filter to constrain the orbital integration and parameter estimation are promising. However, careful analyses of the effects of alternative strategies such as different gravity models and a-priori constraints on other solve-for or consider parameters need to be done to evaluate this technique.

Acknowledgements

Our gratitude is expressed towards the SLR stations in the ILRS network for providing good quality data. During discussions with I Ciufolini and S Kopeikin it was suggested to expand the analysis to the PPN parameter β. This was done after the ILRS workshop and results at the level of 5×10^{-4} are now readily obtained for both parameters. I want to thank L. Iorio for suggestions to improve the text of this report.

References

Bertotti, B., Iess, L., and P Tortora, *"A test of general relativity using radio links with the Cassini spacecraft",* Nature, 425, 374–376, (2003).

Ciufolini, I, Pavlis, E.C. and R. Peron, New Astronomy, 11, 527 (2006).

Iorio, L., In: *The Measurement of Gravitomagnetism*, pp.3-11, Nova Science Publishers, Inc., (2007).

Iorio, L., *"An Assessment of the Systematic Uncertainty in Present and Future Tests of the Lense-Thirring Effect with Satellite Laser Ranging"*, Space Science Reviews, at press, doi: 10.1007/s11214-008-9478-1 (2009).

Lucchesi, D., In: *The Measurement of Gravitomagnetism*, pp.3-11, Nova Science Publishers, Inc., (2007).

McCarthy D.D. and G. Petit. *IERS Conventions (2003) (IERS Technical Note ; 32)*. Verlag des Bundesamts für Kartographie und Geodäsie, Frankfurt am Main, (2004).

Nordtvedt, K., *Equivalence principle for massive bodies. II. Theory*, Phys. Rev., 169, 1017{1025}, (1968).

Will, C. M., and K. Nordtvedt Jr., *Conservation laws and preferred frames in relativistic gravity I*, The Astrophysical Journal 177, 757, (1972).

Preparing the Bernese GPS Software for the analysis of SLR observations to geodetic satellites

D. Thaller (1)**, M. Mareyen** (2)**, R. Dach** (1)**, G. Beutler** (1)**, W. Gurtner** (1)**, B. Richter** (2)**, J. Ihde** (2)

(1) Astronomical Institute, University of Bern (AIUB), Switzerland
(2) Bundesamt für Kartographie und Geodäsie (BKG), Frankfurt/Main, Germany

thaller@aiub.unibe.ch / Fax: +41-31-6313869

Abstract

The Bernese GPS Software is extended to become a full SLR analysis software. As a minimum requirement, the software should be capable to estimate satellite orbits, station coordinates, and Earth rotation parameters from SLR data. The data set of the ILRS Benchmark is used to test the quality of the solutions.
Comparisons with solutions generated by other established ILRS analysis centers and orbit repeatability studies demonstrate the quality that is actually achieved.

1. Introduction

The Bernese GPS Software (Dach et al., 2007) was originally developed to process Global Navigation Satellite System (GNSS) data. Consequently, the program structure and the implemented models (especially for satellite orbits) initially followed the needs for GNSS satellites.

Nevertheless, the software is already capable to compute SLR residuals for given satellite orbits and station coordinates. For this application, CODE (Center for Orbit Determination in Europe) is currently acting as an associated analysis center of the ILRS performing quicklook analyses using SLR measurements to GNSS satellites (two GPS and three of the GLONASS satellites are actually tracked by the ILRS).

In cooperation with Bundesamt für Kartographie und Geodäsie (BKG), the Bernese GPS Software (BSW) is now being generalized in order to be able to analyze SLR observations to geodetic satellites, like Lageos and Etalon, as well. This means, that the major work has to be done in the framework of the orbit modelling and the implementation of SLR-specific parameters (e.g., range biases).

At the moment, the analysis of SLR data with the BSW includes the estimation of station coordinates, Earth rotation parameters (ERP), and satellite orbits (i.e., osculating elements and dynamical orbit parameters). The paper summarizes the actual status of the Lageos-1 orbits using the data set of the ILRS Benchmark.

Processing strategy

Following the specifications for the ILRS Benchmark, we focus on the data set between October 10, 1999 and November 6, 1999, i.e., a time span of 28 days. This data set contains SLR observations of 13 stations to Lageos-1. As it is requested to divide the 28-day orbit into

sub-arcs of 4 days for the dynamical orbit parameters, the processing is performed in two steps:

1. Generation of 4-day normal equation systems (NEQs) based on SLR observations. The NEQs contain the parameters of interest, i.e., osculating elements, dynamical orbit parameters, station coordinates, Earth rotation parameters.
2. Accumulation of the 4-day NEQs of step 1 to a 28-day solution by transforming the osculating elements to one common set, but estimating the dynamical orbit parameters separately for each 4-day interval (see Brockmann (1997) for a detailed description of the procedure).

Several solution types were generated with the BSW. They mainly differ concerning the estimated parameters. An overview of the generated solution types and their characteristics is given in Table 1.

One major difference between the solution types is the set up of dynamical orbit parameters. For solution types B and C only a minimal number of dynamical orbit parameters is estimated, i.e., only an empirical constant along-track acceleration every four days. Solution type D improves the orbit parameterization by additionally estimating 4-day once-per-revolution terms in the radial and cross-track component.

Another difference between the solution types is the handling of the station coordinates and ERPs: The solutions of type B only contain orbit parameters, i.e., station coordinates and ERPs are fixed to their a priori values. Contrary, the station coordinates and ERPs are estimated for solution types C and D using loose constraints of 1 m for these parameters.
The 28-day solutions “B28” and “C28” correspond to the ILRS Benchmark types “B” and “C”, respectively.

In addition, we generated series of solutions covering a shorter time span, i.e., eight, twelve, and 16 days (labelled accordingly in Table 1). Within each series, the solutions were generated using data sets shifted by one day, e.g., the 8-day solutions were computed for the days 1-8, 2-9, 3-10, etc. When comparing two adjacent orbital arcs (e.g., the arcs for days 1-8 and days 2-9) we have seven, eleven and 15 overlapping days in the case of the 8-, 12-, and 16-day solutions, respectively. This allows us to perform orbit repeatability studies for the different solution types.

Table 1: Estimated parameters and their temporal resolution in different solution types.

Solution type	Osculating elements	Along-track constant	Radial once-per-revolution	Cross-track once-per-revolution	Coordinates, ERP
B8	8 d	4 d			fix
B12	12 d	4 d			fix
B16	16 d	4 d			fix
B28	28 d	4 d			fix
C28	28 d	4 d			loose
D8	8 d	4 d	4 d	4 d	loose

Orbit comparisons

As an external validation, the 28-day orbits for the Benchmark types B and C (B28, C28 in Table 1) are compared to the corresponding orbits computed by BKG using the UTOPIA software (developed at CSR, Texas) and by GFZ using EPOS.

Figure 1 shows the residuals in radial, along-track and cross-track components for the comparison of the BSW-derived orbit with that from BKG and GFZ for solution type B. The dark lines represent the mean residual for one revolution. Thus, we see, that the residuals in radial and cross-track components mainly have a once-per-revolution signature, whereas the residuals in along-track additionally have a daily signature. The origin of these differences still has to be investigated.

The residuals of the orbit comparison for solution type C are shown in Figure 2. The conclusions that can be drawn from this comparison are similar to those from the comparison for solution type B.

It is especially important to see that the radial component, what is the major component to be determined by SLR, agrees quite well.

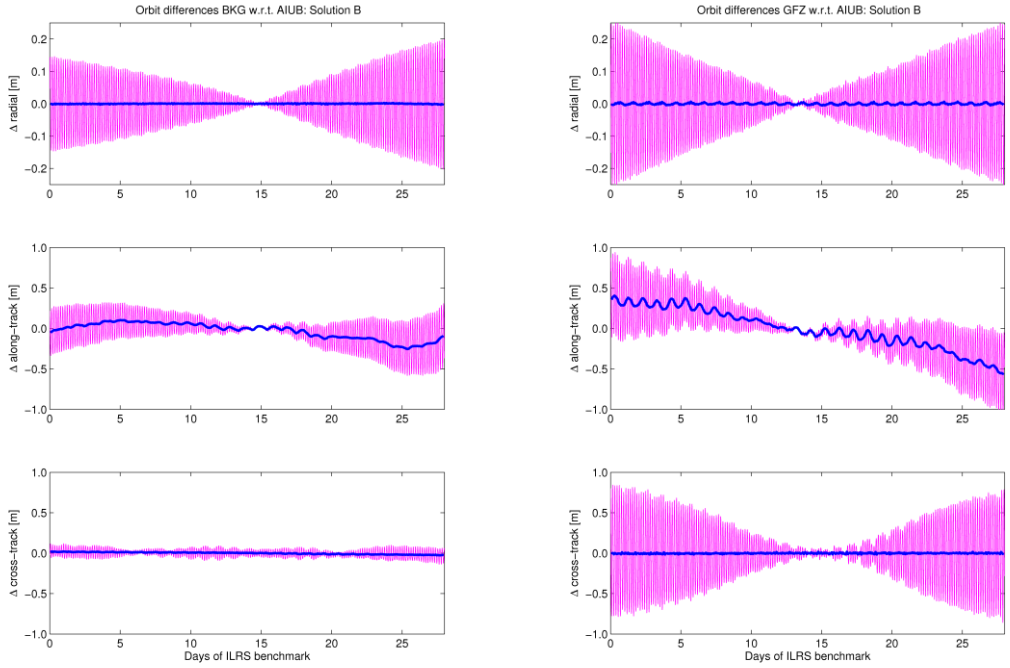

Figure 1. Residuals of orbit comparison for the Benchmark solution type "B" (i.e., solution B28 in Table 1). Left: BKG vs. BSW, right: GFZ vs. BSW (dark line: mean residual over one revolution).

For an internal validation we perform orbit repeatability studies for the 8-, 12- and 16-day solution series of type B, and for the 8-day solution series of type D. As described in section 2, we compare adjacent orbital arcs within one solution type. The RMS of the residuals for each overlapping time span gives the measure for the repeatability. Figure 3 shows the

repeatability for the solution series analyzed. Again, it is important to see that the radial component shows a good repeatability.

The level of the repeatability does not differ much between different arc lengths of one solution type (B8, B12, B16). But the repeatability can be clearly improved by estimating once-per-revolution terms in radial and cross-track direction in addition to constant along-track accelerations (i.e., D8 compared to B8). This behaviour may be an indication that the dynamical orbit parameters absorb deficiencies in the orbit modelling.

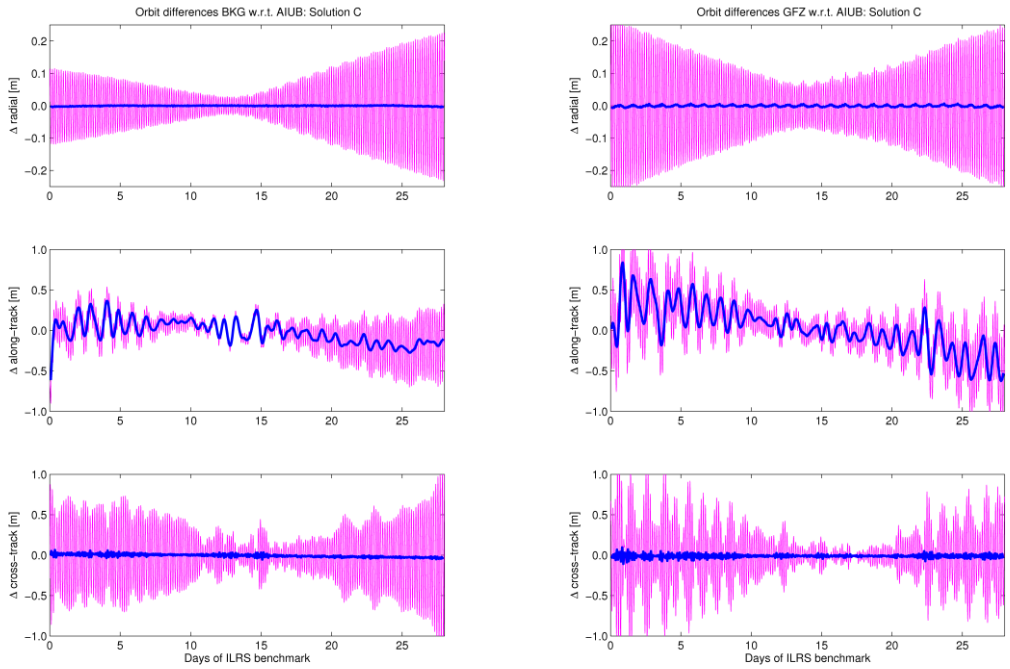

Figure 2. Residuals of orbit comparison for the Benchmark solution type "C" (i.e., solution C28 in Table 1). Left: BKG vs. BSW, right: GFZ vs. BSW (dark line: mean residual over one revolution).

Conclusions

The orbits of Lageos-1 generated with the Bernese GPS Software have a quality that is comparable to that of other ILRS analysis centers. Furthermore, the radial component shows a very good behaviour. This is important to see, because the radial component is the major component to be determined by SLR.

Nevertheless, there are several improvements to be done. The next steps to improve the SLR analysis with the Bernese GPS Software will be:

- Improve/extend the a priori models (e.g., Earth albedo);
- Implement the estimation of range biases according to the specifications of the ILRS;
- Develop a procedure for screening observations in order to detect outliers automatically and reliably.

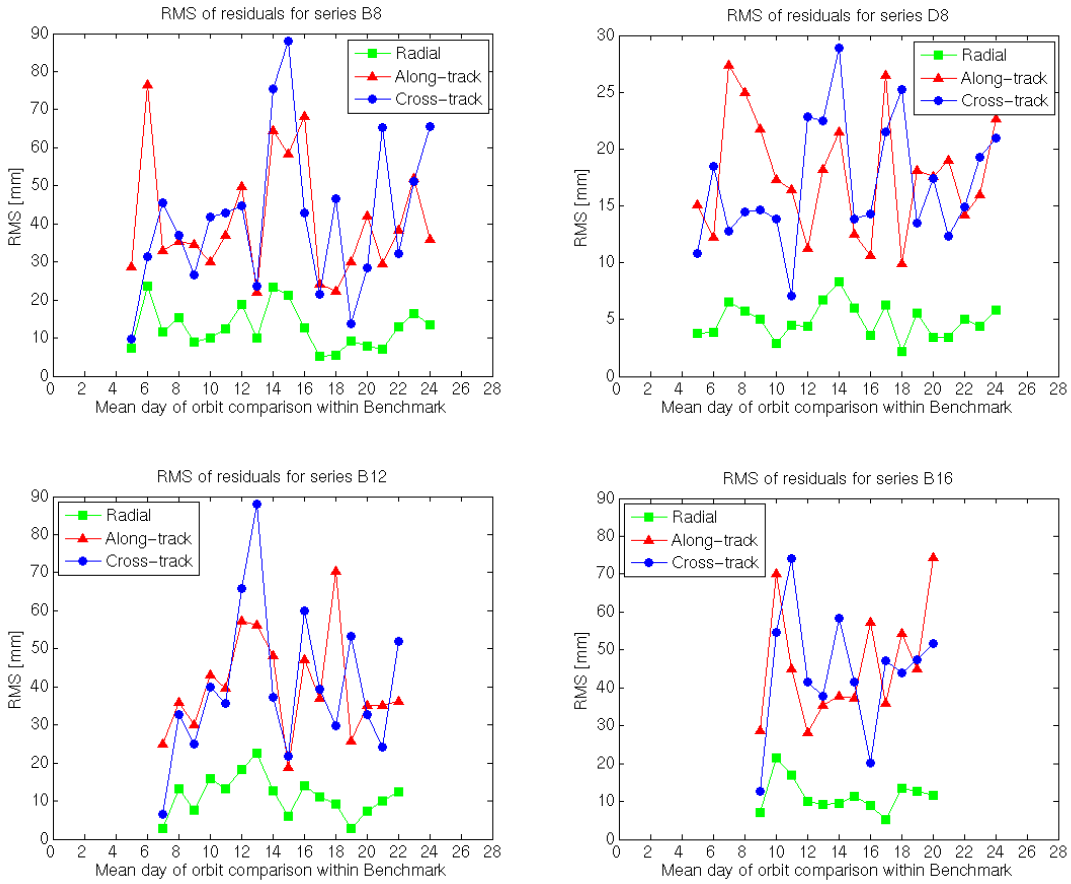

Figure 3. Comparing adjacent orbital arcs for different solution types. Note the different scale of the y-axis for solution D8!

Acknowledgement

We would like to thank Rolf König from GFZ Potsdam for providing the orbits for the ILRS Benchmark generated with EPOS.

References

Brockmann, E. (1997): *Combination of solutions for geodetic and geodynamic applications of the Global Positioning System (GPS)*. Geodätisch Geophysikalische Arbeiten in der Schweiz, Vol. 55, Zürich, Switzerland

Dach, R., U. Hugentobler, P. Fridez, M. Meindl (2007): *Bernese GPS Software Version 5.0*. Astronomical Institute, University of Bern, Switzerland

The methods of converting observation data of SLR between two nearby stations

V. Pap, M. Medvedsky
Main Astronomical Observatory National Academy of Sciences of Ukraine,
E-mail: vic@mao.kiev.ua, medved@mao.kiev.ua

Abstract

There are two methods of converting observations data of satellite laser ranging from one station to another nearby station. The first method is conditionally named analytical and it consists of ordinary geometrical conversation in system of the station A – station B – satellite S. The second method we are called differential and it is based on ephemeris data of the same pass of satellite for each station. We have converted observation data from two Ukrainian SLR station Simeiz 1873 and Katzively 1893 the distance is about 3 kilometers between them. The result of this conversation with Lageos 1 and Lageos 2 at 2004 year for both stations is present in article. On the basis of both algorithms the program has been created.

Introduction

It happens difficult to use observations of two nearby stations during processing of observations of network SLR stations. Especially sharply this question rises at processing of results of observations of a network into which the small amount of stations, for example, to Ukrainian network SLR stations. Thus it is necessary to exclude one of two stations from processing. Otherwise there will be very big correlations between both observations of nearby stations and the end result will be deformed. It would be expedient to process results of observations of two stations presents as observations of one that is not to exclude from processing one of stations. For this purpose it is necessary to transform observations of this station to other station.
In the given work it is presented two methods of transformation of results of observations of one station to another station. The first method is conditionally named by analytical and it is based on simple geometrical transformations to system station A – station B – satellite S. The second method consists of differences between ephemeris for the same passage of the satellites for each stations and addition of this differences to observations one of stations.

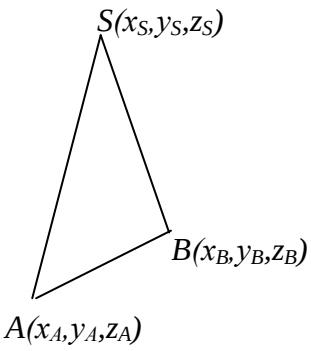

Figure 1. Conditional placing of objects of stations A, B and the satellites S

Analytical method

Start up at us there are two nearby stations A and B and the measured range (distance) from station A to satellite S. It is necessary to transform range of station A to station B. It is possible to find easily distances between them, if all of coordinates are in same frame.

Easier to make it in the Cartesian rectangular system of coordinates, for example, geocentric coordinates. Except coordinates of stations it is necessary to have satellite coordinates in the same frame. For this purpose it is possible to use accurate ephemeris. From geocentric

coordinates of both stations we find distance between stations and topocentric coordinates station B relative to station A. If we will have the topocentric Cartesian coordinates station B and coordinates satellite S, that it is possible to find the distance between station B and satellite S, because these coordinates will be in same frame. We will write down all it by means of mathematical expressions.

The distance between stations will look like:

$$\vec{R} = \begin{pmatrix} X_B - X_A \\ Y_B - Y_A \\ Z_B - Z_A \end{pmatrix},$$

where X_A, Y_A, Z_A and X_B, Y_B, Z_B – geocentric coordinates respectively.

Topocentric coordinates station B rather station A will be calculated by means of such expressions (see [1-3]):

$$M = T_1 \times R,$$
$$N = T_2 \times M$$
$$R_{Top} = \begin{pmatrix} X_{BTop} \\ Y_{BTop} \\ Z_{BTop} \end{pmatrix} = T_3 \times N$$

Where:

$$T_1 = \begin{pmatrix} \cos\varphi & \sin\varphi & 0 \\ -\sin\varphi & \cos\varphi & 0 \\ 0 & 0 & 1 \end{pmatrix}, \; T_2 = \begin{pmatrix} \sin\lambda & 0 & -\cos\lambda \\ 0 & 1 & 0 \\ \cos\lambda & 0 & \sin\lambda \end{pmatrix}, \; T_3 = \begin{pmatrix} -1 & 0 & 0 \\ 0 & -1 & 0 \\ 0 & 0 & 1 \end{pmatrix},$$

φ and λ – latitude and longitude of station A.

Now, it is easily found required distance *SB* if we have the topocentric coordinates station B and satellite S:

$$SB = \sqrt{(X_{STop} - X_{BTop})^2 + (Y_{STop} - Y_{BTop})^2 + (Z_{STop} - Z_{BTop})^2}$$

Differential method

This method is based on calculated ephemeris [4]. Let we again need to transform observations of station A to station B.

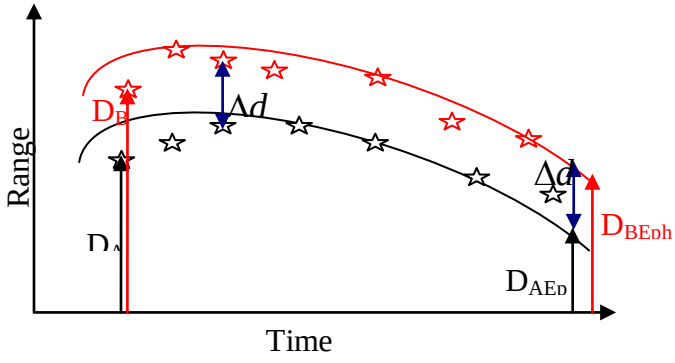

Figure 2. The conditional image of a differential method

For an illustration of a differential method it is possible to use figure 2. Black color is drawn observation and ephemeris of station A. Red colors is drawn ephemeris stations B and points where the observation of station A is transformed.
Δd – shift-size between ephemerides on which it is necessary to shift observation of station A for receive observation of station B.

The essence underlying the method is that find difference between calculated ephemerides for both stations. Then this difference interpolate for the moments of observations station A. And this difference it is added to observations station A. Also we find observation station B. That is:

$$\Delta d = D_{AEph} - D_{BEph} \ ,$$

where D_{AEph} – ephemeris station A, D_{BEph} – ephemeris station B, Δd – the difference of them. Then observations station B will be behind the formula:

$$D_B = D_A + \Delta d \ ,$$

where D_A – the observation of station A.

Comparing methods

For check of correctness of methods real observations of two nearby Ukrainian stations Simeiz 1893 and Katzively 1873, distance between of them is about 3 km, have been used. The observations were taken in the form of files of normal points with the server http://www.cddis.gsfc.nasa.gov [3]. The ephemerides were taken from this site too[4]. It is used for testing the passage of satellites LAGEOS 1 for March, 31st, 2004 and passage of satellite LAGEOS 2 for the July, 10th, 2004 which location was spent by both stations.

To check up correctness of the principle of an analytical method it has been transformed by this method ephemeris station A to station B. The differences between ephemeris station B and transformed ephemeris station And to station B is presented in figure 2. Apparently from figure, the difference between ephemerides makes an order of 10^{-6} meters. It gives the chance to us to assert, that algorithm and the software is developed correctly.

To check up correctness of a differential method so simply it will not turn out. On it already ready results transaformed by both methods were compared. The observations of station Katzively have been transformed to the station Simeiz for all 2004, and we have compared results. Comparison has shown, that the data received by both methods identical to within picoseconds.

Approximation of results

As there are some joint observations of the same passages of satellites it would be expedient to check up how the transformed observation and real observation of station on which transformations of observations were made will be adjust.

[3] ftp://cddis.gsfc.nasa.gov/slr/data/npt/lageos1/2004/
ftp://cddis.gsfc.nasa.gov/slr/data/npt/lageos2/2004/

[4] ftp://cddis.gsfc.nasa.gov/slr/predicts/2004/lageos1/
ftp://cddis.gsfc.nasa.gov/slr/predicts/2004/lageos2/

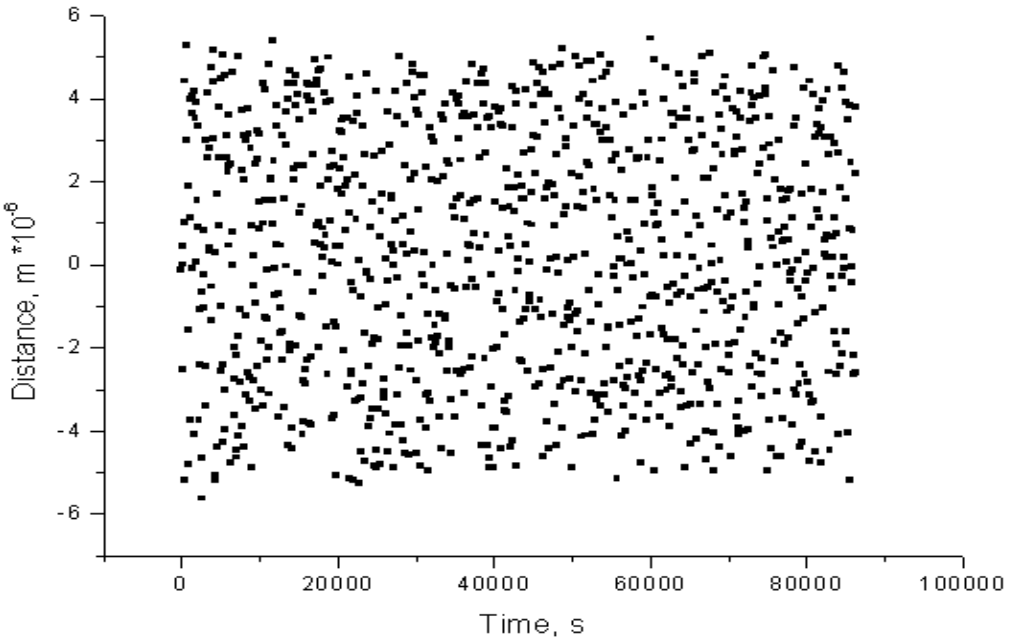

Figure 3. The difference between real ephemeris and transformation ephemeris

The transformed observations of station Katsiveli to station Simeiz are taken for an example. Results it is submitted in figures 4 and 5.

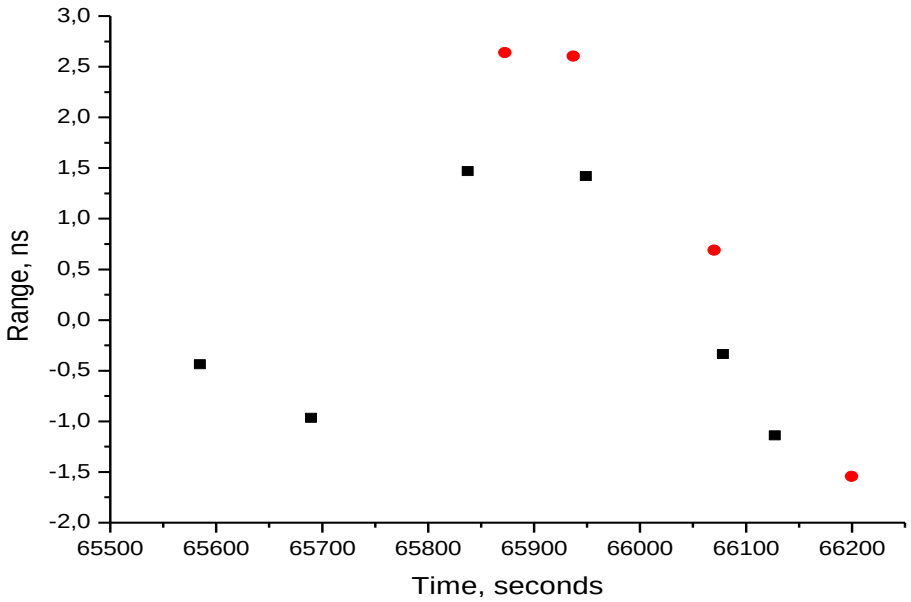

Figure 4. Difference between observations and ephemeris of station Simeiz (black) and difference between transformation observations of station Katzively and ephemeris of station Simeiz (red), satellite LAGEOS 1 for 31.03.2004

Differences between range and ephemeris stations Simeiz are represented for the best perception in figures, but not range in it. Black color represents observations of Simeiz, and red – the transformed observations of station Katzively.

In figure 4 it is visible, that observations of two stations will be to good agreement among themselves. In figure 5 observations will be to good agreement among themselves too, but from this figure follows that ephemeris is inexact. At it is present range bias order 99

nanoseconds, which identical to both stations. On it to avoid the errors connected with ephemeris, it is make better to use a differential method.

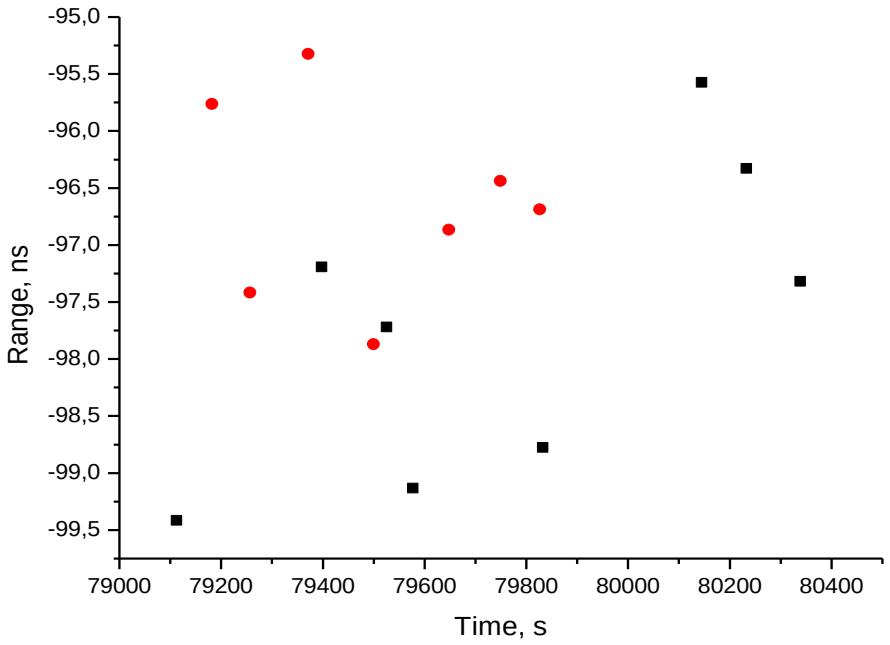

Figure 5. Difference between observations and ephemeris of station Simeiz (black) and difference between transformation observations of station Katzively and ephemeris of station Simeiz (red), satellite LAGEOS 2 for 10.07.2004

Further we have compared, on how many the transformed observations actually differ from the real observations. The observations of station Simeiz for the moments of observations of station Katzively have been interpolated for this purpose at the general intervals and are taken differences between the transformed and interpolated observations. The results it is shown in figure 6 and 7.

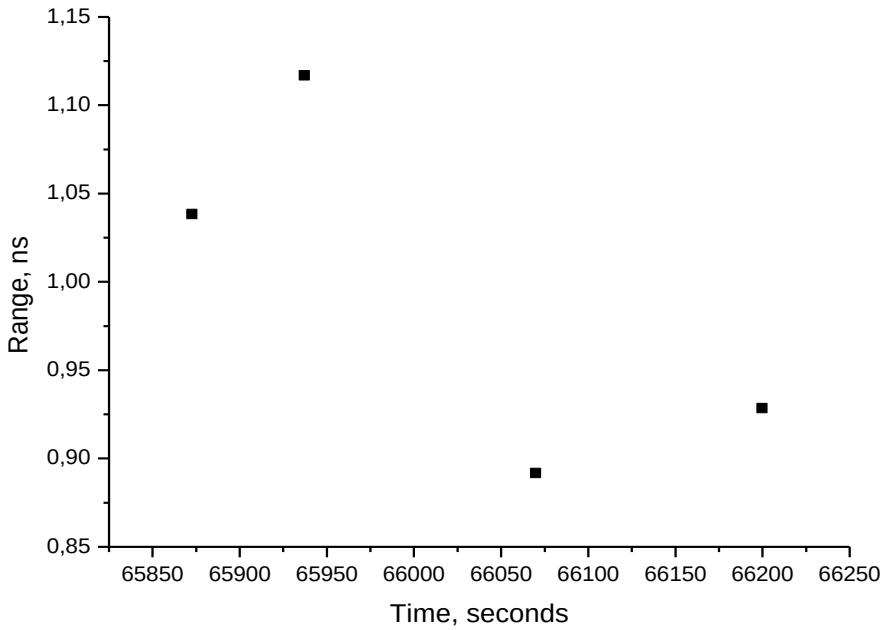

Figure 6. The difference between transformed and interpolated observation, satellite LAGEOS 1 for 31.03.2004

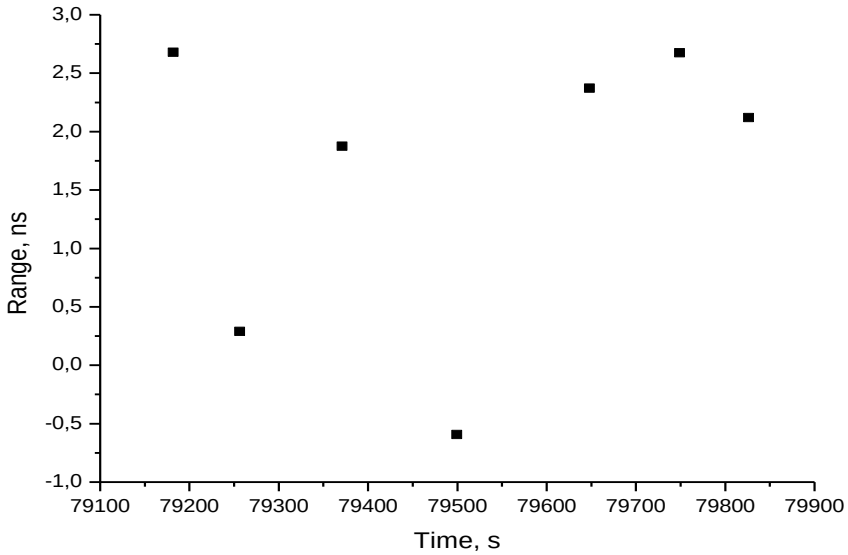

Figure 7. The difference between transformed and interpolated observation, satellite LAGEOS 2 for 10.07.2004

This figures are shown that the difference between real and transformed observations is less then 3 nanoseconds or 45 centimeter in distance.

Conclusion

It is developed two techniques for transformation of observations from one station to other nearby station. Both techniques have identical result. From the mathematical point of view, a differential method is much easier to use. Both techniques it is possible to use in the centers of processing of results of observation. Also both methods can be used for comparison of relative quality of observation, for example, presence time bias, size of range bias. The program for transformation of observation by both methods is developed and it can be used in the centers of processing observations. This program is freeware.

References

1. Abalakin V. *Bases of ephemeridical astronomy*. – Science, Moscow, 1979
2. Abalakin V., Aksenov E., Grebenikov E., Demin V. *Reference manual on the celestial mechanics and astrodynamics*. – Science, Moscow, 1976
3. Podobed V., Nesterov V. *The general astrometry*. – Science, Moscow, 1975
4. Pap V., Medvedsky M. Two methods of transforming observations from one station to another station, *Bulletin of the Ukrainian Centre of determination of the Earth Orientation Parameters № 2, 38 –40.* – VAITE Company, Kyiv, 2007

Estimation of the elastic Earth parameters k_2 and k_3 from the SLR technique

Milena Rutkowska (1)**, Marcin Jagoda** (2)

(1) Space Research Centre, Polish Academy of Sciences, Poland
(2) Technical University , Koszalin, Poland

milena@cbk.waw.pl, mjagodam@o2.pl

Abstract

The global elastic parameters k_2, k_3 associated with the tide variations of the satellite motion are estimated from the Satellite Laser Ranging (SLR) data. The study is based on satellite observations taken by the global network of the ground stations during the period from January 1, 2005 until January 1, 2007 for monthly orbital arcs of satellites Lageos 1 and Lageos 2, separately. The observation equation, contains unknowns which are related to orbital arcs only, some unknowns are common for all arcs and the Earth parameters, can also be estimated. The example is elastic Earth parameters k_2, k_3 which describe tide variations of the satellite motion. The adjusted values k_2 equal to 0.3016 ± 0.0001 and 0.3006 ± 0.0001, k_3 equal to 0.0989 ± 0.0051 and 0.0810 ± 0.0051 for LAGEOS1 and LAGEOS2 tracking data are discussed and compared with geophysical estimations of Love numbers. All computations were performed employing the NASA software GEODYN II (Eddy et al. 1990).

1. Introduction

The attraction of the Earth is the most important force acting upon the artificial satellite. The perturbations produced by the Earth's gravity field evidently belong to the greatest disturbances. Usually, the gravity field and the tide potential (which describe the influence of the conservative forces) in the external point $P(r, \varphi, \lambda)$ of the Earth are given by following expression (1).

$$V = \frac{GM}{r}\left(1 + \sum_{n=2}^{\infty}\sum_{m=0}^{n}\left(\frac{a}{r}\right)^n P_{nm}(\sin\varphi)((C_{nm} + \Delta C_{nm})\cos m\lambda + (S_{nm} + \Delta S_{nm})\sin m\lambda\right) \quad (1)$$

The gravity field is modeled by standard geopotential coefficients C_{nm}, S_{nm} and their tide variations ΔC_{nm} and ΔS_{nm} in time (Eanes et al., 1983) .The tide model (having frequency dependent Love numbers) is computed by a general procedure.

$$\Delta C_{nm} - i\Delta S_{nm} = \frac{k_{nm}}{\sqrt{2n+1}}\sum_{j=2}^{3}\frac{GM_j}{GM_E}\left(\frac{R_E}{r_j}\right)^{n+1} P_{nm}(\sin\Phi_j)e^{-im\lambda_j} \quad (2)$$

where:
$P_{nm}(\sin\varphi)$ - the associated Legendre'a function of degree *n* and order *m*,

GM_j - gravitational parameter for the Moon and Sun,
GM_E - gravitational parameter for Earth.,
R_j - vector from the geocenter to the Moon or Sun,
r, ϕ, λ - vector from geocenter to the station, geocentric latitude and longitude,
k_2 - nominal second degree Love number k_2 equal to 0.3
k_3 - nominal third degree Love number k_3 equal to 0.093 by Longman.

For degree 2 the tide model is computed in two steps. The first step uses a frequency dependent Love number k_2. The changes in normalized second degree geopotential coefficients for step 1 are:

$$\Delta C_{20} = \frac{1}{\sqrt{5}} k_2(0) \frac{R^3{}_E}{GM_E} \frac{GM_j}{r_j^3} P_{20} \sin\varphi_j$$

$$\Delta C_{21} - i\Delta S_{21} = \frac{1}{3}\sqrt{\frac{3}{5}} k_2(1) \frac{R_E^3}{GM_E} \frac{GM_j}{r_j^3} P_{21} \sin\phi_j * \cos\lambda_j \qquad (3)$$

$$\Delta C_{22} - i\Delta S_{22} = \frac{1}{12}\sqrt{\frac{12}{5}} k_2(2) \frac{R_E^3}{GM_E} \frac{GM_j}{r_j^3} P_{22} \sin\varphi_j * \sin 2\lambda_j$$

The above equations are revised in such a way that three different Love numbers $k_2(0), k_2(1), k_2(2)$ for long period, diurnal and semi-diurnal periods are introduced instead of one Love number k_2. If a common nominal number k_2=0.3 is used in equations (2), then the differences between actual and nominal Love numbers must be corrected in step 2 which is described in (Eanes et al., 1983)

The contributions of the degree 3 tides ΔC_{3m} and ΔS_{3m} are computed by a general procedure (2) too. For n=3 m=0 is described by following formula.

$$\Delta C_{30} = \frac{1}{\sqrt{7}} k_3 \frac{R_E^4}{GM_E} \frac{GM_j}{r_j^4} P_{30} \sin\varphi_j \qquad (4)$$

The partial derivative quantities $\frac{\partial\rho}{\partial k_2}$ and $\frac{\partial\rho}{\partial k_3}$ required in expression (5) to estimation of the Love numbers k_2 and k_3 (where ρ is a given SLR measurement) are computed by differentiation of expressions (3,4).
The knowledge of the partial derivatives described above allows to calculate the Love numbers k_2 and k_3 ,using observation equations (5) an iterative process . Initial values used in solution were equal to k_2=0.3 described in IERS Technical Note 21 and k_3 =0.093 (Longman) in (Melchior P, 1978)

$$V_\rho = \sum_{i=1}^{6} \frac{\partial\rho}{\partial\varepsilon}\Delta\varepsilon + \frac{\partial\rho}{\partial k_2}\Delta k_2 + \frac{\partial\rho}{\partial k_3}\Delta k_3 + (O-C) \qquad (5)$$

where:

$\Delta\varepsilon$ - corrections regarded to the satellite arcs,
Δk_2 - correction to the Love number k_2,
Δk_3 - correction to the Shida number k_3,
V_ρ - correction to observation,
$(O-C)$ - observation to satellite minus computed distance between satellite and station.

2. Method of analysis

The study is based on the SLR data of LAGEOS-1 and LAGEOS-2 taken by the global network of SLR stations during the period from 3 January 2005 until 30 December 2006. The database of normal points was processed in 30-day batches. In total 48 orbital arcs were used in the analyses. A preliminary step not reported in this paper, the compression of observations into normal points, was performed for two-minute intervals of LAGEOS-1 and LAGEOS-2 by Crustal Dynamics Data Information System (CDDIS) and EUROLAS Data Center (EDC). Number of normal points used in solution for LAGEOS1 and LAGEOS2 is shown in Fig.1.

The solution was produced employing the software GEODYN II (Eddy et al.,1990). The forces that perturb the satellite orbit needed to be modeled as accurately as possible. The force models used and the reduction of measurements for LAGEOS-1 and LAGEOS-2 are shown in Table 1. The study is based on the station positions published by ITRF2005 referred to the epoch 2000.0.

Table 1. Computation model used in the solution.

DYNAMIC MODEL
Gravity field TEG4 (20,20)
Wahr solid Earth tides NASA/NIMA EGM96 ocean tides
C_R direct solar radiation pressure estimated
Albedo and infrared Earh radiation
Relativistic effects
Accelerations in along-track, cross-track and radial directions (for 5-day intervals)
REFERENCE FRAME
Station coordinates used –ITRF2005 referred to epoch 2000.0
Nutation according to IAU 1980 (Wahr model)
Pole tide
Ocean loading deformation, atmospheric pressure loading deformation
PROCESSING MODE
Normal points provided by CDDIS and EDC
Marini-Murray model for troposphere delay
Center-of-mass correction used
Station dependent data weighted
OBSERVATIONS
LAGEOS-1- 24 arcs normal points (2005.01.03- 2007.01.02)
LAGEOS-2- 24 arcs normal points (2005.01.03- 2007.01.02)
INTEGRATION
Cowell 11-order predictor-corrector; step-size 2 min.

3. Results

The paper presents the global elastic Earth parameters k_2 and k_3 (Love numbers) associated with the tidal variations of satellite orbits estimated for 24 months time interval. The sequential method was adopted for analysis. In the first step, the elastic parameters were adjusted for two orbital arcs. In the next steps, arcs one after the other were included using sequential method. In the each step, the parameters were adjusted once again. The results of analysis are shown in Fig.2 and Fig.3. for k_2 and k_3 separately. The total adjusted value k_2 is equal to 0.3016 ± 0.0001 for LAGEOS1 tracking data and is equal to 0.3006 ± 0.0001 for LAGEOS2 tracking data. The total adjusted value k_3 is equal to 0.0989 ± 0.0051 for LAGEOS1 and 0.0810 ± 0.0051 for LAGEOS2. The discrepancy is at the 0.3% level for k_2 and the 20% level for k_3. The differences from the LAGEOS1 and LAGEOS2 are not significant for k_2 value.

As an example, previous estimation of k_2 by Wahr (1981) provide value equal to 0.299 which have to be corrected.

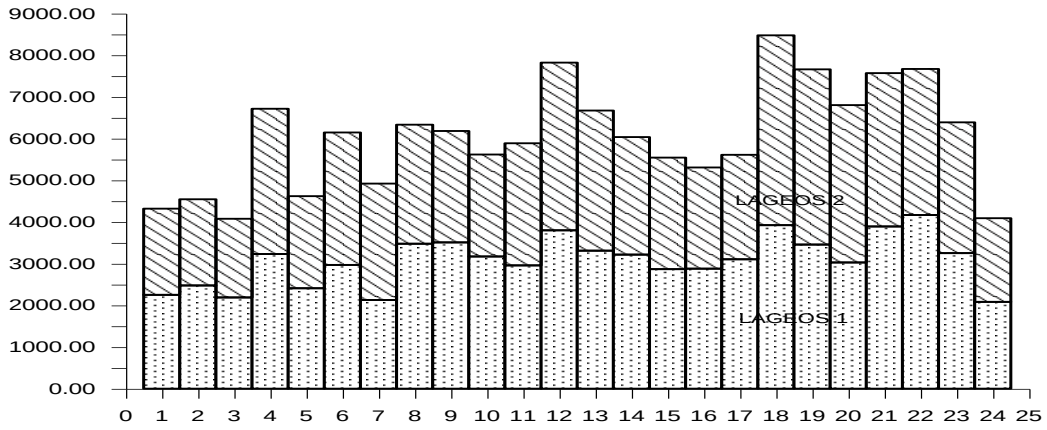

Figure 1. The number of normal points used in solution for LAGEOS1 and LAGEOS2.

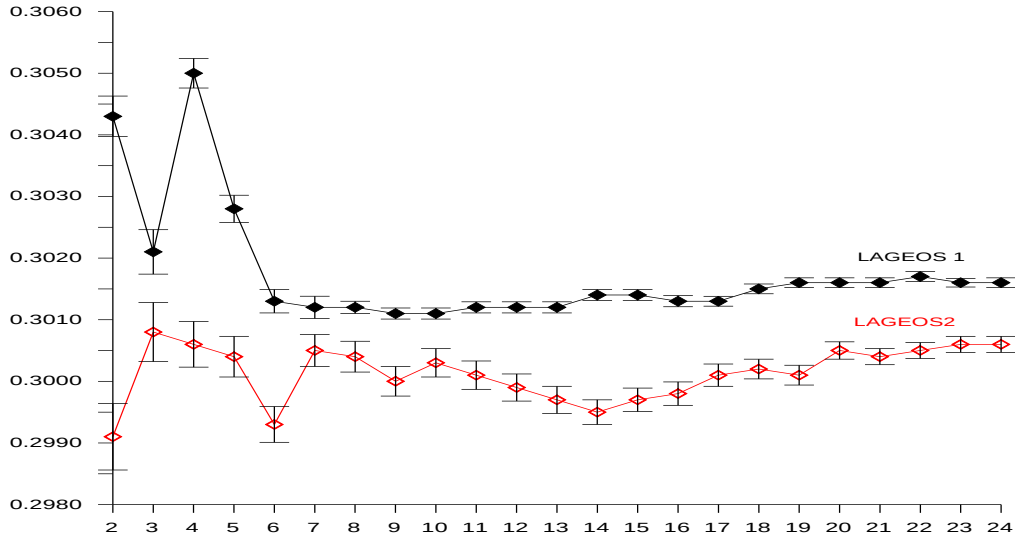

Figure 2. The Love number k_2 estimated from Lageos1 data equal to 0.3016 ± 0.0001 and Lageos2 data equal to 0.3006 ± 0.0001

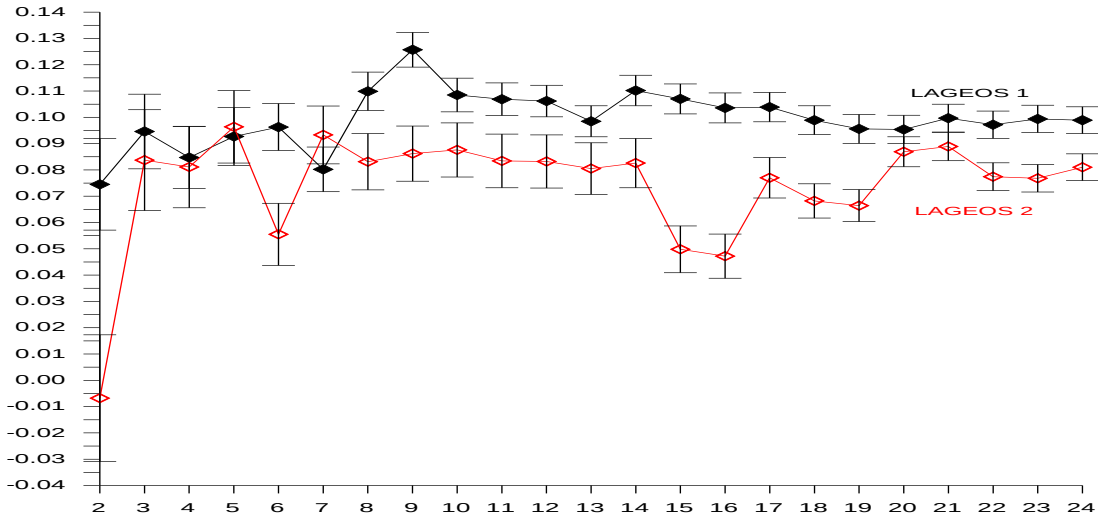

Figure 3. The Love number k_3 estimated from Lageos1 data equal to 0.0989 ± 0.0051 and Lageos2 data equal to 0.0810 ± 0.0051.

4. Conclusions

The SLR tracking data for satellite LAGEOS1 and LAGEOS2 were used to determine the elasticity Earth parameters k_2 and k_3. On the basis of the computations performed it can be concluded that:

- The estimated parameter, Love number k_2 is equal to (0.3016 ± 0.0001 and 0.3006 ± 0.0001) for LAGEOS1 and LAGEOS2 tracking data separately. The good agreement of estimated parameters for both satellites can be seen. Difference is at the level 0.3%.
- The estimated Love number k_3 is equal to (0.0989 ± 0.0051 and 0.0810 ± 0.0051). for LAGEOS1 and LAGEOS2 tracking data separately. Difference is equal to 0.0179, it means at the level 20% value. The discrepancy with value estimated by Longman which is equal to 0.93 (P.Melchior,1978) is agree at the level 5% .
- Stability of estimated elasticity Earth parameter k_2 and their errors became visible for about 23-month time interval (Fig.2). But for k_3, 24-month time interval not allows to obtain stability of solution what is shown in (Fig.3). Probably for number of arc greater than 20 differences are at the level of noise.

4. Acknowledgments

The autors would like to express special thanks to Despina Pavlis, she helped to install new files of data connected with GEODYN II software .

References

Eanes. R, J.Schutz, B. Tapley, Earth and Ocean Tide Effects on Lageos and Starlette, Proceedings of the Ninth International Symposium on Earth Tides, E. Schweizerbartsche Verlagsbuchhandlung, Stuttgart

Eddy W.F., J.J. McCarthy, D.E. Pavlis, J.A. Marshall, S.B. Luthcke, L.S. Tsaoussi: GEODYN II
system operation manual, Vol.1-5, ST System Corp. Lanham MD, USA, 1990.

Melchior. P, The tides of the planet Earth, Pergamon Press.
Wahr J.M, The forced nutations of an ellipsoidal rotating, elastic and oceanless Earth, Geopys. J.R. Astronom. Soc., 64,1981.

IERS, TN 21

IERS, ITRF2005.

The role of Satellite Laser Ranging in the Global Geodetic Observing System

Chairs: Erricos Pavlis and Horst Mueller

Session Summary

The third session of the workshop, entitled “The role of Satellite Laser Ranging in the Global Geodetic Observing System", intended to highlight the central role that SLR plays within GGOS. The session comprised invited and contributed presentations on the significant role of SLR in support of GGOS' goals.

In the opening presentation, R. Gross summarized the main contributions of SLR to the three pillars of geodesy for GGOS. Gross gave examples of the state-of-the-art in the definition of the origin and scale of the ITRF, the long history of SLR series of EOP, the longest of all space techniques, and mass load variations from long wavelength harmonics time series derived from SLR, with comparisons to other techniques (GRACE, GPS, hydrology, etc.).

The second presentation, by C. Sciarretta, demonstrated that the SLR technique evolves and strives to deliver new products that fulfill requirements of the user community. In this case, the focus was on the daily delivery of fresh EOP estimates that can be used to constraint the EOP forecasting process of the NEOS service of IERS.

Following the presentation of this new ILRS product was a talk by T. Springer on ESA’s efforts to harmonize the reduction of GNSS and SLR data with a common analysis package for a combined and consistent estimation of geophysical parameters required by GGOS.

S. Schillak followed with a comparison between GPS- and SLR-derived time series of coordinates over a period of eleven years. The results indicated the general consistency of the results at the few millimeter level. It also demonstrated how well the two techniques compare at sites with data of exceptional quality, and how they can be used to identify problems in either technique when they are co-located and properly and accurately surveyed.

In the final presentation, E. C. Pavlis showed the results of optimization studies in designing the future global geodetic networks that will support GGOS. In particular, the talk focused on the role of SLR and the possible products to be delivered. The presentation stressed the stringent requirements of GGOS and how the synergy of the geodetic techniques will meet this challenge.

The session concluded with two posters. C. Noll presented a global map illustrating the four networks of the space techniques as they exist today. In the second poster, F. Deleflie showed an example of how ILRS can make use of the Virtual Observatory on the web, following the example of astronomy.

The Contribution of Laser Ranging to the Global Geodetic Observing System

Richard S. Gross
Jet Propulsion Laboratory, California Institute of Technology, USA
Richard.Gross@jpl.nasa.gov/ fax: 818-393-4965

Abstract

The Global Geodetic Observing System (GGOS) provides measurements of the time varying gravity, rotation, and shape of the Earth using instruments located on the ground and in space. The key components of GGOS that provide these measurements are the IAG Services, including the ILRS. Earth orientation parameters have been routinely determined from laser ranging observations to the Moon since 1970 and to artificial satellites since 1976, making them the longest available space-geodetic series of Earth orientation parameters. Such long duration homogenous series of accurate Earth orientation parameters are needed for studying long-period changes in the Earth's orientation, such as those caused by climate change. Low-degree time varying spherical harmonic coefficients of the Earth's gravitational field have also been routinely determined from laser ranging measurements to artificial satellites since shortly after the launch of Lageos; the resulting degree-2 zonal coefficient agrees better with models of the gravitational effect of surface geophysical fluids than does that determined by GRACE. Laser ranging measurements also fundamentally contribute to the determination of the terrestrial reference frame by providing its origin and contributing to its scale. Thus, satellite laser ranging is a key component of GGOS. Without satellite laser ranging GGOS would not be able to meet its goal of providing geodetic products accurate to better than a part per billion.

Quality Assessment of the ILRS EOP 'Daily' Product

C. Sciarretta (1)**, V. Luceri** (2)**, G. Bianco** (3)

(1) Telespazio SpA, Roma, Italy
(2) e-GEOS SpA, CGS-Matera, Italy
(3) Agenzia Spaziale Italiana, CGS-Matera, Italy

Abstract

The ILRS Analysis Community has been developing, since several years, global, long term, very accurate geodetic products. In the last few years, even short term (weekly data arcs) and fast updated (every week) geodetic solutions have been produced, conveyed into official ILRS combined 'weekly' product, thus allowing the users to benefit of SSC and EOP estimates which are either accurate and fast. In the case of EOP, the users are provided with daily estimates over a week with a minimum latency, at the generation day, of 4 days and a maximum latency of 11 days. The 'weekly' product performance triggered the generation of a faster, lower latency combined product, now still under testing. This product is labelled 'daily' due to its updating frequency: a sliding window of 7 days worth of data is analyzed daily, reducing the overall product latency to 2 days. In this presentation, the performance of the presently available 'daily' EOP combined product is reported. In particular, the stability and reliability of the product with respect to its latency is analysed, as well as the effect of the combination process.

The ILRS Weekly Solution experience

Since 2004, ILRS has been providing, routinely, the weekly combined *SSC/EOP* solutions mainly to support IERS for the EOP computation, give the scientific community an updated coordinate time series and contribute to the reference frame maintenance. Each weekly solution consists of

- daily estimated ITRF-framed and loosely constrained EOP values (XPO, YPO, LOD)
- a set of loose constrained coordinates for the acquisition network
- several quality evaluation indicators

provided in three different files available at CDDIS and EDC.

At present, eight Analysis Centers (ACs) contribute to the weekly ILRS combined solution issued by the Official ILRS Combination Centers (hereafter CCs): ASI, BKG, DGFI, GA, GFZ, GRGS, JCET, NSGF. ASI-CGS is the Primary ILRS CC and its product (named ILRSA) follows the combination procedure based on the direct combination of loosely constrained solutions (Davies and Blewitt, 2000; Bianco, Devoti, Luceri, 2003). The combination is performed along the lines of the iterative Weighted Least Square technique: each contributing solution plays the role of an ‘observation’ whose residuals with respect to the combined solution must be minimized.

Each Wednesday, the official ILRS combined solutions are issued following the same timeline: the SLR data acquired (Lageos1/2, Etalon1/2) during a 7-day period (Sunday-Saturday) are processed by the ACs and made available to the CCs within Tuesday.

√ Data arc 7 days

√ Generation frequency 1/week
√ EOP estimate age 4-10 days

In Figure 1, a sample (Jan-Oct 2008) of EOP ILRS residuals with respect to the USNO finals values is shown; different age of the estimates are indicated. The relevant overall statistics is reported in Table 1.

Table 1. ILRSA weekly solution EOP residuals wrt USNO EOP "finals.data"

X (mas)		Y (mas)		LOD (0.1ms)	
<res>+/-std	<σ>	<res>+/-std	<σ>	<res>+/-std	<σ>
0.02+/-0.17	0.05	0.04+/-0.17	0.05	0.04+/-0.41	0.12

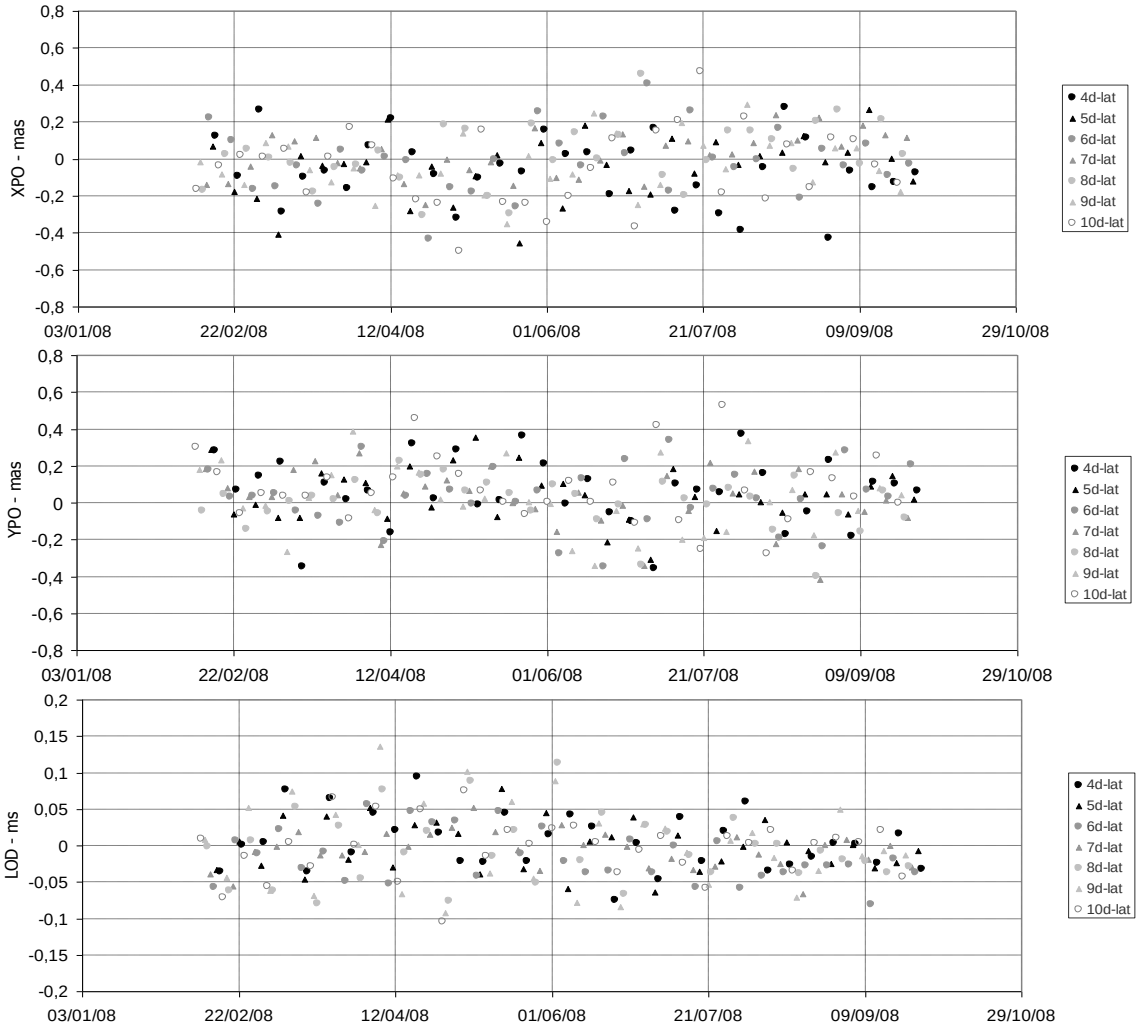

Figure 1. ILRSA weekly solution EOP residuals wrt USNO EOP "finals.data"

An enhanced ILRS product: the Daily Solution

The consolidated, well performing ILRS weekly product (Bianco, Luceri, Sciarretta, 2006) has suggested the concept of a 'rolling' weekly product to be issued daily in order to provide the minimum latency SLR contribution to the IERS EOP estimation.

At day N-1, within midnight UTC, each contributing AC makes available its weekly solution spanning the period [N-8, N-2]; at day N, the CCs generate the combined solution. The following features are common:

√	Data arc	7 days
√	Generation frequency	1/day
√	EOP estimates age	2-8 days

ASI-CGS CC adapted the ILRSA weekly combination strategy to the daily product; only a slight tuning has been performed to allow the proper handling of the USNO "finals.daily" as reference values, due to the necessity of computing a reference value for the most recent LOD estimate, not provided by that EOP series.

Moreover, a careful revision of the combination procedure has been performed, in order to allow the fully automated generation of the solutions, including the reporting, to avoid (or minimize) the daily intervention of the analyst. The automated ILRSA combination procedure, at present, starts every day at 1:30 AM UTC; the starting time may be modified according to ILRS/IERS recommendations.
At present, 5 ACs contribute to the daily ILRS combined solution: ASI, BKG, GFZ, JCET, NSGF.

A preliminary overall assessment of the Daily Solution

February 25th, 2008 may be assumed as the true start date of the pre-operational generation of the daily ILRSA product: that is the first date when all the 5 ACs submitted fully operational solutions after a brief tuning phase. Since then, only few sporadic cases of missing solutions occurred. If late solutions were submitted, they were not analysed to stress the ILRSA combination procedure under realistic operational conditions.

The Core station list, as agreed after the Grasse ILRS AWG (Sep.'07) meeting, is used in the ILRSA daily product. As for the consolidated weekly product, 3d WRMS for all sites is below 10mm, while for the Core sites it is slightly above 7mm.

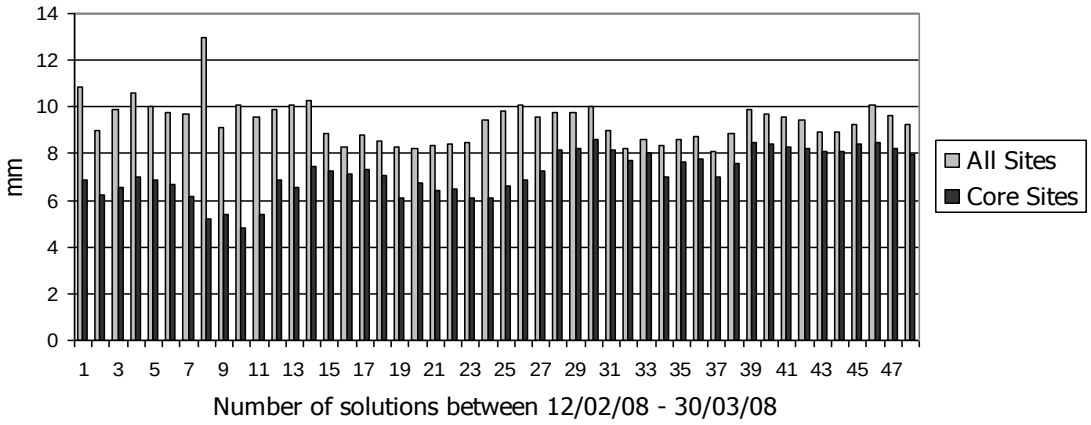

Figure 2. ILRSA daily solution: a sample SSC 3D WRMS wrt SLRF2005

A preliminary quality evaluation of the daily solution results at the start of the pre-operational phase has been made through the cross comparison with IERS EOP C04 and with ILRSA weekly solutions, focussing on the **most recent day EOP estimate**, being that one the most critical from the product latency, and hence efficacy, point of view.

The results, based on a month of solutions, indicate an overall precision level (<σ>) of the last day estimates of the order of 0.10mas/0.026ms and an accuracy level (WRMS(res)) of the order of 0.25mas/0.070ms, roughly twice, twice-and-half larger than the values relevant to the Weekly solution.

Table 2. ILRSA weekly solution EOP residuals wrt USNO EOP "finals.data"

	X (mas)		Y (mas)		LOD (0.1ms)	
	<res>+/-std	<σ>	<res>+/-std	<σ>	<res>+/-std	<σ>
D	0.14+/-0.20	0.10	-0.04+/-0.27	0.10	-0.017+/-0.064	0.026
W	0.08+/-0.13	0.05	-0.03+/-0.12	0.05	-0.004+/-0.052	0.012

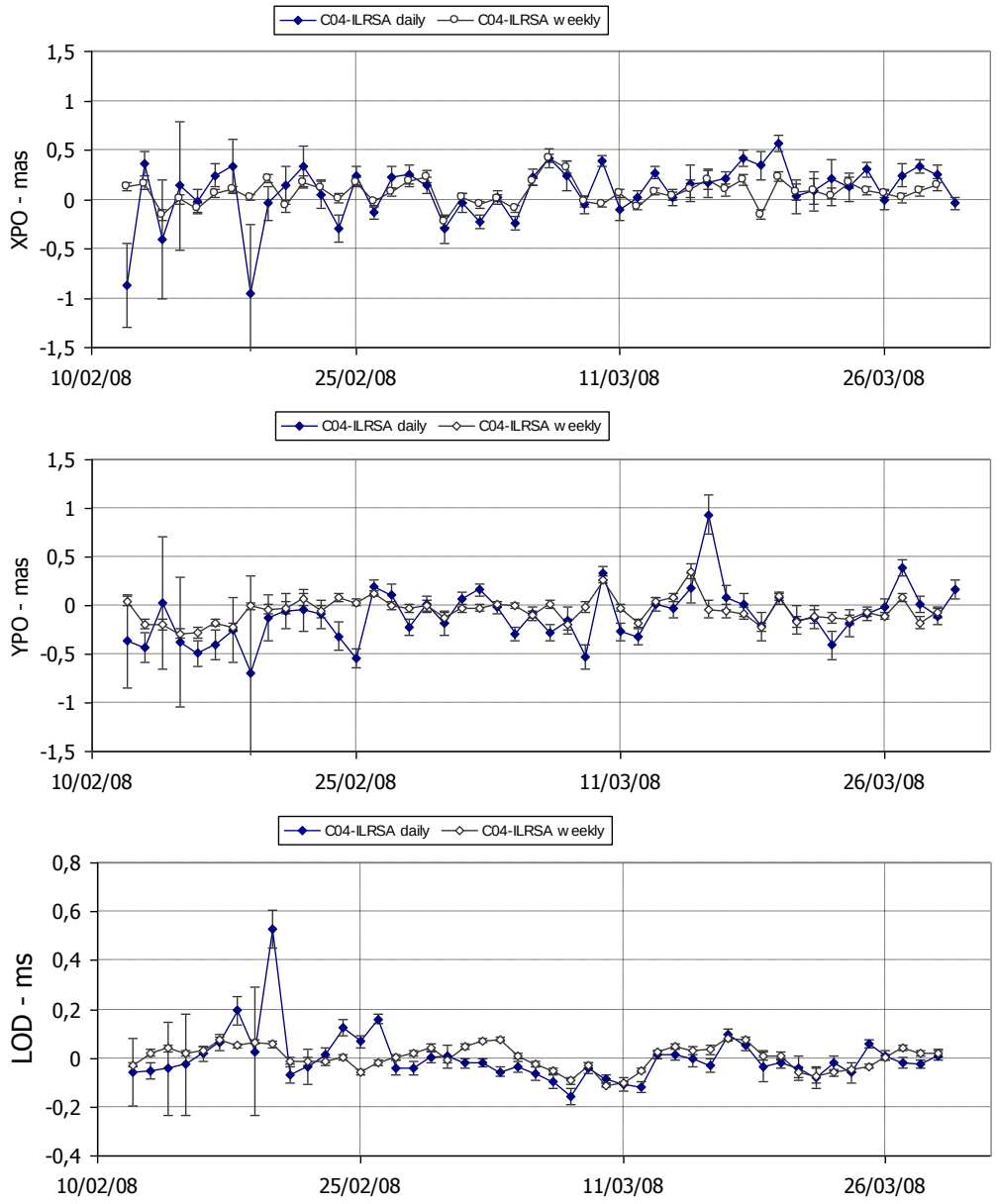

Figure 3. Sample assessment on the 'last day' ILRSA daily EOP estimates

An assessment of the Daily Solution in terms of 'age' of estimates

The accumulation of solutions allows a deeper insight into the performance of the product versus the 'age' of the estimated EOP's, keeping in mind that the potential added value of the daily product is the availability of the fastest EOP, as possible, with the best accuracy level.
Up to October 2008, more than 6 months of individual and combined solutions were available and they have been used to construct EOP time series with the "same age". The quality of the sampled series has been evaluated by computing the relevant statistics for each contributing AC: an **"arc edge"** effect is evident in the x-pole and y-pole estimates (Fig. 4, Fig.5, Fig.6, Fig.7) both in the RMS of the residuals with respect to the USNO "finals.data" and in the estimate uncertainties.

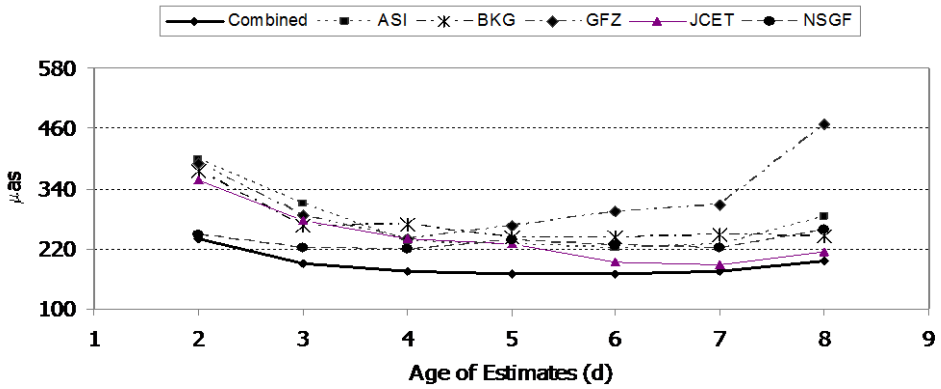

Figure 4. RMS of XPO residuals w.r.t. USNO "finals.data" vs "age"

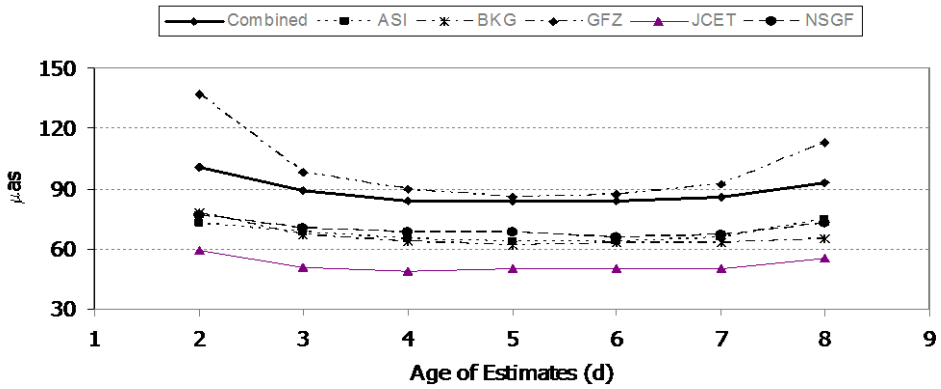

Figure 5. Average uncertainty of XPO estimates vs "age"

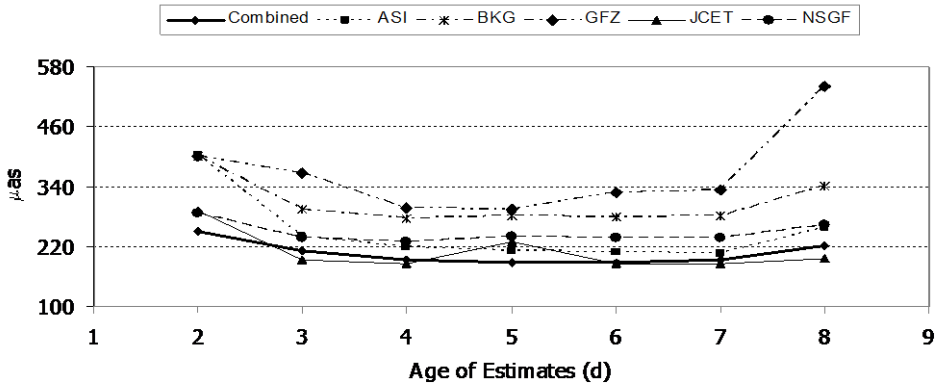

Figure 6. RMS of YPO residuals w.r.t. USNO "finals.data" vs "age"

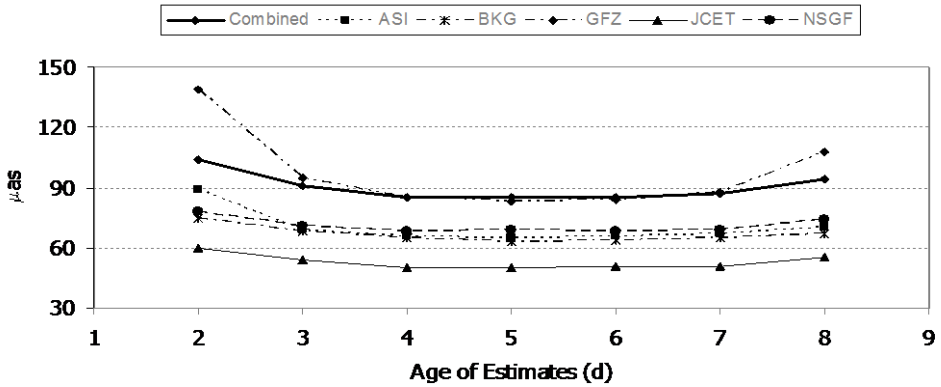

Figure 7. Average uncertainty of YPO estimates vs "age"

The edge effect, also present in the combined weekly product, is a key feature to be investigated to provide the lowest latency (2 days), accurate EOP estimates, that is the primary target of the daily solution product; the combined product mitigates the effect especially in the accuracy of estimates, but their uncertainties, rescaled by the post fit variance factor, are affected both by the imprecision of the contributing estimates and by their discrepancies. The following comments hold:

- part of the "arc edge" effect, for the 'last day' estimates is due to partial lack of observation data: the problem can be overpassed by pushing some hours later the issue epoch of the contributing solutions to collect more data;
- discrepant values among contributing solutions raise the uncertainty and accuracy of the final combined values;
- fine tuning of the analysis strategy should be done by the ACs to mitigate the "arc edge" effect in the contributing solutions, showing different levels of evidence;
- new contributors will improve the quality of the daily product.

It is worth to be noted that the 3-day-old EOP estimates show a good level of accuracy and precision and represent already an operational upgrade of the performance of the weekly solution, providing the same level of accuracy at a homogeneous and faster latency.

Conclusive remarks

At present, ILRS is able to provide daily, in a pre-operational phase, a combined solution with high level quality, daily, EOP estimates, covering a weekly arc, and with a constant latency lower than the minimum latency of the ILRS weekly solution (4 days). The minimum constant latency possible for the product is 2 days; in this extremal case, however, several actions have to be undertaken to mitigate the "arc edge" effect, degrading the potential quality of the 'last day' EOP estimates: adding contributing solutions, revising the length of the data arc, tuning the AC analysis strategies will raise the quality of the product. The 3-day latency EOP estimates, however, can be considered, at present, an optimal trade-off between accuracy and latency requirements.

References

Davies, P., and G. Blewitt, *Methodology for global geodetic time series estimation: A new tool for geodynamics*, Journ. Geophys. Res., Vol. 105, No. B5, pp. 11,083-11,100, 2000.

Bianco, G., Devoti, R., Luceri, V., *Combination of loosely constrained solutions*, Proceedings of the IERS Workshop on Combination Research and Global Geophysical Fluids (Munich, 18-21 Nov 2002), IERS Technical Note 30, 107-109, 2003.

Bianco, G., Luceri, V., Sciarretta, C., *The ILRS Standard Products: A Quality Assessment*, Proceedings of the ILRS Workshop, Canberra, 2006.

ESOC IGS, IDS, and ILRS (Re-) processing

T.A. Springer, M. Otten, I. Romero, C. Flohrer, J. Dow, R. Zandbergen
ESA/ESOC Robert-Bosch-str. 5, Darmstadt, 64289, Germany
Tim.Springer@esa.int

Abstract

This paper gives an overview of the processing and reprocessing activities at the European Space Operations Centre (ESOC) of the European Space Agency (ESA). Within ESOC the navigation support office (OPS-GN) is since many years an analysis centre of the International GNSS Service (IGS). Enabled by enhancements of the Napeos software package the OPS-GN analysis capacities and activities have been expanded significantly since 2008. Thanks to these enhancements OPS-GN is now capable to contribute to the international services for all three satellite geodesy techniques: IDS, IGS, and ILRS. Besides an overview this paper shows selected results of the ongoing processing activities.

Introduction

Early in 2008 ESOC has replaced its old GNSS analysis software with its new software, called ***Napeos***. One of the key design criteria of this new ESOC GNSS analysis software was the reduction of processing time! The software, now fully operational, allows generating a 1-day IGS final solution using 150 stations within 60 minutes on a single core of a Linux PC using the Intel Fortran compiler. On a "quad-core" CPU four jobs can be run simultaneously without any performance loss, meaning that we are able to process 96 days of IGS data per day (24 hours x 4 cores). With this performance, rapid reprocessing of decades of IGS data becomes possible. On a single PC reprocessing of a full year of IGS data takes less than 4 days, so reprocessing 10 years of data will take about 40 days on a single quad-core PC.

Besides efficient GNSS analysis, the Napeos software is also fully capable of processing DORIS and SLR observations. ESOC recently joined the reprocessing activities of the International Doris Service (IDS), and is joining the ILRS reprocessing activities. Our aim is to contribute to all three space geodesy technique services: IGS, IDS, and ILRS with fully reprocessed time series. In our opinion a contribution from one software to all three techniques is unique and of significant value for the next ITRF combination. Our IDS, IGS and ILRS reprocessing has been completed. Only for the ILRS the acceptance of the solution is still pending.

At ESOC the reprocessing of the three individual techniques is considered a ***first step***. Our ***ultimate*** goal is to do a fully combined analysis of the data of all three techniques, and in the future even 4 techniques when adding VLBI. In such a combined analysis the strength of each technique may be used to overcome the weaknesses in the other techniques. In this combination of techniques SLR plays a crucial role as it is the only technique that provides (in principle) unbiased range measurements. Thus SLR is the only technique that provides direct access to the scale of the terrestrial reference frame. In addition SLR is extremely important in validating the orbits of both the IGS and the IDS.

Here will show the status and some selected results from our different reprocessing solutions and provide an overview of our future plans regarding the fully combined reprocessing.

IGS processing

ESOC OPS-GN has been a full analysis centre of the International GNSS Service (IGS) since its very beginning in 1992. In January 2008 a switch to the new ***Napeos*** software was made which gave rise to a significant improvement of the ESOC GNSS processing, both in quality and in speed. The two aspects combined enabled ESOC to participate in the IGS reprocessing. With Napeos the reprocessing of 1 day of IGS data using 150 stations and 32 satellites can be done within 60 minutes on a single core of a Linux PC. Thus on a single "quad-core" machine four jobs can be run simultaneously without any loss of performance. For the reprocessing this means that the reprocessing can advance by 96 days of IGS data per day. With this performance the reprocessing of the full IGS data set from 1994 to 2008 took only 53 days.

ESOC reprocessed all days from 1994 to the end of 2007. The results from 1994 were omitted since the IGS tracking network suffered some severe problems early in this year when "anti-spoofing" was turned on. So ESOC finally submitted only the results from 1995 until the end of 2007 to the IGS. Before submission our products were carefully validated. One important quality measure in the validations was the agreement of the orbit at the day boundary. The ESOC reprocessed orbits are generated using 24 hour arcs. So the difference at the day boundary gives a "worst case" estimate of the satellite orbit quality. Figure 1 shows the results of this day boundary check in the radial direction for each of the years. A steady improvement of the orbit overlap is observed going down to the 20 mm level. This is an excellent result for the overlap of two independent orbit arcs at their arc boundary!

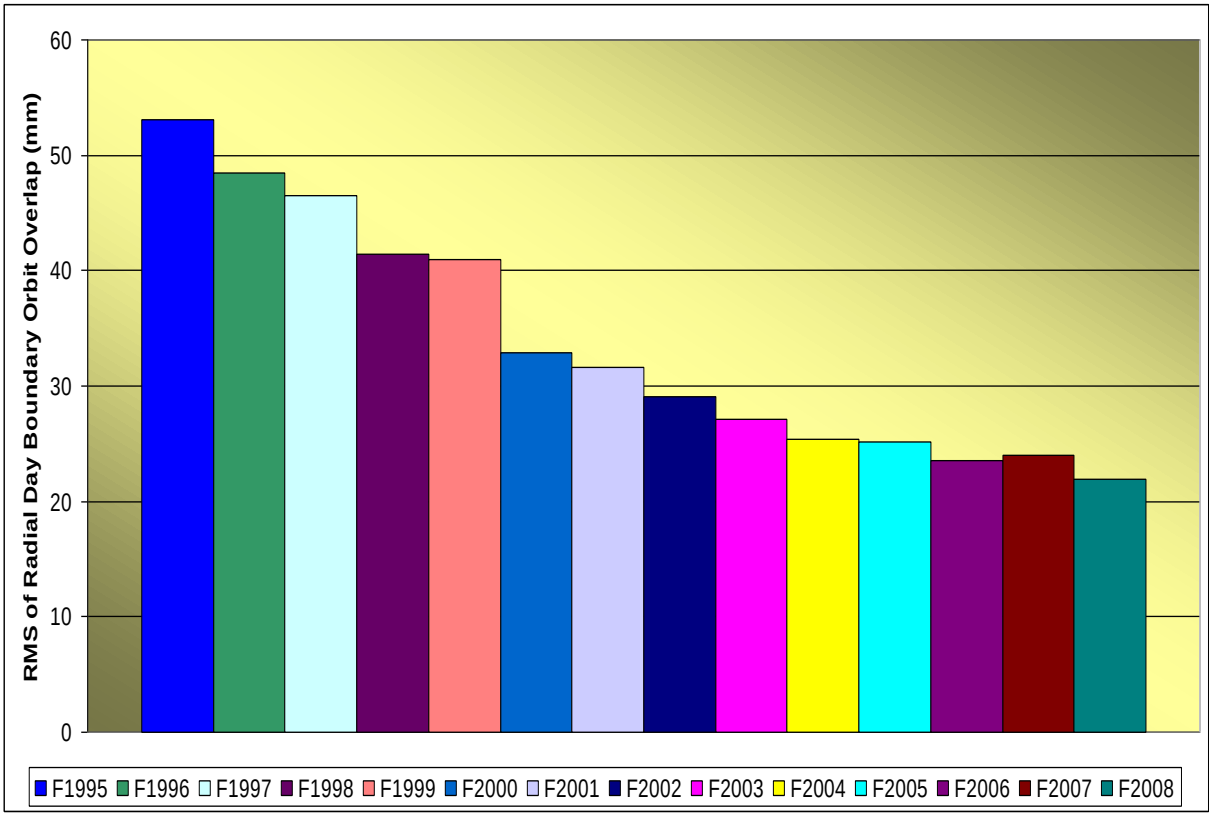

Figure 1. Statistics of Radial Orbit Differences at the Day Boundaries of the ESOC reprocessed IGS orbits for each individual year over the timeframe from 1995 to 2008

Another quality control step was the validation of the orbits against the SLR observations from the GPS satellites 35 and 36 (PRN 5 and 6). The mean and the sigma of this GNSS-orbit versus SLR-observation validation are given in Figure 2.

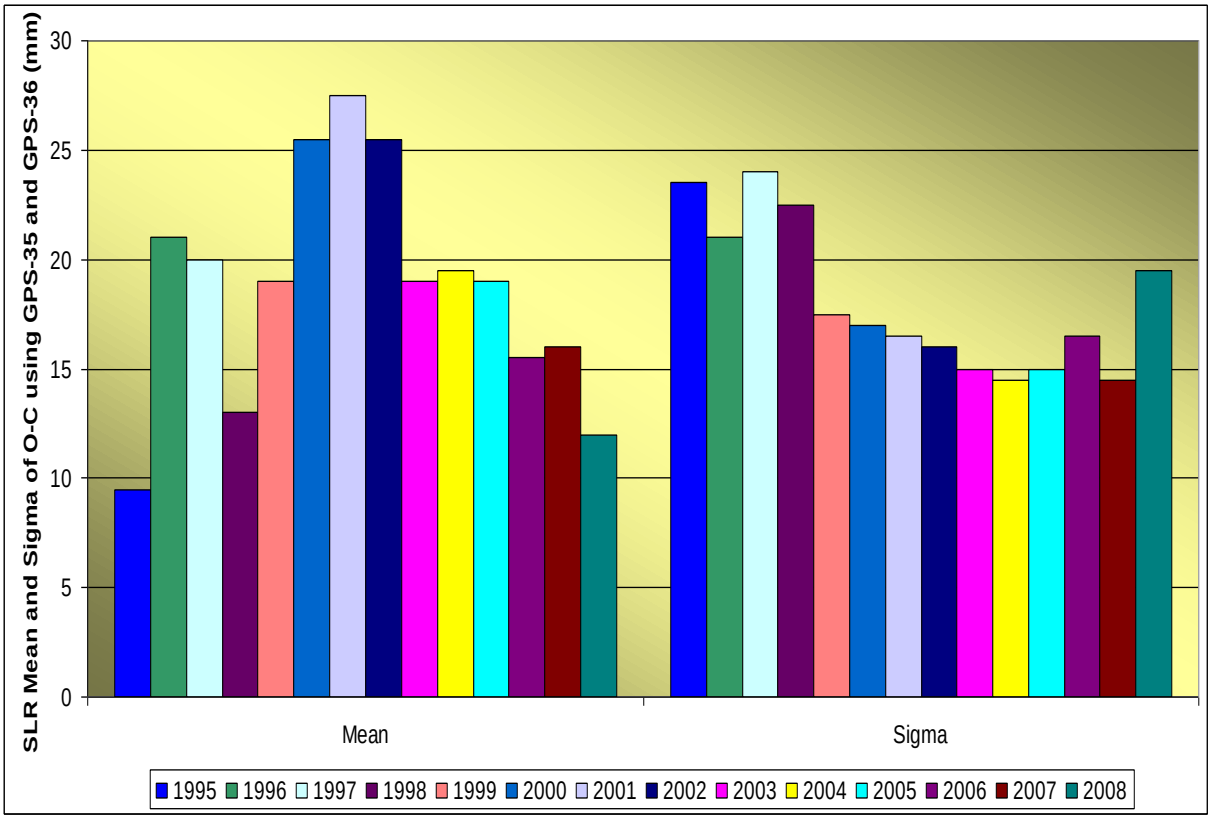

Figure 2. SLR validation of the ESOC reprocessed IGS orbits for each individual year over the timeframe from 1995 to 2008.

Figure 2 shows that the average mean bias between the GPS-orbits and the SLR observations is now at the level of 15 mm whereas the sigma is at a similar level. The agreement between time series of the radial orbit overlap and the sigma of the SLR residuals is quite good. However, the somewhat "erratic" behaviour of the mean of the SLR residuals indicates that for the early years, 1995 to 1998, there may be some biases in the SLR observations. Also the rather high sigma for 2008 may be related to not properly accounting for some of the biases present in the SLR observations.

Another interesting way to look at the SLR residuals it to plot the residuals as function of the latitude and elevation of the Sun with respect to the orbital plan of the satellites, as was done by Flohrer (2008). The results are shown in Figure 3. The figure nicely shows the eclipse period of the satellites, the dark circle in the middle. The reason for this pronounced eclipse effect is mainly because we did not account for the correct attitude of the GPS satellites. Thus the attitude error coupled with the eccentric position of the laser reflector array gives a significant signal for the eclipse phase. Outside the eclipse very little signal may be observed although in the centre of the figure, around 180 degrees latitude, there seem to be more positive residuals whereas around 90 and 270 degrees latitude there seem to be more negative residuals. This could be an indication for a twice per revolution signal. Unfortunately there is little data around 0 and 360 degrees latitude because this reflects the point where the satellite

is in full sunlight and thus would require daylight tracking. Most of the ILRS stations are incapable of daylight tracking of the GPS satellites.

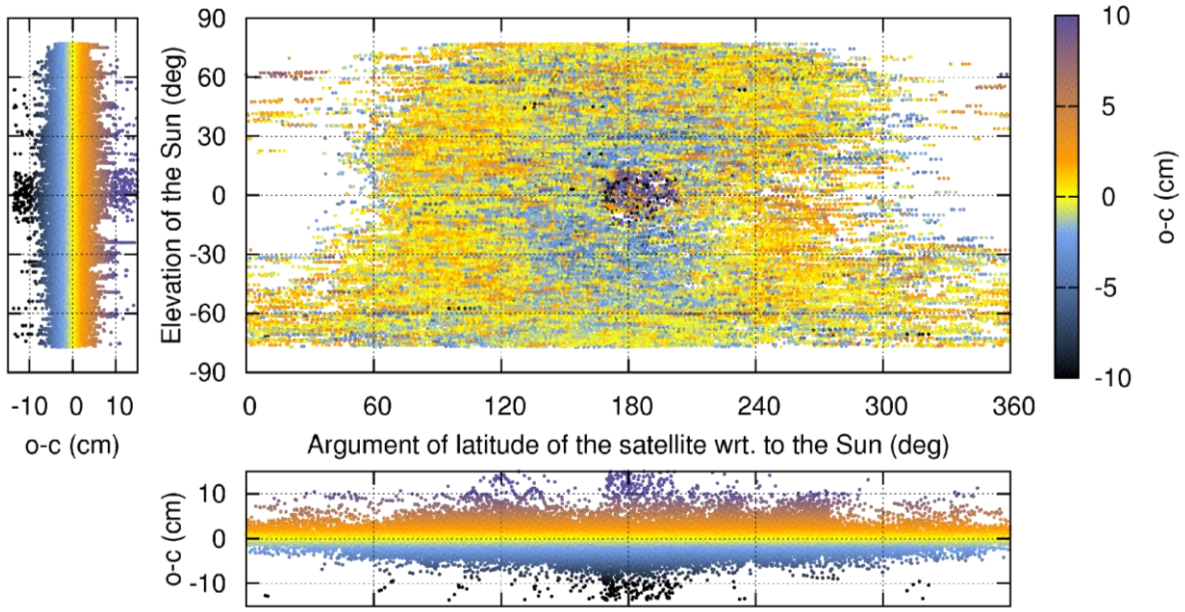

Figure 3. SLR residuals of the GPS satellites as function of latitude and elevation of the Sun with respect to the Orbital Plane, using all SLR observations from the GPS satellites from 1995 to 2008.

The pronounced eclipse effects may also be an explanation for the variability of the mean and the sigma observed in Figure 2. We will have to regenerate the statistics either whilst excluding the eclipse phases of the satellites or whilst correctly accounting for the attitude of the satellites.

IDS processing

The key enablers for ESOC to participate in the DORIS reprocessing were:

- Many years of experience in routine processing of the DORIS data of the ESA ENVISAT mission
- Efficient software, Napeos, including
    - Excellent modelling capability for LEO satellites, and,
    - All tools for generating the required IDS products, e.g., SINEX.

The key challenges in IDS reprocessing are the station and satellite equipment changes. Many stations were refurbished over time because of hardware improvements. However, this leads to discontinuities in the station coordinates. Secondly, there are only few satellites equipped with a DORIS instrument and thus the addition and/or removal of a satellite from such a small constellation has noticeable effects. The positive effect of the hardware changes, or rather improvements, can be observed clearly in Figure 4 which shows the evolution of the residual RMS of the DORIS observations over the entire reprocessing period of 1992 to 2008. The downward trend of the DORIS residual RMS from 1992 to 2006 is mainly caused by hardware improvements of the system. The small jump of the ENVISAT residual RMS

around 2005 is an artefact of the increase of the integration time. Furthermore, the increase of the residual RMS since 2006 is caused by the degradation of the accuracy of the station positions. In this analysis the station coordinates were fixed to the ITRF2005 values. Imperfections of the velocities and a number of new sites thus have a significant effect on the residual RMS. At the same time the figure shows appearance and disappearance of the satellites equipped with DORIS receivers.

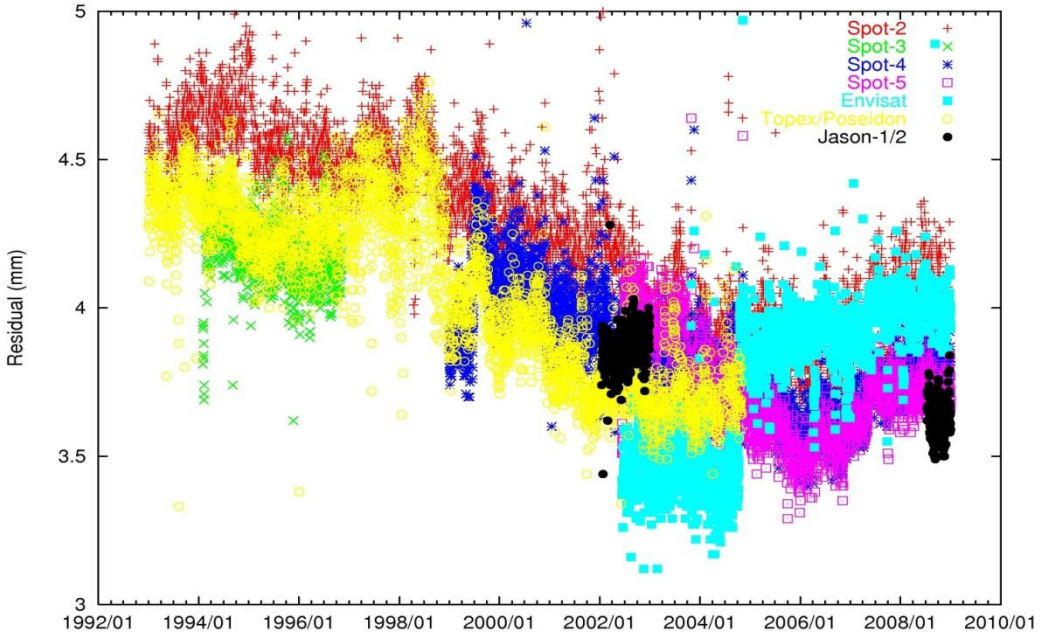

Figure 4. Time Evolution of the DORIS Residual RMS.

ILRS processing

The key enablers for ESOC to participate in the ILRS reprocessing were:

- Many years of experience in routine processing of the SLR data of the ESA missions
  - ERS-1, ERS-2, and ENVISAT
- Experience with processing SLR from GNSS targets
- Efficient software, Napeos, including:
  - Excellent modelling capability for LAGEOS and ETALON targets
  - All tools for generating the required ILRS products, e.g., SINEX files
- ILRS associate analysis centre with as key activities:
  - Prediction centre for several satellites, e.g., Giove-A, Giove-B
  - Analysis of ENVISAT, ERS-1 and ERS-2

The main challenges for ILRS reprocessing are gathering the information regarding the different possible instrumental biases. It has become clear that even for our relatively simple SLR validation of the GNSS satellite orbits, taking into account the different instrumental biases of the ILRS stations is an absolute must. The results in Figure 2 give some indication

regarding the importance of this. Given the fact that the GNSS orbit were generated fully homogenously in terms of modelling and reference frame the significant variation of the observed mean differences must, at least in part, be caused by not properly accounting for the observation biases. After accounting for the observation biases the analysis of the Lageos and Etalon data is actually not very time consuming. Thus ESOC is planning to become a full analysis centre of the ILRS. The benchmark test has been performed and submitted in May 2009. In addition, a full reprocessing of all ILRS historic data since 1993 of both Lageos and both Etalon satellites has been performed. Figure 5 shows the time evolution of the ESOC weekly reference frame solution compared to the ITRF2005 (courtesy of Zuheir Altamimi). The results are very encouraging although the individual station residuals indicate that some station biases were not yet properly accounted for.

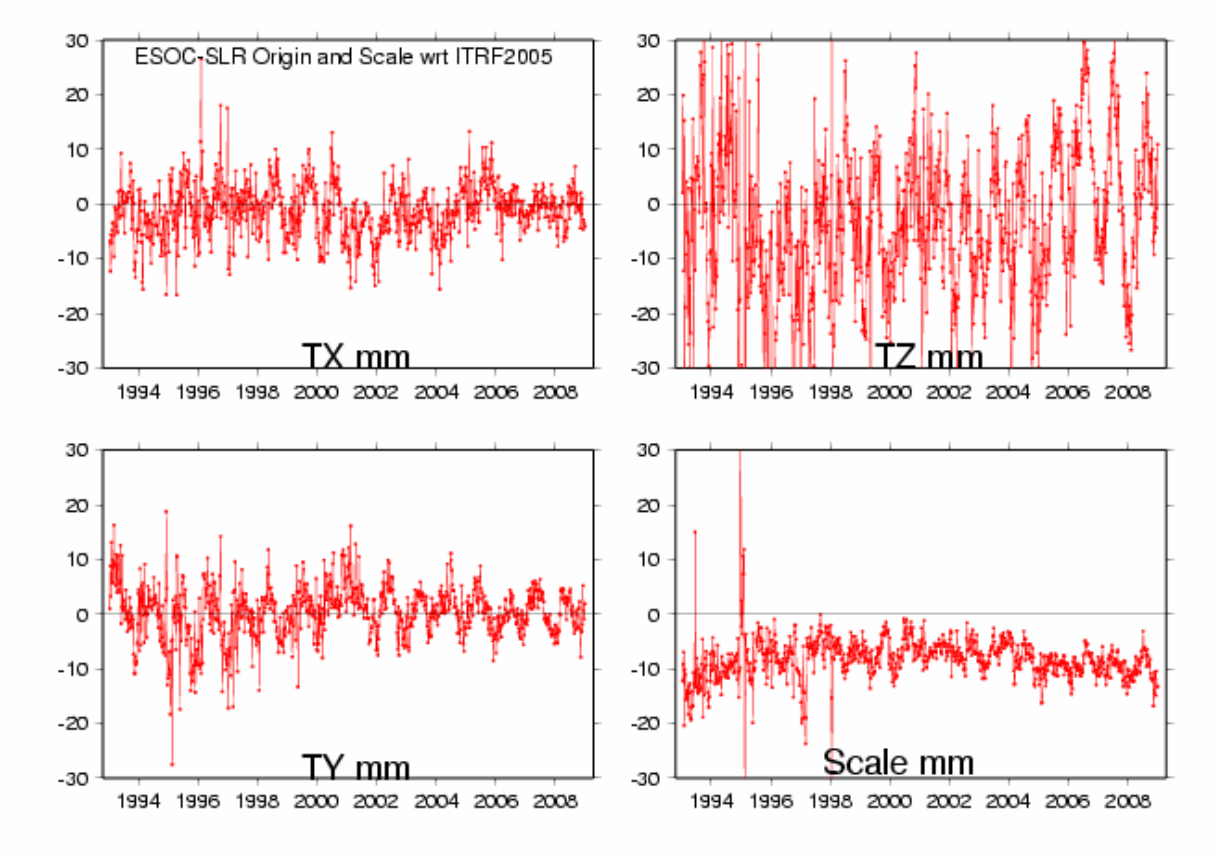

Figure 5. Time Evolution of ESOC ILRS Reference Frame Solutions from 1993 to 2008 (courtesy of Zuheir Altamimi)

Conclusions

ESOC has re-analyzed the historic data of all three satellite geodetic techniques, IDS, IGS, and ILRS using one single piece of software. The results of the ESOC IDS and IGS reprocessing will contribute to the realization of the ITRF2008. Due to the "infamous" ILRS bias issues and the lengthy process of being accepted as an ILRS analysis centre the ESOC ILRS reprocessing results will not be used for the ITRF2008 realization. For future ITRF updates we are convinced that we will contribute to all three space geodetic techniques using our Napeos software.

References

Flohrer, Claudia, *Mutual Validation of Satellite-Geodetic Techniques and its Impact on GNSS Orbit Modelling*, PhD Thesis, Bern, Switzerland, May 2008.

The comparison of the station coordinates between SLR and GPS

S. Schillak, M. Lehmann
Space Research Centre, Polish Academy of Sciences
Astrogeodynamic Observatory, Borowiec, Poland
sch@cbk.poznan.pl

Abstract

The paper presents results of comparison of the station positions and velocities determined by two satellite techniques: SLR and GPS. The coordinates were calculated for the same epochs in the International Terrestrial Reference Frame 2005. The comparison was performed for all stations equipped in the SLR and GPS systems in the period from 1993.0 to 2004.0 without the SLR stations whose system was changed in that time. The final calculations were performed for 12 stations. The coordinates were determined for the epochs on the first day of each month. The analysis included estimation of the station positions stability, and comparison of the positions with those according to ITRF2005, estimation of the station velocities obtained by the two methods SLR and GPS. The NNR-NUVEL1A plate velocity model and ITRF2005 velocities were used for verification of the station velocities. Generally with some exceptions, a good agreement of the station positions and velocities obtained for both techniques. For several stations significant (2-3 cm) differences were detected in the vertical components.

1. Introduction

One of the aims of the Global Geodetic Observing System (GGOS) appointed at the International Association of Geodesy (IAG) to be realised within the next 10 years is unification of the methods, models and parameters of the terrestrial studies. The hitherto made comparisons of the measuring methods based on the global mean results, as presented in subsequent ITRF solutions (Altamimi et al., 2002, Boucher et al., 1997, 2004) do not permit a detail analysis of differences between different techniques. To be able to identify and evaluate these differences, a comparison must be made of the results obtained within the same reference system (ITRS) for the same measuring points, the same reference epoch and – if possible- for the same models and parameters. The comparison should be made for the results collected for a long time, at least 5 years, which is particularly important for determination of the station velocity. The aim that should be achieved in the nearest future is determination of the station position at a global accuracy of 1 mm and the station velocity at a global accuracy of 0.1 mm/year. Direct comparison of the results obtained by different measuring techniques permits a detection and elimination of systematic errors brought by individual techniques and stations. Performance of a good comparison requires a correct transformation of results to a common reference system, accurate tie of the reference points of particular techniques at a given station, long-term observation sequences and high quality of measurements in each measuring technique.

The aim of this study was to compare the positions and velocities of a few stations determined by two different satellite techniques SLR and GPS. The analysis was made for the 12 stations carrying out parallel measurements by SLR and GPS in the period from 1993.0 to 2004.0. The laser stations whose laser system was changed in this period were not taken into account.

2. SLR and GPS Data

Results of laser observations were taken from the database Eurolas Data Centre (EDC) in the form of two-minute normal points of the LAGEOS-1 and LAGEOS-2 satellites (Pearlman et al., 2002). The orbits were calculated by the orbital NASA GEODYN-II program (Pavlis et al., 1998). Normal equations were calculated for each satellite separately for the same monthly arcs. The points over the criterion of 5 σ for each station as well as those below 10 degrees over the horizon were rejected. Also the passes whose systematic deviation exceeded 2.5 σ from systematic deviations in a given month were rejected. The reference stations for orbit determination were 15-16 of those whose results were characterised by the highest accuracy, a large number of normal points and continuity of observations. Ten of those stations were the same over the period of the 11 years of study, while the others were selected according to the quality of observations in a given year. The station coordinates were determined from the normal equations of the two satellites in each arc for one station, while the coordinates of the other stations were taken from the system ITRF2005 (ITRF2005, 2006). The station coordinates were determined for the first day of each month.

As follows from Fig.1a showing the RMS of fit of each monthly arc, a substantial improvement in the quality of observations is visible beginning from 1996. It is a consequence of significant changes in the equipment of the best laser ranging stations. The considerable deterioration of RMS in April 2002 was most probably a consequence of the collision of a micrometeorite with LAGEOS-1 on April 5th, 2002 over the Pacific (Lemoine et al., 2004). Fig. 1b presents the number of normal points used for determination of the monthly arcs.

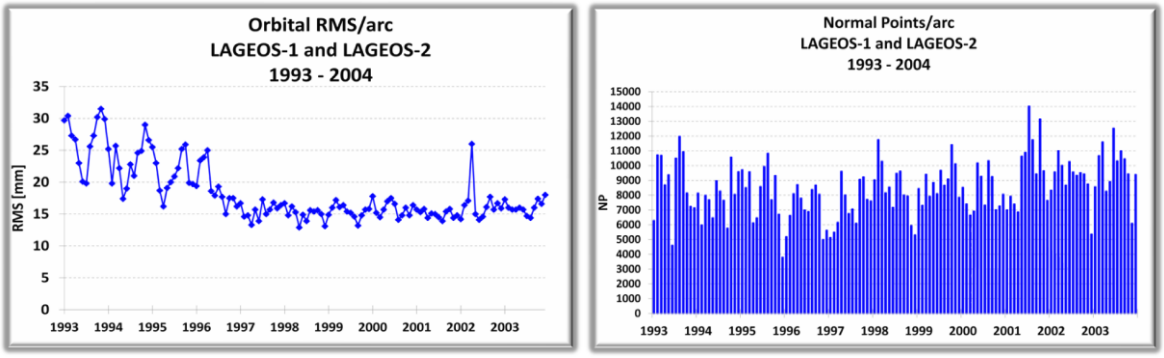

a) b)

Figure 1. a) RMS of fit b) number of normal points
LAGEOS-1 and LAGEOS-2 for the monthly orbital arcs

The geocentric GPS coordinates in the ITRS2005 system over the period 1993.0-2004.0 in the form of daytime series per the 2007.0 epoch was obtained from Dr Michael Heflin from JPL/NASA. The reference frame ITRF2005 was established for each day on the basis of the 7-parameter Helmert transformation. The transformation to the 2000.0 epoch (ITRF2005 epoch) was performed using the velocities given for each station by JPL NASA. The common reference point for SLR and GPS was that of the laser station, i.e. the point of intersection of the rotation axes of the telescope. The tie of the geocentric coordinates ΔX,

ΔY, ΔZ of the reference points of GPS and SLR for a given station was taken from ITRF2005. The GPS coordinates were determined for the epoch of first day of each month, similarly as for SLR.

From the list of SLR and GPS coordinates only those having the common epoch were selected, therefore, from the maximum number of 132 point that can be determined over 11 years the selected number of common points is much lower (Table 1). Some stations, like e.g. that in Beijing, have a low number of common points as they started the GPS observations much later (Beijing since 2000). The last column gives the period of time of common observations, from the first to the last, particularly important for determination of the station velocity. Except the Beijing station this time was close to 8 years, which is sufficient for accurate determination of the station velocity. Because of the changes in the coordinates of the Arequipa station forced by the earthquake in June 2001, two sets of data were given for this station covering the periods before and after the earthquake. The averaged results are given for the period before the earthquake.

Table 1. List of the SLR – GPS stations whose data were taken into account over the period 1993.0 – 2004.0.

STATION	SLR	GPS	NUMBER OF COMMON POINTS	PERIOD (months)
McDonald	7080	MDO1	111	125
Yarragadee	7090	YAR1	109	131
Monument Peak	7110	MONP	76	109
Beijing	7249	BJFS	34	45
Arequipa	7403	AREQ	56/14	87/30
Borowiec	7811	BOR1	96	111
Grasse	7835	GRAS	68	94
Potsdam	7836	POTS	96	110
Shanghai	7837	SHAO	67	99
Graz	7839	GRAZ	116	132
Herstmonceux	7840	HERS	102	130
Wettzell	8834	WTZR	79	94

3. Positions and velocities of the stations

The geocentric SLR and GPS coordinates calculated for the first day of each month were transformed into the topocentric components in the form of deviations from ITRF2005 in the N-S, E-W and vertical (U) directions (Borkowski, 1989). Exemplary results for the stations Yarragadee (7090) and Arequipa (7403) are shown in Fig. 2.

The station velocity is described by the slope of the time dependence of the coordinate components, shown in Fig. 2. According to the model of the tectonic plate motion, no changes are observed in the vertical component of the station position. The results of a few stations revealed considerable (up to 3 cm) differences in the vertical component between the SLR and GPS data. Particularly important are the differences of the two Moblas stations (Moblas-4, Monument Peak and Moblas-5, Yarragadee). The data from these two stations are of substantial importance for determination of orbits from laser observations. The data from a

few other stations shows systematic deviations in the vertical component in some periods (Borowiec, Graz, Grasse, McDonald). The majority of systematic errors in the data obtained by SLR and GPS occur in the vertical direction as it is the fundamental direction of observations. The data for Arequipa (Fig. 2) show a jump change in the horizontal components as a result of the earthquake and a very good agreement in the SLR and GPS results. No jump is noted in the vertical component, but the slow change in the station vertical position is visible for the data obtained by these two techniques immediately before the earthquake.

The quality of the position of a given station can be evaluated on the basis of changes in its coordinates. The change in the position of a station determined for the epoch assumed following from taking into regard the station velocity should be very small, at least for a majority of the stations. The lower the mean square deviation over the period of time studied the more accurate the results of coordinate determinations. The results illustrating the stability of the station position are given in Table 2; the stability of the best stations is at a level of 5 mm. In contrast to the GPS data, the SLR data reveal large differences in the station stability, reaching even up to 3 cm, which is a consequence of the systematic measurement errors of SLR.

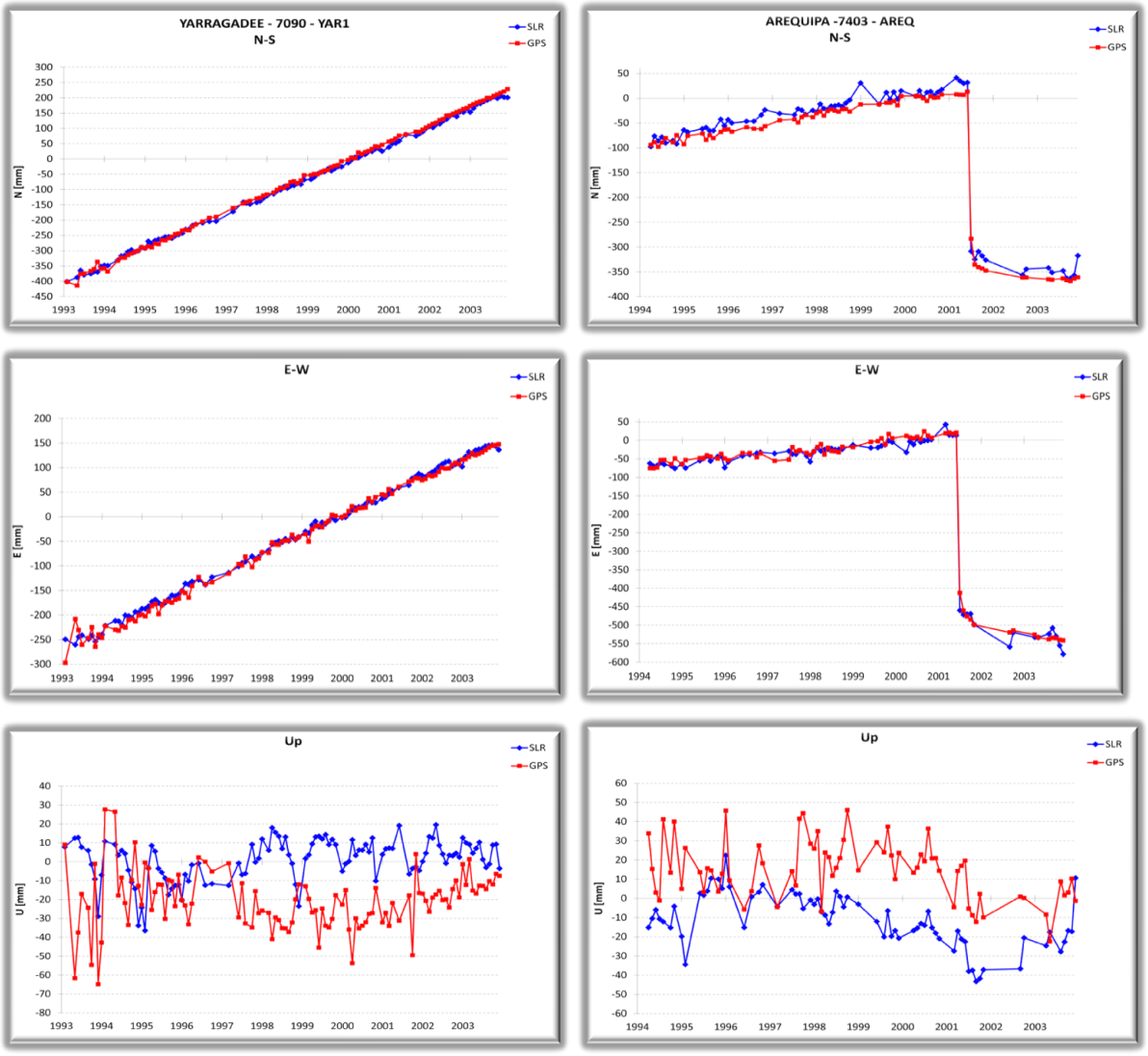

Figure 2. The topocentric coordinates of Yarragadee-left and Arequipa-right (SLR–blue, GPS-red)

Table 2 presents also the differences in the mean coordinates obtained from the SLR and GPS data for the period given in Table 1 for particular stations. The differences expressed in ITRF2005 are also given. The differences between the results of our study and ITRF2005 follow from a bit different period of data averaging, especially for Arequipa, from the differences in data analysis and in criteria of points rejection.

The velocities of the stations were calculated on the basis of the SLR and GPS data by linear regression as the slope of the time dependence of the coordinate components over the time period given in Table 1. The uncertainty of determination of the station velocity ranges from 0.1 mm/year for the best SLR stations and almost all GPS stations to 3 mm/year for the least accurate SLR stations. The results of the station velocities obtained for all stations considered are given in Table 3.

The data presented in Table 3 illustrate a very good agreement between the results obtained by the two methods SLR and GPS for the majority of the stations, the differences do not exceed 1 mm/year. A comparison of these data with those provided by ITRF2005 also indicates a very good agreement, with the differences not exceeding 1 mm/year. No systematic differences are noted in the station velocities determined from SLR and GPS data, both in the geocentric system and horizontal plane.

Table 2. Mean differences in the coordinates obtained by SLR and GPS methods and the stability of the (3D) coordinates determined.

STATION	SLR-GPS [mm]	SLR-GPS ITRF2005 [mm]	STABILITY [mm]	
			SLR	GPS
McDonald	10.3	5.3	8.4	8.2
Yarragadee	13.1	8.5	8.4	11.2
Monument Peak	18.8	8.7	7.6	8.6
Beijing	13.4	13.7	31.6	6.7
Arequipa	18.6	2.9	10.0	10.0
Borowiec	7.0	15.8	17.0	6.4
Grasse	4.4	3.7	10.5	5.9
Potsdam	6.0	4.2	8.4	6.7
Shanghai	18.1	9.5	21.5	9.9
Graz	7.4	2.9	11.7	7.2
Herstmonceux	4.1	11.3	6.8	8.9
Wettzell	3.2	3.7	9.4	5.6

However, there are systematic differences between the velocities of the stations determined by these two methods and those following from the NNR-NUVEL1A plate velocity model (DeMets et al.1994). The NNR-NUVEL1A velocities of all European stations are by 1-2 mm/year lower. The velocities of the Chinese stations are lower by 5 mm/year for Beijing and 10 mm/year for Shanghai. The differences could be explained by the fact that these two stations are localised at the edge of the Eurasia plate or on the Chinese subplate. The analogous differences in the velocities of the stations from the Pacific and Australian plates are small 1-3 mm/year, practically nonexistent for the station from the North American plate. The vertical components of the positions of each station except Beijing change at the velocity below 5 mm/year. No systematic changes are obtained in the velocity of the vertical component depending on the plate. Relatively high velocities obtained for Beijing are a

consequence of the short time of measurements (below 4 years) and large systematic errors of this station.

Table 3. The velocities of the stations.

STATION	PLATE	V_{XYZ} [mm/year]		V_{XYZ} ITRF2005 [mm/year]		V_{NE} [mm/year]		V_{NE} NUVEL [mm/year]	V_U [mm/year]	
		SLR	GPS	SLR	GPS	SLR	GPS		SLR	GPS
Herstmonceux	Eurasia	24.0	24.3	23.8	23.8	24.0	24.2	23.2	-1.1	2.2
Grasse	Eurasia	26.8	26.0	26.0	26.0	26.7	26.0	24.7	2.3	0.3
Graz	Eurasia	27.7	26.5	26.4	26.9	27.4	26.5	24.7	-4.0	1.2
Wettzell	Eurasia	25.5	25.7	25.2	25.6	25.1	25.7	24.3	4.4	1.1
Potsdam	Eurasia	24.4	24.8	24.1	24.2	24.5	24.7	23.9	-0.7	1.8
Borowiec	Eurasia	25.8	25.4	24.7	24.7	25.8	25.4	24.1	-1.5	1.2
Beijing	Eurasia	32.2	31.0	32.2	32.4	29.2	30.6	25.6	-13.5	5.4
Shanghai	Eurasia	33.3	34.5	34.6	34.0	34.5	34.5	25.7	-4.5	0.5
Yarragadee	Australia	68.2	69.7	69.6	69.6	68.4	69.9	71.0	1.3	0.0
Monument Peak	Pacific	43.7	42.3	42.4	42.4	43.6	42.3	46.6	0.4	0.2
McDonald	N. America	14.2	13.1	13.5	13.2	14.1	13.0	13.9	-1.3	1.5
Arequipa	S. America	19.6	19.3	18.9	18.9	19.6	19.4	10.0	-2.0	0.5

4. Conclusions

Analysis of the results obtained by the two satellites methods SLR and GPS has revealed significant differences in the range 1-3 cm in the vertical component of the positions of five stations: Yarragadee, Monument Peak, Arequipa, Shanghai, Herstmonceux (over the period 1999-2004). As the data from these stations are important for the calculations of the satellite orbits the explanation of the origin of these differences has great significance. Similar differences had been noted earlier for different stations but were later eliminated (Grasse 1995-1998, Graz 1993-1996, Beijing 2000-2002, McDonald 1993-2001). An interesting observation is similar change in the station vertical position of Arequipa station prior to the earthquake for results from both techniques GPS and SLR (Fig. 2). The horizontal components of the station position obtained from the SLR and GPS results for all the stations studied are consistent to 5 mm. The coordinates calculated on the basis of the SLR results have shown considerable differences in the station stability, depending on the system.

The station velocities determined on the basis of the data collected by the two methods compared have shown a very good agreement (to less then 1 mm/year), this agreement was also good with the ITRF2005 results. No systematic shift was found between the station velocities calculated on the basis of the data collected by the two methods. Moreover, these station velocities were in good agreement with those following from the NNR-NUVEL1A plate velocity model, although the velocities of the European stations determined according to NNR-NUVEL1A are systematically lower by 1-2 mm/year. The differences in the velocities of the European stations reaching up to 3 mm/year can be considered as real because of their agreement with the analogous differences between those following from NNR-NUVEL1A and ITRF2005. The velocities of the two Chinese stations, Monument Peak and in particular Arequipa differ from those following from NNR-NUVEL1A, however, these differences can be explained by the position of these stations at the edges of the plates.

Further efforts should concern the explanation and elimination of the 2-3 cm differences in the vertical component of the station position between the results calculated from SLR and GPS data. A new system of ITRF coordinates should facilitate solution of this problem.

Acknowledgments

The authors wishes to thanks Dr. Michael Heflin and JPL NASA for GPS Time Series, NASA GSFC for consent to use GEODYN-II program and ILRS and IGS stations for their continuous efforts to provide high-quality SLR and GPS data. This work has been supported by financial resources for science in 2006-2009 as a research project No. 4T12E 007 30.

References

Altamimi, Z., P. Sillard, C. Boucher, 2002, ITRF2000: A new release of the International Terrestrial Reference Frame for earth sciences applications, *Journal of Geophysical Research,* Vol. 107, No. B10, 214.

Borkowski K.M., 1989, Accurate Algorithms to Transform Geocentric to Geodetic Coordinates, Bull. Geod., *63, pp. 50-56.*

Boucher C., Altamini Z., Sillard P., 1997, The 1997 International Terrestrial Reference Frame (ITRF97), IERS Technical Note 27, *Obs. De Paris, Paris.*

Boucher C., Altamini Z., Sillard P., Feissel-Vernier M., 2004, The ITRF2000, *IERS Technical Note No. 31,* BKG, Frankfurt am Main.

DeMets C., Gordon R.G, Argus D.F, Stein S., 1994, Effect of recent revisions to the geomagnetic reversal time scale on estimates of current plate motions, *Geophys. Res. Lett.*, 21, 2191-2194.

ITRF2005, 2006, Available from: http://itrf.ensg.ign.fr/ITRF_solutions/2005/ITRF2005.php

Lemoine J.M., Biancale R., Bourda G., 2004, Processing 18.6 years of Lageos data, *Proc. of 14th International Laser Ranging Workshop,* San Fernando, 7-11.06.2004.

Pavlis D.E., Rowlands D.D., et al., 1998, GEODYN Systems Description, vol. 270 3. NASA Goddard, Greenbelt, MD.

Pearlman M.R., Degnan J.J., Bosworth J.M., 2002, The International Laser Ranging Service, *Advances in Space Research,* Vol. 30, No. 2, pp. 135-143.

SLR and the Next Generation Global Geodetic Networks

E. C. Pavlis, M. Kuźmicz-Cieślak
JCET/UMBC and NASA Goddard, Maryland, USA
epavlis@umbc.edu/Fax: +1-410-455-5832

Abstract

The Global Geodetic Observing System—GGOS, places the utmost importance on the development, maintenance and wide distribution of an International Terrestrial Reference Frame (ITRF) with very stringent accuracy attributes. We present here results from simulation studies aimed at designing optimal global geodetic networks to support GGOS. At present, our goal is an origin definition at 1 mm or better at epoch and a temporal stability on the order of 0.1 mm/y, with similar numbers for the scale and orientation components. These goals are based on extensive deliberations within the Earth science community. In particular, oceanographers, a prime user group that these products are intended for, require this level of accuracy and temporal stability in order to address sea level rise issues with confidence. The stability, integrity and applicability of the ITRF are directly related to how accurately we can account for mass redistribution during the analysis and reduction process of the data used for its development. Long wavelength variations of the gravity field driven by these mass redistributions produce geometric effects that are manifested as changes in the origin and orientation between the instantaneous and the mean reference frame. This insidious coupling between the product and the reference with respect to which the product is generated makes the problem extremely complex and sensitive to systematic errors. An uneven distribution of the stations realizing the ITRF results in biases and distortions in the combined product due to the dissimilarity of the combined networks and their de facto lopsided overlap. Poor geometry results in increased correlations between the similarity transformation parameters, leading again to biased and unstable results. In this presentation, we are examining SLR's contribution in establishing the optimal network along with VLBI, since these two techniques alone are sufficient for this task. Using simulations of geodetic data that we expect to collect with the future geodetic networks, we look at various designs of several co-located networks and the resulting accuracy in the origin, scale and orientation definition of the realized ITRF.

Introduction

Space techniques are indispensable for the development of the terrestrial reference frame and for geodetic metrology. It is well-known and generally accepted that the current state-of-the-art does not meet the science requirements primarily due to the poor area coverage and aging equipment for all of the deployed space geodetic techniques. To meet the stringent future requirements as set forth for the Global Geodetic Observing System—GGOS, 1 mm accuracy in the origin of the reference frame and 0.1 mm/y stability over time [Pavlis et al., 2008], we need to design a new network and deploy modern hardware systems. These observations form the motivation behind the work that is reported here, focusing on the contribution of Satellite Laser Ranging (SLR). We need to clarify that this task is very complicated and involves not only scientific research, but also political and policy-dependent decisions, which evolve over the years and the prevailing socioeconomic conditions. What is thus presented here should be understood as work in progress and not as the final answer to the posed questions.

Technique Signal Source Obs. Type	**VLBI** Microwave Quasars Time difference	**SLR** Optical Satellite Two-way range	**GPS** Microwave Satellites Carrier phase
Celestial Frame UT1	**Yes**	No	No
Scale	**Yes**	**Yes**	Yes
Geocenter	No	**Yes**	Yes
Geographic Density	No	No	**Yes**
Real-time	No	No	**Yes**
Decadal Stability	**Yes**	**Yes**	Yes

Figure 1. Areas where the different space geodetic techniques can contribute to the process of the terrestrial reference frame development.

The future GGOS network

A fundamental premise in the development of the terrestrial reference frame from space geodesy is that none of the available techniques is able to do the job alone. This is shown in some detail in Figure 1, where we consider GPS, SLR and VLBI and some of the most important processes and attributes that one encounters while developing the frame. Based on this observation, it has long been common practice to use a global network that comprises all techniques, in order to benefit from their complementariness. The benefit however can only be gotten if we have a highly accurate connection of the different techniques and in fact, in a reasonably global and uniform distribution. We generally call this connection, the "local ties", i.e. the vectors that connect the reference points which are determined by each technique at each location where more than one technique coexist (are co-located). One very important caveat that we must enforce in the design of the future network then is that we not only try to co-locate the maximum possible number of techniques at each site of the fundamental network, but we also require that their local tie vectors are known and monitored with enough accuracy that they will not compromise the overall quality of the resulting frame. At present, the space geodetic techniques have a very poor overlap, with very few sites with all techniques present (2-3). Even in the case of the two of the most complementary techniques, SLR and VLBI, there were never more than 7-8 such sites. Furthermore, these overlaps are time-dependent, with stations appearing and disappearing over time, resulting in very biased frame realizations due to the lack of redundancy in this aspect of the network. Finally, the situation is further exacerbated by the fact that the SLR and to some extent the VLBI networks, are both biased towards the northern hemisphere, where most of the stations

are located. These are some of the deficiencies that the new design will address and ensure that they will no longer be present in the future network.

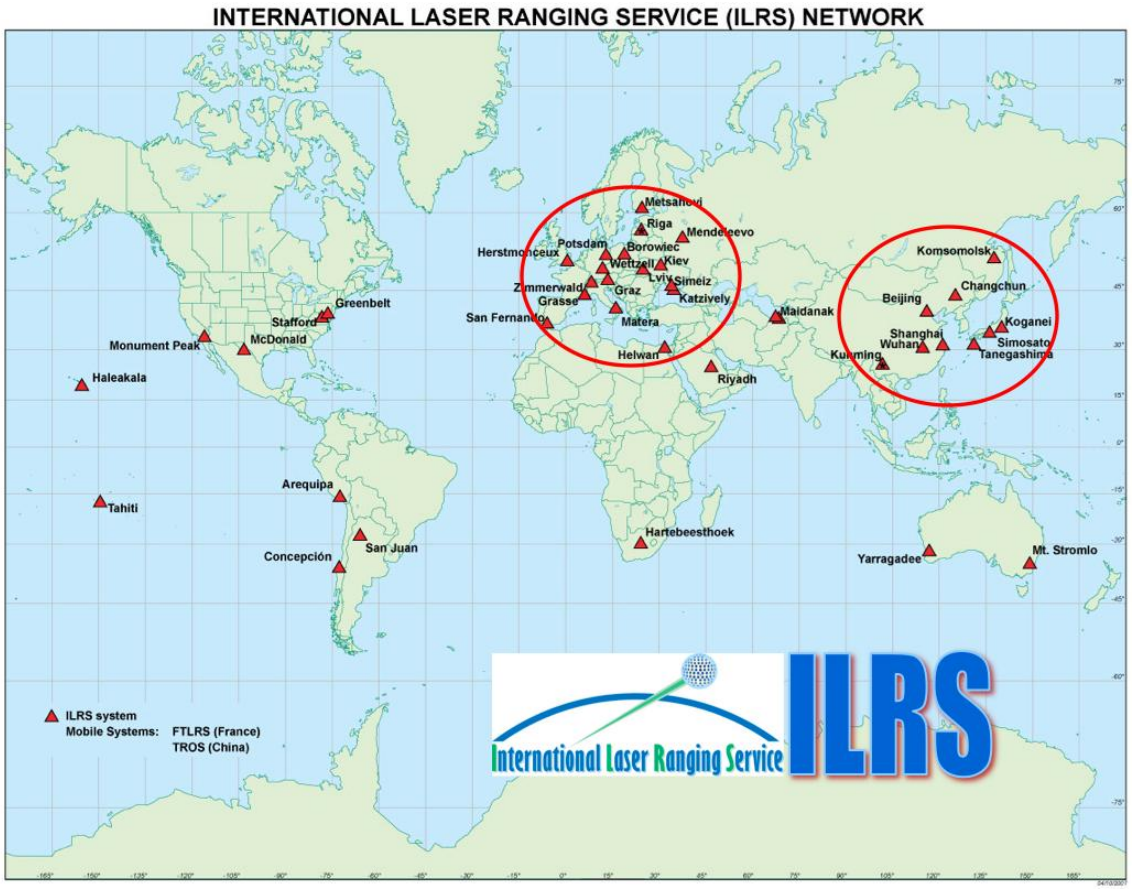

Figure 2. The ILRS SLR-station network of active stations (ca. 2008), with the high concentration of sites over Europe and Asia highlighted.

The SLR network and future developments

It has been already stated that the new network should have a globally uniform site distribution and comprise all available space geodetic techniques. Figure 2 demonstrates the current situation for the SLR network, stressing its extremely lopsided nature. In addition to this observation, one should consider that the majority of the existing hardware was developed several decades ago, and it is kept operational thanks to painstaking efforts of the network engineers. The majority of the current sites require a crew on site while tracking, driving their operational costs to unsustainable levels. The future network will be based on newly designed hardware that addresses all of these issues and many more. The design parameters considered include among others:

- Single photon operational regime;
- Narrow laser divergence;
- Multi-kiloHertz operation (with multiple fires in flight);
- Autonomous, independent operations;
- Improved epoch timing;
- More stable/better defined pointing and ranging calibrations;
- Eye-safe operation, from LEO to GNSS altitude;

- Predictions and collected data submission via the internet (near real-time);
- New applications of these systems beyond Precision Orbit Determination (POD):
  - Satellite surface scanning for spin-axis orientation and rate of rotation;
  - Atmospheric seeing measurements along the laser beam path;
  - kHz Time Transfer (successful tests using AJISAI and the Graz system);
  - kHz LIDAR (under implementation now in Graz);
  - Detection of atmospheric layers, clouds, aircraft vapor trails;
  - …

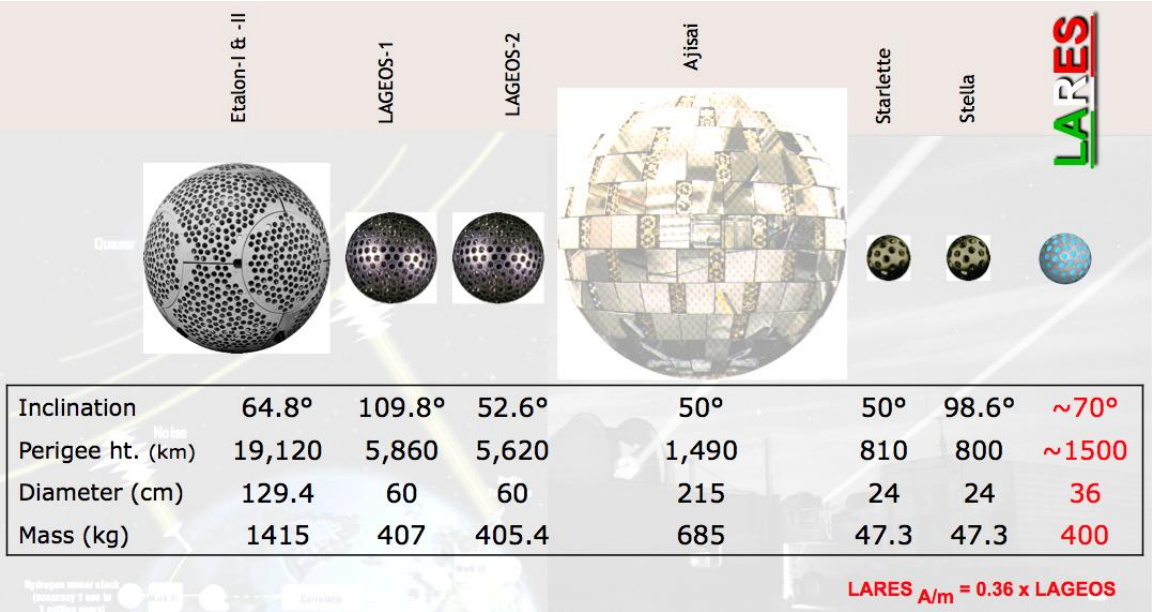

Figure 3. The currently available geodetic targets augmented with the soon-to-be-launched LARES spacecraft.

New studies and engineering tests of retroreflector cornercubes from the same lot that was originally used on some of the existing (in orbit) geodetic satellites, e.g. LAGEOS, ETALON, Starlette, etc., attempt to develop improved models for the center-of-gravity to effective reflection plane offset, for various operational regimes of the present network sites (e.g. signal strength, detection system, etc.). Narrowing down the value of this offset is critical in achieving an accurate, stable and unbiased scale of the SLR network.

Another effort that should have significant implications in the accurate and stable TRF of the future is the launch of additional geodetic targets that have been designed with the GGOS requirements in mind, i.e. for millimeter-level or better geodesy. One such target is LARES (Laser Relativity Satellite), a mission that is in the final stages with a launch date of sometime in late 2010, on ESA's Vega rocket inaugural launch. The LARES mission is an Italian Space Agency (ASI) mission, designed by a consortium of Italian and other universities from several European countries and the US [Ciufolini et al., 2008]. It is expected that the quick and significant improvement in modeling the static and temporal gravity field as a result of the unprecedented GRACE mission [Tapley et al., 2004], will soon allow geodesists to use even some of the much lower than LAGEOS-altitude and above targets for TRF work (i.e. Starlette, Stella, Larets, etc.). When this family of geodetic targets is tapped for TRF work, it will help generate a quasi-inertial frame of reference around Earth,

to be used for the determination of the TRF with high accuracy and using data collected over very short time periods on the order of a week or even less. This extended family of targets is displayed in Figure 3.

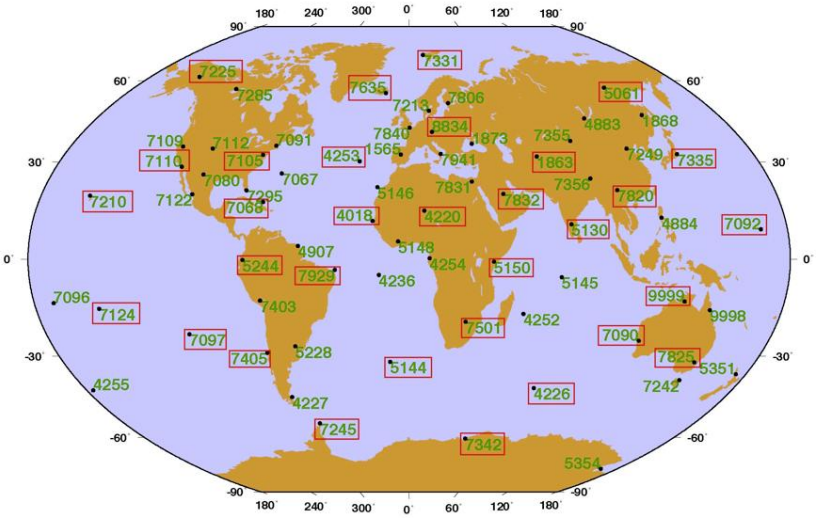

Figure 4. Globally distributed past and present space geodetic sites used in the network simulations. Sites in red rectangles are the maximal 32-site sub-network we examined.

Network Design Studies

NASA has sponsored an activity that included an "Observing System Simulation Experiment (OSSE)", using VLBI, SLR and GPS systems. Under this effort a network simulation capability was developed by the Joint Center for Earth Systems Technology (JCET) with participation from NASA Goddard and the University of Texas. This simulation system has been running since 2008 on NASA's Columbia grid at Ames. Resources supporting this work have been provided by the NASA High-End Computing (HEC) Program through NASA Advanced Supercomputing (NAS) Division at Ames Research Center.

Simulation and Trade-off Studies

First we scoped the size and distribution of co-located VLBI and SLR stations, over a global network that would support the GGOS program goals. These two systems together can define completely the TRF, with no need for external information. We first identified seventy globally distributed sites occupied at present or at some point in time by at least one technique (not necessarily SLR or VLBI), Figure 4. We then selected from this group 32 sites that comprise the maximum size network we would examine, and we then generated three sub-networks of 24, 16 and 8 sites, each one a subset of the previous, (Figure 5), trying to keep as uniform a global distribution as possible for all sub-networks.

The simulations characterize the degradation in the accuracy of the resultant TRF as the size of the network progressively decreases. The currently co-located VLBI and SLR sites are not more than eight. The results indicate that we need 24 – 32 sites to implement and maintain the reference frame to the required level of accuracy (Figure 6). A larger uniform network is required to maintain the stable origin and scale, while orientation can be maintained even with a smaller network, of about 24 sites (Figure 6). Additional future studies will establish reliable limits on the sensitivity of the chosen network to outages of individual sites and

groups. Although such catastrophic outages do not happen often, we need to know how poorly the network will behave when portions become inoperable over extended periods of time.

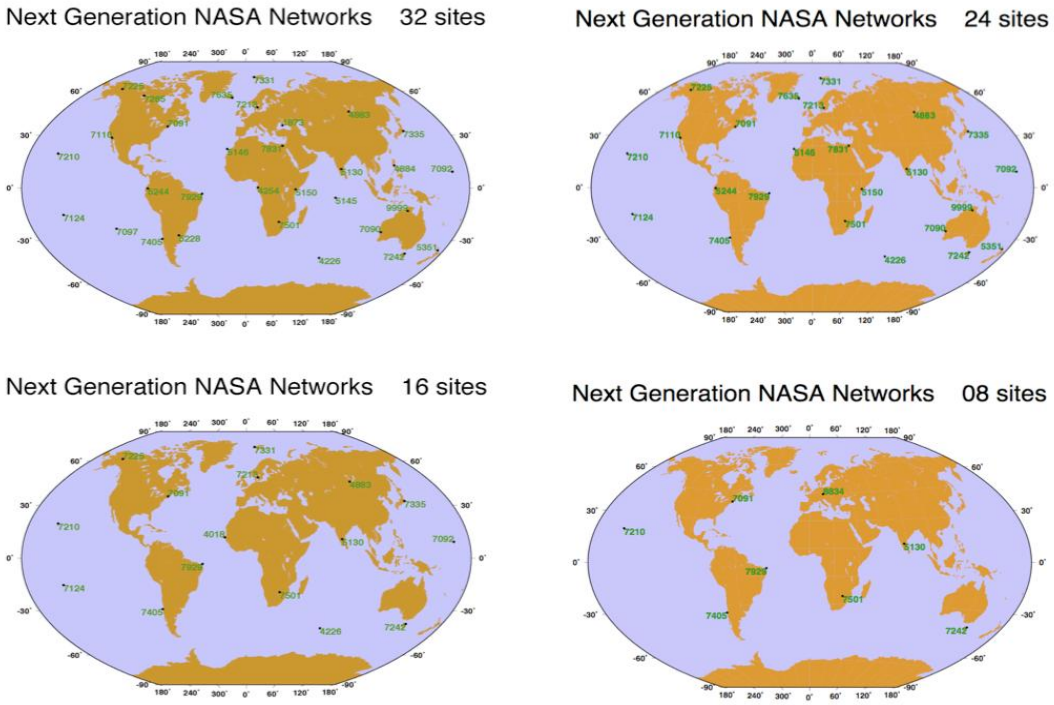

Figure 5. Initial 32-site network and the three variants of 24, 16 and 8 sites used in the simulations.

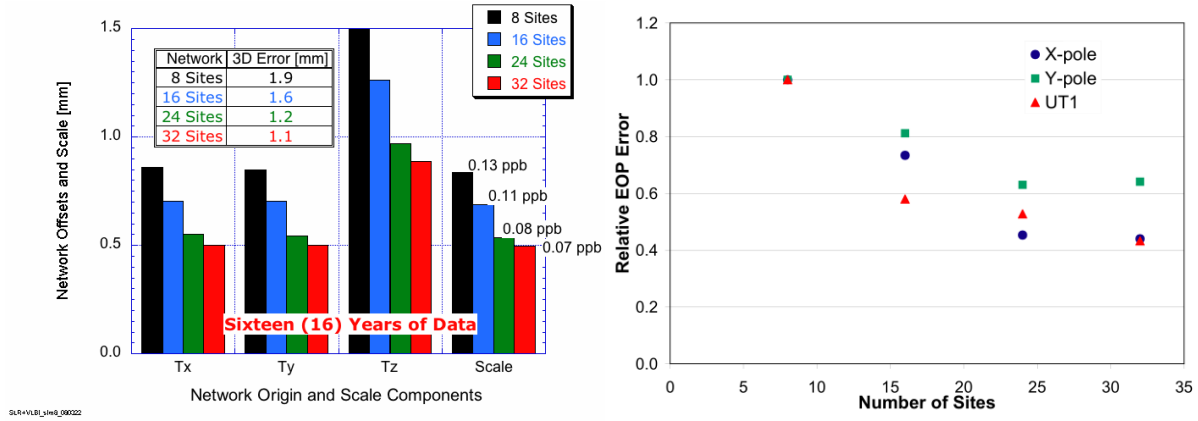

Figure 6. Origin and scale accuracy (left) and orientation accuracy (right) as a function of the size of the defining network.

Conclusions

In order to achieve the accuracy requirements of the GGOS project, it is necessary to redesign our space geodetic networks and to deploy new, automated tracking systems. Simulations that consider an ideal network of co-located SLR and VLBI systems provide guidance in the required size and global distribution of this future network. Examining four alternative networks of 32, 24, 16 and 8 sites, we have reached some initial conclusions.

Firstly, the simulation validates the real world experience with the 8 co-located SLR and VLBI sites. The biggest improvement is seen when going from 8 to 16 sites. The largest impact of an 8-site addition in the origin is seen when going from 16 to 24 sites (~22%), and the least, from 24 to 32 (~8%). Results for a 13-year time span (corresponds to the data record used in the development of ITRF2005) show a 4- or 5-fold improvement compared to what we estimate for ITRF2005. A projection for a 16-year time span (similar to what will contribute to the *ITRF2008* realization) shows that a 32-site network approaches the GGOS goal of accuracy in the origin and scale.

While the above provide some boundary conditions for the design of the future network, we should note that the current study has some significant limitations and these will require additional studies to be done to address them. We currently work with only two geodetic techniques (SLR & VLBI), assuming that GNSS and DORIS will become de facto available for any size of such a fundamental network of core sites. We are currently optimizing the network size on the basis of a constrained system performance and assuming a background model quality that is similar to what is available today. Additionally, we have assumed that we have perfect ties between the two systems (SLR and VLBI), far from what is happening today and certainly an item that deserves careful consideration, given its large contribution to the successful realization of the TRF from multiple techniques. The criterion we use for a successful design is TRF quality: origin, scale and orientation. We eventually need to also consider temporal variations of the TRF parameters, to investigate the ability of the network to determine accurate velocities and maintain a stability of all other attributes over long periods of time. Solutions will be soon repeated with the addition of local tie errors with varied weighting schemes. In the future we plan to use the 16-site network to investigate the effect of choosing alternate sites on the results (varying the uniformity of the network), since the actual realization of any design will meet some very practical problems that will in several cases force us to deviate from the theoretical optimal design.

References

Ciufolini, I., A. Paolozzi and E. C. Pavlis, (2008), "Toward a One Percent Measurement of Frame Dragging by Spin with Satellite Laser Ranging with the LAGEOS, LARES and GRACE satellites", *Space Sci Rev.*, Springer-Verlag, Heidelberg.

Pavlis, E. C. et al., (2008), "Observing Systems Needed to Address Sea-level Rise and Variability", in *Understanding Sea-level Rise and Variability*, Aarup, T., J. Church, S. Wilson, and P. Woodworth (eds.), Blackwell, Oxford (*in press*).

Tapley, B. D., S. Bettadpur, M. Watkins and Ch. Reigber, (2004), "The gravity recovery and climate experiment: Mission overview and early results", Geophysical Research Letters 31 (9).

SLR, GNSS, VLBI, and DORIS Networks: ILRS+IGS+IVS+IDS

Carey Noll
NASA Goddard Space Flight Center, USA
Carey.Noll@nasa.gov/Fax: 301-614-6015

Abstract

The global networks of the International Laser Ranging Service (ILRS), the International GNSS Service (IGS), the International VLBI Service for Geodesy and Astrometry (IVS), and the International DORIS Service (IDS) are the backbone of GGOS. The observations obtained from these global networks provide a continuous monitoring of the International Terrestrial Reference Frame (ITRF). Co-location of two or more techniques at sites is an important aspect for generation of the ITRF as well as providing an assessment of the observation quality, accuracy, and validation of results. As of mid-2008, these networks consisted of 42 laser ranging sites, 407 GNSS sites, 45 VLBI sites, and 58 DORIS sites. The data generated by the stations in these networks, and the products derived from these data, are available from the Crustal Dynamics Data Information System (CDDIS). This poster will illustrate the global coverage of these networks, highlighting inter-technique co-locations.

Scientific Contributions of the ILRS, IGS, IVS, and IDS

The global networks of the IAG's geometric services, the International Laser Ranging Service (ILRS), the International GNSS Service (IGS), the International VLBI Service for Geodesy and Astrometry (IVS), and the International DORIS Service (IDS) are one of the most important components of the Global Geodetic Observing System (GGOS), the observing system of the IAG. It is through these networks that observations are obtained to generate an International Terrestrial Reference Frame (ITRF). These networks currently consist of 42 laser ranging sites, 407 GNSS sites, 45 VLBI sites, and 58 DORIS sites. The networks of the ILRS, IGS, IVS, and IDS are shown in Figure 1.

In addition to the TRF, the ILRS, IGS, IVS, and IDS contribute to many scientific areas:

- Terrestrial Reference Frame (TRF):
  - Station positions and velocities: SLR, GNSS, VLBI, DORIS
  - TRF scale and temporal variations: SLR, VLBI
  - Network densification: GNSS
  - Homogenous network distribution: DORIS
- Celestial Reference Frame: VLBI
- Precise Orbit Determination (POD):
  - Accurate satellite ephemerides: SLR, GNSS, DORIS
  - Calibration and validation for remote sensing missions and instruments: SLR, GNSS
  - Sea level monitoring: SLR, GNSS, DORIS
- Earth Orientation Parameters (EOP):
  - Polar motion and rates: SLR, VLBI, GNSS, DORIS
  - Length-of-day: SLR, GNSS, DORIS
  - UT1-UTC and long-term stability of nutation: VLBI

- Atmosphere:
  - Tropospheric zenith delays: GNSS, VLBI
  - Global maps of ionosphere mean electron content: GNSS, DORIS
  - Limb sounding for global profiles of water vapor: GNSS
- Gravity:
  - Static and time-varying coefficients of the Earth's gravity field: SLR, DORIS
  - Total Earth mass: SLR
  - Temporal variations of network origin with respect to Earth center of mass: SLR
- Timing:
  - Station and satellite clock solutions: GNSS
  - Time and frequency transfer between time laboratories: GNSS
- Fundamental Physics:
  - General relativity and alternative theories: SLR/LLR
  - Light bending, time dilation: VLBI

The co-location of two or more techniques at a single site is important for the computation of this TRF. A co-location site is defined as an installation where two or more instruments are positioned within hundreds of meters of each other. Through co-location, analysts can assess and validate the quality and accuracy of the measurements. As of the fall 2008, over 80 global sites have co-locations of two or more of these space geodesy instruments (2 sites with four techniques, 14 sites with three techniques, and 69 sites with two techniques). Unfortunately, however, not all of these inter-technique co-location vectors are measured with sufficient accuracy for intercomparison/combination purposes.

The data generated by these networks, as well as products derived from these data, are available from the Crustal Dynamics Data Information System (CDDIS, *http://cddis.nasa.gov*). The CDDIS is NASA's active archive and information service of space geodesy data and products and currently serves as a key global data center for the IGS, ILRS, IVS, and IDS as well as GGOS. For over 25 years, the CDDIS has provided continuous, long term, public access to the data and product records required for the terrestrial reference frame to the global Earth Science community.

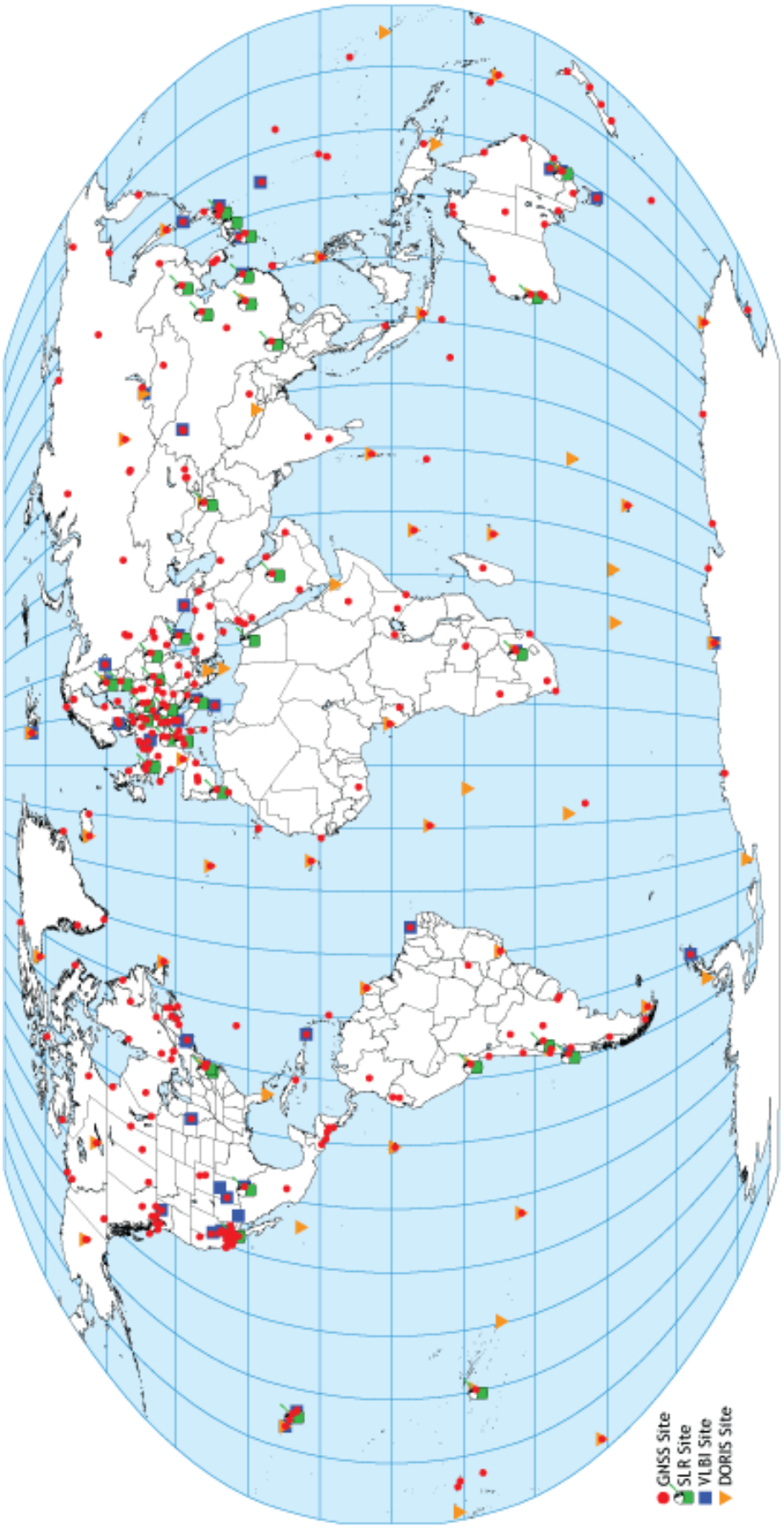

Figure 1. The networks supporting the ILRS, IGS, IVS, and IDS.

The Virtual Observatory in Geodesy and Earth's Sciences: The French activities

F. Deleflie (1)**, S.B. Lambert** (2)**, X. Collilieux** (3)**, C. Barache** (2)**, J. Berthier** (4)**, O. Laurain** (1)**, D. Coulot** (3)**, P. Exertier** (1)**, A.-M. Gontier** (2)

(1) Observatoire de la Côte d'Azur – Geoazur / GRGS, Grasse, France
(2) Observatoire de Paris – SYRTE / GRGS, Paris, France
(3) Institut Géographique National – LAREG / GRGS, Marne la Vallée, France
(4) Observatoire de Paris – IMCCE / GRGS, Paris France

Florent.Deleflie@obs-azur.fr /Fax: +33-4-93405333

Abstract

This paper presents the context of the astronomical Virtual Observatory (VO), an ambitious international proposal to provide uniform, convenient access to disparate, geographically dispersed archives of astronomical data from software which runs on the computer on the astronomer's desktop. The VO could be of interest for the geodetic community: We present the efforts we made in that direction over the last two years.

Introduction

As mentioned on the *International Virtual Observatory Alliance* (IVOA) website (http://www.ivoa.net), the IVOA was formed in June 2002 with a mission to "facilitate the international coordination and collaboration necessary for the development and deployment of the tools, systems and organizational structures necessary to enable the international utilization of astronomical archives as an integrated and interoperating Virtual Observatory. The work of the IVOA focuses on the development of standards. Working Groups are constituted with cross-project membership in those areas where key interoperability standards and technologies have to be defined and agreed upon. The Working Groups develop standards using a process modeled after the World Wide Web Consortium. Recommendations are ultimately endorsed by the Virtual Observatory (VO) Working Group of Commission 5 (Astronomical Data) of the International Astronomical Union (IAU).

Several independent Java-based tools have been developed in the VO framework, that can be used in geodesy and more generally in Earth's Sciences. These tools can either be downloaded and set up in PCs as Java applications, or used through a web browser as Java applets. In particular, some of the tools we started to use with SLR data are "VOPlot" and "TopCat", which are devoted to astronomical data and time series plotting.

1. Basic principles of the Virtual Observatory

1.1. The VO-Table Data Exchange Format

VOTable is the XML-based format for representing astronomical data, recommended by IVOA (e.g. catalogues, as tables of the properties of celestial objects, celestial coordinates, brightness etc.). The VO-Table format has been defined in terms of XML in order to take advantage of computer-industry standards and to utilize standard software and tools. At the same time it is important not to loose the previous investment in astronomy-specific standards, such as the table variants of the *Flexible Image Transport System* (FITS) format.

Also, astronomical tables are rich in *metadata*, which in this context means annotation, interpretable by either computers or humans, both of the tables and the individual columns that they contain. It is important that these metadata should be preserved with the table and the VO-Table has features to permit this.

It is crucial to point out the fact adopting the VO-Table format does not mean giving up of its own data format: the VO-Table format can encapsulate existing files and simply supplies metadata to understand its content and facilitate data exchanges.

1.2. Why choosing the Virtual Observatory

There exists several software packages to treat metadata files, but the so-called "Virtual Observatory", as an ensemble of VO-Table-based software packages, is now widely used within the astronomical community, by several thousand users worldwide. The Virtual Observatory takes advantage on the notion of *Unified Content Descriptors* (UCD) to be inserted into metadata files to describe the data, following the self-descriptive format VO-Table based on these standards and XML. As a consequence, many tools already exist to manage, plot or analyze data supplied in VO-Table format. Converting ones own data in VO-Table format means benefiting of all existing tools, some of them providing a conversion from unformatted data files into the VO-Table format, as well. As a consequence, data will be described non-ambiguously, ensuring further exchange and better understanding between different scientific communities. By the way, the Virtual Observatory provides an easy access to all VO-Table data: they can be registered to a "registry", that means that any user can locate on the web, get details of, and make use of, any resource located anywhere in the IVOA space.

1.3. Using the Virtual Observatory in geodesy ?

VO standards have been developed for Earth-centered or body-centered reference frames in order to extend the VO to Earth and planetary sciences. Nevertheless, some improvements are to be made. Two years ago, our group proposed to the IVOA to adopt standards relevant to the Earth orientation data (polar motion, UT1—UTC, nutation, etc.) and to space geodesy, that were accepted in 2008. In particular, the list of official UCD now contains terms which permit to describe all the products built and analyzed by the ILRS community.

2. Web services developed by our team

2.1. Example in astronomy, and celestial reference frame

It is worth noting that the construction of the Large Quasar Astrometric Catalogue by Souchay & al. (2009) made an extensive use of cross identifications between a dozen of quasar catalogues that were facilitated by the use of VO tools like Aladin. Moreover, the Observatoire de Paris offers the IVS OPAR products and the IERS/ICRS-PC products in VO-Table format, including radio source and station coordinates and EOP time series. It means that all these catalogues and data can be read using VO tools and can be directly compared to any other similar data set contained in the astronomical VizieR database.

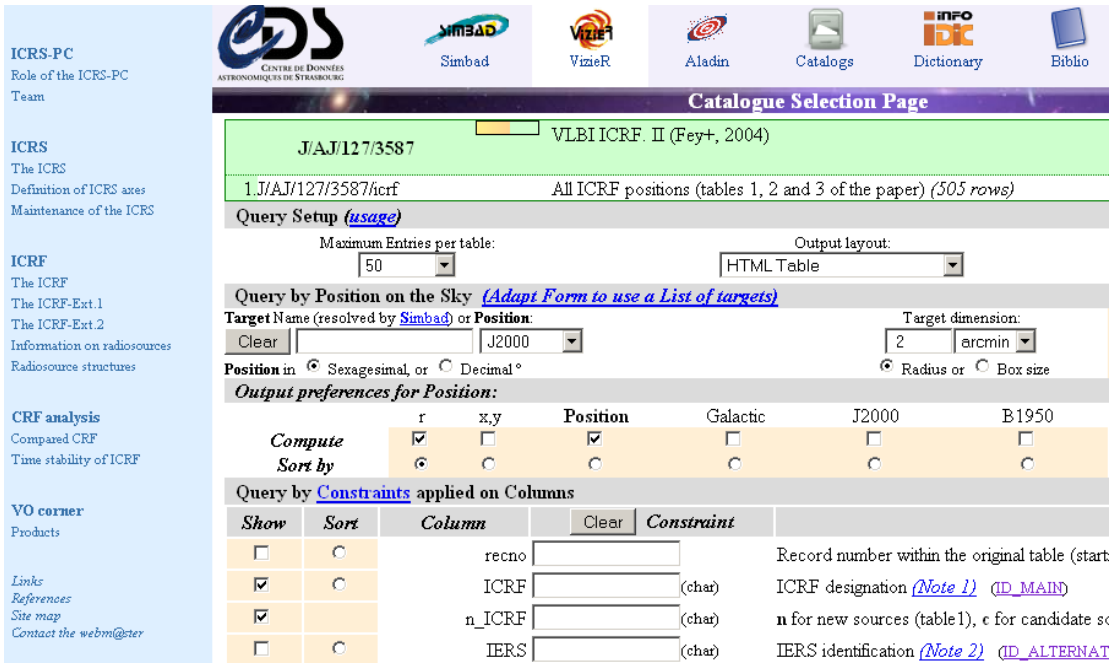

Figure 1. The ICRF–Ext.2 available through the portal of the ICRF product center web site

2.2. Products built by GRGS Analysis Center

GRGS-Grasse geodesy team provides short arc analysis to give an access to satellite orbit error, in particular in the framework of altimetric missions ; time series of observed station position, and of EOP based on SLR data, which are the results of the GRGS ILRS Analysis Center.

The Java applet gives the visualization and the comparison of the consistent EOP and site coordinate time series. Output files are either in ASCII or in VO-Table format.

2.3. International Terrestrial Reference Frame

The ITRF website takes benefit from a cartography host which enables one to visualize the different ITRF networks, spot networks from each technique, the velocity fields of the various ITRF since ITRF94 and also the border of plate tectonics according to two patterns. Also, it enables ones to a point selection in view of accessing to the ITRF coordinates of sub-network at the chosen period. In the close future, ITRF solutions tables will also be provided in VO-Table format, and dynamical tables of coordinates generated by the ITRF website users will also be supplied in VOTable format.

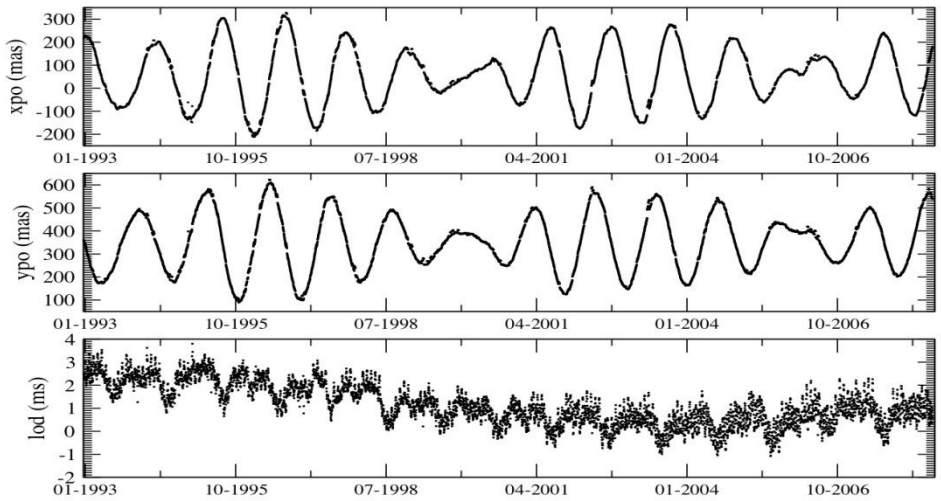

Figure 2. Polar motion, as plotted on the OCA/GRGS Virtual Observatory portal

3. Possible links between VO, GGOS, and the whole ILRS community

To our opinion, the fields related to geodesy that could benefit from the VO concept could be:

- Optimization of the estimation methods: biases, decorrelation of parameters, recognition of orbit's errors (for the determination of the Earth's rotation, its gravity field, reference frames)
- Optimization of the use of data: choice of the orbital configurations, according to altitudes and orbit inclinations, for instance
- New concepts: data combination, or simultaneous inversion of the gravitational field and the station's positions
- Orbital dynamics: improving simultaneously orbital modelling, and the determination of environmental parameters which act on the trajectories (gravitational origin or not)

The systematic use of approaches such as the VO is likely to be generalized in the next few years within various scientific communities. For the geodetic community, we think that projects such as the GGOS projet should investigate to what extent they can follow, or not, the reommendations provided by IVOA (namely: the VO-Table and associated web services).

4. Conclusions

The scientific community working on the field of space geodesy – that is: not only the community belonging to ILRS – can benefit from the VO concept mainly through two points. On the one hand, the concept of metadata (following or not the recommendations provided by IVOA) permits to gather up in a single file some data together with a description supposed to

be exhaustive. This means, for example, that a user can immediately know, when comparing station coordinate time series, if these time series are expressed with respect to an homogeneous and compatible reference frame. If not, and this is the second point to be reminded of, this user can easily transform these time series through web services –providing an interface with classical geodetic software, running on local computers where the web service is set up –, to make these time series compatible.

To our opinion, such tools can give an extraordinary visibility of all data and products built by the ILRS community, and can reinforce in a strong way the links between the Analysis Working Group and the station network. Both corner stones of the SLR technique could discuss in "real time", and it is nice to see that several groups started to develop web services inside the AWG. Obviously, the VO-Table format is not mandatory for such a goal, but "only" a very efficient solution, anyway.

Many new applications can be expected using VO concepts in geodesy and associated fields. It should be very well adapted to use existing tools such as VOPlot, and Top-cat, devoted to data plotting and cross identifications, with SLR data. It would be very challenging to use in our context other tools originally developed for celestial bodies, such as the Aladin software package, an interactive software sky atlas allowing the user to visualize and manipulate astronomical images in multi-wavelength, superimpose entries from astronomical catalogues and so on. Developing such new applications and new web services will be a further step to come. Though we did not participate in the birth of the VO, we have been helping for a few years in the development of standards which permits the inclusion of astrometry and geodesy products in the VO. We now have to systematically deliver geodetic products analyzed by our group following all the recommendations provided by IVOA, fully compatible with the ones provided by ILRS.

5. Web links

Here are some VO and OV-GAFF resources:

The International Virtual Observatory Alliance web site: http://www.ivoa.net

The IERS/ICRS Product Center: http://hpiers.obspm.fr/icrs-pc

French activities: http://grg2.fr/

GRGS-Grasse Web services and data (in English):
http://www-g.oca.eu/heberges/pnaf/OV-GAFF/Webservices/webservices_group_en.html

Technical informations on the VO (in French):
http://www-g.oca.eu/heberges/pnaf/OV-GAFF/Asov/info-techniques.html

ITRF solutions: http://itrf.ensg.ign.fr

References

Souchay, J.; Andrei, A. H.; Barache, C.; Bouquillon, S.; Gontier, A.-M.; Lambert, S. B.; Le Poncin-Lafitte, C.; Taris, F.; Arias, E. F.; Suchet, D.; Baudin, M., *The construction*

of the large quasar astrometric catalogue (LQAC), Astronomy and Astrophysics, Volume 494, Issue 2, pp.799-815, 2009

Lambert, S., F., Deleflie; A.-M., Gontier; P., Berio; C. Barache, *The Astronomical Virtual Observatory and Application to Earth's Sciences*, IVS 2008 General Meeting Proc., 2008

Network and Station Performance

Chairs: Vincenza Luceri and Mark Torrence

Session Summary

The papers in the session can be roughly divided into three main topics:

1) **On-site Data quality control**

   Some stations reported their effort in reaching and keeping the best data quality. Herstmonceux focussed on the separation of the range bias and height signals using other on-site geodetic techniques (GNSS, absolute gravity); the time-of-flight counter effects are evident and the cause still under investigation.

   The Next Generation Satellite Laser Ranging System (NGSLR) was collocated with MOBLAS-7 at GGAO to calibrate the NGSLR event timer and processor. High energy returns were used to calibrate the longer-pulse transmit system built for LRO.

   Starting from the need to trace and correct the unmodeled range bias in 2007, MLRO set a quality control loop in cooperation with data analysts, engineers, operators at the station. A control infrastructure and web based information system was defined to enable a constant monitor of the system parameters.

   Mt Stromlo SLR upgraded its laser power. The station is operated unmanned in all weather conditions and still at its productivity levels.

2) **Data quality control at Analysis Centers**

   A routine quality control system for the ILRS global network is provided by the Hitotsubashi University and numerical tables are available via web, ftp and email. Stations are directly contacted when a bias is evident and encouraged to reply.

   Data analysis activities are carried out at the Changchun site: a bridge between theoretical research and observational work. The LAGEOS 1/2 range and time biases are evaluated.

3) **Models**

   The SLR data from Jason1, Lageos1/2, and TOPEX SLR data have been processed using the latest and most accurate POD models and SLRF2005. Individual SLR station performance and systematic signals have been evaluated and several stations updated in SLRF2005 to obtain LPOD2005.

   Model update is under discussion in the SLR analysis standards. In the near future, a proposal will be done by ILRS to IERS for modification of the analysis standards related to the products contributing to the establishment of the future ITRF.

4) **Network**

   An analysis of the correlation between the TRF datum and the ILRS network geometry has been done with the aim to explain the discontinuity in the SLR scale: further investigation to be done using data simulation

   In September 2009 TanDEM-X was launched to fly with TerraSAR-X in a very close formation.

   Difficulties in the tracking are shown together with possible remedies for the various station types.

Multi-Satellite Daily Bias Report: How to Read and Handle it

Toshimichi Otsubo (1)**, Mihoko Kobayashi** (1)**, Tadahiro Gotoh** (2)**,**
Toshihiro Kubo-oka (2)

(1) Hitotsubashi University, Tokyo, Japan, t.otsubo@srv.cc.hit-u.ac.jp
(2) National Institute of Information and Communications Technology, Koganei, Japan

Abstract

A quality control system for the ILRS global network has been developed utilizing the precise orbit determination technique. Laser-range observation data for as many as 15 satellites are being processed every day within 24 to 48 hours after ranging observations, and the quality control numerical tables are available via web, ftp and email. The analysis reports, formerly provided by National Institute of Information and Communications Technology and currently by Hitotsubashi University, are widely used for detecting and alerting various kinds of problems. The anomaly information is being promptly notified to the laser stations by email.

1. Introduction

It would be ideal if satellite laser ranging data were faultlessly precise, but it is not realistic to demand the 100% of completeness. Data anomaly will occur even if every station pays careful attention to the quality of its observation data. It is, of course, important for a station to minimise the amount of anomalous data, but it is equally or possibly more important to detect and notify problems to the corresponding station managers and observers. When a laser ranging station releases its observation data, in general, it is not possible to locally assess the quality of its own observation data even at a metre or 10-metre level. Therefore quick quality checks from the analysis community have played an important role since the middle of 1990's, partly owing to the evolution of computer network. By giving a quick feedback to the corresponding station, the time span with anomalous data has been significantly shortened.

2. Ten-Year Operation at CRL/NICT/HIT-U

In 1998 we have started automated routine analysis at Communications Research Laboratory (CRL) (Otsubo and Endo, 1998). At the beginning, only three satellites, two LAGEOS satellite and AJISAI, were used for quality check. We gradually increased the number of satellite while the name of the institute being changed from CRL to National Institute of Information and Communications Technology (NICT). In 2007, as the first author moved to Hitotsubashi Univeristy (HIT-U), the routine analysis was also transferred from NICT to the university.

As of November 2008, laser-range observation data for as many as 16 satellites are being processed every day: LAGEOS-1, LAGEOS-2, ETALON-1, ETALON-2, GPS-35, GPS-36, GLONASS-99, GLONASS-102, GLONASS-109, AJISAI, STARLETTE, STELLA, ERS-2, ENVISAT, JASON-1 and JASON-2. SLR-based terrestrial reference frame SLRF2005 has been adopted for the station coordinates since December 2007.

At 21:30 UTC (=6:30 in Japanese Standard Time) every day, the automated analysis run starts and the worldwide observation data are reduced by means of orbit determination using orbit analysis software 'concerto'. This process usually ends around 0h or 1h UTC (9h to 10h in JST) which means the first analysis gets available within 24 to 48 hours after ranging observations. After checking the quantity of observations and the quality of orbit fit for each satellite, the post-fit residuals for the qualified satellites were used to generate pass-by-pass range bias and time bias. Due to this filtering procedure, some of the above 16 satellites are sometimes dropped from the final reports. The final result is assembled to one large text file, typically 300 to 400 kB, and is made available via WWW, FTP and E-Mail. The URL of this website is

http://www.science.hit-u.ac.jp/otsubo/slr/bias/

where the analysis report is updated every day around 0h or 1h UTC. In addition to the weekly report being sent to the SLReport mailing list, the email reporting service is available daily or weekly (every Wednesday) upon request.

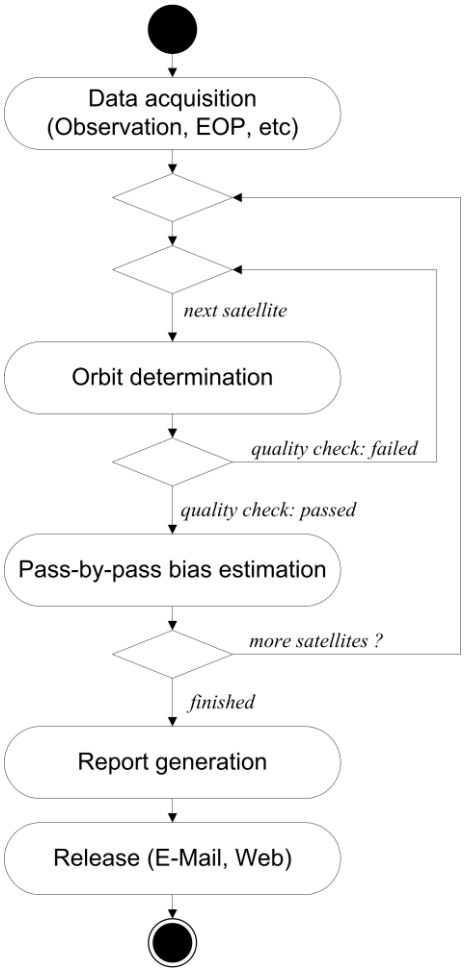

Figure 1. Routine sequence of the daily analysis at Hitotsubashi University.

The whole sequence of the daily procedure is summarised in Fig. 1 (Otsubo, et al., 2008).

3. Manual Check and Communication Issues

In a case of obvious anomaly, we promptly notify it directly to the station. Before sending the alert, we check:

- Is the bias large enough? Is it surely 'their' problem?
- Is the problem continuous, not a one-pass event?
- Has the problem already been solved?
- Who is a contact point of the station?

Then, we send email to the corresponding station manager, mainly based on the station specification webpage in the ILRS website. Since October 2007 when the ILRS workshop was held in Grasse, we also notify it in parallel to Task Force 1 Members. It is therefore very important to keep the ILRS web contents updated. We sometimes had problems in communicating through email when the email addresses of station managers are outdated.

We would be grateful if the contacted station manager gives us a quick reply, just to inform us that he/she has read the notification.

The list below is the cases of actual email notification from January to September of Year 2008. RB, TB and FB mean range bias, time bias and frequency bias, repectively. For the cases in which we received a reply from a station, the cause of large bias is given in round brackets.

[Sep, 2008] 1 or 2 or 3 m RB (laser multipulse)
[Sep, 2008] < 2 m RB (calibration (human) error)
[Jul, 2008] 1.2 km RB (calibration error. System testing.)
[Jul, 2008] 200 ms TB (?).
[Jun-Jul, 2008] 132 m RB (?).
[Jun, 2008] -20 ms TB (hardware & software problem)
[Jun, 2008] 10 ms TB (software?)
[Apr, 2008] Non-existing station ID (human error)
[Feb, 2008] Atm pressure error (wire problem.)
[Feb, 2008] 0.5 to 1.7 km RB (FB?)
[Jan-Feb, 2008] 1 day TB (wrong day?)
[Jan, 2008] 3 m RB (laser multipulse)
[Jan, 2008] 18.6 ms TB (event timer)
[Jan, 2008] < 2 m TB LEO Only (?)

4. Proposal of On-Site Use with Locally Available Information

The analysis report is not just for looking at but also for detailed investigations on various observation conditions.
One example is given in Fig. 2. Herstmoceux station, UK, is currently in the transitional phase from the 10-Hz laser ranging system to the 2-kHz laser ranging system (Gibbs, et al., 2008). According to Herstmonceux's log record, the SCI flag in the ILRS normal point header is "6" for 10 Hz and "7" for 2 kHz. Pass-by-pass range biases during June-September 2008 were plotted in this figure, for JASON-1 and 2 (left) and LAGEOS-1 and 2 (right). The

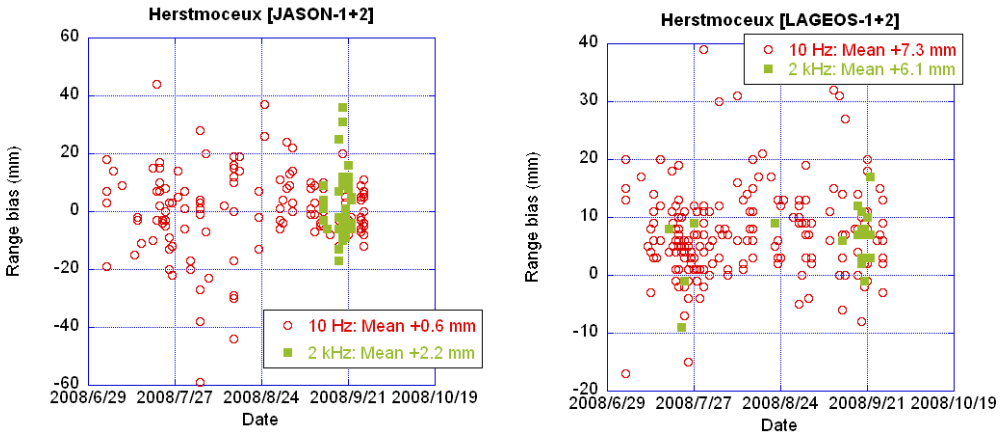

Figure 2. Range bias variation of Herstmonceux during their 10Hz – 2kHz transition.

two graphs show that the range bias has been consistent for both configurations, below 2 mm for both satellite types.

This example is generated using information available in the ILRS normal point format. However, the stations have recorded much more information than publicly available data, for instance, name of observer, time since system activation, room temperature, signal intensity, optical/electrical configuration, etc. We would like to propose the use of the reported bias values with such local information.

5. Conclusions

The daily quality check by CRL/NICT/HIT-U has been played an important role in the ILRS community for detecting unnoticed problems and shortening the period of data anomaly. The wide range of satellites from low orbits of several hundreds of km up to high orbits of GNSS altitudes are being processed and it results in easy and effective problem detection. The quick and direct notification is also a key in this activity. Various 'local' use of bias analysis reports will be possible for detailed tests of various component, and we would like to collaborate any of ILRS stations.

References

1. T. Otsubo, T. Endo, Quick Bias Report for Lageos and Ajisai Data, Proceedings of 11th International Workshop on Laser Ranging, 650-653, 1998.
2. T. Otsubo, M. Kobayashi, T. Gotoh and T. Kubo-oka: "Daily Quality Control System of Satellite Laser Ranging Data for the ILRS Network," Journal of the Geodetic Society of Japan, Vol. 54, No. 2, 69-79, 2008 (in Japanese with English abstract).
3. P. Gibbs, G. Appleby, D. Benham, C. Potter, R.Sherwood, T. Shoobridge, V. Smith and M. Wilkinson, "Herstmonceux - towards kHz ranging and multi-technique status," 16th International Workshop on Laser Ranging, in these proceedings.

Assessment of SLR observation performance using LAGEOS data

Gang Zhao, You Zhao, Mingguo Sun, Huanhuan Yu
Changchun Observatory, NAOC, CAS, China
zhaog@cho.ac.cn; youzhao@cho.ac.cn; sunmg@cho.ac.cn; yuhh@cho.ac.cn

Abstract

From the beginning of 2008, Changchun Observatory has carried out routine short-arc (3-day) orbit determination and station residual analysis on LAGEOS SLR data. Meanwhile, we commence analysis in some aspects of related issues. In this report, the satellite precise orbit determination results and its preliminary applications are presented. Influences of gravity models - JGM-3, EGM96, GGM02C – have been checked and compared. We find these models are nearly equivalent for mm-level orbit determination with maximum difference less than 3%. Results of short-arc orbit determination which show our orbit determination accuracy around 1.2cm with moderate difference are presented. After comparison of SLR stations' observation precision, the TB and RB analysis on some high performance stations and some stations we concerned are presented in detail. The value and variation of terrestrial coordinates of some stations are also computed and discussed. We expect such analysis will build a bridge between our theoretical research and observational work.

1. Introduction

Satellite Laser Ranging (SLR) has experienced continuous and highly development. The application of SLR observation data on space geodesy, geodynamics, and geophysics has obtained fruitful production. LAGEOS-1/2 are two important targets of SLR observation. Precise orbit determination and subsequent residual analysis of orbit RMS on LAGEOS-1/2 are very useful for study on related issues. The accuracy of LAGEOS short-arc orbit determination today is on cm level.

As a productive station, Changchun Observatory (7237) has provided large numbers of SLR observation data with moderate precision for more than 20 years. It has made great and continuously efforts in SLR equipment and technology.[1] How to make use of SLR data and resource of experiential staffs sufficiently is an important issue for our future development. In these two years, Changchun Observatory has begun precise orbit determination making use of SLR data, especially on LAGEOS data. From the beginning of 2008 on, we have realized routine short-arc POD (precision orbit determination) and residual analysis on SLR data of LAGEOS-1/2, which is publicized on our website (www.cho.ac.cn) and is updated around once a week. In this report, we presented preliminary results and application of our SLR POD work.

2. Data processing methodology

Some characters make LAGEOS-1/2 especially suitable targets for satellite POD. Fairly simple and accurate modeling can be easily got from their spherically symmetric figuration. Altitude around 6000 km make the effect of atmospheric drag and high order/degree geopotential coefficients, which are hard to assign exactly, can be safely ignored. Long observation duration over 30 years for LAGEOS-1 and 16 years for LAGEOS-2 – triggered

plenty of detailed investigation on both short-term and long-term POD, so many perturbation factors and parameters had been well defined.
Table 1 demonstrated the properties of LAGEOS-1/2 which were used in POD processing.

Table 1. Satellite characters

	LAGEOS-1	LAGEOS-2
Satellite ID	7603901	9207002
Mass	411 kg	405 kg
CM (center of mass) offset	0.251 m	0.251 m
Cross section	0.283 m^2	0.283 m^2

Table 2. Strategy of POD solution

Numerical Integration	
integrator	Krogh-Shampine-Gordon
step length	fixed-step, 150s
Reference Coordinate System	
inertial	J2000.0
terrestrial	ITRF2000
precession	IAU1976
nutation	IAU1980
Measurement Model	
plate tectonic motion	NNR-NUVEL1
earth solid tides	
rotational deformation	
ocean tide loading	CSR4.0
tropospheric refraction	Marini/Murry model
Dynamical Model	
earth gravity field	JGM-3 30*30
n-body perturbation	JPL ephemerides DE403 (sun/moon)
ocean tide model	CSR4.0+TEG4
relativistic correction	1-body
solar radiation pressure	conical
earth radiation and albedo	
thermal radiator (y-bias)	
empirical drag	
empirical RTN acceleration	
Estimated Parameters	
satellite state vector	3-position, 3-velocity
empirical drag coefficients	
solar radiation pressure coefficients	
earth radiation parameters	
empirical acceleration	R, T, N
earth rotation parameters	xp, yp, dut1/dt

Table 3. Orbit determination precision of three geopotential models

	JGM-3	EGM96	GGM02C
LAGEOS-1	0.012416 m	0.012764 m	0.012607 m
LAGEOS-2	0.012371 m	0.012571 m	0.012258 m
Mean	0.012393 m	0.012667 m	0.012432 m

Dynamical orbit determination is popularly used methodology in satellite POD.[2] Not only orbital elements are solved, but also combined dynamical parameters are estimated during the processing of dynamical orbit determination. For insuring cm-level orbit determination precision, in POD processing on LAGEOS-1/2, models and parameters should be carefully selected. The adopted reference system, perturbing forces and parameters in our POD procedure are listed in Table 2.

The observation data analyzed in this study covered 1200 days from March 1, 2005 to June 12, 2008. Such long duration can level down the effect of some random factors such as short-term bad station performance, and can also check up the stability and reliability of our work. During such a long period, almost every SLR station has observed LAGEOS-1/2. In our study, observation data are included as much as possible with different calculation weights based on historical experience.

3. Gravity field test

Three gravity models are taken into account here for testing availability of our POD method. For the improvement of modern geopotential determination and relatively low degree/order (30*30) necessarily used in LAGEOS-1/2 POD processing, it should be no obvious difference among POD results of different gravity fields.

The test models include JGM-3, which is recommended in IERS conventions 1996[3], EGM96, which is recommended in IERS conventions 2003[4], and GGM02C, which is got from the combination of satellite GRACE and *terrestrial* gravity measurement[5]. We set the resolved arc length 15 days (i.e. 80 arcs in 1200-day duration). The mean values of orbital precision were presented in Table 3.

We can see the difference among these models is on mm level. The maximum difference is 2.21%. In other words, gravity field models have no influence on present cm-level POD. And also, high correlation among RMS of these models was also found. That is to say the selection of any gravity models is equivalent in our investigation.

We also compiled preliminary statistics on quantity and quality of station observation used 15-day-arc data. We find acknowledged high-performance stations, such as Yarragadee, Graz really held good achievements on both quantity and quality. The weighted RMS, i.e. mean orbital residual of data from high-performance stations is around or a bit more than 1.0 cm. For Changchun, the RMS sometimes exceeds 3 cm.

4. Short-arc POD

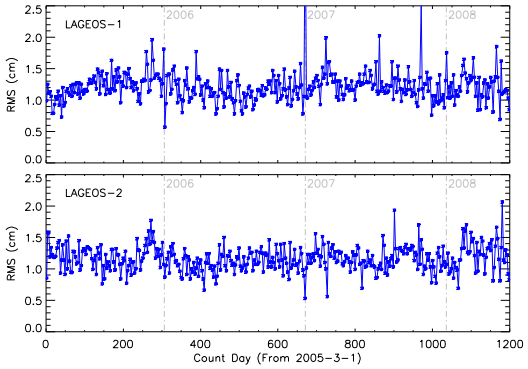

Figure 1. Short-arc orbit determination precision

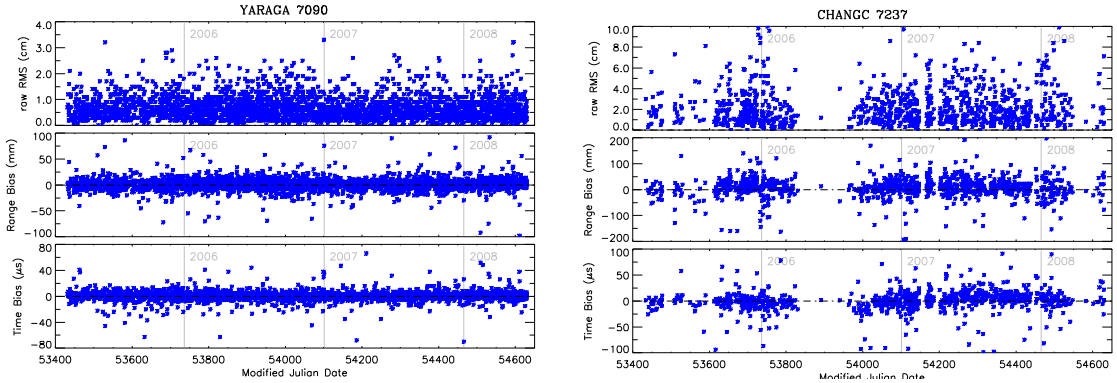

Figure 2. POD RMS, RB, TB of Yarragadee (7090) and Changchun (7237) determined using LAGEOS-1 data

Short-arc (often 3-day) approach is frequently used for the solution of LAGEOS POD, and the cm-level accuracy should be reached, otherwise the POD will lose much of its meaning. We implemented 3-day arc POD on LAGOES-1/2 throughout the whole 1200-day duration with the POD methodology detailedly described above. Figure 1 shows the RMS of each arc. Mean RMS for LAGEOS-1 and LAGEOS-2 is 1.22 cm and 1.17 cm, respectively. But we should also notice large RMS come forth in very few arcs. The reason need to be further investigated.

Based on the results of short-arc POD, we calculated RMS, range bias (RB) and time bias (TB) per arc per station which we concerned. These three indices reflect the difference between observational value and theoretical value of POD from various aspects, and are the most important indices for evaluation of station observation. High performance station held rather low value and Changchun held moderate value on these indices, just like Figure 2 showed.

5. Station coordinates estimation

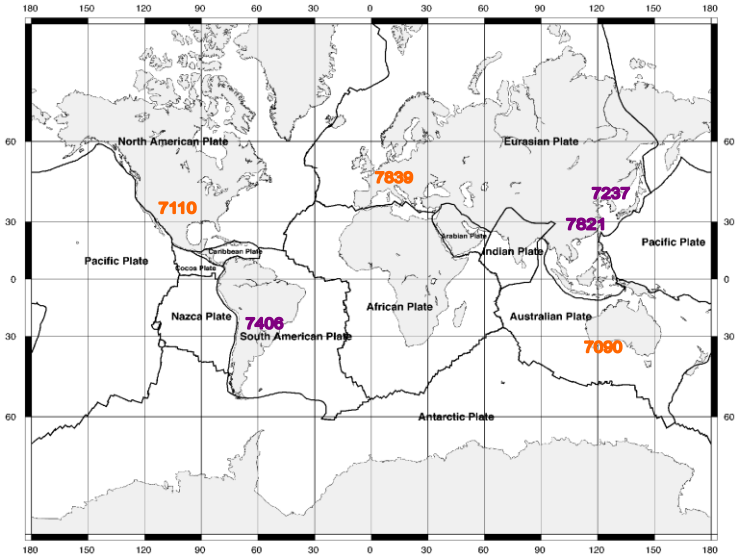

Figure 3. Sketch of location of six station in tectonic plates

A set of terrestrial coordinates of SLR stations was adopted in ITRF 2000 frame and was maintained as input constants during routine POD procedure above. Yet station coordinates vary along with time in some degree.[6] Two reasons required us considered this factor more carefully. First, no well-recommended coordinates provided in ITRF 2000 frame for the SLR stations put into operation in recent years. Second, for all stations, the coordinates are not fixed actually. Even after the influences of geometrical tides, ocean loading and some other factors are eliminated reasonably by modeling, the variations which are difficult to explain at present will also appear in station coordinates. Some suppose the variations are correlated with meteorologic parameters but without confirmation. In POD processing, we found inaccurate value of single station coordinates could put no notable impact on whole orbit determination precision, but could reduce the RMS of the station itself remarkable.

In this step, we set the coordinates of six SLR stations – Yarragadee (7090), Monument Peak (7110), Graz (7839), Changchun (7237), Shanghai (7821) and San Juan (7406) - as estimated parameters. The location of six stations is illustrated in Figure 3. The first four located in quite far away from the boundary of earth tectonic plates. The last two began observing no more than three years, so their coordinates have not been well defined.

The displacement of coordinates along three directions - height, longitude and latitude – was determined. Examples are showed in Figure 4. For all station coordinates, variations are clearly although with different amplitudes. There seems to be periodicities, or quasi-periodicities in variations of coordinates. How to explain them is another complex problem.

6. Summary

Changchun Observatory has the foundation in SLR POD work now. Routine POD and residual analysis on LAGEOS-1/2 has begun from the beginning of 2008. Our present-day orbit determination precision is about 1 to 2 cm.

In the case of our study, the choice of gravity model has slight effect on precision of LAGEOS orbit determination. The influencing magnitude is on sub-mm level.

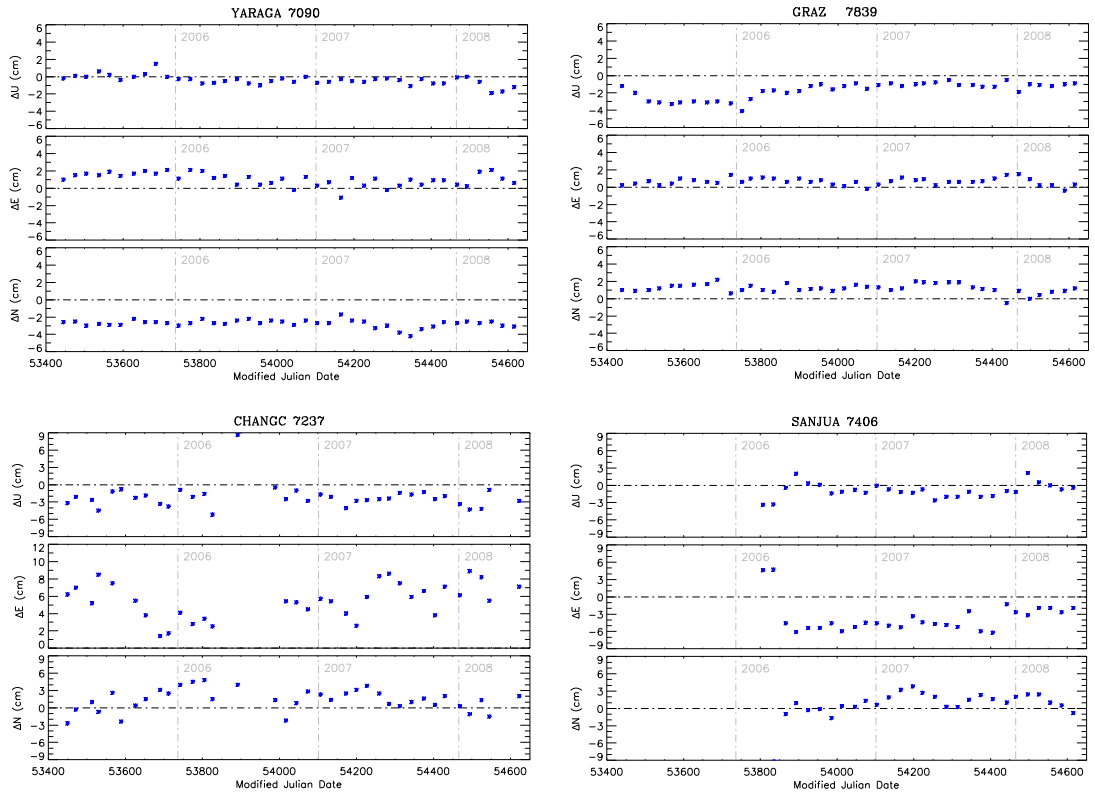

Figure 4. Coordinates of Yarragadee, Graz, Changchun and San Juan determined using LAGEOS-1 data

The station coordinates can also be determined in POD process, and the proper value can do help to improve orbit determination precision. The cause of variability of station coordinates need to be further investigated. What we can do using POD results, how to apply them in relevant geodynamic and geophysical problems, how to combine them with our observational duty, need seriously consideration. We wish the POD work in Changchun will build a bridge to connect theoretical research and observational work.

References

1 Zhao Y., Fan C.B., HAN X.W., et al., *Progress of Changchun SLR*, Proc. of 16th International Workshop on Laser Ranging, Poznan, Poland, 2008

2 Vetter J.R., *Fifty years of orbit determination: development of modern astrodynamics methods***,** Johns Hopkins ApL Technical Digest, Vol. 27, No. 3, 2007

3 McCarthy D. D. (ed.), *IERS Conventions (1996)***,** IERS Technical Note 21, Observatoire de Paris, 1996

4 McCarthy D.D. and Petit G., *IERS Conventions (2003)***,** IERS Technical Note 32, Frankfurt am Main: Verlag des Bundesamts fur Kartographie und Geodasie, p.127, 2004

5 Tapley B., Ries J., Bettadpur S. et al., *GGM02 - An improved Earth gravity field model from GRACE***,** Journal of Geodesy, Vol. 79, p.467–478, 2005

6 Angermann D., GerstlM., Kelm R. et al., *Time evolution of an SLR reference frame***,** Advances in Space Research. Vol. 30, No. 2, p.201–206, 2002

Attempts to separate apparent observational range bias from true geodetic signals

Graham Appleby[1], Matthew Wilkinson[1], Vincenza Luceri[2], Philip Gibbs[1] , Victoria Smith[1]

[1]Space Geodesy Facility, Herstmonceux, UK
[2]e-GEOS, ASI/CGS, Matera, Italy

Abstract

Orbital solutions that include laser range bias naturally produce results that are highly correlated with station height variations. In this paper we investigate features of a long time-series of Herstmonceux LAGEOS and LAGEOS-II range bias solutions derived by the ILRS Primary Combination Centre at ASI. We discuss time-of-flight counter effects apparent in the results as well as attempting to separate bias and height signals using other on-site geodetic techniques including GNSS and absolute gravity.

Introduction

We currently use satellite laser range, GPS and absolute gravity data in a programme for long-term monitoring of the Herstmonceux site. This programme includes analyses of the global laser range observations of LAGEOS and ETALON by the in-house analysis package SATAN, and use of and analysis of GPS data from the global IGS and UK networks that include HERS and HERT, using the GAMIT package (REFERENCE). The UK, non-Herstmonceux GPS data was obtained from the British Isles GNSS Facility (BIGF, http://www.bigf.ac.uk/) located at the IESSG, Nottingham, UK. In addition to the space-geodetic observations, we are operating and analysing data from the FG5 absolute gravimeter that is permanently located in the basement at SGF, with a particular interest in looking into local geology and hydrological loading effects.

Of course, long time-spans of accurate observations are key to the definition of the ITRF. Within the ILRS Analysis Working Group, a programme of re-analysis of LAGEOS data from 1983-date is ongoing, and includes the generation of time series of station range-bias at weekly intervals which has the potential to reveal possible engineering problems. However, because of the high correlation that exists between station height and range bias, the degree of which depends upon the minimum ranging elevation, there is a potential danger of attributing real station-height changes to ranging-system problems. The ideal is to have good on-site QC and not allow system changes to affect range accuracy and also to use orbit-based QC (see, for example, the new daily LAGEOS and ETALON analysis at http://sgf.rgo.ac.uk) that might rapidly detect an unexpected system change. However, recent email exchanges between some ILRS Analysis Centres suggest that some Herstmonceux range accuracy issues have been apparent since early 2007. Here we investigate those issues in the context of the AWG re-analysis work, in particular using the time-series of range bias values.

Range bias solutions (ASI/CGS) for SGF Herstmonceux

Shown in Figure 1 are fortnightly solutions for range bias at Herstmonceux for the period 1983-2008 (Fig. 1a, LAGEOS) and 1992-2008 (Fig. 1b, LAGEOS-II). These have been

estimated recently in a consistent way with a multi-year global geodetic solution at the ASI Space Geodesy Center. For the time-period between 1983 and 1992, a 'Maryland' event timer was used in the SGF ranging system, leading to a single-shot precision of some 45mm. During that period, large systematic range bias of up to 40mm was present and mostly un-removable (Appleby *et al*, 1989). From 1992 to 2007, Stanford counters replaced the Maryland event timer and the 'bias' time series is dominated by a clear seasonal signal, almost certainly representing real height changes at the 10 to 15mm level. However, for this time period, engineering tests at Herstmonceux revealed that up to 8mm range bias is also present in the data, dependent upon satellite range (Gibbs and Appleby, 2006).

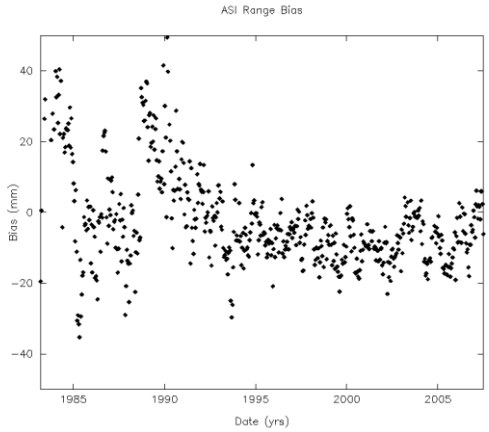

Figure 1a. LAGEOS range-bias

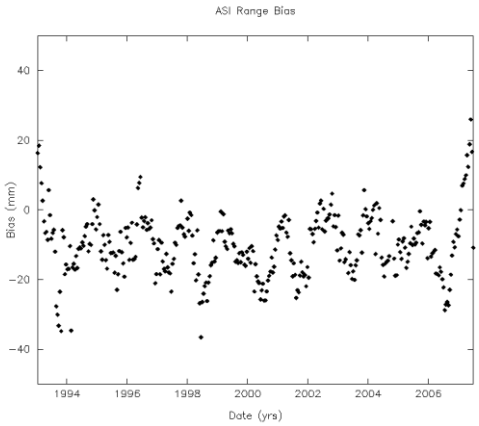

Figure 1b. LAGEOS-II range-bias

In close up, the range-bias series for LAGEOS is shown in Figure 2, where the epochs of removal of the Maryland Event Timer and the Stanford Counters are 1992 and 2007.

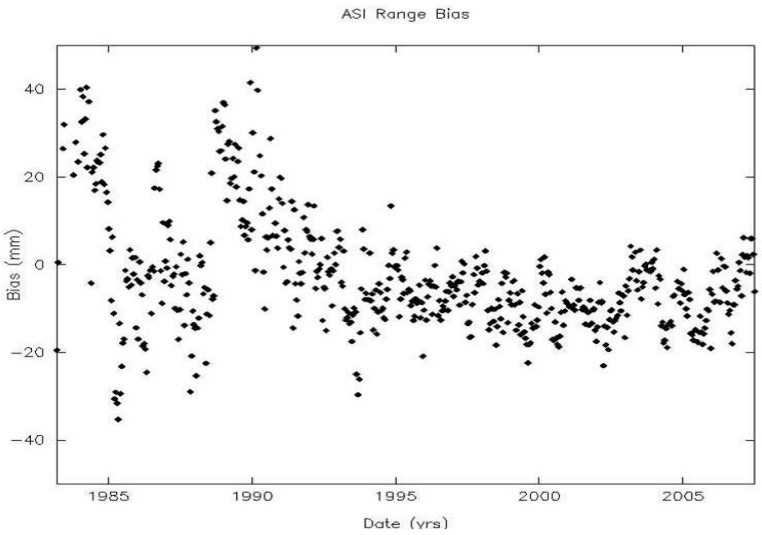

Figure 2. Full time-history of LAGEOS range-bias

Stanford Counters

Work to compare the Stanfords' behaviour at close, target board, and long, satellite, ranges as reported in Gibbs and Appleby (2006), has been extended to include several, mainly European, stations that use or have used the counters. This work was reported at the EGU in

2007 (Appleby, Otsubo and Gibbs, 2007) and discussed within the ILRS Analysis Working Group and the GGOS Unified Analysis Workshop of 2007. Corrections of up to 12mm were recommended for some stations, but with the understanding that the uncertainties of the corrections themselves may reach 5 or even 10mm. These uncertainties are mainly driven by the inherent high-frequency (90MHz) error-curve of amplitude some 50ps in the counters, meaning that estimating the range error especially during target-board ranging is very problematic. The value of such 'calibration' work for the historical data sets from the 'Stanford' stations is currently under review by the AWG.

High-quality event timer

As previously reported (*e.g.* in Gibbs, *et al*, 2006), a high precision event timer based on Thales units was installed in the ranging system on 2007 February 11, with the expectation that from that date the range data should be bias-free at the single mm level. However, the weekly, unconstrained reference-frame solutions carried out using global LAGEOS and ETALON data by the ILRS Analysis Centres, including SGF, suggested that the height of Herstmonceux underwent an abrupt negative change of some 10mm at about the same time, in early 2007, as shown in Figure 3.

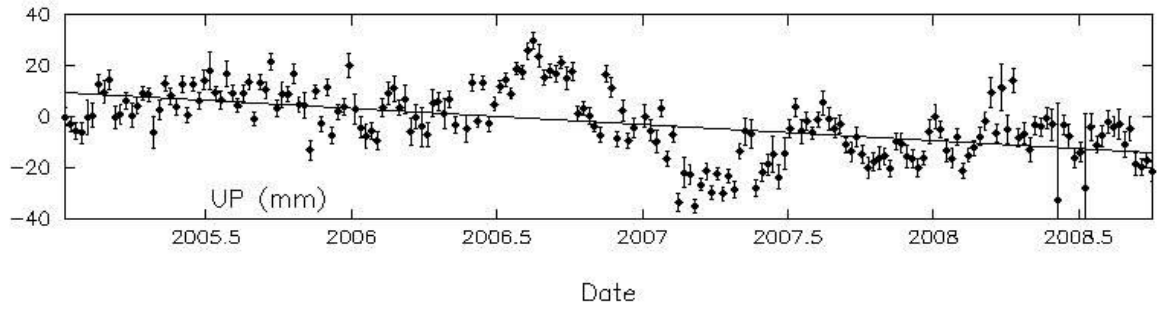

Figure 3. Weekly time-series of height variations at Herstmonceux determined by the SGF AC

Initially, this jump was not recognised as such, especially given the context of the quasi-seasonal height variations apparently related to water-table loading that are the subject of multi-sensor site-stability work currently underway at the Facility. In that work, taking results from 1996 to date, there is a clear relationship between water-table height and station height as shown in Figure 4, but we note here that atmospheric pressure loading, also of course seasonally correlated, has not been removed from the height series and which may be exaggerating the height variations.

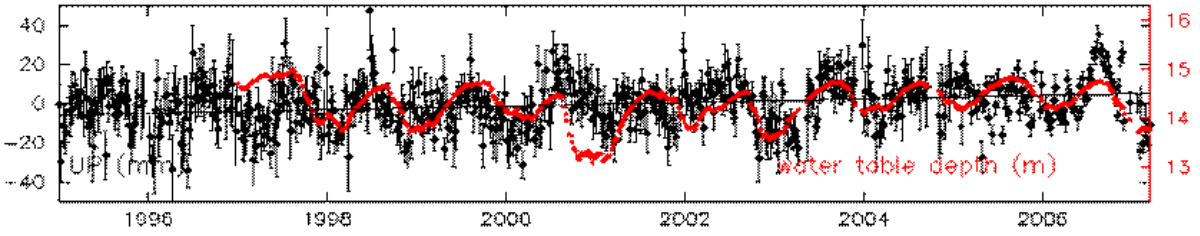

Figure 4. Weekly time-series of height variations and water-table levels at Herstmonceux

Comparison with GPS and absolute gravity

As a further check and interesting comparison of results from closely-situated techniques, we compare the SLR height time series first with that from the long-standing HERS Z12 receiver, using GAMIT to determine weekly coordinate solutions. The two series, with the laser solutions in green and the HERT series in black, are shown in Figure 5, where the mean values of each height series have been removed from the weekly values; seasonal signals are evident in both solutions, and a drop in height relative to the GPS results is suggested by the laser results from early 2007 onwards.

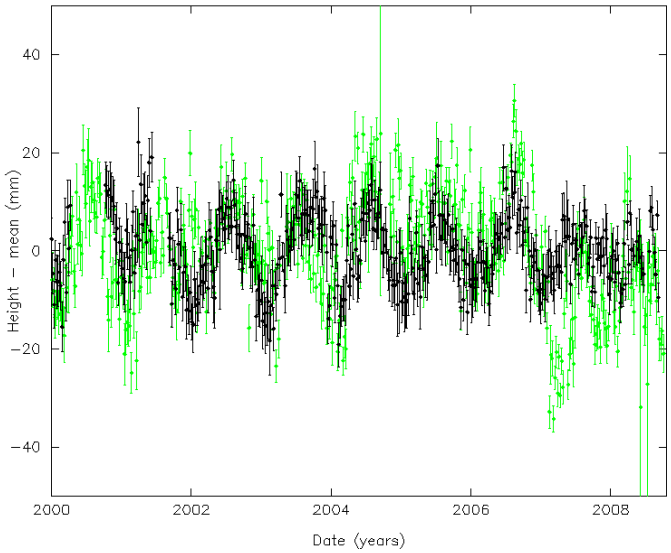

Figure 5. Weekly GPS (HERS, black) and SLR-derived (green) height series

The FG5 absolute gravimeter has been operational in the basement of the Facility since late 2006 to derive weekly values of the local gravitational acceleration from 24-hour sessions centred on mid-GPS week. For this comparison, the resulting series of average gravity variations have been converted to equivalent height changes using an estimated 1μGal = -4.5mm, following Zerbini *et al* (2007).

In Figure 6 we show the results from the beginning of 2006 from all three techniques, with the gravity values in red. During the period of interest from late 2006 through to the end of the comparison, the heights inferred from the gravity results show much less variation that that from the satellite techniques, although the exact nature of the atmospheric correction implicit in the G7 software is yet to be clarified. However and importantly, the gravity data do not see the height change suggested by the laser data.

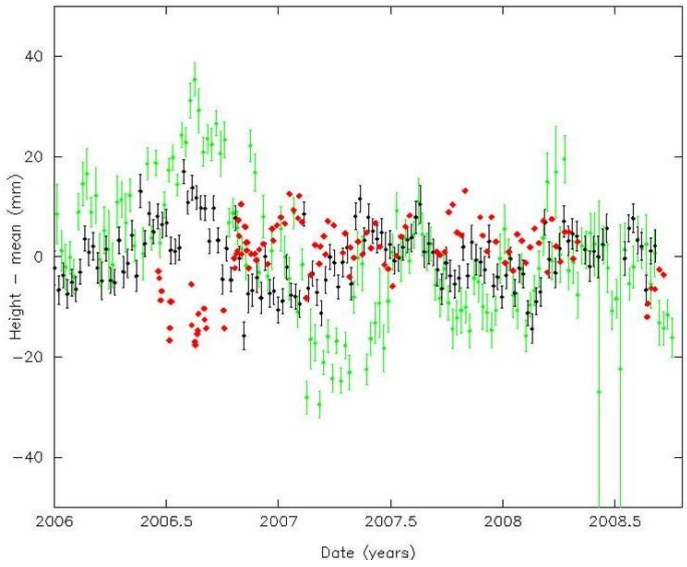

Figure 6. Weekly GPS (HERS, black), SLR (green) and gravity-derived (red) height series

Conclusion

An apparent discontinuity in the laser range data from Herstmonceux, as revealed from range-bias solutions, has been identified and coincides with the introduction of a high-accuracy event timer in 2007 February. Supporting evidence for the existence of the discontinuity in the laser data itself, rather than from a real change in station height, has been obtained from a comparison between the height time series derived from SLR, from on-site GPS and from on-site absolute gravity data. Further work suggests that the laser data ***prior*** to 2007 February is biased by about 12mm, with the modern data essentially bias-free. Correction tables for the Herstmonceux laser data will be issued in due course.

References

Appleby G M**,** Otsubo T and Gibbs P., **"**Further Improvements in Understanding Subtle Systematic Effects in Laser Ranging Observations" (Solicited presentation), *Geophysical Research Abstracts, Vol 9, EGU, 2007*

Appleby, G.M. and Matthews, W.E., "An analysis of range calibration values from the UK SLR system, 1985-1989", Proc. of the 7th International Workshop on Laser Ranging Instrumentation, Matera, Italy, October 2-8, published by OCA/CERGA, Grasse, France, p. 303, 1989.

Gibbs, P., Appleby, G.M., Potter, C.B. "A reassessment of laser ranging accuracy at SGF Herstmonceux", Proc. *15th Int. Laser Ranging Workshop, Canberra*, 2007

King, R., and Bock, Y. "Documentation for the GAMIT GPS analysis software, release 9.9", Mass. Inst. of Technol., Cambridge, 2004.

Zerbini, S., B. Richter, F. Rocca, T. Van Dam, F. Matonti "A Combination of Space and Terrestrial Geodetic Techniques to Monitor Land Subsidence: Case Study, the Southeastern Po Plane, Italy". *Journal of Geophysical Research*, 112, B05401, doi:10.1029/2006JB004338, 2007.

Sub-centimeter SLR precision with the SLRF2005/LPOD2005 network

N.P. Zelensky[2], F.G. Lemoine[1], D.D. Rowlands[1], S.B. Luthcke[1], D.S. Chinn[2], J.W. Beall[3], B.D. Beckley[2], S.M. Klosko[2], P. Willis[4], V. Luceri[5]

[1] NASA Goddard Space Flight Center, USA
[2] SGT Inc , Greenbelt, MD , USA
[3] Raytheon, Greenbelt, MD , USA
[4] Institut De Physique Du Globe De Paris, France
[5] E-GEOS S.P.A, Italy

Abstract

Satellite Laser Ranging (SLR) offers the only unambiguous sub-centimeter range measurement to orbiting satellites. This capability finds many applications in addition to precision orbit determination (POD), which include a unique absolute measure of orbit accuracy, accurate altimeter range calibration, accurate definition of the Earth's center of mass, the most accurate definition of the geocentric gravitational coefficient (GM) and scale of a terrestrial reference network. Achieving sub-centimeter precision requires appropriate modeling of the satellite laser retro-reflector array (LRA) coupled in some cases with appropriate modeling of the satellite-dependant station detector characteristics, a highly accurate terrestrial reference frame, and appropriate attention to possible bias modeling of individual stations. We have processed Jason1/2, Lageos1/2, and TOPEX SLR tracking using the latest and most accurate POD models which include a GRACE-based static gravity, time varying gravity, and the highly accurate ILRS update of the rescaled ITRF2005 SLR complement, SLRF2005. SLRF2005 has been further updated, based on recommendations for the rescaling of ITRF2005, producing LPOD2005. Our analysis evaluates individual SLR station performance and systematic signals as observed from all four satellites. Several primary stations are identified as having significant range biases, which if untreated could lead to degradation in current levels of POD accuracy, and possibly degrade the results for other applications of the SLR measurement.

1. SLR processing and POD strategy

The current GSFC POD strategy allows SLR processing at the 1-cm level for Lageos 1/2 and Jason 1/2, and at the 1.5 cm level for TOPEX/Poseidon (TP) (Figure 1). Tests using the latest Precision Orbit Determination (POD) models have shown progressive improvement of the Lageos, Jason, and TP orbits. Table 1 illustrates improvement for the Jason-1 SLR/DORIS orbit based principally on the improvement in the orbit fit to the SLR data as these models are progressively improved. The culmination of these tests has led to the definition of the current GSFC POD recommended standards (Table 2) (Lemoine et al., 2008).
At this level of processing accuracy, even relatively small errors in station position or the presence of range biases at certain stations can be detected, and as will be shown, can produce significant and systematic orbit error.

2. SLRF2005 and LPOD2005

Upon its release in October 2006 the ITRF2005 SLR complement (Altamimi et al., 2007) offered improved stability and accuracy (Lemoine et al., 2007) over its predecessor,

ITRF2000 (Altamimi et al., 2002). However, several factors prevented the immediate and direct use of ITRF2005 for processing SLR data: 1) the ITRF2005 scale, obtained from VLBI, was not compatible with the inherent SLR scale, 2) many stations with a history of tracking were not included, and new stations since 2005 were missing, 3) there is no official documentation of the biases applied in the ITRF2005 station solution. A complement to ITRF2005, called , ITRF2005s, which adopted the SLR-derived scale was later released, but like the ITRF2005 complement, it did not include all stations, nor reference a station bias history.

The aforementioned issues were solved with the terrestrial reference frame SLRF2005 (Luceri 2008) and with a consistent treatment of SLR biases defined by the ILRS Analysis Working Group. The terrestrial reference frame was obtained combining ITRF2000, ITRF2005 rescaled and a global SLR solution with data from 1993 to 2007 to add the new sites. The well defined set of station biases to be applied when using the SLRF2005 solution was also required. SLRF2005 shows improved POD performance over the ITRF2005s complement (Table 1).

A further improvement to the SLR complement was achieved with LPOD2005 version-9 (Ries 2008), refining four primary and 18 other station position/velocities of the complete SLRF2005 complement. Of special importance to POD is the improvement seen in the four primary stations (Figure 2). In addition to improved residual fits in the four LPOD2005 stations, the majority of stations show lower residuals, indicating an improvement in the Jason-1 orbit using LPOD2005 (Figure 2).

In the POD tests we present herein, we apply a SLRF2005 bias strategy using the SLRF2005 complement and apply the LPOD2005 bias strategy using the LPOD2005 complement. The GSFC bias strategy is consistent with that of LPOD2005 but has been updated to estimate biases for all suspect stations (Table 3).

3. Primary stations with apparent station position/bias error

LPOD2005 significantly improves primary stations Zimmerwald, Riyadh, and Ajacio. LPOD2005 offers a critical improvement for the Zimmerwald station position, where the correct bias history has been applied in the station solution. In contrast, the Zimmerwald bias history was not applied in the SLRF2005 solution. Figure 3 shows the time series of Zimmerwald mean SLR residuals using each of the two complements. The mean SLR residuals reflect the presence of a range bias. The two series diverge following 2006 with the SLRF2005 position indicating the appearance of a bias in the Zimmerwald station from early 2006. In February 2006 the CSPAD detector/Stanford clock were replaced with equipment known to be bias free. It is the LPOD2005 coordinates which show no bias in the data, as expected, when a zero Zimmerwald bias is assumed in the POD processing. Figure 3 illustrates the intimacy between a station solution and the bias history applied when forming that solution, and consequently implies that the same bias history be applied using the new coordinates in subsequent processing of SLR data.

The Riyadh velocity is improved in LPOD2005. Error in velocity will result in the increase in the SLRF2005 position error over time, and this is seen in Figure 4 showing an increase in mean residuals for this station.

Even with LPOD2005 several stations still show mean residual trends, the most prominent of which are Herstmonceux and Wetzell. The presence of such an apparent varied bias history for Wettzel (Figure 5) would make it difficult , if not impossible to achieve a bias-free station solution. The GSFC bias strategy adopts the estimation of a bias/arc for this station (Table 3). The February 12, 2007 appearance of an apparent 1.2cm bias for Herstmonceux was unexpected (Figure 6) and could not be immediately explained. The GSFC strategy was to estimate a bias/arc for this station from February 12, 2007 (Table 3). Subsequently it was determined that an incorrect bias history was applied in the ITRF2005 Herstmonceux station solution. Several months following these tests LPOD2005 (version 11) was updated with a new station position estimate for Herstmonceux.

In the interest of brevity other SLR stations which show less prominent trends in the mean SLR residuals are not presented in this paper. Please see the Zelensky et al., 2008 OSTS presentation for a more complete description.

4. Orbit sensitivity to station position/bias error

A long-term increase in mean SLR residuals is seen in Jason-1 POD using the SLRF2005 complement (Figure 7) and confirmed with Jason-2 POD (Zelensky et al., 2008). The presence of such a trend provides ample warning that the estimation of geodetic parameters or a stable orbit reference for altimetry may be compromised by systematic error. Using LPOD2005 and the GSFC bias strategy (Table 3) the trend in mean residuals is greatly diminished (Figure 7) and the residual fits improved (Table 1).

The orbit differences between SLR/DORIS orbits using SLRF2005 and LPOD2005 show radial rms differences of up to 8-mm / cycle and differences in the mean-Z of up to -15 mm. with a possible trend (Figure 8). Such orbit error is significant for altimeter data analysis, where mm/y levels of accuracy are required for mean sea level trends. Figure 8 illustrates that only a few small primary SLR station position/bias errors are sufficient to degrade the SLR/DORIS precision orbit.

5. Conclusion

The current GSFC POD strategy allows 1-cm SLR processing of the Lageos and Jason satellites. At this level differentiating between station biases and position/velocity error is difficult but critical for further improvements in SLR station position/velocity estimates. Our POD tests have shown that only a few SLR station position/bias errors are sufficient to degrade this level of processing accuracy, and have illustrated that an accounting for a station's explicit bias history is an integral component of any SLR station solution.

SLRF2005 is the ITRF2005s SLR complement expanded for completeness and reflects the inherent TRF SLR-scale. SLRF2005 was the first SLR complement distributed with a bias history. LPOD2005 updates only a small subset of the SLRF2005 stations.

In summary:

- An explicit station bias history should be distributed with every SLR station solution set.
- SLRF2005, based on ITRF2005s, offers a comprehensive station set and explicit station bias history, a significant improvement over the ITRF2005-SLR-scaled station set.

- LPOD2005, based on SLRF2005, significantly improves primary stations Zimmerwald, Riyadh, and Ajacio.
- The use of LPOD2005 significantly improves the Jason SLR/DORIS orbits.
- Even with LPOD2005 several stations still show mean residual trends, the most prominent of which are Herstmonceux and Wetzell. Subsequent to this analysis it was determined an incorrect bias history was applied in the ITRF2005 Herstmonceux solution, and consequently LPOD2005 was updated with a new position for Herstmonceux.
- The generation of a comprehensive station set and the improvement of several station position/velocities, was realized by SLRF2005 followed by LPOD2005. These ITRF releases represent an essential service provided to the SLR community.

References

Altamimi, Z., P. Sillard, and C. Boucher (2002), ITRF2000: A new release of the International Terrestrial Reference Frame for earth science applications, J. Geophys. Res., 107(B10), 2214, doi:10.1029/2001JB000561.

Altamimi, Z., X. Collilieux, J. Legrand, B. Garayt, and C. Boucher (2007), ITRF2005: A new release of the International Terrestrial Reference Frame based on time series of station positions and Earth Orientation Parameters , J. Geophys. Res., 112, B09401, doi:10.1029/2007JB004949.

Lemoine F.G., N.P. Zelensky, S.B. Luthcke, D.D. Rowlands, B.D. Beckley, D.S. Chinn (2007), Improvement of a Complete and Consistent TOPEX and Jason Orbit Time Series, poster, OSTST 2007, Hobart, Tasmania, March 12-15, 2007 http://www.aviso.oceanobs.com/fileadmin/documents/OSTST/2007/lemoine_tpj1_pod.pdf

Lemoine F.G., N.P. Zelensky, D.D. Rowlands, S.B. Luthcke, T.A. Pennington, D.S. Chinn, BD. Beckley, M. Ziebart, A. Sibthorpe, P. Willis, V. Luceri, (2008) Calibration and Validation of the Precise Orbits for OSTM – Extending the TOPEX, Jason-1 and Jason-2 Climate Data Record for MSL Studies, poster OSTST 2008, SB.5-043, Nice., France, November 2008 http://www.aviso.oceanobs.com/fileadmin/documents/OSTST/2008/F.G_Lemoine.pdf

Luceri V, Bianco G. (2008), The temporary ILRS reference frame: SLRF2005, presented at ILRS Fall Meeting, 24-28 September 2007, Grasse www.oca.eu/gemini/ecoles_colloq/colloques/ilrs2007/PresentationsPdf/2_Session.pdf/2.1_Luceri_ILRS_TRF.pdf

Ries J.C. (2008), LPOD2005: a practical realization of ITRF2005 for SLR-based POD, presentation, OSTST 2008, Nice., France, November 2008 http://www.aviso.oceanobs.com/fileadmin/documents/OSTST/2008/oral/ries.pdf and ftp://ftp.csr.utexas.edu/pub/jason/models/coords

Zelensky N.P., F.G. Lemoine, D.D. Rowlands, S.B. Luthcke, D.S. Chinn, J.W. Beall, B.D. Beckley, S.M. Klosko, P. Willis, V. Luceri (2008), Sub-centimeter SLR precision with the SLRF2005 / LPOD2005 network, poster OSTST 2008, SB.5-042, Nice., France, November 2008 http://www.aviso.oceanobs.com/fileadmin/documents/OSTST/2008/Zelensky_1.pdf

Table 1. Significant improvements to GSFC 2008 POD Standards					
test name	Jason-1 SLR/DORIS residual summary cycles 1-21	doris rms (mm/s)	slr (cm)		xover rms (cm)
			mean	rms	
nominal 2007	itrf2005(s)_merged (itrf2000), ggm02c	0.3976	-0.073	1.519	5.730
trf2005	+ slrf2005/dpod2005 (version 1.1)	0.3979	0.086	1.508	5.732
eigen_gl04s	+ switch to eigen gl04s	0.3979	0.081	1.479	5.728
tidal_com/eop	+ tidal CoM (got4.7) & tidal EOP	0.3978	0.073	1.428	5.724
cr_panel	…. + tune Cr=0.929	0.3978	0.074	1.409	5.727
lpod2005	….+ lpod2005 + lra phase map	0.3978	-0.041	1.324	5.725

Table 2. GSFC POD Standards summary (October 2008)	
Reference frame and displacement of reference points	
SLR	SLRF2005 + LPOD2005
DORIS	DPOD2005
Earth tide	IERS2003
Ocean loading	Got4.7 all stations
Tidal CoM &EOP	Got4.7; VLBI high frequency terms
Gravity	
Static	Eigen-Gl04s
Time varying	Linear C20-dot, C21-dot, S21-dot (IERS2003) + 20x20 annual terms from GRACE
Atmospheric	ECMWF, 50x50@6hrs
Tides	Got4.7 (ocean); IERS2003 (Earth)
SLR measurement	
Biases	Consistent with SLRF2005/LPOD2005
LRA/CoM (mm)	TP: model, JA1/2: -49, L1/2: -251 / -245(RGO)

Table 3. GSFC SLR Bias Strategy Summary (November 19, 2008)			
Station		sigma wt cm	Bias treatment
name	number		
mcdo	70802419	10	estimate troposphere scale 950306-960126, 960126-960425, 960435-960508
gorf	71050725	10	estimate time bias/pass 990304 -990308, 9900429-990501
mnpe	71100411	10	estimate range bias/arc 960827-961004
tahi	71240801 71240802	10	estimate range bias/arc 040501-040701
gorf t4	71301403		estimate range bias/arc 920422 → present
holl	72102312	10	estimate time bias/arc 990629 – 990804
chac	72371901	30	estimate pass x pass range bias
beij	72496101	30	apply +40 mm 990304-020305
rich	72951102 72951103 72951501	10	estimate range bias/arc 941124-941214
zimm	78106801	10	apply -18 mm 961215–970709

	(blue)		**apply +68 mm 970709–970717** **apply -64 mm 970730 – 970903** **apply -18 mm 970903-980000** **apply -26 mm 980101-020529** **apply -20 mm 020529-041228** **apply -26 mm 041228-060206**
	88106801 (ir)	**10**	**estimate range bias/arc 020801 - 060621**
	68106801 (green)	**10**	**estimate range bias/arc 080401 → present**
boro	**78113802**	**10**	**estimate range bias / pass 920422- 990722** **estimate tropo bias / arc 920422- 980701**
sfef	**78306901**	**10**	**estimate range bias/arc 920422 → present**
gras	**78353102**	**10**	**estimate range bias/arc 920422 → present**
pots	**78365801**	**10**	**apply +18.5 mm 940101-940130**
simo	**78383602**	**20**	**estimate range bias/arc 920422 → present**
graz	**78393401**	**10**	**estimate range bias/arc 920422 – 960930** **estimate tropo bias/arc 020610 – 021210**
rgo	**78403501**	**10**	**estimate range bias/pass 940113-940121** **apply -2.5 mm 941001-020201** **apply +5.5mm 020201-070210** **estimate range bias/pass 070210 → present**
orrl	**78432502**	**10**	**estimate pass x pass range bias**
mate	**79417701**	**10**	**apply -14 mm 070216 00:00 - 070222 11:00** **apply -28 mm 070222 11:00 - 070706 08:00** **apply -22 mm 070706 08:00 - 070830 00:00** **apply -25 mm 070830 00:00 - 071022 14:00**
wetz	**88341001**	**10**	**estimate range bias/arc 920422 → present**

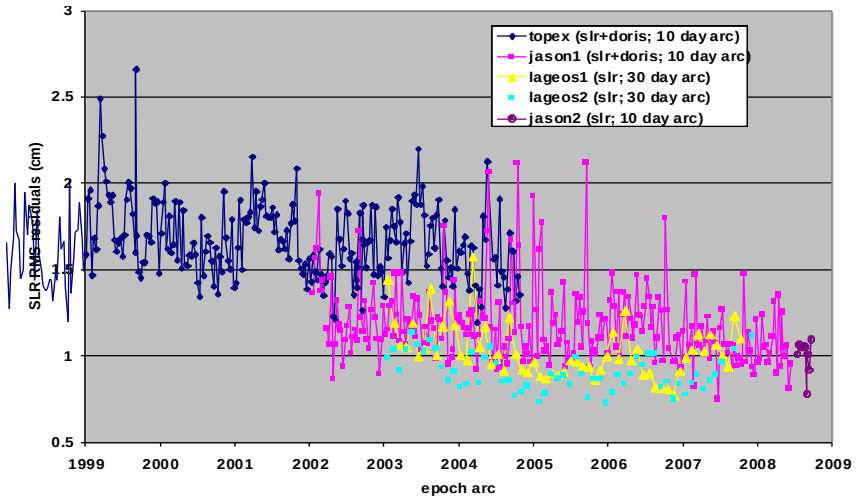

Figure 1. SLR Processing at GSFC

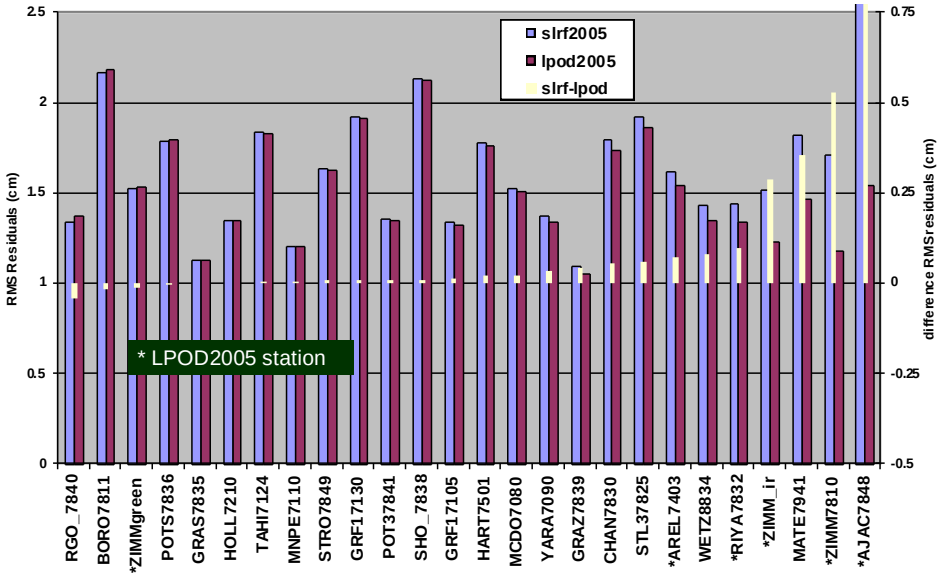

Figure 2. SLRF2005 / LPOD2005 primary station performance over Jason-1 cycles 1-237

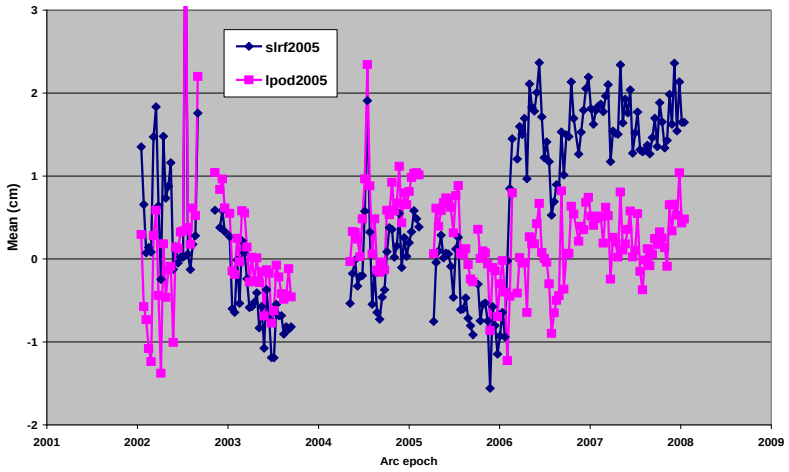

Figure 3. Jason-1 Zimmerwald (blue) mean SLR residuals

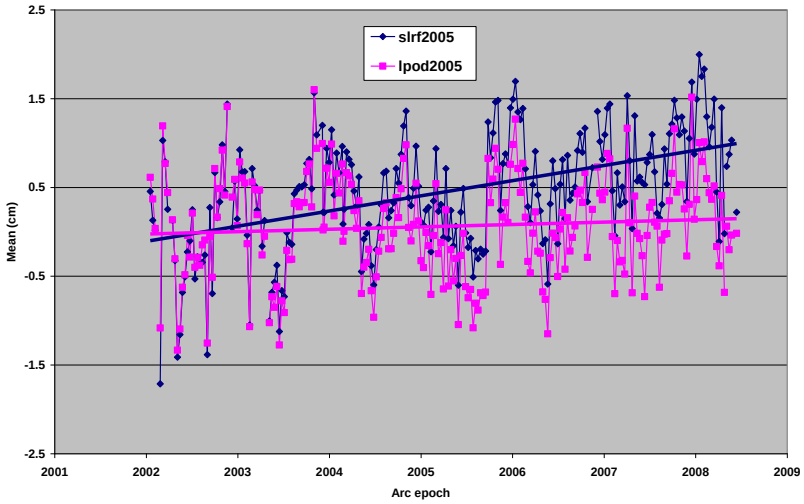

Figure 4. Jason-1 Riyadh mean SLR residuals

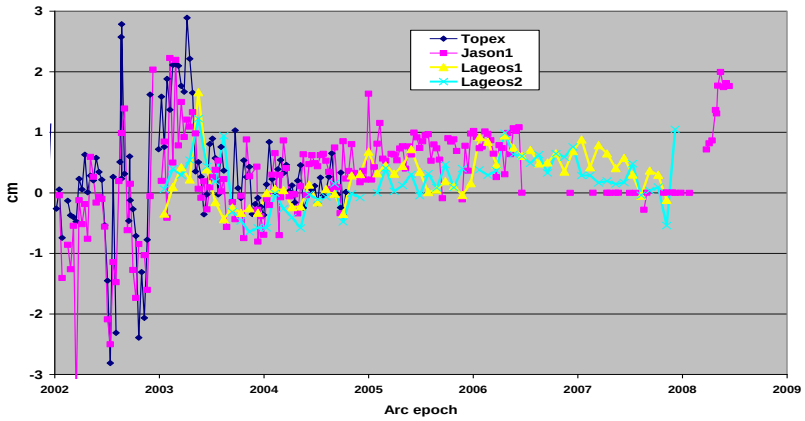

Figure 5. Wettzel mean SLR residuals

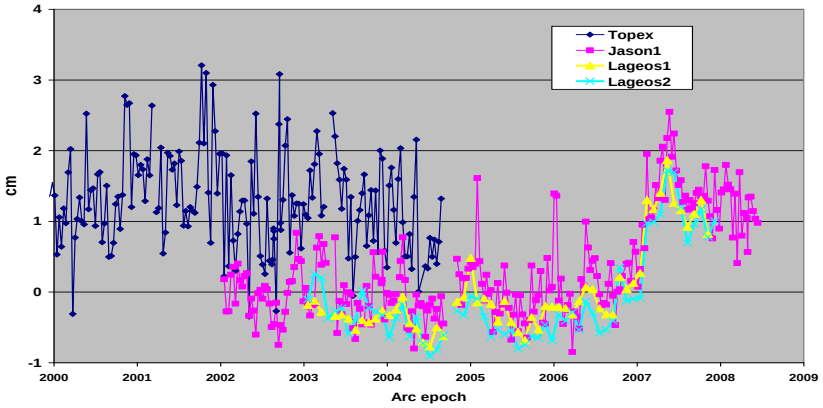

Figure 6. Herstmonceux mean SLR residuals

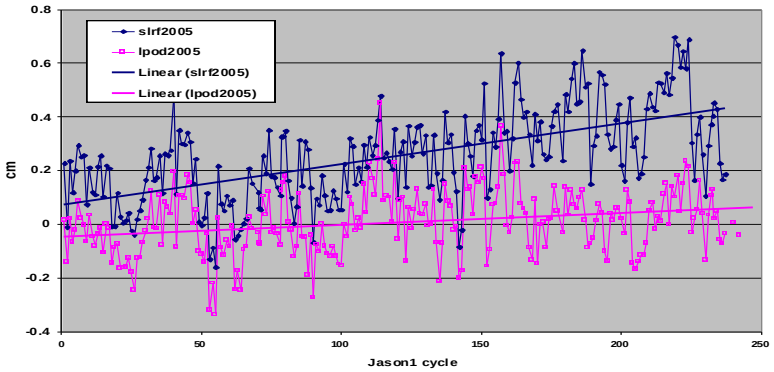

Figure 7. Jason-1 mean SLR residuals

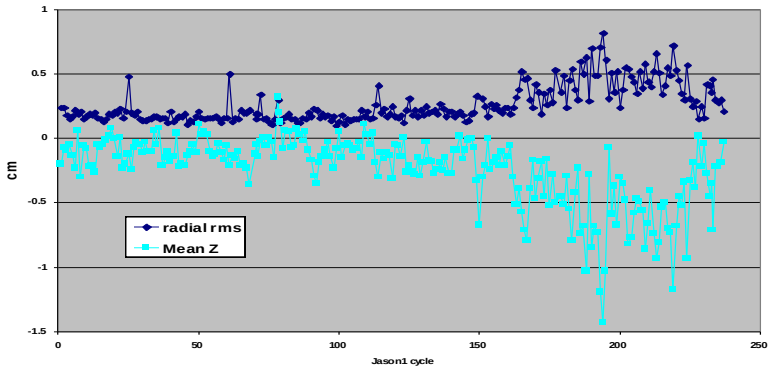

Figure 8. Jason-1 LPOD2005-SLRF2005 SLR/DORIS orbit differences

NGSLR Performance in High and Low Energy Operation

Peter Dunn (1)**, Christopher Clarke** (2)**, Mark Torrence** (3)

(1) Raytheon Information Solutions
(2) Honeywell Technology Solutions Incorporated
(3) SGT Incorporated

peter.j.dunn@raytheon.com

Abstract

The Next Generation Satellite Laser Ranging System (NGSLR) has been designed to track targets at lunar distance as well as Earth-orbiting retroreflector-equipped satellites. NGSLR's eye-safe, single photon, high frequency observations of the closer targets exhibit characteristics of system and satellite signature which must be considered in an effective orbit determination in combination with data collected by other observatories in the global SLR network. To help isolate these features, observations taken by the instrument as the receiver in a two-station configuration with MOBLAS-7 at Goddard Geophysical and Astronomical Observatory (GGAO) have been used to calibrate the NGSLR event timer and processor.
High energy returns from available Earth orbiting satellites have now been used to calibrate the longer-pulse transmit system built into NGSLR to support the up-coming Lunar Reconnaissance Orbiter (LRO) Mission. Special efforts by stations in the tracking network will provide the timing required to construct the lunar observations from signals received at LRO. We will show the results of a continuing analysis of the accuracy and precision of each of the two NGSLR systems observing returns from geodetic satellites ranging in altitude from Larets to Etalon.

Introduction

NGSLR is a single photon multi-kilohertz eye-safe satellite laser ranging system (McGarry 2006).The instrument has conducted operations in several tracking modes, performing two-way ranging to ground targets and satellites, as well as three-way ranging to satellites in its low energy mode. In preparation for one-way ranging to LRO, it has operated in high energy mode and ranged to both ground targets and low and high earth satellites. This paper describes the analysis of the ranging observations to characterize the system and to calibrate it's operation when transmitting at both high and low energy.

Data Analysis for the low energy NGSLR 2 kHz system

The eye-safe laser (~100 micro-Joules at 2 kHz) has tracked targets ranging in altitude from Low Earth Orbiting (LEO) satellites to LAGEOS, and has successfully ranged to GLONASS-95 and GLONASS-l02. A tight laser divergence (4 arc-sec) is used and LEOs are often tracked at below 15 degrees elevation requiring no bias correction.

During the analysis period, a technique described by Degnan et al. (2008) and designed to accommodate the lack of overlap between the transmit and receive beams in the system, was implemented. In this method, the telescope is pointed behind, in the direction of the returning light from the satellite, and Risley Prism wedges are independently controlled to point the

laser ahead to anticipate the arrival of the laser pulse at the target.

NGSLR uses a Q-Peak laser with an output energy of about 50 micro-Joules per pulse at the telescope aperture in a 37 cm diameter beam. The current laser pulse width is about 300 picoseconds and the system generally receives multi-photon returns from the LEO satellites. The receiver system is a high quantum efficiency (32%) Hamamatsu four quadrant detector with a threshold discriminator nominally set to < 0.5 photoelectrons on each quadrant.

The low energy instrument has conducted satellite measurements in two tracking modes. Two-way, single station returns have been received from satellites up to LAGEOS altitude with a conventional SLR configuration using the 2 kHz laser transmitter. These measurements show the characteristics of the target satellite in the single photon regime, and RMS noise levels are limited to a minimum of about 30 mm by the convolution of the transmitter pulse width and the receiver impulse response.

The instrument has also taken measurements as the receiver in a two station (3-way) configuration with MOBLAS-7, a nearby high energy system. This configuration can be used for receiver testing; the higher power of the 4 or 5 Hz transmitting laser allows easier detection of returns from satellites at GPS and ETALON altitudes. The tighter transmitted pulse yields measurements with an RMS noise level closer to 20 mm. When the receiver stop time of the transmitter is considered as well as the transmit time, the 10 mm RMS noise level of the high energy transmitter can be matched, demonstrating the integrity of the eye-safe system's event timer and processor.

The increased number of returns per second from the NGSLR system produces normal points comparable in precision to the higher energy transmitter system and allows the station to autonomously close the tracking loop. Data taken at kilohertz resolution can also be used improve the definition of signals in the returns from satellites which have a strong satellite signature.

Sharing returns from a high energy transmitter

NGSLR receiver performance was calibrated using MOBLAS-7 which transmits shorter multi-photon pulses, with cables connecting the systems. For the case in which MOBLAS-7's own two-way measurements were monitored, the NGSLR Event Timer was triggered on the transmitting systems start and stop pulses. The RMS noise levels of returns detected by NGSLR amounted to 8 mm for ERS-2, 10 mm for Starlette and LAGEOS, and 15 mm for Ajisai.

These levels were consistent with those expected from MOBLAS-7's own system and confirmed the integrity of NGSLR's timing and software. In 3-way configuration, MOBLAS-7 fires and NGSLR only receives, and its threshold discriminator gave a higher detection noise level than MOBLAS-7. In this case the RMS noise levels were found to be 21 mm for ERS-2, 26 mm for Starlette, 21 mm for LAGEOS and 35 mm for Ajisai.

In the conventional 2-way configuration, NGSLR transmits longer pulses than MOBLAS-7, and the RMS noise levels were 30 mm for ERS-2 and Starlette, 35 mm for LAGEOS and 42 mm for Ajisai. The characteristics of a 72 degree elevation Ajisai pass are shown in the Figure 1, which also gives the contribution to the tracking signal from each of the four receiver quadrants. Evidence of both satellite and system signature can be seen in the full-rate

observations, and the normal points, shown in yellow and computed according to ILRS standards, demonstrate precision at the millimeter level.

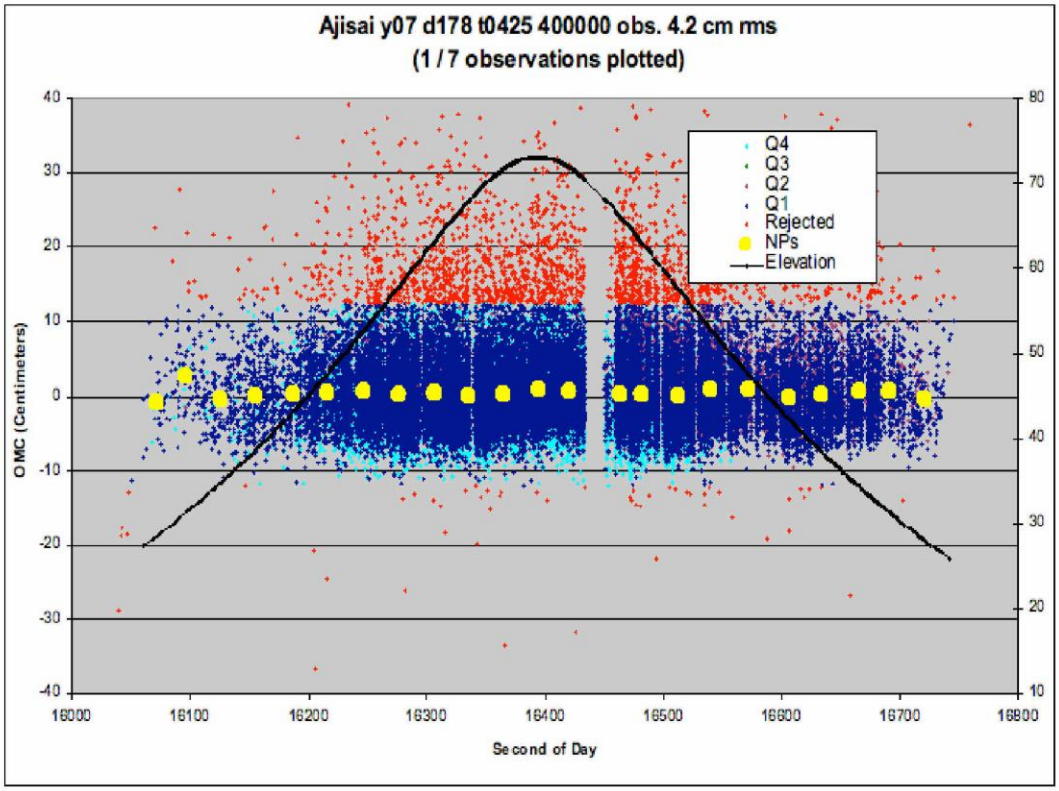

Figure 1. Normal point data compression residuals for an Ajisai pass from NGSLR/2K

In the first three quarters of this year NGSLR has tracked nearly 100 passes, including AJISAI, BEC, JASON, JASON-2, LARETS, STARLETTE, LAGEOS 1 and 2, and GLONASS-102 (McGarry et al., 2008a). Many of these passes were tracked simultaneously with MOBLAS-7, allowing for a calibration of system accuracy.

The following table lists the details of those co-located passes and includes the number of normal points, the RMS of those normal points and statistics associated with the overlap with the data from MOBLAS-7. The mean pass bias between the two systems is seen to be -9.5 mm +/- 4.5 mm for 27 passes of BE-C, Starlette, LAGEOS-1, Ajisai, Jason, Larets, LAGEOS-2, ERS-2 and Envisat. The receiver system was found to exhibit a dependence on the return signal strength which was monitored from ground target calibrations as a function of return rate.

When this system signature was accommodated in the NGSLR data processing, the mean pass bias between the two systems was reduced to 2.5 +/-3.5 mm. Otsubo and Appleby (2003) show that the Ajisai satellite exhibits a large bias of 20 to 30 mm when data from systems receiving low energy returns are compared with those from high energy instruments. When this satellite signature is accounted for, the mean pass bias between the two systems is reduced to -1.1 +/- 3.3 mm. Inter-comparison tracks thus confirm average agreement of a few millimeters between NGSLR and MOBLAS-7 for a number of LEO satellites and LAGEOS.

Satellite	DOY	Accepted Obs.	RMS(mm)	NPTs	NPT RMS (mm)	Mean Pass Bias (mm)	NPT over lap	Peak to Peak (mm)	Mean Pass Bias (mm)	Bias with system function (mm)	Bias with system/ satellite function
BEC	220	63161	35.9	30	1.1	-20.2	7	17	-20.2	4.8	4.8
Starlette	164	7716	32	20	1.8	4.3	19	15.8	4.3	29.3	29.3
Starlette	165	4946	33.1	8	1.6	-56.1	6	28	-56.1	-31.1	-31.1
Starlette	177	70201	31	24	1	-25.4	4	18.1	-25.4	-0.4	-0.4
Starlette	178	93276	32	19	0.6	-33.1	18	42.7	-33.1	-8.1	-8.1
Starlette	234	133693	28.8	17	1	-4.2	10	26.5	-4.2	20.8	20.8
Lageos-1	234	134	40.1	4	5.9	23.2	3	2.3	23.2	-1.8	-1.8
Lageos	247	3959	43.9	23	4.7	45.1	5	15.5	45.1	20.1	20.1
Ajisai	165	601211	43.7	28	0.5	-16.2	4	14.4	-16.2	8.8	-16.2
Ajisai	178	32431	44.4	24	2.7	1.4	17	32.8	1.4	26.4	1.4
Ajisai	193	413332	46.7	28	0.8	4	3	11.3	4	29	4
Ajisai	268	202346	47.5	30	1.1	-18.9	30	53.8	-18.9	6.1	-18.9
Jason	177	24033	30.4	42	2.6	-12.9	21	29.7	-12.9	12.1	12.1
Larets	184	16393	33.9	13	3.2	-48.6	7	51.6	-48.6	-23.6	-23.6
Larets	234	33972	25.3	10	1.1	-24.2	2	20.2	-24.2	0.8	0.8
Larets	268	89535	36.3	16	1.5	-15.4	9	32.3	-15.4	9.6	9.6
Lageos-2	164	4846	32.1	15	2.3	9.6	3	11.7	9.6	-15.4	-15.4
Lageos-2	165	15580	34	18	1.9	22.4	9	20.1	22.4	-2.6	-2.6
Lageos-2	177	2061	49.6	15	3.8	-9.9	14	18.5	-9.9	-34.9	-34.9
Lageos-2	178	1666	47.2	17	5.3	23.5	12	23.8	23.5	-1.5	-1.5
Lageos-2	193	5648	36.8	17	2.5	5.4	12	15	5.4	-19.6	-19.6
ERS-2	177	71341	32.7	24	1.9	-28.4	1	0	-28.4	-3.4	-3.4
ERS-2	184	29398	43.5	17	2.6	-38.9	5	20.8	-38.9	-13.9	-13.9
Envisat	212	8202	30.5	14	2.1	-21.4	5	45.6	-21.4	3.6	3.6
Envisat	226	983	31.5	10	3.8	-31.4	7	15.1	-31.4	-6.4	-6.4
Envisat	234	1458	29.2	14	3.9	8	6	10.3	8	33	33
Envisat	247	2537	33	12	3.9	1.4	3	2.5	1.4	26.4	26.4
								Mean	-9.5	2.5	-1.1
								Std Err.	4.5	3.5	3.3
								Std Dev	23.6	18.5	17.5
								Count	27	27	27

Figure 2. Statistics of passes tracked simultaneously with NGSLR and MOBLAS-7

Data Analysis for the NGSLR/LR system

The NGSLR system can switch from eye-safe laser ranging to high energy transmitting, in order to perform uplink-only ranging to the Lunar Reconnaissance Orbiter (LRO-LR). In this application the laser fire must be controlled to ensure that the pulses arrive at the spacecraft when the Range Window is open. Ground laser fire times are recorded and transmitted to a central facility where they are matched with the spacecraft events to form ranges (McGarry et al., 2008b).

Laser ranging to LRO employs a 28 Hz 30 mJ laser with a wavelength of 532.2 nm, which is matched to the center of the spacecraft's 3 Angstrom LR bandpass filter, and with a pulse width of 5.5 nanoseconds. In this mode, the width of the range gate generator output pulse is modulated to provide an approximately 28 Hz frequency to the laser.

In the first three quarters of this year NGSLR/LR has tracked 26 passes of satellites ranging in altitude from Low Earth Orbit targets to ETALON. Three of these passes were tracked simultaneously with MOBLAS-7, and showed an average difference between the two systems of -11 cm. This level of accuracy will allow the system to improve the orbital knowledge of LRO to support lunar gravity model development.

Satellite	SIC	DOY	Start Time	Accepted Obs.	RMS(mm)	NPTs	Obs/NPT	Skew	Kurtosis	NPT RMS (mm)	Mean Pass Bias (mm)	Overlapping NPTs	Peak to Peak (mm)		
Larets	5557	5	2:31	2214	279.5	10	221	0.3	2.62						
Ajisai	1500	5	3:17	5542	266.8	15	369	0.34	2.76						
Etalon-1	525	5	3:30	276	322.3	6	46	0.12	3.07						
Starlette	1134	5	4:26	4141	240.6	7	591	0.29	2.82						
BEC	317	21	1:30	5170	282.3	27	191	0.38	2.9						
Etalon-1	525	21	1:44	18	316.2	7	2	0.08	4.4						
Ajisai	1500	21	2:59	5388	247.2	21	256	0.25	2.9						
Jason	4378	73	2:02	2109	310.5	17	124	0.43	2.84	37.5					
ERS-2	6178	73	2:54	8701	274.3	27	322	0.31	2.8	18.1					
Jason	4378	74	0:26	27011	296.1	46	587	0.43	2.91	16.4					
Lageos-2	5986	81	3:14	200	357.1	9	22	0.22	2.76	71.8					
Starlette	1134	107	1:38	10459	310.6	10	1045	0.24	2.89	10.5					
Lageos-2	5986	107	1:45	25601	294.1	8	3200	0.42	2.83	14.8					
ERS-2	6178	116	2:06	2093	287.6	17	123	0.31	2.97	30					
Larets	5557	116	3:02	4334	297.6	9	481	0.29	2.8	23.6					
Etalon-2	4146	170	0:39	299	477.4	10	29	0.12	2.5	77.5					
Envsat	6179	170	1:36	2019	341.4	22	91	0.51	2.89	38.8					
Ajisai	1500	170	1:57	23941	266.8	30	798	0.51	3.01	10.1					
Lageos-2	5986	170	3:00	12739	306.6	29	439	0.37	2.84	19.5					
Larets	5557	207	2:29	1217	288.1	9	135	0.27	2.88	26.4	-65.5	5	245.4		
BEC	317	207	3:15	34684	241.9	44	788	0.17	2.87	8.5	-165.1	34	385.6		
Etalon-2	525	207	3:22	3179	237.9	1	3179	0.11	2.71	3.6					
ERS-2	6178	207	2:42	9738	259.3	24	405	0.31	2.82	16.5	-97.4	19	385.1		
Lageos-1	1155	207	3:48	1688	303.3	17	99	0.41	2.76	33.8					
Lageos	1155	248	0:53	294	256.1	8	36	0.39	2.82	44.8					
Envsat	6179	248	2:24	3184	240.6	11	289	0.28	2.83	21.2					

Figure 3. Statistics of passes tracked by NGSLR/LR

References

Degnan, J., McGarry, J., Zagwodzki, T., Varghese, T., *Transmitter Point-Ahead using Dual Risley Prisms: Theory and Experiment,* in this Proceedings, 16th International Workshop on Laser Ranging, Poznań, Poland, October 2008.

McGarry, J., Zagwodzki., T., *SLR2000: The Path Toward Completion,* Proceedings of the 15th International Workshop on Laser Ranging, Canberra, Australia, October 2006.

McGarry, J., Zagwodzki, T.,Varghese, T., Degnan, J., et al, *NGSLR: Sharing Eyesafe Kilohertz SLR with Transponder Ranging,* in this Proceedings, 16th International Workshop on Laser Ranging, Poznań, Poland, October 2008a.

McGarry, J., Zellar, R., Neumann, G., Noll, C., Torrence, M., et al, *Laser Ranging to the Lunar Reconnaissance Orbiter: a Global Network Effort,* in this Proceedings, 16th International Workshop on Laser Ranging, Poznań, Poland, October 2008b.

Otsubo, T , Appleby, G., *System-dependent centre-of-mass correction for spherical geodetic satellites,* Journal of Geophysical Research, 108, B4, 2201,10.1029/2002 JB002209,2003.

Development of quality control tools for the MLRO

G. Bianco (1)**, V. Luceri** (2)**, D. Iacovone** (3)

(1) ASI Centro di Geodesia Spaziale \"G. Colombo\", Italy
(2) e-GEOS SpA, Italy
(3) Sistematica SpA, Italy

giuseppe.bianco@asi.it

Abstract

Starting from the need to trace and correct the unmodeled range bias which arose in the MLRO data during last year, we have developed a control infrastructure and a web based information system which enables us to constantly monitor the system parameters and alert the station operators and data analysists for possible anomalies in quasi real time. This presentation gives a thorough description of what has been done so far.

Challenges of the TerraSAR/TanDEM-X formation

K. Snopek, L. Grunwaldt, R. Koenig
Helmholtz Centre Potsdam,
GFZ German Research Centre for Geosciences
snopek@gfz-potsdam.de

Abstract

In September 2009 TanDEM-X will be launched to fly with TerraSAR-X in a very close formation called helix. The helix means close approaches of the two spacecrafts down to approximately 200 meters at one time in along-track direction, at another time in radial direction. Orbit predictions for both spacecrafts will exhibit the usual accuracy of 2 to 3 m in radial and cross track, and something below 10 ms in along-track within 12 hours after release. Due to the very close formation, the stations need to distinguish between the two targets. We will present the formation scenario and highlight the parts where the constellation exhibits extreme positions for tracking. From this, conclusions are drawn on the difficult situations and possible remedies for the various station types

1. Introduction

TerraSAR-X (TSX) is a German radar satellite launched on June 15th 2007 to provide high quality topographic information for commercial and scientific applications. It flies on a polar, sun-synchronous orbit at the altitude of 514 km. The design lifetime of TSX is 5 years. TanDEM-X (TDX) is a TerraSAR-X add-on for Digital Elevation Measurements (DEM). Its launch is planned for fall 2009 with design lifetime 5 years where 3 years overlap with TSX.

The primary goal of the TSX/TDX mission is to deliver high quality elevation data by means of SAR interferometry. To achieve this, the two satellites will fly in a very close formation called helix. The distances between the two spacecrafts will vary between ±200 m in cross, ±300 m in radial and ±600 m in along track direction. TSX will fly on a stabile orbit and TDX, by means of frequent maneuvers, will fly around TSX. The absolute distance between the two satellites, the baseline, will vary from ~300 to ~600 m. (see Figure 1).

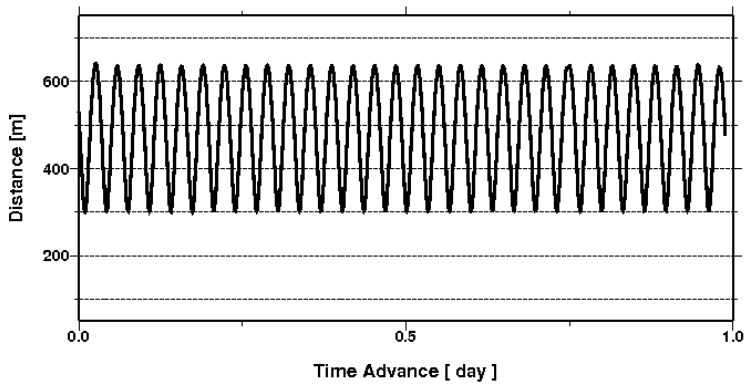

Figure 1. Baseline between TerraSAR-X and TanDEM-X.

Such a close formation imposes new challenges for SLR tracking. Accurate orbit predictions will be needed to allow the stations to distinguish between the two satellites. The stations will probably need to adapt their software and to develop dedicated tracking strategies.

The efforts put into the preparation of the TSX/TDX mission will be rewarded by the unique opportunity of simultaneous tracking of two spacecrafts. Data from simultaneous tracking will be used for the validation of the baseline between the two satellites at millimeter accuracy. The baseline will be determined solely by means of GPS measurements. The millimeter accuracy is the prerequisite to achieve the DEM accuracy requirements. The validation by SLR will be a significant input to the mission.

In the following we present the current prediction quality for TSX and results of performed simulation of SLR tracking of the TSX/TDX formation.

2. TSX Prediction Quality

Good orbit predictions are the basis for successful SLR tracking. GFZ delivers predictions for TSX and will deliver them for TDX. The two satellites are nearby identical from the construction point of view and they will fly in the same orbits. Hence, the analysis of the quality of the predictions for TSX allows us to examine if it will be possible to separate the two satellites in space. We analyzed how much the predicted orbits (PRD) differ from the precise orbits, the so called Rapid Science Orbits (RSO) that we also generate operationally with an accuracy of a few centimeters. We calculated the residuals between PRD and RSO as a function of time. The analysis period covered two months (July and August) in 2008. We also calculated histograms of residuals between PRD and RSO 12 h after the release of the prediction. The predictions are being computed twice a day; therefore 12 h is the longest period of PRD validity. The results of the analysis are given in Figure 2.

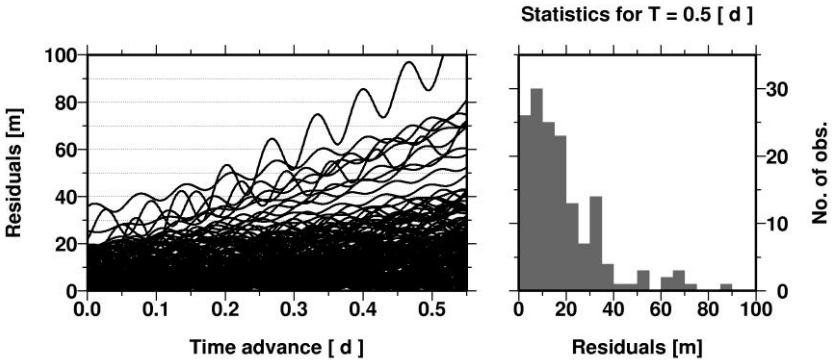

Figure 2. Accuracy of predictions for TerraSAR-X.

It can be seen that the residuals 12 h after release remain usually below 40 m. This is several times smaller than the anticipated distance between the two satellites. So we conclude that the stations will be in the position to easily distinguish between the two satellites.

3. TSX/TDX Simulation

In order to check how the TSX/TDX formation will look from a SLR station point of view we simulated several passes over selected stations locations. Our goal was to answer the following questions: (1) how large will be the angular difference between the two spacecrafts

and (2) will it be possible to track both satellites simultaneously. We assumed that the possibility for simultaneous tracking will occur if the angular difference between TSX and TDX is smaller than 60 arc seconds (as). We simulated SLR passes for 11 SLR stations: Yarragadee, Washington, Arequipa, San Juan, Zimmerwald, Mount Stromlo, Graz, Herstmonceux, Potsdam, Matera and Wettzell. The period of the simulation was one day, which resulted in 35 passes (minimum elevation was 20 deg) and 555 observations. We used the GFZ precise orbit determination software EPOS for our calculations. A sample pass over Potsdam is presented in Figure 3Figure 3.

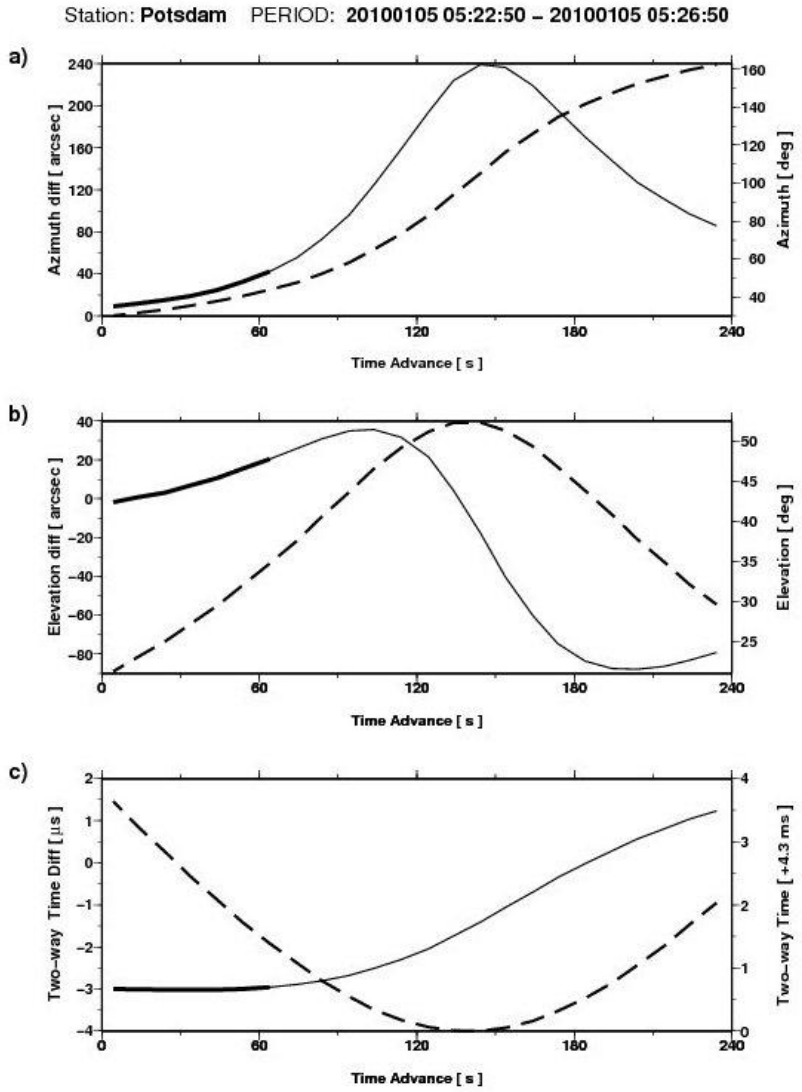

Figure 3. Simulation of a pass of the TSX/TDX formation over station Potsdam. Dashed lines indicate angular coordinates: azimuth and elevation in a) and b) respectively, and two-way travel time to TSX (c). Thin solid lines indicate angular (a,b) or time differences (c) between TSX and TDX as observed by the station. Thick solid lines indicate that the angular difference between the two spacecrafts is smaller than 60 arcs seconds.

Angular differences between TSX and TDX for the pass presented in Figure 3 vary from approximately +10 as to +240 as in azimuth, and from approximately -80 as to +30 as in elevation. Two-way travel time separation is in the order of several microseconds. There

exists the possibility to track both satellites simultaneously for about 60 s. in the beginning of the pass.

Figure 4 shows statistics for all simulated passes. A simultaneous tracking is possible for about 20% of all observations. For these cases, the separation of the two satellites in the two-way travel time is more than 2000 ns. So the separation in range is significant and allows also to distinguish the two spacecrafts.

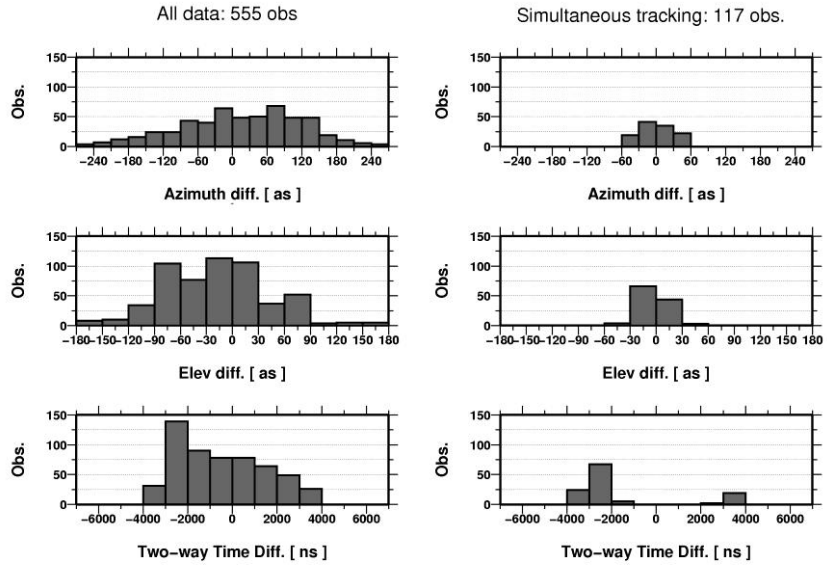

Figure 4. Left side: histogram of differences between TSX and TDX for all simulated observations. Right side: histogram of differences for observations when simultaneous tracking is possible.

4. Conclusions

Our study shows that SLR tracking of the TSX/TDX formation will be a challenging task for the SLR network. The accuracy of the predictions, with updates twice per day, should allow a separation of the two satellites in space. However, very small distances between the two spacecrafts in certain instances will probably urge stations to decide which spacecraft to track during a pass. One can imagine a scenario where stations build a cluster and decide which part of the cluster tracks TSX and which TDX.

Our simulations show also that in a certain percentage of tracks, both spacecraft will be within the transmitting beam at the same time but with a clear separation in range. In these cases, simultaneous tracking will be possible enabling the validation of the baseline between the two satellites at the milimeter accuracy.

Improved Modeling Approaches Towards the mm SLR

E. C. Pavlis, M. Kuźmicz-Cieślak, P. M. Hinkey
JCET/UMBC and NASA Goddard, Maryland, USA
epavlis@umbc.edu/Fax: +1-410-455-5832

Abstract

Accuracy requirements for the International Terrestrial Reference Frame (ITRF) are becoming increasingly more stringent, especially with regards to its origin definition and its scale stability. Satellite Laser Ranging (SLR) contributes unique information on the origin, and along with VLBI, for its absolute scale. Advances in our understanding of the coupling between the sub-components of system Earth require that we revisit our current modeling used in the reduction of SLR data. Over the past few years, the inclusion (or not) in our models of high frequency effects of the temporal gravity signals due to mass redistribution in the terrestrial system, has been a topic of heated discussions at venues such the EGU, AGU and various workshops. With the recent release of numerous products from global circulation models and, satellite and terrestrial observations, we are now able to examine the effect of such improved modeling in the analysis of several years of SLR data. We present results from such analyses and compare them to our nominal results, based on the currently accepted ILRS standards. Depending on the outcome of these tests, we anticipate that in the near future, ILRS will formulate a proposal to IERS for modification of the analysis standards related to the products contributing to the establishment of the future ITRFxx.

Introduction

The International Terrestrial Reference Frame (ITRF) accuracy requirements are becoming increasingly more stringent, driven primarily by those dictated by the Global Geodetic Observing System—GGOS. It is now commonly accepted that the future ITRF should exhibit 1 mm accuracy in the origin of the reference frame at epoch and 0.1 mm/y stability over time [Pavlis et al., 2008]. One of the primary techniques contributing to the development of the ITRF is Satellite Laser Ranging (SLR). SLR determines uniquely the origin of the ITRF and along with VLBI, its scale. For many years now SLR has also observed mass redistribution in the Earth system [Pavlis, 2002], providing unique estimates prior to the launch of GRACE [Tapley et al., 2004]. With the increased maturity in the GRACE products and the proliferation of global fields of atmospheric, oceanic, and hydrological processes, it is now high time to consider the forward modeling of these processes in the analysis of SLR data for the establishment of the TRF. These observations form the motivation behind the work that is reported here, focusing on the possible improvements in the currently adopted standards for SLR data analysis. We will present results form limited tests with various ancillary data sets, demonstrating the level of expected improvement in the results, once these are considered in the a priori model. Although these are presently focused on the analysis of LAGEOS data only, it is planned that in subsequent stages we will extend the most promising model improvements to LEO targets in an effort to make their contribution useful and of acceptable accuracy for inclusion in the development process of the ITRF.

Candidate models under consideration

One of the first improvements to be considered is of course the time varying gravitational signals that GRACE observes at monthly intervals. With several years of GRACE data accumulated by now, it is even possible to derive sufficiently high-resolution models that can be used even during the time period prior to GRACE's launch. In this fashion we can benefit and improve the results from reanalysis of historical SLR data collected long before the GRACE era. In addition or instead if these, we can also consider the inclusion of other models, namely:

- Extended temporal gravity variations
  - NCEP or ECMWF (3 or 6 hr temporal resolution, 0°.25, …)
  - GRACE-derived monthly fields & de-aliasing products
  - Other combinations

- Atmospheric loading (from NCEP or ECMWF)

- Hydrological loading (e.g. GLDAS)

- New ocean tides (e.g. GOT04.7 or more recent) with proper treatment for the atmospheric tides

- Atmospheric refraction from 3-D atmospheric ray tracing (ART) to include atmospheric gradients

- Albedo from global satellite-based fields (higher degree-order seasonal model)

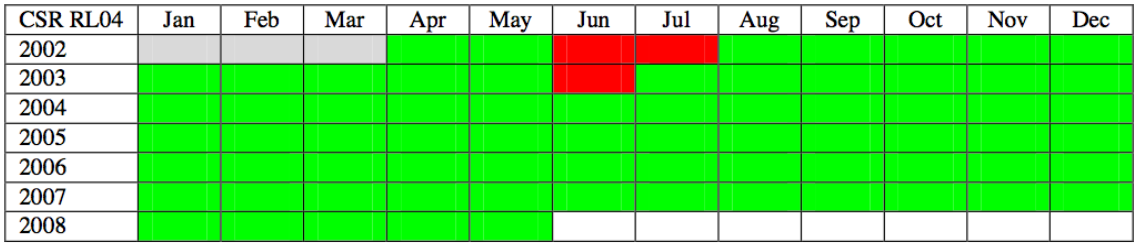

Figure 1. The monthly GRACE fields that were used (green) in this study to derive the analytical model of time varying gravity for very long wavelength (temporal) signals.

The work reported here addressed through limited tests for a few years of LAGEOS and LAGEOS 2 SLR data analysis, the contribution of the GRACE fields, the atmospheric fields from ECMWF, the improved tidal models, and the use of 3-D ART corrections [Hulley and Pavlis, 2007] for the atmospheric refraction instead of analytical models and surface data [Mendes and Pavlis, 2004].

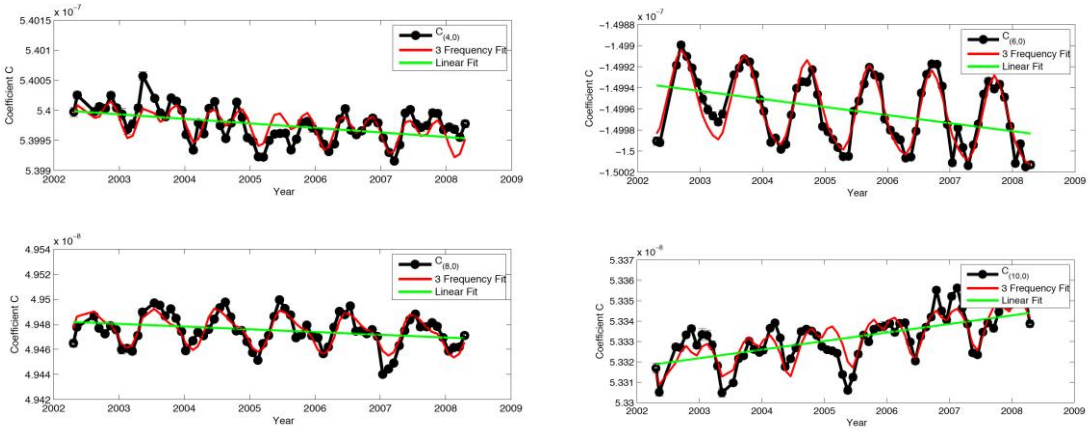

Figure 2. Temporal variations in the even zonal harmonics for degree 4 to 10 observed by GRACE and the linear (green) and harmonic (red) analytical model fitted to them.

GRACE-derived time varying gravitational model

We used the six-year monthly series from CSR's release 4 (RL04) available from April 2002 up to present (Fig. 1), along with the associated de-aliasing product and estimated a set of mean coefficients at epoch 2000.0, along with a secular linear trend and annual, semi-annual and seasonal terms for the entire field to degree and order sixty. Examples of the derived models are shown in Figure 2 for select harmonic coefficients. These coefficients and their variations were then used as the basis for the Precise Orbit Determination (POD) step of the SLR data. The results were then compared to those based on the standard model used for the development of the official ILRS weekly products. In terms of gravitational model, the standard model uses CSR's GGM02C and the tidal model from Goddard, GOT00.2. The current tests used the slightly improved tidal model GOT04.7 that differs from GOT00.2 primarily near the coastlines, which however has implications for the computation of the loading effects, especially for coastal sites.

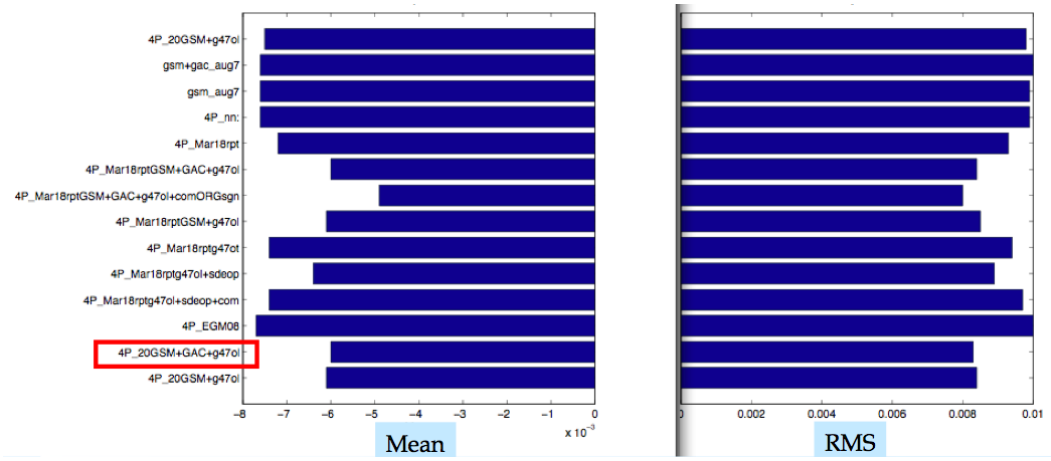

Figure 3. Residual mean and RMS statistics [m] of fits to LAGEOS SLR data collected at Herstmonceux, UK, using a variety of background models for gravity, tides, etc..

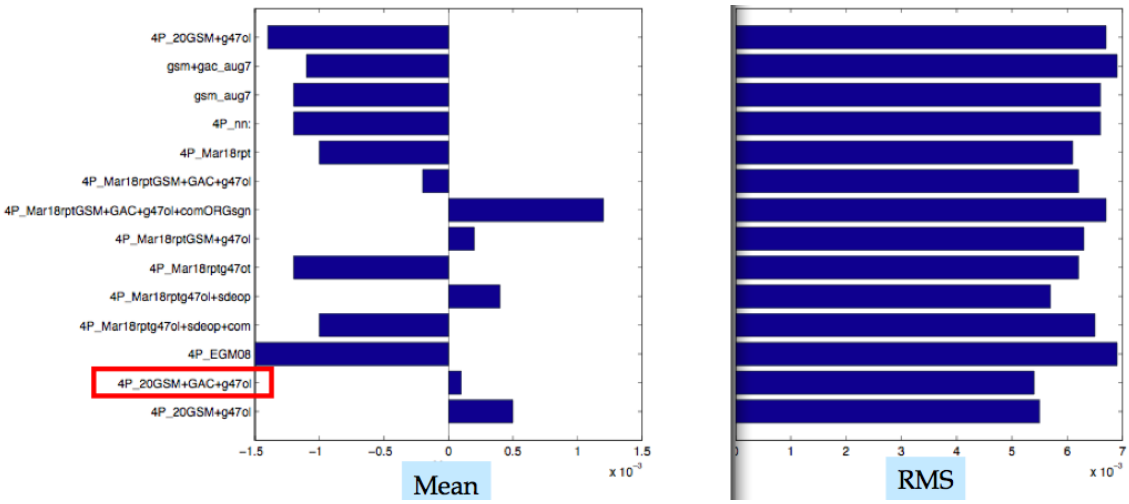

Figure 4. Residual mean and RMS statistics [m] of fits to LAGEOS SLR data collected at Yarragadee, Australia, using a variety of background models for gravity, tides, etc..

Various combinations of improved models were used in reducing the SLR data, each time comparing the mean and RMS residual for each station with respect to those obtained from the standard model as well as the previous tests. We tested each station separately rather than the result for the ensemble of the participating stations in each arc, since not all stations are of equal quality and the ensemble statistics depend largely on the adopted relative weights, something that is a rather subjective process. Our conclusions were drawn primarily from the results of the strong and consistent stations in the network. An example is given in Figure 3 for the Herstmonceux site in UK and for Yarragadee, Australia, in Figure 4.

An examination of the best stations in the network revealed that the preferred model by the data is the one described by the model we fit to the GRACE monthly fields, augmented by the GRACE-supplied de-aliasing and the new Goddard tidal model GOT04.7. Even though there were slight variations between the various sites, the majority vote was for the aforementioned model.

Atmospheric loading modeling

The effect of atmospheric circulation (mass redistribution) was partially modeled through the adopted GRACE-derived gravitational model of the previous section. This is because the modeled effect applies only to the orbit, ignoring entirely the loading effect that modifies primarily the tracking sites' height over the entire spectrum. Using the meteorological global fields of ECMWF we can derive a correction to each station's position due to this loading effect. This has been pioneered as a service since a few years now [Petrov and Boy, 2004], and results are available for various operational and experimental fields from ECMWF (versions v0, v1 and v2), as well as from NCEP:

"v0": 1970/01 - 2002/08: ECMWF Reanalysis (ERA40), with a spatial resolution of 1.125 degrees
"v1": 2000/12 - 2006/12: ECMWF Operational, with a spatial resolution of about 0.350 degrees
"v2": 2005/10 –present: ECMWF Operational, with a spatial resolution of about 0.250 degrees

Because of the existence of these multiple fields, we chose to analyze SLR data in 2001 and 2006, so that we can test the maximum possible set of these fields. The results obtained from

these tests were compared to those obtained without atmospheric modeling, and the statistics of their differences are summarized in Table 1.

Table 1. Statistics of RMS differences for the 2001 & 2006 LAGEOS SLR data reductions with atmospheric loading modeling from various ECMWF releases.

Test Case	Points (weeks)	Mean	Median	RMS	Std Deviation
ΔRMS v0-NO*	52	3.4	2.7	4.45	2.87
ΔRMS v1-NO	104	2.9	2.1	4.31	3.16
ΔRMS v2-NO	52	2.7	1.7	4.09	3.08
ΔRMS v1-v0	*52*	*0.4*	*0.0*	*0.92*	*0.82*
ΔRMS v2-v1	*52*	*1.7*	*1.4*	*2.58*	*1.96*

* NO indicates no atmospheric loading modeling

The top three rows of Table 1 show that any of the three versions of ECMWF fields, when used to derive loading at the tracking sites improves the results with an average reduction in the overall RMS of fit of the order of 3 mm in the mean (or 2 mm median difference), and a similar magnitude of variation about the mean over the tested weeks.

The last two rows compare the three variations of the ECMWF released fields, as "seen" through the orbit filter controlled by SLR tracking data. Evidently, the difference between v0 and v1 is insignificant given the magnitude of the mean and the corresponding RMS. Apparently, going from 1°.125 resolution down to 0°.350 is not making a huge difference. On the other hand, the difference between v1 and v2 is much larger, although that one does not seem statistically significant either when one considers the scatter associated with it. Additionally, the comparison of v1 and v2 is over 2006, when the data that are used to form the ECMWF fields are quite different from those used in 2001 (when we compared the v1 to v0), dominated by global fields obtained from satellite missions. Irrespective of which ECMWF product one uses, it is evident that there is a significant change (improvement) in the fits to SLR data and if one compares this change to the present day state-of-the-art results, the conclusion is that we can no longer afford to not model such effects if our goal is to achieve millimeter or better geodesy.

Advanced refraction modeling

SLR is an optical technique and as such it is not affected greatly by atmospheric refraction as other space geodetic techniques operating in the microwave region of the spectrum. Nevertheless, when we strive for mm-level accuracy, even the otherwise small effects of horizontal gradients in the lower atmosphere must be accounted for. One proven way to do this is to compute refraction corrections along the laser beam path directly from three-dimensional ray tracing through the meteorological fields that are now routinely available. This method was pioneered and tested with the analysis of two years of SLR data by Hulley and Pavlis [2007]. The concept is described in the graphic and equations shown in Figure 5. As discussed in [ibid], the SLR data for 2004-2005 were corrected using refraction corrections obtained using the 3D ART approach, based on three different global fields: ECWMF, NCEP and the satellite observations from the AIRS instrument on board the AQUA NASA platform.

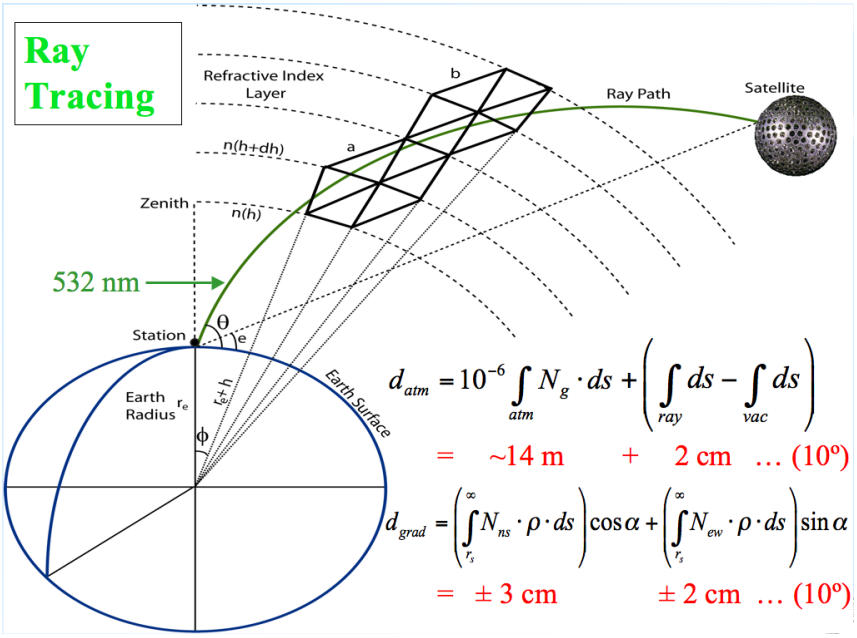

Figure 5. The three-dimensional ray tracing approach to computing the total atmospheric delay along the path of a SLR range observation.

The comparison of atmospheric gradient variations obtained from the three sources agreed in generally very well, however, it is quite apparent when one looks at the results shown in Figure 6 for the Herstmonceux site, that AIRS and ECMWF are in much better agreement than any other pair.

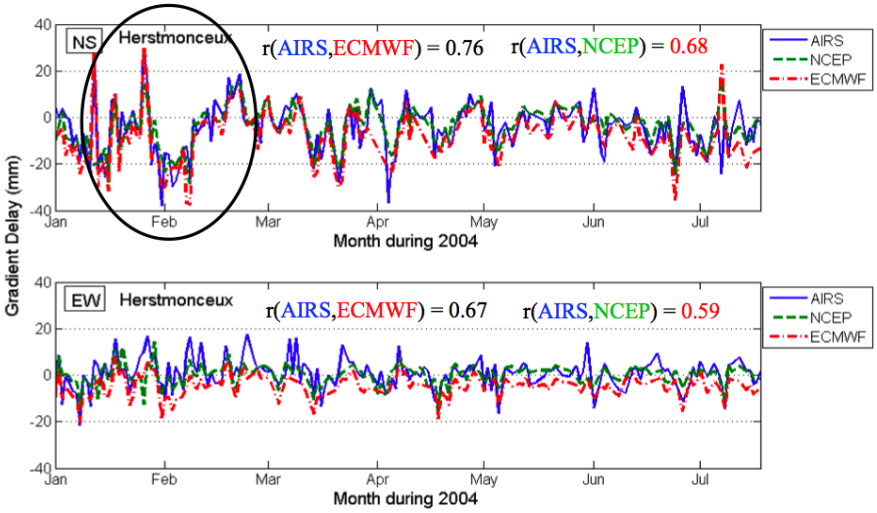

Figure 6. Atmospheric gradients at Herstmonceux during 2004, from three different source fields (AIRS, NCEP and ECMWF).

After applying these corrections to the SLR data, the RMS residual fits improve considerably, indicating the importance of these corrections for future analyses. Statistics of these comparisons are shown in Table 2. From these results it is evident that 3D ART with AIRS-observed meteorological fields is the best approach, explaining almost 25% of the residual variance. An alternate approach where the isotropic delay is modelled through the

analytical model of [Mendes and Pavlis, 2004] and the gradients are obtained from 3D ART is not as effective, explaining only 14% of the variance for the same data.

Table 2. Residual statistics of SLR data corrected with 3D ART atmospheric delays.

Method	**ΔBias (mm)**	**$\Delta\sigma^2$ (%)**
AIRS		
RT_{grad}	0.3 ± 0.3	14.0
RT_{3D}	0.9 ± 1.1	**24.8**
ECMWF		
RT_{grad}	0.1 ± 0.5	10.8
RT_{3D}	0.6 ± 1.2	**22.5**

Conclusions and future plans

The stringent accuracy requirements of GGOS require amongst other the improvement of the a priori models necessary for the reduction of the space geodetic data. One of the most significant errors in techniques sensitive to gravitational variations are the temporal signals caused by the continuous mass redistribution in the Earth system. We have shown that using the available GRACE monthly fields we can generate models for these variations that can be used in orbital modeling along with consistent improved tidal models, to significantly reduce the residual variance. Similarly, the use of meteorological fields to derive the corresponding loading effects at the tracking stations can further explain part of the remaining variance. A final improvement is the computation of the entire atmospheric delay using meteorological fields, especially those obtained from global satellite observations, in order to properly account for the horizontal gradients which are otherwise ignored. Implementing these changes in the future reduction of SLR data will result in significantly improved products with emphasis on consistency over time.

The currently envisioned schedule for the implementation of the new models is to follow the completion of the tests of various models by end of 2008, by which time the ILRS reanalysis for the development of the ITRF2008 should be complete also. Once we have a final version of the ITRF2008 released, we will be ready to begin a re-analysis of the entire LAGEOS 1 & 2 data set from ~1983 to present in 2009, to be ready for a new product that can be used for experimental versions of a new ITRF. With the primary set of satellites completed, we can then apply these models with appropriate resolution to LEO satellites and reduce data over the same period to test their quality for future contributions to the development of the ITRF.

References

Hulley, G. C. and E. C. Pavlis, (2007), A ray-tracing technique for improving Satellite Laser Ranging atmospheric delay corrections, including the effects of horizontal refractivity gradients, *J. Geophys. Res.,* 112, B06417, doi:10.1029/2006JB004834.

Mendes, V. and E. C. Pavlis, (2004), "High-Accuracy Zenith Delay Prediction at Optical Wavelengths", Geophys. Res. Lett., 31, L14602, doi:10.1029/2004GL020308.

Pavlis, E. C., (2002), Dynamical Determination of Origin and Scale in the Earth System from Satellite Laser Ranging, in *Vistas for Geodesy in the New Millennium*, proceedings of the 2001 International Association of Geodesy Scientific Assembly, Budapest, Hungary, September 2-7, 2001, J. Adam and K.-P. Schwarz (eds.), Springer-Verlag, New York, pp. 36-41.

Pavlis, E. C. et al., (2008), "Observing Systems Needed to Address Sea-level Rise and Variability", in *Understanding Sea-level Rise and Variability*, Aarup, T., J. Church, S. Wilson, and P. Woodworth (eds.), Blackwell, Oxford (*in press*).

Petrov, L., and J.-P. Boy, (2004), Study of the atmospheric pressure loading signal in VLBI observations, J. Geophys. Res., 109, B03405, doi:10.1029/ 2003JB002500.

Tapley, B. D., S. Bettadpur, M. Watkins and Ch. Reigber, (2004), "The gravity recovery and climate experiment: Mission overview and early results", Geophys. Res. Lett. 31 (9).

TRF datum and ILRS network geometry

V. Luceri (1)**, G. Bianco** (2)**, C. Sciarretta** (3)**, M. Virelli** (2)

(1) e-GEOS SpA, CGS-Matera, Italy
(2) Agenzia Spaziale Italiana, CGS-Matera, Italy
(3) Telespazio SpA, Roma, Italy

cinzia.luceri@telespazio.com

Abstract

The definition of the ITRF datum is one of the key element to assure a stable reference frame without internal distorsion. The last geodetic reference system ITRF2005 was constructed by combining time series from all the space geodesy techniques. The orientation was constrained to the ITRF2000 orientation at epoch 2000.0 and null orientation rates between the two, the translation and its rate were fixed to the SLR solutions and scale and its rate to the VLBI solutions. The SLR time series was not considered in the scale definition mainly for its discontinuity in the time series.
The SLR network geometry has been identified as a candidate to explain the discontinuity and possible evidences of the network effect will be investigated.

The ITRF datum

The satellite techniques such as SLR, GPS and DORIS are sensitive to the Earth's center of mass, where the ITRF models place the origin of the global geodetic network. SLR is the only one having demonstrated to be able to locate the center of mass relatively to the tracking station network with an accuracy of a few millimetres. Thus the reference frame origin of a SLR loose solution is naturally placed in the Earth's CM; its uncertainty can be measured by the solution degree of looseness.

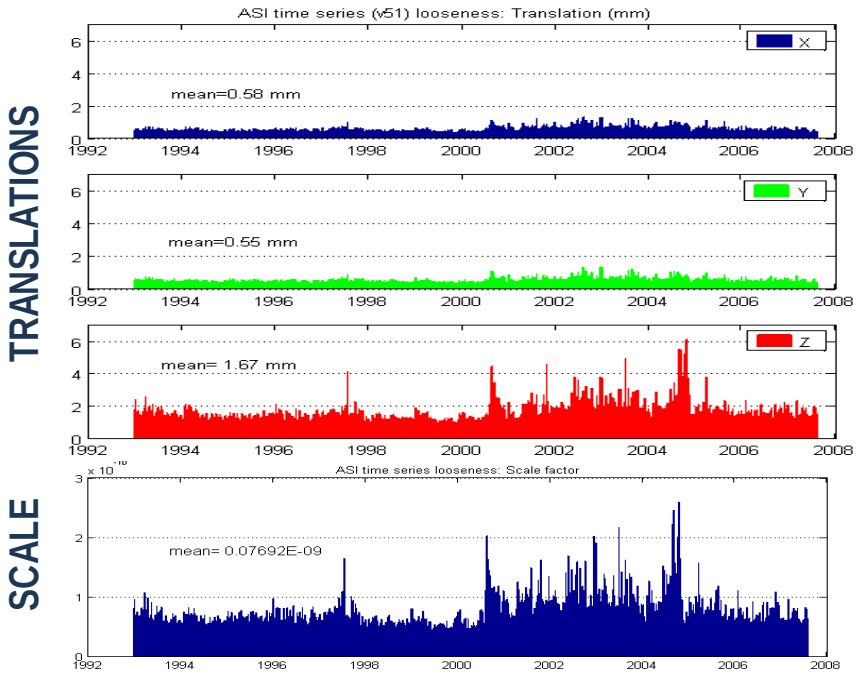

Figure 1. Looseness of the ASI SLR time series

More generally the degree of looseness is the uncertainty of the Helmert parameters of the solution with respect to an 'error free' reference frame and is obtained from: $\mathbf{C}_{\vartheta} = \left(\mathbf{A}^{\mathbf{T}}\mathbf{C}^{-1}\mathbf{A}\right)^{-1}$ (Blewitt, 1998) where C is the solution variance/covariance matrix and A is the Helmert transformation design matrix. Figure 1 is the plot of the time series of the indexes retrieved from the ASI weekly loose solutions of site coordinates and EOP, each bar indicating the value for one week. The mean value is less than on millimetre for the X and Y translation, less than two millimetres for the Z translation.

The time series of the SLR translations, estimated from 1993 on, are quite smooth with variations within one centimeter in X and Y, two centimeters in Z. The ITRF2005 translations and its rates were fixed to the SLR solutions. The situation is a bit different for the scale.

The scale of a frame is dependent on the modeling of some physical parameters: both SLR and VLBI determine the global scale with a higher stability w.r.t. GPS and DORIS. Figure 1 shows the looseness index for the scale: the uncertainty of the SLR scale is less than 0.1 ppb. Despite its accuracy, the scale time series has a discontinuity, roughly around 2002, when compared with VLBI or intrinsically (Altamimi et al., 2007). The direct consequence was that the ITRF2005 scale and its rates were fixed to the VLBI solutions, even if it is much less accurate. Figure 2 is a plot of the scale factor of the ASI SLR solution (in mm at the Earth's surface) compared with ITRF2005 rescaled (rescaling was due to an inconsistency found between SLR and VLBI, soon after revealed as caused by a mismodeling in the VLBI analysis). The purpose of this study is to find the reason of the discontinuity.

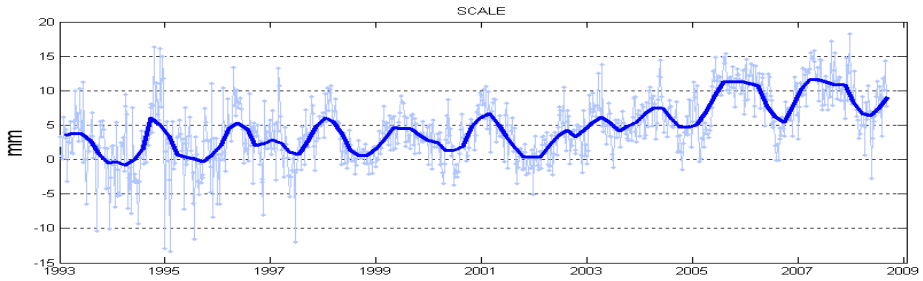

Figure 2. Scale of the ASI SLR time series with respect to ITRF2005

The SLR network

The first candidate identified to explain the scale discontinuity is the network geometry; its lack of spatial uniformity has always been a weakness of the SLR technique. The idea is that the limited number of sites in the network makes it too sensitive to the appearance/disappearance of tracking stations in the years and to the variation of the amount of data tracked by each of them. As a first approach, the number of data acquired by the network tracking the two LAGEOS satellites, from 1993 on, have been computed separately for the two hemispheres: North/South, East/West, +X/-X. Figure 3 shows the amount of data in the years, binned in weekly arcs. The North/South distribution starts changing in 2005 when more data are collected in the southern hemisphere and the balance is better. The data quantity in the East/West is similar until 1999 when more data are collected by the eastern sites, a decrease of "western" data is evident in 2005. The data distribution along X is quite balanced, with a small increase in the positive X. The unbalance of the spatial data coverage led to the idea of a data centroid, a kind of data "center of mass".

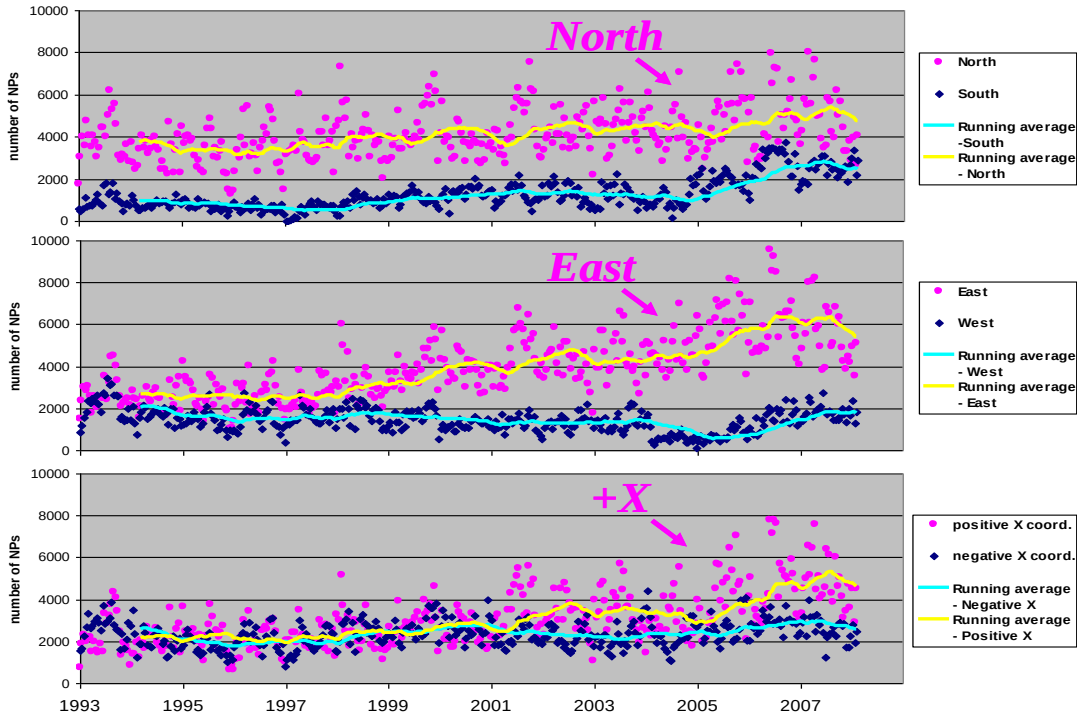

Figure 3. Data distribution in the hemispheres

Data centroid and scale

The weekly time series of the LAGEOS 1/2 *data centroid* has been computed, expressed as coordinates (*dX*,*dY*,*dZ*) in the ITRF reference frame with the following formulas:

$$dX = \sum_i X_i n_i / N_{tot}$$

$$dY = \sum_i Y_i n_i / N_{tot}$$

$$dZ = \sum_i Z_i n_i / N_{tot}$$

where:

X_i , Y_i , Z_i *: X, Y, Z coordinate of the i-th site of the week*

n_i *: number of observations of the i-th site of the week*

N_{tot} *: total number of observations in the week*

We expect a centroid position close to the ITRF origin if the data distribution is spatially well balanced.

Figure 4 is the plot of the centroid coordinates together with the running mean of the values. The time series are quite flat until 2001: the X and Y component close to zero and an obviously positive Z (2-3 km far from the ITRF2005 origin). Afterwards, the centroid moves in the positive XY quadrant and in 2008 the Z coordinate becomes smaller, close to X and Y. The centroid migration in the space and in the XY plane is represented in Figure 5.
Its position in 2008 is more distant from the ITRF origin than in 1993, in a direction of 45 degrees from the Greenwich Meridian: the distribution of the data is worse in terms of geographic coverage along the longitude.

Looking at the plots of the scale variations and the centroid migration, the similarities are evident for the X and Y coordinates. The correlation coefficients between the centroid coordinates and the scale have been computed:

scale/X = 0.32
scale/Y = 0.45
scale/Z = 0.06

and confirm the uncorrelation with the Z coordinates, i.e. with the North/South data distribution.

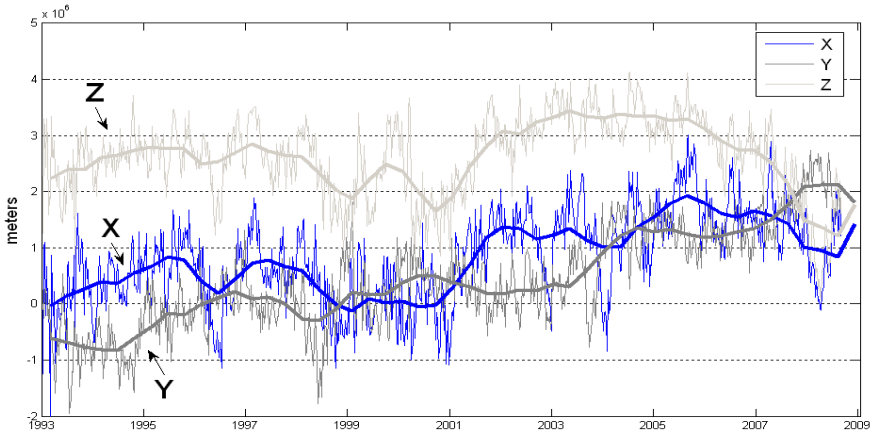

Figure 4. Data centroid coordinates

The correlation between the scale and the length of the centroid vector is 0.27 but, if we consider the vector projection on the equator, the correlation increases up to 0.45.
In Figure 6 the distance, in the XY plane, is plotted together with the scale, expressing the Y-axis for the distance in meters at the right, the Y-axis for the scale in mm (at the Earth's surface) on the left.

Conclusion

The study of the network geometry in terms of geographic data coverage has put in evidence the unbalanced data distribution since 2001-2002, above all due to the increase of data in the East hemisphere not balanced by data collected in the western part of the world. The correlation coefficients show a possible effect of the longitudinal data distribution on the scale to SLRF2005 while there is no evidence of the North/South data distribution influence. The concept of the data centroid can be useful to monitor the data homogeneity and for the network update, in the definition of the location of new sites.
Further investigations will be done with network simulation to assess the correlation between the scale and the data centroid and to check the reliability of scale estimation, above all in the cases of non uniformity.

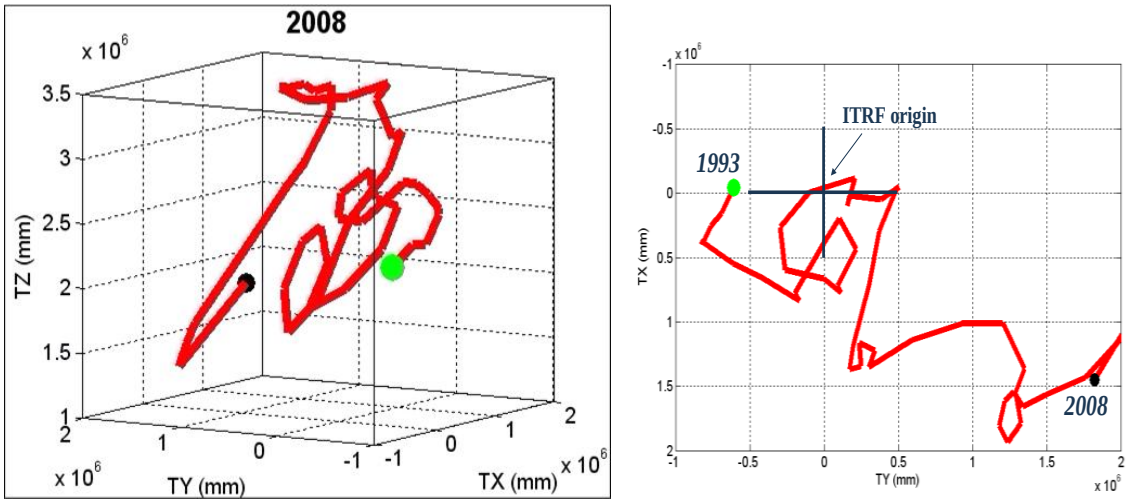

Figure 5. Centroid motion (3-D and XY plane)

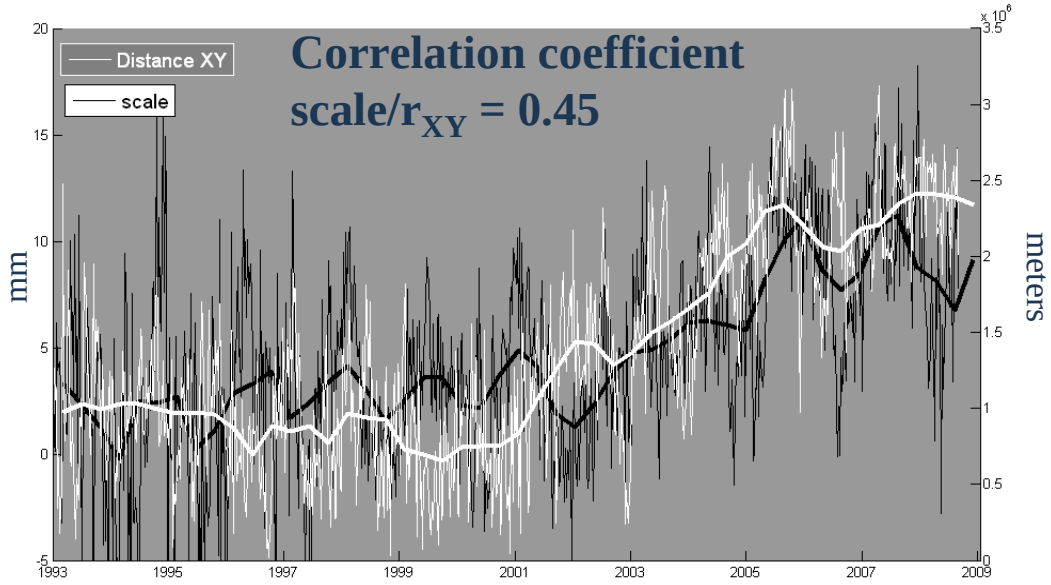

Figure 6. Centroid XY distance and scale

References

Blewitt G., GPS data processing methodology: from theory to applications, in *GPS for Geodesy*, P.J.G. Teunissen and A. Kleusberg editors, Springer, 2nd edition, p. 231-270, 1998.

Altamimi, Z., X. Collilieux, J. Legrand, B. Garayt, and C. Boucher (2007), ITRF2005: A new release of the International Terrestrial Reference Frame based on time series of station positions and Earth Orientation Parameters, J. Geophys. Res., 112, B09401, doi:10.1029/2007JB004949.

Assessing Tracking Performance of High Satellites at Mt Stromlo SLR Station

C.J. Moore
EOS Space Systems, Canberra, Australia.
cmoore@eos-aus.com /Fax: +61 2 6287 2951

Abstract

An analysis of changes to tracking productivity of high satellites following the 2007 laser power upgrade at Mt Stromlo SLR Station is presented. This analysis uses data obtained from tracking Giove A and other satellites during June-August 2008 and contrasts the results with similar data obtained during May-August 2006. The results show that the increase in power level has subsequently allowed the station to operate unmanned in all weather conditions and still maintain productivity levels.

Introduction

In mid 2006, Mt Stromlo SLR station undertook an analysis of tracking productivity primarily based on the recently launched Giove A satellite (Moore, 2006). Since that time, the station has been subject of some significant changes in equipment and procedures. These include;

- June/July 2007 – Laser power upgraded from approximately 400 to 1200 mW. Pulse energy increased from 13 to 20 mJ and the fire rate from 30 to 60Hz.
- December 2007 – facility cooling systems upgrade.
- April 2008 – 1m telescope coudé mirrors replaced.
- From July 2007 – automated (all weather) tracking.

This paper describes a re-assessment of the productivity performance of Mt Stromlo SLR station in light of these changes based on a comparison of recent Giove A tracking performance with the earlier study, and analysis of other productivity statistics using a number of high earth orbit (HEO) satellites, such as the Etalon and Glonass satellites, and the geostationary ETS8 satellite. An analysis of productivity for all routinely tracked satellites is also presented.

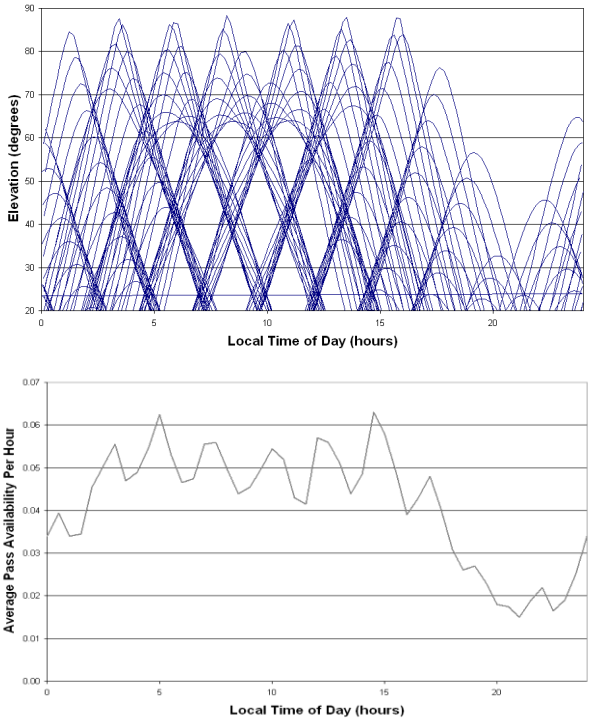

Figure 1. Giove A pass availability, May-August 2008.

Performance Factors

Of primary interest is the change in productivity performance of the station resulting from the

increase in laser power, but such assessment is compounded by other factors including;

1. Changed operational mode – before the upgrade tracking was operator (manual) control, generally with no dome window in place. After the upgrade, tracking has been automatic through the glass dome window.
2. Effects of weather – A very significant period of overcast weather experienced in the months soon after the upgrade.
3. Coude mirror replacement – Most mirrors in the coude path were replaced after the upgrade due to significant degradation of the coatings.
4. Changed tracking priorities – fewer Giove A tracking periods to accommodate more Giove B, Etalon, Glonass, and ETS8 passes.

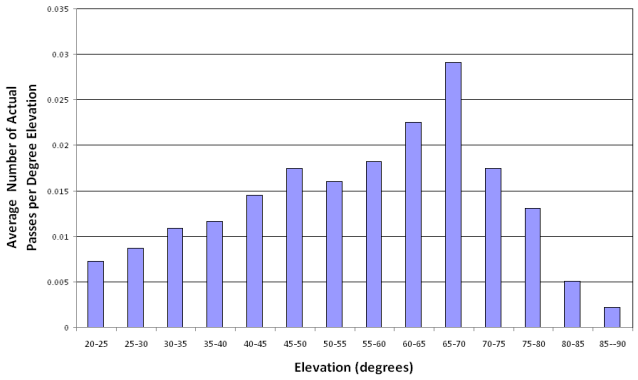

Figure 3a. Available Giove A passes versus elevation.

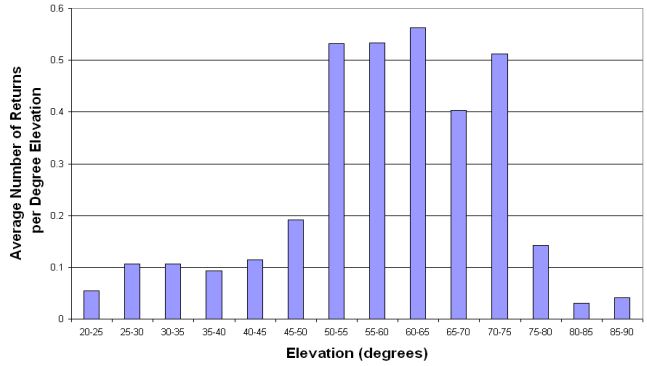

Figure 3b. Giove A productivity versus elevation.

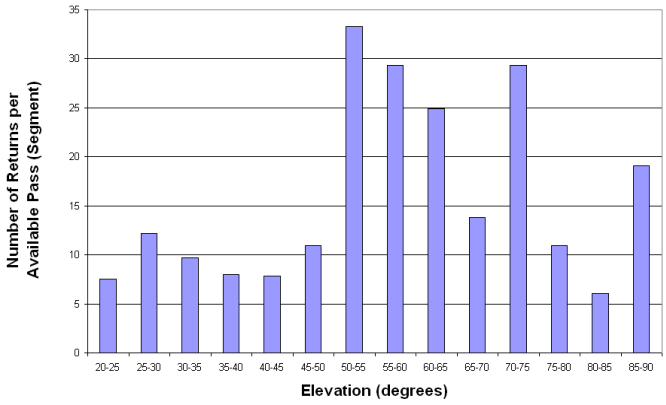

Figure 3c. Giove A normalized productivity versus elevation.

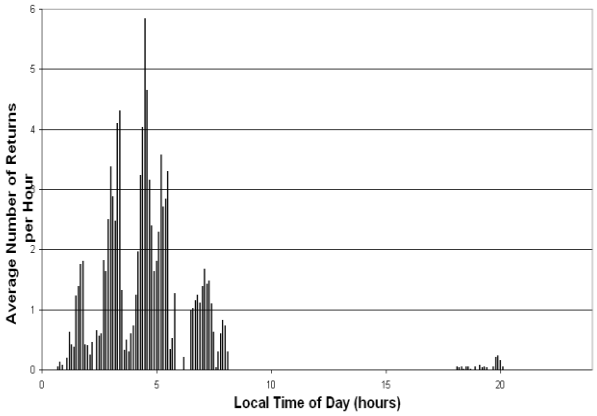

Figure 2. Giove A passes tracked, May-August 2008.

Giove A Analysis

Giove A tracking data obtained during May – August 2008 were analysed in the same manner as the May-August 2006 data (Moore, 2006). As illustrated in Figures 1 and 2 the distribution of Giove A passes were quite different between the two periods, with successful tracking confined to the early hours in the day in the latter period. Few passes are tracked during daylight periods and there was a lack of evening passes. A distribution of actual passes tracked in the latter period is shown in Figure 2.

To allow comparisons to be drawn with the results of Giove A tracking in 2006, factors such as pass availability and elevation were normalized as shown in Figures 3a, 3b and 3c.

The results indicate that low elevation productivity was a little higher in 2008, mid-elevation values were similar for the two periods and high elevation productivity in 2008 were perhaps a little less then 2006. Given the relatively few

data and variability in atmospheric conditions, these results imply that there was a very similar level of performance between the two periods, noting that Giove A was generally tracked through the dome window in 2008, but not in 2006.

Table 1. Productivity Statistics for the Glonass and Etalon satellites.

Statistic	Satellite	May-Aug 2006	May-Aug 2008
Normal Points per Pass	*Glonass*	*10-12*	*12-13*
	Etalon	*9-12*	*10-15*
Returns per Normal Point	*Glonass*	*20-40*	*50-80*
	Etalon	*20-30*	*20-60*
Returns per Pass	*Glonass*	*300-600*	*500-1000*
	Etalon	*100-300*	*300-600*

HEO Productivity

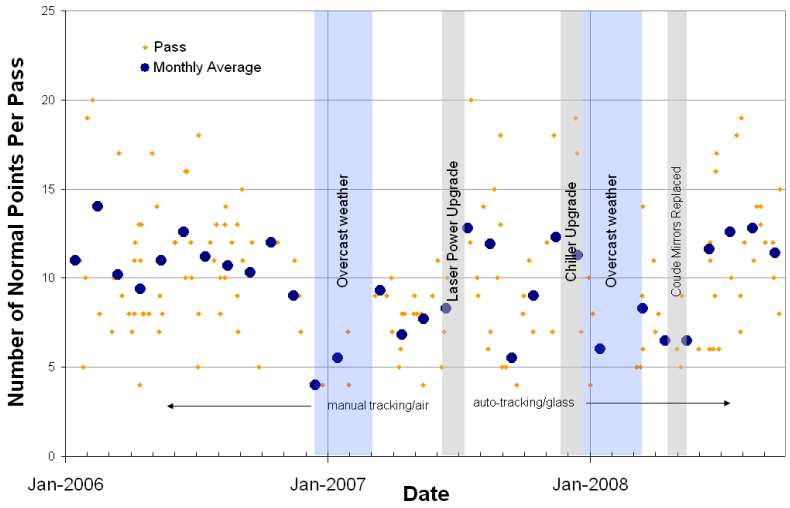

Figure 4a. Number of normal points per pass from January 2006 to September 2008 for the Glonass satellites.

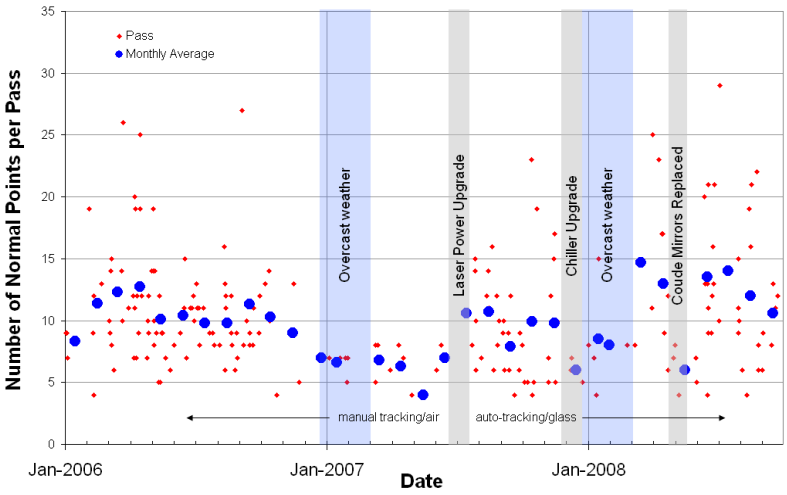

Figure 4b. Number of normal points per pass from January 2006 to September 2008 for the Etalon satellites.

Table 1 shows a summary of the productivity statistics for the Glonass and Etalon satellite passes during the May-August periods in 2006 before changes were made and 2008 after such changes, and corresponding to the Giove A analysis periods. For these satellites and periods, the productivity in the latter period was at least as good as the earlier period and by some measures, significantly better. Improvements of up to100% in maximum returns per normal point and returns per pass are evident.

To determine the impact of the various factors described in the introduction that might affect the station performance, data from all Glonass and Etalon satellite passes throughout the whole

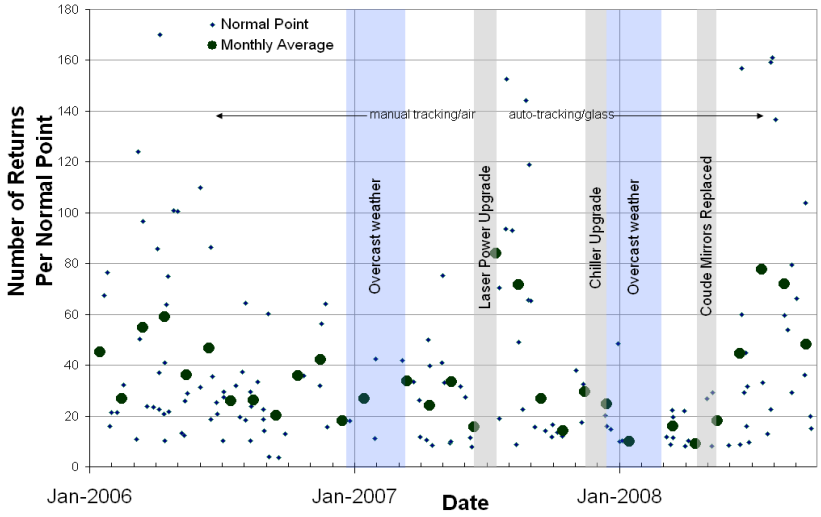

Figure 5a. Number of returns per normal point for the Glonass satellites.

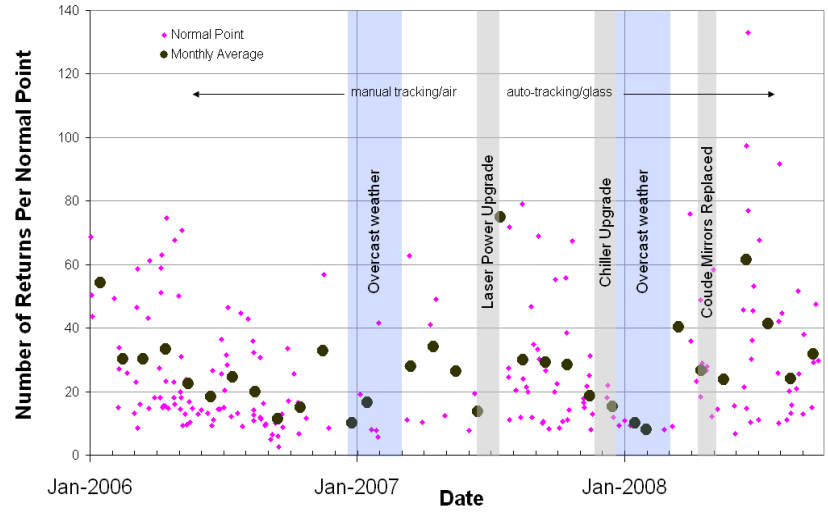

Figure 5b. Number of returns per normal point for the Etalon satellites.

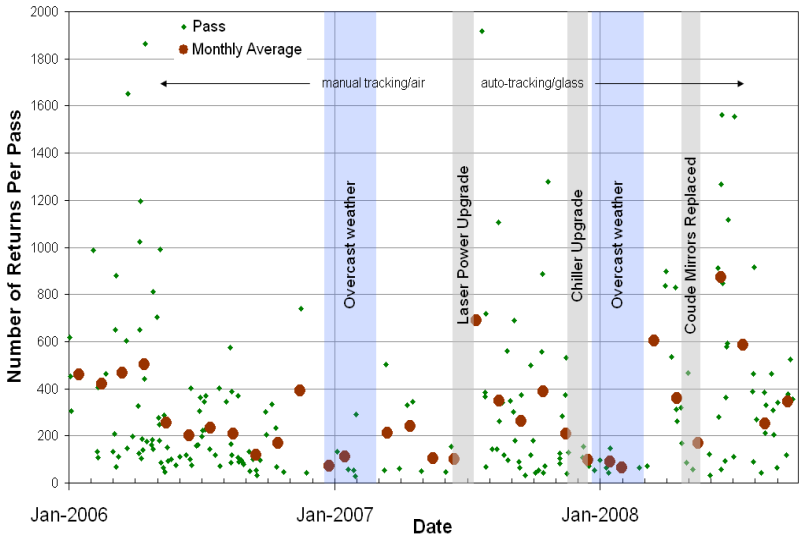

Figure 6a. Number of returns per pass for the Glonass satellites.

period January 2006 to September 2008 were analysed. Figures 4, 5 and 6 show the results of these analyses together with identification of the various events and milestones where conditions changed significantly.

These figures show both monthly averages (large symbol) and daily passes or normal points (small symbol).

The number of normal points per pass, shown in Figure 4, the number of returns per normal point, shown in Figure 5, and the number of returns per pass, shown in Figure 6 for Glonass and Etalon satellites increased in all cases immediately in the 1-2 months immediately after the power upgrade.

However this trend was interrupted by station maintenance activities and a period of particularly overcast skies. From May 2008 the increase in productivity (in comparison to 2006) is quite evident, but by this time the coude mirrors had also been replaced. It is not clear to what impact the deterioration of the coatings on these mirrors had on the longer term productivity, but they may have contributed to the apparent long term downward trend evident during 2006 and 2007.

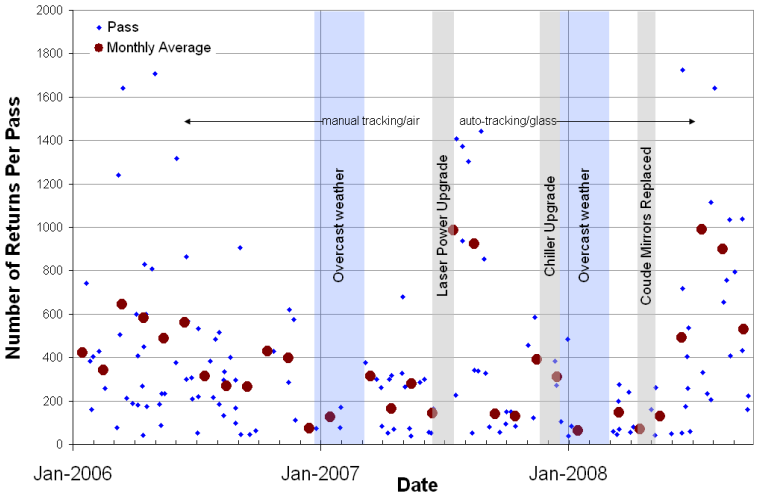

Figure 6b. Number of returns per pass for the Etalon satellites.

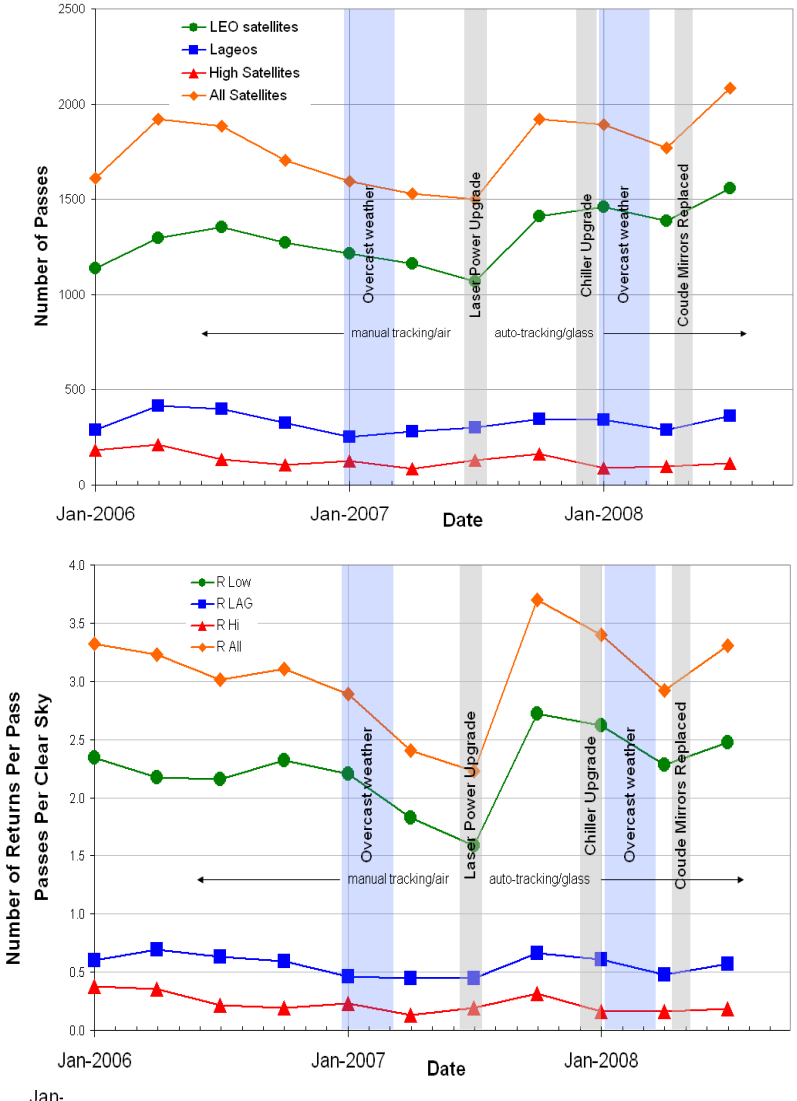

Figure 7. Mt Stromlo productivity for low earth orbit, high earth orbit, Lageos and all satellites. *Top*; quarterly averages of the number of passes per day and *bottom*; quarterly averages of the number of passes per clear sky

General Productivity

Figure 7 summarizes some continuous combined productivity statistics for the period January 2006 to September 2008. It is clear from this figure that there was an improvement in the average number of LEO satellite passes per day resulting from the laser power upgrade, and correspondingly an improvement in overall results. Immediately following the upgrade, a slight improvement in Lageos productivity in clear sky conditions is also apparent. More significantly, it is clear that the overall productivity of both Lageos and high earth satellites after the power upgrade was at least maintained despite the change to auto-tracking which requires that ranging is performed with the enclosure window in place.

Geostationary Satellite Productivity

In early 2007, the Japanese Aerospace Exploration Agency (JAXA) requested a number of Western Pacific Laser Tracking Network (WPLTN) stations, including Mt Stromlo, to undertake routine tracking of their recently launched geostationary satellite, ETS-8. At a range of approximately 37,000 km from the station, only manual tracking with the enclosure window removed

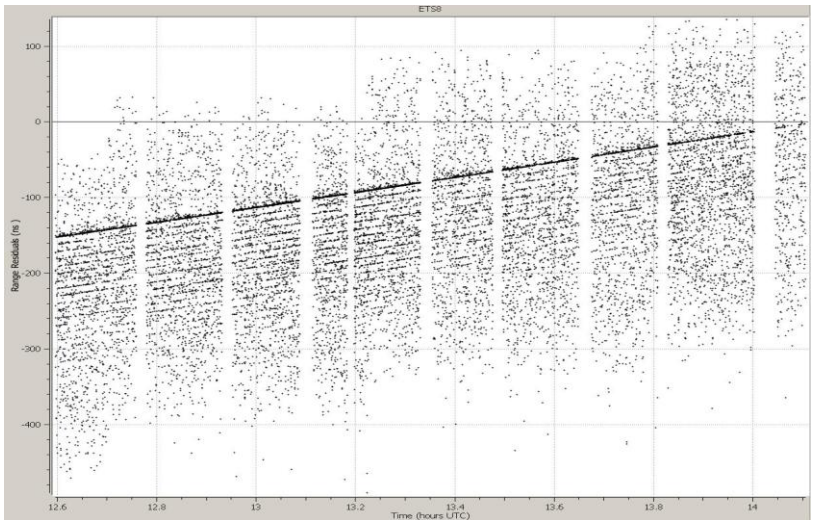

Figure 8. Residual plot of returns from tracking ETS-8 at 37000 km over a number of hours on the 11th September 2008. Even returns from pre-pulses ('tramtracks') can be observed.

was feasible. Even though the satellite was successfully tracked prior to the laser power upgrade (in very good seeing conditions), the signal was very marginal. After the upgrade, there was at least a three-fold increase in the signal return rate, which subsequently allowed routine clear sky tracking to be carried out. Figure 8 shows the residuals from such a tracking period in September 2008, where return rates exceeded 0.6% (primary signal only) or 3% including all pre-pulses and the signal-to-noise exceeded 10%. It was observed that during ranging with the enclosure window in the optical path, a signal was observable but again was quite marginal. In this configuration, a successful search for such a signal would have been very difficult to achieve.

Conclusion

Moore (2006) estimated that an increase in the link budget by a factor of at least 2, and more probably 4, was necessary to maintain productivity levels if the station was to operate in its "all weather" configuration appropriate for automated and unmanned operations. This is due to the requirement that ranging be performed through an 18mm glass enclosure window.

Subsequent to a laser power upgrade in mid 2007 which increased the link budget by roughly a factor of 3, operations have been largely performed in this all-weather configuration and auto-tracking mode. The evidence has shown that although confounded by some periods of overcast weather and other changes to the station, that productivity levels for high satellites such as Giove A, etc. has been maintained as predicted, and even improved for lower orbit satellites.

Also without the upgrade, it is doubtful that the station could have made a significant contribution to the tracking of the geostationary satellite, ETS-8.

Acknowledgement

The author would like to thank his colleagues, John Luck for help in collating many of the productivity statistics and Peter Wilson for assistance in tracking ETS-8.

References

Moore, C.J. *A Summary of Observations of Giove A, taken from Mt Stromlo SLR Station*. Proceedings of the 15th International Workshop on Laser Ranging, pp. 203-209, Canberra, 2006.

Lunar and Interplanetary Laser Ranging

Chairs: Jürgen Müller and Tom Murphy

Session Summary

In the lunar laser ranging (LLR) and interplanetary laser ranging session, we had nine talks and two posters---dramatically up from a single talk two years ago.
Sergei Kopeikin gave an invited talk about reference frames for lunar ranging analysis, with an emphasis on not misinterpreting gauge-dependent terms as physical effects. Tom Murphy reported on two years of APOLLO operation, showing high photon rates and evidence for one-millimeter performance. Liliane Biskupek presented recent efforts to understand earth orientation using 38 years of LLR data. Simone Dell'Agnello described (for Doug Currie) the science attainable by and tests related to emplacement of next-generation (large) corner cubes on the lunar surface. A trio of talks by Jan McGarry, Anthony Mallama, and Chris Clarke detailed the capabilities of one-way ranging to the lunar reconnaissance orbiter (LRO). The talks focused on technical parameters/capabilities, pointing strategies and verification, and scheduling/prediction logistics, respectively. Jerry Wiant described the preparations taking place at the McDonald Observatory for ranging to LRO---with the persistent theme that Randy Ricklefs has already done most of the software preparation. Finally, Maria Zuber spoke about the science deliverables one may achieve via interplanetary laser ranging, including the success stories of ranging to the MESSENGER and Mars Orbiter spacecraft, as well as plans for LRO. In addition, Wasilla Zerhouni and Tomasz Niedzielski displayed posters pertaining to using LLR for celestial pole determination, and the minimum duration necessary for sea level rise determination, respectively.

Millimeter Laser Ranging to the Moon: a comprehensive theoretical model for advanced data analysis

Sergei M. Kopeikin
Department of Physics and Astronomy
University of Missouri-Columbia, MO 65211, USA
kopeikins@missouri.edu/Fax: +1-573-882-4195

Abstract

Lunar Laser Ranging (LLR) measurements are crucial for advanced exploration of the evolutionary history of the lunar orbit, the laws of fundamental gravitational physics, selenophysics and geophysics as well as for future human missions to the Moon. Current LLR technique measures distance to the Moon with a precision approaching 1 millimeter that strongly demands further significant improvement of the theoretical model of the orbital and rotational dynamics of the Earth-Moon system. This model should inevitably be based on the theory of general relativity, fully incorporate the relevant geophysical/selenophysical processes and rely upon the most recent IAU standards. We discuss new methods and approaches in developing such a mathematical model. The model takes into account all classic and relativistic effects in the orbital and rotational motion of the Moon and Earth at the millimeter-range level. It utilizes the IAU 2000 resolutions on reference frames and demonstrates how to eliminate from the data analysis all spurious, coordinate-dependent relativistic effects playing no role in selenophysics/geophysics. The new model is based on both the locally-inertial and barycentric coordinates and extends the currently used LLR code. The new theory and the millimeter LLR will give us the opportunity to perform the most precise fundamental test of general relativity in the solar system in robust and physically-adequate way.

Lunar Laser Ranging

The dynamical modeling for the solar system (major and minor planets), for deep space navigation, and for the dynamics of Earth's satellites and the Moon must be consistent with general relativity. Lunar laser ranging (LLR) measurements are particularly crucial for testing general relativistic predictions and advanced exploration of other laws of fundamental gravitational physics. Current LLR technologies allow us to arrange the measurement of the distance from a laser on the Earth to a corner-cube reflector (CCR) on the Moon with a precision approaching 1 millimeter [1, 2]. There is a proposal to place a new CCR array on the Moon [3], and possibly to install other devices such as microwave transponders [4] for multiple scientific and technical purposes. Successful human exploration of the Moon strongly demands further significant improvement of the theoretical model of the orbital and rotational dynamics of the Earth-Moon system. This model should inevitably be based on the theory of general relativity, fully incorporate the relevant geophysical processes, lunar libration, tides, and should rely upon the most recent standards and recommendations of the IAU for data analysis [5].

LLR technique is currently the most effective way to study the interior of the Moon and dynamics of the Moon-Earth system. The most important contributions from LLR include: detection of a molten lunar core and measurement of its influence on the Moon's orientation along with tidal dissipation [6-9]; detection of lunar free libration along with the forced terms

from Venus [10] and the internal excitation mechanisms [11]; an accurate test of the strong principle of equivalence for massive bodies [12, 13] also known as the Nordtvedt effect [14, Section 8.1]; and setting of a stringent limit on time variability of the universal gravitational constant and (non)existence of long-range fields besides the metric tensor [15]. LLR analysis has also given access to more subtle tests of relativity [16-19], measurements of the Moons tidal acceleration [20-22] and geodetic precession of the lunar orbit [23, 24], and has provided orders-of-magnitude improvements in the accuracy of the lunar ephemeris [25-29] and its three-dimensional rotation [30, 31]. On the geodesy front, LLR contributes to the determination of Earth orientation parameters, such as nutation, precession (including relativistic geodetic precession), polar motion, UT1, and to the long-term variation of these effects [32, 33].

LLR also contributes to the realization of both the terrestrial and selenodesic reference frames [34, 35]. The satellite laser ranging (SLR) realization of a dynamically-defined inertial reference frame [36] in contrast to the kinematically-realized frame of VLBI [37, Section 6], offers new possibilities for mutual cross-checking and confirmation [33] especially after the International Laser Ranging Service (ILRS) was established in September 1998 to support programs in geodetic, geophysical, and lunar research activities and to provide the International Earth Rotation Service (IERS) with products important to the maintenance of an accurate International Terrestrial Reference Frame
(ITRF) [38].

Over the years, LLR has benefited from a number of improvements both in observing technology and data modeling [39]. Recently, sub-centimeter precision in determining range distances between a laser on Earth and a retro-reflector on the Moon has been achieved [1, 2]. As precision of LLR measurements was gradually improving over years, enormous progress in understanding evolutionary history of the Earth-Moon orbit and the internal structure of both planets has been achieved. With the precision approaching 1 millimeter and better, accumulation of more accurate LLR data will lead to new, fascinating discoveries in fundamental gravitational theory, geophysics, and physics of lunar interior [40] whose unique interpretation will intimately rely upon our ability to develop a systematic theoretical approach to analyze the sub-centimeter LLR data [28, 41].

EIH Equations of Motion in N-body Problem

Nowadays, the theory of the lunar motion should incorporate not only the numerous Newtonian perturbations but has to deal with much more subtle relativistic phenomena being currently incorporated to the ephemeris codes [25, 42-44]. Theoretical approach, used for construction of the ephemerides, accepts that the post-Newtonian description of the planetary motions can be achieved with the Einstein-Infeld-Hoffmann (EIH) equations of motion of point-like masses [45], which are valid in the barycentric frame of the solar system with time coordinate, t, and spatial coordinates, $x^i \equiv \boldsymbol{x}$.

Due to the covariant nature of general theory of relativity the barycentric coordinates are not unique and are defined up to the space-time transformation [46-48]

$$t \;\mapsto\; t - \frac{1}{c^2}\sum_B \nu_B \frac{GM_B}{R_B}\,(\boldsymbol{R}_B \cdot \boldsymbol{v}_B)\;, \tag{1}$$

$$\boldsymbol{x} \;\mapsto\; \boldsymbol{x} - \frac{1}{c^2}\sum_B \lambda_B \frac{GM_B}{R_B}\boldsymbol{R}_B\;, \tag{2}$$

where summation goes over all the massive bodies of the solar system *(B* = 1,2, ... , *N); G* is the universal gravitational constant; *c* is the fundamental speed in the Minkowskian space-time; a dot between any spatial vectors, $\boldsymbol{a} \cdot \boldsymbol{b}$, denotes an Euclidean dot product of two vectors $\boldsymbol{a}$ and $\boldsymbol{b}$; M_B is mass of a body B; $\boldsymbol{x}_B = \boldsymbol{x}_B(t)$ and $\boldsymbol{v}_B = \boldsymbol{v}_B(t)$ are coordinates and velocity of the center of mass of the body B; $\boldsymbol{R}_B = \boldsymbol{x} - \boldsymbol{x}_B$ is a relative distance from a field point $\boldsymbol{x}$ to the body B; ν_B and λ_B are constant, but otherwise free parameters being responsible for a particular choice of the barycentric coordinates. We emphasize that these parameters can be chosen arbitrary for each body B of the solar system. Physically, it means that the space-time around each body is covered locally by its own coordinate grid, which matches smoothly with the other coordinate charts of the massive bodies in the buffer domain, where the different coordinates overlap.

If the bodies in N-body problem are numbered by indices *B,* C, *D,* etc., and the coordinate freedom is described by equations (1)-(2), EIH equations of motion for the body *B* have the following form [46]

$$a_B^i \;=\; \sum_{C\neq B}\left[F_{BC}^i + \frac{4-2\lambda_C}{c}\,(\boldsymbol{v}_B \times \boldsymbol{H}_{BC})^i - \frac{3-2\lambda_C}{c}\,(\boldsymbol{v}_C \times \boldsymbol{H}_{BC})^i\right] \tag{3}$$

where E^i_{BC} is called the gravitoelectric force, and the terms associated with the cross products $(\boldsymbol{v}_B \times \boldsymbol{H}_{BC})^i$ and $(\boldsymbol{v}_C \times \boldsymbol{H}_{BC})^i$ are referred to as the gravitomagnetic force [49].

The gravitoelectric force is given by

$$E^i_{BC} \;=\; \left(-\frac{GM_C}{R^3_{BC}} + \frac{GM_C}{c^2}\mathcal{E}_{BC}\right) R^i_{BC}\;, \tag{4}$$

and the gravitomagnetic force is

$$H^i_{BC} \;=\; -\frac{1}{c}\,(\boldsymbol{V}_{BC} \times \boldsymbol{E}_{BC})^i = \frac{GM_C}{c}\,\frac{(\boldsymbol{V}_{BC} \times \boldsymbol{R}_{BC})^i}{R^3_{BC}}\;, \tag{5}$$

where $\boldsymbol{V}_{BC} = \boldsymbol{v}_B - \boldsymbol{v}_C$. The first term in right side of equation (4) is the Newtonian force of gravity, and the post-Newtonian correction

$$\begin{aligned}\mathcal{E}_{BC} \;=\; -\frac{1}{R^3_{BC}}\Bigg\{ & 3(-1+\lambda_C)v_B^2 + 3(1-2\lambda_C)(\boldsymbol{v}_B \cdot \boldsymbol{v}_C) - (1-3\lambda_C)v_C^2 \\ & -\frac{3}{2}\left(\frac{\boldsymbol{R}_{BC}\cdot\boldsymbol{v}_C}{R_{BC}}\right)^2 - 3\lambda_C\left(\frac{\boldsymbol{R}_{BC}\cdot\boldsymbol{V}_{BC}}{R_{BC}}\right)^2 - (5-2\lambda_B)\frac{GM_B}{R_{BC}} - (4-2\lambda_C)\frac{GM_C}{R_{BC}} \\ & + \sum_{D\neq B,C} GM_D\left(\frac{1+2\lambda_C}{2R^3_{CD}} - \frac{\lambda_C}{R^3_{BD}} + \frac{3\lambda_D}{R_{BD}R^2_{BC}} - \frac{3\lambda_D}{R_{CD}R^2_{BC}}\right)(\boldsymbol{R}_{BC}\cdot\boldsymbol{R}_{BD})\Bigg\} \\ & + \sum_{D\neq B,C} GM_D\left[\frac{4}{R_{BC}R^3_{CD}} + \frac{\lambda_C}{R_{BC}R^3_{BD}} - \frac{\lambda_C}{R_{CD}R^3_{BD}} - \frac{7-2\lambda_D}{2R_{BD}R^3_{CD}} + \frac{1-2\lambda_D}{R^3_{BC}R_{CD}} + \frac{4-\lambda_D}{R^3_{BC}R_{BD}}\right]\;,\end{aligned} \tag{6}$$

2.
As one can see, the gravitomagentic force (5) is proportional to the gravitoelectric force (4) multiplied by the factor of V/c, where V is the relative velocity between two gravitating bodies. EIH equations (3)-(5) differ from the equations of the PPN formalism 1969ApJ...158...81E employed in particular at JPL for actual calculation of the ephemerides of the major planets by the fact that the right side of equation (3) has been resolved into radius-vectors and velocities of the massive bodies and does not contain second derivatives (accelerations). This elimination of the high-order time derivatives from a perturbed force is a standard practice in celestial mechanics for calculation of the perturbed motion.

Barycentric coordinates x_B and velocities v_B of the center of mass of body B are adequate theoretical quantities for description of the world-line of the body with respect to the center of mass of the solar system. However, the barycentric coordinates are global coordinates covering the entire solar system. Therefore, they have little help for efficient physical decoupling of the post-Newtonian effects existing in the orbital and rotational motions of a planet and for the description of motion of planetary satellites around the planet. The problem stems from the covariant nature of EIH equations, which originates from the fundamental structure of space-time manifold and the gauge freedom of the general relativity theory.

This freedom is already seen in the post-Newtonian EIH force (3)-(6) as it explicitly depends on the choice of spatial coordinates through parameters λ_C , λ_D . Each term depending explicitly on λ_C , λ_D in equations (3)-(6), has no direct physical meaning as it can be eliminated after making a specific choice of these parameters. In many works on experimental gravity and applied relativity researches fix parameters $\lambda_C = \lambda_D = 0$, which corresponds to working in harmonic coordinates. Harmonic coordinates simplify EIH equations to large extent but one has to keep in mind that they have no physical privilege anyway, and that a separate term or a limited number of terms from EIH equations of motion can not be measured - only coordinate-independent effects can be measured [46].

Recently, there was a lot of discussions about whether LLR can measure the gravitomagnetic field H^i_{BC} [18, 19, 51-53]. The answer to this question is subtle and requires more profound theoretical consideration involving the process of propagation of the laser pulses in a curved space-time of the Earth-Moon system. We are hoping to discuss this topic somewhere else. Nevertheless, what is evident already now is that equation (3) demonstrates a strong dependence of the gravitomagnetic force on the choice of coordinates. For this reason, by changing the coordinate parameter λ_C one can eliminate either the term $(\boldsymbol{v}_B \times \boldsymbol{H}_{BC})^i$ or $(\boldsymbol{v}_C \times \boldsymbol{H}_{BC})^i$ from EIH equations of motion (3). It shows that the strength of the factual gravitomagnetic force, as it appears in the equations of motion, is coordinate-dependent, and, hence, a great care should be taken in order to properly interpret the LLR "measurement" of such gravitomagnetic terms in consistency with the covariant nature of the general theory of relativity and the theory of astronomical measurements in curved space-time [48, 54-57].

The Gauge Freedom

The primary gauge freedom of EIH equations of motion is associated with the transformations (1)-(2) of the barycentric coordinates of the solar system, which are parameterized by parameters v_C and λ_C . However, the post-Newtonian force in the lunar equations of motion admits additional freedom of coordinate transformations. This *residual* freedom remains even after fixing the coordinate parameters v_C and λ_C in equations (3)-(6). It is associated with the fact that the Earth-Moon system moves in tidal gravitational field of the Sun and other planets, which presence in the local frame of the Earth-Moon system indicates

that the local background space-time is not asymptotically-flat. The residual freedom remains in making transformations of the local coordinates attached to the Earth-Moon system. It induces the gauge transformation of the metric tensor and the Christoffel symbols and changes the structure of the post-Newtonian terms in EIH equations of motion of the Earth-Moon system that is not associated with the parameters v_C and λ_C .

Thus, we face the problem of investigation of the residual gauge freedom of the lunar equations of motion, which goes beyond the choice of the barycentric coordinates by fixing a specific value of the gauge parameter λ_C in equations (3)-(6). This freedom is naturally associated with the choice of the local coordinates of the Earth-Moon barycentric frame as well as the geocentric and selenocentric reference frames. Proper choice of the local coordinates removes all non-physical degrees of freedom from the metric tensor and eliminates spurious (non-measurable) terms from the post-Newtonian forces in the equations of relative motion of the Moon with respect to the Earth. If one ignores the residual gauge freedom, the gauge-dependent terms will infiltrate the equations of motion causing possible misinterpretation of LLR observations. This problem is similar to that one meets in cosmology, where the theory of cosmological perturbations is designed essentially in terms of the gauge-independent variables so that observations of various cosmological effects are not corrupted by the spurious, coordinate-dependent signals [58]. The residual gauge degrees of freedom existing in the relativistic three-body problem (Sun-Earth-Moon), can lead to misinterpretation of various aspects of gravitational physics of the Earth-Moon system [51, 59], thus, degrading the value of extremely accurate LLR measurements for testing fundamental physics of space-time and deeper exploration of the lunar interior [28].

The residual gauge freedom of the three body problem was studied by Brumberg and Kopeikin [60], Klioner and Voinov [61], and Damour, Soffel and Xu [62]. They found that the post-Newtonian equations of motion of a test body (artificial satellite) can be significantly simplified by making use of a four-dimensional space-time transformation from the solar barycentric coordinates $\boldsymbol{x}^\alpha = (ct,\boldsymbol{x})$, to the geocentric coordinates $\boldsymbol{X}^\alpha = (cT, \boldsymbol{X})$

$$T = t + \frac{1}{c^2}A(t,\boldsymbol{r}_E) + \frac{1}{c^4}B(t,\boldsymbol{r}_E) + O\left(\frac{1}{c^5}\right), \tag{7}$$

$$X^i = x^i - x^i_E(t) + \frac{1}{c^2}C^i(t,\boldsymbol{r}_E) + O\left(\frac{1}{c^4}\right), \tag{8}$$

where the gauge functions $A(t,\boldsymbol{x})$, $B(t,\boldsymbol{x})$, $C^i(t,\boldsymbol{x})$ are polynomials of the geocentric distance $\boldsymbol{r}_E = \boldsymbol{x} - \boldsymbol{x}_E(t)$ of the field point $\boldsymbol{x}$ from the Earth's geocenter, $\boldsymbol{x}_E(t)$. Coefficients of these polynomials are functions of the barycentric time t that are determined by solving a system of ordinary differential equations, which follow from the gravity field equations and the tensor law of transformation of the metric tensor from one coordinate chart to another [63]. Contrary to the test particle, the Moon is a massive body, which makes the exploration of the residual gauge freedom of the lunar motion more involved. This requires introduction of one global (SSB) frame and three local reference frames associated with the Earth-Moon barycenter, the geocenter, and the center of mass of the Moon (selenocenter). It should be clearly understood that any coordinate system can be used for processing and interpretation of LLR data since any viable theory of gravity obeys the Einstein principle of relativity, according to which there is no preferred frame of reference [64-66]. Accepting the Einstein principle of relativity leads to discarding any theory of gravity based on a privileged frame (aether) [67] or admitting a violation of the Lorentz invariance [68]. The class of scalar-tensor theories of gravity, which have two PPN parameters – β and γ [14, 69], is in agreement with the

principle of relativity and it has been investigated fairly well [70, 71].

The principle of relativity also assumes that an arbitrary chosen, separate term in the post--Newtonian equations of motion of massive bodies can not be physically interpreted as straightforward as in the Newtonian physics. The reason is that the post-Newtonian transformations (1)-(2) and (7)-(8) of the barycentric and local coordinates, change the form of the equations of motion so that they are not form-invariant. Therefore, only those post-Newtonian effects, which do not depend on the frame transformations can have direct physical interpretation. For example, the gauge parameters v_C and λ_C entering transformations (1)-(2) and EIH equations (3)-(5) can not be determined from LLR data irrespectively of their accuracy because these parameters define the barycentric coordinates and can be fixed arbitrary by observer without any relation to observations.

Towards a New Lunar Ephemeris

Existing computer-based theories of the lunar ephemeris [25, 42-44] consist of three major blocks:

(1) the barycentric EIH equations (3)-(6) of orbital motion of the Moon, Earth, Sun, and other planets of the solar system with the gauge parameters $v_C = 1/2$, $\lambda_C = 0$ - the standard PPN coordinates;

(2) the Newtonian rotational equations of motion of the Moon and Earth;

(3) the barycentric post-Newtonian equations of motion for light rays propagating from laser to CCR on the Moon and back in standard coordinates with the gauge parameters $v_C = 1/2$, $\lambda_C = 0$.

This approach is straightforward but it does not control gauge-dependent terms in EIH equations of motion associated with the choice of the gauge-fixing parameters v_C and λ_C. Particular disadvantage of the barycentric approach in application to the lunar ephemeris is that it mixes up the post-Newtonian effects associated with the orbital motion of the Earth-Moon barycenter around the Sun with those, which are attributed exclusively to the relative motion of the Moon around the Earth. This difficulty is also accredited to the gauge freedom of the equations of motion in three-body problem and was pointed out in papers [60, 62, 72]. Unambiguous decoupling of the orbital motion of the Earth-Moon barycenter from the relative motion of the Moon around the Earth with apparent identification of the gauge-dependent degrees of freedom in the metric tensor and equations of motion is highly desirable in order to make the theory more sensible and to clean up the LLR data processing software from the fictitious coordinate-dependent perturbations, which do not carry out any physically-relevant information and may accumulate errors in numerical ephemerides of the Moon and the Earth.

This goal can be rationally achieved if the post-Newtonian theory of the lunar motion is consistently extended to account for mathematical properties offered by the scalar-tensor theory of gravity and the differential structure of the space-time manifold. Altogether it leads us to the idea that besides the global barycentric coordinates of the solar system one has to introduce three other local reference frames. The origin of these frames should be fixed at the Earth- Moon system barycenter, the Earth's center of mass (geocenter), and the Moon's center of mass (selenocenter). We distinguish the Earth-Moon barycenter from the geocenter because the Moon is not a test particle, thus, making the Earth-Moon barycenter displaced from the geocenter along the line connecting the Earth and Moon and located approximately

1710 km below the surface of the Earth. Mathematical construction of each frame is reduced to finding a metric tensor by means of solution of the gravity field equations with an appropriate boundary condition [41]. The gauge freedom of the three-body problem is explored by means of matching the set of the metric tensors defined in each reference frame in the overlapping domains of their applicability associated with the specific choice of boundary conditions imposed in each frame on the metric tensor. This matching procedure is an integral part of the equations defining the local differential structure of the manifold [73, 74], which proceeds from a requirement that the overlapping space-time domains covered by the local reference frames, are diffeomorphic.

The primary objective of the multi-frame post-Newtonian theory of the lunar ephemeris is the development of a new set of analytic equations to revamp the LLR data processing software in order to suppress the spurious gauge-dependent solutions, which may overwhelm the existing barycentric code at the millimeter accuracy of LLR measurements, thus, plunging errors in the interpretation of selenophysics, geophysics and fundamental gravitational physics. Careful mathematical construction of the local frames with the post-Newtonian accuracy will allow us to pin down and correctly interpret all physical effects having classical (lunar interior, Earth geophysics, tides, asteroids, etc.) and relativistic nature. The gauge freedom in the three-body problem (Earth-Moon-Sun) has been carefully examined in our paper [41] by making use of a scalar-tensor theory of gravity and the principles of the analytic theory of relativistic reference frames in the solar system [63, 75, 76] that was adopted by the XXIV-th General Assembly of the International Astronomical Union [5, 77] as a standard for data processing of high-precision astronomical observations.

The advanced post-Newtonian dynamics of the Sun-Earth-Moon system must include the following structural elements:

1. construction of a set of astronomical reference frames decoupling orbital dynamics of the Earth-Moon system from the rotational motion of the Earth and Moon with the full account of the post-Newtonian corrections and elimination of the gauge modes;
2. relativistic definition of the integral parameters like mass, the center of mass, the multi pole moments of the gravitating bodies;
3. derivation of the relativistic equations of motion of the center-of-mass of the Earth-Moon system with respect to the barycentric reference frame of the solar system;
4. derivation of the relativistic equations of motion of the Earth and Moon with respect to the reference frame of the Earth-Moon system;
5. derivation of the relativistic equations of motion of CCR on the Moon (or a lunar orbiter that is deployed with CCR) with respect to the selenocentric reference frame;
6. derivation of the relativistic equations of motion of a laser with respect to the geocentric reference frame.

These equations must be incorporated to LLR data processing software operating with observable quantities, which are proper times of the round trip of the laser pulses between the laser on the Earth and CCR on the Moon. The computational advantage of the new approach to the lunar ephemeris is that it separates clearly physical effects from the choice of coordinates. This allows us to get robust measurement of true physical parameters of the LLR model and give them direct physical interpretation. The new approach is particularly useful for comparing different models of the lunar interior and for making the fundamental test of

general theory of relativity.

Acknowledgments

This work has been supported by the Research Council Grant No. C1669103 of the University of Missouri-Columbia and by 2008-09 faculty incentive grant of the Arts and Science Alumni Organization of the University of Missouri-Columbia.

References

[1] J. Battat, T. Murphy, E. Adelberger, C. D. Hoyle, R. McMillan, E. Michelsen, K. Nordtvedt, A. Orin, C. Stubbs, and H. E. Swanson, APS Meeting Abstracts p. 12.003 (2007).

[2] T. W. Murphy, E. G. Adelberger, J. B. R. Battat, L. N. Carey, C. D. Hoyle, P. Leblanc, E. L. Michelsen, K. Nordtvedt, A. E. Orin, J. D. Strasburg, et al., *Publ. Astron. Soc. Pacific* **120**, 20 (2008), 0710.0890.

[3] D. G. Currie, C. Cantone, W. D. Carrier, S. Dell'Agnello, G. Delle Monache, T. Murphy, D. Rubincam, and R. Vittori, LPI Contributions **1415**, 2145 (2008).

[4] P. L. Bender, J. E. Faller, J. L. Hall, J. J. Degnan, J. O. Dickey, X. X. Newhall, J. G. Williams, R. W. King, L. O. Macknik, and D. O'Gara, in *Astrophysics from the Moon,* edited by M. J. Mumma and H. J. Smith (1990), vol. 207 of *American Institute of Physics Conference Series,* pp. 647-653.

[5] M. Soffel, S. A. Klioner, G. Petit, P. Wolf, S. M. Kopeikin, P. Bretagnon, V. A. Brumberg, N. Capitaine, T. Damour, T. Fukushima, et al., *Astron.* J. *(USA)* **126**, 2687 (2003), astro-ph/0303376.

[6] J. G. Williams, *Geophys. Res. Lett.* **34**, 3202 (2007).

[7] J. G. Williams, D. H. Boggs, J. T. Ratcliff, C. F. Yoder, and J. O. Dickey, in *Lunar and Planetary Institute Conference Abstracts* (2001), vol. 32 of *Lunar and Planetary Inst. Technical Report,* p. 2028.

[8] J. G. Williams, D. H. Boggs, C. F. Yoder, J. T. Ratcliff, and J. O. Dickey, J. *Geophys. Res.* **106**, 27933 (2001).

[9] J. G. Williams, D. H. Boggs, and J. T. Ratcliff, in *Lunar and Planetary Institute Conference Abstracts* (2008), vol. 39 of *Lunar and Planetary Inst. Technical Report,* p. 1484.

[10] J. G. Williams, X. X. Newhall, C. F. Yoder, and J. O. Dickey, in *Lunar and Planetary Institute Conference Abstracts* (1996), vol. 27 of *Lunar and Planetary Inst. Technical Report,* p. 1439.

[11] N. Rambaux, J. G. Williams, and D. H. Boggs, in *Lunar and Planetary Institute Conference Abstracts* (2008), vol. 39 of *Lunar and Planetary Inst. Technical Report,* p. 1769.

[12] J. G. Williams, R. H. Dicke, P. L. Bender, C. O. Alley, D. G. Currie, W. E. Carter, D. H. Eckhardt, J. E. Faller, W. M. Kaula, and J. D. Mulholland, Physical Review Letters **36**, 551 (1976).

[13] J. Muller and K. Nordtvedt, *Phys. Rev. D* **58**, 062001 (1998).

[14] C. M. Will, *Theory and Experiment in Gravitational Physics* (Cambridge: Cambridge University Press, 1993).

[15] K. Nordtvedt, in *Gyros, Clocks, Interferometers ...* : *Testing Relativistic Gravity in Space,* edited by C. Liimmerzahl, C. W. F. Everitt, and F. W. Hehl (2001), vol. 562 of

Lecture Notes in Physics, Berlin Springer Verlag, pp. 317-329.
[16] J. Mueller, M. Schneider, M. Soffel, and H. Ruder, *Astrophys.* J. *Lett.* **382**, L101 (1991).
[17] J. Muller, K. Nordtvedt, and D. Vokrouhlicky , *Phys. Rev. D* **54**, 5927 (1996).
[18] J. G. Williams, S. G. Turyshev, and T. W. Murphy, International Journal of Modern Physics D **13**, 567 (2004), arXiv:gr-qc/0311021.
[19] M. Soffel, S. Klioner, J. Muller, and L. Biskupek, *Phys. Rev. D* **78**, 024033 (2008). [20] O. Calame and J. D. Mulholland, Science **166**, 977 (1978).
[21] H. Xu and W. Jin, Shanghai Observatory Annals **15**, 129 (1994).
[22] J. Chapront, M. Chapront-Touze, and G. Francou, *Astron. Astrophys.* **387**, 700, (2002).
[23] B. Bertotti, 1. Ciufolini, and P. L. Bender, Physical Review Letters **58**, 1062 (1987).
[24] J. O. Dickey, X. X. Newhall, and J. G. Williams, Advances in Space Research **9**, 75 (1989).
[25] G. Y. Li, H. B. Zhao, Y. Xia, F. Zeng, and Y. J. Luo, in IAU Symposium (2008), vol. 248 of IAU Symposium, pp. 560-562.
[26] X. X. Newhall, E. M. Standish, Jr., and J. G. Williams, in Dynamics, Ephemerides, and Astrometry of the Solar System, edited by S. Ferraz-Mello, B. Morando, and J.-E. Arlot (1996), vol. 172 of IA U Symposium, pp. 37-44.
[27] S. M. Kudryavtsev, Highlights of Astronomy **14**, 472 (2007).
[28] S. M. Kopeikin, E. Pavlis, D. Pavlis, V. A. Brumberg, A. Escapa, J. Getino, A. Gusev, J. Muller, W.-T. Ni, and N. Petrova, Advances in Space Research **42**,1378 (2008), 0710.1450.
[29] E. M. Standish, in Recent Developments in Gravitation and Cosmology, edited by A. Macias, C. Liimmerzahl, and A. Camacho (2008), vol. 977 of American Institute of Physics Conference Series, pp. 254-263.
[30] J. Chapront, M. Chapront-Touze, and G. Francou, Astron. Astrophys. **343**, 624 (1999).
[31] J. G. Williams, D. H. Boggs, J. T. Ratcliff, and J. O. Dickey, in Lunar and Planetary Institute Conference Abstracts, edited by S. Mackwell and E. Stansbery (2003), vol. 34 of Lunar and Planetary Inst. Technical Report, p. 1161.
[32] J. Muller, J. G. Williams, and S. G. Turyshev, in Lasers, Clocks and Drag-Free Control.' Exploration of Relativistic Gravity in Space, edited by H. Dittus, C. Liimmerzahl, and S. G. Turyshev (2008), vol. 349 of Astrophysics and Space Science Library, pp. 457-472.
[33] J. Muller, M. Soffel, and S. A. Klioner, Journal of Geodesy **82**, 133 (2008).
[34] C.-L. Huang, W.-J. Jin, and H.-G. Xu, Shanghai Observatory Annals pp. 169-175 (1996).
[35] C. Huang, W. Jin, and H. Xu, Journal of Geodesy **73**, 125 (1999).
[36] E. M. Standish and G. Williams, in Inertial Coordinate System on the Sky, edited by J. H. Lieske and V. K. Abalakin (1990), vol. 141 of IAU Symposium, pp. 173-180.
[37] H. G. Walter and O. J. Sovers, Astrometry of fundamental catalogues: the evolution from optical to radio reference frames (Berlin, Heidelberg: Springer-Verlag, 2000).
[38] D. J. Pearlman, M.R. and J. Bosworth, Advances in Space Research **30**, 135 (2002).
[39] F. Meyer, F. Seitz, and J. Mueller, in Society of Photo-Optical Instrumentation Engineers (SPIE) Conference Series, edited by U. Schreiber, C. Werner, G. W. Kamerman, and U. N. Singh (2002), vol. 4546 of Society of Photo-Optical Instrumentation Engineers (SPIE) Conference Series, pp. 154-159.
[40] T. W. Murphy, E. L. Michelson, A. E. Orin, E. G. Adelberger, C. D. Hoyle, H. E. Swanson, C. W. Stubbs, and J. B. Battat, International Journal of Modern Physics D **16**, 2127 (2007).
[41] S. Kopeikin and Y. Xie, ArXiv e-prints (2009), 0902.2416.
[42] M. Chapront-Touze and J. Chapront, Astron. Astrophys. **124**,50 (1983).
[43] E. M. Standish, JPL 10M 312.F-98-048, Jet Propulsion Laboratory (1998).

[44] E. V. Pitjeva, Sol. Sys. Res. **39**, 176 (2005).
[45] A. Einstein, L. Infeld, and B. Hoffmann, The Annals of Mathematics **39**, 65 (1938).
[46] V. A. Brumberg, Essential Relativistic Celestial Mechanics (New York: Adam Hilger, 1991).
[47] M. H. Soffel, Relativity in Astrometru, Celestial Mechanics and Geodesy (Berlin: Springer, 1989).
[48] V. A. Brumberg, Relativistic Celestial Mechanics (Moscow: Nauka (in Russian), (1972).
[49] K. Nordtvedt, International Journal of Theoretical Physics **27**, 1395 (1988).
[50] F. B. Estabrook, Astrophys. J. **158**, 81 (1969).
[51] S. M. Kopeikin, ArXiv General Relativity and Quantum Cosmology e-prints (2007), gr-qc/0702120.
[52] T. W. Murphy, Jr., K. Nordtvedt, and S. G. Turyshev, Physical Review Letters **98**, 071102 (2007), gr-qc/0702028.
[53] T. W. Murphy, Jr., K. Nordtvedt, and S. G. Turyshev, Physical Review Letters **98**, 229002 (2007), 0705.0513.
[54] V. A. Brumberg, in ASSL Vol. 86: IA U Colloq. 56: Reference Coordinate Systems for Earth Dynamics, edited by E. M. Gaposchkin and B. Kolaczek (1981), pp. 283-294.
[55] J. L. Synge, Relativity based on chronometry (Recent Developments in General Relativity, 1962), pp. 441-448.
[56] J. L. Synge, Relativity: The general theory (Series in Physics, Amsterdam: North-Holland Publication Co., -c1964, 1964).
[57] L. Infeld and J. Plebański, Motion and Relativity (Oxford: Oxford University Press, 1960).
[58] V. F. Mukhanov, H. A. Feldman, and R. H. Brandenberger, Phys. Rep. **215**, 203 (1992).
[59] S. Kopeikin, ArXiv e-prints (2008), 0809.3392.
[60] V. A. Brumberg and S. M. Kopejkin, Nuovo Cimento B Serie **103**, 63 (1989).
[61] S. A. Klioner and A. V. Voinov, Phys. Rev. D **48**, 1451 (1993).
[62] T. Damour, M. Soffel, and C. Xu, Phys. Rev. D **49**, 618 (1994).
[63] S. M. Kopejkin, Celestial Mechanics **44**, 87 (1988).
[64] V. A. Fock, The Theory of Space, Time and Gravitation (New York: Pergamon Press, 1959).
[65] L. D. Landau and E. M. Lifshitz, The classical theory of fields (Oxford: Pergamon Press, 1975).
[66] C. W. Misner, K. S. Thorne, and J. A. Wheeler, Gravitation (San Francisco: W.H. Freeman and Co., 1973).
[67] C. Eling, T. Jacobson, and D. Mattingly, in Deserfest: A Celebration of the Life and Works of Stanley Deser, edited by J. T. Liu, M. J. Duff, K. S. Stelle, and R. P. Woodward (2006), pp. 163-179.
[68] A. Kostelecky, APS Meeting Abstracts p. 13.00001 (2008).
[69] T. Damour and G. Esposito-Farese, Classical and Quantum Gravity **9,** 2093 (1992).
[70] S. Kopeikin and 1. Vlasov, *Phys. Rep.* **400,** 209 (2004), gr-qc/0403068.
[71] S. A. Klioner and M. H. Soffel, *Phys. Rev. D* **62,** 024019 (2000), gr-qc/9906123. [72] J.-H. Tao, T.-Y. Huang, and C.-H. Han, *Astron. Astrophys.* **363,** 335 (2000).
[73] L. P. Eisenhart, *Differential Geometry* (Princeton: Princeton University Press, (1947).
[74] B. A. Dubrovin, A. T. Fomenko, and S. P. Novikov, *Modem Geometry* (New York: Springer-Verlag, 1984).
[75] V. A. Brumberg and S. M. Kopejkin, in *ASSL Vol. 154*: *Reference Frames,* edited by J. Kovalevsky, 1. 1. Mueller, and B. Kolaczek (1989), pp. 115-141.
[76] T. Damour, M. Soffel, and C. Xu, *Phys. Rev. D* **43,** 3273 (1991).
[77] S. M. Kopeikin, in *American Institute of Physics Conference Series* (2007), pp. 268-283.

APOLLO: Two Years of Science Data

T. W. Murphy, Jr.[1], E. G. Adelberger[2], J. B. R. Battat[3], C. D. Hoyle[4], R. J. McMillan[5], E. L. Michelsen[1], C. W. Stubbs[6], H. E. Swanson[2]

[1]University of California, San Diego, La Jolla, CA, USA
[2]University of Washington, Seattle, WA, USA
[3]Massachusetts Institute of Technology, Cambridge, MA, USA
[4]Humboldt State University, Arcata, CA, USA
[5]Apache Point Observatory, Sunspot, NM, USA
[6]Harvard University, Cambridge, MA, USA

tmurphy@physics.ucsd.edu

Abstract

APOLLO is a newly operational lunar ranging experiment aimed at achieving one-millimeter range precision in an effort to better probe the nature of gravity. After two years of operation, we can characterize its performance as obtaining return rates at least an order-of-magnitude higher than previous stations, attaining a resultant random uncertainty at the few-millimeter level. Such precision presents a new challenge to model capabilities, which will lead to improved scientific knowledge.

Introduction

The Apache Point Observatory Lunar Laser-ranging Operation (APOLLO) was established in an attempt to push lunar laser ranging (LLR) capabilities to a new regime of one-millimeter range precision as a way to advance tests of general relativity. LLR has long stood at the forefront of testing general relativity, boasting the best tests to date of the strong equivalence principle, time-rate-of change of Newton's gravitational constant, geodetic precession, the inverse-square law, and gravitomagnetism (see Williams et al., 1996; Murphy et al., 2007). Therefore, extending the precision capability of LLR promises to advance our understanding of gravity in a number of ways. In addition to improving our knowledge of gravity, LLR offers insight into properties of the lunar interior, earth orientation, and tidal processes on Earth.

The Instrument

APOLLO is installed on the 3.5 meter astronomical telescope at the Apache Point Observatory in southern New Mexico at an altitude of 2780 meters. The telescope has a median image quality—including atmospheric seeing—below 1.5 arcsec, and is competitively scheduled for a variety of astronomical observations. A detailed description of the apparatus appears in Murphy et al. (2008). Here, we just summarize the principal features. APOLLO consists of:

- A 20 Hz, 90 ps pulse, 115 mJ/pulse, Nd:YAG laser operating at 532 nm
- A 16-element avalanche photodiode array detector, in 4×4 format, spanning 1.4 arcseconds on a side
- A 16-channel timing system with 25 ps resolution and 15 ps jitter
- Identical optical path/electronics fiducial corner cube measurement at the single-photon level

- Automation for remote operability and environmental self-control

APOLLO is typically allocated approximately 8–10 one-hour slots of telescope time per lunar month, typically allowing a few dozen normal point measurements to the various reflectors each month. The observations are primarily performed by R. McMillan, either at the site or remotely, with another APOLLO member participating in the observation and ready to assume control of the operation if necessary.

Performance

The large aperture and good atmospheric conditions at the site permit APOLLO to detect multiple photons per pulse, thus necessitating the multiple-element detector array. Record yields may be characterized by photons per shot or photons per unit time, and characterized by maximum net yield or maximum net rate. Table 1 summarizes the results below. Note that a number of the records were obtained on the last day of the conference in Poznan.

Table 1: Summary of APOLLO record runs

Reflector	Date	Laser Shots	Photons detected (× prev. record)	Photons/minute (× prev. record)	Phot/shot
Apollo 11	2008-10-17	5000	4497 (26×)	1079 (65×)	0.90
Apollo 14	2008-10-17	5000	7606 (36×)	1825 (69×)	1.52
Apollo 15	2008-10-17	5000	15730 (26×)	3775 (67×)	3.15
Lunokhod 2	2008-09-22	5000	750 (11×)	180 (31×)	0.15

Aside from Lunokhod 2—which no longer performs as well as the Apollo reflectors, there is a remarkable consistency in the peak rate seen per reflector compared to that of the previous record runs. APOLLO appears to have record rates roughly two-orders of magnitude higher than the previous records (all obtained from OCA). Given more time, APOLLO will almost certainly improve on the records presented here. Since it is APOLLO's goal to improve precision by an order-of-magnitude—and this requires two orders-of-magnitude higher photon number if the result is statistically dominated—the photon performance of APOLLO is encouraging.

Figure 1 shows returns from Apollo 15 and 11 on 2007 November 19, in which 2346 and 3731 photons were recorded, respectively. In a temporary scheme to minimize the effect of first-photon bias, our current data reduction excludes pulses delivering multiple photon detections. Thus the plots in Figure 1 only display 1155 and 1041 photons that arrived as single-photon detections. Because the moon was at the same libration angle for both sets of data (taken minutes apart), and the arrays are both aligned to point at the mean-earth position within 1°, we can see immediately the smaller physical size of the Apollo 11 array.

The statistics of returning photon packets from the moon are subject to variations from—among other things—speckle interference from atmospheric turbulence. The illumination pattern on the moon is a complex and random array of hot-spots and valleys, numbering roughly D/r_0 across (thus this number squared for total number of speckles), where D is the diameter of the laser beam and r_0 is the atmospheric Fried parameter, such that the atmospheric seeing scale is λ/r_0. For APOLLO, $D/r_0 \approx 20$, and is larger in bad seeing. The result is that many pulses deliver

very strong returns when a "hot-spot" happens to land on the lunar reflector. Because we have a multiple-photon detector, we can verify these statistics.

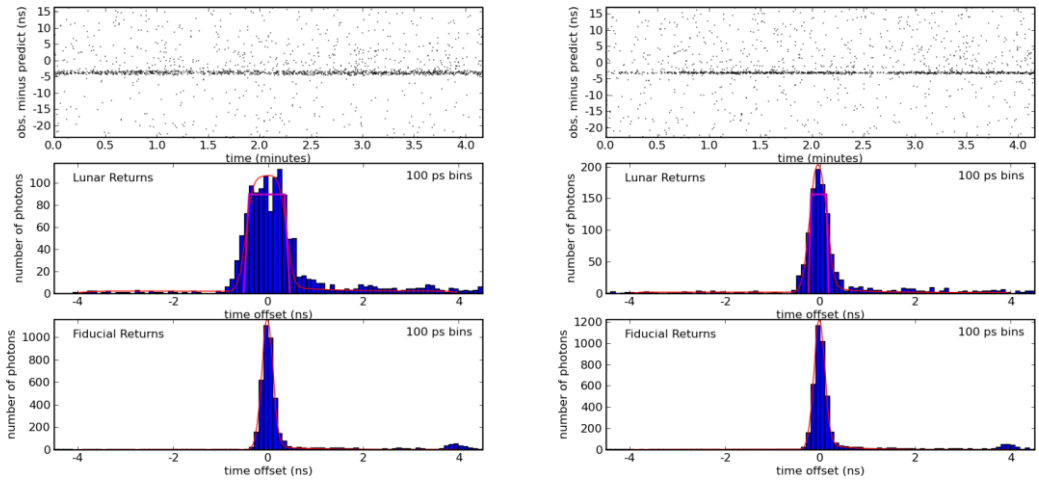

Figure 1. 5000-shot runs on Apollo 15 (left) and Apollo 11 (right) on 2007 November 19. The total yields for the two runs are 3371 and 2346 photons, respectively—though only 1155 and 1041 are shown here. The lower histogram is the local (ficucial) corner cube, showing a 120 ps standard deviation. A functional fit to the fiducial is convolved with the trapezoidal response from the lunar array (shown superimposed on the lunar return) to form a fit-function for the lunar return. Note that the Apollo 11 array is obviously physically smaller than the Apollo 15 array.

For example, the 5000-shot Apollo 15 observation pictured in Figure 1 resulted in 702 shots with zero photons, 1062 shots with one photon, 471 shots with two photons (thus 942 photons), 225 shots with three, 98 with four, 47 with five, 27 with six, 13 with seven, 3 with eight, and finally 1 shot returning nine photons. This adds to a total of 3592 photons (selection criterion slightly more restrictive than the one that produces estimate of 3731 photons used above). This means over 70% of detected photons arrived in bundles of more than one photon. If the distribution followed a Poisson behavior, a return of 3592/5000, or a mean of 0.718 per pulse would deliver only 51% of photons in multi-photon returns, and would not be expected to produce more than one return with as many as 5 photons, out of 5000 trials. Strictly speaking, the proper distribution in an APD detector is binomial, because any given element will either report a detection or not, but is not capable of reporting the detection of more than one photon in a single element.

We can ask the question: Does APOLLO have *enough* detector elements—are we missing any events? Figure 2 addresses this question. It is clearly seen that the lunar distribution does not adhere to either Poisson or binomial statistics, being "top-heavy" with strong returns from speckle. But even for the strong run pictured, where 81% of the lunar returns arrived in multi-photon packets, the distribution terminates naturally before we run out of detector elements. Thus we can be reasonably assured that we are catching all the detectable photons with APOLLO, and therefore can anticipate being able to correct for multi-photon bias. Note also the remarkable adherence of the fiducial data to binomial statistics. At every data point (save the cross-over at $n = 3$), the data identifies with the binomial point rather than the Poisson point. This provides additional reassurance that we understand our device statistics.

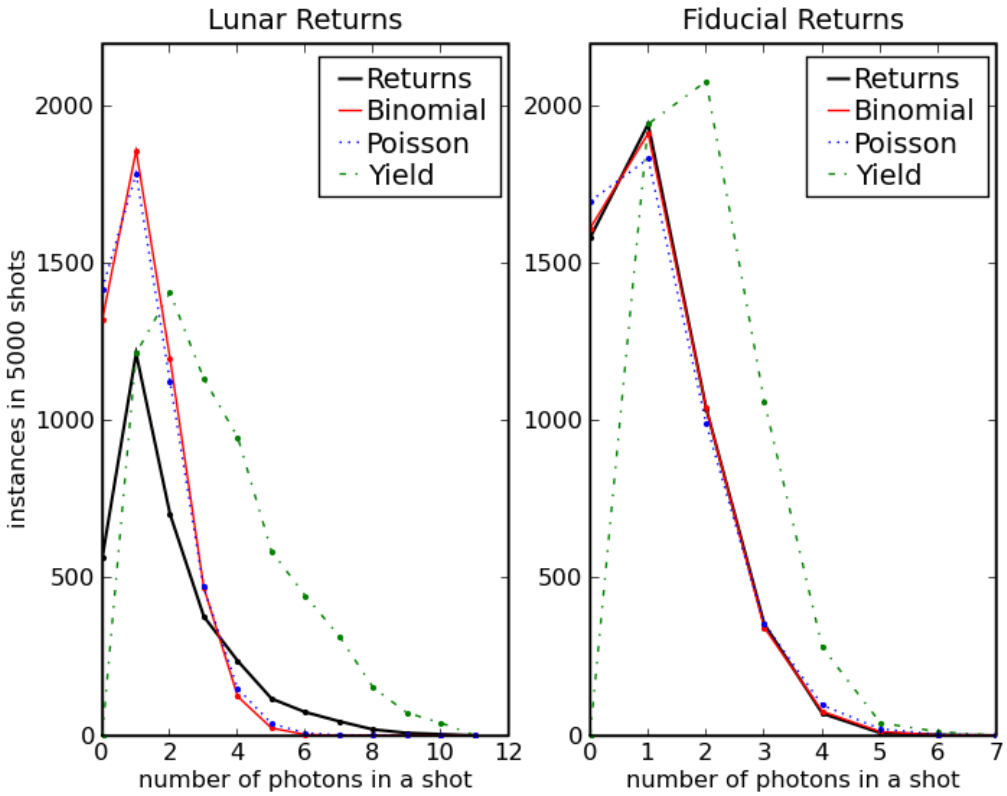

Figure 2. Study of photon count statistics for both the lunar and fiducial returns. In the lunar case, the return rate average was 1.26 photons per shot, with 81% of photons in multi-photon packets. For the fiducial, the average was 1.08 photons per shot, 64% in multi-photon clusters. In each, measured returns (number of shots with that number of photons) are thicker black lines, and comparative binomial and Poisson distributions are shown in red solid and blue dotted lines, respectively. The green dash-dot line is a multiplication of the return (black) line by the number of photons, to represent the total photon number as a function of photons per shot. While the binomial and Poisson distributions are very similar, the fiducial data clearly picks out the binomial distribution as correct (in fact, the black line is largely hidden by the red one).

Precision Assessment

High photon yield is *necessary* for achieving high precision, but it is not in itself *sufficient*. In the worst-case libration angle of 10°—resulting in the greatest array-induced spread—the standard deviation of lunar return photons may be 450 ps, as depicted for Apollo 15 in Figure 1. One millimeter one-way determination corresponds to 6.7 ps of round-trip time, which would necessitate approximately a 70-fold increase in precision over that offered by a single photon, requiring 4900 photons. APOLLO can clearly achieve the requisite photon number, but there may be other instrumental errors that preclude APOLLO from reaching its one-millimeter precision goal. Where random uncertainty is concerned, APOLLO appears to me reaching the millimeter mark, as illustrated by Figure 3.

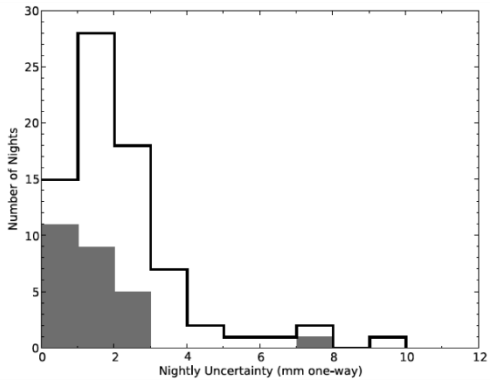

Figure 3. Summary performance of APOLLO normal points, averaged per night per reflector. The median is 1.8 mm for all data (2006 April through 2008 February), though for "recent" data (shaded: 2007 September through 2008 February) the median is lower, at 1.1 mm.

Ultimately, one must compare against a model that contains all relevant physics, the parameters of which are determined by a least-squares fit to the data. But no model has yet demonstrated one-millimeter LLR fidelity. So for the short term, we must find alternate means of assessment. One way to explore the data quality is by comparing against the prediction used for data acquisition. The prediction we use is only good to a round trip of about 1 ns (150 mm one-way) over the long term. But within a one-hour observation block, the departure from truth is reduced to a behavior that is almost entirely linear with time. Thus we can look for scatter or otherwise nonlinear departures of APOLLO data from the prediction. Such analysis was extensively pursued in Battat et al., (2009), and here we only summarize the results.

We have applied two methods to seek possible deviations from linear behavior. The first is to break strong runs into segments, applying our data reduction analysis to each segment in turn. The second is to look at the trend of normal points from the same reflector taken over a one-hour observation period. In short, we have not yet seen deviations from linear performance for either method. The scatter we see is consistent with our estimated errors based solely on the standard deviation of the return profile divided by the square root of the number of photons constituting the measurement. This is not a conclusive statement about APOLLO accuracy: the remaining linear trend may not be wholly due to prediction inadequacy, and the night-to-night variations are not probed by this method. At the least, it is a reassuring check on the performance.

A separate indicator that the APOLLO estimated uncertainties are approximately correct is the behavior of the residuals against the LLR model employed by the Jet Propulsion Laboratory (JPL). APOLLO is frequently able to make several rounds among the reflectors within a single one-hour session. When APOLLO data is downweighted to 15 mm uncertainty per normal point, the post-fit residuals show coherent clustering by reflector, the spread of points for a given reflector being consistent with the original normal-point uncertainty estimates, but in disagreement with other reflectors. This is symptomatic of a lunar orientation offset. When APOLLO data is fit at full weight, the model is able to eliminate the spread from one reflector to the next, indicating that the APOLLO data contains true coherence that is useful to the model, well below the 15 mm level. This is a point of further reassurance, but does not in itself address longer-term systematics. For this, we must pursue further model development.

Unsolved Mysteries

Despite the high photon return from APOLLO, we still have a signal deficit compared to expectations. We reported in the proceedings from the 15th International Workshop on Laser Ranging that a careful attempt to calibrate the signal strength fell a factor of 12–16 short, even with knowledge of the beam footprint on the lunar surface. This work was based on a maximum photon rate of 0.6 photons per pulse—far exceeded by now. But the narrow-band filter used at the time was calculated for 35% transmission, whereas the current filter has a transmission > 90%. The net effect is that we still have a factor of ten discrepancy, though we will continue to look for ways in which we may have misunderstood our system.

Potentially associated with the signal deficit is a pronounced performance gap near full moon. When the moon is within 15° of full, we have difficulty acquiring any signal at all, and not because of increased background. The actual signal level is down by a factor of 15 or more compared to the rates we see away from full moon (we closed the gap somewhat since the Poznan presentation, when the gap was a factor of 100). Meanwhile, the background rate goes from 0.15 photons per gate across 16 channels (thus 0.01 per gate per channel) to about 1.0 photons per gate across all channels (thus < 0.1 per channel per gate). The background trend as a function of lunar phase is smooth and well-behaved, reaching a peak at full moon with no discontinuities in behavior near full moon.

References

Battat, J. B. R., Murphy, T. W., Adelberger, E. G., Gillespie, B., Hoyle, C. D., McMillan, R. J., Michelsen, E. L., Nordtvedt, K., Orin, A. E., Stubbs, C. W., & Swanson, H. E., "The Apache Point Observatory Lunar Laser-ranging Operation (APOLLO): Two Years of Millimeter-precision Measurements of the Earth-Moon Range," *Publications of the Astronomical Society of the Pacific*, **121**, 29–40, (2009)

Murphy, T. W., Adelberger, E.G., Battat, J. B. R., Carey, L. N., Hoyle, C. D., LeBlanc, P., Michelsen, E. L., Nordtvedt, K., Orin, A. E., Strasburg, J. D., Stubbs, C. W., Swanson, H. E., & Williams, E., "The Apache Point Observatory Lunar Laser-ranging Operation: Instrument Description and First Detections," *Publications of the Astronomical Society of the Pacific*, **120**, 20–37, (2008)

Murphy, T. W., Nordtvedt, K., & Turyshev, S. G., "Gravitomagnetic influence on gyroscopes and on the lunar orbit," *Physical Review Letters*, **98**, 071102, (2007)

Williams, J. G., Newhall, X. X., & Dickey, J. O., *Physical Review D*, **53**, 6730, (1996)

Relativity and Earth Orientation Parameters from Lunar Laser Ranging

L. Biskupek, J. Müller
Institut für Erdmessung, Leibniz Universität Hannover, Germany
biskupek@ife.uni-hannover.de, mueller@ife.uni-hannover.de

Abstract

Lunar Laser Ranging (LLR) is carried out for more than 39 years. Several Newtonian and relativity parameters of the Earth-Moon system can be fitted in a global adjustment with high accuracy. Here, we just give a few examples for gravitational physics parameters, but mainly focus on Earth orientation parameters (EOP). In the global adjustment long-term lunisolar nutation coefficients for different periods (18.6 years, 9 years, 1 year, 182.6 days, 13.6 days) are determined and compared with results from studies of other analysis centres and values of the MHB2000 model (Mathews et al., 2002). Furthermore, the post-fit residuals of the global adjustment are investigated by the daily decomposition method to study variations in $\Delta UT0$ and latitude $\Delta\phi$. In our recent LLR analysis, also different EOP series are applied as input and their effect on the Earth-Moon parameters is investigated.

Model and Analysis

At the Institut für Erdmessung (IfE) the existing model to analyse LLR data is based on Einstein's theory of gravity. It is fully relativistic and complete up to the first post-Newtonian ($1/c^2$) level (Müller et al., 2008). The Barycentric Celestial Reference Frame (BCRF) is the central frame of the analysis. The basic observation equation for the station-reflector distance is defined in this system and the station and reflector coordinates have to be transformed from their respective reference frames (the terrestrial (TRF) or selenocentric (SRF) reference frame) into the inertial frame. In the transformation, the Earth orientation parameters are used for the Earth and the libration angles, computed by numerical integration, for the Moon. The Earth-Moon distance is obtained by numerical integration of the corresponding equation of motion, considering many Newtonian and relativistic contributions.

In our LLR analysis, two groups of parameters for the Earth-Moon system (ca. 180 in total) are determined by a weighted least-squares adjustment of the observations. The first group are the so-called Newtonian parameters, e.g.,

- initial position and velocity of the Moon,
- parameters of physical librations of the Moon,
- coordinates of LLR observatories and retro-reflectors,
- orbit and mass of the Earth-Moon system,
- lunar gravity field,
- long-periodic nutation parameters,
- the lag angle, indicating the lunar tidal acceleration.

Figure 1 shows the annually averaged weighted post-fit residuals of the standard solution with data from Jan. 1970 to Mar. 2008 (16230 normal points). Up to the middle 80ies, the precision of the LLR measurements and analysis model is about 20-30 cm. From 1985 on, more stations started to track the Moon and the residuals decreased. In the last years, only two stations, one with reduced accuracy, observed the Moon, so that

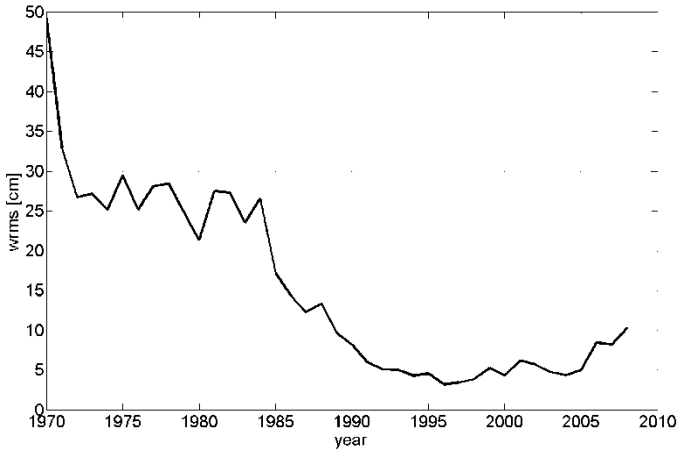

Figure 1. Weighted post-fit residuals (observed minus computed Earth-Moon distance) annually averaged

the residuals increased again. For more details see (Müller et al., 2008). The post-fit residuals of this solution are further investigated w.r.t. Earth orientation parameters, see below.

Relativity

By extending the standard solution, it is possible to solve for parameters related to general relativity, like the temporal variation of the gravitational constant (Müller and Biskupek, 2007), metric parameters as well as the strong equivalence principle and preferred-frame effects (Soffel et al., 2008). The latter can be related to gravito-magnetic effects in the solar system constraining possible deviations from Einstein's theory. (Müller et al., 2008) carried out dedicated sensitivity studies to analyse the potential of LLR to determine specific gravitational physics parameters. Recent results for some selected relativity parameters including realistic errors are given in table 1.

Table 1. Values from LLR for some relativistic parameters and their realistic errors

Nordtvedt parameter η (test of the strong equivalence principle)	$(6 \pm 7)\ 10^{-4}$
time variable gravitational constant $\dot{G}/G$ [yr^{-1}] $\ddot{G}/G$ [yr^{-2}]	$(2 \pm 7)\ 10^{-13}$ $(4 \pm 5)\ 10^{-15}$
preferred frame parameters α_1 α_2 (coupled with velocity of the solar system)	$(-4 \pm 9)\ 10^{-5}$ $(2 \pm 2)\ 10^{-5}$
preferred frame parameter α_1 (coupled with dynamics within the solar system)	$(1.6 \pm 4)\ 10^{-3}$

Nutation

As mentioned in the first section, amplitudes of long-term nutation coefficients can be determined by the analysis of LLR data as part of the global adjustment. The IAU 2000

nutation model is described in the IERS Conventions 2003 (McCarthy and Petit, 2004) as a series for nutation in longitude $\Delta\psi$ and obliquity $\Delta\varepsilon$, referred to the mean ecliptic of date:

$$\Delta\psi = \sum_{i=1}^{N} \left(A_i + A_i^{'} t\right) \sin\left(ARG\right) + \left(A_i^{''} + A_i^{'''} t\right) \cos\left(ARG\right) \quad (1)$$

$$\Delta\varepsilon = \sum_{i=1}^{N} \left(B_i + B_i^{'} t\right) \cos\left(ARG\right) + \left(B_i^{''} + B_i^{'''} t\right) \sin\left(ARG\right) \quad (2)$$

with t in Julian centuries from epoch J2000 and $ARG = \sum_{j}^{5} N_j F_j$, N_j: integers, F_j: Delaunay parameters.

Table 2. Nutation coefficients from MHB2000 model

period	A_i [mas]	B_i [mas]	A_i'' [mas]	B_i'' [mas]
18.6 years	-17206.42	9205.23	3.34	1.54
182.6 days	-1317.09	573.03	-1.37	-0.46
13.6 days	-227.64	97.85	0.28	0.14
9.3 years	207.46	-89.75	-0.07	-0.03
1 year	147.59	7.39	1.18	-0.19

The model is composed of 678 lunisolar and 687 planetary terms with in-phase and out-of-phase components and their time variations. Basis is the REN2000 nutation solution (Souchay et al., 1999) for the rigid Earth, which is convolved to the nutation model MHB2000 for the non-rigid Earth applying the transfer function of (Mathews et al., 2002). The MHB2000 model is relied on the solution of linearised dynamical equations for each forcing frequency, adding contributions from non-linear terms and other effects not included in the linearised equations. The model improved the IAU 1980 nutation theory by the incorporation of mantle anelasticity, ocean tide effects and electromagnetic couplings of the mantle and the solid inner core to the fluid outer core. Table 2 gives the largest terms of the MHB2000 nutation model. There, the non-time-dependent components for the in-phase (A_i, B_i) and out-of-phase (A_i'', B_i'') parts of nutation in longitude and obliquity are shown.

Table 3. Nutation coefficients from our LLR computation

period	A_i [mas]	B_i [mas]	A_i'' [mas]	B_i'' [mas]
18.6 years	-17201.93	9203.41	3.84	3.88
182.6 days	-1316.88	572.98	-3.25	-0.98
13.6 days	-230.54	99.26	0.16	0.31
9.3 years	207.13	-90.75	1.63	-0.21
1 year	146.83	7.86	0.27	-0.58

Analogue to table 2 the same components were fitted in the global adjustment of our LLR analysis. Table 3 gives the preliminary results. The components, which are marked in grey, show the largest differences between the MHB2000 model (Tab. 2) and our LLR analysis (Tab. 3). These are not completely understood yet, but they are also seen in similar way in the analysis of other groups (Williams, 2008) and must be further investigated.

Earth rotation from LLR data

Post-fit residuals from the global adjustment of the LLR analysis can be further investigated to determine corrections for the components of Earth rotation parallel to a change in longitude ($\Delta UT0$) and latitude (variation of latitude $\Delta\phi$). The latter one was also used to iteratively improve the results of the global standard solution.

To determine $\Delta UT0$ and $\Delta\phi$ from LLR data, the post-fit residuals are sorted by station-reflector combinations and merged in daily sets. One set must include the minimum of three station-reflector pairs. Out of 16230 observations, 1179 daily sets for the station OCA in Grasse and 752 daily sets for the station McDonald in Texas were found. These sets are analysed in a least-squares adjustment (daily decomposition method, see (Dickey et al., 1985)) applying the following model:

$$r(t) = r_{\Delta UT0} + r_{\Delta\phi} + r_n, \tag{3}$$

where the post-fit residuals of the global adjustment are assumed to be caused by contributions from universal time

$$r_{\Delta UT0} = 2\,\Delta UT0\; r_E\; \cos\phi \sin H\; \cos\delta, \tag{4}$$

from variation of latitude

$$r_{\Delta\phi} = 2\,\Delta\phi\; r_E \left(\sin\phi \cos\delta \cos H - \sin\delta \cos\phi\right), \tag{5}$$

and a part containing other effects r_n like systematic ranging errors and model errors. $\Delta UT0$ and $\Delta\phi$ enter the respective equation as

$$\Delta UT0 = \Delta UT1 + \tan\phi \left(x_P \sin\lambda + y_P \cos\lambda\right) \tag{6}$$

and

$$\Delta\phi = x_P\; \cos\lambda - y_P \sin\lambda \tag{7}$$

with the declination δ and hour angle H of the Moon and the latitude ϕ, longitude λ and radius r_E of the Earth. The pole coordinates x_P/y_P and $\Delta UT1$ are also used for the transformation between the celestial and terrestrial systems in our global fit. There in addition, the long-periodic, diurnal and sub-diurnal effects of the ocean are corrected according to the IERS Conventions 2003.

Moreover, the effect of different EOP series, serving as initial values in our LLR analysis, was investigated. The EOP series IERS EOP C04 (Gambis, 2004) and COMB2006 (Gross, 2007) were used as input for the global standard solution. Then, the post-fit residuals were analysed to determine corrections for universal time $\Delta UT0$ and variation of latitude $\Delta\phi$. Both EOP series were obtained from the combination of "operational" EOP series derived from the various space-geodetic techniques VLBI (Very Long Baseline Interferometry), GPS (Global Positioning System), SLR (Satellite Laser Ranging) and LLR as well as optical observations, see (Gambis, 2004; Gross, 2007). Additionally, in the C04 series DORIS

(Doppler Orbitography and Radiopositioning Integrated by Satellite) data were included. Differences between the series are caused by different time spans, filter techniques to combine the data and the treatment of tidal effects. In the C04 series periods from 5 days to 18.6 years are corrected by the model of (Defraigne and Smits, 1999), in the COMB2006 series periods from 5 days to 35 days are corrected using the procedure of (Yoder et al., 1981). Comparison of the two series (C04 minus COMB2006) shows large differences in the period between 1970 and 1982 in all components (x_P, y_P and $\Delta UT1$). From 1982 on, the differences decrease more and more, for polar coordinates it is near zero now. For $\Delta UT1$ the difference is only a few microseconds today, because of the different treatment of the tidal effects.

As an example, figure 2 shows the resulting $\Delta\phi$ for McDonald when using the different EOP series. The daily solutions (dots), calculated with (5), are smoothed by a spline filter. The curves of the two calculations show large differences in the 70ies and middle 80ies, the period where the two EOP series show large differences, too. From the middle 80ies on, when both EOP series are very similar, also the results are very similar here.

In a next step, these spline-interpolated $\Delta\phi$ values were iteratively used as corrections in the global adjustment. Two calculations were made for both EOP series (figure 3 shows the corresponding results): One as reference without the estimated $\Delta\phi$ values (solid lines) and one with the $\Delta\phi$ correction applied (dotted lines). As in the previous figures, it can be seen, that again in the time span from the middle 80ies on, where the EOP series are very similar, also the residuals are very similar. It is furthermore obvious, that the residuals can not really be improved by using the $\Delta\phi$ correction, because the input EOP series are already very accurate. In the time span up to the 80ies, the residuals using the COMB2006 series are smaller than those based on the C04. It seems, that the COMB2006 series fits better to the LLR analysis than the C04 series. But also here, the results of the global adjustment can not really be improved by applying the determined $\Delta\phi$ correction.

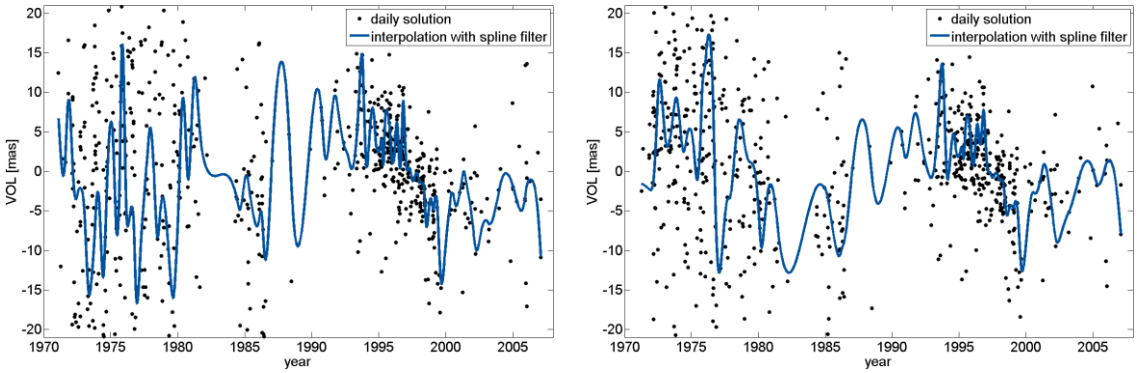

Figure 2. Results for $\Delta\phi$ when using the EOP series C04 (left) and COMB2006 (right) as input in the global adjustment

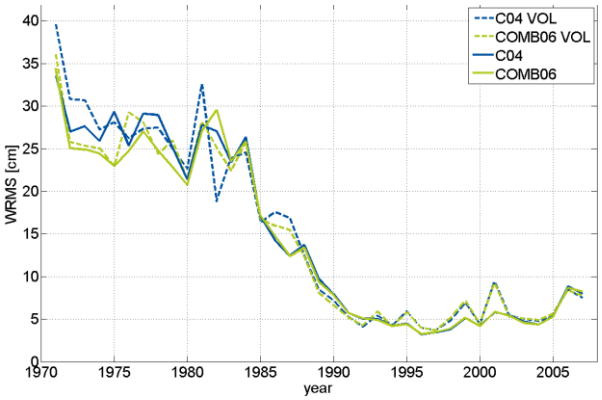

Figure 3. Results of using the $\Delta\phi$ corrections in the global adjustment

Conclusions

A 38-year LLR data set has been analysed to determine Newtonian as well as gravitational physics parameters with high accuracy, impressively confirming Einstein's theory.

The results of long-periodic nutation coefficients determined from LLR analysis show differences to the MHB2000 model for some of the coefficients. These differences are also seen by other analysis centres, but can not be explained yet and must be further investigated. In a next step, the results from LLR shall be directly compared to VLBI nutation results.

The investigation and determination of the EOP correction parameter $\Delta\phi$ based on different EOP input series is possible with the daily decomposition method. Using these values in the next iteration step of the LLR analysis, however, does not significantly improve the residuals. Obviously, the input EOP series are already of very good quality, especially from the middle 80ies on. In a future step other filters, apart from the spline filter, will be tested. Also values for length of day *LOD* will be calculated to compare them with *LOD* results from VLBI.

Acknowledgments

Current LLR data are collected, archived and distributed under the auspices of the International Laser Ranging Service (ILRS) (Pearlman et al., 2002). We acknowledge with thanks, that the more than 39 years of LLR data, used in these analyses, have been obtained under the efforts of personnel at the Observatoire de la Cote d'Azur in France, the LURE Observatory in Maui, Hawaii, the McDonald Observatory in Texas as well as the Apache Point Observatory in New Mexico.

We would also like to thank the DFG, the German Research Foundation, which funded this study (project MU 1141/6-2) within the research unit FOR584 "Earth rotation and global dynamic processes".

References

Defraigne, P., Smits, I., *Length of day variations due to zonal tides for an inelastic earth in non-hydrostatic equilibrium*, Geophys. J. Int., 139, p. 563-572, 1999

Dickey, J.O., Newhall, X.X., Williams, J.G., *Earth Orientation From Lunar Laser Ranging and an Error Analysis of Polar Motion Services*, J. Geophys. Res. (B11), 90, p. 9353-9362, 1985

Gambis, D., *Monitoring Earth orientation using space-geodetic techniques: state-of-the-art and prospective*, J. Geod., 78, p. 295-303, 2004

Gross, R.S., *Combinations of Earth orientation measurements: SPACE2006, COMB2006, and POLE2006*, JPL Publication, no. 07-05, 2007

Mathews, P.M., Herring, T.A., Buffett, B.A., *Modeling of nutation and precession: New nutation series for nonrigid Earth and insights into the Earth's interior*, J. Geophys. Res. (B4), 107, p. 10.1029/2001JB000390, 2002

McCarthy, D.D., Petit, G. (eds.), *IERS Conventions (2003), IERS Technical Note No. 32*, Verlag des Bundesamts für Kartographie und Geodäsie, Frankfurt am Main, 2004

Müller, J., Biskupek, L., *Variations of the gravitational constant from lunar laser ranging data*, Class. Quan. Gravity, 24, p. 4533-4538, doi: 10.1088/0264-9381/24/17/017, 2007

Müller, J., Williams, J.G., Turyshev, S.G., *Lunar Laser Ranging Contributions to Relativity and Geodesy*, in: Lasers, Clocks and Drag-Free Control: Exploration of Relativistic Gravity in Space, eds: Dittus, H., Lämmerzahl, C., Turyshev, S.G., Springer, 349, p. 457-472, 2008

Pearlman, M.R., Degnan, J.J., Bosworth, J.M., *The International Laser Ranging Service*, Adv. Space Res., 30, p. 135-143, doi: 10.1016/S0273-1177(02)00277-6, 2002

Soffel, M., Klioner, S., Müller, J., Biskupek, L., *Gravitomagnetism and lunar laser ranging*, Phys. Rev. D, 78, p. 024033, 2008

Souchay, J., Loysel, B., Kinoshita, H., Folgueira, M., *Corrections and new developments in rigid earth nutation theory - III. Final tables "REN-2000" including crossed-nutation and spin-orbit coupling effects*, Astron. Astrophys. Suppl. Ser., 135, p. 111-131, 1999

Williams, J.G., priv. communication, 2008

Yoder, C.F., Williams, J.G., Parke, M.E., *Tidal Variations of Earth Rotation*, J. Geophys. Res., 86, p. 881-891, 1981

A Lunar Laser Ranging Array for NASA's Manned Landings, the International Lunar Network and the Proposed ASI Lunar Mission MAGIA

D.G.Currie (1)**, S.Dell'Agnello** (2)**, G.O.Delle Monache** (2)**, T.Murphy** (3)**, R.Vittori** (4)**, D.Carrier** (5)**, C.Cantone** (2)**, M.Garattini** (2)**, A.Boni** (2)**, M.Martini** (1)**, C.Lops** (2)**, N.Intaglietta** (2)**, G.Bellettini** (6)**, R.Tauraso** (6)**, R.March** (7)**, G.Bianco** (8)**, D. Rubincam** (9)

(1) University of Maryland (UMD), College Part (UMCP), MD, USA
(2) Laboratori Nazionali di Frascati (LNF) dell'INFN, Frascati (Rome), Italy
(3) University of California at San Diego, CA, USA,
(4) Italian Air Force, Rome, Italy
(5) Lunar Geotechnical Institute, Lakeland, FL, USA
(6) University of Rome Tor Vergata and INFN-LNF, Rome, Italy
(7) CNR-IAC and INFN-LNF, Rome, Italy
(8) ASI-Space Geodesy Center (CGS), Matera, Italy
(9) NASA Goddard Space Flight Center, Greenbelt, MD, USA

Abstract

Over the past forty years, Lunar Laser Ranging (LLR) to the Apollo Cube Corner Reflector (CCR) arrays deployed on the surface of the Moon has supplied almost all of the significant tests of General Relativity (GR), that is, it has evaluated the PPN parameters and addressed, for example, the possible change in the gravitational constant and the self-energy of the gravitational energy. In addition, it has provided significant information on the composition and origin of the Moon through measurement of its rotations and tides. Initially the Apollo lunar arrays contributed a negligible portion of the error budget used to achieve these results. Over the decades, the performance of ground stations has greatly improved so that the ranging accuracy has improved by more than two orders of magnitude. Now, after forty years, the existing Apollo retroreflector arrays contribute significantly to the limiting error to the range measurements. The University of Maryland, which was the Principal Investigator for the original Apollo arrays, is now proposing a new approach to the lunar laser CCR array technology. The investigation of this new technology is currently being supported by two NASA programs (LSSO, the Lunar Sortie Scientific Opportunities, and CAN, a NASA Lunar Science Institute Cooperative Agreement Notice) and by INFN. Thus, after installation on the next lunar landing, the new arrays will reduce the contribution of the lunar emplacement by more than two orders of magnitude, from the centimeter level to the micron level. The new fundamental physics and the lunar physics that this can provide will be discussed. In the design of the new array, there are three major challenges: 1) Address the thermal and optical effects of the absorption of solar radiation within the CCR 2) Reduce the transfer of heat from the hot housing and from the rapid temperature changes of the regolith to the CCR and 3) Define a method of emplacing the CCR package on the lunar surface such that it is stable over the lunar day/night cycle. The design approach, the computer simulations using Thermal Desktop and the housings of the new CCR that have been built by INFN-LNF will be presented. Thermal and optical vacuum testing will be conducted at the "Satellite/lunar laser ranging Characterization Facility" (SCF) at INFN-LNF, Frascati. Finally, we also discuss the innovations over the Apollo arrays and current satellite retroreflector packages. This new concept for a CCR for Lunar Laser Ranging is being considered for the NASA Manned Lunar Landings, for the NASA Anchor Nodes of the

International Lunar Network and for the MAGIA lunar orbiter mission proposed to the Italian Space Agency.

Second Generation Lunar Laser Ranging for the 21st Century

The three Apollo and the Lunakhod arrays have provided the best evaluation of General Relativity of any experiment. In particular, LLR gives the most accurate measurements of the De Sitter effect in GR (PPN parameter □) and of Yukawa-like deviations from the $1/r^2$ force-law. Together with laboratory tests at very small distances, LLR gives the most accurate test of the Weak Equivalence Principle (EP). It also allows for a unique, 10^{-4}-level test of the Strong EP. The EP is the heart of GR. Current limits are shown in Table 1, together with the tighter constraints that can be reached with a 2nd generation CCR array.

Table 1. Limits on gravity tests based on current, first generation LLR data and expected physics reach for second generation LLR.

Phenomenon	1st Generation Limit with current LLR accuracy	2nd Generation Limit with 1 mm LLR	2nd Generation Limit with 100 ⌈m LLR	Measurement Time scale
Weak Equivalence Principle, WEP (⊗a/a)	10^{-13}	~ 10^{-14}	~ 10^{-15}	2 yr
Strong Equivalence Principle, SEP (Nordvedt parameter)	4×10^{-4}	~ 10^{-5}	~ 10^{-6}	2 yr
Gdot/G	10^{-12}/yr	~ 10^{-13}/yr	~ 10^{-14}/yr	4 yr
Geodetic Precession (PPN param. ®)	~ 5×10^{-3}	5×10^{-4}	~ 5×10^{-5}	6-10 yr
Deviations from $1/r^2$ (Yukawa parameter ⟨)	10^{-10}	~ 10^{-11}	~ 10^{-12}	6-10 yr

In 2006 a 2nd generation LLR experiment (LLRA21, Lunar Laser Ranging Retro-reflector Array for the 21st Century) has been proposed to LSSO, target to manned landings, by a US-Italy team led by UMCP (PI is D. G. Currie) and co-led by INFN-LNF. The Italian team participates at zero cost for NASA. In 2006, INFN-LNF and UMCP also proposed a robotic version of the project,

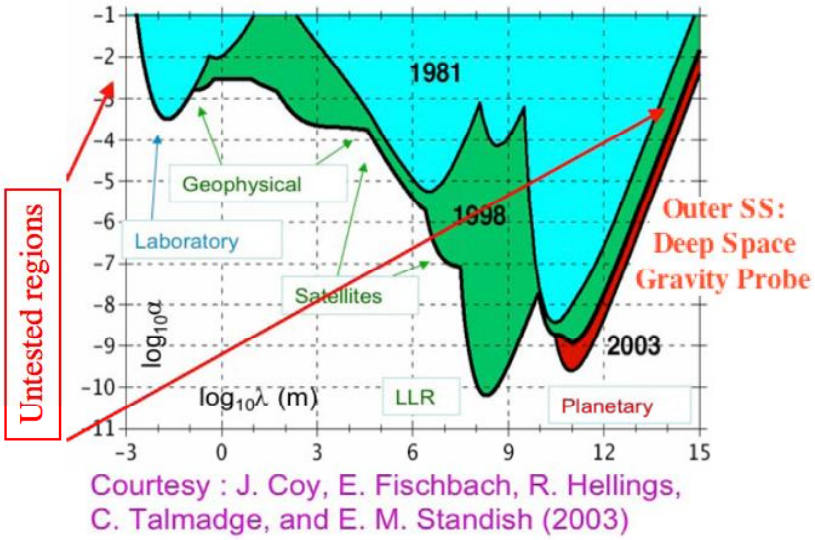

Figure 1. Limits on Yukawa deviations from the $1/r^2$ force-law.

MoonLIGHT (Moon Laser Instrumentation for General relativity High-accuracy Tests) for an ASI Study (Observation of the Universe from the Moon). For NASA and ASI we developed a new LLR payload capable of improving the space segment contribution to LLR by a factor 100 or more. This will be achieved by replacing the 38mm Apollo CCRs with a sparse array of single, 100mm CCRs, separated by few tens of meters in order that their laser returns yield separate signals on the Earth detectors. Such an array will not suffer from the time broadening of the return pulse from the Apollo arrays due to the Moon librations. This effect currently dominates the error budget and limits the LLR accuracy to ~2 cm (see Fig. 2). Note that the replacement of the Apollo CCRs must be followed by improvements of the ground segment of LLR, that is, of the atmospheric corrections, hydrogeological loading of the Earth crust, laser pulse length, laser readout electronics, etc. In the decades following the Apollo missions, the wide geodesy, planetology and laser-user communities made very significant progress in their fields, which allowed for the major success of 1st generation LLR shown in Fig. 2.

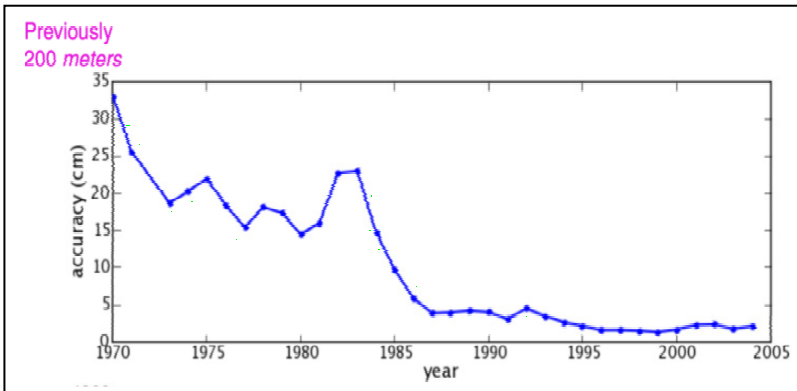

Figure 2. Historical accuracy of 1st generation LLR.

SCF thermal testing of the LSSO CCR was done in 2008 (fig. 3) at INFN with the measurement of the CCR solar absorptivity (3-4%). This drives the thermal distortions of the optical far field diffraction pattern back to the Earth. The CCR has been manufactured with 0.2 arcsec dihedral angle offsets specs, a factor 2.5 tighter than the standard. The FFDP test of the CCR inside the SCF is planned for spring of 2009. This SCF-Test is an effective and innovative tool for precision experimental tests of gravity, GNSS and space geodesy [1].

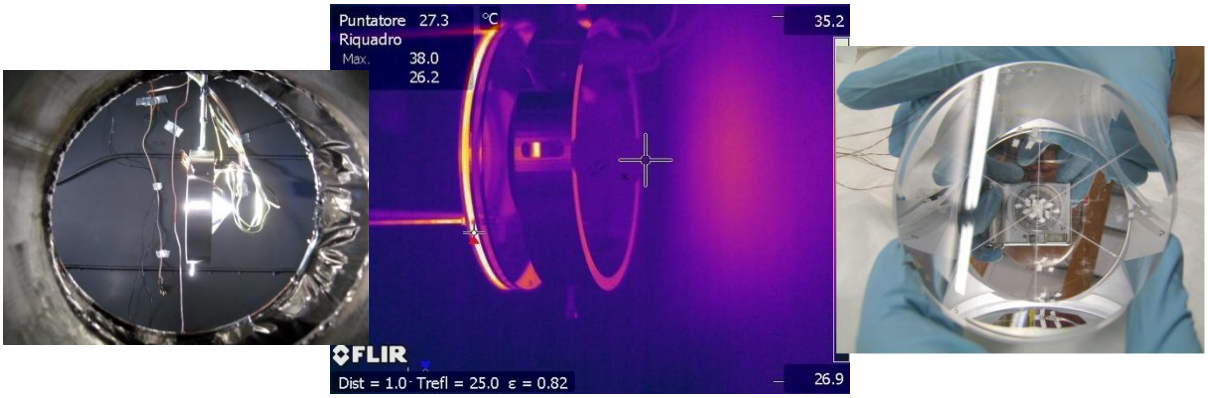

Figure 3. LSSO CCR (top left). Thermal test in SCF: bottom left photo and right (IR photo).

A new theory that can be tested with 2nd generation LLR is the braneworld theory of [2]. This is a unified quantum theory of weak gravity at horizon scales, which explains the apparent acceleration of the universe without Dark Energy and predicts a correction to the Moon

geodetic precession by about 1mm/orbit. The GR geodetic precession is about 3m/orbit and is currently well measured with a precision of 2 cm. This braneworld theory cannot be tested with 1st generation LLR but it will be weill in the domain of an LLRA21/MoonLIGHT array.

The International Lunar Network (ILN)

On July 24, 2008 space agencies (including ASI) met for the 2nd time at NASA-AMES and signed a Statement of Intent (SoI) to establish a network of 6 to 8 nodes of agreed core instruments deployed with robotic missions [3]. Agency representatives are called the ILN Steering Group, chaired by J. L. Green, Director of NASA SMD/Planetary Science Division. Working groups were also formed with members of the international scientific community designated by the national space agencies: Core Instrument Working Group (CIWG, in which INFN-LNF participates); Communications; Enabling Technologies, particularly devoted to the generation of power on the Moon; Site Selection, to be formed in spring 2009.

NASA is preparing a mission, now in Phase A, to establish four initial "Anchor Nodes" with a single ATLAS V launch no earlier than 2016. The US science definition team (SDT) completed a final report, which foresees a "baseline mission" with four core instruments per node (in priority order: seismometer, heat-flow probe, E&M sounding, CCR) and a "floor" mission only one instrument (the seismometer). The report also states: *The SDT recommends that the Anchor Nodes operate as part of a larger network for a minimum of six years to capture the 6-year lunar tidal period.* It is not clear which country will lay the 1st ILN node.

The SDT specs for the CCR are: ~10cm diameter, ~1Kg reflector weight (with ~1Kg extra weight for the CCR deployment). The CCR developed for LSSO and studied for ASI meets these specs, and it could be a natural candidate for the ILN (if expectations on the space FFDP performance are confirmed by SCF-Testing and further modeling). To get the factor >100 improvement we need the capability of emplacing the payload as described below and shown in fig. 5 and 6. Thus, a synergy is possible with the any drilling work, like the one required for the heat-flow experiment. A description of our work has been submitted by UMCP on Dec. 19, 2008, in response to the Request for Information (RFI) issued by NASA for its Anchor Nodes. Other responses to this RFI have been submitted by the Italian scientific community.

Additional missions, which could contribute to the ILN are MoonLITE by the BNSC and Selene-2 by JAXA, both now in Phase A. MoonLITE includes a relay satellite and 5 penetrator payloads for geophysics studies. Selene-2 includes one orbiter and two landers.

We report some conclusions of the CIWG work at the 3rd ILN meeting, which took place in Yokohama (Japan) on March 12-13, 2009. The CIWG finalized its Term of Reference, defined the ILN as "few-msec simultaneous and/or multi-site measurements", identified areas of common participant interest and finalized a list of four core science/instrument:

- Seismometry
- Heat flow
- E&M sounding
- Laser Ranging for Lunar Geodesy and Test of General Relativity.

The CIWG also identified a list of "outer" core science/instrument list: (i) Exploring unsampled lithology; (ii) VLBI to measure the Moon rotation; (iii) New astronomy from the

Moon (including radio observations from the far side); (iv) New Fundamental Physics (including unified theories like [2] and strange quark matter [4]).

Unlike for US Anchor Nodes, the above ILN lists are not prioritized. All landing site activities will require knowledge of the geological context (ie, it will required a Camera). The CIWG and the ILN Steering Group agree that this is a living list and that to finalize its work the CIWG will produce a White Paper to be approved at the next ILN meeting (the 4th).

We believe that in the long-term the ILN nodes will define the International Moon Reference System (IMRF), referenced to the ITRF: near (far) side nodes will be referenced with respect to the ITRF by direct LLR and radio/mw measurements (relay satellites); ILN nodes will also provide an absolute altitude reference to orbiters instrumented with a laser or radio altimeters.

Thermal Design and Emplacement of the Payload for NASA's LSSO and the ASI Study

Particular care has been devoted to the payload thermal design and to the choice of the materials used for the CCR mounting cavity. This assembly drawing of the inner housing illustrates the mounting of the CCR (designed to withstand the launch environment and yet have a very low thermal conductivity) and the internal screen to prevent the hot housing from radiating heat to the CCR and thus degrading the FFDP. The internal screen is coated, inside and out, with polished gold with <2% emissivity).

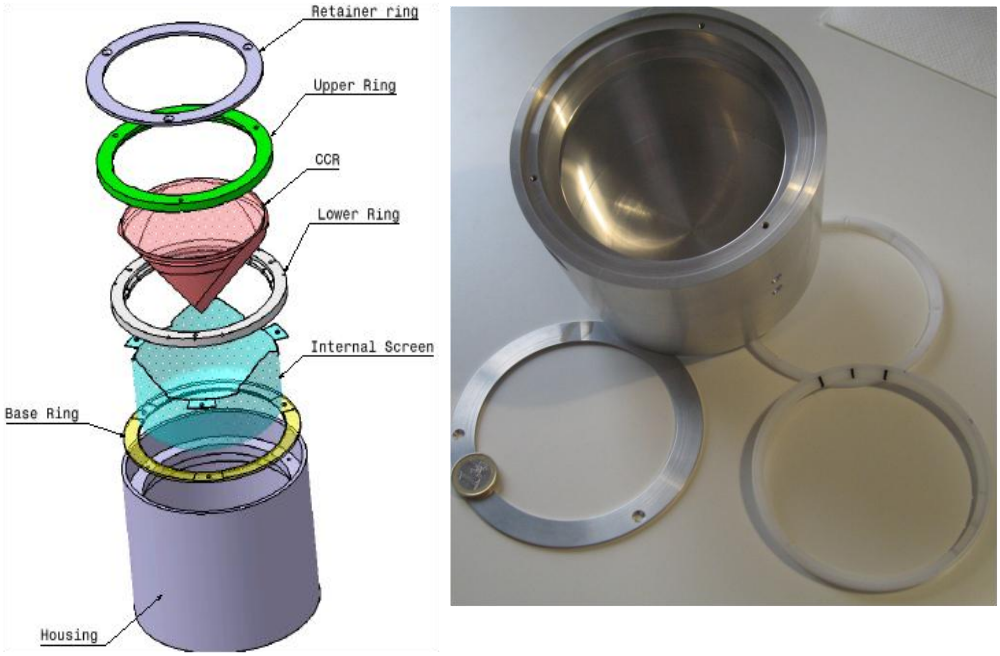

Figure 4. Illustration (photo) of 2nd (1st) CCR housing built at LNF show at left (right). The lower ring (to be made of KEL-F plastic) has line inserts (in black) to reduce heat flow from the cavity to the tabs of the CCR. This is an improvement of the Apollo and LAGEOS design.

The emplacement of the latter into the lunar soil will be done with an Invar or ULE foot, inserted ~1m meter deep into the regolith, where the temperature has only a few degree K excursion. A 2m×2m thermal blanket will be deployed around the CCR to stabilize locally the environment. We are performing detailed simulations to model the temperature distribution in the regolith to address the effect of the proposed MLI thermal blanket. The purpose of this thermal blanket is to isolate the regolith mounting of the CCR from the

thermal and mechanical effects of the lunar day/night cycle in the regolith. Simulations indicate that the temperature under the blanket changes very little.

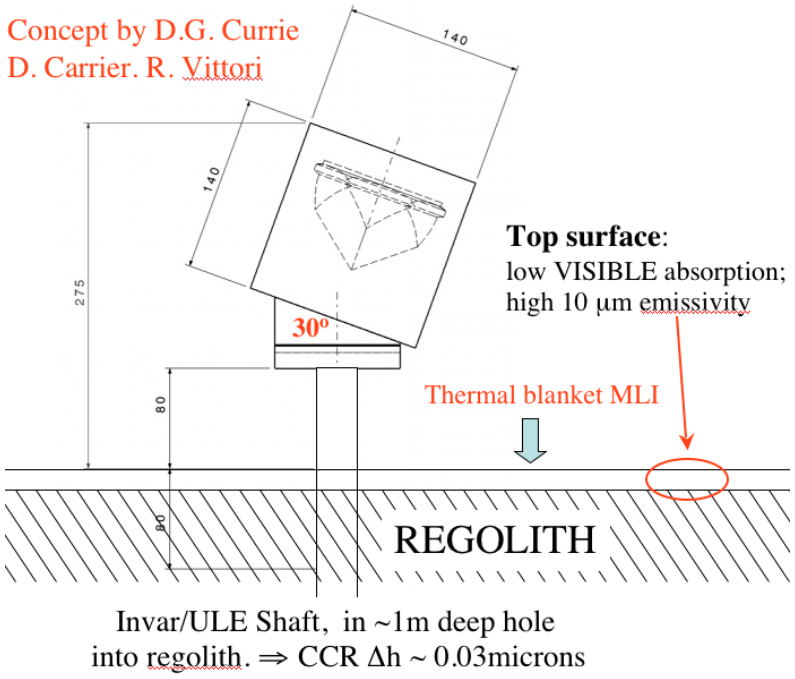

Figure 5. Emplacement concept developed for NASA's LSSO and the ASI Study.

The concept of fig. 5 is to be completed by an outer shield (Mushroom or "Bubbola", in Italian), which surrounds the inner housing and optimizes the response to the external thermal environment (solar and IR radiation from regolith). It absorbs little of the solar radiation and has a high emissivity on the top. The angle prevents strong heating from the lunar regolith. The bottom is close to the surface to shield the portion of the thermal blanket under the outer housing from the solar radiation.

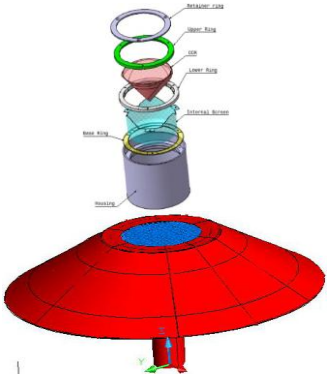

Figure 6. Inner housing, outer Bubbola

The ASI Lunar Orbiter Mission MAGIA

In February 2008 ASI approved for Phase A five proposals presented in response to its call for "Small Missions" issued in 2007. One of these is MAGIA (Missione Altimetrica Gravimetrica GeochImica Lunare), an altimetry, gravimetry and geochemistry lunar orbiter mission. The MAGIA Principal Investigator is A. Coradini of INAF-IFSI Rome, Prime Contractor is Rheinmetall Italia S.p.A.

Using two retroreflector, atomic clock, acceleratometer and radio science payloads, INFN and UMCP proposed for MAGIA the improved measurement of the gravitational redshift, a precursor test of the functionality of the MoonLIGHT CCR and a direct measurement of the position of the selenocenter with respect to the ITRF. The latter will reference the altimetry and the gravity models of MAGIA to the ITRF, thanks to the precise and absolute positioning granted by two onboard CCR arrays. The redshift measurement will provide a high-level

validation of the gravity model built with the MAGIA radio science experiment and the accelerometer. In the future the Moon altimetry model will be needed to select landing sites, while the gravity model will ensure that spacecrafts can safely navigate to and return from the Moon. Concerning the ILN goals, the MAGIA PI expressed the hope that the science goals of current and future orbiter missions and of the ILN be kept complementary and synergetic.

The Phase A study was completed and the proposal for the following B/C/D/E/F Phases was submitted to ASI in December 2008. MAGIA is now awaiting the ASI decision.

Acknowledgments
We thank NASA and INFN-LNF for supporting this Program in the last 3 years and ASI for supporting the 2007 MoonLIGHT Study. We also wish to warmly thank A. Coradini and C. Baldetti of INAF-IFSI Rome, C. Dionisio and A. Di Salvo of Rheinmetall Italia for their many useful suggestions and friendly collaboration and technical help.

References

[1] *Creation of the New Industry Standard Space Test for Laser Retroreflectors for GNSS, Fundamental Physics and Space Geodesy: the SCF-Test*, S. Dell'Agnello, G. O. Delle Monache, D. G. Currie, R. Vittori, et al, INFN-LNF Report LNF-09/02(P).
[2] *The Accelerated Universe and the Moon*, Dvali, G., Gruzinov, A., Zaldarriaga, M., Phys. Rev. D 68 024012 (2003).
[3] *Statement of Intent of the International Lunar Network*, promoted by NASA and signed at NASA-AMES on July 24, 2008 by many Space Agencies, including ASI.
[4] *Cosmic separation of Phases*, E. Witten, Phys. Rev. D, 272 (1984).

Laser Ranging to the Lunar Reconnaissance Orbiter: a Global Network Effort

Jan McGarry (1)**, Ronald Zellar** (1)**, Gregory Neumann** (1)**, Carey Noll** (1)**,**
Mark Torrence (2)**, Julie Horvath** (3)**, Christopher Clarke** (3)**,**
Randall Ricklefs (4)**, Michael Pearlman** (5)**, Anthony Mallama** (6)

(1) NASA Goddard Space Flight Center
(2) SGT Incorporated
(3) Honeywell Technology Solutions Incorporated
(4) University of Texas at Austin
(5) Harvard-Smithsonian Center for Astrophysics
(6) Raytheon Information Solutions

Jan.McGarry@nasa.gov/ +1-301-614-5867

Abstract

The Lunar Reconnaissance Orbiter (LRO) will launch in early 2009 carrying multiple instruments for lunar study including the NASA Goddard Space Flight Center built Lunar Orbiter Laser Altimeter (LOLA). Also part of the mission will be the Laser Ranging (LR) instrument, which consists of a 2 cm aperture receive telescope mounted on the High Gain Antenna and a fiber optic bundle from this aperture to one of the LOLA detectors. Laser Ranging to LRO is an uplink-only measurement where ground stations time-tag their laser fires and LOLA measures the receive times to better than 10 centimeter precision with sub-centimeter resolution. This information will be used to improve the orbital knowledge which in turn will support the lunar gravity model development.
While NASA's Next Generation Laser Ranging System (NGSLR) is the primary ground station for LR, multiple International Laser Ranging Service (ILRS) stations will also be supporting this historic mission, providing much better coverage than a single station could provide. Data from all of the participating ILRS stations will be sent to the LOLA Science Operations Center (SOC) where ground fire events will be matched with LOLA events and ranges produced. Coordination of the global effort will be at the Goddard Space Flight Center, where predictions and schedules will be created, data archived (CDDIS), and an LR science product generated (LOLA SOC).

Introduction

This paper provides the status of the preparations for global LR support, and gives an overview of the scheduling, data-transfer, and real-time LR website feedback from the spacecraft.

LOLA's Earth Range Measurement

LOLA uses one of its five detectors to measure events coming from Earth. The Earth Window is the time when the detector is gated on, and this occurs in the first 8 milliseconds of every one of LOLA's 28 hz cycles. LOLA does not fire its lunar laser until approximately 9 milliseconds into the 28 hz cycle to avoid any collision between Lunar and Earth events.

LOLA's 28 hz cycle is synchronized to the raw spacecraft Mission Elapsed Time (MET). When the MET second rolls over, the spacecraft 1 pps signal is sent and LOLA's first 28hz cycle begins. The LRO Mission Operations Center (MOC) keeps track of the relationship between MET and UTC. At launch the knowledge will be better than +- 3 millseconds. This information should improve by several orders of magnitude shortly into the data-taking part of the mission.

The LOLA LR measurement is made with a single-stop timer. Because of the large field of view of the LR telescope (30 milliradians), the noise power can be 5 nanoWatts or greater when the High Gain Antenna is pointed to a fully sunlit Earth. The onboard software will increase the threshold to compensate for this high noise power but it cannot reduce it completely. For high noise situations ground station laser pulses that arrive early in LOLA's Earth Window will have a higher probability of being detected than those arriving later in the window.

The LOLA onboard software performs signal processing on the LR events at one second intervals using Poisson statistics to determine the ground pulses from noise. The software should be able to recognize signals from stations firing synchronously at rates of 7 hz or greater. The LOLA energy monitor should also register when ground system pulses are detected in the Earth Window.

Participating Stations

NGSLR will be the primary LRO laser ranging station and will fire at LRO every opportunity that the Moon is above 20 degrees elevation at the station, LRO is on the near side of the Moon, there is no local precipitation, and the LRO Go/No-Go flag is set for "go". NGSLR fires synchronously to LOLA at 28 hz, meaning that NGSLR uses the MOC supplied UTC to MET conversion, takes into account the range to the spacecraft, and only fires its laser when the resultant pulse would arrive at the spacecraft when the LOLA Earth Window is open.

McDonald Laser Ranging Station (MLRS), operated by the University of Texas at Austin under a contract with NASA, will also participate in LRO-LR. MLRS will fire asynchronously at their normal 10 hz rate which will ensure a minimum of 2 events per second in the LOLA Earth Window. MLRS will fire at LRO in a non-interference basis with SLR operations.

Other NASA associated stations that may provide support are MOBLAS-5 in Australia and MOBLAS-6 in South Africa. A modification to the MOBLAS systems to more precisely time the fires is being worked. The timing will be done with a separate computer and timing card so as not to interfere with SLR operations. The MOBLAS systems will fire asynchronously at 5 hz which will ensure a minimum of 1 event per second in the LOLA Earth Window.

Proposals have been received from Zimmerwald in Switzerland, Herstmonceux in Great Britain, Mount Stromlo in Australia, and Wettzell in Germany. All have been accepted for participation and two have formally signed agreements with the LRO project. All of the stations are expected to try synchronous ranging to LRO. Most of the stations have to operate in a configuration different from SLR in order to prevent possible damage to the LOLA detector. Agreed upon configurations will be listed in all of the formal Agreements.

Table 1. Participating stations and their characteristics. LRO-LR requirements are for an energy density of 1 to 10 femtoJoules per square centimeters at the spacecraft. Stations marked with an asterisk (*) do not yet have a final configuration agreed upon for ranging to LRO.

	Synch to LOLA?	Firerate (Hz)	# / sec in LOLA window	Expected energy at LRO (fJ per sqcm)
NGLSR	Yes	28	28	2 to 5
MLRS*	No	10	2 to 4	1 to 10+
Zimmerwald	Yes	28	28	1 to 3
Herstmonceux	Yes	7 or 14	7 or 14	1 to 3
Wettzell*	Maybe	7 or 10	2 to 7	1 to 10+
Mt Stromlo*	Yes	28	28	1 to 10+
MOBLAS	No	5	1 to 2	1 to 3

Station Scheduling

Each week an LR schedule will be generated which will give the requested firing times for each of the participating stations. Each system will decide which of the times they can support. Stations are requested not to fire at LRO outside of the scheduled times.

Initially only one station will be scheduled at any given time. This will allow the LOLA Science Team to work individually with each system's data and will also allow each system to test out the LR website feedback from LOLA (discussed later in this paper).

Eventually two or more stations may be scheduled during overlapping periods. Since LOLA is a single stop system, only the first event in the Earth Window will register and therefore multiple 28 hz stations would be competing for the same single stop in each window.

Data Products and Flow

LRO predictions will be generated by the NASA Goddard Space Flight Center Flight Dynamics Facility (FDF). These predictions are in the ILRS standard Consolidated Prediction Format (CPF). LRO will be in a polar orbit at approximately 50 km above the surface of the Moon. The predictions give the rectangular coordinates of the spacecraft's location from the center of the Earth in an Earth rotating coordinate system. The accuracy of these predictions will be better than 4 km (3D, 3 sigma). Predictions will be updated daily and will span a 10 day period of time. Only organizations that have signed Agreements with the LRO Project will be given access to the predictions.

The normal satellite CPF software as found on the ILRS website (Ricklefs 2006) can be used to generate pointing angles and range from the predictions. The LRO predictions as supplied are already point-ahead predictions, so the on-site software should not attempt to correct these predictions to make them point-ahead.

LRO fire times, weather information, and ancillary data from all stations will be sent into the LRO project in the new ILRS Consolidated Ranging Data Format (CRD) with the exception of the MOBLAS systems which will use an internal Transponder Data Format (iTDF). The CRD format can be found on the ILRS website (Ricklefs 2008). NGSLR will format its data

in both iTDF and CRD formats. All LRO ground station data will be sent through Honeywell at Goddard Corporate Park where it will be grouped together and placed on CDDIS (Noll 2007). The LOLA SOC will pick up the ground system fires and match those with the LOLA event times to form one-way ranges to LRO. These one-way ranges will be placed back on CDDIS where they will be available to all of the participating organizations.

The information to convert UTC to MET and back is contained in the SCLK files. One file contains piecewise continuous linear functions relating the spacecraft UT to UTC. A second file contains an offset between spacecraft UT and the raw spacecraft MET. These files are only needed for stations that will fire synchronously to LOLA. After launch the information in the SCLK files is expected to change very infrequently.

Similar to ICESat, LRO-LR will have a Go/No-Go file that the LRO mission will use to control the firing of the ground stations (Gurtner 2005). The Go/No-Go flag is expected to be turned to "nogo" only during calibrations, maneuvers or emergencies, or any time that the High Gain Antenna is not facing Earth.

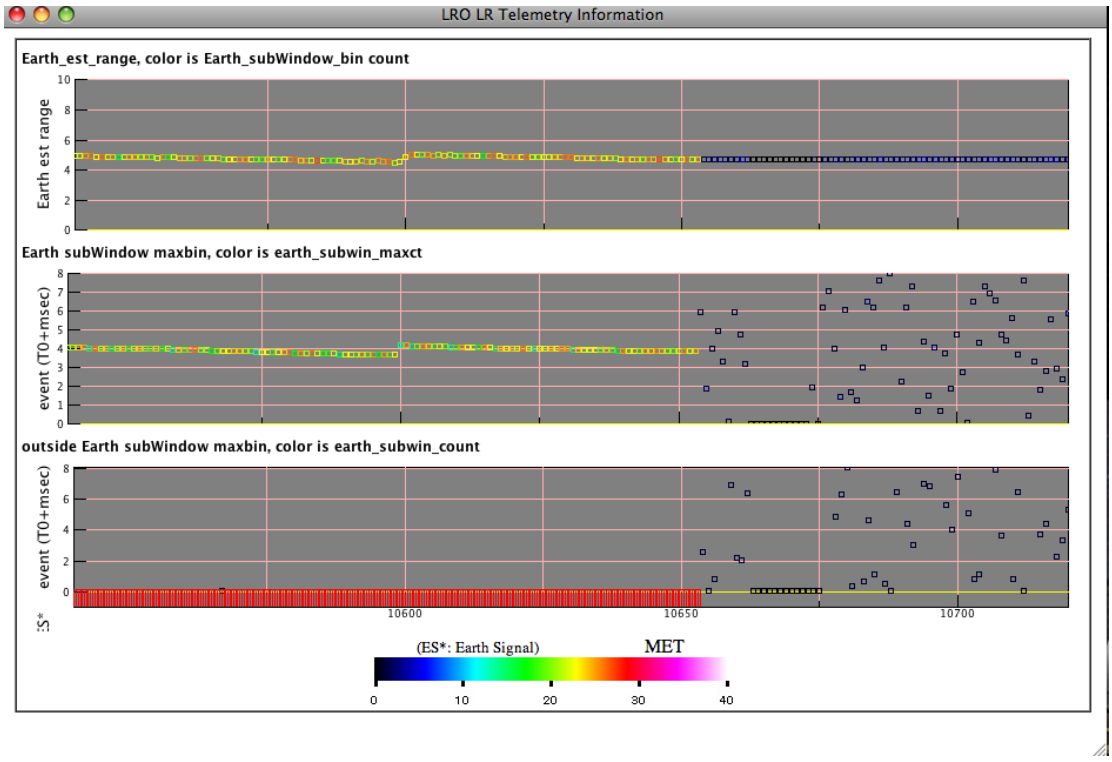

Figure 1. LRO-LR website displaying LOLA one second signal processing information of Earth Window data. The vertical axis is the Earth Window in milliseconds. The horizon axis is elapsed time in seconds. The dots in the top window represent LOLA's estimated location of the ground signal in the window. The color of each dot shows the number of receive events in that estimate. The middle window gives similar information but with a different signal processing which can pick up weak results from ground stations. The lower window attempts to capture receive events from a second ground station. Also shown in the lower window is the signal flag (red mark if LOLA believes LR signal is present). Real-time data flows from right to left. The left half of this plot shows LR signal events as seen by LOLA. The signal stops about half way through this plot and from then on the plot contains only noise.

Feedback to Stations

The LOLA signal processing and energy monitor information will be sent down in the LOLA House-Keeping (HK) packets in real-time. The HK packets will flow to the LOLA SOC where the relevant information will be displayed to a website as shown in Figure 1 (Torrence 2009). This information should be less than 30 seconds stale. The ground stations can make use of this website to determine if their pulses are being detected at LOLA. Synchronous stations, especially those with 28 hz fires, should be able to use the signal processing information, while all stations can make use of the energy information.

This website will also display the data received from each station over the past week so that each station can determine if all of its data is getting to the LOLA SOC.

Summary and Acknowledgements

LRO-LR laser ground stations will not only be supporting LRO and lunar science, but they will be taking some of the ILRS's first steps into planetary laser ranging. The LRO-LR Team and the LOLA Science Team would like to thank all of the ground stations who are participating in this mission.

The authors would like to thank the LOLA Principal Investigators, David Smith and Maria Zuber, for their support of laser ranging to LRO, and a special thanks to the LR Instrument Scientist, Xiaoli Sun, for his initial concept of LRO-LR, and for his continued technical support.

The launch is currently scheduled for late May 2009 with LR operations expected to start about a month later.

References

Gurtner, W., *Restricted Laser Tracking of Satellites*, http://ilrs.gsfc.nasa.gov/satellite_missions/restricted.html, May 2005.

Noll, C., Torrence, M., Seemueller, W., *Laser Ranging Archiving and Infrastructure Support through the ILRS Data Centers and Web Site*, 15th International Workshop on Laser Ranging, Canberra, Australia, October 2006.

Ricklefs, R., *Consolidated Laser Ranging Prediction Format*, http://ilrs.gsfc.nasa.gov/products_formats_procedures/predictions/cpf.html, Feb 2006.

Ricklefs, R., Moore, C., *Consolidated Laser Ranging Data Format*, http://ilrs.gsfc.nasa.gov/products_formats_procedures/crd.html, June 2008.

Torrence, M., *LRO-LR website*, http://lrolr.gsfc.nasa.gov, 2009.

Pre-Launch Testing of NGSLR Ranging to LRO

Anthony Mallama (1,2)**, Jan McGarry** (1)**, Tom Zagwodzki** (1)**,**
Jack Cheek (1,2), **Christopher Clarke**(1,3)

(1) NASA Goddard Space Flight Center
(2) Raytheon Company
(3) Honeywell Technical Solutions Inc.

anthony.mallama@gmail.com

Abstract

A comprehensive test program for NASA's Next Generation Satellite Laser Ranging (NGSLR) system is being conducted as the development phase nears completion. A subset of those tests pertaining specifically to tracking the Lunar Reconnaissance Orbiter (LRO) spacecraft fall into three functional categories, namely, (1) the telescope must track LRO, (2) LRO must be scheduled as the highest priority target, and (3) NGSLR software is correctly modified for LRO. This document describes the subtest of LRO-related tests and focuses on three examples to demonstrate testing procedures. The LRO testing program has been successfully completed and NGSLR is prepared for operational tracking once the spacecraft is lunar orbit and is ready to receive laser pulses from Earth stations.

1. Introduction

NGSLR will be used for one-way ranging to LRO with the goal of providing an improved lunar gravity field and a precise spacecraft orbit. Data from the Lunar Orbiter Laser Altimeter (LOLA) instrument can then be referenced to the orbit to facilitate high accuracy surface mapping.

NGSLR has a 28 Hz, 50 milli-Joule laser for tracking LRO, in addition to the 2000 Hz eye-safe laser for Earth orbiting satellites. The laser ranging telescope is mounted on the high gain antenna which normally points toward the Earth. A fiber optic bundle carries light from the ranging telescope to the LOLA receiver. Meanwhile, the telescope for altimetry points to nadir, and thus the receiver can be used for altimetry and ranging. The 28 Hz LOLA duty cycle has separate time windows for receiving lunar reflected pulses from its own laser and Earth pulses. Thus, one testing criteria is that NGSLR pulses will arrive at LRO during the 8 milli-second Earth window.

The overall testing program for NGSLR has 137 elements including 19 that pertain specifically to tracking LRO. Each of the 19 LRO tests falls into to one of three functional categories described in section 2 and each includes a set of criteria for success. Testing procedures involve operating the NGSLR system, running test scenarios, and comparing logged data with expected results. Interplanetary calculations make use of SPICE software, ephemeris kernels and clock files. Simulation is being used in order to complete the test program before the spacecraft is launched.

The following tests will be described in some detail. In section 3, the arrival time of laser pulses during the Earth window will be demonstrated using SPICE calculations. Section 4 illustrates the results of manually controlling the laser fire offset and frequency. Finally, in

section 5 correct and accurate telescope pointing will be validated using photographic images of the Moon taken through the NGSLR telescope.

2. Functional Test Categories

There are three levels of requirements recognized in the overall testing plan for NGSLR. The highest one is identified as mission level or level 1, and the requirement to track LRO is number 8 of all the NGSLR mission requirements. Thus, the test numbers in this document all begin with '8' in conformance with the general testing plan.

Proceeding directly from the LRO mission requirement are the following functional level requirements, also known as level 2: 8.1, the telescope must track the LRO spacecraft; 8.2, LRO must be scheduled as the highest priority target; and 8.3, NGSLR software is correctly modified for LRO.

Testing level requirements, level 3, follow from the functional requirements listed above. The hierarchy from mission through test requirements is shown below.

8. Lunar Reconnaissance Orbiter Requirements
    - 8.1 The telescope must track the LRO spacecraft
        - 8.1.1 The telescope commanded pointing is correct
        - 8.1.2 The telescope actual pointing is correct
    - 8.2 LRO must be scheduled as the highest priority target
        - 8.2.1 When the Moon is above 20 degrees LRO is scheduled
        - 8.2.2 LRO is scheduled as the highest priority target
    - 8.3 NGSLR software is correctly modified for LRO
        - 8.3.1 Laser pulses hit the LR receiver in the LOLA Earth window
        - 8.3.2 The software functions correctly when no returns are received
        - 8.3.3 No satellite search takes place
        - 8.3.4 Biases are not applied automatically
        - 8.3.5 LRO is the sole target and it is tracked whenever scheduled
        - 8.3.6 Manual control of laser fire including offset and frequency
        - 8.3.7 All fires are recorded
        - 8.3.8 Output data is in ITDF format
        - 8.3.9 The LRO-LR web site is displayed to the operator
        - 8.3.10 SCLK data can be input
        - 8.3.11 Laser parameters are automatically switched
        - 8.3.12 Go/NoGo restrictions are correctly processed
        - 8.3.13 The time of the laser fire is correct
        - 8.3.14 Signal processing parameters are correct for LRO
        - 8.3.15 The percentage of laser fires missing is acceptable

The following sections illustrate the procedures and results for tests 8.3.13, 8.3.6 and 8.1.2.

3. The Time of the Laser Fire is Correct (Test 8.3.13)

For this test the laser fire times from a log file were used as input to a SPICE program that used an SCLK file to compute their arrival time in the LOLA duty cycle. This cycle, illustrated in Figure 1, shows that the Earth window opens near the start of the cycle and ends approximately 9 milliseconds later.

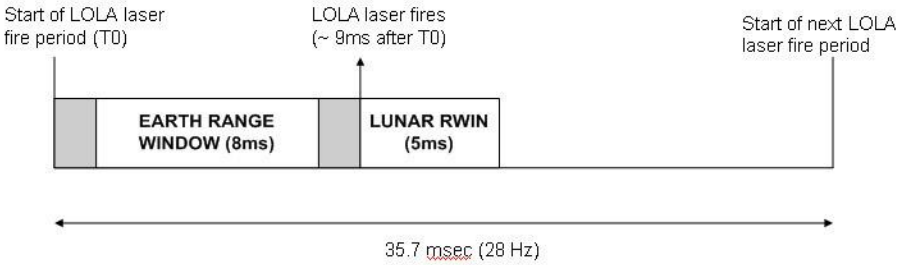

Figure 1. The LOLA duty cycle showing the location of the Earth Range Window.

The data portion of an SCLK file is shown below where the columns represent ticks of the spacecraft clock, ET seconds elapsed since the epoch of J2000, and the ratio of the rates of the spacecraft clock and ET, respectively.

SCLK01_COEFFICIENTS_85 = (
0.0000000000000E+00 3.1579264184000E+07 1.0000000010000E+00
1.5485503275008E+13 2.6786929218400E+08 1.0000000010000E+00)

Procedures:
1. Capture laser fire time.
2. Compare with off-line calculation.
3. Verify SCLK data usage.

Results
1. Captured fire times in two log files.
2. In Figure 2 and statistics below form the comparison.
3. Statistics: 99% of pulses arrive at 5.0 +/- 0.1 msec

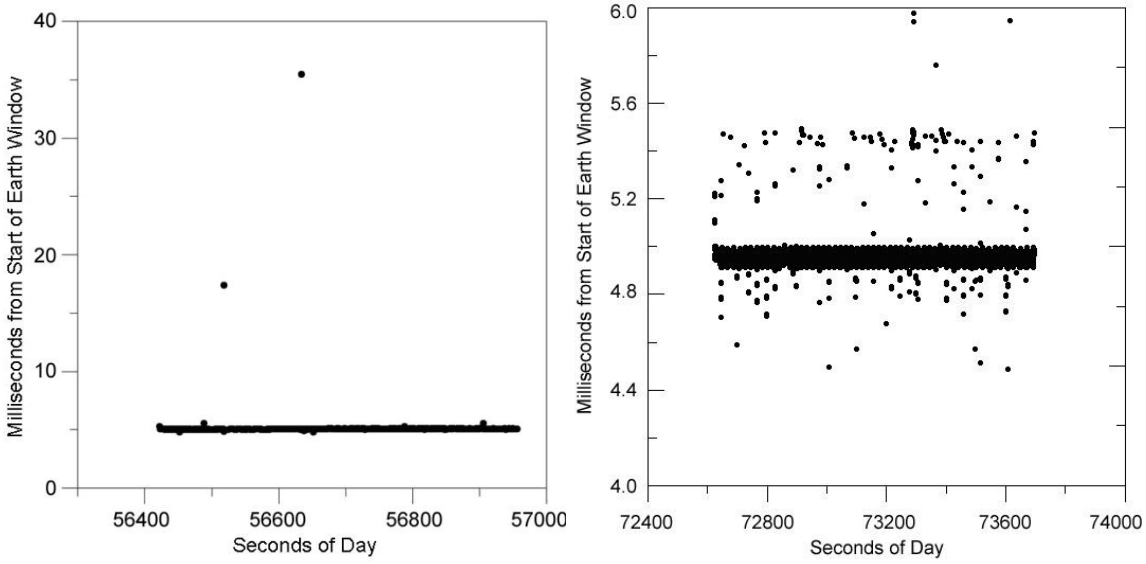

Figure 2. Two data sets of arrival times of pulses in the LOLA duty cycle.

4. Manual Control of Laser Fire Including Offset and Frequency (Test 8.3.6)

Offsets can be commanded from +35.7 milliseconds to minus that same magnitude and the frequency can be changed from +100 microseconds per second to minus that magnitude. The test is to analyze fire times when offset and frequency changes occurred and to compare commanded and measured values.

Procedures:
1. Identify the LRO pass.
2. Manually adjust the laser fire offset and frequency (both separately and together) and record those adjustments.
3. Verify that the log and message files recorded the manual offset and frequency adjustments.

Results:
1. Ran a simulated track of LRO on 2006 August 21 at 18:50.
2. Commanded a comprehensive set of frequency and offset changes.
3. Shown in Figure 3 on the left are offset of +2, 0 and -2 milliseconds versus time. On the right are the intervals between fires during a frequency change versus time.

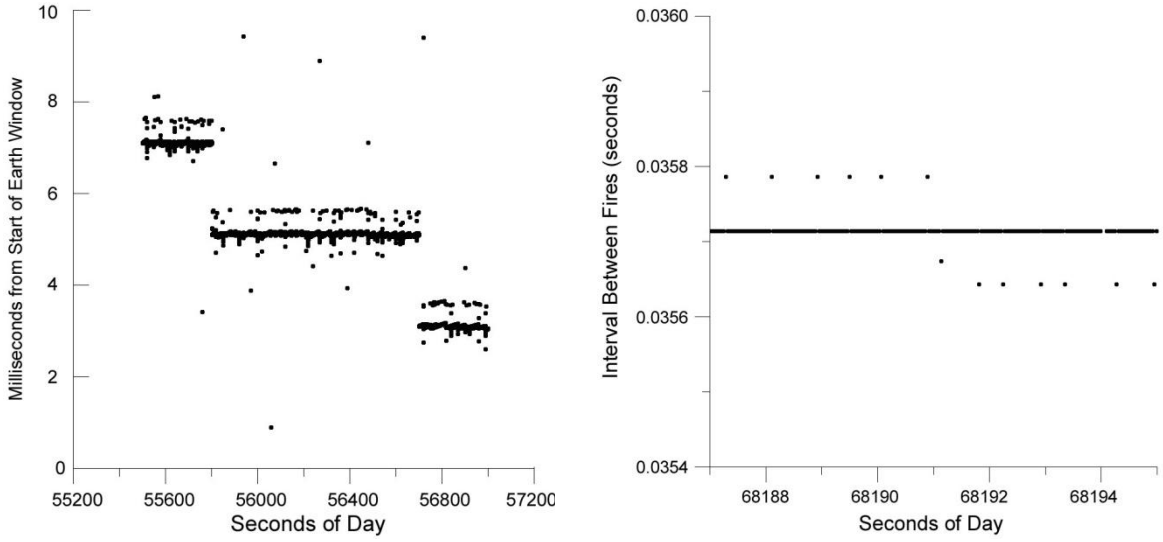

Figure 3. Left – arrival times of pulses. Right – interval between fires.

5. The Telescope Actual Pointing is Correct (Test 8.1.2)

In this test the pointing of the NGSLR telescope was verified using images of the Moon captured during a simulated LRO track.

Procedures:
1. Request Flight Dynamics Facility for dummy LRO pass including STK output
2. Run the pass and image the Moon with the star camera
3. Compute actual pointing based on identification of lunar craters
4. Record the differences in the sense 'actual minus STK'
5. Compute the statistics of the difference

Results:

Steps 1 and 2 were completed as specified.
Steps 3 and 4 are illustrated in Figures 4 and 5, and were augmented by a comparison of 'actual minus SPICE'.
Step 5. The statistics measured in arc seconds are in Table 1.

Table 1. Pointing differences of NGSLR versus STK and SPICE

Comparison	Root-mean-square Difference	Largest Difference
NGSLR versus STK	3.2	5
NGSLR versus SPICE	2.4	4

Intermediate results from Steps 3 and 4 are described below.

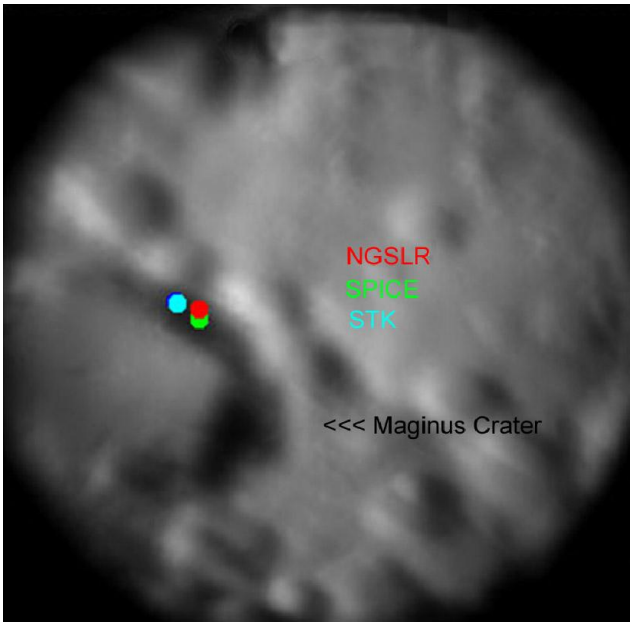

Figure 4. This image of a portion of the Moon was captured with the NGSLR star camera. The red dot indicates the location of the telescope pointing. Identification of lunar features, such as the crater Maginus in this case, and auxiliary information allowed the SPICE and STK positions to be superposed on the images as well.

SPICE coordinates were computed in a separate program. The main SPICE kernels were (1) NGSLR position from custom generated kernel, (2) Earth and Moon positions from DE421, (3) LRO position from a special orbit kernel obtained from FDF, and (4) the Lunar 'Mean Earth' reference frame. The SPICE point-ahead correction, XCN+S, was used. This corresponds to the transmission case computed with a converged Newtonian light time correction and stellar aberration applied.

The resulting lunar coordinates were then plotted on a USGS airbrushed shaded relief map that had been warped to correspond with the Unified Lunar Coordinate Network, ULCN2005. The sample image in Figure 5 (left) shows the plotted location of coordinates computed from the SPICE program. This location was then transposed to the NGSLR image of the Moon.

Finally, STK positions were transposed straight from images generated by the STK program. STK images indicate the position of LRO directly, as shown in Figure 5 (right).

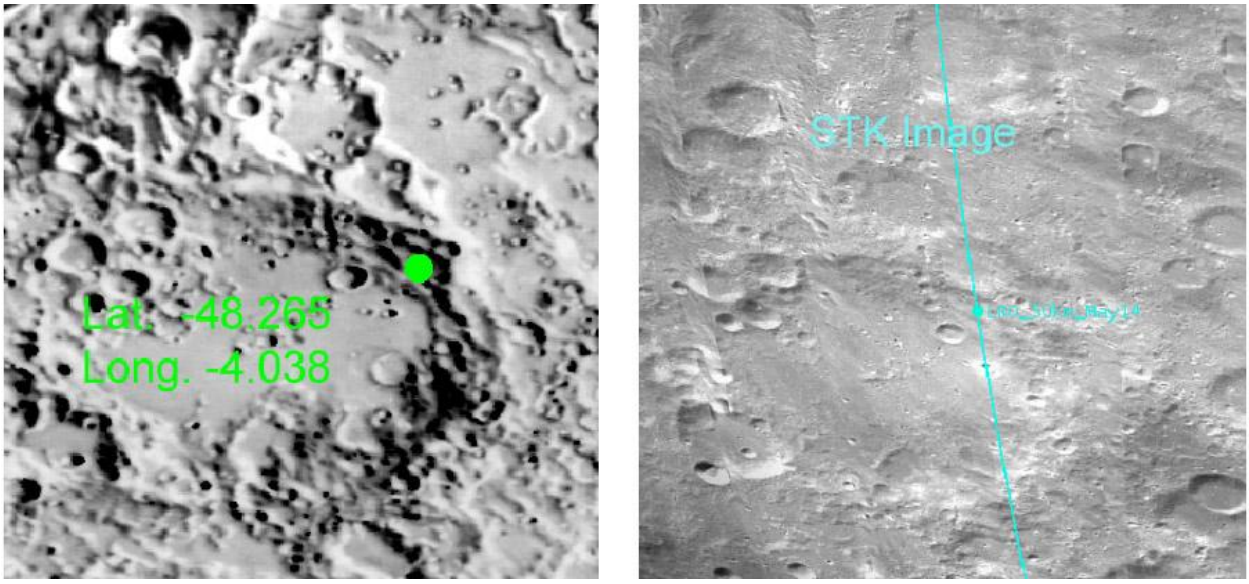

Figure 5. SPICE (left) and STK (right) coordinates plotted.

Laser Ranging (LR) Lunar Reconnaissance Orbiter (LRO) Data Flow and Scheduling

Christopher Clarke (1)**, Julie Horvath** (1)**, Jan McGarry** (2)**, Carey Noll** (2)**, David Carter** (2)**, Greg Neumann** (2)**, Mark Torrence** (3)

(1) Honeywell Technology Solutions Incorporated
(2) NASA Goddard Space Flight Center
(3) SGT Incorporated

Christopher.Clarke@honeywell.com

Abstract

The Lunar Reconnaissance Orbiter (LRO), soon to be launched in early 2009, will present new challenges to the NASA and ILRS communities, by adding new requirements for scheduling, data format, and data flow. These new requirements are necessary to help ensure the success of the on-board Lunar Orbiter Laser Altimeter (LOLA) payload instrument. The NGSLR and other approved ILRS sites will conduct one-way ranging to the lunar-orbiting spacecraft to meet the intensive orbit determination requirements needed to develop a new lunar gravity field. NASA and HTSI have coordinated with the LR-LRO mission and LOLA payload experiment team to establish new processes to meet the new data operations and data requirements. This paper will detail the coordination efforts for all LR-LRO scheduling activities for the approved ILRS sites, the coordination of all LR-LRO fire data reception at the HTSI Data Operations Facility, and all LR-LRO data delivery to NASA's CDDIS and LOLA Science Operations Center (SOC).

Introduction

This paper describes the LR-LR data products, scheduling requirements, and the data transfer time tables and schematics.

LR-LRO Data Products

The LR-LRO data products will include predictions in the Consolidated Prediction Format (CPF), LR fire time data in the Consolidated Laser Ranging Data Format (CRD) or an internal Transponder Data Format (iTDF), and combined ground fire and spacecraft event normal points in the CRD.

GSFC Flight Dynamics Facility (FDF) will generate the predictions daily. The prediction files will be in the CPF and contain ten days of predictions. They will be delivered to, and accessed on, a secure location to the CDDIS. The predictions will be used to generate station visibilities, and station schedules, and used for real-time tracking. Stations using the predictions for real-time tracking should not apply any point-ahead corrections because the time of flight of to the satellite is accounted for when generating the predictions.

LR LRO fire-time data will be generated at the LR sites in the CRD or iTDF. The data will be delivered to the ILRS Data Operations Centers (HTSI,EDC). The data in the CRD should be named with an ".frf" extension to differentiate it from other types of data in the CRD. Once at the HTSI Data Operations Facility, the fire data will be compiled together hourly,

compressed with UNIX compression, and delivered to a secure location in the CDDIS. The LOLA Science Team will combine the ground fires with corresponding spacecraft events and generate normal points in the CRD.

The format details for CRD and CPF can be found on the ILRS web-site (Ricklefs 2006, Ricklefs 2008). Format details for the iTDF can be found on LRO-LR web-site. (McGarry, 2006)

ILRS LR-LRO Schedules

A combined Global LR-LRO schedule will be generated for all approved ILRS tracking stations. This schedule will contain suggested ranging opportunities for each tracking station. A station may not range to LRO outside the suggested opportunities. The schedules will generate every Friday for the following Monday – Sunday week and will be delivered to and may be accessed from a secure site on the CDDIS.

LRO predictions in the CPF will be used to the generate schedule. An initial set of station visibilities will be generated based on a 20 degree minimum tracking elevation, then portions of visibilities will be eliminated when LRO is behind the moon and when LRO is in with a sun angle restriction for a station. From these visibilities a global schedule will be generated based on station priorities and the High Gain Antenna schedule (WOTIS). If LRO is visible to two or more stations, then only the station with the highest priority will be scheduled. If the two or more stations have the same highest priority then all stations with that priority will be scheduled. The WOTIS may be used to determine if the LRO high gain antenna is pointed at S-Band system that is "near-by" to a LR station. Each LR station will have a corresponding set of S-Band systems that are determined to be "near-by". If a "near-by" S-Band system is not scheduled during an LR station's tracking opportunity then the station may not be scheduled. The WOTIS will be delivered from the LRO Mission Operations Center (MOC) to LRO SOC then stored in a secure site on the CDDIS.

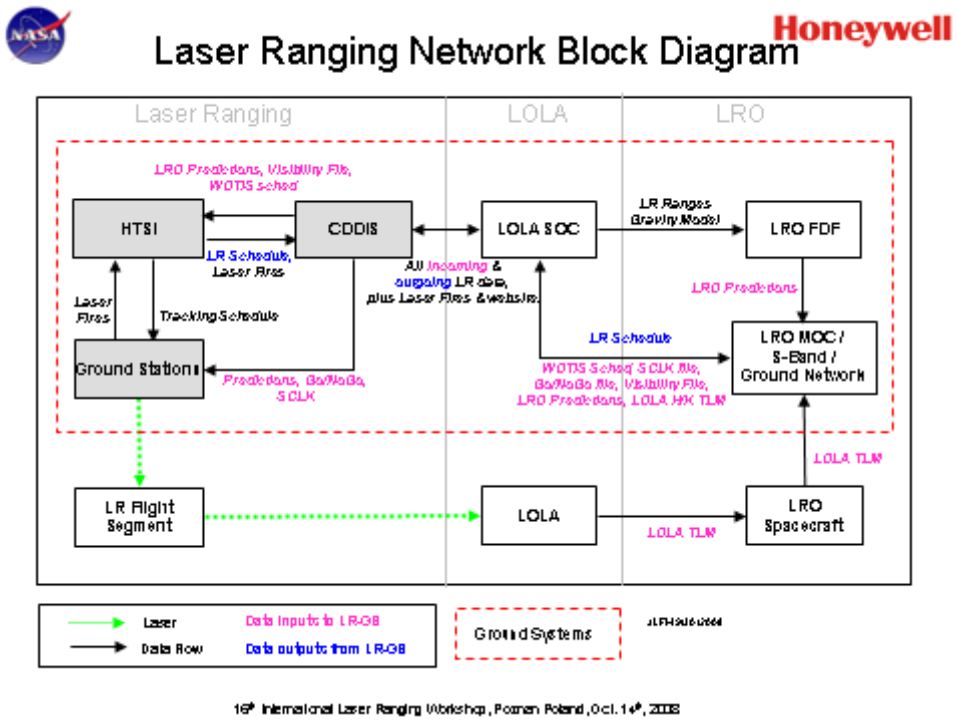

Figure 1. LR-LRO Laser Ranging Network Diagram

Summary

The ILRS stations approved to range to LRO will generate fire data in the CRD or iTDF and send it to ILRS Data Operations Centers (HTSI, EDC). Combined global schedules will generated that include all approved ILRS stations. All LR_LRO products (predictions, fire data, normal points, and combined station schedules) will be hosted at a secure site on the CDDIS. The LR-LRO data flow schematic is displayed in Figure 1.

References

Ricklefs, R., *Consolidated Laser Ranging Prediction Format,* http://ilrs.gsfc.nasa.gov/products_formats_procedures/predictions/cpf.html, Feb 2006.

Ricklefs, R., Moore, C., *Consolidated Laser Ranging Data Format*, http://ilrs.gsfc.nasa.gov/products_formats_procedures/crd.html, June 2008.

McGarry, *Internal Transponder Data Format*, http://lrolr.gsfc.nasa.gov/docs/ITDF_112006.pdf, October 2006

LRO Operations at the MLRS

J. R. Wiant[1], R. L. Ricklefs[2], Peter J. Shelus[2]

[1]McDonald Observatory, The University of Texas at Austin
[2]Center for Space Research, The University of Texas at Austin

jrw@astro.as.utexas.edu

Abstract

The University of Texas at Austin's McDonald Laser Ranging Station (MLRS) is one of the first stations that is slated to participate in a one-way ranging experiment with the Lunar Reconnaissance Orbiter (LRO) in 2009. The experiment will entail the laser illumination of the LRO spacecraft by the MLRS and making precise and accurate time of fire measurements. This poses several interesting challenges that involve pointing, tracking, data format definitions, and unique operational procedures. Some heretofore unanswered questions concerning the MLRS telescope beam divergence and tracking stability must be answered. The newly defined ILRS Consolidated laser Ranging Data (CRD) format will be implemented and tested, and procedures will be established to insure proper handling of LRO schedules, predictions, processing and data distribution.

Introduction

The Lunar Reconnaissance Orbiter (LRO) will perform laser altimetry of the moon from lunar orbit and improve lunar gravity field modeling. To provide orbital accuracy at the required several-cm level, substantial amounts of one-way laser ranging data is needed [1]. MLRS has been selected as one of the primary laser stations to track LRO. To support the required operations, data accuracy, and data volume, a number of MLRS pointing, tracking, beam-divergence, software, and procedural issues must be resolved prior to the 2009 launch.

Hardware Issues

LRO will not be visible in the MLRS telescope, so accurate blind pointing is required. However, absolute pointing of the MLRS telescope is around 10 arcsec, which is not accurate enough for blind pointing to LRO. MLRS has decades of experience tracking lunar retro-reflectors and will apply the same technique to improve LRO pointing to 1-2 arc-seconds. These techniques involve offsetting to LRO from lunar features, possibly using the XY stage. Once LRO data has been acquired, the observer will re-center as needed using the same techniques for the 60 minute "passes." It has been shown that MLRS can track high satellites hands-off to a few arc-seconds over 15 minutes, implying that LRO tracking will be quite manageable.

Delivering only an appropriately low power laser pulse to LRO is critical to the safety of the LOLA detector pointing back towards earth. Power delivered to the spacecraft's detector depends on laser transmit power, seeing, and beam divergence. Beam divergence (controlled by defocus of the MLRS telescope) has been poorly known, and now needs to be better understood. Ranging high satellites (Glonass) using high laser power and high detector amplification while manually scanning through the laser beam along track and across track gives the MLRS beam divergence as modified by the atmospheric seeing. (Due to the

extreme power and amplification, this data is not suitable for scientific use, and does not "leave the station.")

Tests with a collimated laser beam (focus = 0 on an arbitrary scale) show that the beam-width at the spacecraft matches the seeing estimate. Using a LAGEOS-level defocussed beam (-100 on the same scale) with Glonass shows a beam divergence of 7-16 arc-seconds greater than seeing. Using LAGEOS beam divergence and a laser energy of 60 mJ should deliver the proper power level at LRO. Additional tests of MLRS telescope optical path losses and laser power levels will be performed with Goddard employees to gain more knowledge of power output from the end of the telescope.

Other laser-related issues need to be addressed as well. First, the optimal laser fire rate for LRO is 28Hz, synchronized with the LOLA detector's earth window opening. However, MLRS will fire at 10 Hz as usual, as it is not possible to convert our existing laser to 28Hz (or probably even 14Hz) operations. The MLRS ranging detector will be used during LRO ranging to gather internal calibration data and the laser firing time. Assessing the one-way system calibration is being worked out. Finally, the compatibility of the MLRS laser transmit wavelength with the LOLA detection wavelength (532 nm) had to be assured, something that tests have confirmed.

Another issue to be worked out with Goddard personnel is the maintenance of the proper level of timing stability (1 part in 10^{-12}) over each hour of ranging. The existing crystal clock used for fire time control may or may not be stable at this level.

Software Tasks

The MLRS ranging acquisition software must be modified to handle some unique aspects of LRO ranging. First, ranging software must allow any target to be treated either as a lunar laser ranging (LLR) or satellite laser ranging (SLR) target through a set-up file. This will allow offset pointing from lunar features to LRO as is done for lunar retro-reflectors. The CPF prediction file "target type" (SLR, LLR, or transponder) must be passed in the raw data to trigger transponder processing in reduction software. Also, the LRO go/no-go flag, which specifies whether there are exceptions that preclude ranging, must be read and acted upon. These changes have all been accomplished.

For greater control over unintended high-power irradiation of LRO, go/no-go flags are being implemented for each of the lunar corner cube reflectors. The LRO mission will set the appropriate flag to "no-go" during the times LRO flies over the corner cube array. We are awaiting the ftp address of these files so that they can be added to our list of go/no-go flag files.

Similarly, the MLRS data reduction software requires several changes. First, the LRO predictions and schedule must be downloaded and processed. The go/no-go flags described above are downloaded by this system and passed to the ranging acquisition computer. Also, LRO must be recognized by "target type" in raw data, as noted above, to allow unique transponder processing to occur. During data reduction, the LRO data must be converted to CRD-formatted files. While most of these tasks have been accomplished, we are still working on defining and applying one-way calibrations, as noted above. Finally, LRO data will flow automatically to our Operations Center, HTSI, without any additional software changes.

Procedural Changes

The last area in which changes will occur are in the realm of procedures. To range LRO successfully and safely, the MLRS crew must check the integrated target schedule for LRO availability (1 hour out of every 2 while the moon is above horizon – and while we are allowed to range LRO). The laser power and the telescope focus must then be set manually to LRO levels prior to ranging (although software and hardware may be changed to make this task more dependable). Despite the fact that there are no photon returns from LRO, operator feedback is critical to obtaining data. Feedback will come from the LRO website's near-real-time (<30 seconds delay) graphical display which shows laser hits in the LRO earth window as a function of time.

Conclusion

Our build-up to LRO tracking has required addressing lingering questions about MLRS's pointing, tracking, and beam divergence. Additional impact on hardware, acquisition software, reduction software, and crew procedures have been or are being addressed.

Acknowledgments

We would like to thank NASA for support of LRO preparations through NASA contract NNG06DA07C.

References

Smith, D., Zuber, M., Torrence, M., McGarry, J., and Pearlman, M., *Laser Ranging to the Lunar Reconnaissance Orbiter (LRO)*, Proceedings of the 15th International Workshop on Laser Ranging, pp 468-471, Canberra, Australia, 2006.

One-Way Ranging to the Planets

Maria T. Zuber[1], **David E. Smith**[2]
[1]MIT, [2]NASA-GSFC, USA
zuber@mit.edu

Abstract

Often the increase in mission complexity of flying an active laser system to the planets limits the opportunities for attempting laser tracking of planetary spacecraft. The best and most accurate method is generally considered to be the transponder approach that involves active laser systems at both ends of the link. But because of the increased complexity, risk and cost of a two-way system we have been forced to consider the value of a one-way measurement in which most of the complexity and costs are at the Earth terminal, and therefore more palatable and "fixable" should issues arise. This was the choice for LRO and hence the development of the LR system which was minimal in cost and required almost no additional spacecraft resources. The advantage of "one-way" is clear for distances of several AU if the issues of precision versus accuracy can be resolved and the opportunities for flight are greater.

The contribution of LLR data to the estimation of the celestial pole coordinates

Wassila Zerhouni, Nicole Capitaine, Gerard Francou
SYRTE, Observatoire de Paris, CNRS, UPMC
wassila.zerhouni@obspm.fr, nicole.capitaine@obspm.fr, gerard.francou@obspm.fr

Abstract

This presentation is focused on the use of Lunar Laser Ranging data for the determination of the direction of the Celestial Intermediate Pole (CIP) in the Geocentric Celestial Reference System (GCRS).
We have first calculated the residuals of LLR observations over a period of 38 years, using the
IAU 2000A-2006 model of precession nutation (i.e. MHB 2000 nutation of Mathews et al. 2002 and P03 precession of Capitaine et al. 2003) and the CIO based procedure. Secondly, we have estimated the corrections to the X, Y coordinates of the CIP based on the IAU 2000A-2006 model every 70 days. Thirdly, we have compared the results with the VLBI celestial pole offsets.

Introduction

The Lunar Laser Ranging technique consists in determining the round-trip travel time of light pulses between a transmitter on Earth and reflectors on the surface of the Moon. It has may applications in various domains including astronomy, lunar science, geodynamics, and gravitational physics.

The main purpose of this paper is to focus on the application of the Lunar Laser Ranging technique in the field of the Earth rotation, especially for the determination of the celestial pole coordinates. We have first calculated the LLR residuals. Second, we have determined the corrections to the celestial pole coordinates and finally compared these corrections with the VLBI estimations.

Calculation and analysis

For the calculation of the residuals, we have used the LLR data from both stations of McDonald and CERGA over periods spanning 1969–2006 and 1984–2005, respectively. Figure 1 shows the residuals obtained for Grasse station. We have separated the figure into two parts in order to see the improvement of the residuals (i.e. since 1987).

Then, we have calculated the corrections to the celestial pole coordinates with respect to the IAU 2006-2000A model of precession nutation (i.e. MHB 2000 as the nutation model and P03 as the precession model) every 70 days. We have used the CIO procedure and the SOFA 2007 routines (see at www.iau-sofa.rl.ac.uk). Figure 2 represents the DX, DY corrections to the celestial pole coordinates obtained with this computation. It shows that from LLR observations, it is possible to have a reliable estimation of the corrections to the celestial pole coordinates (DX, DY).

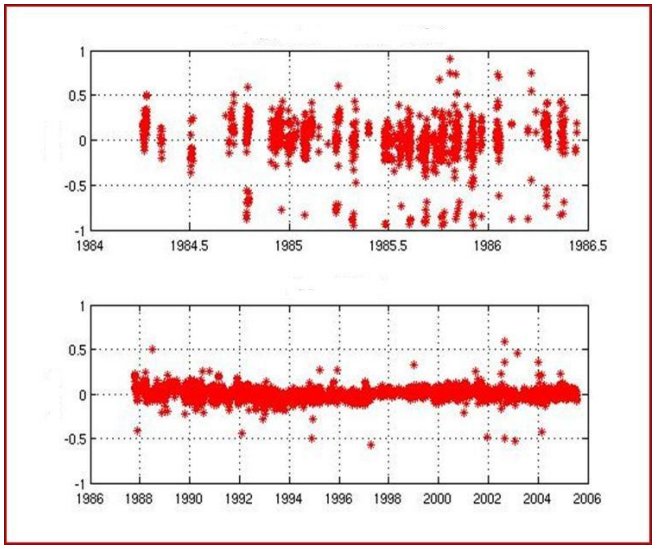

Figure 1. LLR residuals of Grasse station from 1984 to 2006 (in meters)

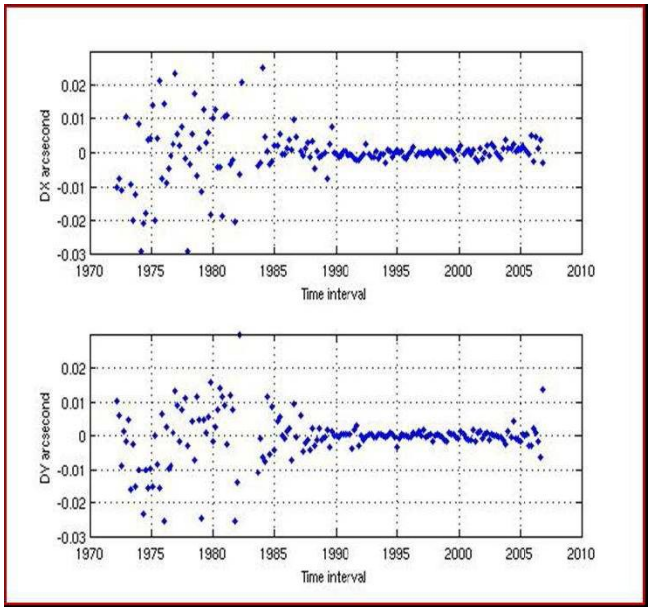

Figure 2. DX, DY corrections to the celestial pole coordinates (LLR data, IAU 2006-2000A precession nutation model) expressed in arcsecond.

Finally, we have calculated the VLBI celestial pole offsets with respect to the IAU 2006-2000A model of precession-nutation using the IVS combined solution (ivse08q1.eops). This solution is given with respect to the IAU 2000A model of precession nutation. In order to be consistent with our work, i.e. to refer the celestial pole offsets to the IAU2006-2000A model, we have used Eq.1 from Capitaine and Wallace (2006; Eq. (41)) which expresses the difference between the IAU2006 and IAU2000 precession models. The results are represented on Fig.3.

$$XIAU2006 - XIAU2000 = 155t - 2564t^2 + 2t^3 + 54t^4$$
$$YIAU2006 - YIAU2000 = -514t - 4t^2 + 58t^3 - 1t^4 - 1t^5 \quad \text{(Eq.1)}$$

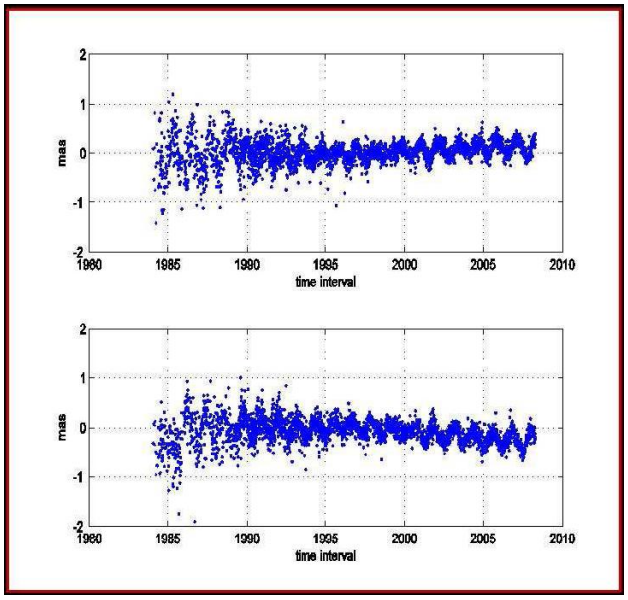

Figure 3. VLBI pole offsets with respect to the IAU 2006-2000A model of precession nutation

Comparing Fig.2 and Fig.3 shows that in both cases there is a significant improvement of the estimation since 1990. It also shows that the estimation of the celestial pole offsets is determined with better precision using VLBI observations.

Conclusion

The determination of the corrections to he celestial pole coordinates using LLR observations is less accurate with a factor 10 than in the VLBI determination. It is due to the imperfect distribution of the LLR observations. However, the interest of using LLR data for such estimations is that it provides independent estimations and a reference to another celestial reference system. A combination of the two techniques will be appropriate in order to improve the calculations.

References

Capitaine, N., Wallace, P.T., and Chapront, J. 2003, "*Expressions for IAU 2000 precession quantities"*, Astron. Astrophys., 412, 567-586.

Capitaine, N., Wallace, P.T 2006, "*High precision methods for locating the celestial intermediate pole and origin*", Astron. Astrophys., 450, pp.855-872.

Chapront, J., Chapront-Touzé, M. and Francou, G. 1999, "*Determination of the lunar orbital and rotational parameters and of the ecliptic reference system orientation from LLR measurements and IERS data"*, Astron. Astrophys., 343, 624-633.

Chapront, J., Chapront-Touzé, M. and Francou, G. 2002, "*A new determination of lunar orbital parameters precession constant and tidal acceleration from LLR measurements"*, Astron.-Astrophys., 387, 700-709.

Mathews, P.M., Herring, T.A., and Buffet, B.A. 2002, J.Geophys. Res, 107(B4), 10.1029/2001JB00390. McCarthy, D. D. 1996, IERS technical Note 21: IERS Conventions (1996).

IERS Conventions 2003, IERS technical Note 32, ed. D. D. McCarthy & G. Petit.

SOFA: www.iau-sofa.rl.ac.uk.

Website: hpiers.obspm.fr/eop-pc/models/fcn/index.

Analysis and prediction of altimetric sea level variations during El Niño, La Niña and normal conditions

T. Niedzielski (1,2)**, W. Kosek** (1)

(1) Space Research Centre, Polish Academy of Sciences, Poland
(2) Institute of Geography and Regional Development, University of Wrocław, Poland

niedzielski@cbk.waw.pl /Fax: +48 71 3729372

Abstract

Recent developments in satellite altimetry are due to precise tracking and determining the satellite orbits. This is attained by such techniques as: Satellite Laser Ranging (SLR), Doppler Orbitograhy and Radiopositioning Integrated on Satellite (DORIS), and Global Positioning System (GPS). These techniques were adopted by American-French altimetric missions TOPEX/Poseidon (T/P), and Jason-1 (J-1). Satellite altimetry provides the accurate sea surface height (SSH) measurements. The SSH estimates and the long-term mean sea level are used to compute sea level anomaly (SLA) data. The SLA time series describe the dynamic sea level change. The SLA data provide the knowledge about the large-scale ocean circulation, including El Nino/Southern Oscillation (ENSO). The altimetric data obtained from T/P and J-1 measurements are used to compute the spectra of the SLA data as well as amplitudes of the most energetic oscillations in sea level variation as a function of latitude and longitude. These spectra and amplitudes were computed by the Fourier Transform Band Pass Filter (FTBPF). The SLA time series are often used to determine the trend of sea level change. These estimates may be derived both globally and regionally (for the dissimilar ocean areas). It is also possible to predict SLA data. The SLA predictions are computed using the combination of polynomial-harmonic least-squares and autoregressive models. The SLA forecasts can be used to predict ENSO events, because El Nino and La Nina signals are very well visible in SLA time series.

Introduction

The objective of this paper is to provide a comprehensive review of different approaches to the analysis of altimetric sea level change. In particular, the main focus is put on the relation between the regional sea level fluctuation and El Niño/Southern Oscillation (ENSO). It is now known that ENSO may cause extreme rise and fall of sea level in the vicinity of east and west equatorial Pacific. The magnitude of such variations may reach even 40 cm in respect to the long-term mean sea level. The analysis of sea level change includes both exploring the time series and forecasting. Exploring aims at detecting and understanding long-term and short-period variations in the sea level change. Prediction studies, on the other hand, use dissimilar models to determine the future sea level.

Long-term sea level change is usually described by a linear trend, fitted globally for the entire ocean and locally for selected ocean areas. Many authors calculated the rate of global sea level change using different data sets. They use both tide gauge time data (e.g. Gornitz and Lebedeff, 1987; Peltier and Tushingham, 1989; Douglas, 1991) and altimetric time series (e.g. Kosek, 2001; Leuliette et al., 2004). The rate of global sea level change determined from tide gauge records vary between 1.2 to 2.4 mm/year, depending on the data time span and the number of tide gauges under study. On the other hand, the rate of global sea level rise

estimated using the altimetric time series are of the order of 2.8-3.5 mm/year depending mostly on the data time span. The minimum time span of altimetric data required to obtain the statistically significant trend with the probability close to 1 was found to be of 4.3 years (Niedzielski and Kosek, 2007). The rate of local sea level rise is very high in the western Pacific and may exceed 20 mm/year (Kosek, 2001). On the other hand, there is a fall of sea level (less than 10 mm/year) in the middle and eastern Pacific (Kosek, 2001).

Short-period oscillations are also present in sea level fluctuations. Nerem et al. (1994) found annual and semi-annual oscillations in sea level change. Their amplitudes depend on geographic region. Kosek (2001) found 183, 120, 90, 62, 37, 30 days oscillations in sea level fluctuations depending on the geographic region and determined the amplitudes of these harmonic terms. Niedzielski and Kosek (2005) also confirmed that the most energetic harmonic oscillations in global sea level change recorded by TOPEX/Poseidon altimetric satellite were annual and semi-annual components.

The above-mentioned findings lead to a better understanding of sea level variation and enable to determine both long-term and short-period predictions of sea level change. Warrick et al. (1996) forecasted that the global sea level may rise from 20 to 70 cm up to 2070. Röske (1997) predicted short-period sea level fluctuations by means of artificial neural networks. Chen et al. (1997) utilized the global hydrologic model to forecast annual and semi-annual non-steric sea level variation. Niedzielski and Kosek (2005) used time series methods to predict global sea level data obtained by TOPEX/Poseidon measurements. They have also predicted local sea level change in the east equatorial Pacific during ENSO and normal conditions (Niedzielski and Kosek, 2008).

In this paper we present and review our scientific results on the altimetric sea level change. We focus on long-term and short-period variations as well as on the prediction studies. The particular emphasis is put on the influence of ENSO on the local sea level change.

Methods

The mathematical methods used in our analyses to process altimetric sea level fluctuations can be divided into three groups. First, the long-term changes were analysed combining the stepwise simulation approach with testing statistical hypotheses. Second, the short-period oscillations in sea level change were extensively analysed by the signal processing techniques. Third, the prediction studies were performed using deterministic and stochastic time series modeling techniques.

Testing statistical hypotheses was used as a tool for detecting the statically significant trend in sea level rise. In fact, the main goal was to estimate the minimum sample size, i.e. the minimum data time span, required to obtain the statistically significant trend. The Cox-Stuart test for trend was utilized to test the null hypothesis of no trend in the data against the alternative hypothesis corresponding to the inclining trend. For details we relate to McCuen (2003). The stepwise algorithm was used to apply the Cox-Stuart test for different subsets of global sea level change time series. This allowed us to calculate the sample size for which the statistical significance of trend could be attained.

To analyse short period oscillations in sea level change the Fourier transform band pass filter (FTBPF) was applied (Kosek 2001). This filter enables computation of wideband oscillations with the power concentrated near some chosen central frequency. An oscillation computed by

this filter has variable amplitude so this technique can be applied to compute time-variable amplitude spectra. It this paper this filter was applied to compute the averaged amplitudes of the chosen most energetic seasonal and subseasonal oscillations.

Forecasting sea level change was based on the polynomial-harmonic least-squares model and the stochastic uni- and multivariate autoregressive models. The deterministic polynomial-harmonic model described the trend, annual, and semi-annual components. The autoregressive model was fit to the residuals in order to predict its irregular variation. In particular, the irregularities in sea level change are driven by ENSO and thus can be captured by stochastic processes. The predictions were validated using root mean square error (RMSE) and mean absolute value (MAE). Different data time spans were selected to validate the forecasts. The global mean sea level change was predicted using uni- and multivariate autoregressive models fitted to the differenced data (Niedzielski and Kosek, 2005) and using polynomial-harmonic models combined with the univariate autoregressive models (Niedzielski and Kosek, 2008). Local sea level fluctuations were predicted on a grid scale using polynomial-harmonic model supported by the univariate autoregression (Niedzielski and Kosek, 2008).

Data

For the analysis, the gridded sea level anomaly (SLA) data recorded by TOPEX/Poseidon and Jason-1 altimetric satellites were chosen. SLA time series is calculated as the difference between the sea surface height (SSH) and the long-term mean sea level. The sampling interval of these data corresponds to one satellite cycle approximately equal to 10 days. The maximum data time span was 10.01.1993 - 14.07.2003, however for the computation of the mean prediction errors the time series was truncated in 2002. The spatial latitude-longitude resolution is of 1^o x 1^o. The spatial coverage includes all longitudes and is constrained to latitudes from 65^o S to 65^o N. Both global (averaged) and local (certain geographic regions) SLA data are processed in the analyses.

Results

In accordance with Niedzielski and Kosek (2007), for the purpose of the trend analysis the global mean SLA time series from TOPEX/Poseidon and Jason-1 were merged to cover the time period 10.01.1993 -14.07.2003. In the common observational period the data were combined and the bias between the two was removed. Two data sets were analysed independently: (1) the global mean SLA time series, and (2) the non-seasonal global mean SLA data, i.e. the difference between the global mean SLA time series and the corresponding least-squares model for annual and semi-annual harmonic components. The Cox-Stuart test supported by the above-mentioned stepwise iterative procedure was applied. Thus, the minimum time span of altimetric data required to obtain the statistically significant trend in sea level rise was estimated. The results indicated that at least 4.3 years of the data time span were needed to capture the trend with the probability close to 1 (Tab. 1). This data time span becomes higher if the least-squares model is not subtracted from the SLA data (Tab.1). It was also noted that it was not possible to detect acceleration in SLA data, because of too short data time span.

Table 1. The minimum time span of altimetric data required to detect a statistically significant trend in sea level rise. Source: Niedzielski and Kosek (2007).

Data	Minimum sample size [cycles]	Minimum sample size [years]
Global SLA	203	5.5
Non-seasonal global SLA	160	4.3

Following Kosek (2001), the mean amplitudes of oscillations were computed using the above-mentioned FTBPF amplitude spectrum for gridded SLA data. The 30, 62, 90, 120, 182, 365 day oscillations were detected and the spatial variation of their mean amplitudes was determined for the entire geographic coverage provided by TOPEX/Poseidon and Jason-1 (Fig. 1). It is clearly seen that the annual, semi-annual and triennial oscillations are the most energetic at the equatorial regions as well as north-west Pacific ocean. The annual oscillation is also energetic in north-west Atlantic region, and the semi-annual oscillation has the greatest amplitudes in the west and east equatorial Indian ocean. Big amplitudes of the 62-day oscillation are caused mostly by inaccurate modeling of M_2 tide amplitudes in some coastal regions. Some equidistant spots above the equator in the central Pacific ocean for the 30-day oscillation represent the tropical instability waves or Legeckis waves (Cox, 1980) with the amplitudes of the order of 1 cm.

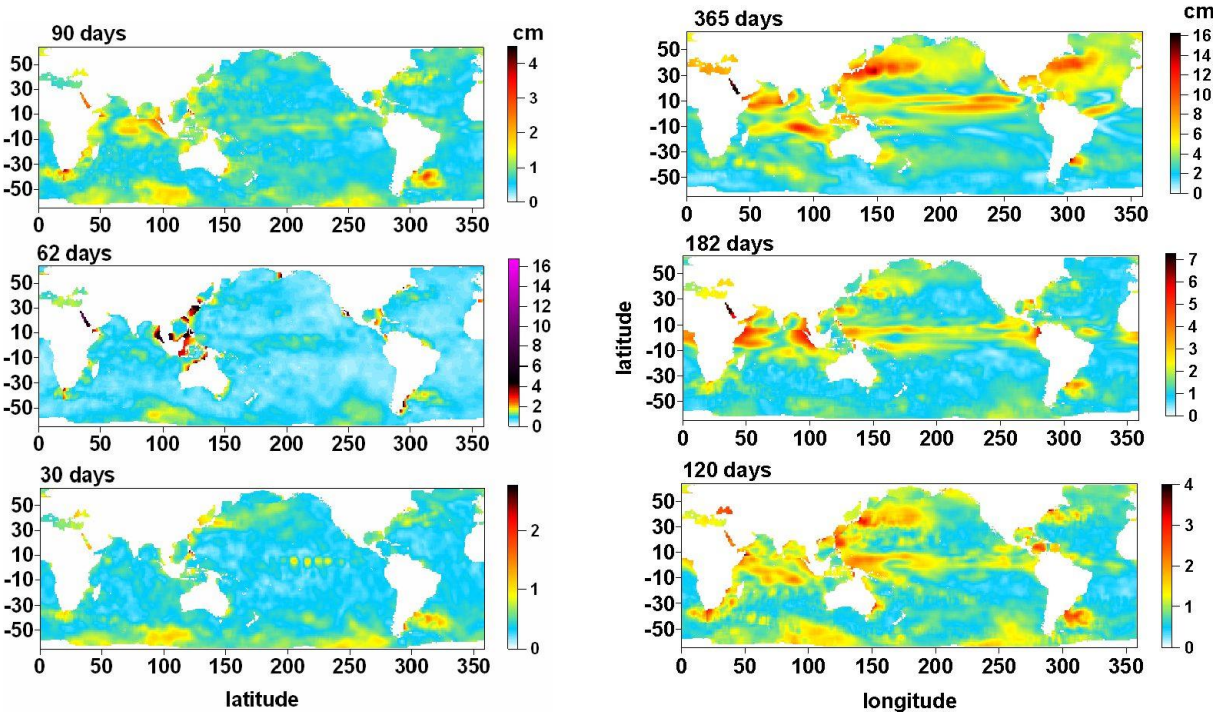

Figure 1. Mean amplitudes of 90, 62 and 30-day oscillations (left column) and 365, 182 and 120-day oscillations (right column) computed by the FTBPF in the SLA data of TOPEX/Poseidon and Jason-1.

The deterministic SLA prediction was based on the 3-step (1-month) extrapolation of the polynomial-harmonic least-squares model consisted of the trend, annual, and semi-annual

oscillations. This model provided the reasonable overall fit to the data. The stochastic forecast of the SLA residuals (the data minus polynomial-harmonic model) was based on the 3-step ahead autoregressive prediction. The prediction of global SLA data can only be used as the general future scenario (Niedzielski and Kosek, 2005; 2008). However, the prediction of local sea level change in the eastern equatorial Pacific determined using both polynomial-harmonic model extrapolation and the autoregressive prediction was considered particularly useful in forecasting ENSO signal (Niedzielski and Kosek, 2008). The significant reduction in the prediction error was observed and hence the potential applicability of altimetric data in ENSO studies was highlighted (Tab. 2).

Table 2. The SLA prediction error reduction for ENSO and normal conditions.

Validation period	Ratio between the RMSE and maximum amplitudes of the signal
El Niño 1997/1998	~1/3
La Niña 1998/1999	~1/4
Normal conditions	~1/6

Conclusions

The trend of sea level change may be detected with the probability close to 1, for small significance levels of the Cox-Stuart test after 160 satellite cycles (approx. 4.3 years). The 30, 62, 90,120,182, 365-day oscillations of SLA data are estimated. Most of the energy of the annual, semi-annual, and triennial oscillations are concentrated in the equatorial regions of the Pacific, Indian and Atlantic oceans. The combination of a polynomial-harmonic model and an autoregressive model allows one to improve the accuracy of SLA predictions in the east equatorial Pacific in respect to those computed by means of a pure polynomial-harmonic model. This improvement is noticed during El Niño, La Niña and normal conditions.

Acknowledgements

The research is financed by the Polish Ministry of Education and Science under the project No 4 T12E 039 29. Tomasz Niedzielski was supported by the Foundation for Polish Science within the Start Programme (stipends for young researchers) and by European Union within the Marie-Curie Actions. The authors thank the Center for Space Research, University of Texas at Austin, USA for providing the T/P and J-1 data. The authors of R 2.0.1., a Language and Environment 2004 and the additional packages are acknowledged.

References

Chen, J.L., Wilson, C.R., Chambers, D.P., Nerem, R.S., Tapley, B.D., *Seasonal global water mass budget and mean sea level variations*, Geophys. Res. Lett. 25, 3555—3558, 1998.

Cox, M., *Generation and Decay of 30 day waves in the numerical model of the Pacific*, J. Physical Oceanography 10, p. 11681—11686, 1980.

Douglas, B.C., *Global sea level rise*, Journal of Geophysical Research 96, p. 6981—6992, 1991.

Gornitz, V., Lebedeff S., *Global sea-level changes during the past century*, In: Nummedal D. et al. (Eds.) Sea-level fluctuation & coastal evolution. Soc. Econ. Paleontol. Miner. Spec. Publ. 41, p. 3—16, 1987.

Kosek, W., *Long-term and short period global sea level changes from TOPEX/Poseidon altimetry*, Artificial Satellites 36, p. 71—84, 2001.

Leuliette, E.W., Nerem, R.S., Mitchum, G.T., *Calibration of TOPEX/Poseidon and Jason Altimeter Data to Construct a Continuous Record of Mean Sea Level Change*, Marine Geodesy 27, p. 79—94, 2004.

McCuen, R.H., Modeling Hydrologic Change, Statistical Methods, Lewis Publishers, Boca Raton, London, New York, Washington, D.C., 2003.

Nerem, R.S., Schrama, E.J., Kobylinsky, C.J., Beckley B.D., *A preliminary evaluation of ocean topography from the TOPEX/POSEIDON mission*, Journal of Geophysical Research 99(C12), p. 24565—24583, 1994.

Niedzielski, T., Kosek, W., *Multivariate stochastic prediction of the global mean sea level anomalies based on TOPEX/Poseidon satellite altimetry*, Artificial Satellites 40, p. 185—198, 2005.

Niedzielski, T., Kosek, W., *A required data span to detect sea level rise*, In: Weintrit, A. (Ed.), Advances in marine navigation and safety of sea transportation, p. 367—371, Gdynia Maritime University, Gdynia, 2007.

Niedzielski, T., Kosek, W., *Forecasting sea level anomalies from TOPEX/Poseidon and Jason-1 satellite altimetry*, Journal of Geodesy, DOI: 10.1007/s00190-008-0254-5, 2008.

Peltier, W.R., Tushingham, A.M., *Global sea level rise and the Greenhouse Effect: might they be connected?* Science 244, p. 806—810, 1989.

Röske, F., *Sea level forecasts using neural networks*, Ocean dynam. 49, p. 71—99, 1997.

Warrick, R.A., Le Provost, C., Meier, M.F., Oerlemans, J., Woodworth, P.L., *Changes in sea level*, In: Houghton, J.T., Meira Filho, L.G., Callander, B.A., Harris, N., Kattenberg, A., Maskell, K., (Ed.) *Climate change 1995. The science of climate change*, p. 361—405, Cambridge University Press, Cambridge, 1996.

NASA NGSLR Precise (~ 1 ns) Transmit Epoch Timing to On-Station Time Reference for LRO Transponder Support

Thomas Varghese (1)**, Jan McGarry** (2)**, Thomas Zagwodzki** (2)

(1) Cybioms Corporation, Rockville, Maryland USA
(2) NASA Goddard Space Flight Center, Greenbelt, Maryland USA

Abstract

The LRO transponder measurement requires the participating ranging stations to time tag the data to the station very accurately and peg the timing measurements to a stable clock that has excellent short term stability of <5 ns over the lunar orbit period of ~1 hour. The latter capability is achieved using a free running Cesium clock that has demonstrated excellent short term stability. This paper highlights the accurate time tagging to better than 1 ns to the station 1pps timing standard. For LRO transponder measurements, NGSLR uses a multimode, 50 mJ, q-switched laser that has a pulse width of 5.5 ns. NGSLR uses a standard high speed photodiode for its START detection and a Quad MCP-PMT based single photoelectron threshold receiver system for its STOP detection with a single photoelectron jitter of ~30 ps. However, the use of the above laser results in a significantly larger (>1ns) 1- for all timing measurements performed with this STOP receiver. Furthermore, Quad MCP-PMT at the high gain setting is extremely sensitive to large photon flux with adverse impact on its lifetime. We have devised a technique to precisely measure the timing and time tagging using the START photodiode as the common detector. Using this technique, measurements done on the external target can be transferred to an internal target for routine performance monitoring. This technique allows the operator to monitor the station performance during the 1-way ranging and ensure that the on-station time tagging is performing smoothly through the real-time internal calibration performance monitoring. The NGSLR had multiple path ways for performing the time tagging measurement; although both gave stable results within the error budget, the new pathway that was laid out was superior to the existing one as it provided a single stable unambiguous Transmit-Receive reference point for the eye-safe kilohertz laser and the high energy LRO laser. These measurements show that accurate sub-nanosecond time tagging is possible and the primary limitation is strictly the short term stability of the clock over the time interval of interest for the transponder. Details of the technique and the results are included.

The poster can be viewed at http://lrolr.gsfc.nasa.gov/lrolr_pubs.html.

High Repetition-Rate Systems

Chairs: Georg Kirchner and Jan McGarry

Session Summary

The number of high repetition rate SLR systems continues to increase with each Workshop. The kHz "club" started operationally with the Graz station which has now six years of continuous 2 kHz operations with excellent results including high reliability and stability.
Herstmonceux is moving into kHz operations with a laser similar to Graz; and NGSLR expects to be operational with their eyesafe 2 kHz laser in 2009.
Potsdam already has the 2 kHz laser, and is finishing now the 2 kHz control system.
China has installed kHz laser systems (3 mJ / 532 nm / 1 kHz) in five of their stations, and at least 2 of them (Shanghai and Changchun) are operational since autumn 2009. Beijing will install a 2 kHz laser end of 2009.
Russia now has a station at 300 Hz with data delivery just started.
Zimmerwald is getting excellent results operationally with their 100 Hz laser, and TIGO's operation, also at 100 Hz, is showing increasing results.

This session showed that high repetition rate systems provide the ability to do several things that lower rate systems are not well suited for. These include the ability to do eyesafe laser ranging with a much reduced energy level as is shown with the NGSLR system whose laser currently outputs less than 100 microJoules. The higher repetition rate systems can also retrieve the optical response of the retro-reflector arrays when coupled with single photon detection. With higher return rates of kHz lasers, millimeter accuracy is possible from centimeter targets. Other areas that benefit from kHz data are the determination of satellite spin rate as shown from the analysis of the Graz system data, and LIDAR data which can be obtained as a by product of SLR operations.

Not in this session, but other planned uses for high repetition rate SLR are determining atmospheric "seeing" and planetary transponder ranging.

Development of Any Frequency Fire Rate SLR Control System

Cunbo FAN, Xue DONG, Xingwei HAN, You ZHAO
Changchun Observatory/NAOC, CAS, China
fancb@cho.ac.cn; dongx@cho.ac.cn; hanxw@cho.ac.cn; youzhao@cho.ac.cn

Abstract

This paper presented the high repetition-rate control system which was developed by Changchun SLR group. The system can make the SLR system work at from several hertz to more than 2 kilohertz frequencies. The real-time control hardware and software under Windows XP environment are introduced in detail. The hardware control circuit includes three parts: accurate timing part, range gate control part and laser firing control part. A 2 KHz laser which borrowed from Wuhan was used to work together with the control system to test the performance. The experimental results show that the any frequency fire rate control system can work very well at or less than 2 KHz. If there is a suitable high repetition rate laser instrument (up to several KHz), Changchun SLR system can work at that frequency now.

Key words: Any Frequency, Windows XP, SLR, Real-Time

1. Introduction

SLR was sprung up at 1960s, and has been developed rapidly during these decades [1]. With the development of scientific technique, the applications in SLR technologies have been widely used, the accuracy has been higher, and the method has been updated rapidly. At the end of 1990s, National Aeronautics and Space Administration (NASA) commenced researching Kilohertz SLR research, but have not completed yet. At 2004, Graz observatory in Austria achieved 2 KHz SLR for the first time, and we could easily drawn a conclusion from the date size and accuracy observed that Kilohertz SLR has some considerable advantages compared with traditional low frequency SLR [2, 3]. High frequency SLR does increase data number largely, from which the accuracies of normal point and orbit determination could be improved, and it would be the important direction for SLR in the future.

The capability of Changchun SLR system was improved in 1990s, its single shot precision has been less than 2 cm, and it also achieved 10Hz SLR owing to A032-ET at the end of 2006 [4]. Now Changchun observatory is under the development of Kilohertz SLR, and has already completed hardware and software subsystems at from several hertz to more than 2 kilohertz frequencies under Windows XP environment. This new system has been applied in Changchun SLR system only at 20Hz due to lack of Kilohertz laser, and if there is a suitable high repetition rate laser instrument (up to several KHz), Changchun SLR system can work at that frequency now.

2. Hardware design

The hardware control system is mainly composed of three parts: accurate timing part, range gate control part and laser fire control part.

Accurate timing part needs standard 1pps signal and 10MHz signal to support its normal running, which are provided by HP58503A GPS time and frequency receiver. The time is 24 hours display and it is synchronized every second to ensure the dependability of the timing subsystem.

Range gate control part calculates and generates range gate signals. The method used in this system is different from that in the old 10Hz frequency system. 10Hz SLR system uses three same counters, and the three counters generate gate signals circularly. As the rate being doubled, the number of counters will become two times of the old size. It is unimaginable for KHz system designing in the same method. While the new design of range gate control system for any frequency only needs a piece of range gate circuit, which depends on timing system and range gate value being calculated. But the real time of control system is highly needed.

In detail, the range gate signals depend on the main pulse. Once the main pulse signal is detected, the range gate signal is allowed to be generated. At this moment, read the accurate time-tag from timing system, calculate the range gate, put it into the FIFO buffer, and send the range gate at the corresponding time to produce range gate signal.

The method used in firing control part is similar with that in range gate control part. But one problem should be considered additionally, that is, the range measurement may be corrupted when a transmitted laser pulse is close to the received one, being called back scatter. By virtue of higher frequency, the time interval between main pulse and return pulse is greatly decreased, and some main pulse may be sent at the meantime the return pulse is back. In that case, the detector can not receive return pulse normally. The solution is that, the laser fire signal be delayed for 50us if the back scatter is appeared. The control system frame is shown as figure 1.

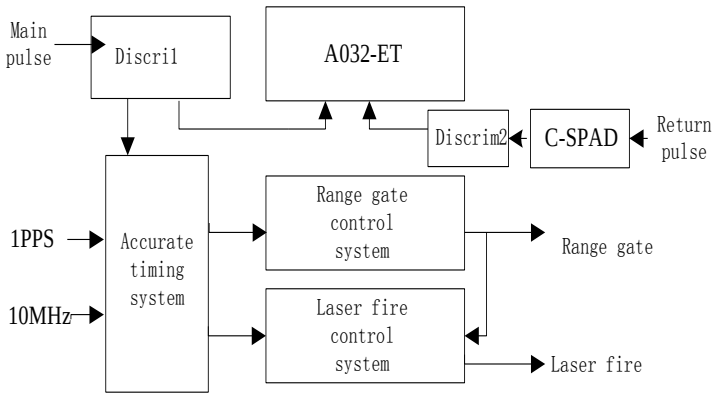

Figure 1. Control system Frame

In figure 1, 1PPS signals and 10MHz signals are provided by HP58503A GPS time and frequency receiver, and range gate control system is used to produce the range gate and laser fire control system to produce laser fire. ISA bus is used to transfer the data in real-time between PC computer and control circuit.

3. Application program design

The software is compiled in VC++6.0 language, running under Windows XP environment. Windows XP is a multiply users' operating system, thence its real-time capability is not as well as single user's operating system such as DOC. To guarantee the real-time capability of control system, the main control program is running in a dependent thread, completing the following functions, such as data calculation, range gate and fire control, data collection, and tracking control and display. While the interface capability provided by Windows XP is well. The runtime environment as follows: Windows XP, CPU Pentium 4 3.0, Resolution 950*680, Main memory 1G. The software flow chart is in figure 2.

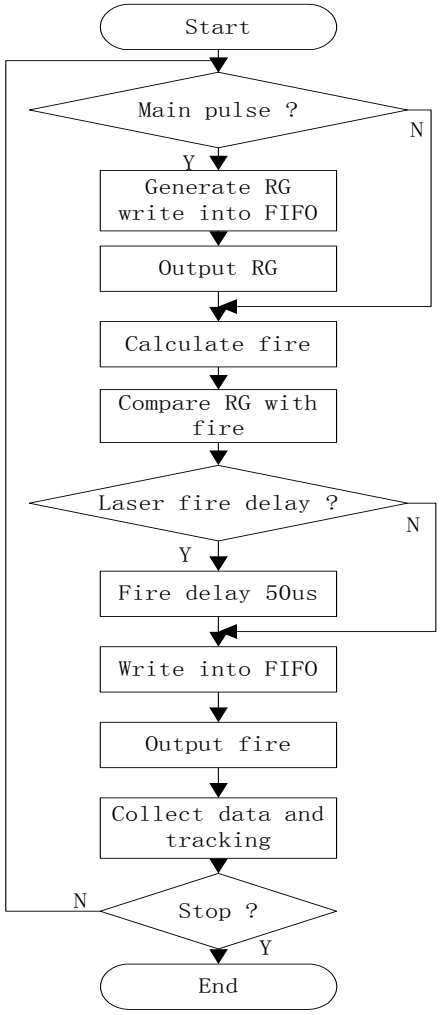

Figure 2. Software flow chart

Software flow in one circle is departed in three steps: 1) In the first step, the range gate control circuit waits for a main pulse, calculates the rang gate and write it into the FIFO buffer, and sends out the rang gate signal at the corresponding time. 2) In the second step, the laser fire control circuit calculates the fire time according to the frequency, compares the fire time and the range gate time worked out in the first step, if the back scatter would happen, the fire time would be delayed by 50us, writes the fire time into the FIFO buffer, and sends out the fire signal at the corresponding time. 3) In the last step, the software collects all kinds of

observed data, including time, azimuth, altitude, range of satellite and so on, achieving the track control.

4. Main performances of Laser

There is a very important instrument in kilohertz SLR system——the laser. It could influence the quality of data greatly. The laser used in changchun kilohertz system was borrowed from Wuhan, and its specifications was shown in table 1. The appearance is shown in figure 3.

Table 1. Laser Specifications

Model	DS20-532
Wavelength	532 nm
Average Power @ 10 kHz	18 Watts
Nominal Pulse Width @ 10 kHz	40 ns
Pulse Energy @ 10 kHz	1.8 mJ
Beam Mode	TEM_{00} - M^2 < 1.1
Polarization	100:1 Vertical
Beam Diameter	1.0 mm
Beam Divergence	1.6 mrad
Pulse-to-Pulse Instability	<3% rms
Long-Term Instability	+/- 3%
Pointing Stability	< 25 μrad
Pulse Repetition Rate	500 to 10kHz

Figure 3. Appearance of the laser

5. Results and analysis

Figure 4 shows real-time tracking interface. The fire rate is 2 KHz. From the picture we can see that the hardware circuits run well such as fire control circuit and range gate control circuit, and the software could complete all works such as collection data and tracking.

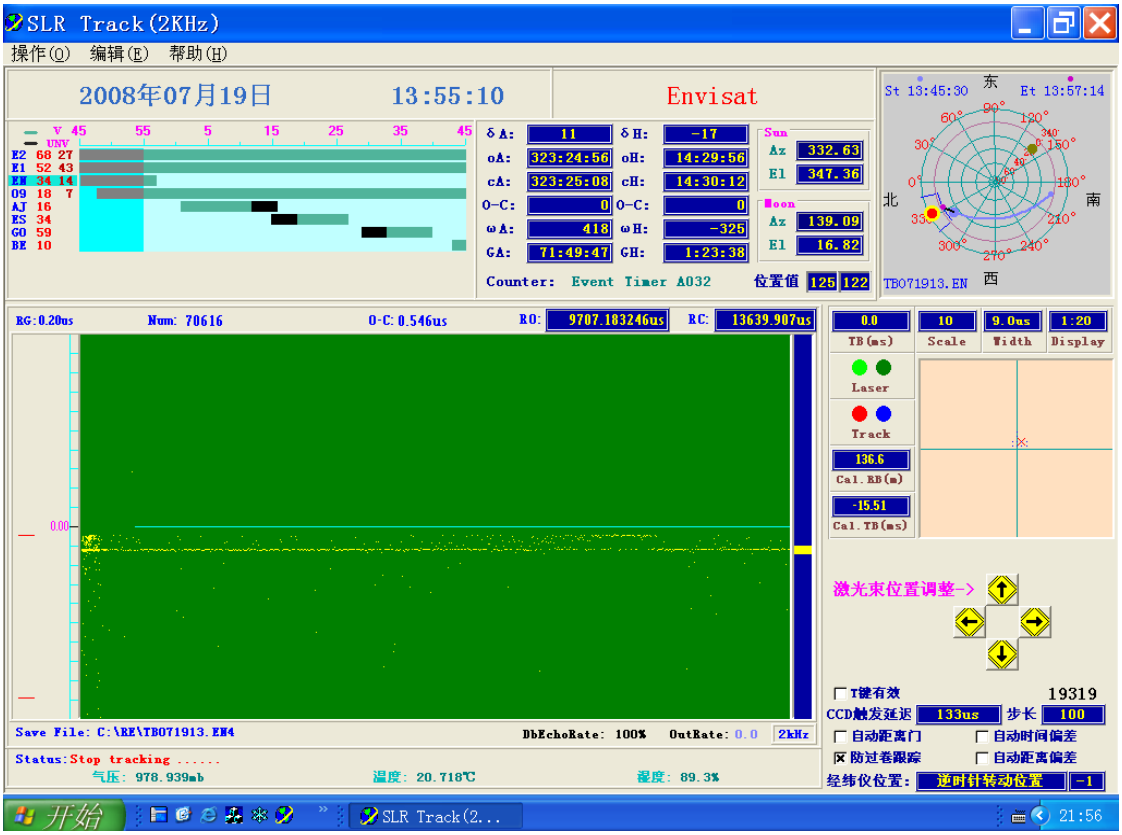

Figure 4. Real-time tracking interface in 2KHz

6. Conclusion

We can draw a conclusion from the experiment above changchun KHz SLR system that it provides good practicability, strong dependability, and wide compatibility. If there is a suitable high repetition rate laser instrument (up to several KHz), Changchun SLR system can work at that frequency now.

7. Acknowledgements

The author gratefully acknowledges the support of the stuff in SLR group, Changchun observatory. Thanks to the very kind people Tangyong Guo lending us the laser, so we can accomplish our KHz research; many thanks to G. Kirchner and some other people from Graz station.

References

1. Ye S. H., Huang C., *Astrogeodynamics*, Ji Nan: Shandong Science Technology Press, 2000
2. Lukas Kral, Karel Hamal, Ivan Prochazka, Georg Kirchner. *Present Status of the Graz KHz SLR System*. Proceedings of KHz SLR Meeting, 2004 Oct. 27-29, Austria.
3. Lukas Kral, Karel Hamal, Ivan Prochazka, Georg Kirchner. *Instrumentation for Creating KHz SLR Timing Systems*. Proceedings of KHz SLR Meeting, 2004 Oct. 27-29, Austria
4. Dong X., *The research on Event timer in Satellite Laser Ranging application*, Master degree thesis. Beijing: Graduate University of Chinese Academy of Sciences, 2007.

The Experiment of kHz Laser Ranging with Nanosecond Pulses at Shanghai SLR

Zhang Zhongping, Yang Fumin, Wu Zhibo, Zhang Haifeng, Chen Juping, Qin Si, Li Pu
Shanghai Observatory, Chinese Academy of Sciences, Shanghai, China
zzp@shao.ac.cn /Fax:+86-21-64696290

Abstract

The paper presents some progress on kHz ranging at Shanghai SLR station:
1) design and build a range gate generator with 5ns resolution based on a FPGA chip for kHz ranging;
2) measure time of laser flight with a Riga A032-Event Timer;
3) complete kHz control system made up of two computers: One is for registering start and stop events and matching them, displaying O-C, identifying returns, storing results; another is for tracking and controlling, range gating;
4) establish pre-processing software for handling kHz data on Windows Operating System.
In April 2008, we borrowed a diode-pumping Q-switched Nd: YAG laser with 50ns pulse width, 2 mJ in 532nm and 1kHz repetition from North China Research Institute of Electro-Optics (NCRIEO) in China. This paper gives the preliminary results of 1KHz satellite ranging with the ns-pulses laser.

Introduction

We have got the support from national natural science foundation and Chinese Academy of Sciences to research on kHz SLR and borrowed a kHz laser with long pulse width from NCRIEO. The experiment has been designed with the purpose of testing our design of kHz control system: range gate generator board, event timer, control software and data acquisition, data processing capability. On Apr.26 2008, we successfully got returns from Ajisai satellite for the first time with kHz system. Within the following week, the experiment has been done at ERS-2, Lageos etc. with 2mJ energy, 50ns pulse width laser.

KHz Laser

The main specifications of kHz laser made by NCRIEO are listed in Table 1.

Table 1. Main specifications of the kHz laser

Repetition rate	Up to 10kHz
Pulse width	50ns
Energy per pulse	2mJ @ 532nm
Divergence	6mrad
Size	52*17*12cm

The optical structure of the kHz laser system is shown in Figure1 and Figure 2

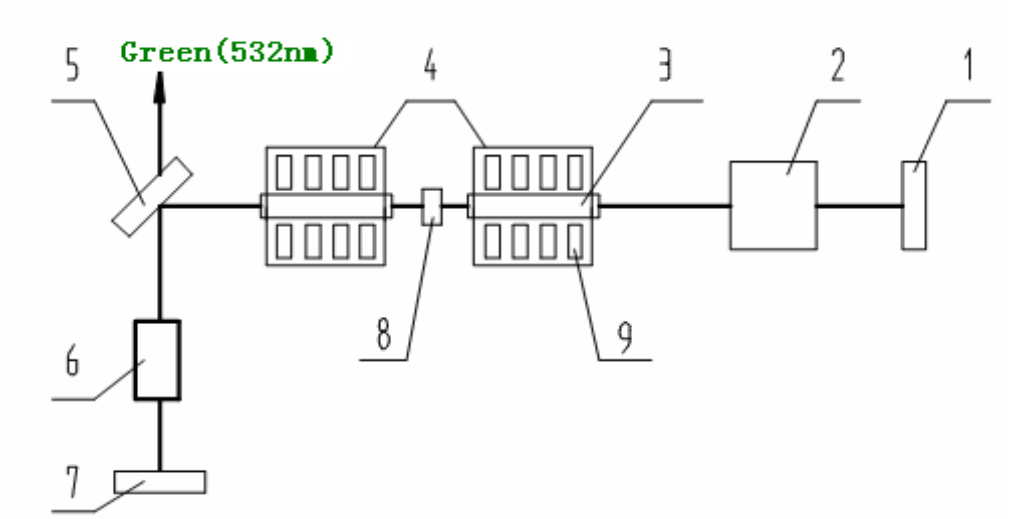

1, 7 HR concave mirror; 2. acousto-optic device; 3 .Nd:YAG rod;
4. focus lamp cavity; 5. output coupling mirror; 6. SHG; 8. polarimeter;
9. diode array

Figure 1. The optical structure of the kHz laser system

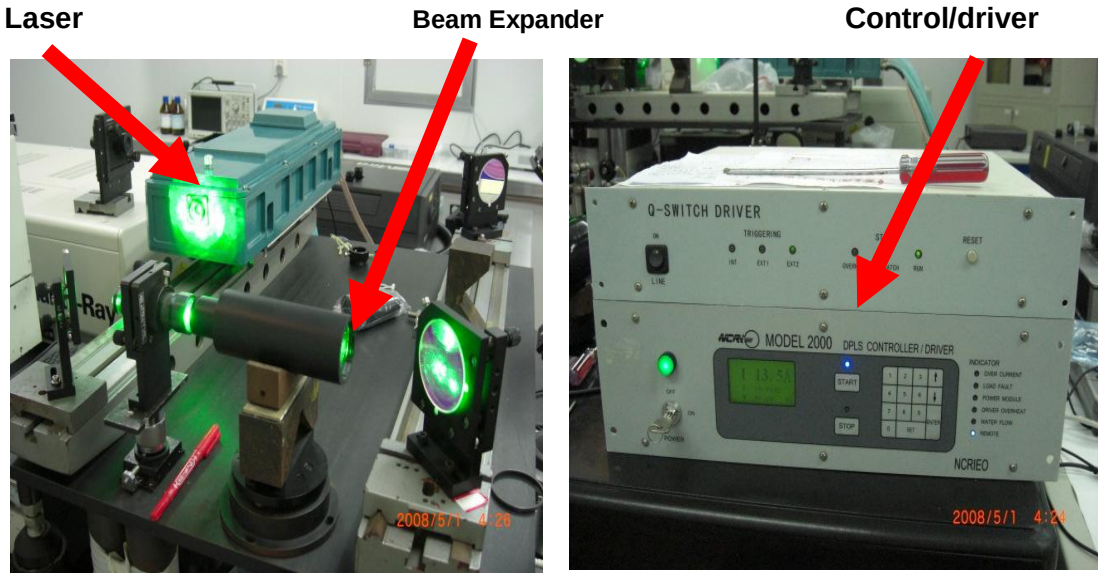

Figure 2. The kHz laser in operation

Event Timer (ET)

We develop the A032-ET functions to adapt for kHz ranging and develop our own data acquisition software with Visual C++, according to the library functions which defines device-specific function. Table 2 lists the specification of A032-ET. Figure3 and Figure 4 show how to use A032-ET.

Table 2. The specification of A032-ET

Single shot RMS	<10ps
Measurement rate	up to 10kHz
FIFO	12000 time-tags
Communication port	EPP

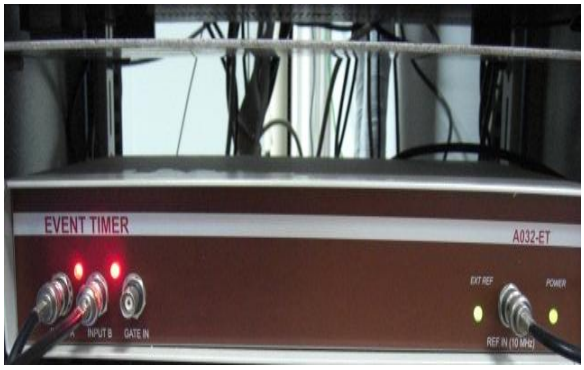

Made by Riga, Latvia

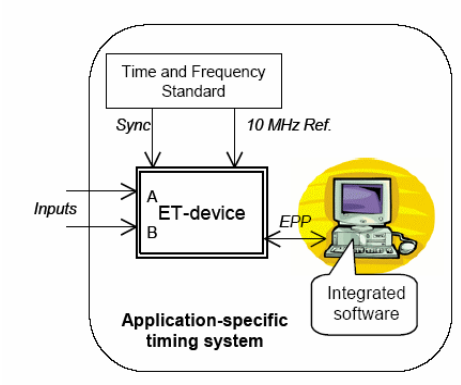

A032-Event Timer EPP mode

Figure 3. The timing system for SLR based on A032-ET

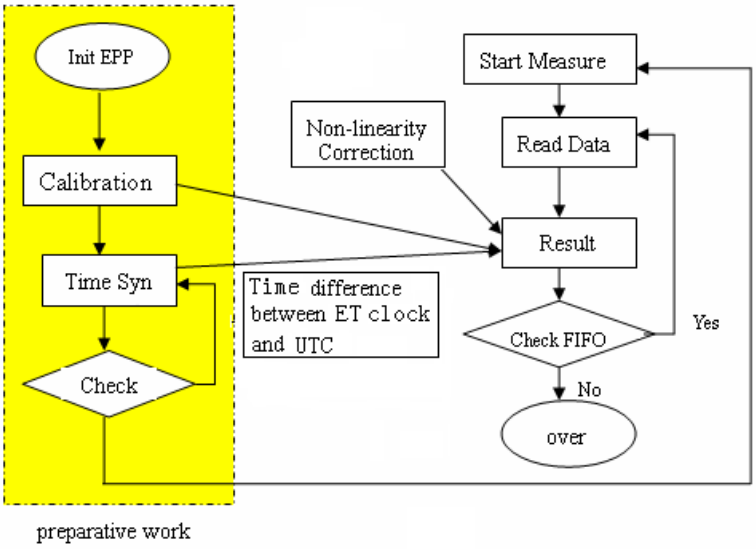

Figure 4. The schematic control diagram for A032-ET

kHz Range Gate Generators (RGG)

We have two RGGs: one from Graz with parameter of 0.5ns resolution, 1ns accuracy, 512 buffers and ISA mode, another developed by our group with 5ns resolution, 1024 buffers and EPP mode.

At the beginning phase of the experiment, Graz board is used. After that, we use our own RGG board to measure several satellites. Figure5 shows the layout of our RGG. The Real Time clock module synchronizes to UTC with 5ns resolution.

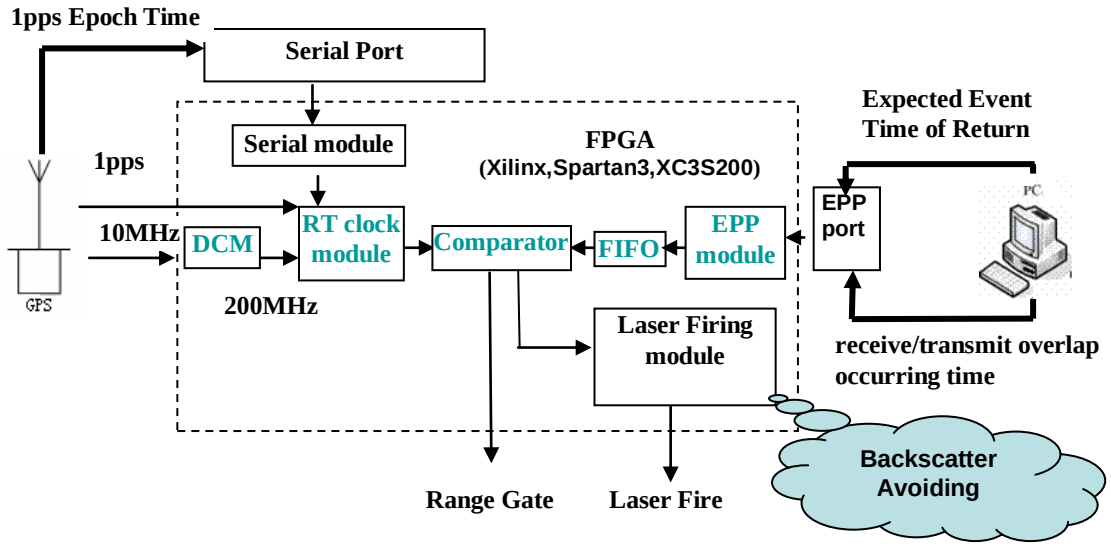

Figure 5. Layout of Shanghai's Range Gate Generator

If expected event time of return equals to real time, then range gate is generated. If receive/transmit overlap occurring time equals to real time, then backscatter avoiding function of laser firing module will start. The timing sequences of backscatter avoiding are shown in Figure6. If the delay between expected epoch time of return and laser firing is less than defined time interval, e.g.100us, then backscatter avoiding module will shift the following laser firings by another defined time interval backward, e.g.120us.

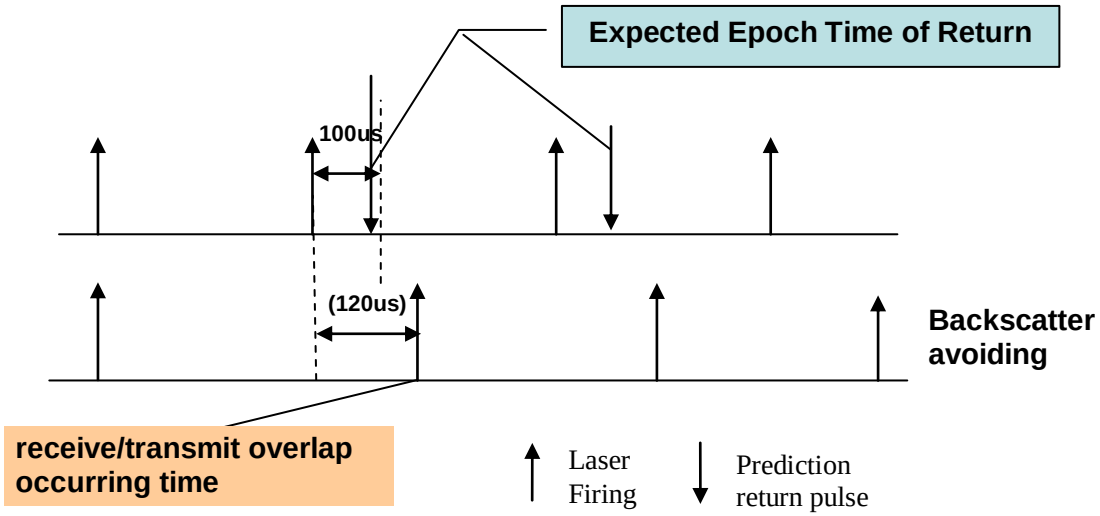

Figure 6. Timing sequences of backscatter avoiding

KHz Control Software System

Due to high real-time in kHz SLR controlling, we adopt two computers in the experiment in Windows OS: One computer is used for communicating with ET, recording start and stop events, and matching them, identifying, displaying range residual (O-C), storing data, etc. The software interface is shown in Figure8; Another computer is used for track and control which includes laser firing, range gating, receive/transmit overlap avoiding, etc. The software interface for this computer is shown in Figure9. During the experiment, the two computers communicate with each other via RS232. Block diagram of kHz system is shown in Figure 7.

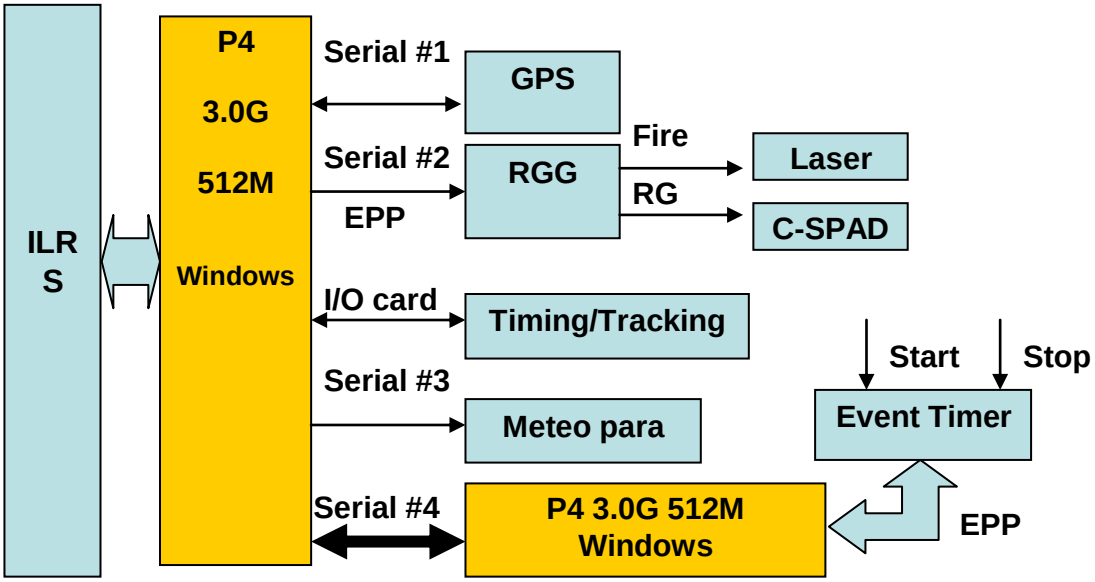

Figure 7. Block diagram of kHz system

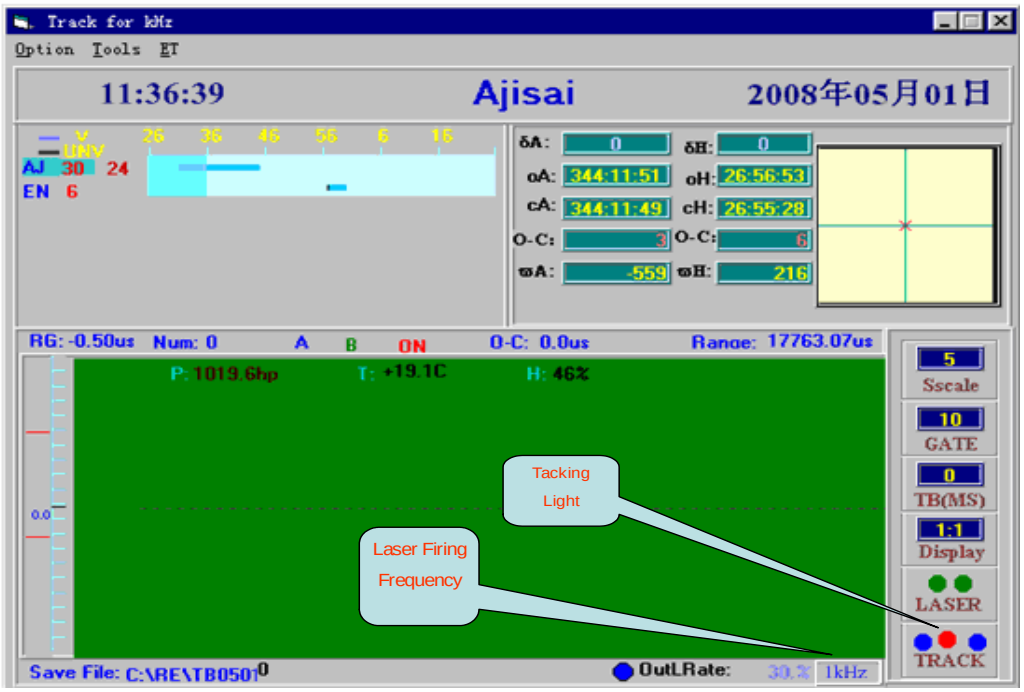

Figure 8. Real-time tracking interface for tracking, firing…

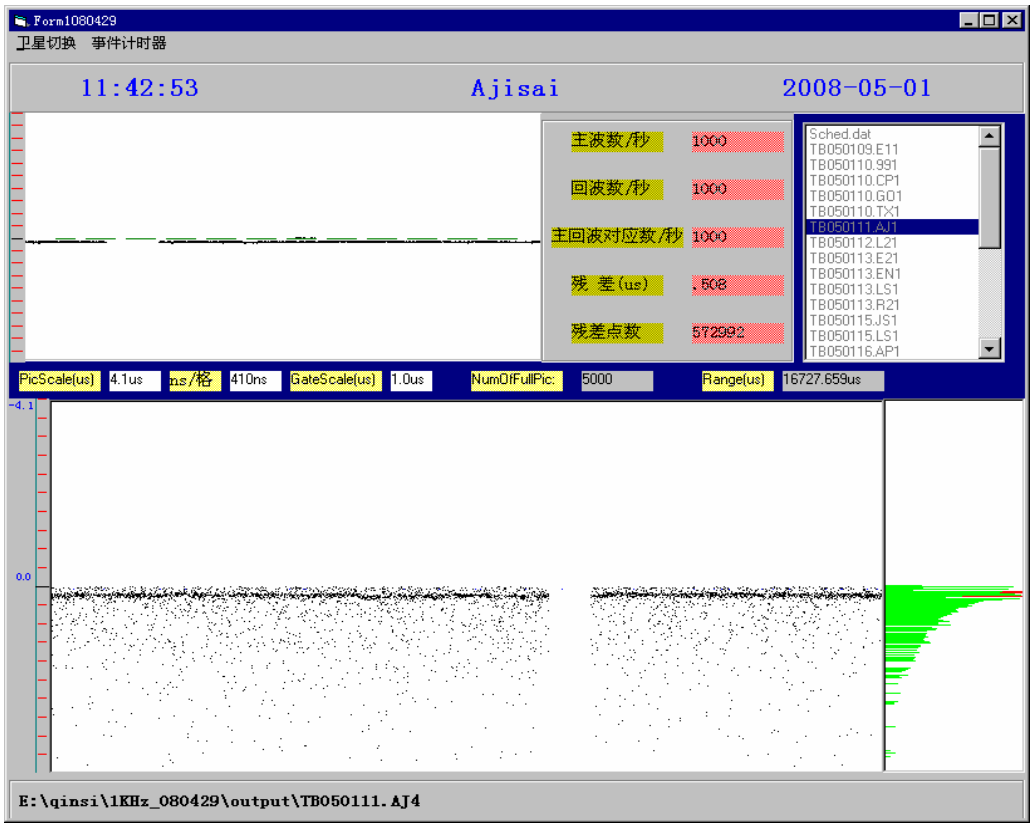

Figure 9. Another computer's real-time interface

Although kHz SLR control is highly real-time, we put expected epoch time of return into RGG in advance to ensure that kHz control software will run well in windows OS. Time sequencing diagram of writing RGG is shown as Figure10.

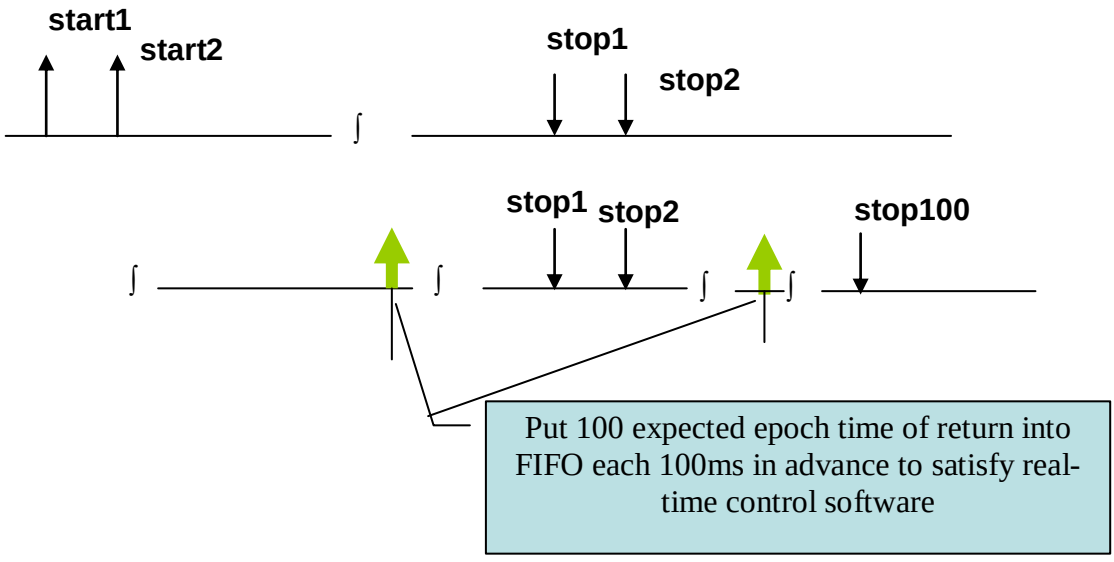

Figure 10. Time sequencing diagram of writing RGG

Data Pre-Processing

Because it takes a lot of time to display all observation data measured with 1kHz, we have developed a new data pre-processing program to process all data and only a part of them are displayed. This method increases the displaying speed without affecting the result. Comparison between the two ways of date displaying is shown in Figure 11.

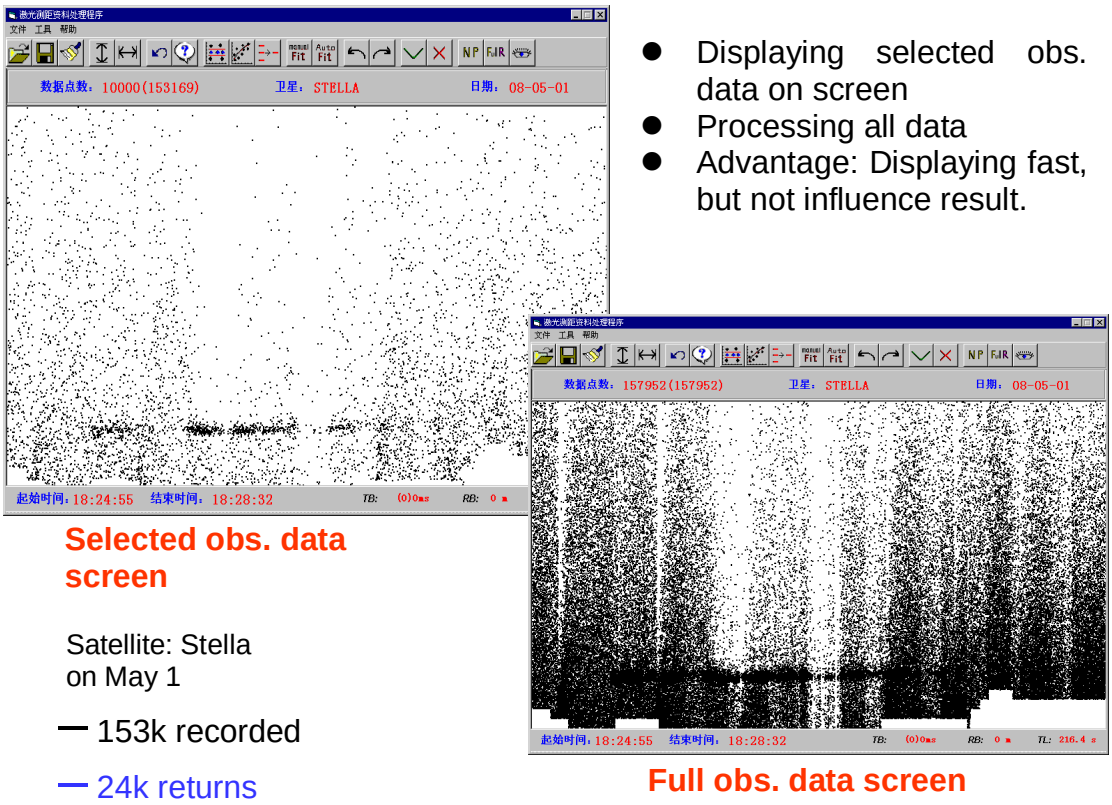

Figure 11. Method of Data Pre-Processing

Experiment Results

Since Apr.26 2008, we have successfully got returns from LEO satellites (Ajisai, Stella, BeaconC, ERS-2, Envisat, etc.) and Lageos with our kHz system, real-time interface for Lageos ranging is shown in Figure 12. Table 3 lists our kHz experiment results.

Table 3. kHz SLR returns vs. Routine SLR at Shanghai station

Satellite	KHz SLR		Routine SLR
	Recorded	Returns	Returns
Ajisai	618k	190k	1500
Stella	153k	24k	500
BeaconC	81k	42k	800
Lageos1	900k	60k	1000

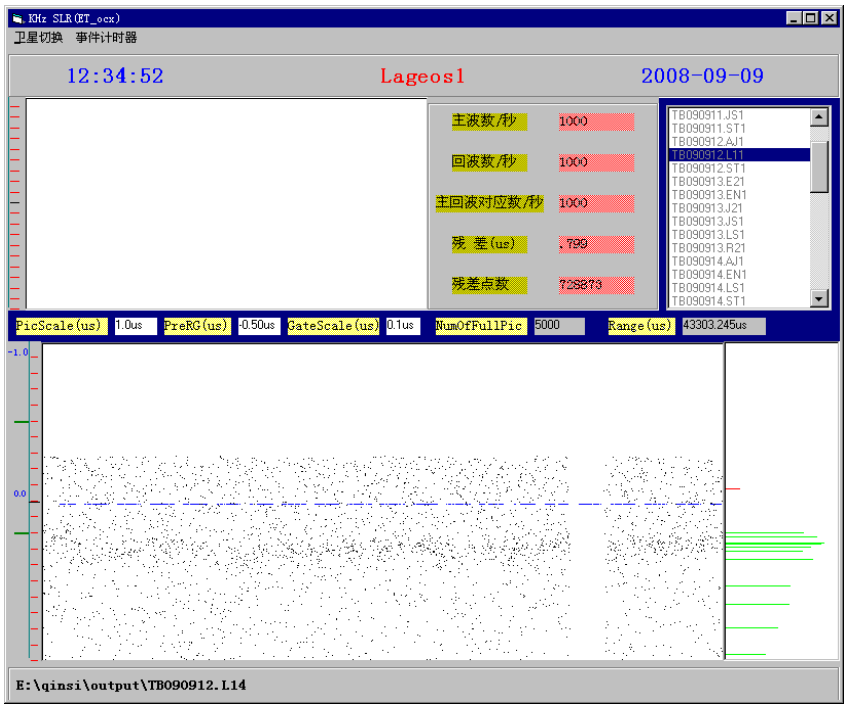

Satellite: Lageos-1 on Sep. 9

─ 900k recorded

─ 60k returns

Figure 12. Real-time interface for Lageos ranging

Summary and future plans

We have successfully obtained returns from satellites (Ajisai, Stella, BeaconC, ERS-2, Envisat, Lageos, etc.) by using a kHz laser with long pulse width. The experiment shows that our kHz control system works fine and promise fully. Now fund has been gotten from China government to purchase a kHz laser with short pulse width next year, and then high-precision routine kHz ranging will be started.

References

[1] V. Bespal'ko, E. Boole, V. Vedin, *THE MODEL A032-ET OF RIGA EVENT TIMERS*, 15th International Workshop on Laser Ranging, Canberra, Australia, 15-20 October, 2006

[2] G. Kirchner, F.Koidl, *Graz KHz SLR System: Design, Experiences and Results*,14th International Workshop on Laser Ranging, San Fernando, Spain, 7-11 June, 2004

[3] G. Kirchner, SLR Graz: *The RGG (Range Gate Generator)*, ILRS kHz Technical Meeting, Graz, Austria, October 27-29, 2004

[4] G. Kirchner, *Real Time Return Detection*, ILRS kHz Technical Meeting, Graz, Austria, October 27-29, 2004

NGSLR: Sharing Eye-safe Kilohertz SLR with Transponder Ranging

Jan McGarry (1), **Thomas Zagwodzki** (1), **Thomas Varghese** (2), **John Degnan** (3), **John Cheek** (4), **Christopher Clarke** (5), **Peter Dunn** (4), **Anthony Mallama** (4), **Anthony Mann** (5), **Donald Patterson** (5), **Randall Ricklefs** (6)

(1)NASA Goddard Space Flight Center
(2) Cybioms Corporation
(3) Sigma Space Corporation
(4) Raytheon Information Systems
(5) Honeywell Technology Solutions Incorporated
(6) University of Texas at Austin

Jan.McGarry@nasa.gov / +1-301-614-5867

Abstract

NASA's Next Generation Satellite Laser Ranging System (NGSLR) is expected to be operational in early 2009. The system is currently ranging with the eyesafe laser (~100 microJoules at 2 khz) to targets ranging in altitude from Low Earth Orbiting (LEO) satellites to LAGEOS, and has successfully ranged to GLONASS-95 and GLONASS-102. Satellite passes are normally tracked using a tight laser divergence (4 arcsec) with hands-off operation, and requiring no bias correction. Many LEOs have been tracked down below 15 degrees elevation. The telescope is pointed behind, in the direction of the returning light from the satellite, and the Risley Prism wedges are independently controlled to point the laser ahead to where the satellite will be when the laser pulse arrives.
With a simple drop-in mirror, toggle switch, and single cable change, the system can switch from eyesafe laser ranging to ranging with the 50 milliJoule, 28 hz, 6 nanosecond pulsewidth laser. This higher power laser was added to the system to perform uplink-only ranging to the Lunar Reconnaissance Orbiter (LRO-LR). For LRO the laser fire is controlled to ensure that the pulses arrive at the spacecraft when the Range Window is open and can accept events. Ground laser fire times are recorded and transmitted to a central facility where they are matched with the spacecraft events to form ranges.

Introduction

NGSLR is expected to be operational in a few months, performing two-way ranging to satellites and one-way ranging to LRO. This paper describes the current system status, the modifications needed to perform one-way ranging to LRO, and future work to make the system more automated with enhanced performance.

Eyesafe Ranging Configuration and Status

NGSLR is a single photon multi-kilohertz eyesafe satellite laser ranging system (McGarry 2006). NGSLR uses a Q-Peak laser with an original output energy of 120 microJoules per pulse which has degraded over the last several years to less than 100 microJoules per pulse. A 50% transmission loss through the telescope means that the current system is outputting about 50 microJoules per pulse at the telescope aperture in a 37 cm diameter beam.

The current laser pulse width is about 300 picoseconds. The software controls the laser fire rate which is varied between 1.96 khz and 2.0 khz to prevent collisions between outgoing and incoming laser pulses when the detector is gated on. The hardware also provides an added measure of protection by blanking the detector for 50 microseconds after the laser fires.

The laser divergence is currently set at 4 arcseconds (full width) for all satellite ranging. Currently NGSLR receives multi-photon returns from the LEO satellites.
Future plans are to vary the divergence as a function of the satellite. Low earth orbiting (LEO) satellites would have a larger divergence (~8 arcseconds) while the LAGEOS and Global Navigational Satellite Systems (GNSS) would continue with the 4 arcsecond divergence.

The current receiver system is a high quantum efficiency (32%) Hamamatsu four quadrant detector with a constant fraction discriminator (CFD) on each quadrant. The threshold setting on the discriminators is nominally set to < 0.5 photo-electrons.

The telescope is pointed behind to allow the quadrant information to be used for angular correction. The transmitted beam is independently pointed ahead by a Risley Prism pair (Degnan 2008). This allows the system to operate during the daylight with both a narrow beam divergence and a narrow receiver field of view, even when the two do not overlap. The full width fields of view used are 25 arcseconds for night, 16 arcseconds for twilight, and 11 arcseconds for daylight.

The Xybion mount continues to perform well consistently closing the tracking loop to 1 arcsecond. The 22 term mount model provides absolute pointing at the 2-3 arcseconds level after star calibrations.

Over the last several months the system has demonstrated robust tracking of satellites from LEO to LAGEOS in day as well as night, with night tracks of GLONASS-95 and GLONASS-102.

Much of the system is automated, but the station currently requires a single operator to track satellites.

Satellite Laser Ranging Results

The engineering team currently performs the tracking operations for NGSLR which occurs a few hours every week. Over the last two months NGSLR has tracked 27 passes, including AJISAI, BEC, JASON, JASON-2, LARETS, STARLETTE, LAGEOS 1 and 2, and GLONASS-102. Inter-comparison tracks show centimeter level agreement between NGSLR and MOBLAS-7 for all satellites (Dunn 2008).

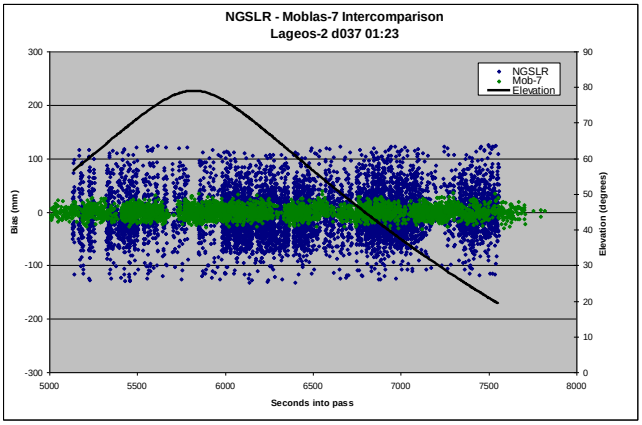

Figure 1. NGSLR full-rate ranges (blue: wide envelop) versus MOBLAS-7 ranges (green: narrow envelop) for a February 6th, 2009 LAGEOS-2 pass.

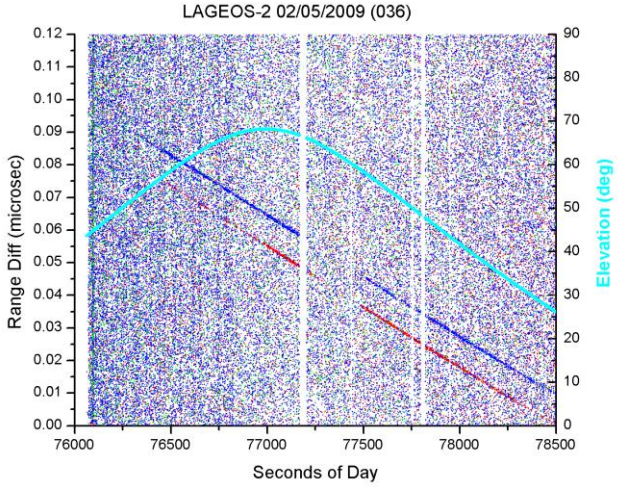

Figure 2. Daylight LAGEOS-2 OMC plot showing returns in two of NGSLR's four quadrants. Length of tracking segment is ~ 40 minutes.

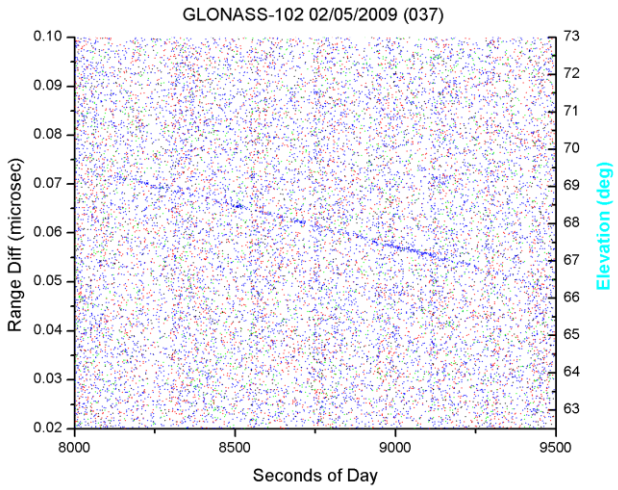

Figure 3. Night GLONASS-102 pass with returns in single quadrant. Length of tracking segment is ~ 30 minutes. Elevation of mount was > 60 degrees.

Accommodating Laser Ranging to LRO

Laser ranging to LRO requires a 28 hz 30+ milliJoule laser with a wavelength that is matched to the center of the spacecraft's 3 Angstrom LR bandpass filter. The pulse width is required to be less than 8 nanoseconds (FWHM). Two lasers were purchased from Northrop Grumman Space Technology Cutting Edge Optronics and characterized. They have a wavelength of 532.2 nm and an output energy capability of up to 50 milliJoules with a pulse width of 5.5 nanoseconds. One laser was installed in NGSLR and the other is the system spare. The onboard LR filter was tilt tuned to center it around the 532.2 nm wavelength.

The LRO laser is mounted on an upper level breadboard above the NGSLR optical bench and coupled into the telescope with a removable aperture share mirror. This mirror allows for easy switching back and forth between the eyesafe 2khz laser and the LRO laser and permits use of common receiver and alignment optics and electronics, allowing the system to track satellites with either laser. The two lasers also share a common start diode. A single cable swap is required to move from one laser to the other on the start discriminator.

Because the LRO laser is not eyesafe, an aircraft avoidance radar and associated electronics were added to NGSLR. This Laser Hazard Reduction System (LHRS) provides a means of detecting aircraft and shutting off the laser before the aircraft intersects the transmitted laser beam. The radar can detect aircraft out to a range greater than the nominal ocular hazard distance. It is the same unit used on the NASA MOBLAS and TLRS systems.

The software must control the time of the laser fire to ensure that each pulse arrives at the spacecraft when the Earth detector gate is open (McGarry 2008). NGSLR uses the Range Gate Generator (RGG) to command the laser fire times. The HTSI built RGG outputs at a 2 khz frequency with the software commanding (1) the delay of the outgoing pulse from the start of each 2khz interval and (2) the width of the outgoing TTL pulse to the laser. The software modulates the width of the RGG output pulse to provide an approximately 28 hz frequency to the laser.

Because of the critical nature of the timing measurement it was determined that the Truetime GPS steered Rubidium station timing was not an adequate source for the 10 Mhz external input to the Event Timer. This is because the steering puts jumps in the otherwise smooth fire time differences when the GPS steering occurs. To eliminate this issue a Cesium Oscillator (Symmetricom model 4310) was added to the system. This unit now provides the 10 Mhz input to the system Event Timer for all operations (SLR and LRO), while the Truetime continues to provide station time-keeping. Special processing for LRO ensures that only the Cesium drives the timing for the hour long LRO passes.

The block diagram in Figure 4 shows the NGSLR system with the additions for LRO.

Operations during LRO-LR

NGSLR is expected to operate whenever the moon is above 20 degrees elevation, LRO is on the near side of the moon, the spacecraft High Gain Antenna (HGA) is pointed at earth, and there is no precipitation. This implies operational shifts that would need to cover as much at 10 hours per day 7 days a week. Operations are expected to last for over a year. We are still working on the shift scheduling, but we will have 3 trained operators to cover NGSLR and

one MOBLAS-7 shift, and we will have multiple people from the engineering development team to fill in for sick days, holidays, and other times.

The period of LRO's orbit is approximately 2 hours. Passes last for approximately one hour. The alternate hour will be used at NGSLR to do eyesafe satellite laser ranging.

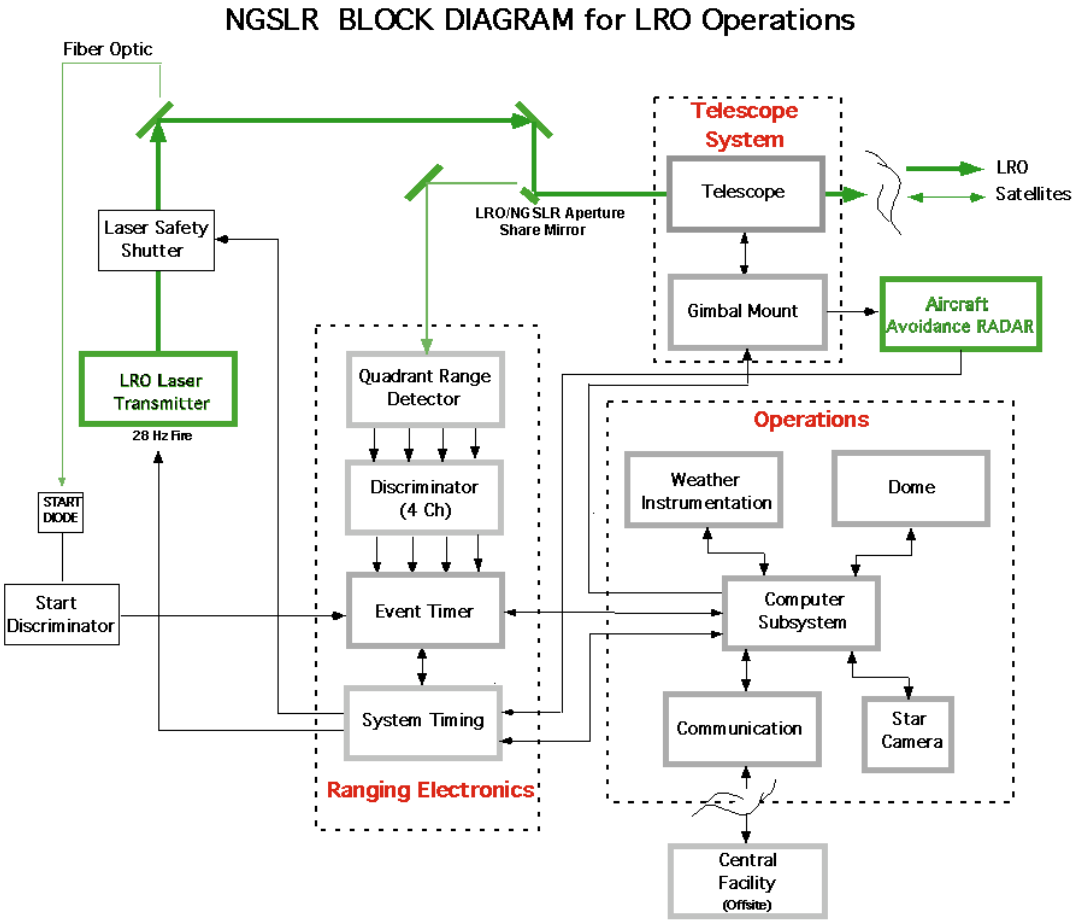

Figure 4. Block diagram of NGSLR system. Changes for LRO-LR include additional laser (28hz) with software control of fire via RGG, aircraft avoidance radar, and drop in mirror to allow switching between LRO and eyesafe lasers**.**

Remaining to Complete at NGSLR

To complete the automated eyesafe satellite laser ranging at NGSLR, we will be replacing the Q-Peak laser with a new laser designed and built in-house at GSFC by D. B. Coyle based on his previous work on the injection seeded ring cavity (Coyle 2008). This laser will give us a variable energy output level from eyesafe to up to 2 milliJoules of output energy per pulse, allowing us to more easily range to the navigational satellites such as GPS and GLONASS while maintaining our ability to do eyesafe ranging. This laser will be tested in NGSLR during the month of March and will be completed and installed permanently later in 2009.

Automated closed-loop tracking of satellites will be the focus of our efforts after NGLSR completes collocation with MOBLAS-7 in the next couple of months. Included in this work

is equalizing the quadrant noise counts, upgrading the signal processing, and completing the algorithms to convert the quadrant signal counts to mount drive information. We expect to have this work completed in late 2009 or early 2010.

Several of the optics on the transceiver bench have been automated, but the rest also need to be added to the software control, as do the detector and camera shutters.

The modifications required for LRO-LR are complete and successfully tested (Mallama 2008).

Summary and Acknowledgements

NGSLR has been in development since the late 1990s utilizing many novel technologies that required in depth analysis and engineering. This last year has seen the fruition of this development work. We have made great strides in system robustness, daylight ranging capability, and data accuracy, and we expect to be operational in a few months. The system is capable of being completely automated and we will continue to work toward this end.

At the same time, we have performed the required system modifications for LRO-LR and successfully tested them. We will begin operational ranging to LRO later this year, demonstrating that NGSLR is capable of both earth orbiting satellite and planetary transponder laser ranging.

NGSLR SLR development is being funded by the NASA/HQ Science Mission Directorate. Funding for LR modifications and operations is provided by the LRO Project. The authors would like to thank John LaBrecque of NASA/HQ for his continued support of the SLR work. We would also like to thank David Carter of NASA/GSFC code 450 for all of his efforts on behalf of NGSLR.

References

Coyle, D., Kay, R., Degnan, J., Krebs, D., Injection seeded diode pumped regenerative ring Nd:YAG amplifier for spaceborne laser ranging, Meas. Sci. Technol. 5**,** 136–143, 1994.

Degnan, J., McGarry, J., Zagwodzki, T., Varghese, T., *Transmitter Point-Ahead using Dual Risley Prisms: Theory and Experiment,* in this Proceedings, 16th International Workshop on Laser Ranging, Poznan, Poland, October 2008.

Dunn, P., Clarke, C., Torrence, M., *NGSLR Performance in High and Low Energy Operation*, in this Proceedings, 16th International Workshop on Laser Ranging, Poznan, Poland, October 2008.

Mallama, A., McGarry, J., Zagwodzki, T., Cheek, J., *Pre-Launch Testing of NGSLR Ranging to LRO,* in this Proceedings, 16th International Workshop on Laser Ranging, Poznan, Poland, October 2008.

McGarrry, J., Zagwodzki., T., *SLR2000: The Path Toward Completion*, Proceedings of the 15th International Workshop on Laser Ranging, Canberra, Australia, October 2006.

McGarry, J., Zellar, R., Neumann, G., Noll, C., Torrence, M., et al, *Laser Ranging to the Lunar Reconnaissance Orbiter: a Global Network Effort*, in this Proceedings, 16th International Workshop on Laser Ranging, Poznan, Poland, October 2008.

Transmitter Point-Ahead using Dual Risley Prisms: Theory and Experiment

John Degnan (1)**, Jan McGarry** (2)**, Thomas Zagwodzki** (2)**, Thomas Varghese** (3)

(1) Sigma Space Corporation
(2) NASA Goddard Space Flight Center
(3) Cybioms

John.Degnan@sigmaspace.com /Fax +01-301-577-9466

Abstract

For maximum detection efficiency and solar noise rejection, eyesafe photon-counting Satellite Laser Ranging (SLR) systems rely on narrow transmit beams and receiver FOV's. Because of the finite velocity of light, the transmit and receive FOV centers are angularly separated by up to 11 arcseconds in SLR and by several tens of arcseconds in interplanetary laser transponders or communications systems. We have successfully implemented and tested a dual Risley prism beam steerer for "Transmitter Point Ahead" (TPA) compensation in NASA's Next Generation Satellite Laser Ranging (NGSLR) System

Introduction

Conventional multiphoton SLR systems typically employ coaligned transmitters and receivers. The combination of high pulse energies, large transmitter beam divergences and even larger receiver fields-of-view ensure that a sufficient number of photons are reflected off the target and into the receiver to exceed the multiphotoelectron detection threshold. The latter is set sufficiently high (3 to 4 pe) to minimize false alarms under high solar background conditions. In contrast, eyesafe photon-counting systems operating at 532 nm in daylight must operate with over 3 orders of magnitude lower pulse energies, tight transmitter beam divergences to concentrate more of the transmitted light onto the satellite, and narrow receiver fields-of-view to reduce the solar background and improve the contrast between signal and solar noise.

As a consequence, the transmit and receive FOV's may no longer overlap if the point-ahead angle is sufficiently large. Thus, NASA's Next Generation Satellite Laser Ranging System (NGSLR, formerly known as SLR2000) is designed to point the receive telescope where the satellite was at the time the photons were reflected and independently point the transmitter ahead to where the satellite will be when the subsequent pulse arrives at the satellite (see Figure 1).

Overview of NGSLR Transceiver

The overall design and operation of the NGSLR transceiver has been described in prior workshops [Degnan, 2004], but a short overview is needed here to comprehend the nature of the Transmitter Point-Ahead" (TPA) issue. Figure 2 provides a schematic of the NGSLR transceiver optical bench. The transmitter is input to a computer-controlled 5-element Special Optics beam expander which controls the final beam divergence while maintaining a constant beam spot size at the telescope exit aperture (for eye safety). This is followed by a Matched Dual Risley Prism Pair, which implements the TPA feature, and a passive T/R switch

consisting of an entrance polarizer, Faraday Isolator, half-wave plate and an exit polarizer. The reflected beam off the exit polarizer then passes through a 3-power beam expander and is reflected off the telescope pit mirror into a four mirror Coude system and an az-el tracking mount with a 40 cm aperture, x10.16 magnification, off-axis primary telescope.

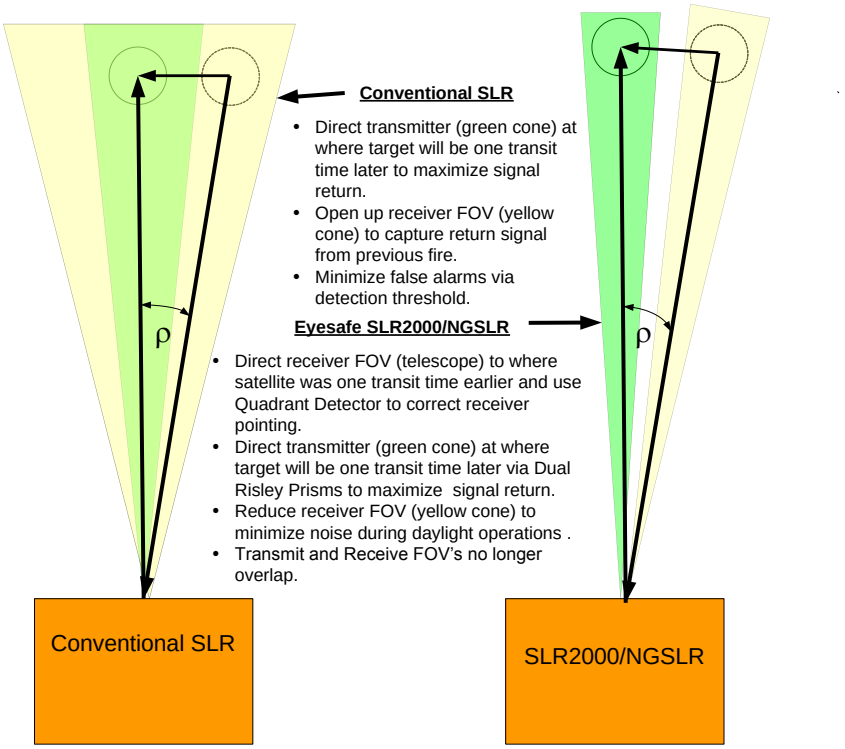

Figure 1. A comparison of conventional multiphoton SLR operations with that of the photon-counting SLR2000/NGSLR station.

Received photons are transmitted with high efficiency through the T/R switch (along two polarization paths) through the spectral and spatial filters to a quadrant MicroChannel Plate PhotoMultiplier Tube (MCP/PMT). Under full automated operation, signal count imbalances in the four quadrants are used to center the receive FOV on the "apparent" position of the satellite. The "apparent" position differs from the "true" position by the angular distance the satellite travels during the one-way transit of the reflected photons from the spacecraft to the station.

Coordinate Systems

The point-ahead angles expressed in the azimuth and elevation coordinates of the telescope, $\Delta\alpha$ and $\Delta\varepsilon$ respectively, are obtained from the orbit prediction program and are equal to the satellite angular rates in each axis multiplied by the roundtrip transit time of the light pulse. As shown in Figure 3a, we choose to express the TPA angle in polar coordinates as an angular magnitude, ρ, and direction, β_{AE}, as measured from the instantaneous telescope azimuth axis.

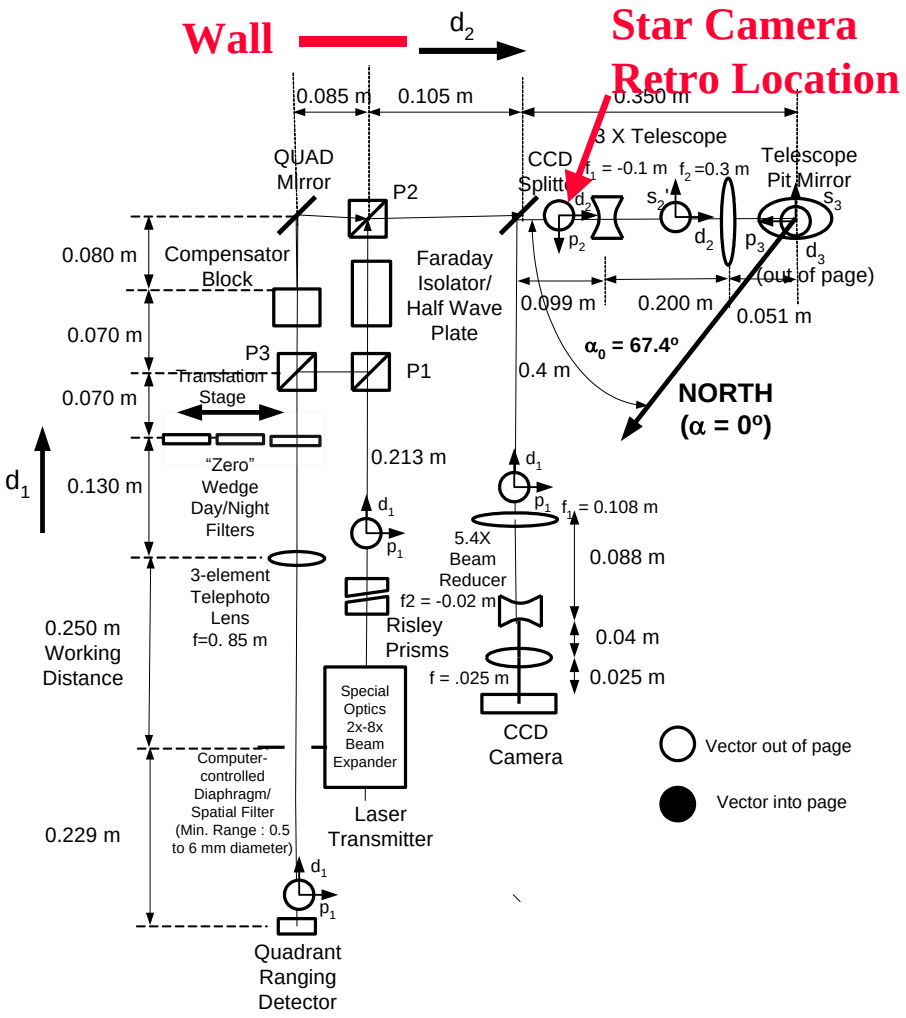

Figure 2. Block diagram of the NGSLR transceiver optical bench. The positions of the "wall" and "star camera retro location", referred to in the Experimental Validation Section , are superimposed in red.

Theoretical Predictions via Ray Tracing

Converting these az-el offsets into the proper rotation angle commands for the two Risley prisms requires that we properly account for the complex and time-dependent coordinate transformations that are imposed by the various optical components and the axis rotations of the Coude mount as the transmitted pulse travels from the Risleys to the exit aperture of the telescope. This was accomplished theoretically through "ray tracing" as described in a detailed internal report [Degnan, 2005]. We obtain for the rotation angle commands

$$\theta_5^c = \theta + \beta_{AE} + a\cos\left(\frac{\rho}{2R}\right) = \frac{\pi}{2} - \theta - \beta_{AE} + \frac{1}{2}a\cos\left[1 - \frac{(m_t\rho)^2}{2\delta^2}\right] \quad (1a)$$

$$\theta_6^c = \pi - \theta - \beta_{AE} + a\cos\left(\frac{\rho}{2R}\right) = -\frac{\pi}{2} + \theta + \beta_{AE} + \frac{1}{2}a\cos\left[1 - \frac{(m_t\rho)^2}{2\delta^2}\right] \quad (1b)$$

where the Coude θ-parameter

$$\theta = \alpha - \alpha_0 - \varepsilon + \frac{\pi}{2} = \alpha - \varepsilon + 22.5^o \qquad (2)$$

takes into account the effect of the tracking mount on the orientation of the final TPA deflection. The parameters appearing in the above equations are: the instantaneous azimuth and elevation angles, α and ε; a system specific azimuthal correction defined as the angle the input/output beam of the transceiver makes with the North direction as measured with a compass, α_0 =67.5^o (see Figure 2); the overall effective magnification of the transmit beam following the Dual Risley Prisms, m_t = 28.21; and the deflection angle produced by a single wedge, $\delta \sim (n\text{-}1)w$ = 15.6 arcmin, where n is the index of refraction and w is the wedge angle. The second form of the equations in (1) are currently used in the operational algorithms.

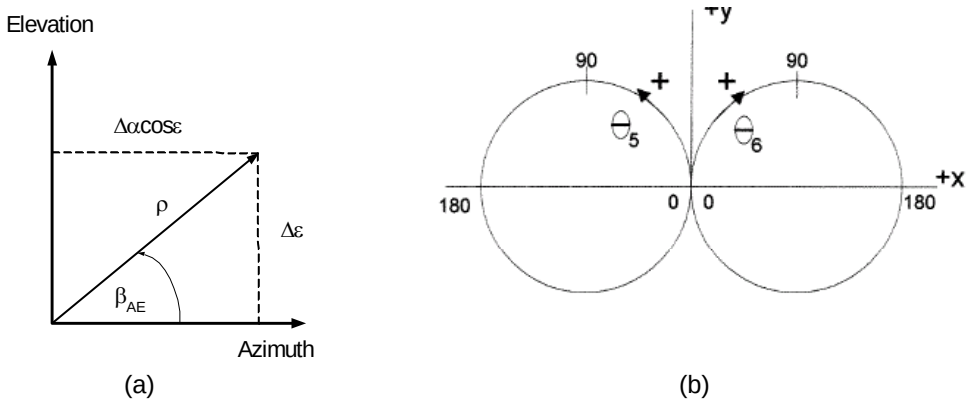

Figure 3. (a) TPA coordinate definitions in the instantaneous azimuth-elevation plane of the primary telescope. (b) Within the dual Risley unit, one wedge (θ_5) is rotated in a CCW direction from a "home" position along the positive x-axis while the second (θ_6) is rotated in a CW direction from a "home" position along the negative x-axis.

Experimental Validation

A simple, but low angular resolution, test was conducted by projecting the output of the dual Risley prism pair onto the "wall" directly behind the Risleys (see Figure 2) and at the telescope exit aperture for a fixed value of azimuth (α= 90^o) and elevation (ε = 22.5^o) as a function of the commanded values of ρ and $\beta_{AE.}$ In the experiments of Figure 4, ρ was constant at 10 arcsec, except for point J (ρ =0), while β_{AE} took on the values 0,90,180, and 270^o (F,G,H,I). As expected from (2), the telescope aperture pattern is rotated by θ = 90^o with respect to the wall pattern and the angular deviations are smaller by a factor m_t =28.21.

Finally, for optimum performance, one must correct for any rotational angle biases between the "home" positions of the servo motor drivers and the corresponding wedge orientation. Retroreflecting the outgoing transmitter pulse from a point in the common transmit/receive path on the optical bench (labeled "Star Camera Retro Location" in Figure 2) into the focal plane of the star calibration camera, with a resolution of ~0.5 arcsec per pixel, allowed us to achieve the necessary angular sensitivity. The various parameters in the theoretical model were adjusted to give the "best" agreement with experiment as illustrated in Figure 5, where the abscissa and ordinate values correspond to the pixel numbers in the star camera.

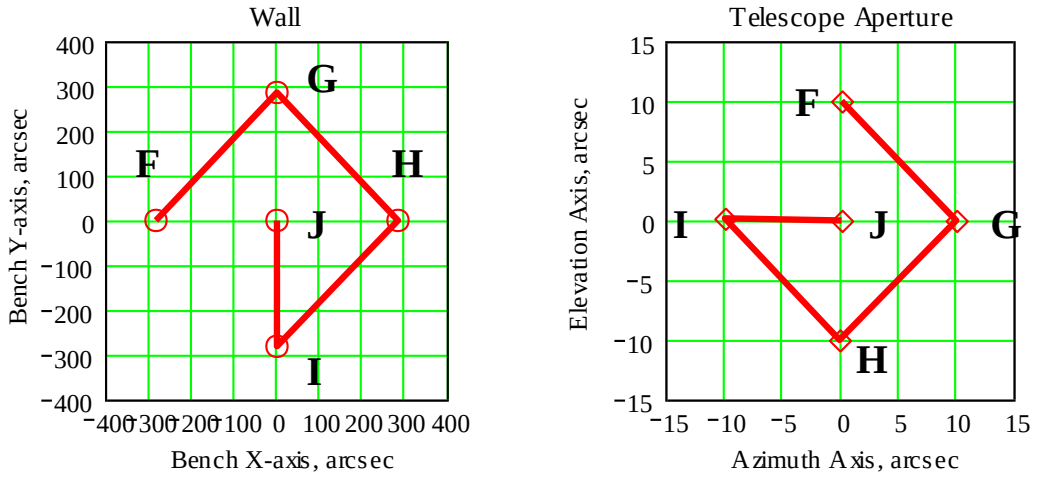

Figure 4. Projections of the deflected beam on the "wall" and at the telescope exit aperture. The pattern at the exit aperture is rotated by 90° in agreement with (2) for α =90° and ε=22.5°.

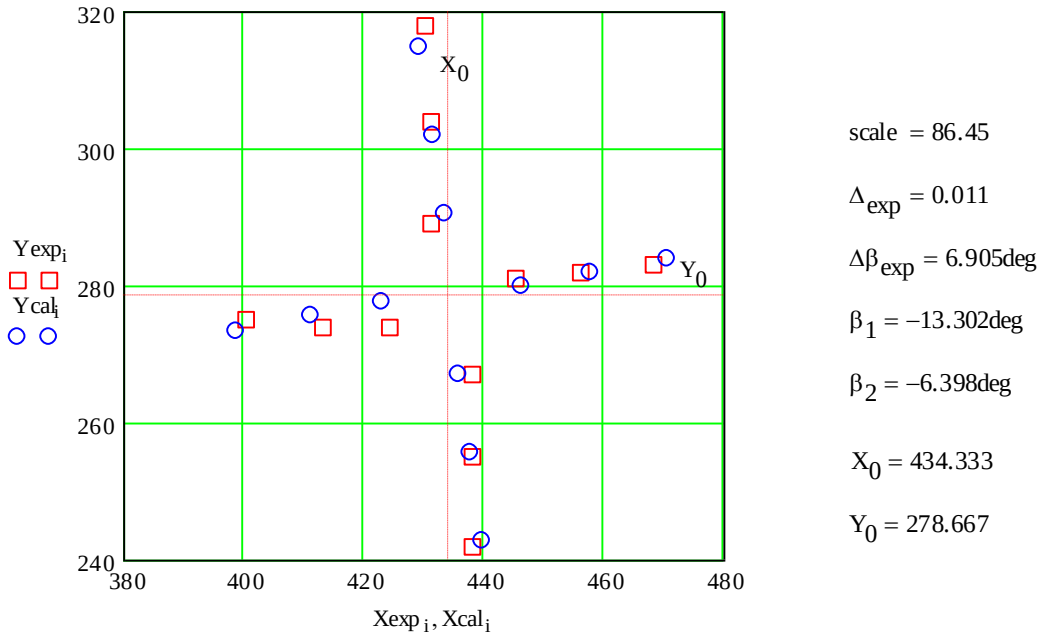

Figure 5. Star camera **c**omparison of theory (blue diamonds) with experiment (red squares). Each major division (20 pixels) corresponds to slightly less than 10 arcsec.

The numerical values to the right of the plot correspond to the "best fit" values of the theoretical parameters to the experimental data. "Scale" is related to the mean deflection angle of each prism and sets the overall size of the pattern. Δ_{exp} is the fractional difference between the two wedge angles (1.1%), and the non-zero value is responsible for the open area near the origin defined by X_o and Y_o (intersecting vertical and horizontal red dashed lines) since, as mentioned previously, ρ cannot equal zero for unequal wedges. The parameters β_1 and β_2 are the rotational biases between the stepper motor "home" positions and the thick part of the wedge (i.e. direction of the individual wedge deflection), while $\Delta\beta_{exp}$ is simply the difference between the two rotational biases.

Summary

The development of the point-ahead algorithms for NGSLR was approached through an iterative combination of theoretical ray analyses and experiment until we achieved agreement. During the star camera experimentation, we found that the wedge angles of the two prisms differ by about 1.1%, implying that true "zero" deflection can never be achieved. However, ignoring this difference in the point-ahead algorithm produces an acceptable maximum transmitter pointing error of about 1.5 arcsec for small ρ. For larger ρ, the errors are typically sub-arcsecond. To avoid this small discrepancy in the future, tighter matching of the prism angles will be required.

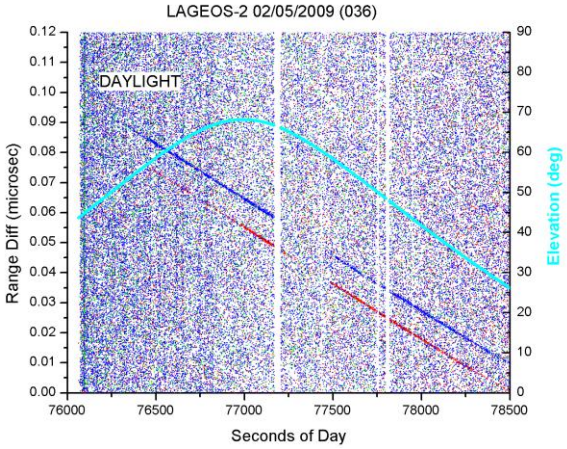

Figure 6. Daytime LAGEOS pass with time of day on the abscissa. The straight red and blue curves give the satellite returns in 2 of 4 quadrants offset by a fixed 100 nsec time delay. The magenta curve gives the satellite elevation on the right ordinate.

Since the workshop, we have successfully tracked LEO's and LAGEOS in daylight with the Dual Risley TPA-mechanism active and the telescope pointing the receiver open loop to the apparent position of the satellite. Figure 6 shows a daylight LAGEOS pass which used a $\pm$ 2 arcsec transmit beam and a $\pm$ 5.5 arcsec receiver FOV. Maximum point-ahead for this pass was 7.8 arcsec. The blue and red lines in the plot correspond to the orbital fit from two different detector quadrants; the quadrants are offset from each other by 100 nsec so that all quadrant returns can be recorded by the Event Timer, which has a nominal 60 nsec deadtime. The absence of two quadrants in the plot is the result of not yet activating the closed loop pointing system (an upcoming NGSLR milestone) which attempts to derive receiver pointing corrections by balancing the count rates in the four detector quadrants.

Similar transmitter point-ahead systems and algorithms will be required for future interplanetary laser transponder and communications systems where the link margins are weak and ρ can take on values of several tens of arcseconds.

References

Degnan, J. , 2004, "Ray Matrix Approach for the Real Time Control of SLR2000 Optical Elements", Proc. 14th International Workshop on Laser Ranging, San Fernando, Spain, June 6-10.

Degnan, J., 2005 ,"Ray Matrix Analysis for the Real-Time Control of Automated SLR2000 Subsystems", Sigma Space Corporation Internal Report, October.

Impact of Receiver Deadtime on Photon-Counting SLR and Altimetry during Daylight Operations

John J. Degnan
Sigma Space Corporation
John.Degnan@sigmaspace.com /Fax: +01-301-577-9466

Abstract

The dominant noise source in photon-counting SLR and altimetry systems is the solar background during daylight operations. We discuss the relevant attributes of Single Photoelectron Avalanche Diodes (SPADs) and Microchannel Plate Photomultipliers (MCP/PMTs) for these applications. Using a solar noise model based on a stratified spherical shell atmosphere, we compute the expected background count rates under a variety of atmospheric conditions for two pertinent instruments, i.e. NASA's NGSLR (SLR2000) system and the Cross Track Channel Lidar Altimeter proposed for the ICESat-II Mission. We discus the relevant merits of the various detector types and the role various types of pre-detection noise filters can play.

Background Noise Sources for SLR and Laser Altimetry

Sources of background noise for SLR include detector dark counts, solar scattering off the atmosphere, and laser backscatter from instrument optics or the local atmosphere. In laser altimetry, one must also add solar scatter off the surface being interrogated.

Detector dark counts are spontaneous and random photon events that occur in a darkened environment without any apparent external stimulus. Dark count rates are generally lower in the visible wavelength regime and increase as one moves the operating wavelength deeper into the near infrared (NIR). Dark count rates can often be reduced by cooling the detector.

Solar photons enter the receiver by scattering off objects within the receiver Field-of-View (FOV) and are by far the dominant source of noise during daylight operations. In SLR, these photons are scattered by atmospheric constituents, such as molecules, aerosols, fog, clouds, etc. In altimetry, one has an additional, and usually dominant, solar contribution from the surface lying within the receiver FOV.

Another source of photon noise is laser backscatter off the instrument optics and/or nearby atmosphere. This is of special relevance to monostatic photon-counting systems, such as NASA's Next Generation Satellite Laser Ranging (NGSLR) station, when atmospheric scatter from the outgoing pulse falls within the temporal receive gate of a previous pulse. NGSLR periodically varies the laser pulse repetition rate slightly in an attempt to avoid this temporal overlap and has the additional option (not currently implemented operationally) of isolating the receiver from backscatter using a high speed, liquid crystal, optical gate [Degnan and Caplan, 2006]. Bistatic systems, whose transmit and receive FOV's are spatially isolated out to some range due to separate non-coaxial optical systems, are far less vulnerable to this type of backscatter noise.

Photon-Counting Detectors and Limitations

Kilohertz photon-counting SLR and altimetry systems employ either Single Photon Avalanche Photodiodes (SPADs) or MicroChannel Plate PhotoMultiplier Tubes (MCP/PMTs) as detectors. Both detector types have high quantum efficiencies (40% to 55%) at the 532 nm SLR wavelength. When used in the near infrared (NIR), commercially available Geiger-mode SPAD's and MCP/PMT's have traditionally been plagued by relatively low efficiencies (<4%) and high dark counts when compared to their visible counterparts. More recently, however, MIT Lincoln Laboratories has reported on passively-quenched NIR APD arrays with about 55% efficiency at 1064 nm. Similarly, Hamamatsu has recently introduced a cooled NIR MCP/PMT with QE's as high as 18% (10% is nominal).

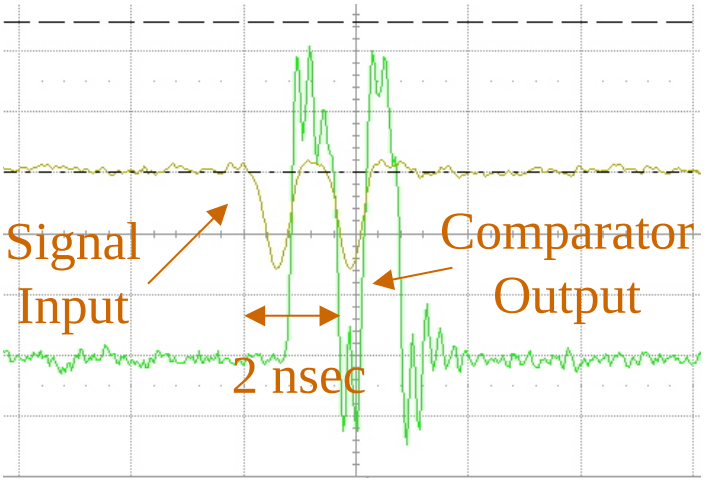

Figure 1. Sigma Space Corporation has built a 50 channel timing board with a timing precision of ± 93 psec (±1.4 cm) and a recovery time of about 1.6 nsec as part of a 100 beam, airborne 3D imaging lidar. The waveforms demonstrate the ability of the timing receiver to resolve input signals separated by only 2 nsec.

SPADs are further divided into passively or actively quenched subgroups with vastly different recovery times following a photon event. Passively-quenched SPADs (PQ-SPADs) have recovery times on the order of 1.6 microseconds, which essentially makes them "single-stop per pulse" devices for most lidar applications. Actively quenched SPADs (AQ-SPADs) , on the other hand, typically have recovery times on the order of 50 nsec. In contrast, MCP/PMTs have vanishingly small recovery times (< 2 nsec), but this inherent advantage is not always maintained by the backend timing electronics. In NASA's NGSLR system, for example, the HTSI-built timing electronics recovery time is comparable to that of an actively-quenched SPAD receiver, whereas the combined MCP/PMT detector and timing electronics in Sigma's 100 beam 3D Imaging Lidar [Degnan et al, 2007] has a much shorter recovery time, about 1.6 nsec. Fast recovery times also enhance the performance of laser altimeters measuring surface topography through semi-porous obscurations, such as tree canopies, ground fog, clouds, dust, etc.

Impact of Solar Noise on Photon-Counting Detectors

High solar background rates can reduce the probability of detecting the signal if the detector or receiver have recovery times, τ_d, comparable to or greater than the mean time between solar photon arrivals. In general, the solar photon count rate, $\dot{n}$, will cause the mean signal count rate from the satellite or the ground to be reduced by a factor

$$SCRF = \exp\left(-\dot{n}\tau_d\right) \qquad (1)$$

which corresponds to the Poisson probability that a solar count will not be detected within a receiver deadtime interval prior to a signal "event". In Figure 2, we plot the "Signal Count Reduction Factor" (SCRF) as a function of solar background rate for the three photon-counting detectors discussed previously, i.e. the PQ-SPAD, AQ-SPAD, and MCP/PMT.

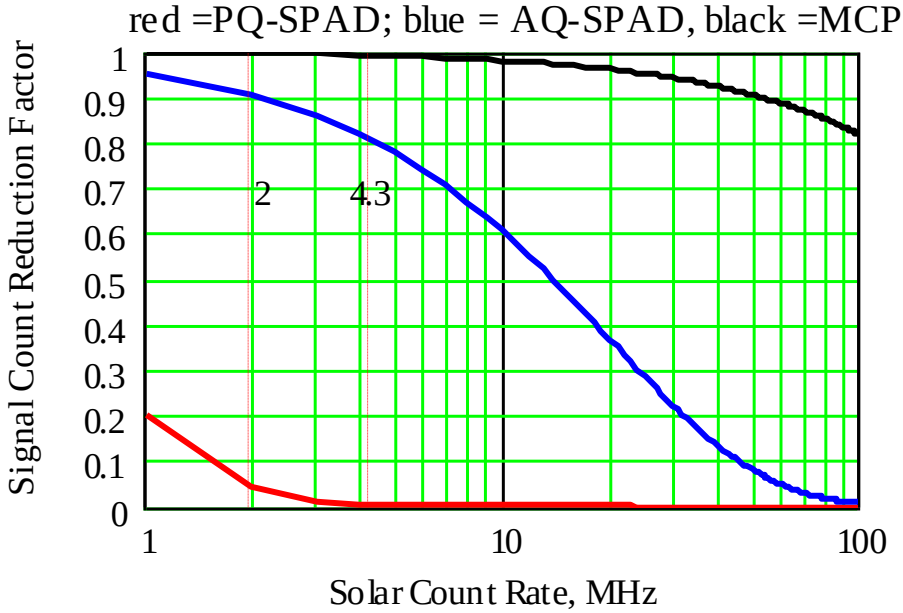

Figure 2. Signal count reduction factor vs solar count rate for three common photon-counting detectors: red = PQ- SPAD (1600 nsec), blue = AQ-SPAD (50 nsec), and black = MCP/PMT (2 nsec).

MCP/PMTs have one disadvantage relative to AQ-SPADs. High solar background rates can: (1) cause the microchannel plates to temporarily exceed their current limits (typically 100 to 200 nA) and reduce responsivity; and (2) reduce microchannel plate photomultiplier lifetime by extracting excessive charge from the microchannels. SPAD lifetimes do not appear to be limited by total charge extraction but rather by malfunctions in their associated electronics.

High solar background rates also reduce the *signal contrast* [Degnan, 2002a], analogous to Signal-to-Noise Ratio in multiphoton lidars, making the satellite or surface returns more difficult to identify against the background. Unless the noise can be successfully filtered pre-

detection or edited out via near real-time post-detection algorithms [Degnan, 2002a], ultralow contrast can add significantly to in situ data storage and transfer requirements.

Solar Noise Models for SLR and Altimetry

In performing the numerical studies presented here, we have employed a simple closed-form solar noise model, which assumes isotropic scattering in a stratified spherical shell atmosphere [Degnan, 2002b]. For photon-counting SLR systems, the solar count rate is given by

$$\dot{n} = \frac{\eta_q \eta_r}{h\nu} \frac{N_\lambda(\Delta\lambda)\Omega_r A_r}{4\pi} \left\{ \sec\theta_t T_0^{\sec\theta_t} \left[\frac{1 - T_0^{\sec\theta_s - \sec\theta_t}}{\sec\theta_s - \sec\theta_t} \right] \right\}$$
$$\cong \frac{\eta_q \eta_r}{h\nu} \frac{N_\lambda(\Delta\lambda)\Omega_r A_r}{4\pi} \left\{ T_0^{\sec\theta_t} \ln\left(\frac{1}{T_0^{\sec\theta_t}} \right) \right\} \qquad (2)$$

where, for NGSLR, η_q =0.28 is the MCP/PMT detector counting efficiency, η_r = 0.4 is the throughput efficiency of the receiver optics, $h\nu$ is the laser photon energy, N_λ is the exo-atmospheric spectral irradiance at the laser wavelength (0.2W/m^2-A^o-ster @ 532 nm), $\Delta\lambda$ = 3A^o is the FWHM bandwidth of the spectral filter, A_r = 0.126m^2 is the telescope receive area, Ω_r is the receiver solid angle, T_0 is the one-way atmospheric transmission at zenith, θ_s is the solar zenith angle, and θ_t is the target (satellite) zenith angle. The *atmospheric factor* in {brackets} is plotted for NASA's NGSLR System versus the satellite zenith angle in Figure 3. The four plots correspond to T_0= 0.8, 0.6,0.4, and 0.2 and the curves within each plot correspond to different solar zenith angles. The black curve in each graph is a plot of the approximate expression in (2) which is generally valid for T>0.6 and θ_t< 60^o.

From Figure 3, one can conclude that an Atmospheric Factor (AF) = 0.5 is a "worst case" value for target zenith angles less than 70^o. In Figure 4, we plot (2) for NGSLR with AF = 0.5 to obtain a worst case noise count as a function of the receiver half-angle FOV, ω, which is related to the receiver solid angle by $\Omega_r = \pi\omega^2$. Since the NGSLR timer has a 60 nsec deadtime (comparable to an actively-quenched SPAD), it will lose 10% or more of the target data for ω >5.3 arcsec.

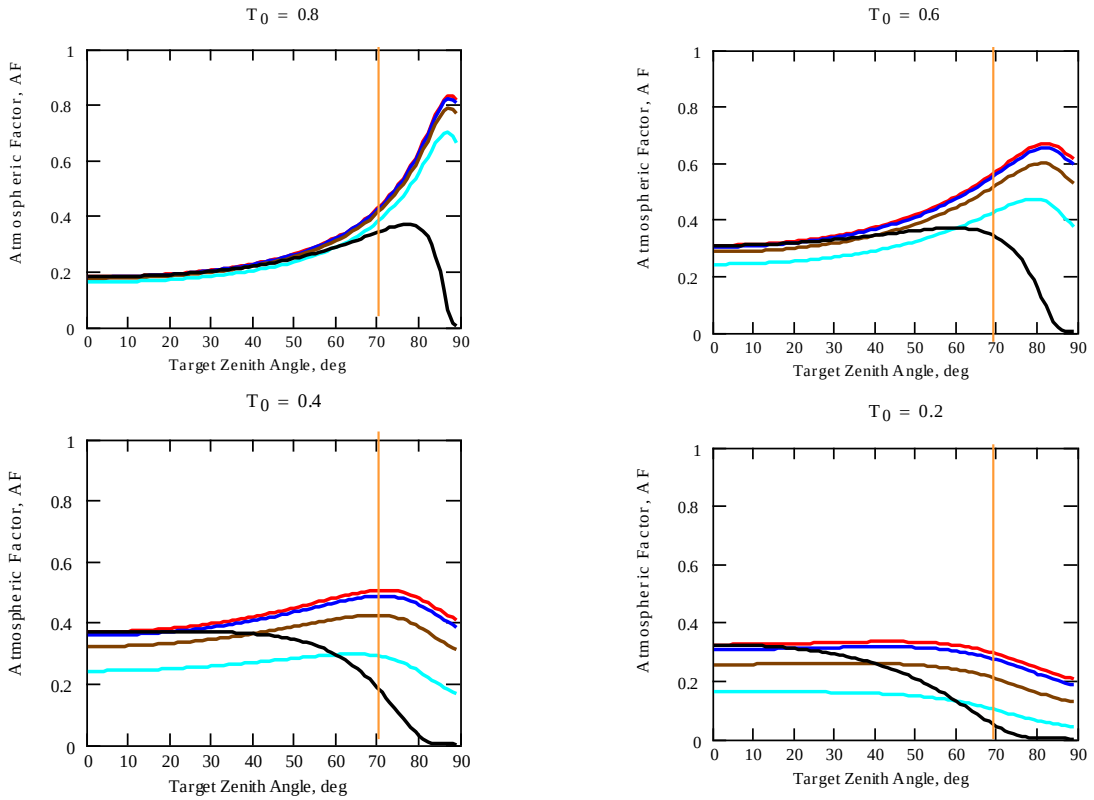

Figure 3. Plots of the atmospheric factor in (2) for NASA's NGSLR system vs target (satellite) zenith angle. The four graphs correspond to four different zenith atmospheric transmissions (T_0 = 0.8, 0.6, 0.4, and 0.2) while the curves within each figure correspond to different solar zenith angles in degrees, i.e. θ_s = 0 (red), 20 (blue), 40 (brown), and 60 (magenta). The black curves correspond to the approximate expression in (2) which is only valid for high transmissions (T_0 >0.6) and lower target zenith angles (θ_t <60°).

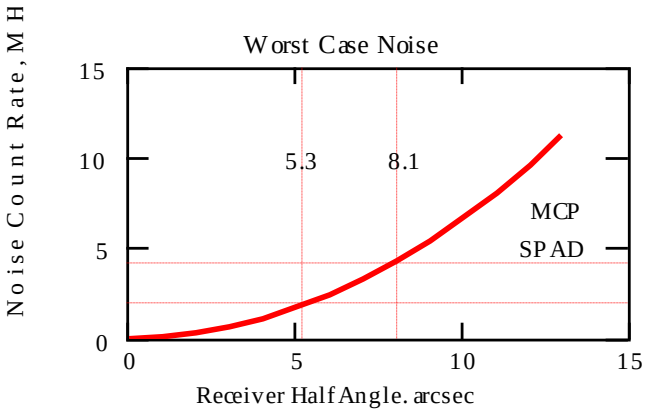

Figure 4. Solar noise count rate vs NGSLR receiver FOV half angle assuming a worst case atmospheric factor, AF =0.5. For a nominal half angle of 5.3 arcsec, approximately 10% of the satellite data will be lost due to the slow recovery time of the HTSI timing receiver, which negates the inherent recovery time advantage of NGSLR's MCP/PMT.

For laser altimetry, we have the following expression for the solar count rate due to the combined scattering off the surface and intervening atmosphere [Degnan, 2002a]

$$\dot{n} = \left[\frac{\eta_q \eta_r}{h\nu}\right]\left[\frac{N_\lambda^0(\Delta\lambda)\Omega_r A_r}{\pi}\right]\left[\rho T_0^{1+\sec\theta_s}\cos\psi + \frac{1-T_0^{1+\sec\theta_s}}{4(1+\sec\theta_s)}\right] \quad (3)$$

where ρ is the surface reflectance and ψ is the angle between the surface normal and the Sun. For this example, we consider the photon-counting, Cross Track Channel (CTC) Lidar proposed by Sigma to fly alongside the primary GLAS-II lidar on NASA's ICESat-II Mission and described elsewhere in these Proceedings [Degnan, 2008]. The CTC is designed to generate 16 parallel tracks of surface profile data as in Figure 5a. The plots in Figure 5b assume a nominally flat ($\psi \sim \theta_s$), high reflectance (ρ =0.94), Lambertian ice/snow surface, and a receiver solid angle per channel of $\Omega_r = 2\text{x}10^{-9}$ ster , corresponding to a 30 m diameter ground spot at 600 km altitude. As in ICESat-1, the green channels share the 1 m telescope (A_r = 0.736 m^2) with the primary 1064 nm lidar, and an additional 25 pm etalon filter in the receiver reduces the solar count rate by an additional factor of 10 relative to the 250 pm GLAS "coarse" spectral filter. The etalon extends tube life by a similar factor by reducing the overall charge transfer rate from photocathode to anode , but the transmission peak of the etalon filter must actively track the laser transmitter wavelength. Cloud cover is included in the atmospheric transmission T_0, which, in Figure 5b, is varied from 1.0 (no atmosphere) to 0 (thick clouds). In the latter case, neither the lidar nor solar rays can penetrate to the surface.

.

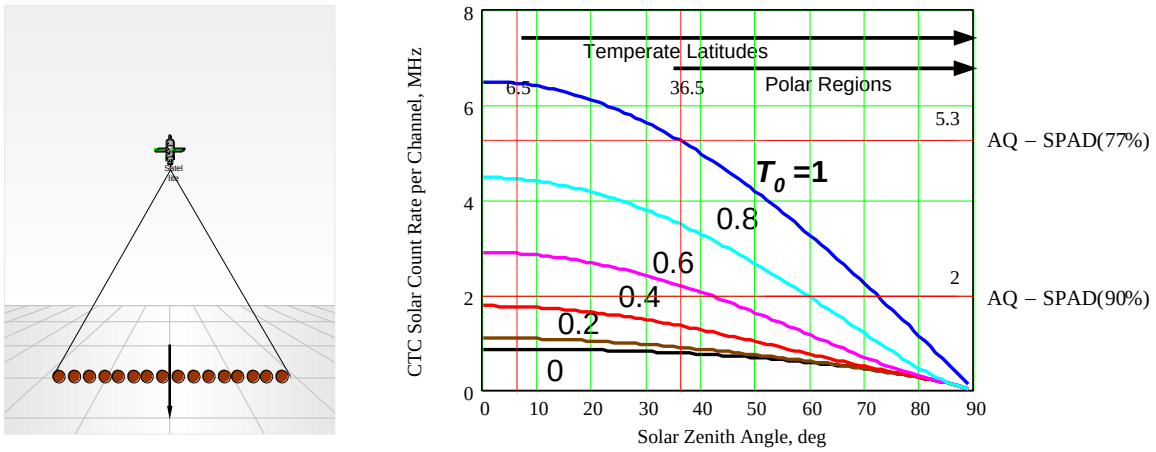

(a) (b)

Figure 5. (a) CTC 16 beam lidar concept; (b) Solar background rate for a single CTC channel with the 25 pm GLAS etalon over a Lambertian ice/snow surface as a function of solar zenith angle and the one-way zenith atmospheric transmission, T_0. In the polar regions (LAT>60^o), the minimum solar angle is 36.5^o, and the SCRF is reduced to about 77% for the AQ-SPAD in extremely clear atmospheres.

The Role of Pre-Detection Filtering

There are four pre-detection filtering techniques that can be employed [Degnan, 1993]:

1. **Spectral** – choose narrowband filters trading off between bandwidth, optical throughput, and added operational complexity

2. **Spatial** – use minimum receive FOV consistent with transmitter divergence, telescope image quality, and transmit/receive co-boresight stability.
3. **Temporal** – use range gates to only accept returns from the region of interest and reject other regions.
4. **Amplitude** – choose receiver detection thresholds to eliminate background "false alarms" in high SNR systems.

As can be seen from (2) and (3), the solar count rate seen by the detector can only be reduced through the use of spectral ($\Delta\lambda$) and/or spatial (Ω_r) filtering.

Temporal filtering, or range gating, has no effect on the SCRF as defined by (1) unless the range gate can be set very narrow, i.e. to a small fraction of the mean time between solar counts. Temporal filtering can, however, lower the mean current in an MCP/PMT, preventing the MCP from reaching saturation, preserving responsivity, and extending MCP/PMT lifetime.

Since by definition photon-counting systems detect single photon events, amplitude filtering is not generally applicable except for eliminating low-level electronics noise. It was determined analytically that raising the detection threshold above 1 pe (amplitude filtering) for the CTC application resulted in a significant loss of surface data without providing commensurate noise reduction benefits.

Summary

The combined detector/receiver recovery time determines the maximum tolerable noise count rate in photon-counting lidars. During night operations, when the noise background is dominated by detector dark counts , Microchannel Plate Photomultipliers (MCP/PMTs) and Single Photon Avalanche Diodes (SPADs) are predicted to work equally well for "single stop applications", which include SLR, transponders, or altimetry over unobscured terrain. During daylight operations, however, the target return rate will be substantially reduced if the mean time between solar counts is not much greater than the recovery time of the overall receiver. The solar background count rate can only be managed by limiting the telescope aperture or optical throughput, spatial field-of-view, and/or spectral filter bandwidth. Temporal filtering (range gating) has no impact on recovery time limitations of SPAD's unless the gate can be set very narrow relative to the mean arrival time between solar photons, but gating can prevent microchannel plate saturation in an MCP/PMT, preserve responsivity, and significantly extend tube life. Gating also reduces data storage and/or transmission requirements, and aids the post-detection filtering process. It was determined that raising the detection threshold above 1 pe (amplitude filtering) results in a significant loss of target data without providing commensurate noise benefits. Photon-counting systems, such as NASA's NGSLR/SLR2000 station and a proposed multichannel spaceborne altimeter on ICESAt-II, the Cross Track Channel Lidar, were used as examples to illustrate these important effects.

References

Degnan, J., "Millimeter Accuracy Satellite Laser Ranging: A Review", in Contributions of Space Geodesy to Geodynamics: Technology, D. E. Smith and D. L. Turcotte (Eds.), AGU Geodynamics Series, Volume 25, pp. 133-162, 1993.

Degnan, J., "Photon-Counting Multikilohertz Microlaser Altimeters for Airborne and Spaceborne Topographic Measurements", Journal of Geodynamics, 34, pp. 503-549, November, 2002a,.

Degnan, J. "Asynchronous Laser Transponders for Precise Interplanetary Ranging and Time Transfer", Journal of Geodynamics , pp. 551-594, November, 2002b.

Degnan, J., Caplan, D. 2006, "Performance of a Liquid Crystal Optical Gate for Suppressing Laser Backscatter in Monostatic Kilohertz SLR Systems", Proc. 15th International Workshop on Laser Ranging, Canberra, Australia, October 16-20.

Degnan, J., Wells, D., Machan, R., Leventhal, E., "Second Generation 3D Imaging Lidars Based on Photon-Counting", SPIE Optics East , Boston, MA, September 9-12, 2007.

Degnan, J., 2008, "Globally Contiguous, High Resolution Topographic Mapping of Planets and Moons via Photon-Counting", these Proceedings.

High speed Pockels Cell shutter and the Herstmonceux MCP-PMT detector

Matthew Wilkinson and the NERC Space Geodesy Facility team

Abstract

Daytime kHz satellite laser ranging at the NERC Space Geodesy Facility in Herstmonceux, UK experiences a large amount of daylight noise. The C-SPAD detector in operation needs a minimum delay of 50ns after gating to avoid any range measurement error and only one detection is made for each laser fire. Therefore a noise point detected in this post-gating time period is a lost opportunity for a satellite laser measurement. An estimate of the loss for Lageos and HEO satellites due to daytime noise varies from 20% to as high as 50% of shots fired.

Introducing a high speed Pockels cell shutter before the C-SPAD allows the detector to be armed in darkness. The shutter then opens ~10ns before the satellite track, resulting in a reduced amount of daytime noise and an increased number of successful return signal detections. The polarisers in the Pockels cell however reduce the return signal intensity by a factor of more than 50%.

Advantages and practical considerations for this application are discussed and compared with an alternative fast gating MCP-PMT detector.

The NSGF SLR system uses a C-SPAD detector and consequently makes only one detection per laser fire. Also the C-SPAD must be armed 50-100ns before an observation to avoid any bias in the range measurement due to characteristics of the detector, as shown in figures 1 and 2.

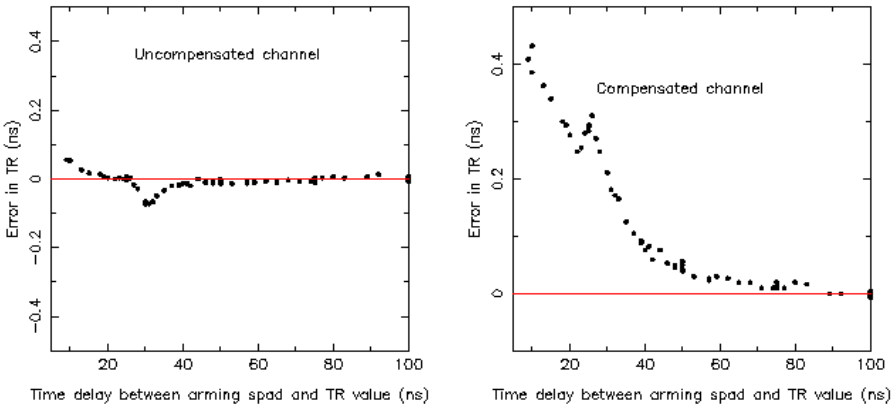

Figures 1 and 2. Range bias variation of the uncompensated and compensated C-SPAD channels with time of observation after gating.

Once armed, if the C-SPAD detects a noise point before the arrival of the satellite return signal then the opportunity to observe the satellite from that laser shot is lost. Furthermore, in comparison to the Nd:YAG laser, the new kHz laser system has a greatly reduced signal to

noise ratio with much more sampling. Therefore, daylight noise is much more apparent in the range gate window and has a more significant impact on daytime observing.

The C-SPAD will make a detection within a few hundreds of nanoseconds during normal daylight operations. To reduce daytime noise the return path includes an oven controlled daylight filter that allows a narrow spectrum of 0.14nm FWHM centred at 532.1nm. Peak Transmission is 68.04%. Nevertheless daytime noise still reaches the detector and figure 3 shows the proportion of lost laser shots due to daylight detections for a Champ. Less than 10% of laser shots result in detected noise in the first 20 nanoseconds after arming the detector. After 100 ns about 40% of shots are lost to daytime nose and about 70% of shots are lost in 250 ns. The drop in percentage lost seen toward the end of the pass is due to the satellite being detected and ND filters being added in front of the C-SPAD.

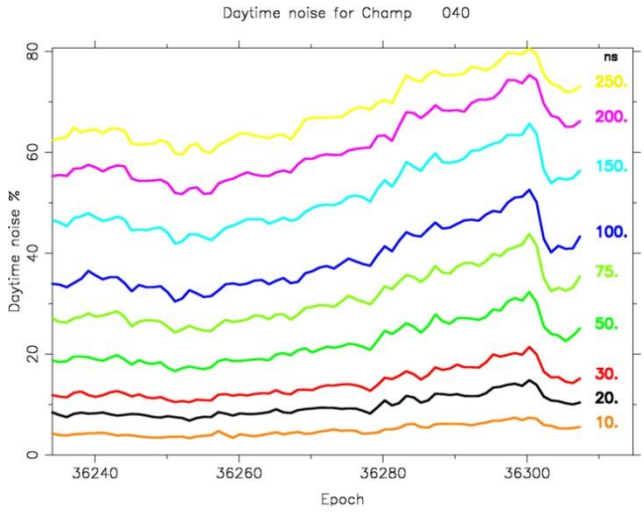

Figure 3. The percentage of lost observation opportunities due to daytime noise detection during a Champ pass during the first 10, 20, 30, 50, 75, 100, 150, 200 and 250 nanoseconds after the gating of the C-SPAD.

Introducing a very fast shutter before the C-SPAD will allow it to fully arm in darkness. The shutter can then be opened much closer to the satellite track (~10ns). This could turn a 50% loss to a 10% loss.

Suitably Fast Shutters

Physical - Spinning disc or resonant forks opening and closing a physical barrier matched in phase. However, it would be demanding to match the kHz frequency and phase of the returning signal.

Liquid Crystal Display - Cell containing long molecules aligned at each surface and 90 degrees apart. Polarised light is rotated through the cell with no applied voltage. Cell becomes opaque when a voltage is applied as the molecules align to the electric field. However, the shutter needs to open in a few nanoseconds and the LCD is too slow with transition times of > 10 μs.

Electro-optic - Pockels cell shutter using fast switching of polarisation to block and transmit light. However, more than 50% of returning signal is lost.

Acousto-optic - A piezoelectric device transmits a sound wave through a quartz crystal to produce a diffraction grating. This grating then deflects light. However, the speed of the shutter is limited to the speed of sound in the crystal and it is only fast enough if the return signal beamwidth is very small ~ 1 micron.

The best option is an electro-optic Pockels cell shutter, which can switch between transmission and blocking very quickly, about 1 ns. Light is polarised before entering the Pockels cell crystal and is blocked by an opposing polariod on the other side. To transmit the light a high voltage is applied to the Pockels cell which rotates the polarisation of the light and allows it to then pass through the second polariod and reach the detector. However, the major disadvantage of introducing a Pockels cell shutter before the C-SPAD is the loss of signal intensity due to Malus's Law. For a perfect polariser aligned by θ to polarised light of intensity I_0, the output intensity equals: $I = I_0\cos^2\theta$. Only the intensity component that is parallel to the polariser's transmission axis is transmitted. Unpolarised light consists of a random mixture of polarisations with an average of $\cos^2\theta$ from 0 to 90°, which equals ½. Therefore the intensity of unpolarised light through a perfect polariser is reduced by half. Polarisers are not perfect and so transmission is less than 50%, although calcite glass polarisers can achieve close to 50% transmission.

Furthermore, the Pockels cell must be electronically switched at high voltage. This reduces gating time to 10-15ns. The Pockels cell will not block all wavelengths of light, but this is not a problem as it would be positioned after the dichroic mirror in the return path and experience mostly green light.

Conclusion

A very fast shutter would benefit Lageos and HEO SLR by reducing daytime noise. The best shutter option is a Pockels cell and all of the obstacles encountered in planning for the installation have been overcome. The disadvantage of this shutter is a 50% loss of return signal. The advantage is the close gating that reduces the number of lost shots due to daytime noise.

An Alternative Detector?

Instead of installing a Pockels cell shutter, an alternative detector option is available that would give the same advantage of close gating. An MCP-PMT detector can be gated even quicker than a Pockels cell shutter. Also this detector has much less dark noise compared to the SPAD.

The choice of the most suitable MCP-PMT detectors lies between two similar but slightly different detector specifications. The first is the Photek PMT210 S2. It has very fast gating, a quantum efficiency of 12% and 30ps jitter. Such a device is on loan from Photek and is undergoing testing at Herstmonceux. Alternatively the Hamamatsu MCP-PMT R5916U-64 has very fast gating, a quantum efficiency of 40% and 110ps jitter. A similar detector was recently installed at the Borowiec SLR station.

The New 100-Hz Laser System in Zimmerwald: Concept, Installation, and First Experiences

Werner Gurtner, Eugen Pop, Johannes Utzinger
Astronomical Institute, University of Bern, Switzerland

Abstract

In spring 2008 we replaced the Titanium-Sapphire laser by a new 100 Hz Nd:YAG system. One of the requirements for the new laser was a high flexibility in the actual firing rate and epochs to allow for synchronous operation in one-way laser ranging experiments. Firing order and range gate generation are controlled by a Graz-provided PC card with field-programmable gate array. The protection of the receiver from backscatter through our monostatic telescope was realized with a synchronized rotating shutter. First experiences show a very stable operation of the laser without any re-adjustment needs for many months, a much better efficiency regarding return rates to high satellites, and a single shot rms to well-defined targets of about 5 mm in single-photon mode.

Introduction

From 1996 till 1997 the Satellite Laser Ranging facility at the Zimmerwald Observatory was completely renovated: The 50-cm bistatic telescope was replaced by a 1-meter monostatic dual-purpose (SLR and astrometry) telescope and a new two-color Titanium-Sapphire laser was installed. The following years proved the new system to be very productive and efficient. Supported by an increased automation of the system Zimmerwald gradually moved to the top group of SLR stations with respect to the collected data volume. One of the major reasons to go for a dual-color system was the expectation to use the observations in the two wavelengths (423 nm and 846 nm) for the more precise determination of the atmospheric refraction correction (tropospheric delay). However, it turned out that small system-dependent systematic errors (or rather their differences between the two colors) were too large to allow the direct determination of the tropospheric delay with the necessary precision. Nevertheless the second color (infrared) helped to detect and to identify the order of magnitude of such remaining systematic errors and it extended the operation capabilities of SLR e.g., with respect to unfavorable atmospheric conditions because of the better transparency for infrared light.

After ten years of operation the laser system became more and more difficult and expensive to maintain, fatal failures were to be expected. Thanks to the combined support of different institutions (University of Bern, Federal Office of Topography, Swiss National Science Foundation) we could evaluate, order, and finally install a new laser system, ready for operation in April 2008.

Evaluation of the New Laser System

The major requirements for the new system were

- minimum intervention by our staff (e.g., no daily realignments etc)
- fully automatic and remotely controllable
- continuous, uninterrupted operation for weeks in a row
- high single-shot precision (few millimeters)

- suited to support future transponder missions, if possible
- ready for two-color ranging
- about 1 Watt average output power per color

Reliable operation and minimum intervention asked for a solid state diode-pumped laser of a rather high repetition rate, i.e. between about 100 Hz and a few kHz, which seems to be the range within which diode-pumped lasers may deliver the requested average power at the requested pulse length.

The single-shot precision under single-photon conditions mainly depends on the precision of the time of flight measurement (counter, event timer) and the pulse length of the laser pulses. We opted for a pulse length of about 40 ps FWHM, equivalent to a RMS of about 2.5 mm in range.

Future transponder missions will most certainly be designed around the second harmonic of the wavelength of the Neodyne:YAG lasers, i.e. 532 nm. Titanium:Sapphire lasers will therefore not be suited.

Routine two-color ranging however is currently only feasible with Titanium-Sapphire lasers in the two wavelengths 423 nm and 846 nm, where suitable detectors are available. We are not aware of detectors for the primary wavelength of Nd:YAG (1064 nm) that fulfill the requirements for high-precision SLR at this date.

One Watt average output power corresponds to 500 μJ @ 2 kHz or 10 mJ @ 100 Hz.. The Graz two-Kilohertz-system outputs about 400 μJ with a pulse length of < 10 ps.

Before we issued a call for participation we already decided upon the wavelengths: Regarding the rather moderate advantages of a two-color system (experience we had with our own system) and the possible impact of the use of transponders on lunar and interplanetary missions we limited our evaluation to a system capable of generating a wavelength of 532 nm.

As the 1-m ZIMLAT telescope used for both SLR and astrometric observations is monostatic w/r to SLR (identical transmit and receive paths between the transmit/receive switch situated in the basement of the telescope dome and the telescope primary mirror) we have to protect the detectors from the backscatter of the transmit beam by a fast enough electro-optical or mechanical shutter or a polarization-based optical device. Low-loss electro-optical shutters seem difficult to obtain, polarization-based devices need enough space on the optical table and mechanical shutters at one or two kilohertz with the necessary duty factor (<1/10, i.e. < 1 part closed, 10 parts open) might be impossible to build. Our call for tender (issued December 2006) specified either 100 Hz or 1-2 kHz but stated that we would select among 100-Hz bids only, if present.

Finally we selected a 100 Hz Nd:YAG system offered by Thales Laser , France.

The New Laser System

The new Thales System was installed in March/April 2008. Together with a fatal failure of the old system end of January 2008 we suffered from interruption of SLR operation of about three months.

Table 1. Major characteristics

Manufacturer	Thales Laser, France
Technology	Diode pumped solid state Nd:YAG laser
Pulse generation	SESAM technology oscillator (**SE**miconductor **S**aturable **A**bsorber **M**irror)
Wavelengths	1064 + 532 nm
Pulse rate	90-110 Hz, adjustable with external trigger Additional decimation with pockels cell
Configuration	Oscillator (TimeBandwidth), regenerative amplifier, doublepass amplifier
Pulse energy	21 mJ @ 1064 nm before doubling 9 mJ @ 532 nm
Pulse width	58 ps (FWHM)
Pulse contrast	< 1/200
Beam diameter	8 mm
Stability of energy	< 1%
Pointing stability	< 5 arc sec

Two specifications could not be met:

1. The pulse width had to be increased to nearly 60 ps because of non-linearity problems in the amplifier
2. Originally we intended to have the possibility to use the remaining infrared after the second harmonic generation (about 50 % of the original beam) for two-color ranging, provided a suitable detector were available. However, the beam quality of the infrared component of the beam after the SHG was insufficient. It was decided to modify the setup in order to bypass the SHG with a selectable fraction of the infrared in case of two-color or infrared-only operation.

Figure 1 shows the major components and the paths of the beams before, after and around the second harmonic generator.

The pump diodes can be triggered with a variable rate between approximately 9 and 11 ms in steps of 10 microseconds, the variability of which is limited by thermal stability conditions. By means of the pockels cell selecting the pulses to be attenuated the actual firing rate can be decimated by any additional integer factor[5].

All major laser commands (e.g., power on, status request, power off) can be issued over a TCP/IP connection between the station computer and the manufacturer-provided laser control

[5] *For the upcoming LRO one-way ranging experiment the laser will be fired at approximately 14 Hertz, i.e. with a basic pump rate of 10.200 ms ≈ 98 Hertz and a decimation factor of 7.*

PC. This LabView–based control program also allows interactive manual control of all laser parameters.

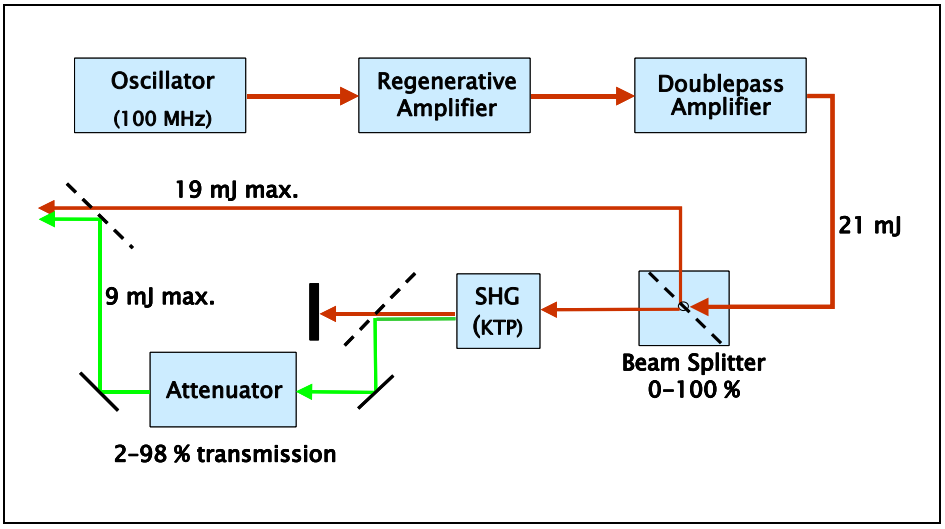

Figure 1. Laser Main Components

Laser trigger signals for pump diodes and enabling/disabling signals for the pockels cell as well as the signals for range gate generation and rotating shutter control (see below) are generated by the FPGA card prepared and programmed by the Technical University of Graz.

Other Components

Transmit/receive switch

Originally we used a perforated mirror as transmit/receive switch: The laser transmit beam entered the Coudé path through an eccentric hole of a coated glass plate. The received pulse, filling the full aperture (with the exception of the center part shadowed by the secondary mirror of the telescope) was reflected by the front face of the 45-degree mirror into the receiving path.

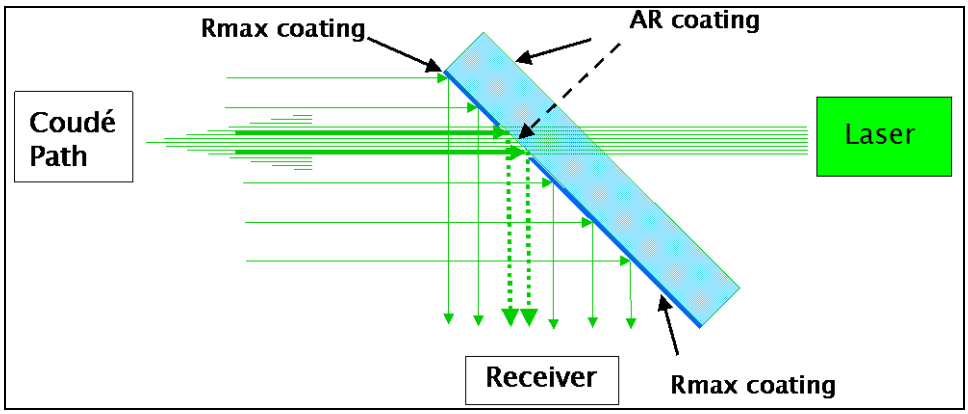

Figure 2. Transmit/receive switch

The hole in the mirror had two distinct disadvantages: It was rather difficult to manufacture and it did not reflect the received beam from a calibration corner cube outside of the dome.

We found a manufacturer that agreed to specially coat the glass plate with

- an anti-reflective coating on the back side (towards the laser)
- a reflective coating on the front face with the exception of the portion where the transmit beam passes the glass plate
- an anti-reflective coating on the front face where the transmit beam passes the glass plate. This portion is also used to separate a small percentage of the received calibration pulse into the receiving path.

Rotating shutter

The rotating shutter has to protect the receiver from the backscatter of the transmitted laser beam during satellite ranging. It opens the receiving path for the time of reception only. The duration of the opening has to include the uncertainty of the opening and closing instants, but it should be short enough to allow the processing of return pulses as close to start pulses as possible.

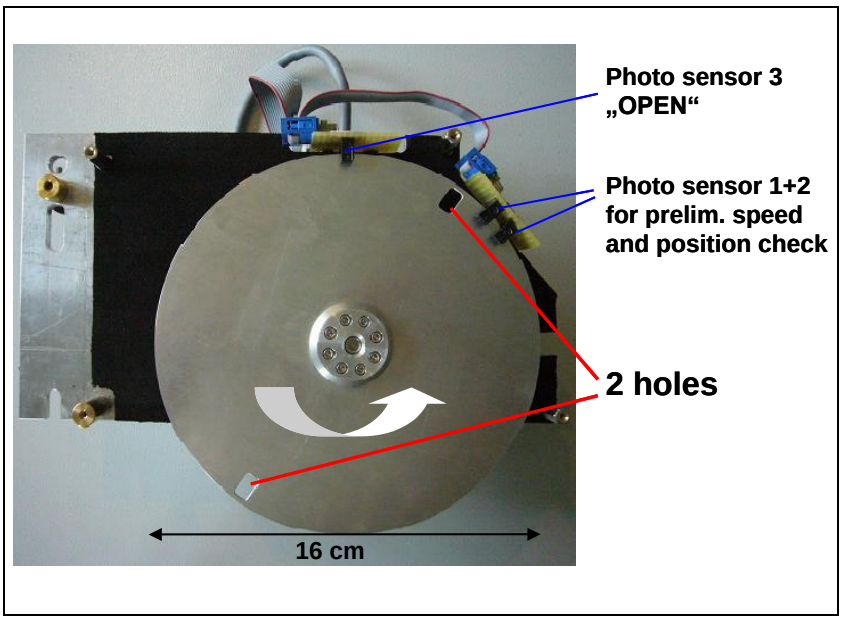

Figure 3. Rotating Shutter

The shutter is realized by a thin aluminum disk with two diametrically opposed holes of 6 mm diameter each at a radius of 70 mm. It is driven by a DC servo motor with integrated controller operated in stepper mode at a frequency of approximately 50 Hz (=3000 rpm), precisely synchronized with the actual firing rate of the laser (see above). The shutter is placed very close to an intermediate focus of the received beam used for the limitation of the field of view with a pin hole.

The shutter is open during about 300 µs with an uncertainly w/r to the expected time of reception of ±50 µs. Frequency and phase are controlled and commanded by a PC via the FPGA card mentioned above.

A hardware-implemented safety monitor assures that the shutter is not unintentionally open at firing time: It checks speed and position two milliseconds before firing time and blocks the laser if a conflict between transmit and receive pulse is to be expected by disabling the Regen pockels cell of the laser and closing a fast mechanical safety shutter within the Regen.

FPGA PC Card

The PC card containing a field-programmable gate array (FPGA) was built and programmed by F. Koidl of the TU Graz.

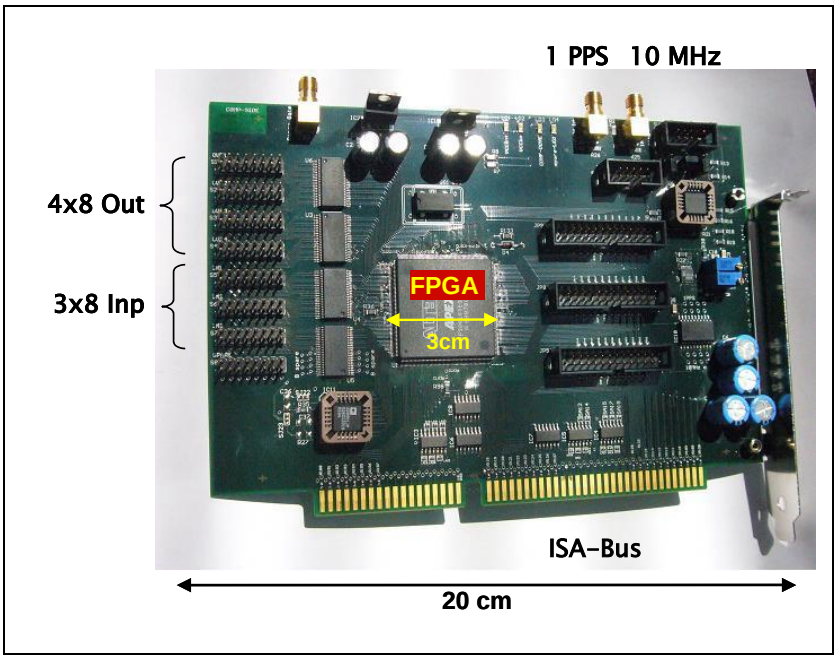

Figure 4. FPGA Card

Its main functions are

- the generation of
  - pulses to control the Laser firing rate (periods of 9 to 11 ms at a resolution: 10 µs)
  - pulses for the range gate (epoch and duration (resolution: 5 ns)
  - frequency for the rotating shutter control
  - Laser firing pre-pulses (rotating shutter safety monitoring)
- the measurement of
  - the current epoch (resolution: 1µs)
  - the epoch of the shutter's open position (resolution: 1µs)
- to make available
  - control register to enable Laser pump diodes, the Pockels cell, safety shutter etc
  - several auxiliary I/O channels

It is mounted in the dual-boot (DOS and Windows XP) PC used for control and data collection. The actual control program is written in MS-Fortran, communication with the FPGA is performed through registers on the I/O page of the DOS system.

Overlap Avoidance
Conflicts between transmit and receive pulses have to be avoided to protect the receiver from the backscatter. This can be achieved by

1. cutting all conflict zones from the satellite passes (losing about 5 percent of the pass duration in our configuration)
2. adjusting the firing epochs several times by inserting short delays during the conflict zone (Graz solution)
3. changing the firing rate once to "jump" over a conflict zone. During a short time (approximately the current flight time) after the change laser firing has to be stopped.

We selected option 3 with the possibility to switch to the simplest option one, if desired.

First Experiences

Laser Stability
Only one slight re-adjustment of the regenerative amplifier was necessary after five months of operation.

Ranging to a well-defined target
Ranging to Champ, Grace A/B, Envisat and similar satellites with well-defined corner cube signal structures show a single-shot RMS of 5 to 6 mm.

The system is always tuned to operate in single-photon mode by automatic adjustment of a the return rate to about 5 to 15 percent by a variable neutral density filter in the receiving path.

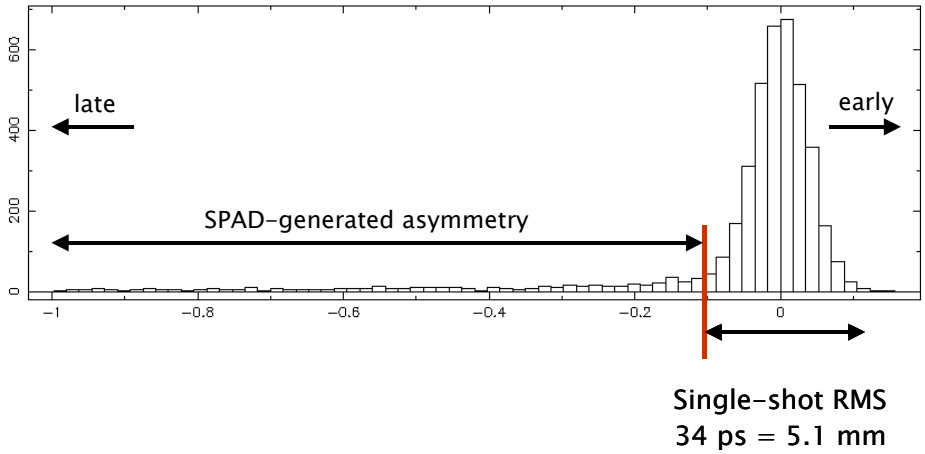

Figure 5: Champ: Distribution of returns

Ranging to Lageos 1 and 2
The target signal structure of the Lageos satellites distorts the observed time of flight distribution and increases the apparent RMS of single-shot observation, as can be seen in Figure 6.

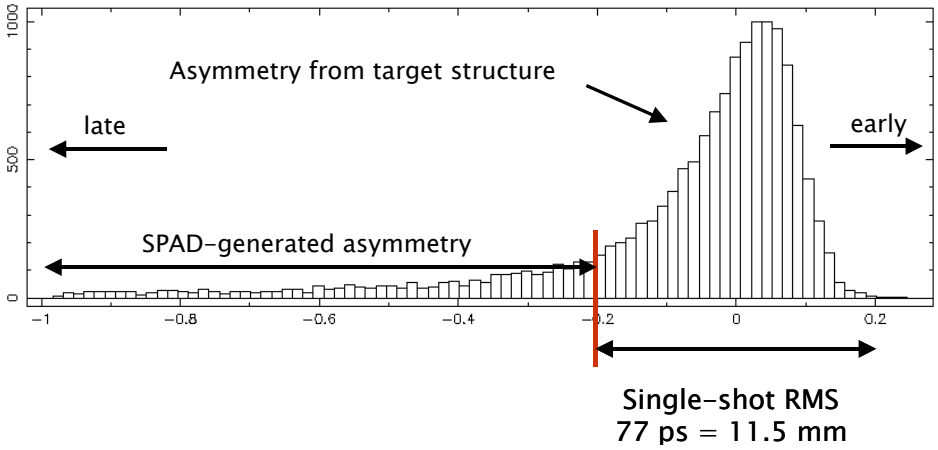

Figure 6. Ranging to Lageos 1 and 2

Performance to GNSS satellites

A sample pass of a Glonass satellite shows up to about 4000 returns per normal point corresponding to a return rate of 13 percent maximum.

Table 2. Normal point statistics of a Glonass pass

Bin Number	Number of Obs per Bin	Residual (ns)	RMS	Residual (mm)	RMS
1	575	0.007	0.007	1.0	1.1
2	1348	0.000	0.005	0.0	0.7
3	1320	0.003	0.005	0.5	0.7
4	786	-0.018	0.006	-2.8	0.9
5	1312	-0.001	0.003	-0.2	0.5
6	2434	-0.002	0.002	-0.3	0.4
7	970	-0.003	0.004	-0.5	0.7
8	1918	0.003	0.003	0.5	0.4
9	3884	0.001	0.002	0.2	0.4
10	3577	-0.002	0.002	-0.3	0.4
11	3769	0.002	0.002	0.4	0.3
12	3074	-0.001	0.002	-0.2	0.4
13	2217	0.004	0.003	0.7	0.4
14	3302	0.001	0.002	0.1	0.3
15	2832	-0.002	0.002	-0.4	0.3
16	3040	0.000	0.002	0.0	0.3
17	1703	0.003	0.003	0.4	0.4
18	1589	-0.006	0.003	-0.9	0.4
19	1691	-0.002	0.003	-0.2	0.4
20	3460	0.005	0.002	0.7	0.3
21	2594	-0.009	0.002	-1.3	0.3
22	2699	0.001	0.002	0.1	0.3

Conclusions

The new laser system fulfills nearly all our expectations. We are certain that we will continue to produce as much if not significantly more SLR data of even higher quality as before April 2008.

16 years of LAGEOS-2 Spin Data - from launch to present

Daniel Kucharski[a], Georg Kirchner[b], Franz Koidl[c]

Space Research Institute, Austrian Academy of Sciences

a) Lustbuehelstrasse 46, A-8042 Graz, Austria. phone: +43–316–873-4653, daniel.kucharski@oeaw.ac.at
b) Lustbuehelstrasse 46, A-8042 Graz, Austria, phone: +43–316–873-4651, georg.kirchner@oeaw.ac.at
c) Lustbuehelstrasse 46, A-8042 Graz, Austria, phone: +43–316–873-4654, franz.koidl@oeaw.ac.at

Abstract

Satellite Laser Ranging (SLR) stations measure distance to the satellites equipped with Corner Cube Reflectors (CCRs). These range measurements contain information about spin parameters of the spacecraft. We present 15 years of LAGEOS-2 (15580 values) spin period determination. The measurements have been made by standard 10 Hz SLR systems and the first 2 kHz SLR system from Graz (Austria). The obtained data allowed calculation of the initial spin period of the satellite: 0.906 s. Long time series of the spin period values show that the satellite's slowing down rate is not constant but is oscillating with a period of 578 days. The results presented here definitely prove that the SLR is a very efficient technique able to measure spin period of the geodetic satellites.

1. Introduction

LAGEOS-1 (L1) and LAGEOS-2 (L2) are spherical, passive geodynamic satellites. They are identical in construction: spheres of 60 cm radius, equipped with 426 corner cube reflectors (CCRs). The parameters of the missions are presented in table 1.

Table 1. Mission parameters.

	LAGEOS-1	LAGEOS-2
Sponsor	United States	United States and Italy
COSPAR ID	7603901	9207002
Launch Date	May 4, 1976	October 22, 1992
Inclination	109.84 degrees	52.64 degrees
Eccentricity	0.0045	0.0135
Perigee	5,860 km	5,620 km
Weight	406.965 kg	405.38 kg

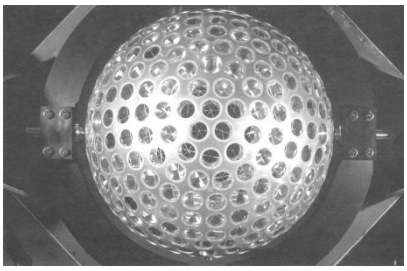

Figure 1. LAGEOS-2 (Courtesy of Italian Space Agency).

The spin parameters of these satellites were investigated using photometric (Bertotti and Iess, 1991, Otsubo et al., 2004) and SLR (Satellite Laser Ranging) measurements (Otsubo et al., 2000b, Bianco et al., 2001, Kucharski et al., 2007), however only for a certain epoch time or for very short time periods. These results then have been used for the mathematical model LOSSAM (LAGEOS Spin Axis Model) (Andrés et al., 2004), which describes and predicts the spin parameters of L1 and L2. Information about spin period value and spin axis orientation helps to verify and improve models of the orbital perturbations (Andrés et al., 2004). Better models can improve the accuracy of the orbital analysis, which in turn results in more accurate investigation of the geodynamical parameters of the Earth (geocenter position, polar motion etc.).

2. Satellite spin measure techniques

Spin parameters of the passive satellites can be investigated with 2 techniques: photometry and SLR. The photometry determines epoch times of flashes caused by sunlight, and reflected from the outer surfaces of the CCRs. This technique works only at night, with the satellite illuminated by the sun, and only with spin periods below about 100 s for LAGEOS type satellites.

The second technique measures the distance to the satellites with laser. The laser pulses transmitted from the SLR station are reflected by the CCRs back to the receiver telescope at the SLR system. The spinning satellite frequently shows the same pattern of the CCRs to the station, thus engraving a frequency signal on the SLR data. This signal can be obtained by spectral analysis (Lomb 1976) of the unequally spaced range residuals (measured – predicted satellite range) data (Otsubo et al., 2000a). The resulting spectra contain frequency peaks with values depending on the spin rate of the satellite and the number of CCRs involved.

SLR can measure spin periods of satellites during day and night, regardless to the Sun – satellite – station geometry (as it is with photometry), and without any additional equipment. With the kHz SLR system it is possible to measure spin parameters from LEO (Low Earth Orbit), like Gravity Probe - B (Kirchner et al., 2008) to HEO (High Earth Orbit), like ETALONs (Kucharski et al., 2008), from very slow spinning objects like LAGEOS-1 (Kucharski et al., 2007) to fast spinning like AJISAI (Kirchner et al., 2007). Table 2 shows the main differences between the previous Graz 10 Hz and the new Graz 2 kHz SLR system. This new system is able to detect return pulses with single or multiple photons, resulting in up to > 1 million measurements per pass of LAGEOS-2, even with its low energy per laser shot (400 µJ).

Table 2. Key parameters of Graz SLR system.

Graz Laser System	10 Hz Laser before 2003/10/9	2 kHz Laser after 2003/10/9
Wavelength	532 nm	532 nm
Repetition rate	10 Hz	2 kHz
Energy/Pulse	30 mJ	400 µJ
Pulse width	35 ps	10 ps

3. Spin period determination

Since the beginning of SLR measurements to LAGEOS-2, many stations send full rate data to the International Laser Ranging Service (ILRS) Data Centers (Pearlman et al., 2002). We spectrally analyzed all available data sets, and got frequency spectra for all of the passes. Only spectra with visible signal peaks of power more than 10 were accepted for further processing. This criterion allowed calculating spin period since 23rd of October 1992 (1 day after launch). The 426 CCRs on the satellite are arranged in 20 rings (with different number of prisms). The different rings are the source of multiple frequency signals (spectral peaks; fig. 2), detectable with Lomb analysis. The values of these peaks are a result of the number of CCRs on the corresponding ring and the spin rate of the satellite; additional peaks can be caused by superposition of a signal produced by two neighboring rings.

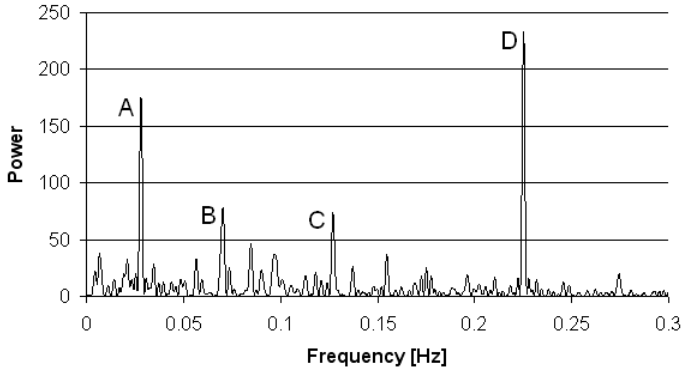

Figure 2. Result of spectral analysis of a kHz pass: LA2 of 15th March 2004.

Fig. 2 presents spectral peaks of a Graz kHz SLR observation of L2, taken on 15th of March 2004. The signal peaks can be recalculated into spin period by formula period = N / frequency, where N is a multiplication factor. In order to obtain the period of the body we were changing the N factor (from 3 to 32) and comparing the result value with LOSSAM predictions. The best agreement criterion allowed us to find out that the D peak is generated by the ring or rings equipped with 32 CCRs (142.3 s = 32 / 0.2249 Hz). The most powerful peak of each single pass – together with its correlated number of CCRs – was used to determine the spin period. However, it must be emphasized that the detected frequency signal is an apparent one; the changing station - satellite geometry during the pass is influencing the detected signal. This work thus presents apparent spin period values as detected by each SLR station. Without knowing the satellite's spin axis orientation it is not possible to properly correct the measured apparent spin period value and get a true spin period of the satellite. However, over a large number of passes, this effect may be considered to average out and should not affect our conclusions regarding long-term spin period behavior.

Fig. 3 shows spin period of L2 (from 1992-10-23 to 2007-08-15, 15580 points) derived from the global SLR full rate data. The resulting spin period data series were divided into time slots of 0.25 years. Spin period values within the slots were approximated with linear function, and spin period residuals to this function were obtained. The RMS of the residuals of every time slot is presented on fig. 4.

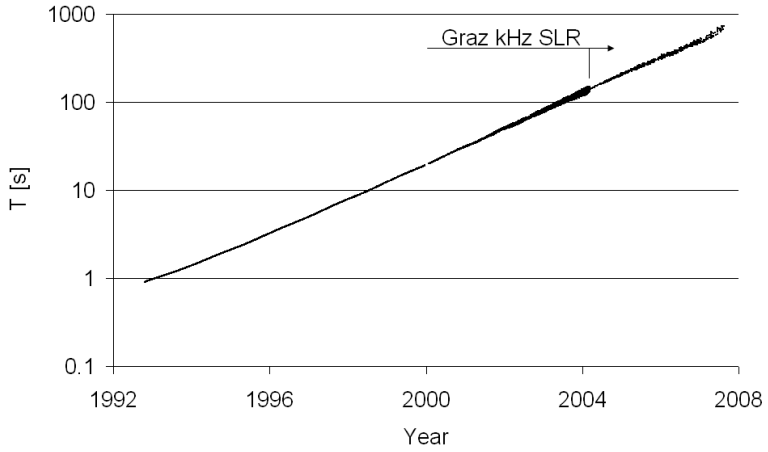

Figure 3. Spin period of L2 (logarithmic scale) derived from SLR data.

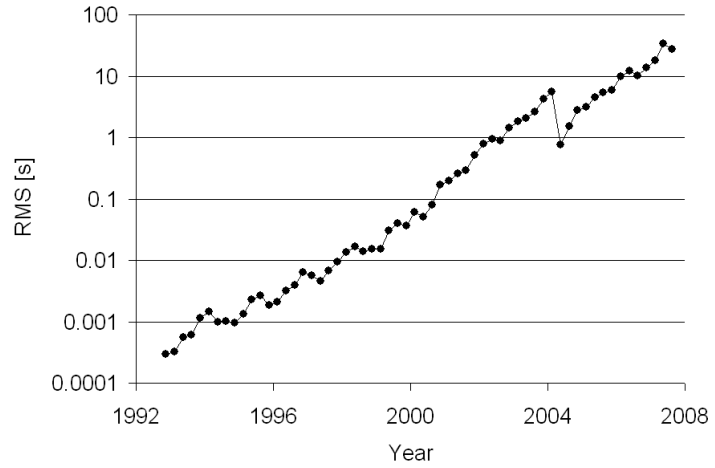

Figure 4. RMS of spin period residuals calculated with a quarter of a year step.

With a slowing down of the satellite the RMS of spin period residuals is increasing with an exponential trend. The number of full rotations of the satellite per pass is decreasing with an exponential trend, thus the frequency signal detected by SLR station gets poorer from pass to pass. The significant improvement of the RMS occurs when the Graz kHz data started to be used. Two hundred times more measurements per pass allow calculation of spin period values with an order of magnitude better accuracy than the 10 Hz SLR systems can give. The Graz kHz SLR data allowed extension of the investigated period for L2 for another 4 years, from 2003 to 2007. While spectral analysis of L2 passes failed for 10-Hz-stations after 2003 (spin period significantly above 100s), the last spin period value for L2 using Graz kHz data was 721 s (15th of August 2007).

4. Determination of initial spin period

Such a long time trend of spin period data allow determination of initial spin period value T_0. We used 137 spin period values measured during the first 30 days after the launch. These values were approximated with a linear function T = 0.00089012Y + 0.90604 [s]. The function points to an initial spin period value of T_0 = 0.906 s; the spread of the spin period points around the linear trend function is RMS = 0.000228 s.

5. Slowing down of LAGEOS-2

To investigate the continuity of the spin period increase, we calculated the differences between the values separated by given number of days D (±1%) and plotted them as percentage of actual spin period dT. We have processed a set of investigations with increasing the D number from 10 to 500 with a step of about 10%. The result for D = 500 and 90 days are presented on fig. 5 and 6. The results obtained for every D value were spectrally analyzed. By setting D = 500 days it is possible to investigate the main trend of the spin period changes. Graz kHz SLR data (visible at the end of the chart) allowed to complete the trend function (2nd degree polynomial) and to calculate its maximum (at about 2002.5). For D = 90 days (fig. 6) spectral analysis gives a peak which is indicating a period of T_{90} = 578 days.

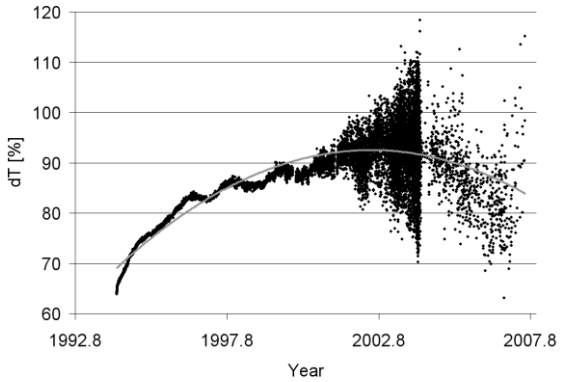

Figure 5. L2 spin period changes: percent of change between points separated by 500 days and 2nd degree polynomial main trend function.

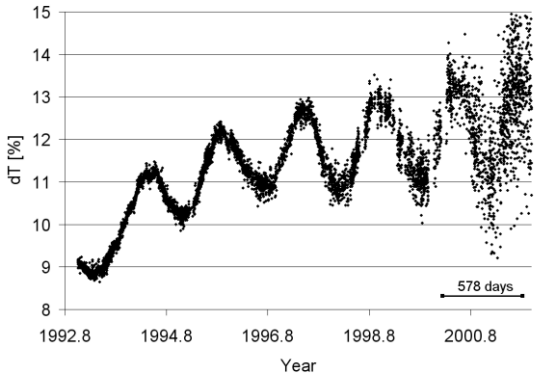

Figure 6. L2 spin period changes: percent of change between points separated by 90 days. Oscillation period: 578 days.

Spectral analysis of dT gives also a good signal for D = 30 days (fig. 7) of a value T_{30} = 103 days. These oscillations are visible up to 2 years after launch.

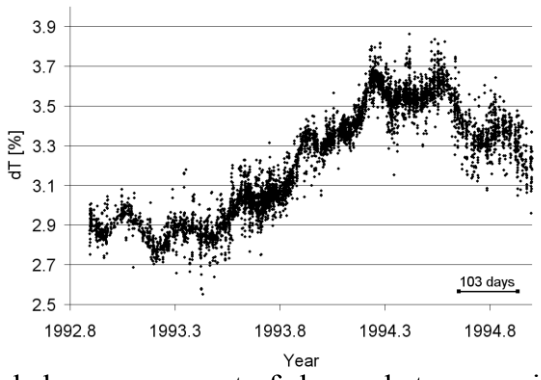

Figure 7. L2 spin period changes: percent of change between points separated by 30 days Oscillation period: 103 days.

6. Conclusions

Satellite Laser Ranging allows determination of spin period of a passive satellite LAGEOS-2. In this paper we used all available laser measurements of all SLR stations to derive spin period values of 15 years for L2 (15580 points). Due to the increasing L2 spin period, only Graz kHz SLR data - with its high repetition rate and 10 ps pulse width - permitted calculation of L2 spin period after 2003; this kHz data also yields an order of magnitude higher accuracy. The values presented here are in very good agreement with the LOSSAM model. Up to now, only 463 spin rate measurements of L2 have been made by photometry, until this technique had to be stopped at the end of 2002 for L2, because of too long spin periods of the both satellites.

The accuracy of spin period determination depends on the number of satellite's full revolution during the single pass and it is decreasing with en exponential trend. However, it is good enough to process detailed analysis of the satellite's slowing down rate. The oscillations of the slowing down rate can be caused by gravitational torque acting on the satellite. The period of the oscillations depends on an angle between the angular velocity vector and the spin axis vector of the satellite.

The evolution of satellite spin periods gives information about forces acting on the spacecraft, and causing perturbation of its orbit. The first-time accurate determination of long series of such spin period values can be used to upgrade models of all those forces.

7. References

Andrés, J.I., Noomen, R., Bianco, G., Currie, D.G., Otsubo, T. Spin axis behavior of the LAGEOS satellites. J. Geophys. Res., 109, B06403, doi: 10.1029/2003JB002692, 2004.

Bertotti, B., Iess, L. The rotation of LAGEOS. J. Geophys. Res., 96 (B1), 2431-2440, 1991.

Bianco, G., Chersich, M., Devoti, R. et al. Measurement of LAGEOS-2 rotation by satellite laser ranging observations. Geophys. Res. Lett., 28(10), 2113–2116, 2001.

Kirchner, G., Hausleitner, W., Cristea, E. Ajisai Spin Parameter Determination Using Graz Kilohertz Satellite Laser Ranging Data. IEEE Trans. Geosci. Remote Sens., 45 (1), 201-205, 2007.

Kirchner, G., Kucharski, D., Cristea, E. Gravity Probe-B: New Methods to Determine Spin Parameters from kHz SLR Data. IEEE Trans. Geosci. Remote Sens, doi:10.1109/TGRS.2006.00675, 2008.

Kucharski, D., Kirchner, G., Schillak, S., et al. Spin determination of LAGEOS-1 from kHz laser observations. Adv. Space Res., 39(10), 1576-1581, doi:10.1016/j.asr.2007.02.045, 2007.

Kucharski, D., Kirchner, G., Cristea, E. ETALON spin period determination from kHz SLR data. Adv. Space Res., 42(8), 1424-1428, doi:10.1016/j.asr.2007.08.030, 2008.

Lomb, N.R. Least-squares frequency analysis of unequally spaced data. Astrophysics and Space Science 39, p. 447-462, 1976.

Otsubo, T., Amagai, J., Kunimori, H., Elphick, M. Spin Motion of the AJISAI Satellite Derived from Spectral Analysis of Laser Ranging Data. IEEE Transactions on Geoscience and Remote Sensing, Vol. 38, No. 3, pp. 1417-1424, 2000a.

Otsubo, T., Gibbs, P., Walters, D.G., Wood, R. Determination of LAGEOS spin motion from photometric observation. 12th International Workshop on Laser Ranging (Matera), 2000b.

Otsubo, T., Sherwood, R.A., Gibbs, P., Wood, R. Spin motion and orientation of LAGEOS-2 from photometric observation. IEEE Trans. Geoscience and Remote Sensing, 42, 1, 202-208, doi:10.1109/TGRS.2003.817191, 2004.

Pearlman, M.R., Degnan, J.J., and Bosworth, J.M. The International Laser Ranging Service. Adv. Space Res., 30(2), 135-143, DOI:10.1016/S0273-1177(02)00277-6, 2002.

kHz Single Photon Ranging: A Precise Tool to Retrieve Optical Response of Satellites

Toshimichi Otsubo (1)**, Philip Gibbs** (2)**, Graham M. Appleby** (2)

(1) Hitotsubashi University, Japan,
2-1 Naka, Kunitachi, Tokyo 186-8601 Japan
(2) Space Geodesy Facility, Natural Environment Research Council, UK
Herstmonceux Castle, Hailsham, East Sussex BN27 1RN United Kingdom

t.otsubo@srv.cc.hit-u.ac.jp

Abstract

Single-photon laser ranging has been proven to be useful for retrieval of optical pulse shapes of satellite returns. kHz single-photon ranging with a 10-ps-pulse laser currently realised at Herstmonceux is much more powerful than 10-Hz laser ranging to precisely retrieve a optical pulse shape, with just one passes. A new "deconvolution" approach is examined for quick and precise retrieval of satellite optical responses.

1. Introduction: Single photon laser ranging

Single photon detection policy, originated at Herstmonceux, UK, in early 1990's, has demonstrated to be a precise satellite-laser-ranging method to relate a post-fit residual profile and a centroid of residuals with the modeled optical response. It results in less ambiguous determination of satellite centre-of-mass corrections, compared with high- or variable-energy detection policy. For instance, Otsubo and Appleby (2003) numerically simulated the optical responses from spherical satellites such as LAGEOS, AJISAI and ETALON, and presented single (=stable) centre-of-mass corrections for single-photon stations and variable centre-of-mass corrections for multiple-photon stations.

Meanwhile, following successful development of 2-kHz laser ranging systems in Graz, Austria, and also in Greenbelt, USA, the 10-Hz laser ranging system at Herstmonceux is being upgraded to a 2-kHz system (Gibbs, et al., 2008). Herstmonceux station continues its single photon detection policy with the 2-kHz system, which means that it will be the first "kHz and single photon" station in the world. This paper deals with the early 2-kHz observation data obtained at Herstmonceux and some numerical test results.

2. Residual histogram: 10Hz vs 2 kHz

The post-fit full-rate residuals of single photon observations enable us to retrieve the whole optical response from a retroreflector array.

Fig. 1 shows a typical full-rate residual profile when tracking AJISAI satellite with a 10-Hz (strictly speaking, up to 14-Hz) laser ranging system at Herstmonceux. This station always controls return rate low, less than 15% per pulse, so that the number of detected photoelectrons is zero or one, which is known as single photon ranging. This results in

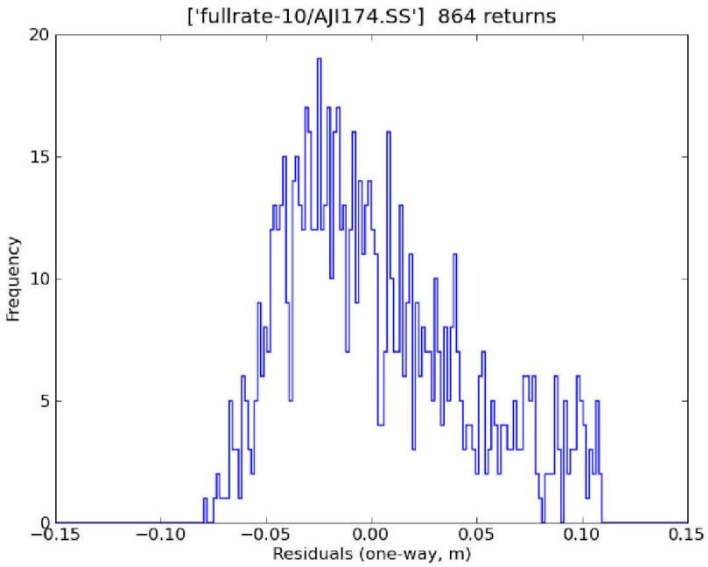

Figure 1. Full-rate residual histogram of an AJISAI pass observed by the 10-Hz system at Herstmonceux, around 21 h UT, 19 June 2000.

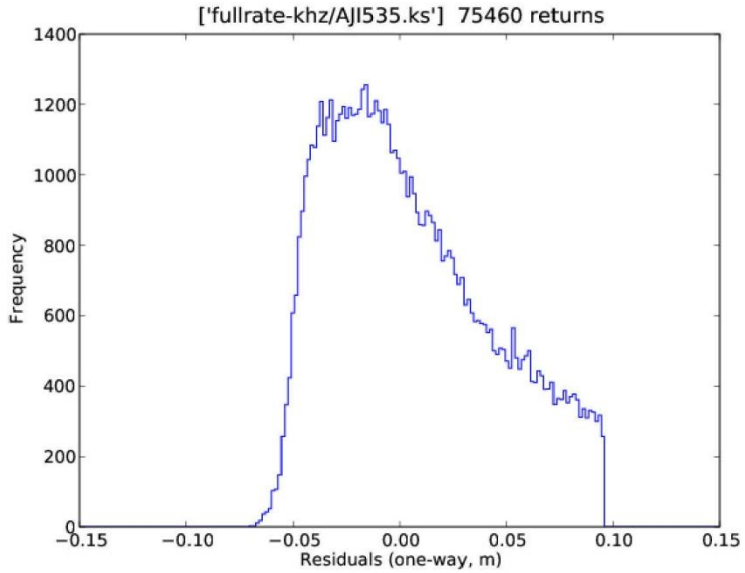

Figure 2. Full-rate residual histogram of an AJISAI pass observed by the 2-kHz system at Herstmonceux, around 7h UT, 18 February 2008.

a significantly reduced number of returns especially for low satellites that produce strong signals, compared with multiple-photon systems. The number of full-rate returns per AJISAI pass (10 to 15 minutes) is usually less than 1000, although it transmits much more laser shots to the satellite. As Fig. 1 indicates, the shape of a residual histogram is not very stable and it is not realistic to use such one-pass data for the studies of satellite optical response. Otsubo and Appleby (2003) had to accumulate a hundred of passes to generate a residual histogram, but it was not ideal to mix months of observations as the system characteristics would change.

kHz laser ranging provides a new solution to this situation. The number of laser shots becomes more than 100 times and, in the case of strong-return satellites like AJISAI, the return rate does not change so much. As a result, the number of full-rate returns potentially gets 100 times higher, and the histogram profile is much smoother as seen in Fig. 2.

In addition to the number of returns, it should be noted that the narrower laser pulse width (~ 10 ps in comparison to ~ 100 ps of 10-Hz laser) and the better timing precision of a new event timer (7 ps; in comparison to 35 ps of old time interval counter) of the kHz laser system and the consequent small observation noise are also useful for the histogram analysis.

3. "Deconvolution" approach

Let us assume these three functions:

- *f*: a residual profile oflaser ranging to a single-reflector target
- *g*: a residual profile of laser ranging to a target to be studied
- *p*: an average optical response function of a target to be studied

where it is clear that *g* is expressed as a convolution of *f* and *p*. In the extreme case of ultimate 0-ps of system noise (*f*), the observed residual profile *g* would completely agree with the optical function *p*.

Preceding studies such as Otsubo and Appleby (2003) adopted a convolution approach where a satellite-ranging residual scatter is assumed to be equal to the system noise convolved with the optical response of the onboard retroreflector array. Various p_{model}'s have to be generated in advance based on the various assumption on the optical response, and the function f_{obs} is then convolved with each p_{model}, which yields various g_{model}'s. The best p_{model} is chosen when a convolved function g_{model} agrees best with the observed g_{obs}. Note that the subscript *"model"* indicates that the function is created by numerical simulation and the subscript *"obs"* indicates that the function is based on observations.

With 2-kHz data, it could be also a realistic way to apply a deconvolution approach. Deconvolution numerical computation requires frequency domains of functions *f*, *g* and *p*, whereas the convolution numerical computation is easier and more straightforward. From the observed residual histograms f_{obs} and g_{obs}, their frequency domains F_{obs} and G_{obs} can be obtained. Then the frequency domain of *p* is simply given as:

$$P_{obs} = F_{obs} / G_{obs},$$

Then a low-pass (high-cut) filter needs to be applied for P_{obs} . Finally, the time domain p_{obs} can be obtained and that is the retrieved response function.

This algorithm does not require any modeled *p* functions, and makes it possible to obtain the 'observed' response function of p_{obs}. Fig. 3 shows an example of deconvolution test, using an ERS-2 residual profile for f_{obs} and an AJISAI residual profile for g_{obs} both of which are formed by just one pass observed on the same day and processed without chopping the tail. The numerically deconvolved function p_{obs} is also shown in the bottom graph of Fig. 3. Its full-width half-maximum (FWHM) width is 71 mm which is close to 66 mm obtained in our preliminary optical simulation of AJISAI's retroreflector array.

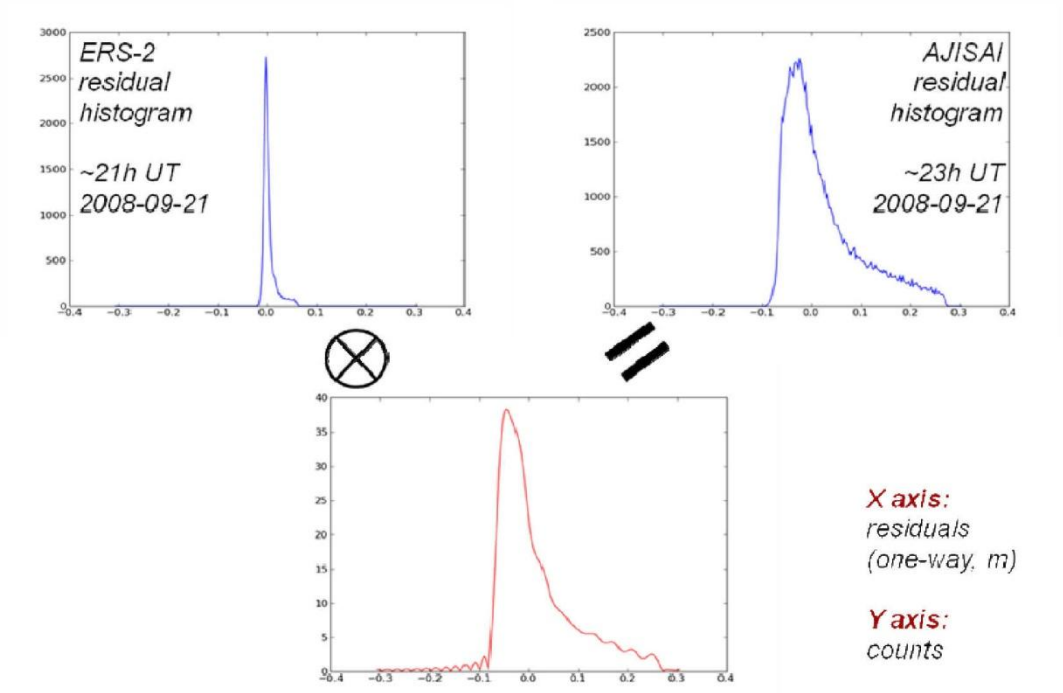

Figure 3. Deconvolution test of AJISAI satellite. Top left: ERS-2 residual histogram for f_{obs}. Top right: AJISAI residual histogram for g_{obs}. Bottom: "deconvolved" response function p_{obs}, FWHM = 71 mm.

4. Conclusions and future studies

Single photon laser ranging data are becoming a more powerful tool for retrieving the satellite optical response function with kHz laser ranging. As demonstrated by recent 2-kHz single-photon laser-ranging data from Herstmonceux, one hundred times more data with kHz observations nicely covers up for the longstanding issue-fewer amount of returns.

A new 'deconvolution' approach has been tested for retrieving the satellite optical response function. It worked reasonably well with AJISAI data.

However, there are two issues remaining before fully utilize this approach. First, this method is very sensitive to leading or tailing noise points and the choice of low-pass filter criteria. The bottom graph of Fig 3 shows many small wobbles before the leading edge. It is not easy to reduce these due to this problem. The other issue is that this approach cannot be so powerful for the small-signature satellites as for AJISAI. When the function g_{obs} is not very different from f_{obs} like LAGEOS or STARLETTE, the deconvolved method does not precisely produce the retrieved response function. It will be useful in the future work to accumulate a large number of passes to overcome these problems and fully utilize the deconvolution approach.

Acknowledgement

We would like to all members of NERC Space Geodesy Facility, Herstmonceux, UK, for

developing a kHz laser ranging system, and for providing us with early fullrate data o bserved by the new system.

References

1. T. Otsubo, G. M. Appleby, System-dependent centre-of-mass correction for spherical geodetic satellites, Journal of Geophysical Research, 109, B4, 9-1-9-10, 2003.
2. P. Gibbs, G. Appleby, D. Benham, C. Potter, R.Sherwood, T. Shoobridge, V. Smith and M. Wilkinson, "Herstmonceux - towards kHz ranging and multi-technique status," 16th International Workshop on Laser Ranging, in these proceedings.

Millimeter Ranging to Centimeter Targets

Georg Kirchner, Damiel Kucharski, Franz Koidl
Austrian Academy of Sciences, Institute for Space Research, Graz
Georg.Kirchner@oeaw.ac.at; Daniel.Kucharski@oeaw.ac.at;
Franz.Koidl@oeaw.ac.at

Abstract

Spherical satellites like LAGEOS-l, LAGEOS-2 or AnSAI introduce a significant satellite signature (> 300 mm for AnSAI, > 80 mm for LAGEOS) into SLR data, if the return signal cannot be kept at a constant level (which is difficult to achieve due to fast pointing fluctuations etc.). These variations cause a significant scatter of the NPs around any assumed mean reflection point.

kHz SLR however allows - due to its inherent data density - an easy and accurate determination of the "leading edge" (LE) of returns (those returns coming from the nearest retros). Using this LE as a reference line, and accepting only returns between LE and LE + 20 mm, the scatter of NPs is reduced from several em to less than 1 mm.

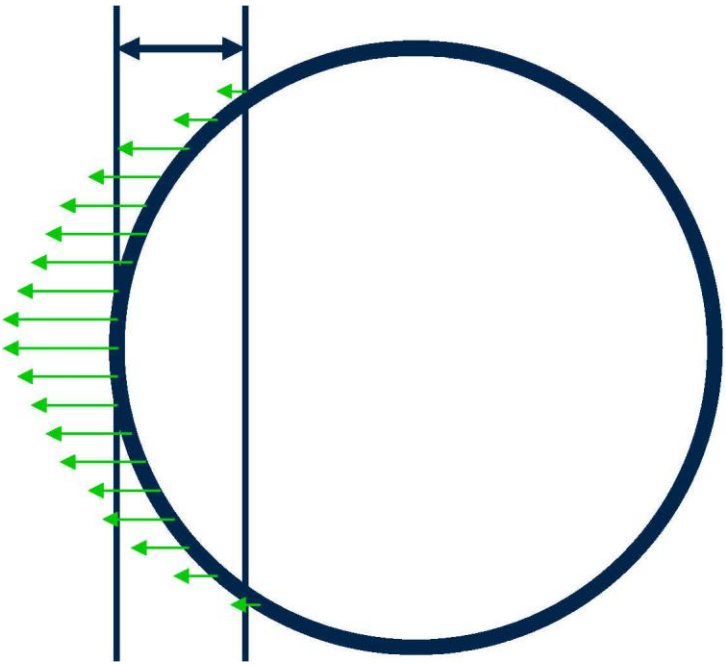

The Problem

The "reflective depth" of spherical satellites is up to 80 mm for LAGEOS, and up to 300 mm for AnSAI. This introduces a corresponding scatter of returns, potentially reducing the precision of SLR measurements.

One possible way to get better precision from such targets is to restrict return energy to single photons only; however, this requires a strict reduction of return rates (below the quantum efficiency of the detector) - which in tum requires additional hardware (ND filters), software (to keep returns rates within limits during ranging), observer training etc. However, this will reduce also significantly the number of returns per pass - loosing a major advantage of kHz systems - while still resulting in a certain amount of multi-photon returns within this SPE data set.

A possible solution

With the Graz 2 kHz SLR system, we are NOT controlling or limiting return signal energy; our observers are instructed only to achieve the maximum possible number of returns for each pass and each satellite. This results in a large amount of returns per pass (can be more than 1 million returns per pass for AnSAI and LAGEOS), but also produces large variations

of data density, mean reflection points etc.; using such data sets to form Normal Points creates large scatter within the "reflective" depth of these satellites.

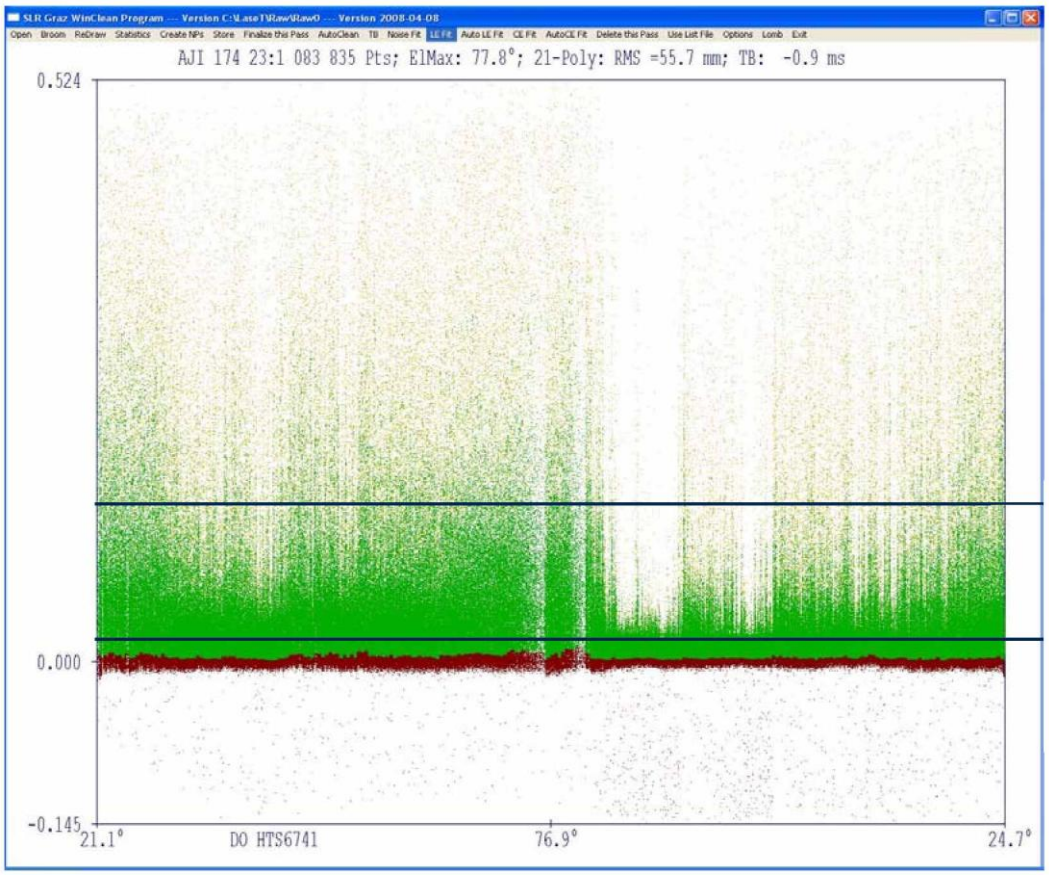

To use the inherent accuracy of our kHz system, but still keeping the operational simplicity and the high return rates, we are using now the "Leading Edge" (LE) of the returns as a reference line, and accept only returns from the first 20 mm reflective depth during post processing. Returns from behind this 20 mm limit are rejected. Although this method reduces the total amount of accepted returns (average reduction: about 30%), it offers significant improvements:

- Simple operation of the kHz system: Just try to get as many returns as possible ©
- ALL returns are accepted during tracking; no ND filters, no return rate reduction for SPE etc.
- Clearly visible "Leading Edge" line; used as reference line (e.g. for polynomial fits)
- 20 mm limit: Thus ALL NPs are located at a constant 10 mm distance from LE
- ALL NPs therefore need the same - CONSTANT - CoM correction;
- NP scatter is now significantly reduced: From ± 17 mm to ± 0.4 mm (AJISAI)

This method can be applied in principal for all spherical satellites; however, there are restrictions when using LE for post processing of other spherical satellites:

- Etalon: LE is applied, however there is no depth limit set (because anyway inherently SPE returns)
- Starlette / Stella: LE not applicable; although the satellites are now synchronized (no inertial spin), we still see the apparent spin; this causes bigger variations of nearest retro distances, and would affect NP positions if LE is applied.

With standard post processing (AJISAI, 2007, Graz), the NPs show large scattering of ± 17.6 mm due to big variations in data density. Since day 065 / 2008, we changed to "Leading Edge" post processing: All NPs are now at 10.6 mm ± 0.4 mm from LE.

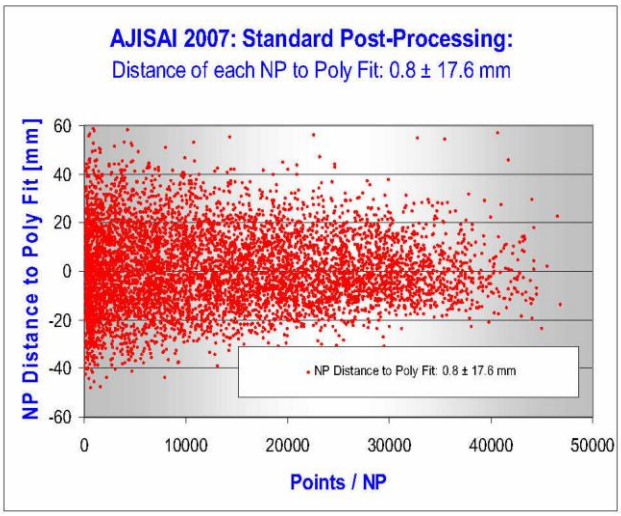

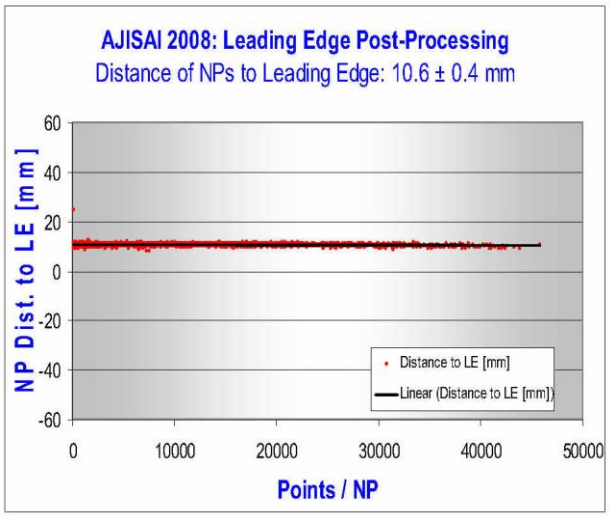

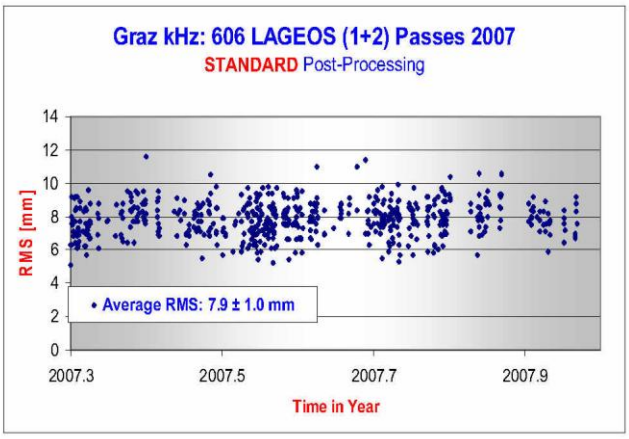

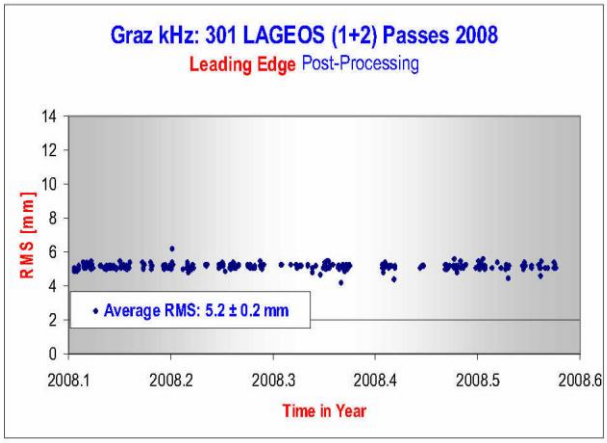

Similar effects can be seen for the resulting pass RMS: Large scattering of 15.8 ± 6.1 mm has been reduced now with the LE method to 5.3 ± 0.2 mm for AJISAI.

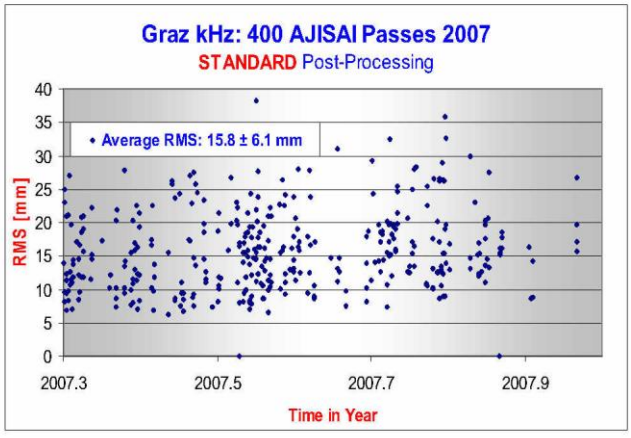

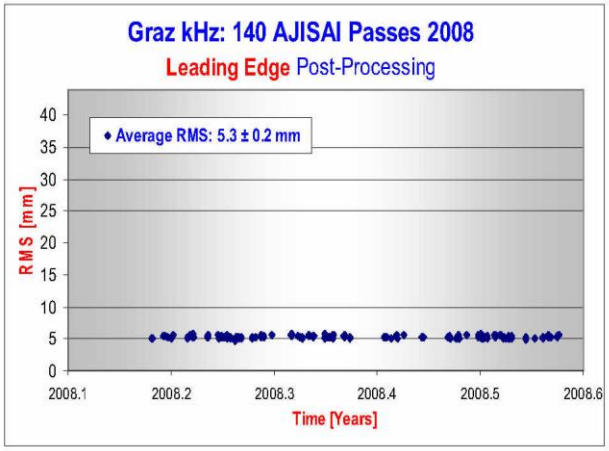

For LAGEOS, the LE has the same effects; shown here is the reduction of the pass RMS; from 7.9 ± 1.0 mm with standard post processing, to 5.2 mm ± 0.2 mm for the LE method.

Graz kHz SLR LIDAR: First Results

Georg Kirchner, Franz Koidl, Daniel Kucharski
Institute for Space Research
SLR Station Graz / Austria

Abstract

Following an idea presented by NERC in Canberra 2006, we developed a kHz SLR LIDAR for the Graz station: Photons of each transmitted laser pulse are backscattered from clouds, atmospheric layers, aircraft vapour trails etc. A Single-Photon Counting Module (SPCM), installed in the main receiver telescope, detects these photons. Using our FPGA card, these detection times are stored with 100 ns resolution (15 m slots in distance). Event times of any number of laser shots can be accumulated in up to 4096 counters (according to> 60 km distance).
The LIDAR distances are stored together with epoch time and telescope pointing information; any reflection point is therefore determined with 3D coordinates, with 15 m resolution in distance, and with the angular precision of the laser telescope pointing.
First test results to clouds in full daylight conditions - accumulating up to some 100 laser shots per measurement - yielded high LIDAR data rates (> 100 points per second) and excellent detection of clouds (up to 10 km distance at the moment). Our ultimate goal is to operate the LIDAR automatically and in parallel with the standard SLR measurements, during day and night.

Hardware

To detect the backscattered photons, we use a Single Photon Counting Module (SPCM) from Micro Photon Devices (www.micro-photon-devices); the Peltier cooled 100 urn diode has a rather low dark noise of about 500 Hz, and is operated in ungated mode. A standard 0.3 nm interference filter transmits about 35 % of the laser wavelength, rejecting most of the daylight background noise.
For the first tests, the device was installed in the main telescope; a mirror switched between SLR or LIDAR measurements. In the next step however, the SPCM will get its own small telescope (15 em diameter), and will be operated in parallel to all SLR activity.

A separate Graz FPGA card has been programmed to do the hardware job (fig.l): The output pulses are counted in up to 4096 counters, according to their "range slot"; each counter integrates only the photons of its dedicated 15 m range bin. For each cycle, the number of shots to be integrated can be set between 1 and up to 65535 (i.e. up to 30 seconds @ 2 kHz).

The resulting counter contents after each cycle are shown on the Real-Time screen of our kHz SLR system (fig. 2); the rather strong reflections from clouds are clearly visible, even in the daylight conditions.

After each cycle, the counter data is stored, together with all relevant telescope pointing information, for later evaluation.

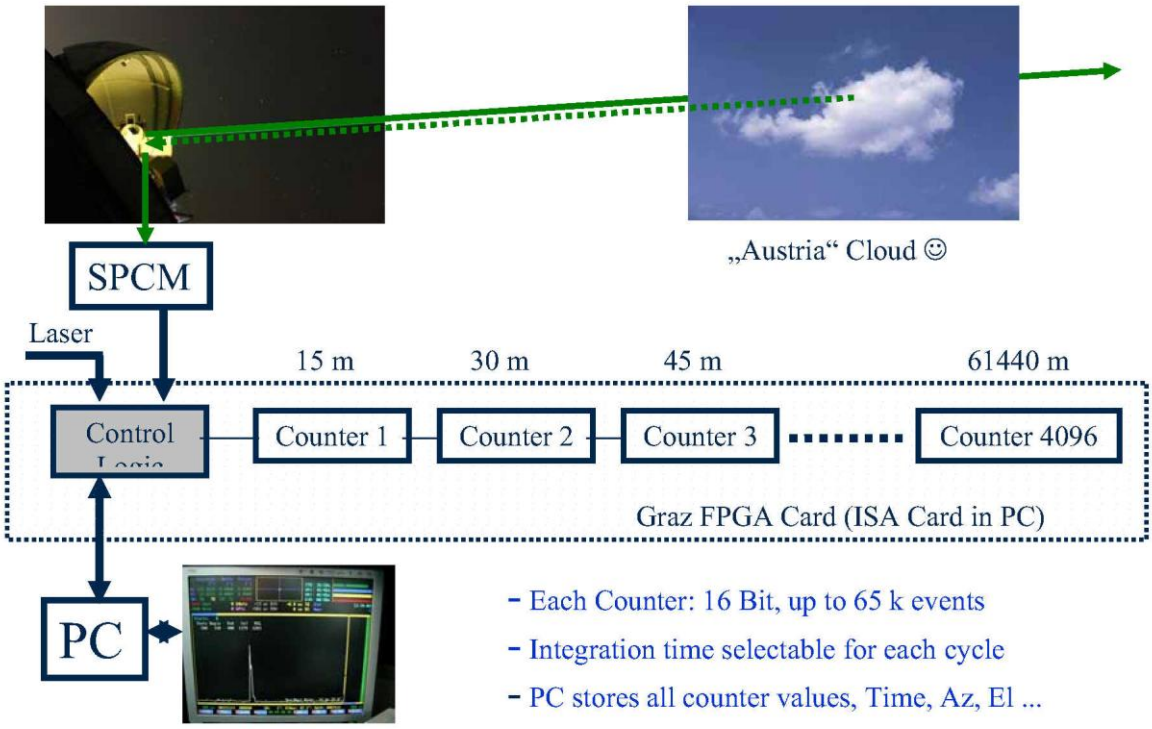

Figure 1. Schematics of Graz kHz LIDAR Hardware

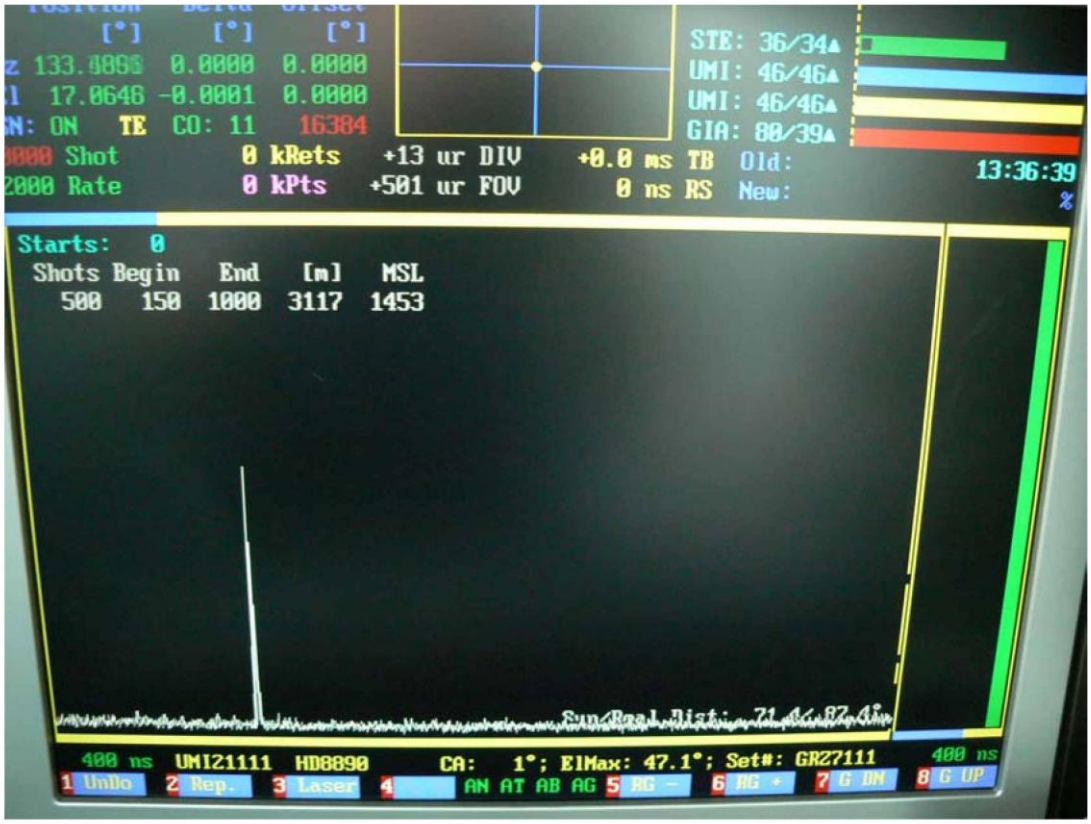

Figure 2. Real Time Dsiplay of Graz kHz LIDAR: A strong backscatter signal at 3117 m distance, from a cloud in 1453 m altitude (MSL); full daylight, single photon detection

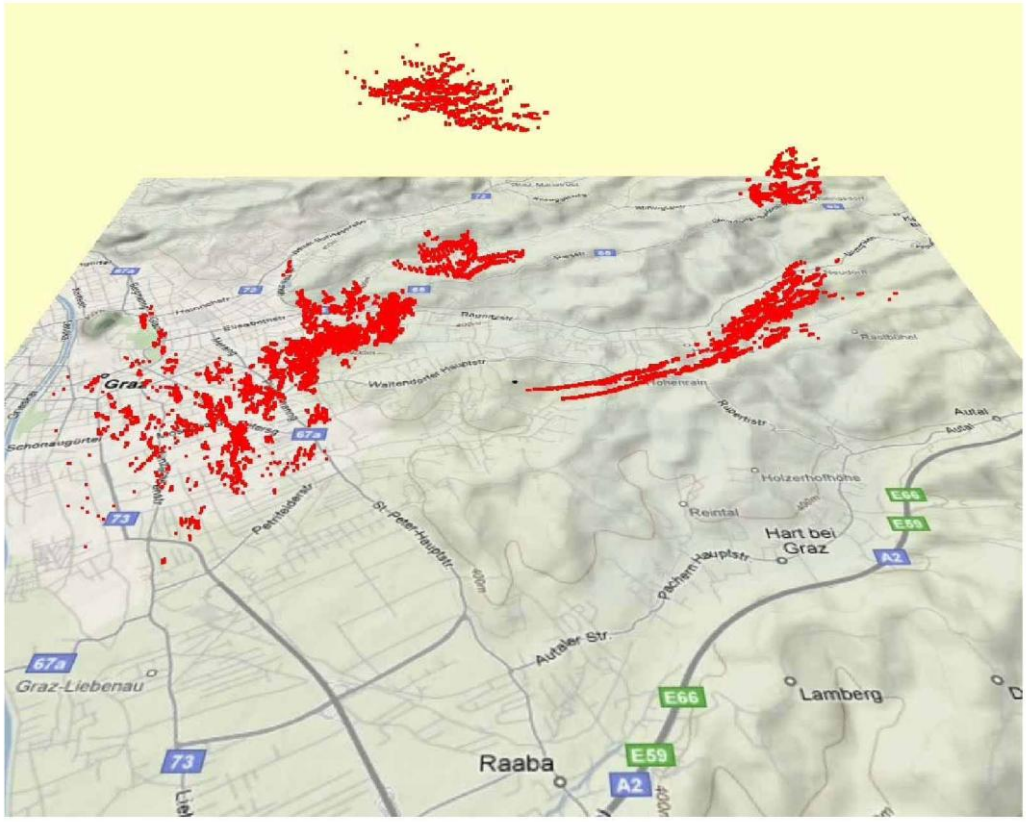

Figure 3. LIDAR scans of several clouds around the SLR Station Graz (black dot in centre)

Future Goals

We intend to operate the kHz SLR LIDAR fully automatically day and night, mainly in parallel to all SLR activities; it will collect - as a by-product to SLR - some information about atmosphere, layers, clouds, inversions, aircraft vapor trails etc. We also hope to get some correlation between SLR return rates, and atmospheric backscatter.

Outside SLR activity, dedicated scans could map dimensions and increase of cumulonimbus clouds, measure cloud top altitudes, determine wind speeds in altitudes of aircraft vapor trails, and similar items.

Medium Resolution Digital Event Timer and Range Gate Generator in Graz FPGA Card

F. Iqbal (1)**, G. Kirchner** (2)**, F. Koidl** (2)

(1) PhD Fellowship – Higher Education Commission of Pakistan
Presently at TU Graz, PhD Study
(2) Austrian Academy of Sciences, Space Research Institute, Graz

farhat_ieee@yahoo.com; Georg.Kirchner@oeaw.ac.at; Franz.Koidl@oeaw.ac.at

Abstract

For our kHz Satellite Laser Ranging (SLR) system in Graz, we developed a fast response, medium resolution Event Timer to determine laser firing times; and a digital Range Gate Generator to activate the Single Photon Avalanche Detector (C-SPAD). The Event Timer has a resolution of 250 ps, and determines the Event Times within 20 ns; the Range Gate Generator produces a range gate pulse with 500 ps resolution, and better than 1 ns accuracy. Both devices are fully digital, and are implemented within an FPGA circuit. These devices can be used in the present 2 kHz SLR system, as well as in future higher repetition rate SLR systems.

Introduction

An SLR system consists of a laser, a telescope, a – single or multiple - photon detector (in Graz: C-SPAD) and a time of flight (TOF) measurement device. The TOF can be measured with 2 different methods: With a simple time interval counter, or with event timers.

Time interval counters are not applicable for kHz SLR, because due to the high repetition rate (some kHz) there are always more than 1 pulse – up to 300 pulses for high orbit satellites for a 2 kHz SLR system – simultaneously traveling between SLR station and satellite.

Event timers determine laser firing epochs and epochs of the returns independently; these epochs are used to calculate the TOF. Because the ultra high precision Graz E.T. (< 2.5 ps) needs about 400 µs to fix the event time (Kirchner et al, 2000), we developed a much faster (20 ns response time), but medium resolution (250 ps) event timer within the FPGA, dedicated – and accurate enough - for range gating purposes.

Figure 1. Graz ISA PC Card; FPGA containing Event Timer and Range Gate Generator

After detecting a laser start pulse event time, the expected return event time is calculated, and loaded into the Range Gate Generator; which then activates the detector short before arrival of the return photon(s). While this is done at present with a combination of a digital 100-ns-resolution FPGA counter PLUS a programmable analog delay chip, we implemented now a fully digital Range Gate Generator into the FPGA - using a 5-ns-course counter, and a 500 ps vernier – to improve linearity and stability.

Both devices were implemented within the Altera FPGA Apex 20K chip on the Graz FPGA card (fig. 1).

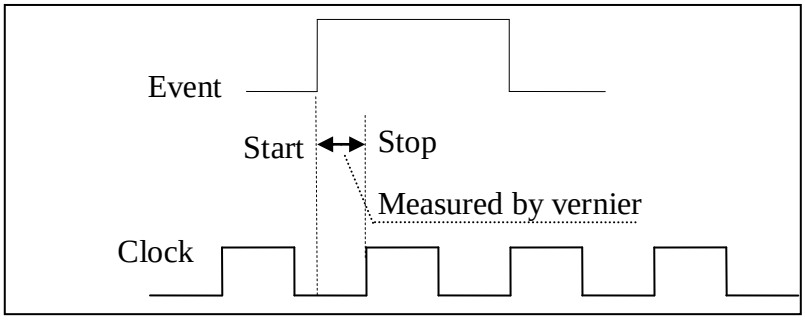

Figure 2. A digital vernier interpolates between 5 ns clock pulses.

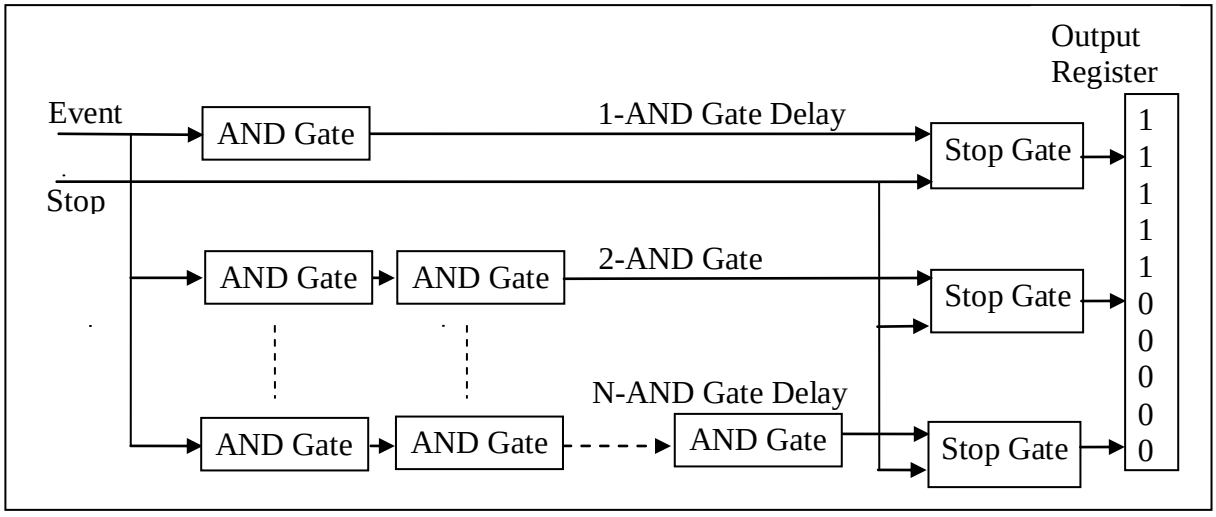

Figure 3. Event timer unit, using chains of AND delay gates of increasing length.

Event Timer Implementation

The fast response digital event timer is implemented using a well known vernier method. This method uses a 200 MHz counter and a vernier for the 5 ns intervals. The vernier uses standard AND gates with 250 ps transit time per gate (fig. 2). To implement a series of identical, cascaded delay gates we had to disable the automatic optimization of the Quartus Compiler for the Altera FPGA device.

The event pulse (e.g. Laser Start Pulse) starts traveling through several parallel chains of AND Gates; each chain consists of an increasing number of AND gates; the next following 5 ns clock pulse is used as a STOP pulse for this simple vernier (fig. 4). If the start pulse

reaches the end of a chain BEFORE the STOP pulse, a "1" is latched into an output register; if not: a "0"… (Fig. 3). The bits in this output register represent a measure for the 0-5 ns interpolation; together with the latched actual reading of the 200 MHz coarse clock this forms a 250 ps resolution event time.

We implemented this event timer into the Graz ISA card FPGA and optimized its floor plan layout to achieve best linearity and uniform resolution. Simulation of such a circuitry gives promising results for the required speed and resolution of this Event Timer (fig. 4).

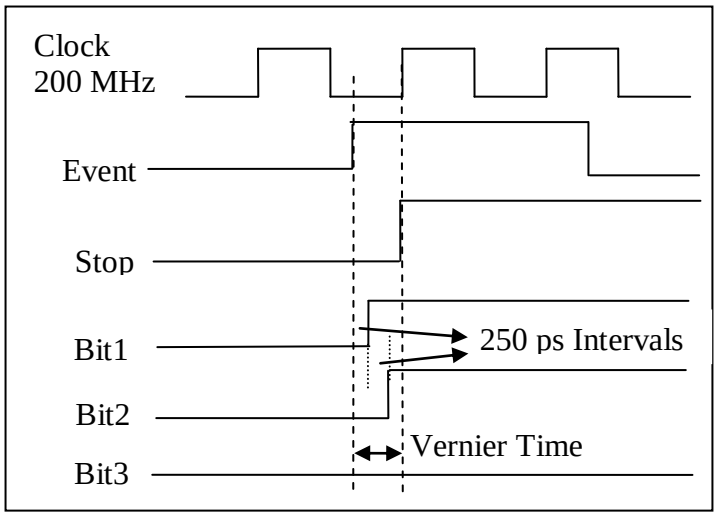

Figure 4. (A) Vernier measurement, interpolating 5 ns intervals.

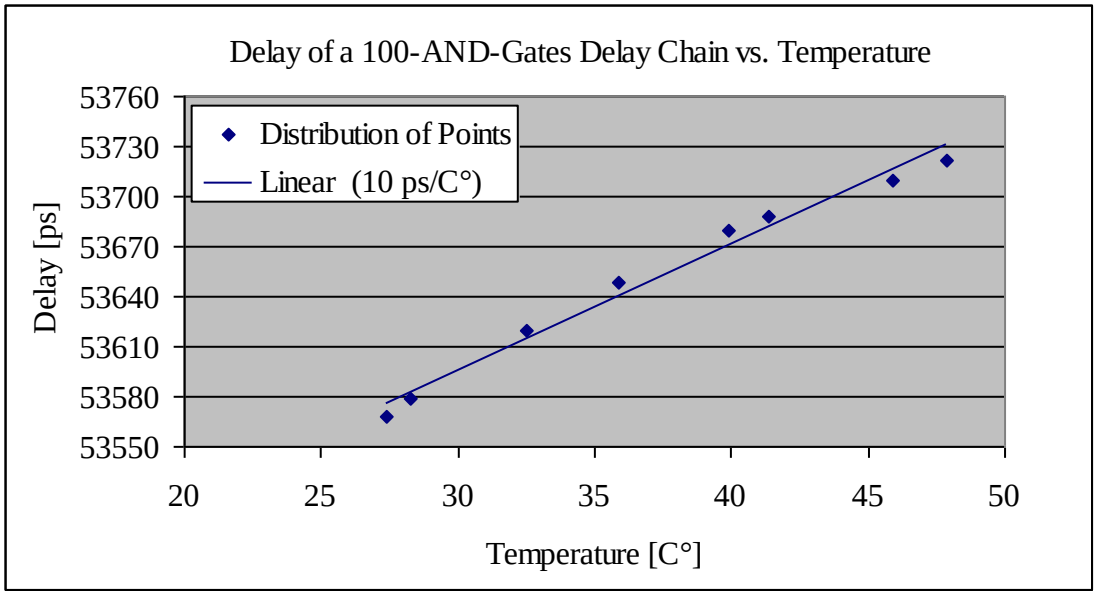

Figure 5. Delay of a 100-AND-Gates Delay Chain vs. Temperature.

Event Timer Experiment and Conclusions

We tested the temperature drift of a 100-AND-gate delay chain; it drifted with about 10 ps/C° (Fig. 5), which is quite acceptable considering the required resolution, and the location of the PC / ISA Card / FPGA in the air conditioned laser room.

To evaluate the FPGA event timer linearity, (fig 6: Test setup) we compared its results with those of our ultra high precision (1.2 ps resolution, < 2.5 ps non-linearity) Graz E.T. (Kirchner et al, 2004). The differences between both showed an RMS of 260 - 290 ps(fig.7).

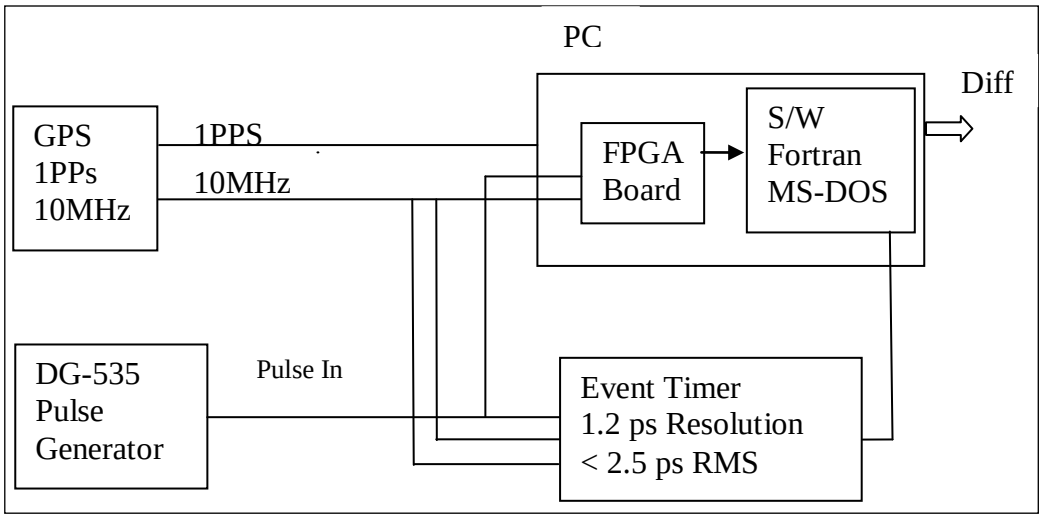

Figure 6. Test setup to compare Graz E.T. and FPGA ET measurements

Although an event timing accuracy of < 300 ps is fully sufficient for the purpose of Range Gate Epoch determination, we tested possible improvements by implementing 4 such Event Timer Units in parallel (**fig** 7) into the FPGA. All 4 event times are read by PC and averaged there; this average reduces the FPGA event timer jitter to 217 ps RMS (fig. 8).

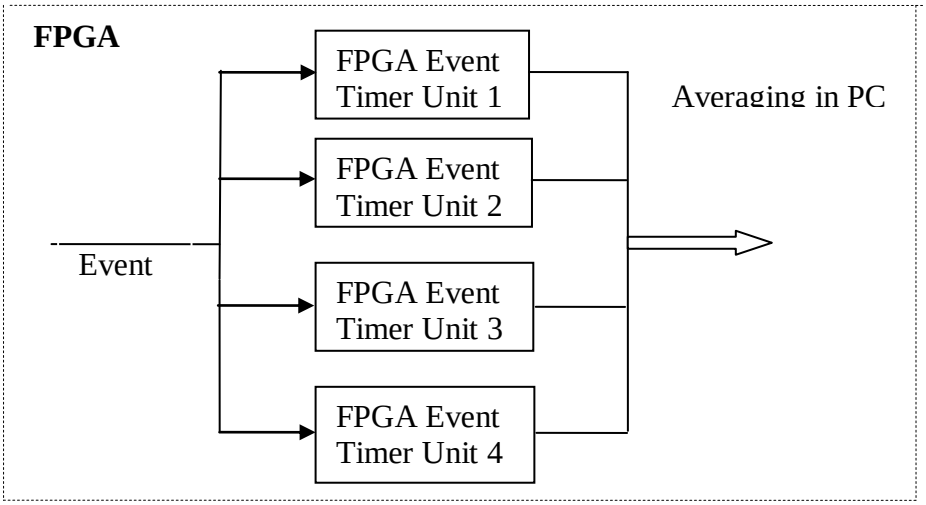

Figure 7. 4 Parallel Event Timers.

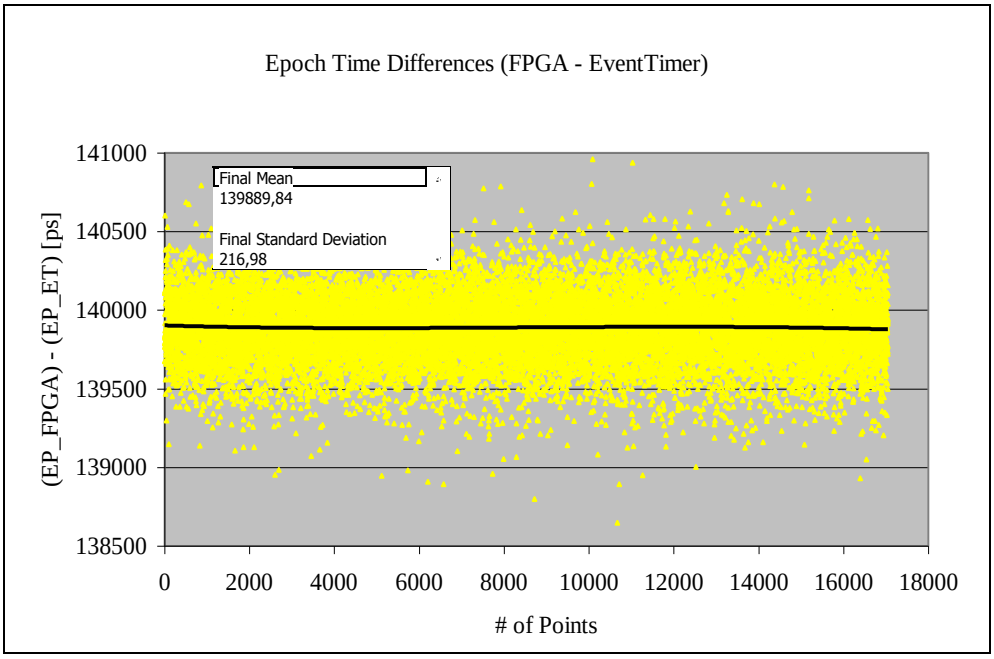

Figure 8. 4 Parallel Event Timers: Standard deviation of 217 ps

Conclusion: Resolution and non-linearity of a single FPGA Event Timer unit is more than adequate for our purpose; for even better resolution, a multi-channel Event Timer can be implemented. Due to its very high speed, it is well suited for the existing 2 kHz SLR system and also for systems with significantly higher repetition rates.

Range Gate Generator

We used a 200MHz clock and a chain of AND gates to implement a Range Gate Generator (programmed via PC) - which generates a range gate pulse short before the actual return of the laser photons - with a resolution of 500 ps and an accuracy of < 1ns.

The start pulse (fig.8) travels through the chain of AND gates. The output of each gate switches its associated D-Flip-Flop as soon as the start pulse has passed; only ONE out of these D-Flip-Flops is activated by the pre-programmable selection logic, and generates the Range Gate pulse (fig. 9).

Experiments and Conclusions

We implemented a test setup using a DG535 Pulse Generator, a Stanford SR620 Time Interval Counter, and a GPS system (1 pps) to test the linearity of the Range Gate Generator.

We tried 3 different placements (floor plan layouts; both manual placements and/or automatical placements of the AND gates and D-Flip-Flops within the logical cells) of the Range Gate circuitry inside the FPGA to find the optimum linearity (Fig.10); the selected final placement has the best R-squared value ("R2" in fig. 10) and linearity.

Conclusion: The Graz ISA PC Card with FPGA now contains also a 250-ps resolution event timer and a fully digital Range Gate Generator. Both are used to speed up the RG setting for present 2KHZ SLR systems.

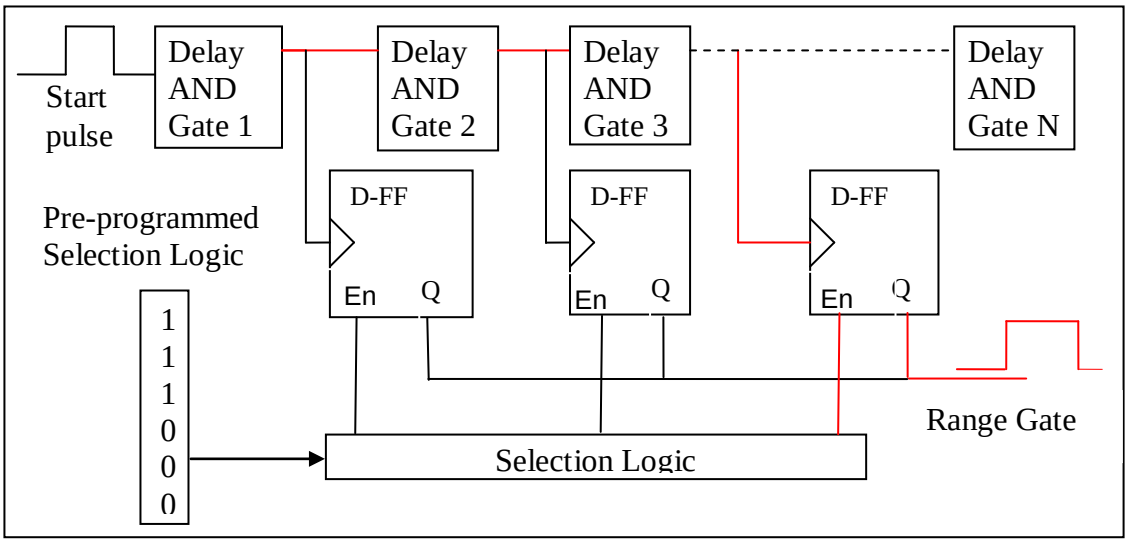

Figure 9. Block Diagram of Digital Range Gate Generator.

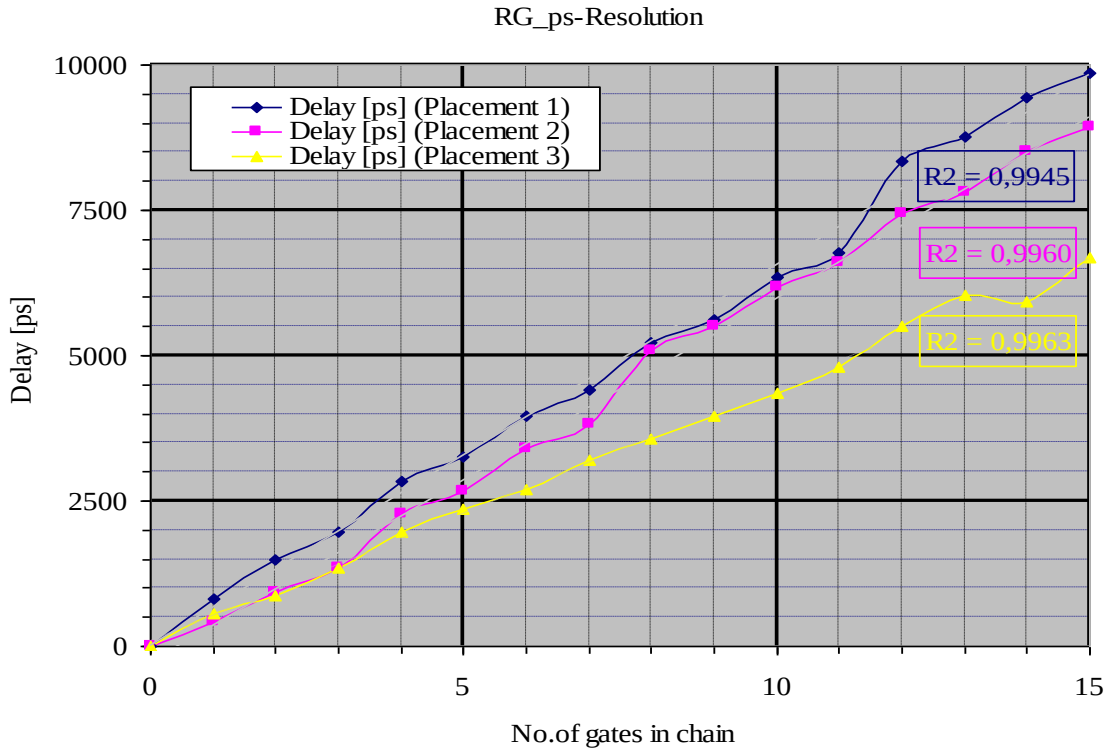

Figure 10. Delay Time (ps) vs. Delay Chain Length – different placements of AND gates and D-Flip-Flops to optimize linearity.

References

Kirchner G., Koidl F. (2000): *Graz Event Timing System;* Proceedings of 14th Int. Workshop on Laser Ranging, Matera, Italy.

Kirchner G., Koidl F. (2004): *Graz kHz SLR system: Design, Experiences and Results* Proceedings of 14th Int. Workshop on Laser Ranging, San Fernando / Spain.

Development of the Electronic Circuit in High Frequency SLR Based on FPGA

Chong CHEN[1,2], Cunbo FAN[2], Zhenwei LI[2], Xue DONG[2,3], You ZHAO[1,2]

[1]National Astronomical Observatories, CAS, 100012, China
[2]Changchun Observatory, NAOC, CAS, 130117, China
[3]Graduate University of Chinese Academy of Sciences, Beijing

Abstract

Increase of the laser firing frequency will significant improve the performance of Satellite Laser Ranging (SLR) system. To meet the requirement of high frequency SLR, an implementation of control circuit in single FPGA chip was designed and developed in this paper. SOPC (System On Programmable Chip) system was proposed to solve these problems. To realize the system, a control circuit custom component was designed and simulated. Then, the component was integrated into a SOPC system. Cooperated with software, the circuit has the ability to control the SLR system running at high frequency. Finally, the system was simulated in the Quartus software and NIOS IDE provided by Altera and implemented in an Altera EP1S10 development kit.

Key words: High Frequency Satellite Laser Ranging, Rang Gate, Firing Control

1. Introduction

The running frequency of tradition satellite laser ranging (SLR) system was limited by the control circuit and other components of system; the frequency was determined by the following equation: F=C/2R. Here the constant C is the speed of light and R is the distance between satellite and station. We can find out that the running frequency will suffer a significant decrease when observing high orbit targets. When it concerned to synchronous satellite, the system only can complete 4.17 ranging per second. Also, with the application of event timer, some station keep its system running at the constant frequency of 10 Hz in spite of the target distance, but the quantity of date is still low. Increasing the running frequency of the system is an efficient method to solve this problem. The trend of new generation SLR system is developing the system able to running at the frequency of Kilo-Hz, called KHz SLR system. Not only increase the quantity of observation data, the benefits of KHz SLR also include the improvement of Normal Point (NP) precision. To increase the running frequency of the SLR system, several improvements need to be conduct to the current system, and one of the most important parts of these improvements is the redesign of control circuit. The function of the control circuit in SLR system is to generate the Rang Gate (RG) signal for time filter and the fire signal for laser. Time filter is a specific filter widely used in SLR observation, which means to generate a RG signal to control the photon receiver (SPAD in our station). With the application of time filter, the SPAD will only active just several nano-second before the return photon arrive, the noise in other time will not influence the SPAD. For the reason of complexity, the currant design method is no longer useful for new generation control circuit. In this paper, we present a method to integrate KHz SLR control circuit into single FPGA chip. Based on the introduction of SLR system in Changchun Observatory, we discussed and described the details about the design method and experiment

result of this implementation, which is meaningful for Changchun Observatory to update its system available to conduct KHz observation.

2. Main problem faced by the control circuit of high frequency SLR

Different from currant SLR control circuit, to meet the requirement of high frequency SLR, the control circuit should solve the following two problems:
(1). Overlap of start and return impulse: between the start and return of one impulse, there are amounts of new impulse on its flight, which means that the flight time of these impulses was overlapped at some level. Each impulse needs a RG signal, the number of RG data buffered in the circuit can be calculate trough the following equation: N= 2fR/C. Here f is the frequency of laser, R is the range between satellite and station, C is the speed of light. Above equation indicates that, if the system running at the frequency of 2KHZ, then the number overlapped impulse can reach to more then 480 when observer synchronous satellite. If we use counters, as currant control circuit did, to generate the RGs, more then 480 counters will be implemented, which is unpractical. In this paper, we use FIFO to buffer the return time of each impulse and comparer to generate the RG signal.
(2). Backscatter: laser impulse will be scattered by the atmosphere, some photons will be reflected back and receive by the telescope, and this phenomenon was named backscatter. Normally, the backscatter will last about 100 us after the laser pulse was send out. When backscatter happens, the noise will disable the receive equipment (SPAD), which will greatly decrease the efficiency of the SLR system. To solve this problem, the control circuit should generate the fire signal appropriately to avoid the return photons.

3. The hardware block-figure and the software flowchart of the control circuit

Basically, there are two schemes for implement the circuit. The fist scheme is design a circuit without microcontroller, all the prediction and control instruction is operated by the host computer. The advantage of this method is that the hardware design will be much easier. The drawback of this scheme is that we should transplant the whole software to a real-time operation system from the currant windows platform, because the time remained for computer to complete the prediction is limited. Take a 2 KHz system for example, in the worst situation, the time between two laser pulses is 400 us, in this short time computer should not only give the prediction result but also complete the operation of system control and ranging data process/display. The scheme employed in this paper for the circuit implementation is to construct a embed system, which includes a micro processor, to execute the prediction operation. This scheme releases the burden of host computer. Therefore, the circuit can access specific resource to complete the calculation with real-time processing requirement. The currant software can be used for high frequency observation with little modify.

Figure 1 is the block figure of whole control circuit system, the host computer send the Ephemeris to the embedded system in FPGA chip, because the transmission will be completed before the observation, there are no strict requirement for the speed, we can transmit it through RS-232 serial communication. A SOPC system was integrated into the FPGA chip, which was composited by several IP components provided by Altera, and a custom component designed by us. All this components was bridged trough Avalon-bus.

For the reason that FPGA chip will loss its configuration information within power off, we use a FLASH ROM to storage the data to configure the device. For the limitation of inner

storage space in FPGA, we add SDRAM as system memory. Also, we design a custom component using VHDL, it communicate with other components through Avalon-bus. The components input signal includes 10 MHz, PPS and start pulse; most of the control signals act as the custom components output. Because the voltage level of TTL and CMOS was incompatible with each other, we need the voltage level transformation chip to guarantee the signal to be correctly identified.

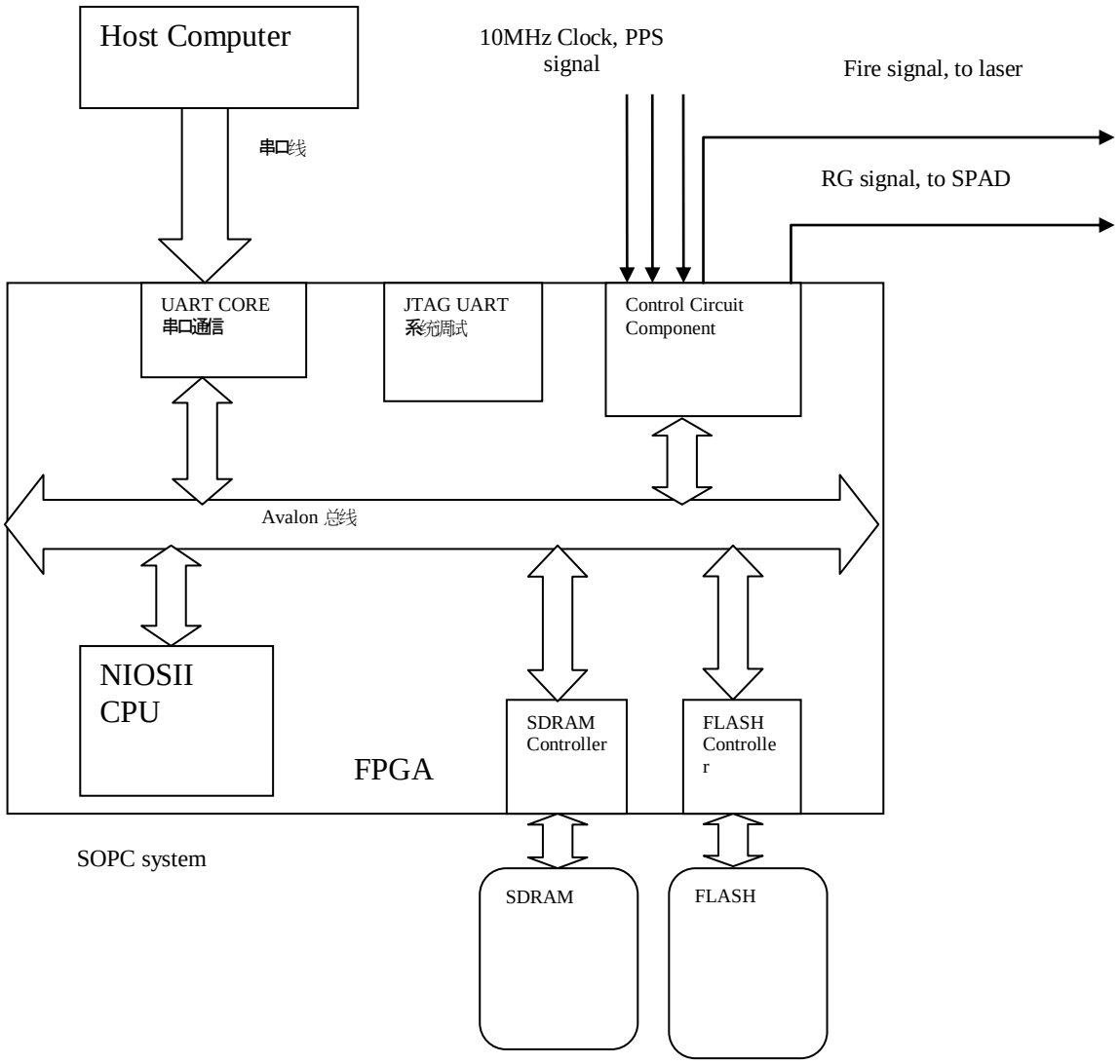

Figure 1. Hardware block diagram

3.1 Flow-Chart of software

Firstly, for the reason that interpolation is used to calculate the return time, we should consider the time sync between UTC (which was used in ephemeris) and the inner clock of control circuit. So, after complete the transmission of ephemeris, the host computer read the currant second of UTC from GPS and transmits it to the circuit, then the circuit begins to count in the next second.

In host computer, the software operation related to the control circuit is very simple; firstly the computer transmits the ephemeris to the circuit, and then transmits the currant second data.

Figure 2 presents the flow-chart of control circuit, it can be described as follow: firstly read the RS-232 UART port, storage the ephemeris to the inner and outside memory, after the transmission is completed, active the "running registration" of custom components, then the components begin to fire the laser, at the same time, the NIOS CPU begin to check the statue bit of this component to determine whether the start pulse occurred, if yes, CPU will read the registered happen time of start pulse, calculate the return time and write it to the component. If the observer want to change the target, reset the CPU, system will waiting for new transmission of ephemeris.

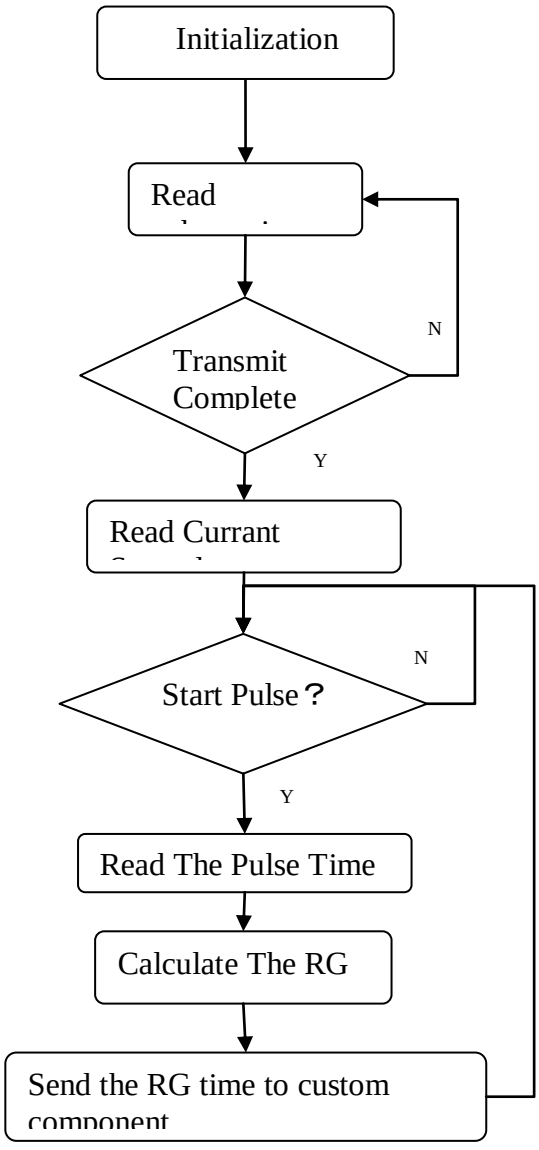

Figure 2. Software in embed system

4. Design, simulation and experiments of custom components

4.1. Fire module

Suppose the system running at the frequency of 1 KHz, we divide the 10 MHz clock with the parameter of 10,000 (we can change the divide parameter to let the system running at any frequency), get the 1 KHz signal for fire. But if we send this signal directly to laser, it is possible that the black scatter region will overlap with the return photons.

From the ephemeris, we know the time when the return photons will arrive, base on this assumption, there is a simple method to avoid backscatter: we generate two fire signals, on without any delay; the other was delayed with 100 us. Figure 3 describes the principle of this method, from the figure, we can see that every fire signal will cause a "backscatter region" of about 100 us, to avoid backscatter, we choose only one pulse as output signal, depend on whether the return photons will be interfered by the backscatter noise. To be more practical, if the return will happens in the fist pulse's backscatter region, pulse two will be send out, in the contrast condition, the first pulse will be send out.

This method requires a state-signal to indicate whether the return photons will be interfered by the backscatter. The circuit in the RG module will generate it and more details will be discussed in the following section of this paper. Figure 4 presents the block diagram of fire module; the function of each pin can be described as follow:

Clk: 10 MHz input clock.

Shift: Control signal, from RG module, indicate whether the return is in the backscatter region of pulse 1.
CLR: reset.
Main_pulse: fire signal.

The delay unit we implemented is a synchronize state-machine. After trig by a rise-edge, the counter of the unit will keep counting until the number reach a constant, and then the unit will output a pulse with 1-clock cycle width.

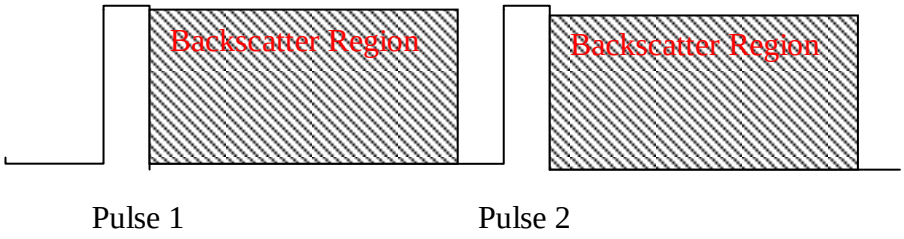

Figure 3. The principle of Avoid backscatter

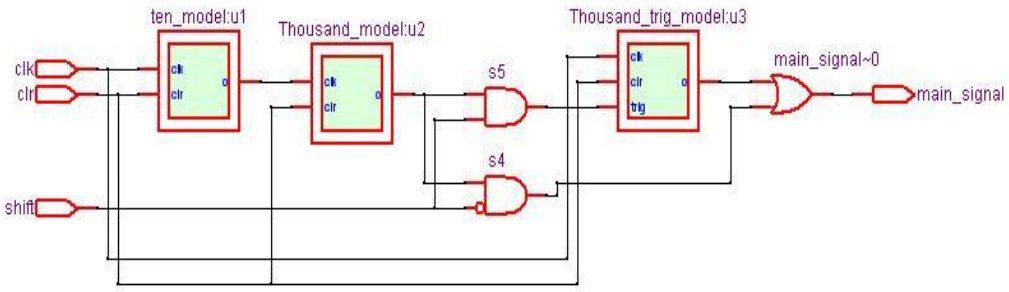

Figure 4. The block diagram of fire module

4.2. RG module

Figure 5 is the block diagram of RG module, to describe it more clearly; we simplified the diagram and neglect several minor signals. The "counter" unit is a multi-usage unit, it provide the system clock, meanwhile register the start pulse time. When the laser firing, the start pulse time was registered by "counter" and read by NIOSII CPU, after the return time is calculated, it will be send to FIFO. Contemporarily the FIFO already buffered numerous of RG time, the output of FIFO is the RG time for next return; this data will be compared with currant time. If the two numbers are equal, the compare will send out a RG signal, the signal also feedback to FIFO to update its output.

The output of FIFO also subscribed with the decimal part of the counter output, the result will be compared with the constant derived from the following equation: N= ζ /T. Here ζ is the "backscatter sustain time" and T is the period of clock. If R<N, the shift signal will be active.

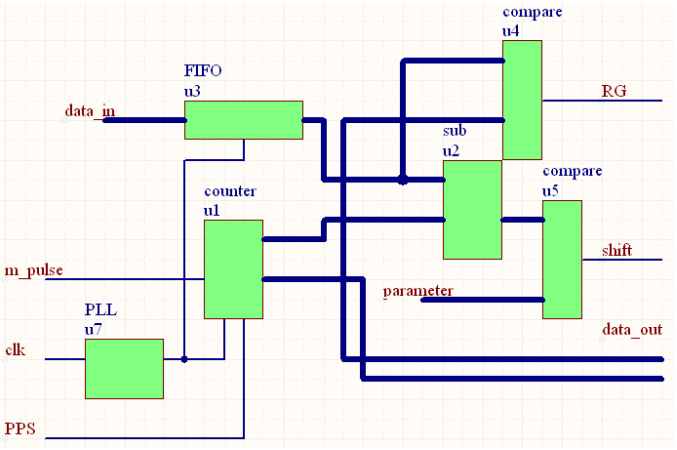

Figure 5. The block diagram of RG module

4.3 Implementation and simulation

All the above design was described by VHDL, synthesis and routed by Quartus II software provided by Altera cooperation, the target device is Stratix 1s10 FPGA. After complete the design flow, we simulated the above design using Quartus II simulator. Figure 6 and figure 7 is the simulation result.

The input waveform file includes input signal m_pulse, PPS (second) and CLK (clock for SOPC system), clk1 (10 MHz external clock), at first active period of wr, set the whole bits of control word to '1', enable the component to running. In every follow active period of wr, write RG time in the input port, in this simulation, we write 4 RG time, 1 ms, 2 ms, 3 ms and 4 ms. After a while, we assign several active periods to the rd signal, In more then one periods, the adr input is '0' (output the decimal part of start pulse time), and in other periods is '1' (output the remain part of the start pulse time). Chipselect signal is always high. Figure 6 is beginning of the simulation, we can see that the m_pulse signal was registered, and the rddate output is correct.

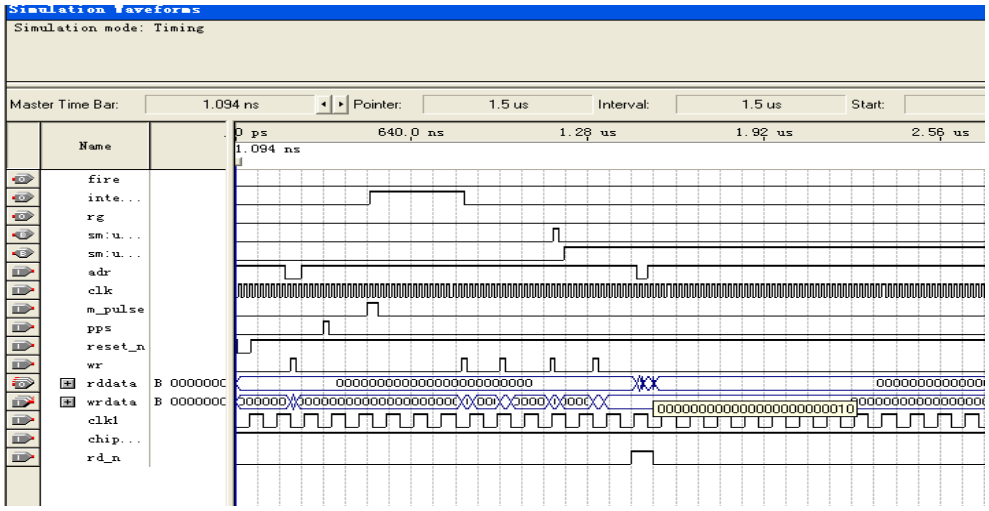

Figure 6. The beginning of simulation

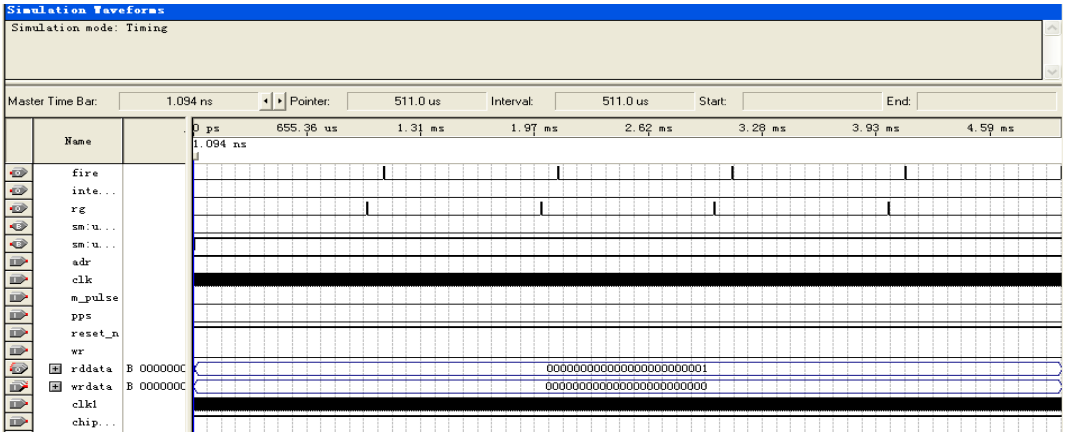

Figure 7. The whole simulation result in the 5 ms time scale.

Figure 7 is the whole simulation result in the 5 ms time scale. We can find out that the RG signal was generated correctly at 1 ms, 2 ms, 3 ms and 4 ms after PPS signal was active, all the fire signal avoid the backscatter region.

The above simulation only verify the performance of our design within 5 ms. With the application of no-sign subtracter, when the system time "cross the second", the circuit can still calculate the number of clock periods between currant time and the predicted arrive time of return photons, then generate the "sift" signal correctly.

5. Hardware implementation and precision

We realize the system in a 1S10 development board from Altera, the documents about this board can be find in Altera website. The board has a RS-232 UART connector and two 14-pin headers for 3.3/5.0 volt prototype connector. So we can build a daughter card with the connector to SPAD, laser and 10 MHz clock in one side and the 14-pin slot in the other side, then insert this card upon the develop board. The SPAD, laser and 10 MHz clock will link to FPGA board with this daughter card. The host PC and FPGA board will be connected with a serial communication cable.

6. Summary

Frequency increase will significantly improve the performance of SLR system, we design a new control circuit which can running at KHz frequency. By integrate a SOPC system in signal FPGA; the circuit can complete the prediction independently after the ephemeris was successfully transmitted. To guarantee the efficiency, the circuit can shift the laser-fire signal automatically to avoid backscatter. The circuit is experimented in a 1S10 develop board, the future work is to implement the circuit in a PCB board designed by ourselves and use it to enable the SLR system in Changchun Observatory running at KHz frequency.

References

1. Kirchner, G., *Rang Gate Generator at GRAZ*, Proceedings of the kHz SLR Meeting, Graz, Austria, October, 2004
2. Altera Corporation., *NiosII Software Development Handbook*.
3. Altera Corporation., *Stratix Device Handbook.*
4. Altera Corporation., *Quartus Handbook Volume 4, SOPC builder*.

Pulse repetition rate optimization in SLR stations to provide minimum systematic error of ranging

M.A. Sadovnikov
Science-Research Institute for Precision Instrument Engineering (IPIE) Moscow
natalia.n@g23.relcom.ru / Fax: +7(495)2349859

Abstract

An analytical model of single-photon satellite laser ranging (SLR) is presented, allowing to estimate the systematic error of ranging caused by fluctuations of photon numbers in the return pulse. It is demonstrated that with a sufficiently small number of photoelectrons in the in the pulse the return pulse intensity fluctuations practically do not affect the ranging systematic error value. It is also demonstrated that this error value may be reduced to a given level by reduction of the number of photoelectrons in the pulse and increase of the repetition rate. An estimate of the minimum required pulse repetition rate is presented.

Background

The basic sources of random errors in time-of-flight (TOF) measurements with a low and fluctuating photon number in the return pulse are:

- The finite pulsewidth (defining the uncertainty in the moment of the return signal photon arrival and corresponding photoelectron appearance)
- Fluctuations of the photoelectrons travel time during their avalanche multiplication in the photodetector (transit time jitter).

The RMS return pulsewidth $2\sigma_t$ is defined not by the laser pulsewidth only, but also by the shape, attitude and dimensions of the target retroreflector array (signature effect). Particularly, the duration of return pulses from LAGEOS and GLONASS retroreflector arrays may vary from 100 ps to 400 ps. The RMS value σ_j of transit time jitter when single-photon returns are detected may vary from 10 ps to 50 ps (depending on the photodetector type and operation mode). Therefore, when single photoelectrons are generated by the return pulse, the one-shot ranging precision, with the above conditions, will be no less than 8…40 mm (correspondingly).

The random errors may be somewhat reduced (about two or three times) by increasing the average number of primary photoelectrons in the photodetector pulse, e.g. by increasing the laser pulse energy. However, a systematic ranging error appears thereby, caused by decrease of the mean delay between the optical signal and the first primary photoelectron generation moment, as well as by decrease of the mean detector transit time.

The RMS ranging error may be reduced by averaging of the multiple TOF measurement results; however, the systematic error cannot be reduced by averaging. In some cases, the systematic error may considerably exceed the RMS error.

Elimination of the systematic error may be achieved by using a high-repetition-rate laser transmitter [1] with a low pulse energy, providing generation in the photodetector of much less than one primary photoelectron per transmit pulse.

Estimation of the systematic ranging error

To estimate the systematic error value, it is necessary to analyze the temporal variations of the return pulse arrival time (Figure 1).

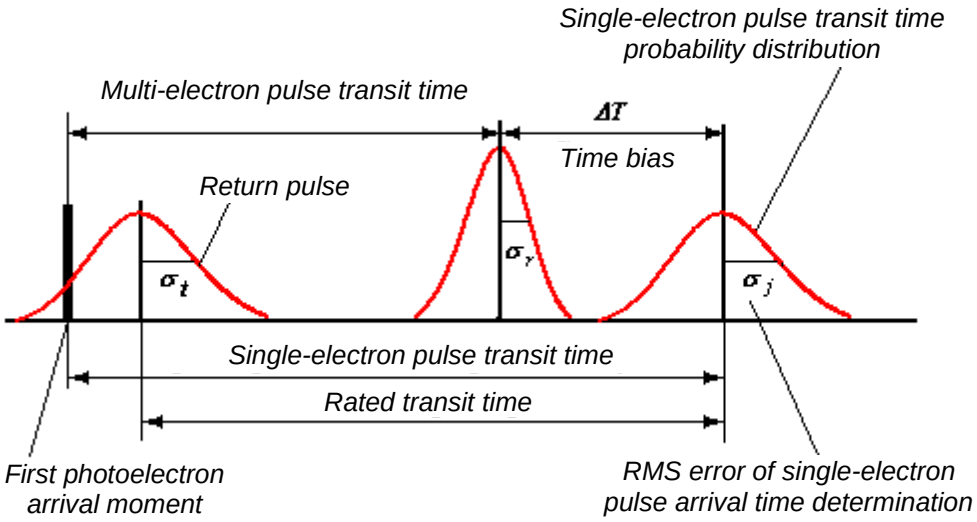

Figure 1. Temporal variations of return pulse arrival time

The process of charge carrier avalanche multiplication is started by the first generated photoelectron within the optical return pulse time limits. The corresponding time moment relative to the optical return pulse centroid varies randomly, and depends on the number of photons in the pulse. The pulse transit time in the photodetector also varies randomly, and also depends on the number of photons (and related photoelectrons) in the pulse. With an increase of the photon (and photoelectron) number, the delay in the photodetector output pulse arrival time is reduced because of the earlier first photoelectron generation as well as because of the detection transit time reduction.

If the return signal intensity does not fluctuate, the probability of n photoelectrons detection in the pulse is defined by the Poisson law:

$$P(n, n_{se}) = \frac{n_{se}^{n}}{n!} \cdot \exp(-n_{se}) \qquad (1)$$

where n_{se} is the average number of photoelectrons generated by the return pulse. In this case, with a Gaussian approximation of the return pulse shape, the probability density of the first photoelectron appearance time distribution may be presented as follows:

$$p_p(t_1, n_{se}) = \frac{n_{se}}{\sqrt{2\pi}} \cdot \frac{\exp(-t_1^2/2)}{1-\exp(-n_{se})} \cdot \exp\left[-\frac{n_{se}}{\sqrt{2\pi}} \int_{-\infty}^{t_1} \exp(-x^2/2)dx\right] \qquad (2)$$

where t_1 is the first photoelectron appearance time normed to the return pulse half-width σ_t. In Figure 2, the $p_p(t_1,n_{se})$ function shape is shown for different values of n_{se}.

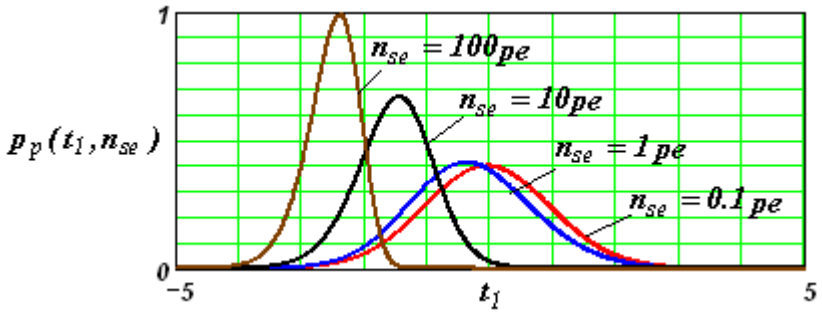

Figure 2. Probability density of the first photoelectron appearance time for non-fluctuating return signals

With $n_{se} << 1$, the curve of probability density of the first photoelectron appearance time has the same shape as the optical return pulse, and the appearance time has a zero mathematical expectation, i.e. the mean time of the first photoelectron appearance corresponds to the return pulse centroid. With an increase of n_{se}, the mean first photoelectron appearance time delay is reduced, thus causing a systematical ranging error which may be estimated from the expression:

$$\Delta t_{tr} = \int_{-\infty}^{\infty} t_1 \cdot p_p(t_1, n_{se}) \cdot dt_1 \qquad (3)$$

where Δt_{tr} is the systematic ranging error normed to the return pulse half-width. If the return signal intensity fluctuates, the probability density of the first photoelectron appearance time $p_b(t_1, n_{se})$ may be determinated from the expression:

$$p_b(t_1, n_{se}) = \int_{0}^{\infty} p_p(t_1, n) \cdot p(n) \cdot dn \qquad (4)$$

where $p(n)$ is the return pulse intensity probability density.

In a common case, the optical return pulse intensity fluctuations are caused by the atmosphere turbulence at the upward and downward laser beam propagation path, as well as by interference effects arising when the laser pulse is reflected by multiple cube corner reflectors in the retroreflector array [2]. There are sufficient theoretical and experimental data providing the possibility of adequate numerical estimation of the resulting probability density taking into account the turbulent atmosphere effects as well as the specle effects caused by reflection from multiple cube corners. However, for analytical estimations it would make sense to use an approximation of the resulting probability density in the form of an exponential distribution:

$$p(n) = \frac{1}{n_{se}} \cdot \exp\left(-\frac{n}{n_{se}}\right) \qquad (5)$$

In this case, the probability of n photoelectrons detection in the return signal pulse is defined by the Bose-Einstein distribution:

$$P(n, n_{se}) = \frac{1}{1+n_{se}} \cdot \left(\frac{n_{se}}{1+n_{se}}\right)^{n} \qquad (6)$$

and the probability density of the first photoelectron appearance time calculated in accordance with the equation (4) has a form shown in Figure 3:

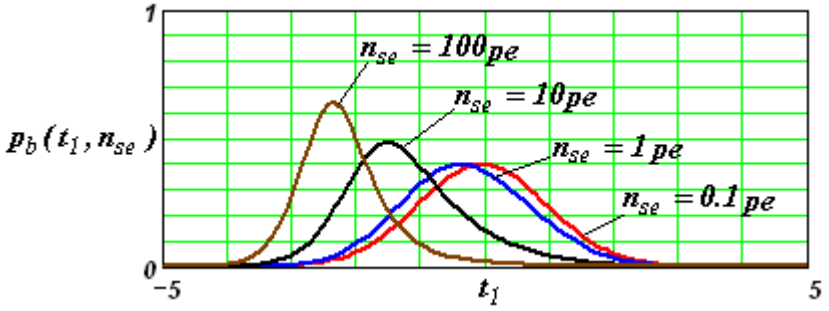

Figure 3. Probability density of the first photoelectron appearance time for fluctuating return signal pulses

From the expressions (1-6) one may calculate the systematic ranging error ΔT_{tr} caused by change in the first photoelectron appearance time on the average number of photoelectron in the pulse. The dependence is shown in Figure 4:

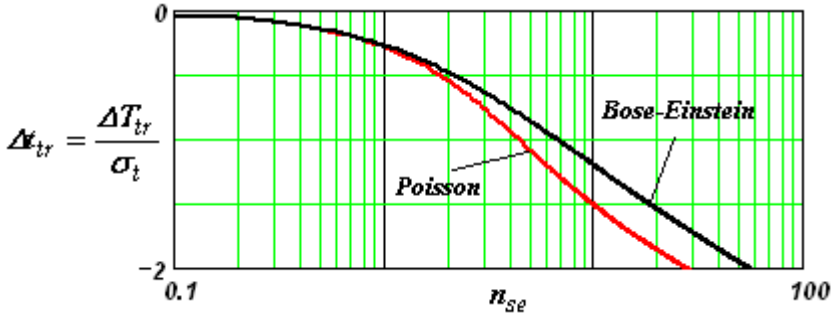

Figure 4. Estimated time bias caused by first photoelectron appearance time variations

One may see from the curves that when the average number of photoelectrons in the pulse is more than 6, the systematic error of measurements (time bias) is always more than σ_t. The σ_t behavior at low n_{se} values will be analyzed below.

For a quantitative estimation of the photoelectrons number in the pulse effect on the transit time, it is worth while to use the results presented in [3]. In this publication, a model is proposed of the avalanche buildup process in the photodetector. In accordance with this model, the transit time is interpreted as the mean time needed for duplication of the number of charge carriers multiplied by the number of duplications needed for exceeding the threshold value of the comparator in the SLR station receiver. In this case, the transit time bias dependence on the average number of photoelectrons in the pulse is defined by the expression:

$$\Delta T_r = \frac{\sigma_j}{\ln 2} \cdot \left[\frac{\sum_{n=1}^{\infty} P(n, n_{se}) \cdot \ln(n)}{\sum_{n=1}^{\infty} P(n, n_{se})} \right] \qquad (7)$$

where σ_j is the RMS deviation of the transit time value for the single-electron pulse. In Figure 5, the dependence is shown, calculated in accordance with (7) for fluctuating and non-fluctuating return signals:

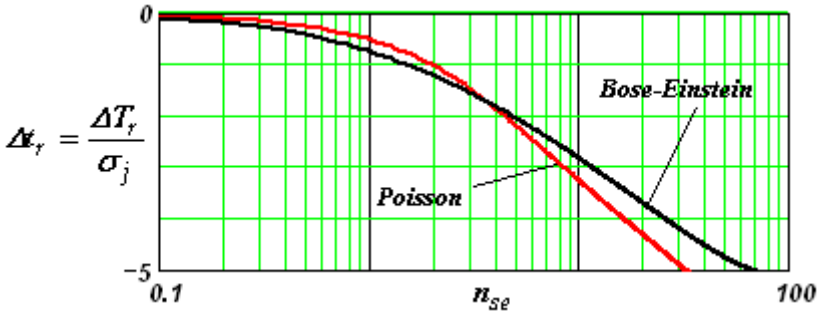

Figure 5. Estimated time bias caused by pulse transit time variations in the photodetector

The systematic ranging error here dominates over the σ_j value already when the average number of photoelectrons in the return signal is more than 2.

Estimation of the required average number of photoelectrons in the return signal pulse

The resulting bias in the return signal pulse arrival time, in accordance with the relationship (3) and (7), may be presented as:

$$\Delta T_{bias} = \sigma_t \cdot \Delta t_{tr} + \sigma_j \cdot \Delta t_r \qquad (8)$$

To retain resulting bias below a certain level, the average number of photoelectrons in the pulse should be small enough. In Tables 1 and 2, permissible values are presented of the average photoelectrons number in the pulse, calculated in accordance with (8) for permissible values of range estimation bias 0.3 mm and 0.6 mm (correspondingly).

Table 1. Permissible bias of estimation: ΔT_{bias} = 2 ps, σ_j = 20 ps

Pulsewidth		**50 ps**	**120 ps**	**240 ps**	**480 ps**
$\mathbf{n_{se}}$	**Poisson**	0.123	0.074	0.041	0.017
	Bose-Einstein	0.077	0.053	0.033	0.015

Table 2. Permissible bias of estimation: ΔT_{bias} = 4 ps, σ_j = 20 ps

Pulsewidth		**50 ps**	**120 ps**	**240 ps**	**480 ps**
$\mathbf{n_{se}}$	Poisson	0.250	0.157	0.094	0.047
	Bose-Einstein	0.163	0.116	0.077	0.042

The following conclusions may be drawn from the calculation results:

- The effect of intensity fluctuations on the ranging systematic error decreases with decrease of the average number of photoelectrons in the return signal pulse.

- At $n_{se} \leq 0.05$, the ranging systematic error does not exceed 0.6 mm for return pulsewidth less than 400 ps.
- At $n_{se} \leq 0.02$, the ranging systematic error does not exceed 0.3 mm for return pulsewidth less than 400 ps.

Estimation of the required pulse repetition rate

To provide the SLR station operation at a sufficiently small n_{se} level, it is necessary to meet the requirement:

$$F \geq \frac{f_{se}}{n_{se}} \qquad (9)$$

where F is the laser pulse repetition rate, and f_{se} is the mean value of return signal photoelectron generation frequency in the SLR station receiver (i.e., the average number of signal-initiated photoelectrons per second).

The mean frequency of signal photoelectron appearance depends on the average laser power and may be determined from the equation:

$$f_{se} = \frac{\eta}{h\nu} \cdot \frac{4P_{av}}{\pi\theta_t^2} \cdot \sigma \cdot \frac{A_r}{4\pi R^4} \cdot \tau_{opt} \cdot \tau_{atm} \qquad (10)$$

where η is the photodetector quantum efficiency, $h\nu$ is the quantum energy, P_{av} is the laser average power, θ_t is the laser transmitter output beamwidth, σ is the equivalent retroreflector array cross-section, A_r is the receive telescope aperture area, R is the target range, τ_{opt} is the optical system transmission, and τ_{atm} is the two-way atmosphere transmission.

For a compact SLR station with an average laser power of about 1 W (e.g. for the SAZHEN-TM SLR station) the f_{se} value is about 10 sec^{-1} with a GLONASS satellite being the target, and about 100 sec^{-1} with a LAGEOS. For SLR stations having the same average power but a 0.5 m-diameter aperture, the f_{se} value is usually between 200 and 2000 sec^{-1}. Hence, to provide $n_{se} \leq 0.5$ a corresponding pulse repetition rate of 4 kHz to 40 kHz is necessary.

The requirement for the pulse repetition rate value may be mitigated by reducing the f_{se} value, e.g. by an increase of the laser beamwidth; however, the SLR station productivity will be thereby less, because the f_{se} value is the maximum return rate and hence a decrease of this value will increase the time necessary to obtain a sufficient number of individual range measurements.

Thus, to eliminate the ranging systematic errors with a simultaneous increase or retaining of the station productivity, it is desirable to use laser pulse repetition rates of several tens of kHz.

References

1. V.P. Vasiliev, V.D. Shargorodsky. Precision Satellite Laser Ranging using high-repetition-rate lasers. Electromagnetic Waves and Electronic Systems. vol.12, No.7, 2007

2. J.L. Bufton, S.T. Ramakrishna, L.S. Taylor. Scintillation statistics caused by atmospheric turbulence and speckle in satellite laser ranging. Applied Optics, vol.16, No.8, 1977
3. E Samain. Timing of optical pulses by photodiode in the Geiger mode. Applied Optics, vol.37, No.3, 1998.